The effect of mineral addition on the pyrolysis products derived from typical Highveld coal

L Roets

21562628

Dissertation submitted in fulfilment of the requirements for the degree of **Master** in **Chemical Engineering,** at the Potchefstroom Campus of the North-West University.

Supervisor: Prof JR Bunt (NWU)

Co-supervisors: Prof HWJP Neomagus (NWU)

Prof CA Strydom (NWU)

Dr D van Niekerk (Sasol)

November 2014

Even in literature and art, no man who bothers about originality will ever be original: whereas if you simply try to tell the truth (without caring twopence how often it has been told before) you will, nine times out of ten, become original without ever having noticed it.

❖ C.S. Lewis

Declaration

I, Leon Roets, hereby declare that the dissertation entitled: ***"The effect of mineral addition on the pyrolysis products derived from typical Highveld coal"***, submitted in fulfilment of the requirements for the degree of Master in Chemical Engineering, is my own work except where acknowledged in the text, it has been language edited as required and has not been submitted to any other tertiary institution in whole or in part.

I understand that the copies, handed in for examination, is the property of the university.

Signed at Potchefstroom on the **12th** day of November 2014.

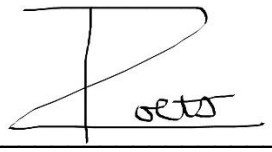

Leon Roets (Student)

21562628

University number

Acknowledgements

"No man is an island,
Entire of itself,
Every man is a piece of the continent,
A part of the main."
- John Donne –

Without a team effort this dissertation would never have seen the light. The author hereby wishes to acknowledge and thank everyone involved during the course of this study and would like to send out a special word of gratitude to the following:

- My study leaders, Professors John Bunt, Hein Neomagus, Christien Strydom and Dr Daniel van Niekerk for their guidance, assistance and willingness to help. Their critical evaluation of my work ensured that I reach my full potential during the course of this investigation. Words cannot put enough value to your assistance.
- The NRF and SARChI Coal chair for financial support with respect to this investigation.
- Mr Jan Kroeze, Mr Adrian Brock and Mr Ted Paarlberg for their assistance and manufacturing of the retorts and additional accessories for the pyrolysis experiments.
- Another word of appreciation to Dr Daniel van Niekerk for assistance and training with regard to the use and interpretation of the analyses of the tars (Simdis, GC-MS, GC-FID and SEC-UV).
- Sasol Infrachem® for performing Simdis, GC-MS and GC-FID on the generated tar samples.
- Mr Ben Ashton for his assistance with the XRD analyses of the raw coal samples.
- Mr Gregory Okolo for his assistance and training with regard to BET analyses of the coal fractions and generated chars.
- Mrs Wena Jansen van Vuuren for handling the bookings regarding the use of the TGA, acid washing laboratory and DRIFT apparatus. Thank you for your friendly assistance.
- Ms Rudelle White for assistance and training regarding the use of the TGA and DRIFT apparatus.
- Ms Jackie Collins for training regarding the acid washing of coal.
- Mr Adolph Kleynhans (final year student) for his assistance regarding the pyrolysis experiments on the raw and acid washed coal fractions.

- Mr Frikkie Conradie and Mr Hennie Coetzee for their assistance and training regarding the use of the GC for gas analyses.
- Mrs Sanet Botes, Mrs Eleanor de Koker and Ms Benice de Wit for the placement of orders, handling of finances and other arrangements.
- Mr Nico Lemmer for laboratory assistance and good conversations.
- Mr Shawn Liebenberg of the Statistical Consultancy Service (SCS) at the NWU for his assistance with the data and statistical interpretation thereof.
- Another word of gratitude towards Prof John Bunt who mentored me over a course of three years, who always remained hopeful and always believed in my abilities. Thank you for who you are, the way you do things and the way in which you guided me through this process. It was only a privilege.
- My residence and all its residents, Patria Manskoshuis. It was only a privilege to serve you all. Thank you for six years of pride, brotherhood, respect and self-belief. The albatross will always stay in my heart.
- The two house committees of Patria Manskoshuis who supported me throughout this study. Tienie van Wyk, Estiane de Lange, Adolph Kleynhans, Marinus Pawson, Nicol Goodwin, Elric Pretorius, Jan-Ben Wiese, Bennie Genis, Louis Potter, Barry Cronje, Louis Vorster, Dawid Labuschagne, Willie Blignaut, Marnus Gerber, Jaco de Klerk and Dirk van der Merwe. Thank you for the friendship, the good laughs and all the fun times.
- Mr Hendri Swanepoel, Mr Johan van Heerden, Mr Marco Pretorius, Mr Kobus Dannhauser and Mr Riaan Venter for their friendship and never ending belief in me.
- My housefather and a mentor in life, Mr James Stoffberg. Thank you for your support and that you taught me what it means to be a man.
- My parents and my brother for their love, moral support and guidance. You are the cornerstone on which my life house is built; without you nothing would have been possible.
- All teachers, mentors, individuals and persons who have affected my life thus far in any way. In the end it is your perception on life that determines the glasses through which you view all things else. Thank you for your contribution.

Soli Deo gloria

Quotes

Anon. 2014. Available at http://www.goodreads.com/quotes/tag/research?page=2. Date of access: 8 September 2014.

Pictures

Part 1:

Anon. 2014. Available at http://hqwallpapers.org/wallpapers/l/1920x1080/7/, macro_minerals_ 1920x1080_6478.jpg Date of access: 8 September 2014.

Part 2:

Anon. 2014. Available at http://www.oldhamsolidfuels.co.uk/wp-content/uploads/2013/04/coal.jpg Date of access: 8 September 2014.

Part 3:

Anon. 2014. Available at http://hqdesktop.net/wallpapers/l/1920x1080/110/architecture_cityscapes_factories_landscapes_refinery_1920x1080_109978.jpg Date of access: 8 September 2014.

Part 4:

Anon. 2014. Available at http://www.sharewallpapers.org/d/686088-1/oil+refinery+plant+in+bahrain.jpg Date of access: 8 September 2014.

Abstract

Mineral matter affect various coal properties as well as the yield and composition of products released during thermal processes. This necessitates investigation of the effect of the inherent minerals on the products derived during pyrolysis, as pyrolysis forms the basis of most coal utilisation processes. A real challenge in this research has been quantifying the changes seen and attributing these effects to specific minerals. Thus far it has been deemed impossible to predict product yields based on the mineral composition of the parent coal. Limited research regarding these aspects has been done on South African coal and the characterisation of pyrolysis products in previous studies was usually limited to one product phase. A novel approach was followed in this study and the challenges stated were effectively addressed.

A vitrinite-rich South African coal from the Highveld coal field, was prepared to an undersize of 75 µm and divided into two fractions. HCl/HF acid washing reduced the ash yield from 14.0 wt% d.b. to 2.0 wt% d.b. (proximate analysis). Pyrolysis was carried out with the North-West University (NWU) Fischer Assay setup at 520, 750 and 900°C under N_2 atmosphere and atmospheric pressure. The effect of acid washing and the addition of minerals on the derived pyrolysis products were evaluated.

Acid washing led to lower water and tar yields, whilst the gas yields increased, and the char yields were unaffected. The higher gas yield can be related to increased porosity after mineral removal as revealed by Brunauer-Emmett-Teller (BET) CO_2 adsorption surface area analysis of the derived chars. Gas chromatography (GC) analyses of the derived pyrolysis gases indicated that the acid washed coal fraction (AW TWD) derived gas contained higher yields of H_2, CH_4, CO_2, C_2H_4, C_2H_6, C_3H_4, C_3H_6 and C_4s when compared to the gas derived from the raw coal fraction (TWD). The CO yield from the TWD coal was higher at all final pyrolysis temperatures. Differences in gas yields were related to increased tar cracking as well as lower hydrogen transfer and de-hydrogenation of the acid washed chars. Analyses of the tar fraction by means of simulated distillation (Simdis), gas chromatography mass spectrometry (GC-MS) –flame ionization detection (–FID) and size exclusion chromatography with ultraviolet (SEC-UV) analyses, indicated that the AW TWD derived tars were more aromatic in nature, containing more heavier boiling point components, which increased with increasing final pyrolysis temperature. The chars were characterised by proximate, ultimate, X-ray diffraction (XRD), X-ray fluorescence (XRF), diffuse reflectance infrared Fourier-transform (DRIFT) and BET CO_2 analyses.

Addition of either 5 wt% calcite, dolomite, kaolinite, pyrite or quartz to the acid washed fraction (AW TWD) was done in order to determine the effect of these minerals on the pyrolysis products. These minerals were identified as the most prominent mineral phases in the Highveld coal used in this study, by XRD and quantitative evaluation of minerals by scanning electron microscopy (QEMSCAN) analyses. It was found that mineral activity decreased in the order calcite/dolomite>pyrite>kaolinite>>>quartz. Calcite and dolomite addition led to a decrease in tar yield, whilst the gas yields were increased. Markedly, increased water yields were also observed with the addition of calcite, dolomite and pyrite. Kaolinite addition led to increased tar, char and gas yields at 520°C, whilst the tar yield decreased at 750°C. Pyrite addition led to decreased tar and gas yields. Quartz addition had no noteworthy effect on pyrolysis yields and composition, except for a decrease in char yield at all final pyrolysis temperatures and an increased gas yield at 520°C. Regarding the composition of the pyrolysis products, the various minerals had adverse effects. Calcite and dolomite affected the composition of the gas, tar and char phases most significantly, showing definite catalytic activity. Tar producers should take note as presence of these minerals in the coal feedstock could have a significant effect on the tar yield and composition. Kaolinite and pyrite showed some catalytic activity under specific conditions. Model coal-mineral mixtures confirmed synergism between coal-mineral and mineral-mineral interactions. Although some correlation between the pyrolysis products derived from the model coal-mineral mixtures and that of TWD coal was observed, it was not possible to entirely mimic the behaviour of the coal prior to acid washing.

Linear regression models were developed to predict the gas, tar and char yields (d.m.m.f.) with mineral composition and pyrolysis temperature as variables, resulting in R^2 coefficients of 0.837, 0.785 and 0.846, respectively. Models for the prediction of H_2, CO, CO_2 and CH_4 yields with mineral composition and pyrolysis temperature as variables resulting in R^2 coefficients of 0.917, 0.702, 0.869 and 0.978, respectively. These models will serve as foundation for future work, and prove that it is feasible to develop models to predict pyrolysis yields based on mineral composition. Extending the study to coals of different rank can make the models universally applicable and deliver a valuable contribution in industry.

Keywords: Mineral matter/minerals, pyrolysis, devolatilisation, acid washing, demineralisation, tar, char, gas, empirical modelling, South African coal

Opsomming

Mineraalinhoud het ‘n effek op verskeie eienskappe van steenkool sowel as op die opbrengs en samestelling van die produkte wat vrygestel word tydens termiese prosesse. Dit maak dit nodig om navorsing te doen om vas te stel wat die effek van die inherente minerale op die pirolise produkte is, omdat pirolise die basis vorm van meeste steenkoolprosesse. ‘n Groot uitdaging in hierdie navorsing tot dusver was om die veranderinge wat gesien word te kwantifiseer end it toe te skryf aan spesifieke minerale. Tot dusver is dit as nie moontlik beskou om die piroliseproduk-opbrengste te voorspel afhangend van die mineraalinhoud van die steenkool nie. Beperkte navorsing ten opsigte van hierdie aspekte is tot dusver op Suid-Afrikaanse steenkool gedoen en die karakterisering van die piroliseprodukte in vorige studies was gewoonlik beperk tot een produkfraksie. ‘n Unieke benadering is in hierdie studie gevolg en die gemelde uitdagings is effektief aangespreek.

‘n Vitriniet-ryke Suid-Afrikaanse steenkool van die Hoëveld-steenkoolveld was voorberei tot ‘n grootte kleiner as 75 µm en verdeel in twee fraksies. HCl/HF wassing het die asinhoud verminder van 14.0 gewigs% d.b. tot 2.0 gewigs% (relatiewe analise). Pirolise was uitgevoer met behulp van die Noordwes Universiteit (NWU) se Fischer opstelling by 520, 750 en 900°C onder ’n N_2-atmosfeer en atmosferiese druk. Die effek van suurwas en die byvoeging van minerale op die afgeleide piroliseprodukte was ondersoek.

Suurwas van die steenkool het tot laer water- en teer-opbrengste gelei, terwyl die gasopbrengs verhoog het en die sintel-opbrengs onveranderd was. Die hoër gasopbrengs is verwant aan die verhoogde porositeit na mineraalverwydering soos aangedui deur Brunauer-Emmett-Teller (BET) CO_2 adsorpsie-oppervlakarea-analises op die sintelopbrengste. Gaschromatografie (GC) analises van die pirolisegasse het aangedui dat die suurgewasde steenkoolfraksie (AW TWD) -gasse hoër opbrengste van H_2, CH_4, CO_2, C_2H_4, C_2H_6, C_3H_4, C_3H_6 en C_4s gehad het, terwyl die rou steenkoolfraksie (TWD) ‘n hoër opbrengs van CO gehad het by alle finale pirolise temperature. Analise van die teerfraksie deur gesimuleerde distillasie (Simdis), gaschromatografie-massaspektrometrie (GC-MS) en vlam-ionisasie-deteksie (FID) en grootte-uitsluitingschromatografie met ultraviolet (SEC-UV) -analises het aangedui dat die AW TWD tere meer aromaties van natuur was, met meer hoër kookpunt-komponente wat toegeneem het met toename in finale pirolisetemperatuur. Die sintels is gekarakteriseer deur relatiewe-, totale-, X-straaldiffraksie (XRD-), X-straalfluoressensie (XRF-), diffuse reflektansie infra-rooi-Fourier-transform (DRIFT-) en BET- CO_2 adsorpsie-analises.

Die byvoeging van of 5 gewigs% kalsiet, dolomiet, kaoliniet, piriet of kwarts by die suurgewasde fraksie (AW TWD) is gedoen om te bepaal wat die effek van hierdie minerale op die piroliseprodukte is. Hierdie minerale was die prominentste mineraalfases soos geïdentifiseer deur XRD en kwantitatiewe evaluasie van minerale deur skandeerelektronmikroskopie (QEMSCAN)-analise. Mineraalaktiwiteit neem af in die volgorde kalsiet/dolomiet>piriet>kaoliniet>>>kwarts. Kalsiet- en dolomite-byvoeging het tot ‘n afname in teeropbrengs gelei, terwyl die gasopbrengs verhoog het. ‘n Merkbare toename in wateropbrengs is ook waargeneem met die byvoeging van kalsiet, dolomiet en piriet. Kaoliniet-byvoeging het tot verhoogde teer-, sintel en gasopbrengs by 520°C gelei, terwyl die teeropbrengs afgeneem het by 750°C. Piriet-byvoeging het tot ‘n afname in teer en gas gelei. Kwarts-byvoeging het geen noemenswaardige effek op die pirolise-opbrengste en -samestellings gehad nie, behalwe ‘n afname in sintelopbrengs en toename in gasopbrengs by 520°C. Ten opsigte van die samestelling van piroliseprodukte het die onderskeie minerale wisselende effekte getoon. Kalsiet en dolomiet het die samestelling van die gas-, teer- en sintelfases noemenswaardig beïnvloed, wat ‘n aanduiding van definitiewe katalitiese effek was. Teervervaardigers moet daarop let dat die teenwoordigheid van hierdie minerale in die steenkoolvoer ‘n merkwaardige effek op die teeropbrens en samestelling kan hê. Kaoliniet en piriet het katalitiese aktiwiteit onder sekere kondisies getoon. Model-steenkool-mineraal-mengsels het die wisselwerking tussen steenkool-mineraal en mineraal-mineraal interaksies bevestig. Alhoewel daar sekere korrelasie tussen die piroliseprodukte van die model steenkool-mineraalmengsels en van TWD-steenkool gevind is, was dit nie moontlik om die gedrag van die steenkool voor suurwas te mimiek nie.

Lineêre regressiemodelle is ontwikkel om die opbrengste (droë, mineraalvrye basis) te voorspel van gas, teer en sintels met mineraalsamestelling en pirolise-temperatuur as funksies. Die R^2 koeffisiënte is gevind om 0.837, 0.785 en 0.846 onderskeidelik te wees. Modelle vir die voorspelling van H_2, CO, CO_2 en CH_4 is ontwikkel met mineraalsamestelling en pirolisetemperatuur as funksies. Die R^2 koeffisiënte was 0.917, 0.702, 0.869 en 0.978, onderskeidelik. Hierdie modelle sal as basis dien vir toekomstige werk, en bewys dat dit moontlik is om modelle te ontwikkel wat die pirolise-opbrengste voorspel, gebaseer op die mineraalsamestelling van die steenkoolvoer. Uitbreiding van die studie na steenkool van verskillende rang kan die modelle universeel toepaslik maak en ‘n waardevolle bydrae aan die industrie lewer.

Kernwoorde: Minerale, pirolise, suurwasing, suurloging, demineralisasie, teer, sintel, gas, empiriese modellering, Suid-Afrikaanse steenkool.

Publications and Conferences

Publications

Roets, L., Bunt, J.R., Neomagus, H.W.J.P. and Van Niekerk, D. 2014. An evaluation of a new automated duplicate-sample Fischer Assay setup according to ISO/ASTM standard and analysis of the tar fraction. *Journal of Analytical and Applied Pyrolysis,* 106: 190-196.

Conferences

Roets, L., Bunt, J.R., Neomagus, H.W.J.P. and Van Niekerk, D. 2014. Evaluation of an automated duplicate-sample Fischer Assay setup according to ISO/ASTM standard and analysis of the tar fraction. *6th International Freiburg Conference on IGCC & XtL Technologies, Coal Conversion and Syngas*, 19-22 May, Dresden/Radebeul, Germany.

Table of Contents

List of figures

List of tables

Nomenclature

Acronym	Description
A-B	Alkyl-benzenes
ACE	Associated Chemical Enterprises
a.d.	Air dry basis
A-I	Alkyl-indenes
Aliph.	Aliphatic compounds
A-N	Alkyl-naphthalenes
ANOVA	Analysis of variance
A-P	Alkyl-phenols
Arom. E & E	Aromatic ethers and esters
ASTM	Ameican Society for Testing and Materials
AW-Cal	Acid washed coal with 5 wt% calcite addition
AW-Dol	Acid washed coal with 5 wt% dolomite addition
AW-Kao	Acid washed coal with 5 wt% kaolinite addition
AW-Pyr	Acid washed coal with 5 wt% pyrite addition
AW-QZ	Acid washed coal with 5 wt% quartz addition
AW TWD	Acid washed coal sample
BET	Brunauer-Emmett-Teller adsorption
BTX	Benzene, toluene, xylene
CCSEM	Computer controlled scanning electron microscopy
C.I.	Confidence interval
C^{13} NMR	Carbon-13 Nuclear Magnetic Resonance
C.V.	Calorific value
CTL	Coal-to-liquids
d.a.f.	Dry, ash free basis
d.b.	Dry basis
DRIFT	Diffuse Reflectance Infrared Fourier-transfrom spectroscopy
DTG	Differential thermogravimetry/thermogravimetric
DV	Dependent variable
EPMA	Electron probe micro-analyser
FBDB gasifier	Fixed-bed dry-bottom gasifier
FBP	Final boiling point
FC	Fixed carbon
FFAP	Free fatty acids phase
FFF	Fossil Fuel Foundation
FTIR	Fourier transformed infrared spectroscopy
GC	Gas chromatograph / chromatography
GC-FID	Gas chromatography with flame ionization detection
GC-MS	Gas chromatography mass spectrometry

Acronym	Description
HM	High ash percentage mineral mixture and acid washed coal mixture
HPLC	High pressure liquid chromatography
IBP	Initial boiling point
ICP	Inductive-coupled plasma
IR	Infrared
ISO	International Standard Organization
LCP's	Liquid crystalline polymers
LD-MS	Laser desorption mass spectrometry
LM	Low ash percentage mineral mixture and acid washed coal mixture
L.O.I.	Loss on ignition
MALDI-MS	Matrix assisted laser desorption/ionization mass spectrometry
MI	Maceral index
Mixed	Mixed aliphatic and aromatic compounds due to co-elution
m.m.b.	Mineral matter basis
m.m.f.b.	Mineral matter free basis
MS	Mass spectrometry
MSCs	Molecular sieving carbons
N-	Nitrogen heteroatoms
NMP	N-methyl-2-pyrrolidinone
NMR	Nuclear magnetic resonance
NWU	North-West University
PAHs	Poly aromatic hydrocarbons
PBN	Poly(butylene terephtalate)
PEN	Poly(ethylene naphthalate)
PONA	Paraffins, olefins, naphthenes and aromatics
Prox	Proximate
PTFE	Polytetrafluorethylene
QEMSCAN	Quantitative Evaluation of Minerals by SCANning electron microscopy
R & D	Research and Development
RID	Reffractive index
RINT	Reactive inertinite
ROM	Run-of-mine
RSF	Reactive semifusinte
SABS	South African Bureau of Standards
SANS	South African National Standard
SEC	Size-exclusion chromatography
SEC-UV	Size-exclusion chromatography ultraviolet fluorescence spectroscopy
Simdis	Simulated distillation
TCD	Thermal conductivity detector
TG	Thermogravimetric / thermogravimetry
TGA	Thermogravimetric Analyser
TL	Total liptinite
TV	Total vitrinite
TWD	Highveld coal

Acronym	Description
TWD-Cal	Highveld washed coal with 5 wt% calcite addition
TWD-Dol	Highveld washed coal with 5 wt% dolomite addition
TWD-Kao	Highveld ashed coal with 5 wt% kaolinite addition
TWD-Pyr	Highveld washed coal with 5 wt% pyrite addition
TWD-QZ	Highveld washed coal with 5 wt% quartz addition
Ult	Ultimate
UV	Ultraviolet
UV-F	Ultraviolet fluorescence spectroscopy
vol.%	Volume percentage
WABP	Weighed average boiling point
WCA	World Coal Association
WCI	World Coal Institute
wt%	Weight percentage
XRD	X-ray diffraction
XRF	X-ray fluorescence

Roman symbols

Symbol	Description	Dimension
B_{1-7}	Gas bag parameters	m
B_i	General constant for yield models	-
C_i	Constant for temperature value in yield models	-
C_j	Constant for mineral loading value in yield models	-
HV	Heating value / Gross calorific value	MJ/kg
INR	Reactive inertinite content (mineral matter free basis)	vol.%
INT	Inertinite content (mineral matter free basis)	vol.%
LIP	Liptinite content (mineral matter free basis)	vol.%
M	Inherent moisture	wt%
m	mass	g
MI	Maceral index	-
MM	Mineral matter	wt%
MW	Molecular weight	g/mol
R	Molar gas constant	J/K/mol
RMI	Reactive maceral index	-
R_r	Mean random vitrinite reflectance	%
T	Temperature	°C or K
V	Volume	m^3
VIT	Vitrinite content (mineral matter free basis)	vol.%
VM	Volatile matter	wt%
VM_j	Volatile matter contribution of maceral, j	wt%
Y	Yield	wt%
Y_j	Content of maceral, j in the coal	vol.%
Y_m	Content of residual macerals in the coal	vol.%

Greek symbols

Symbol	Description	Dimension
Φ_j	Fractional volatile matter content of maceral, j	-
Φ_m	Fractional volatile matter content of residual macerals	-
ζ_j	Percentage contribution of maceral, j	%
ρ	Density	kg/m^3

Glossary

Pyrolysis

The thermal process by which coal undergoes destructive distillation to form char, volatile liquids (containing tars, oils and aqueous compounds) and gaseous products in the absence of oxygen.

AW TWD

Refers to the acid washed fraction of the Highveld coal sample used in this study.

TWD

Refers to the coal sample obtained from the Highveld coal field after beneficiation. This coal is usually exported and characterised by a low (12-15 wt%) ash content.

Part 1 – Background and motivation

Chapter 1: General introduction

Chapter 2: Literature review

"The measure of greatness in a scientific idea is the extent to which it stimulates thought and opens up new lines of research."

— Paul A.M. Dirac

Chapter 1: General Introduction

This Chapter motivates an investigation into the effect of mineral matter on the pyrolysis product yields of a typical South African Highveld coal. A brief introduction and motivation is provided in Section 1.1, which outlines the importance of coal, and the extent to which pyrolysis is influenced by mineral matter and why the investigation of pyrolysis products could provide insight into this matter. Section 1.2 provides a subsequent formulated problem statement, which is further scrutinized with regard to research objectives in Section 1.3. The chapter is concluded in Section 1.4 with the scope of the investigation, whilst Section 1.5 provides detail with regard to the outline of this dissertation.

1.1. Background and motivation

1.1.1. Coal and its applications

Coal has supplied half of the world's energy over the last decade (WCA, 2012; WCI, 2005). In South Africa coal supplies 74-75% of the country's total energy. 92% of electricity is generated by coal-fired power plants and 30% of the country's fuel is provided by coal-to-liquid (CTL) plants (FFF, 2013; Malumbazo *et al.*, 2012; Department of Mineral Resources, 2009; Cairncross, 2001). Coal is not only used as petrochemical and energy sources, but is also used in non-fuel applications such as: (1) the production of metallurgical coke and activated carbon, (2) the production of aromatic chemicals from coal tars, (3) the manufacturing of binder pitch from coal tar pitch, and (4) the production of polymers, fertilizers and even cosmetics from coal by-products to name a few applications (Ahmad *et al.*, 2009a; Jiang *et al*., 2007; Schobert and Song, 2002; Chen *et al.,* 1997; Domínguez, 1996; Longwell *et al*., 1995; Schobert, 1990). Processes used for the preparation of these products include combustion, gasification, carbonization and liquefaction (Ahmad *et al*., 2009a; Liu *et al.*, 2004; Li *et al.*, 2004; Ôztas and Yürüm, 2000; and Mondragon *et al.*, 1999).

1.1.2. Pyrolysis products and mineral matter present in coal

Pyrolysis is the initial step in most coal conversion processes and it is largely dependent on the properties of the coal (Wang *et al.*, 2013; Hu *et al.,* 2004; Chen *et al.,* 1997; Solomon and Hamblen, 1985). Pyrolysis is the thermal process by which coal undergoes destructive distillation to form char, volatile liquids (containing tars, oils and aqueous compounds) and gaseous products in the absence of oxygen (Bell, 2011; Bunt & Waanders, 2008; Kandiyoti *et al*., 2006; Samaras *et al.,* 1996; Schobert, 1990; Lowry, 1945). Devolatilisation and pyrolysis

are sometimes used synonymously (Hattingh, 2012); however devolatilisation usually refers to the process of destructive distillation in the presence of oxygen. Pyrolysis products may provide much information with regard to the parent coal. Many of the structural elements are preserved in the tar fraction which constitutes 50 – 80% of the released volatiles (Solomon and Hamblen 1985; Gavalas, 1982).

Coal has very complex and heterogeneous in structure, containing various organic and inorganic species (Cakal *et al.,* 2007; Ward, 2002, Schobert, 1990). The inorganic fraction contains the various minerals, of which over 125 have been identified (Vassilev & Vassileva, 1996, Schobert, 1992). Most of these minerals (about 100) are described as trace minerals (minerals present in a very low concentration with grain sizes smaller than 10 μm), with only a few considered to be of significance (Vassilev & Vassileva, 1996). The most common major minerals in bituminous coal are: quartz, kaolinite, gypsum, pyrite, calcite, illite and feldspars (Gornostayev *et al.*, 2009; Nel, 2009; Prinsloo, 2008; Kabe *et al*., 2004; Cairncross, 2001; Vassilev *et al*., 1995). The minor minerals as reported by Prinsloo (2008) and Vassilev *et al*. (1995) include cristobalite, montmorillonite, mica, chlorite, zeolites, hematite, goethite, diaspore, borite, apatite, brucite, barytocalite, dolomite, siderite, marcasite, jarosite, alunite and hexahydrite, amongst others.

The mineral matter that is present in coal plays a large role during thermal processes which coal may undergo (Ahmad *et al.,* 2009a; Samaras *et al.*, 1996). Coal properties such as heating value, coal rank, reaction rate and ash content may be affected by the mineral matter content (Samaras *et al.,* 1996). The mineral matter may also affect final product yields due to the effect on the secondary pyrolysis reactions, as well as affect the composition of these products as has been observed during tar production (Hattingh, 2012; Ahmad *et al.,* 2009a; Liu *et al.,* 2004; Chen *et al.,* 1999; Velegol *et al.,* 1997; Samaras *et al.,* 1996; Franklin *et al.,* 1982a).

The catalytic effect of some minerals present in coal has been extensively studied in combustion, liquefaction and pyrolysis experiments (Reichel *et al.,* 2013; Fei *et al.,* 2012; Ahmad *et al.,* 2009a; Ahmad *et al*., 2009b; Yan *et al.,* 2005; Karaca*,* 2003; Lemaignen *et al.,* 2002; Ôztas and Yürum, 2000; Chen *et al.*, 1999; Mondragon *et al.,* 1999; Samaras *et al.,* 1996; Morgan and Jenkins, 1986a and 1986b; Franklin *et al.,* 1982a and 1982b; Yaw *et al.,* 1980; Schafer, 1979a, 1979b and 1980). However, little work has been done on South African coal. Some authors are of the opinion that the prediction of catalytic activity from the amount and composition of particular inorganic components appears unlikely to be feasible (Lemaignen *et al.*, 1999). This statement will be challenged in this study.

From a catalytic gasification perspective, the inorganic components provide the advantage that they are already present in the coal matrix, they are well dispersed and coal-mineral interactions are present, which is usually not the case with added catalysts (Schobert, 1992; Franklin 1980). A better understanding of the catalytic effect of the present inorganic matter will thus assist in more cost-effective operations and more consistency in product yields and composition. An additional motivation for this study is provided by Franklin (1980), stating that the effect of minerals needs to be determined in order to compare effects observed with coal rank and differences in petrography, with the effect of varying mineral content accounted for. When considering the fact that pyrolysis is a step which is so dependent on coal properties, a detailed understanding of the effect of mineral matter on the pyrolysis products will provide valuable insight (Solomon & Hamblen, 1985).

Sasol's CTL plants (as example) use Fixed-bed Dry-bottom technology in Lurgi gasifiers to convert coal to synthetic gas (syn-gas) and liquid products (WCI, 2009; WCI, 2005). Approximately 30 million tons of bituminous coal is processed in the Fischer-Tropsch process (WCI, 2009; WCI, 2005; Kandiyoti *et al*., 2006; Coetzer & Keyser, 2003). The raw gas that leaves the gasifier is quenched with recycled gas liquor to condense the oils and tars and remove the particulate matter (Leckel, 2011). The liquor is upgraded and separated into aqueous and hydrocarbon fractions for further processing. The residual products, characterized by a low hydrogen-to-carbon ratio and high nitrogen, oxygen and polynuclear aromatic contents, are upgraded in a tar refinery (Leckel, 2011; Erasmus & Scholtz, 2002). The aromatics retained from the refinery are of importance to boost the octane and diesel density in the final fuel pool of the low-temperature Fischer-Tropsch facility (Leckel, 2011; Leckel, 2008; Leckel, 2006). The tar is also beneficial for complementing the hydrotreated high-temperature Fischer-Tropsch distillate and provides synergies for a final, marketable diesel (Leckel, 2011).

The market value as well as production efficiency of tar is negatively affected by large compositional variances (Leckel, 2011; Ahmad *et al.*, 2009; Schobert & Song, 2002). In order to utilize tar effectively for the production of chemicals a better understanding of the composition and the properties of coal that affect this composition is needed (Leckel, 2011). Mineral matter has been shown to be responsible for product shifts in the various pyrolysis products (Reichel *et al.,* 2013; Fei *et al.,* 2012; Ahmad *et al.,* 2009a; Ahmad *et al*., 2009b; Yan *et al.,* 2005; Karaca*,* 2003; Lemaignen *et al.,* 2002; Ôztas & Yürum, 2000; Chen *et al.*, 1999; Mondragon *et al.,* 1999; Samaras *et al.,* 1996; Morgan & Jenkins, 1986a and 1986b; Franklin *et al.,* 1982a and 1982b; Yaw *et al.,* 1980; Schafer, 1979a, 1979b and 1980).

1.2. Problem statement

From Section 1.1 it is evident that it will be beneficial to understand the effect of the mineral matter present in coal on the pyrolysis products formed during thermal processing of coal. Research with regard to the effect of coal mineral matter on the pyrolysis products has been conducted by numerous researchers (Reichel *et al.,* 2013; Fei *et al.,* 2012; Ahmad *et al.,* 2009a; Ahmad *et al*., 2009b; Yan *et al.,* 2005; Karaca*,* 2003; Lemaignen *et al.,* 2002; Ôztas & Yürum, 2000; Chen *et al*., 1999; Mondragon *et al.,* 1999; Samaras *et al.,* 1996; Morgan & Jenkins, 1986a and 1986b; Franklin *et al.,* 1982a and 1982b; Yaw *et al.,* 1980; Schafer, 1979a, 1979b and 1980). Most of this work has been performed on lignite-rich coal and brown coals in the subbituminous group using thermogravimetric analysers (TGAs) and other bench-scale methods (Liu *et al.,* 2004a; Ôztas & Yürum, 2000; Chen *et al*., 1999; Samaras *et al.,* 1996). Although most of these studies refer to the effect of mineral matter on the composition of the pyrolysis products, the methods of addition and/or removal of these minerals are sometimes unclear. There is also a lack in detailed characterisation of the effect of the individual minerals on pyrolysis products (Liu *et al.,* 2004a; Chen *et al.,* 1999; Samaras *et al.,* 1996).

1.3. Objectives of investigation

The main objective of this investigation is to determine the effect of mineral matter on the pyrolysis products derived from a typical South African (Highveld) bituminous coal. This objective should be accompanied by quantification of the effect of the individual minerals added. In order to achieve this, the following objectives have been identified:

i. Characterisation of a typical Highveld (South African) coal by means of chemical, mineralogical, structural and petrographic analyses as to provide detailed information with regard to the make-up of the coal structure and changes seen after acid washing.

ii. Determine the effect of acid washing on the pyrolysis product yield and composition by pyrolysis experiments (520, 750 and 900°C) and characterisation of the different pyrolysis products.

iii. Determine the effect of the addition of individual minerals (in significant quantities to ensure measurements above the detection limits of the analysis), to acid washed coal on the pyrolysis product yield and composition by pyrolysis experiments, and characterisation of the different pyrolysis products at the respective pyrolysis temperatures (520, 750 and 900°C).

iv. Measure the effect of the make-up of coal-mineral mixtures similar to the original coal prior to acid washing and evaluation of the pyrolysis product yields and compositions at the respective pyrolysis temperatures (520, 750 and 900°C).

v. Statistical evaluation of the obtained data and derivation of predictive models for char, tar and gas yields at the respective pyrolysis temperatures (520, 750 and 900°C).

Characterisation of pyrolysis products will include: gas chromatography (GC) analysis of the gas yield, gas chromatography-mass spectrometry (GC-MS), size exclusion chromatography (SEC-UV) and simulated distillation (simdis) analyses of the tar yield and proximate, ultimate, x-ray fluorescence and XRD analyses of the char yield.

1.4. Scope of investigation

In order to meet the objectives of the investigation, a specified scope for the investigation was constructed. A washed Highveld bituminous coal was prepared by a comminution process, of which a fraction was acid washed. The NWU Fischer assay setup was used for pyrolysis experiments (Roets *et al.* 2014, Bean, 2013). Pyrolysis experiments were done at three temperatures (in order to investigate the changes occurring over a large pyrolysis temperature range). Minerals added included: calcite, dolomite, kaolinite, pyrite and quartz. These minerals were identified from previous studies conducted on the mineral composition of South African coals (Bunt *et al.,* 2012a; Hattingh *et al.*, 2011; Matjie *et al.*, 2011; Van Dyk *et al.,* 2009; Matjie & Van Alphen, 2008; Everson *et al.,* 2008; Matjie *et al.,* 2008; Matjie *et al.,* 2006; Van Dyk, 2006). The effect of these minerals on the pyrolysis products derived from the acid washed coal sample was studied based on product yield and by proven analytical techniques. Figure 1-1 indicates the research methodology followed in this study. The aim of this study is to quantify the effect of the addition of minerals on the pyrolysis products derived from typical Highveld coal.

This study can be divided into five main sections:

- Coal preparation and characterisation - crushing and milling, acid washing, chemical and petrographic analyses and mineral analyses (XRF,XRD, QEMSCAN);
- Pyrolysis experiments I – effect of acid washing on the pyrolysis product yield and composition.
- Pyrolysis experiments II – effect of mineral addition to the acid washed coal sample on the pyrolysis products yield and composition.
- Pyrolysis experiments III – effect of the addition of mineral mixtures (to simulate the original mineral matter present in the coal sample, prior to acid washing) on the pyrolysis products yield and composition.

- Development of predictive models from the input from the pyrolysis experiments (I-III).

The dependence of the pyrolysis stage on the coal characteristics necessitates the need for thorough characterisation of the coal sample. Therefore chemical analyses consisting of proximate, ultimate, calorific value, XRF, XRD, and QEMSCAN analyses were performed.

Structural analyses consisted of BET and DRIFT analyses, whilst thermogravimetric analysis was done in order to obtain decomposition characteristics. Petrographic analyses included maceral composition and vitrinite reflectance analyses.

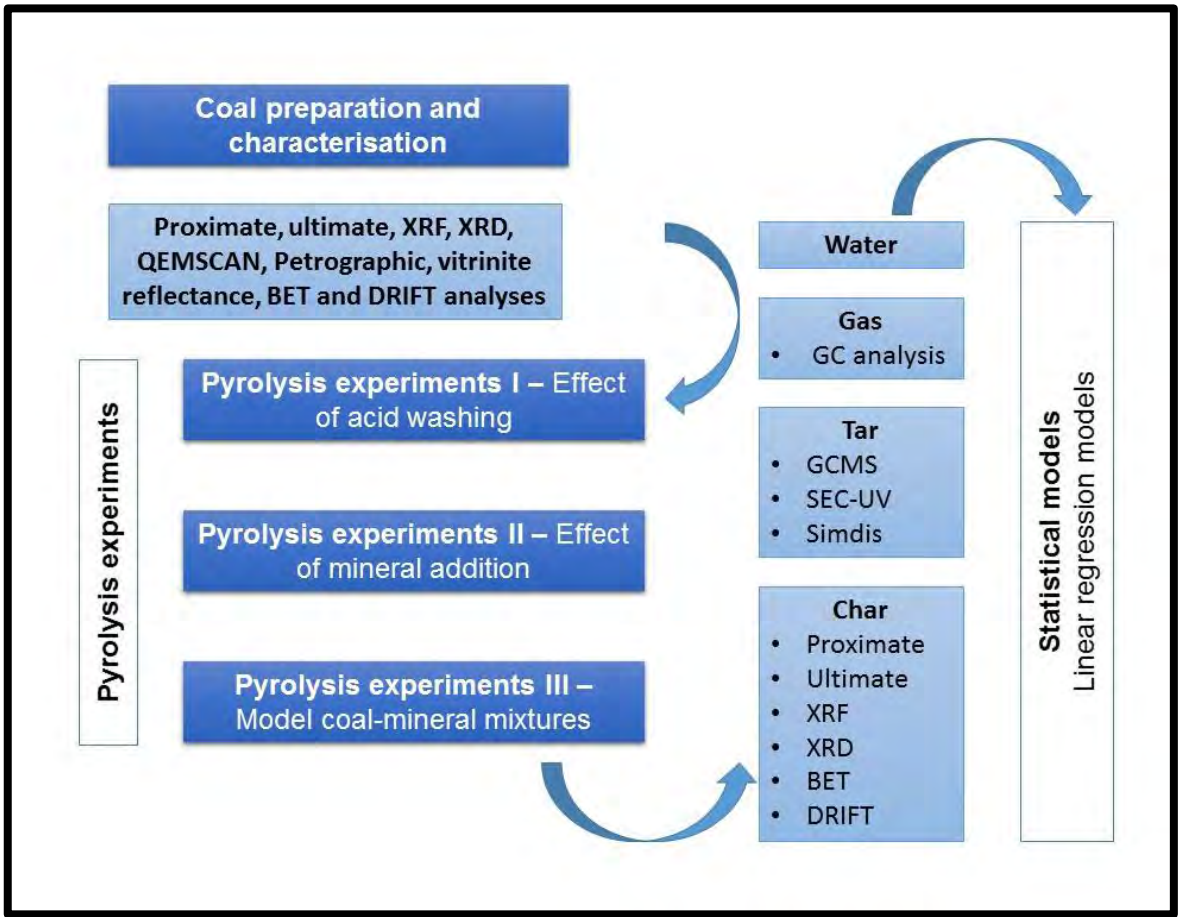

Figure 1-1 Scope of investigation.

The pyrolysis experiments were conducted with the aid of the NWU Fischer Assay setup which is a duplicate sample, automated electrically heated setup. The setup was modified to also sample the gas fraction along with the tar, aqueous and char fractions. The setup was operated at 520°C, 750°C and 900°C, which is not part of the conventional Fischer Assay operation (SANS, 1974). The pyrolysis products were characterised by the methods as indicated in Figure 1-1. Predictive models were developed with the aid of SPSS software by linear regression.

1.5. Outline of dissertation

Figure 1-2 provides an outline of the dissertation. The dissertation can be divided into 4 parts: Part 1: Background and Motivation, Part 2: Coal and mineral characterisation, Part 3: Pyrolysis product yields and composition, and Part 4: Conclusions and recommendations. A brief, but thorough background will be given with regard to previous studies conducted on the effect of minerals on pyrolysis yield and composition as well as other relevant topics in Chapter 2. Chapter 3 will provide insight into the coal and mineral properties as obtained from the various characterisation techniques. Chapters 4 to 7 deal with the pyrolysis experiments and the characterisation of the pyrolysis products. Chapter 8 concludes the study and makes recommendations for future work.

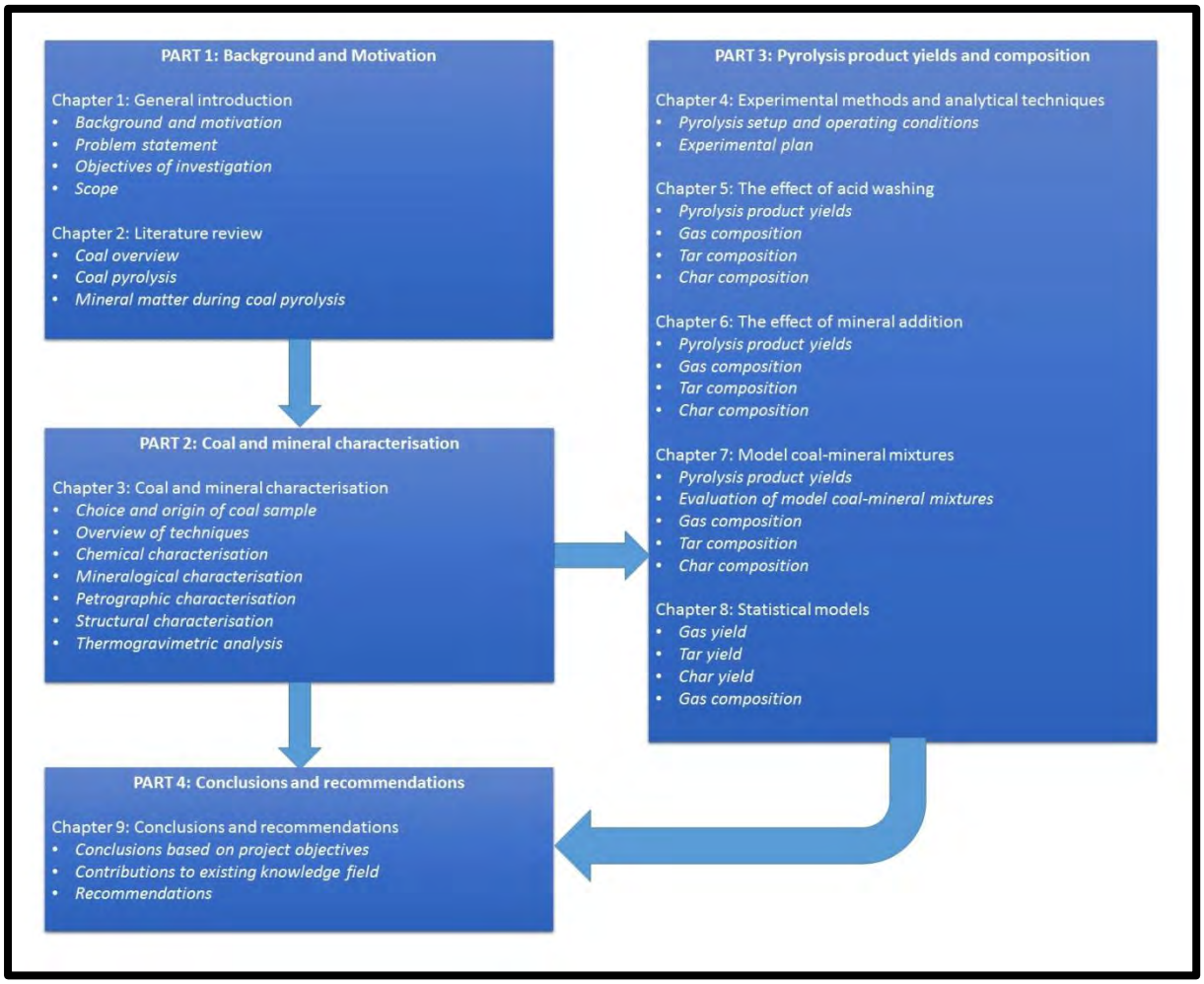

Figure 1-2 Outline of dissertation

Chapter 2: Literature review

The focus of this study is to determine the effect of the mineral matter addition on the pyrolysis products derived from a typical South African Highveld coal. This section of the dissertation will provide a brief background with regard to the specific coal type and minerals present within coal (Section 2.1). Coal pyrolysis and factors affecting pyrolysis will be discussed in detail in Section 2.2, with the main focus on the effect of mineral matter on the pyrolysis products given in Section 2.3. The review will then be summarised as to highlight the most relevant information with regard to the current investigation (Section 2.4). It is not within the scope of this study to provide a full review of all available literature, and therefore the author aimed to provide only the most relevant information.

2.1. Coal overview

Coal is generally described as a sedimentary rock that transformed from plant debris to peat, due to biological conversion, and thereafter was transformed by metamorphic geological changes during burial (Bell *et al*., 2011; Bowen & Irwin, 2008, WCI, 2005; Kandiyoti *et al*., 2006; Kabe *et al*., 2004; Falcon & Ham, 1988). It can be divided into two distinct fractions – an organic fraction that is referred to as the coal maceral, whilst the other is the inorganic fraction consisting mainly of the mineral matter (Oboirien *et al*., 2011; Van Niekerk *et al.,* 2010; Cakal *et al.,* 2007; Borah *et al.,* 2005; Huggins, 2002; Ward, 2002; Gosiewska *et al*., 2002; Hutton & Mandile, 1996; Shirazi *et al.,* 1995, Schobert, 1990).

The organic fraction of coal is characterised by maceral groups, which are remnants of the original plant debris from which it fossilized (Bell *et al.,* 2011; Kandiyoti *et al.,* 2006). The main maceral groups include: vitrinite (remains of various plant matter such as bark, stems and roots); liptinite (cuticles, spores, resin and algal remains); and inertinite (oxidized plant material, fungal remains and fossilized charcoal) (Bell *et al.,* 2011; Van Niekerk *et al.,* 2010; Van Niekerk *et al.,* 2008; Kandiyoti *et al.,* 2006; Kabe *et al*., 2004; Falcon & Ham, 1988). Macerals and submacerals are identified by their reflectance and morphology, but they also differ in chemical and physical attributes (Van Niekerk *et al.,* 2010; Kandiyoti *et al.,* 2006). The mineral matter can be identified by analytical techniques such as X-ray diffraction (XRD) and computer-controlled scanning electron microscopy (CCSEM) (Govender, 2005; Huggins, 2002; Ward, 2002; Hutton & Mandile, 1996).

2.1.1. Highveld coal

Coal in Southern Africa is hosted in coal seams in Permian-aged rocks of the Karoo Super group (Cairncross, 2001). The Karoo basin is a retroarc foreland basin with two large coal fields forming part of the Vryheid Formation, known as the Witbank and Highveld coalfield (Pinetown *et al.*, 2007; Cairncross, 2001). The Highveld coal field is the second most productive, and its coal dates from the Permian age. It is mined extensively in the Mpumalanga Province of South Africa for use in the production of synthetic fuels via Lurgi fixed bed gasification at Sasol – which uses 30 million tons a year of coal for its processes (Saghafi *et al.,* 2008; Pinetown *et al.*, 2007; Van Dyk *et al.,* 2006; Jeffrey, 2005; Wagner & Hlatshwayo, 2005). The importance of this coal field is increasing due to the depleting Witbank reserves (Jeffrey, 2005). These coals are characterized by a medium to high volatile matter content (12-32%), moisture content of 2-6%, and ash content of 8-35% (Saghafi *et al.,* 2008; Pinetown *et al.*, 2007; Wagner & Hlatshwayo, 2005).

Table 2-1 Characteristics of the Highveld coalfield coal seams (Adapted from Jeffrey, 2005).

Seam no.	Type of coal	Ash content wt% d.b.	Gross Calorific value (MJ/kg) d.b.
2	Low-grade bituminous Better quality bituminous, good washability (Leandra)	22-35	20-23 27
4	Low-grade bituminous Upper 1-2 m Lower 3-4 m	20-35 40 21	18-25 15 23
4 Upper	Low grade bituminous	25	22
5	Better quality bituminous	19	>25

The Highveld Coal field consists of 5 seams, with a sixth seam occurring very seldom (Wagner & Hlatshwayo, 2005). The seams are numbered from the base upwards, and the number 4 lower seam is the seam from which most coal is mined. The coal is typified by high ash content and there are two mines that provide an export washed coal product (Jeffrey, 2005; Wagner & Hlatshwayo, 2005). Typical mineral matter content of a Highveld coal seam was reported on a mineral matter only basis, and is characterized by kaolinite (43.7%), followed by quartz (24.7%), pyrite (8.5%), calcite (7.82%) and dolomite (7.1%) (Pinetown *et al.*, 2007; Buhmann, 1991). A significant proportion of crystalline inorganic matter is present in Highveld coal of which most of the minor mineral phases appear to be detectable by XRD of the raw coal

(Pinetown *et al.*, 2007). Table 2-1 summarises the characteristics of the different seams of the Highveld coalfield (adapted from Jeffrey, 2005).

2.1.2. Mineral matter present in coal

There are two distinct forms of mineral matter present within coal - 1) the inherent mineral matter within the coal particles, and 2) the adventitious inorganic material remaining external to the coal particles (Oboirien *et al.*, 2011; Tomeczek & Palugniok, 2002; Chen *et al.*, 1999; Shirazi *et al.,* 1995). The latter can be classified as silicates, sulphides, sulphates, phosphates, carbonates and other minerals (Prinsloo, 2008; Ward, 2002; Chen *et al.*, 1999). More than 125 minerals have been found in coal, of which 100 are described as trace minerals (minerals present in a very low concentration with grain sizes smaller than 10 µm) (Vassilev & Vassileva, 1996; Schobert, 1992; Schobert, 1990). Table 2-2 provides a list of minerals commonly found in coal (Gornostayev *et al.,* 2009; Nel, 2009; Prinsloo, 2008; Kabe *et al*., 2004; Tomeczek & Palugniok, 2002; Ward, 2002; Cairncross, 2001; Chen *et al.*, 1999; Bolat *et al.,* 1998; Vassilev & Vassileva, 1996; Vassilev *et al*., 1995). The major minerals from Table 2-2 are: quartz, kaolinite, gypsum, pyrite, calcite, illite, feldspar, sulphate, dolomite, ankerite and siderite (Gornostayev *et al.*, 2009; Nel, 2009; Prinsloo, 2008; Kabe *et al*., 2004; Cairncross, 2001; Bolat *et al.,* 1998, Vassilev & Vassileva, 1996; Vassilev *et al*., 1995).

The presence of mineral classes in decreasing order of significance are: silicates > carbonates > oxyhydroxides > sulphides > sulphates > phosphates > others (Vassilev & Vassileva, 1996, Schobert, 1990). For earlier research regarding mineral matter present in coal refer to the work of Franklin, (1980), Ward, (1977), Gluskoter, (1975), Watt (1968). Ode, (1963), Nelson, (1953), and Lessing, (1925).

The inorganic minerals present in coal are strongly dependent on the geological location, and hence varies a lot (Ahmad *et al.,* 2009a). From previous studies conducted on South African bituminous coal it has been reported that kaolinite, quartz, pyrite, calcite, dolomite and illite/muscovite are the most commonly found minerals (Bunt *et al.,* 2012a; Hattingh *et al.*, 2011; Matjie *et al.*, 2011; Van Dyk *et al.,* 2009; Matjie & Van Alphen, 2008; Everson *et al.,* 2008; Matjie *et al.,* 2008; Pinetown *et al.* 2007; Matjie *et al.,* 2006; Van Dyk, 2006, Wagner & Hlatshwayo, 2005).

Table 2-2 Minerals found in coal (Prinsloo, 2008; Tomeczek & Palugniok, 2002; Ward, 2002; Chen *et al.*, 1999; Gornostayev *et al.*, 2009; Nel, 2009; Prinsloo, 2008; Kabe *et al.*, 2004; Cairncross, 2001; Bolat *et al.*, 1998; Vassilev & Vassileva, 1996; Vassilev *et al.*, 1995)

Mineral	Formula	Mineral	Formula
Silicates		Hematite	Fe_2O_3
Quartz	SiO_2	Zircon	$ZrSiO_4$
Chalcedony	SiO_2	**Phosphates**	
Cristobalite	SiO_2	Apatite	$Ca_5F(PO_4)_3$
Clay minerals:		Crandalite	$CaAl_3(PO_4)_2(OH)_5.H_2O$
Kaolinite	$Al_2Si_2O_5(OH)_4$	Gorceixite	$BaAl_3(PO_4)_2(OH)_5.H_2O$
Illite	$K_{1.5}Al_4(Si_{6.5}Al_{1.5})O_{20}(OH)_4$	Goyazite	$SrAl_3(PO_4)_2(OH)_5.H_2O$
Muscovite	$KAl_2(AlSi_3O_{10})(F,OH)_2$	Monazite	$(Ce,La,Th,Nd)PO_4$
Smectite	$Na_{0.33}(Al_{1.67}Mg_{0.33})Si_4O_{10}(OH)_2$	Xenotime	$(Y,Er)PO_4$
Chlorite	$(MgFeAl)_6(AlSi)_4O_{10}(OH)_8$	**Carbonates**	
Zeolite	$(Na/K)_2/(Ca/Mg)Al_2Si_3O_{10}.2H_2O$	Calcite	$CaCO_3$
Interstratified clay minerals		Aragonite	$CaCO_3$
Feldspar	$KAlSi_3O_8$; $NaAlSi_3O_8$; $CaAl_2Si_2O_8$	Dolomite	$CaMg(CO_3)_2$
Tourmaline	$Na(MgFeMn)_3Al_6B_3Si_6O_{27}(OH)_4$	Ankerite	$(Fe.Ca,Mg)CO_3$
Analcime	$NaAlSi_2O_6.H_2O$	Siderite	$FeCO_3$
Clinoptilolite	$(NaK)_6(SiAl)_{36}O_{72}.20H_2O$	Dawsonite	$NaAlCO_3(OH)_2$
Heulandite	$CaAl_2Si_7O_{18}.6H_2O$	Strontianite	$SrCO_3$
Sulphides		Witherite	$BaCO_3$
Pyrite	FeS_2	Alstonite	$BaCa(CO_3)_2$
Marcasite	FeS_2	**Sulphates**	
Pyrrhotite	$Fe_{(1-x)}S$	Gypsum	$CaSO_4.2H_2O$
Sphalerite	ZnS	Bassanite	$CaSO_4.0.5H_2O$
Galena	PbS	Anhydrite	$CaSO_4$
Stibnite	SbS	Alunite	$KAl_3(SO_4)_2(OH)_6$
Millerite	NiS	Barite	$BaSO_4$
Other		Coquimbite	$Fe_2(SO_4)_3.9H_2O$
Anatase	TiO_2	Jarosite	$KFe^{3+}_3(OH)_6(SO_4)_2$
Rutile	TiO_2	Rozenite	$FeSO_4.4H_2O$
Boehmite	Al.O.OH	Szomolnokite	$FeSO_4.H_2O$
Brucite	$Mg(OH)_2$	Natrojarosite	$NaFe_3(SO_4)_2(OH)_6$
Goethite	$Fe(OH)_3$	Thenardite	Na_2SO_4
Crocoite	$PbCrO_4$	Glauberite	$Na_2Ca(SO_4)_2$
Chromite	$(Fe,Mg)Cr_2O_4$	Hexahydrite	$MgSO_4.6H_2O$
Clausthalite	PbSe	Tschermigite	$NH_4Al(SO_4)_2.12H_2O$

2.2. Coal pyrolysis

A hydrogen-rich volatile fraction consisting of gases, vapours, condensable tar and a carbon rich solid fraction, (called char), form when coal is exposed to high temperatures (above 320°C). At these temperatures covalent carbon bonds, such as the carbon bonds with oxygen, nitrogen or sulphur break, in an oxygen free environment (Bell, *et al*., 2011; Ahmad *et al.*, 2009a; Liu *et al.,* 2004a; Coetzer & Keyser, 2003; Chen *et al.,* 1997). This process is known as pyrolysis. Coal pyrolysis forms the basis for almost all other conversion processes, and is therefore, regarded as the most important aspect of coal behaviour (Ahmad *et al.*, 2009a; Liu *et al.*, 2007b; Liu *et al.*, 2004a; Li *et al.*, 2004; Ôztas & Yürüm, 2000; Mondragon *et al.*, 1999; Schlosberg, 1985). This subject has been extensively studied by various researchers (Bell, *et al*., 2011; Ahmad *et al.*, 2009a; Liu *et al.,* 2004a; Li *et al.*, 2004; Coetzer & Keyser, 2003; Ôztas & Yürüm, 2000; Mondragon *et al.*, 1999; Chen *et al.,* 1997; Franklin, 1980; Howard, 1980; Suuberg, 1977; Anthony & Howard, 1976; Anthony, 1974). A review of older literature is contained in the work of Howard (1963).

Pyrolysis is important due to the major influence it has on the development of char reactivity during gasification, and the high-value products such as: activated carbon, electrode carbon, form coke, smokeless fuel (clean conversion technologies) and liquid chemicals, that can be produced from its constituents (Wang *et al*., 2013; Zhao *et al*., 2011; Hu *et al.,* 2004; Lemaignen *et al.,* 2002; Chen *et al.,* 1997; Longwell *et al*., 1995). It is a complex process with many parallel and/or sequential reactions taking place. Each reaction taking place produces a reactive solid, as well as liquid and gaseous intermediates, which in turn leads to secondary reactions with new intermediates and final products (Bell *et al*., 2011; Ledesma *et al.*, 2000). A description of the process that leads to the formation of the above stated products is provided in numerous studies (Bell *et al.,* 2011; Borah *et al.,* 2005). Early pyrolysis work, studying the product evolution and total yields, was done by various authors around 1970 and later (Franklin, 1980; Suuberg *et al.,* 1980, 1979, 1978a and 1978b; Anthony, 1974; Anthony *et al.,* 1976, 1974a and 1974b; Anthony & Howard, 1974).

Coals consist of aromatic and hydro-aromatic building blocks, held together by bridging groups such as methylene groups, etherial oxygen, and sulphur between the building blocks and functional groups at their periphery (Borah *et al.,* 2005). During pyrolysis, vulnerable functional groups are removed as volatiles, the cross links or bridges rupture, and the hydroaromatic building blocks are converted to other aromatic blocks, and in the end to small carbon crystallites (Bell *et al.,* 2011; Borah *et al.,* 2005). The last process involves dehydrogenation and condensation reactions. The breaking of weak cross links also allows the building blocks to align better. Two types of simultaneous processes can be described during pyrolysis: (1)

rapid release of volatiles coming primarily from the destruction of carboxyl, carbonyl, alcoholic, hydroxyl, phenolic hydroxyl, lactones, anhydrides and ester-like oxygen functional groups at the periphery of the aromatic and hydroatomic components of the coal matrix; (2) the less rapid release of volatiles coming primarily from hydrogen produced during the conversion of hydroatomic portions to aromatic building blocks (Borah *et al.,* 2005). The first reaction is characteristic of low temperature pyrolysis, said to be centred at 435°C by Borah *et al.* (2005). All of these reactions take place with different reaction rates. The efficiency and product quality are affected by coal type (morphology and petrographic composition), particle size, properties such as mineral constituents, caking ability and operating conditions, i.e. heating rate, final temperature, pressure and the composition of the gaseous atmosphere surrounding the particle during pyrolysis (Ahmad *et al.*, 2009a; Van Dyk *et al.*, 2006a; Yan *et al.*, 2005; Kandiyoti *et al.,* 2006; Lemaignen *et al.,* 2002).

2.2.1. Valuable products produced from coal pyrolysis

The gas fraction typically contains species such as H_2, CO, CH_4, C_2H_6 (ethane) and C_2H_4 (ethylene) (Fuentes-Cano *et al.,* 2013; Reichel *et al.*, 2013; Neves *et al.,* 2011; Gómez-Barea *et al.*, 2010; Zhang *et al.,* 2010; Wang *et al.*, 2013; Wen *et al.,* 2009, Mill, 2000; Hayashi *et al.,* 1992; Xu & Tomita, 1989; Nelson *et al.,* 1988). This fraction can be upgraded by methanation (Speight, 1994) and some of the gaseous components (Syngas – mostly H_2 and CO) are used by companies like Sasol for the production of liquid fuels (Leckel, 2011). The liquid products obtained from coal pyrolysis need to be upgraded to be of commercial value (Hattingh, 2012, Speight, 1994, Schlosberg, 1985).

The light oil and tar fraction are of specific importance. It constitutes 50-80% of the mass loss that occurs during pyrolysis in the form of volatiles (Gavalas, 1982), and provides a lot of information regarding the thermal breakdown of coal (Casal *et al.,* 2008; Kandiyoti *et al.,* 2006; Ibarra *et al.,* 1989). It is also a valuable source of high value chemicals (Jiang *et al.,* 2007; Menéndez *et al.*, 2000, Schobert, 1990). It is during the second stage of coal thermal breakdown (350-550°C) that a dark coloured viscous liquid, known as tar, is formed (Schobert, 1990; Lowry, 1945).

The light oil product produced during pyrolysis may contain BTX (benzene, toluene and xylene) as well as alkanes, cycloalkanes, olefins and a large range of aromatic species (Leckel, 2011; Speight, 1994). Processes such as acid washing, fractional distillation and extraction can be used to produce products such as cumene, synthetic phenol, acetone, benzol and olefins amongst others (Leckel, 2011; Schobert & Song, 2002; Speight, 1994). The most valuable products that can be obtained from the tar product derived from pyrolysis include: phenol, naphthalene, phenatrene, pyrene, biphenyl, cresol and pyridene (Jiang *et al.,*

2007; Menéndez *et al*., 2000; Schobert & Song, 2002; Speight, 1994; Schobert, 1990). The molecular entities in tar can also be used in the manufacture of coal tar fuels, refined tars, tar pitch and creosote (Speight, 1994).

Phenol is a very versatile product that can be derived from coal tar. Its uses include phenolic resins such as Bakelite and Novolacs, adipic acid, alkyl-phenols, caprolactam, catechol, and monomers such as bisphenol A and 2,6 xylenol for the manufacture of aromatic polymers and engineering plastics (Schobert and Song, 2002). Naphthalene is used for chemicals, speciality chemicals and solvents to produce materials such as decalins, polyethylene naphthalene (PEN), polybutylene terephtalate (PBN) and liquid crystalline polymers (LCPs) (Jiang *et al.,* 2007; Menéndez *et al*., 2000; Schobert & Song 2002; Song & Schobert, 1993; Song & Moffat, 1994; Schobert, 1990). 2,6 Xylenol can be used to manufacture polyphenylene oxide which has excellent electrical properties whilst being heat and chemical resistant (Leckel, 2011; Schobert & Song, 2002; Song & Schobert, 1993). Anthrancene, which can also be derived from tar products has been used widely in industrial applications such as dyestuff, anthraquinone and pyromellitic dianhydride (Jiang *et al.,* 2007; Kandiyoti *et al*., 2006; Menéndez *et al*., 2000, Schobert, 1990; Song & Schobert, 1993). Coal tar pitches can in turn be used for the manufacture of carbon fibres and other carbon products such as mesocarbon microbeads (Jiang *et al.* 2007; Domínguez, 1996; Song & Schobert, 1993).

The char residue produced during pyrolysis is also important for further processing. It has high reactivity and can be considered a smokeless fuel (Chen *et al.,* 1997; Longwell *et al*., 1995; Speight, 1994). It can also be used as a reductant in the metallurgical industry, used to produce activated carbon and molecular sieving carbons (MSCs). These products are used in water purification, food processing, gold recovery and gas separation (Chen *et al.,* 1997; Longwell *et al*., 1995; Schobert & Song, 1995).

Tars are complex and consist of various compounds, of which the yields are effected by various factors, such as: operating conditions, particle size and mineral constituents of the parent coal (Leckel, 2011, Schobert, 1990). These variations will also cause shifts in the production of the products as listed above; therefore it is of importance to find a means to assist operators in predicting tar yield and composition, as well as ensuring optimum production of the coal-derived products during thermal processing.

2.2.2. Coal characteristic properties affecting pyrolysis

2.2.2.1. Coal rank

Coal rank dictates various properties of coal, as well as the quality and quantity of volatile products released during pyrolysis (Smith *et al.,* 1994; Speight, 1994). Coal properties that

depend on coal rank include: elemental composition, functional-group composition, molecular weight, plasticity, bridging material, porosity, hydrogen bonding, catalytic species and minerals, and chemically unbound constituents such as methane and other hydrocarbons (Solomon & Hamblen, 1985).

Total volatile yield has been shown to be dependent on elemental and functional group composition, and the total yield decreases with an increase in coal rank (Borrego *et al.,* 2000; Smith *et al.,* 1994). Tars derived from lower rank coals have been found to contain shorter alkyl chain aromatics due to a decrease in the aliphatic branches (Iglesias *et al.,* 2001).

2.2.1.2. Maceral composition

Gondwanaland (Southern Hemisphere) coals are mostly bituminous, and due to the higher inertinite concentrations, the volatile and tar yields are lower (Kandiyoti et al., 2006). For South African coals, volatile and tar releases decrease in the following order: liptinite > vitrinite > inertinite (Kandiyoti *et al.,* 2006; Van Niekerk *et al.,* 2008).

2.2.1.3. Minerals and catalytic species

Coal contains various minerals which appear to have catalytic effects on product yields and quality (Liu *et al.,* 2004a; Ôztas & Yürum, 2000; Chen *et al.*, 1999; Samaras *et al.,* 1996; Franklin *et al.,* 1982a). The effect of these mineral species will be reviewed in detail in Section 2.3.

2.2.3. Operating conditions affecting pyrolysis

The operating conditions under which pyrolysis occurs has a large effect on the product yield and quality. They include: operating temperature, heating rate and holding time, operating pressure, pyrolysis atmosphere and particle size limitations (Kandiyoti *et al.,* 2006; Schlosberg, 1985).

2.2.2.1. Operating temperature

Operating temperature seems to be the most important operating condition affecting pyrolysis product yield and quality (Hu *et al.*, 2004). Thermal bond scission increases with an increase in temperature, and a higher tar yield can thus be expected with an increase in pyrolysis temperature up to a certain maximum value (525-600°C) for heating rates of 5-10°C/min (Liu *et al.*, 2004a; Ôztas & Yürüm, 2000, Franklin, 1980; Yaw *et al.*, 1980; Anthony, 1974). The changes occurring in coal with regard to volatile products can be summarized as follows (Ahmad *et al.,* 2009a; Kandiyoti *et al.,* 2006; Ôztas & Yürüm, 2000; Chen *et al.,* 1999; Taupitz, 1977):

- Acidic groups are freed from the coal structure (300°C).

- Cleavage of long chain aliphatic and etheric bridges (300-350°C).
- Scission of covalent bonds (310-350°C) with a larger volume of hydrocarbons and other gases evolving.
- Increased sample weight loss (350-400°C).
- Cleavage of aryl-alkyl ether and ethylene bridges (>400°C).
- Breaking of anhydrite groups and aryl-aryl etheric and methylene bridges increases (500°C).
- Sulphur content in tar decreases with an increase in temperature.
- Heating favours de-alkylation reactions, leading to the formation of more methane rich gaseous products.
- Yields of other hydrocarbons also increase with an increase in temperature due to the secondary thermal cracking of volatiles as long as they are within the reactor.

Table 2-3 Temperature regions in coal pyrolysis (Adapted from Ladner, 1988)

Temperature range (°C)	Reactions	Products	Application
< 350	Mainly evaporation	Water and volatile organics	Fundamental studies
400 – 750	Primary degradation	Gas, tar and liquor	Smokeless fuels and chemicals
750 – 900	Secondary reactions	Gas, tar, liquor and additional H_2	Smokeless fuels and chemicals
900 – 1100			Metallurgical coke and chemicals
> 1650	Cracking	Acetylene and carbon black	Uneconomic

Table 2-4 Product yields for low- and high temperature pyrolysis (Adapted from Hattingh, 2012).

Product (wt% d.b.)	Temperature range	
	400 – 750°C	**900 – 1100°C**
Gas	7.6	17.2
Liquor	13.0	2.5
Light oils	1.4	0.8
Tar	8.0	4.5
Char	70.0	75.0

Table 2-3 indicates the temperature regions in coal pyrolysis. It can be observed that there is a definite difference in product quality and quantity of the pyrolysis products derived at different temperatures. This can also be observed from Table 2-4, i.e. high temperature pyrolysis favours the formation of lower molecular weight species due to secondary gas-phase

degradation reactions (Sert *et al.,* 2011; Kandiyoti *et al.,* 2006, Mill *et al.*, 2000; Ladner, 1988; Nelson *et al.,* 1988).

2.2.2.2. Heating rate and holding time

Rapid heating leads to the overtaking of pyrolytic events, and thus the stages do not finish reacting (Kandiyoti *et al*., 2006). It is important that the heating rate allows for the completion of reactions under investigation when studying the changes occurring during pyrolysis. Higher heating rates increase volatile yields by 6-8% (Gibbins-Matham & Kandiyoti, 1988). Increases in volatile yield also lead to an increase in tar yield, i.e. because tar survives better through higher heating rates (when internal pressure increases due to bubble build-up within the particle) and forces the tar precursors out (Gibbins-Matham & Kandiyoti, 1988; Gray, 1988). Thus, higher heating rates suppress the retroregressive repolymerisation reactions that are thought to occur, thus yielding more tar (Gray, 1988).

Pyrolysis conversion increases with pyrolysis holding time up until an optimum between heating rate and final temperature is reached (Ôztas & Yürüm, 2000). This ensures that there is no overlap of pyrolysis events, and that reactions are completed (Kandiyoti *et al*., 2006).

2.2.2.3. Operating pressure and atmosphere

Recondensation of tar occurs under atmospheric pressure conditions, and therefore an increased tar yield is observed when reducing the pressure (Kandiyoti *et al.*, 2006). Thus, tar precursor material is lost through re-polymerization; and gas and char, and perhaps light tar are produced (Kandiyoti *et al*., 2004). External pressure thus works against the internal forces driving the tar out, by decreasing the flow and diffusion of volatiles to the external surfaces of particles, and the diffusion of the volatiles to the surrounding gas. (Kandiyoti *et al*., 2006; Gavalas, 1982; Yaw *et al.*, 1980, Franklin, 1980; Anthony, 1974).

2.3.1.5. Particle size limitations

Particle size has a definite effect on the amount of volatiles produced due to the fact that the thermal conductivity of the mass of sample starts to play an increasing role instead of the environment in which the particle reacts (Kandiyoti *et al*., 2006; Gavalas, 1982). Decreased weight loss can be expected with an increase in particle size, i.e. lower pyrolysis yields (Franklin, 1980; Anthony, 1974).

2.3. Mineral matter and coal pyrolysis

Mineral matter that is present in coal plays a large role during heat treatment processes, such as gasification and pyrolysis, and has been studied extensively (Ahmad *et al.,* 2009a; Yu *et al.*, 2009; Yan *et al.*, 2005; Liu *et al.,* 2004a; Karaca, 2003; Lemaignen *et al.,* 2002; Tsubouchi & Ohtsuka, 2002; Ôztas & Yürüm, 2000; Chen *et al.,* 1999; Velegol *et al.,* 1997; Samaras *et*

al., 1996; Gryglewicz, 1995; Otake & Walker, 1993; Miura *et al*., 1989; Morgan & Jenkins, 1986a, 1986b; 1983; Franklin *et al.,* 1982a; 1982b; Franklin *et al.,* 1981; Franklin, 1980). Coal properties such as heating value, coal rank, reaction rate and ash content may be affected by the mineral matter content (Samaras *et al.,* 1996). The mineral matter also affects final product yield and composition (Ahmad *et al.,* 2009; Liu *et al.,* 2004a; Chen *et al.,* 1999; Velegol *et al.,* 1997; Samaras *et al.,* 1996; Franklin *et al.,* 1982a; 1982b). It can be responsible for up to 45% of the total volatile yield in coal, depending on the coal type, particle size, thermal process and amount and type of mineral matter present (Slaghuis *et al.,* 1991). It has a profound effect on coal reactivity, and in the catalisation of gasification reactions (Ye *et al.*, 1998; Miura *et al.*, 1989). Mineral matter is also responsible for various technological problems such as fouling, slagging and inconsistency with regard to product yield and composition (Pusz *et al.,* 1997). This section will discuss the effect of minerals on the pyrolysis products, with specific focus on the major minerals present in Highveld coal. The effect of mineral matter on pyrolysis yields from coal only received attention from around 1980, with little work focusing on this subject earlier (Franklin, 1980).

2.3.1. Effect of acid washing

In order to determine the effect of minerals on coal pyrolysis products, one needs to consider how coal behaves without these minerals present. In order to achieve this goal, acid washing (also referred to as demineralisation, acid leaching or acid treatment) can be done (Franklin, 1980; Bishop & Ward, 1958). Low temperature ashing has also been suggested as an alternative (Gluskoter, 1965). Demineralisation is a process in which the mineral matter is removed from a coal sample by means of acid leaching (Samaras *et al.*, 1996). Various studies have been conducted in order to determine which acids are most effective in leaching coal mineral matter (Yan *et al.,* 2005; Liu *et al.*, 2004a; Ôztas & Yürüm, 2000; Bolat *et al.,* 1998; Adanez & De Diego, 1993). A combination of acid leaching and washing processes is used (Yan *et al.,* 2005; Liu *et al.*, 2004a; Ôztas and Yürüm, 2000; Bolat *et al.,* 1998; Adanez & De Diego, 1993). It was found that hydrochloric acid (HCl) effectively reduces mineral matter, whilst hydrofluoric acid (HF) is effective in dissolving the aluminium and silicon compounds (Bolat *et al.*, 1998). Pyritic compounds are not effectively removed by these acids and therefore ferric ions have been used to remove pyrite (Wu & Steel, 2007), as well as HNO_3 extraction (Franklin, 1980; Edwards *et al.,* 1958).

2.3.1.1. Methods

Minerals can be washed from coal in three ways: (1) selective leaching of minerals and examination of the remaining coal-mineral compound under pyrolysis, (2) leaching of most minerals to obtain a carbon compound as close as possible to being “mineral-free” and

addition of individual minerals to this compound to determine their effect, and (3) use of a model carbon compound such as activated carbon or graphite with the addition of individual minerals to determine their effect (Lemaignen *et al.,* 2003; Yaman *et al.*, 2001). All of these methods have limitations. Selective leaching can be effective for some groups of minerals, but it won't be effective in the removal of specific mineral compounds (Lemaignen *et al.*, 2003). For example, aluminium and silicon species will leach out together, with maybe the sulphide compounds remaining intact. In case (2) the added minerals will differ in dispersion and speciation from the original mineral constituents and impregnated salts, and may therefore react differently (Lemaignen *et al.*, 2003). Case three will be challenging as coal has a very heterogeneous and complex structure; thus it is unrealistic to assume the model carbon compound to be an accurate representation of the coal structure without mineral constituents (Lemaignen *et al.*, 2003). It thus appears that from the 3 scenarios given the best option to study the effect of mineral matter on coal pyrolysis products in this study will be realised when applying case (2). Thorough mineralogical analyses by means of XRF ash analyses, XRD and QEMSCAN will be needed.

2.3.1.2. Changes in pyrolysis product yield and composition

Due to the effect of minerals on coal reactivity, the removal thereof leads to various changes within the coal structure, as well as in the reactivity and emissions of the coal particles (Strydom *et al.,* 2011). This process may change the nature of the chemical functional groups on the coal surface and the morphology of the coal (Lemaignen *et al.,* 2003). The effect of acid washing and/or addition of minerals on the products of pyrolysis was studied extensively (Reichel *et al.,* 2013; Fei *et al.,* 2012; Nisar *et al.,* 2011; Sert *et al.,* 2011; Ahmad *et al.,* 2009a; Ahmad *et al*., 2009b; Yan *et al.,* 2005; Liu *et al.,* 2004a; Liu *et al.,* 2004b; Karaca*,* 2003; Wu *et al.,* 2003; Sciazko & Kubica, 2002; Tsubouchi & Ohtsuka, 2002a; Tsubouchi and Ohtsuka, 2002b; Ôztas & Yürüm, 2000; Chen *et al.*, 1999; Mondragon *et al.,* 1999; Samaras *et al.,* 1996; Otake & Walker, 1993; Morgan & Jenkins 1986a and 1986b; Franklin *et al.,* 1983; Franklin *et al.,* 1982a and 1982b; Yaw *et al.,* 1980; Schafer 1980, 1979a and 1979b). The relevant studies are summarised in Table 2-5.

There are various discrepancies in the literature between what the expected effects of acid washing on the pyrolysis product yields and composition can be due to differences in coal type, acid washing method used, and pyrolysis setup. From the onset it is important that these effects are taken into account when results are compared.

Table 2-5: Summary of studies done on the effect of mineral matter on coal pyrolysis products

Coal type	Pyrolysis process	Apparatus / Operating conditions	Minerals studied and effect found	Effect of removal / addition	Authors
German brown coals	Medium pyrolysis	Fixed bed reactor with vertically movable tube furnace at 300-700°C at a heating rate of 45-122K/min	No addition, just acid washing.	Small increase in char yield, whilst the tar yield showed different behaviour for different coals, increase in water yield and decrease in gas yield.	Reichel *et al.,* 2013
Chinese lignite and high swelling ratio high-sulphur bituminous Chinese coal	Medium pyrolysis	Tubular fixed bed reactor at 600/900°C in a N_2 atmosphere at a heating rate of 15°C/min	No addition, just acid washing.	The synergistic effect of pyrolysis products with blends of high swelling ratio bituminous coal and lignite.	Fei *et al.,* 2012
Top Seam Sibi and Sore Range Quetta coals from Pakistan	Medium pyrolysis	Open type tubular pyrolyser coupled to a gas chromatograph with FID over a temperature range of 500°C to 800°C at 32°C/min.	No addition, just acid washing.	The effect of inherent mineral contents on the pyrolysis product yields.	Nisar *et al.,* 2011
Makarwal Pakistani lignite-rich sub-bituminous coal (raw and acid washed)	Flash pyrolysis	Shimadzu PYR-2A micro furnace pyrolyser at 500-770°C, N_2 atmosphere, over 3 minutes in a flash pyrolysis unit	No addition, just acid washing.	Removal of minerals led to a decrease in yields of total volatiles. Tar and liquid yields decreased, whilst gas yield increased.	Ahmad *et al.* 2009a
Makarwal Pakistani lignite-rich sub-bituminous coal (raw and acid washed)	Flash pyrolysis	Shimadzu PYR-2A micro furnace pyrolyser at 500-770°C, N_2 atmosphere, over 3 minutes in a flash pyrolysis unit	Effect of addition of Na_2CO_3, K_2CO_3, $CaCO_3$, $MgCO_3$, Fe_2O_3 and $CaSO_4$	Decrease in pyrolysates after acid washing, with further decrease in pyrolysates after mineral addition.	Ahmad *et al.,* 2009b
Eleven Chinese coals (raw and acid washed)	Medium pyrolysis	Fixed bed quartz reactor at 600-1200°C (rank, temperatures, acid washing) 400-1300°C (effect of different mineral species during Chinese Fushun coal pyrolysis) in a He atmosphere with a	Addition of $Fe(C_5H_5)$, $AlCl_3$, $Ca(OH)_2$, KOH, $MgCl_2$, NaOH and TiO_2 as catalyst precursors.	The effect of ranks, temperatures and the major inherent mineral species on the nitrogen distributions	Yan *et al.* 2005

Coal type	Pyrolysis process	Apparatus / Operating conditions	Minerals studied and effect found	Effect of removal / addition	Authors
		heating rate of 20 K/min over 45 minutes.		during fixed-bed pyrolysis at low heating rates.	
Shenfu subbituminous coal and Huolingele lignite (raw and acid washed)	Slow pyrolysis	Thermogravimetric analysis at 110-800°C in an N_2 atmosphere with a heating rate of 10 K/min	Al_2O_3, CaO and K_2CO_3 addition	Effect of minerals on reactivity and kinetics of coal pyrolysis.	Liu *et al.* 2004a
Chinese Yima coal	Medium pyrolysis	Fixed bed reactor at 350-650°C at a 50°C interval.	No addition, just acid washing.	Determine the effect of mineral matter on the pyritic and organic sulphur removal during pressurized coal pyrolysis	Liu *et al.* 2004b
Turkish lignite	Fast pyrolysis – slow pyrolysis	Fixed bed reactor at 250-800°C at time intervals of 120-1800s in a N2 atmosphere	No addition just acid washing	Determine the effect of mineral matter on the pyritic and organic sulphur removal.	Karaca, 2003
Longannet and La Jagua coals (raw and acid washed)	Flash pyrolysis	High pressure wire mesh reactor at 1000°C, with varying pressure of 0.1 - 1 MPa in a He atmosphere at 1000°C/s heating rate over 10s.	Impregnation with Ca, K, Na and Fe salts	Influence of acid washing and impregnation with Ca, K, Na and Fe salts on their pyrolysis and CO_2-gasification.	Lemaignen *et al.* 2003
Six coals	Slow pyrolysis	Fixed bed reactor at 1000°C at a heating rate of 2.5°C/min in a He atmosphere	Fe addition as FeOOH and Ca addition as $Ca(OH)_2$	The effect of acid washing and addition of Ca and Fe catalyst on N_2 formation during coal pyrolysis and on char gasification.	Wu *et al.*, 2003
Bituminous (Wieczorek mine) and brown (Belxhatow mine) coals	Slow pyrolysis	Circulating fluid-bed reactor at 800-900°C	Dolomite addition 5 wt%	The effect of dolomite addition on sulphur, chlorine and hydrocarbons distribution in the fluid-bed mild gasification of coal	Sciazko & Kubica, 2002

Coal type	Pyrolysis process	Apparatus / Operating conditions	Minerals studied and effect found	Effect of removal / addition	Authors
Four low rank German, Russian, Indonesian and Chinese coals.	Slow pyrolysis	Fixed bed quartz reactor. Pyrolysis at 10°C/min up to 1350°C under a He atmosphere.	$Ca(OH)_2$ addition for Ca^{2+} loading after acid washing.	The formation of N_2 during pyrolysis of Ca-loaded coals.	Tsubouchi & Ohtsuka, 2002a
Ten coals from different countries with carbon content <80 wt%.	Slow pyrolysis	Fixed bed quartz reactor. Pyrolysis at 10°C/min up to 1350°C under a He atmosphere.	$Ca(OH)_2$ addition for Ca^{2+} loading after acid washing.	Nitrogen release during high temperature pyrolysis of coal and catalytic role of calcium in N_2 formation without volatile matters.	Tsubouchi & Ohtsuka, 2002b
Zonguldak bituminous coal and HCl/HF washed samples (Vitrinite rich)	Fast pyrolysis	Mettler TA 3000 differential scanning calorimeter at 300-500°C, N_2 atmosphere, heating rate of 50 K/min over 60 minutes	No addition, just acid washing.	Volumetric swelling ratios of char and the extent of cross-linking in the macromolecular network of chars.	Ôztas & Yürüm, 2000
Low rank Indonesian coal	Slow pyrolysis	Fixed bed quartz reactor at 850-1100°C at a heating rate of 10°C/min	Mg-, Ca-, Sr- and Ba-loading to acid washed coal as hydroxides	N_2 formation during fixed bed pyrolysis of Mg-, Ca-, Sr- and Ba- loaded coals in an inert atmosphere.	Tsubouchi *et al.*, 2000
Hongmiao Chinese lignite (raw and acid washed and pyrite removed)	Slow pyrolysis	Fixed bed reactor at 450-650°, 3 MPa pressure, H_2 and N_2 atmospheres, heating rate of 10K/min	No addition, just acid washing.	Effect of minerals on sulphur distribution during hydropyrolysis	Chen *et al.* 1999
Colombian coals	Medium pyrolysis	Fixed bed pyrolysis reactor at 800°C at a heating rate of 30 K/min in a N_2 atmosphere.	No addition, just acid washing.	H_2S evolution during coal pyrolysis and the effect of mineral matter and morphological changes.	Mondragon *et al.,* 1999.
Greek lignite rich coal (partially acid washed)	Slow – Fast pyrolysis	Thermogravimetric balance at 700 / 800 / 900°C in an N_2 atmosphere with varying heating rates of 10/50/100 K/min	Selective acid washing.	Effect of partially acid washed coal samples during gasification by carbon dioxide.	Samaras *et al.* 1996

Coal type	Pyrolysis process	Apparatus / Operating conditions	Minerals studied and effect found	Effect of removal / addition	Authors
Texas lignite rich coal (raw and acid washed)	Slow pyrolysis	Silica boat in a horizontal tube furnace at 1000°C in a N_2 atmosphere at a heating rate of 5°C/min	Na, K, Mg, Ca, and Ba salts loaded acid washed coal samples.	Changes in major gases (CO_2, CO, H_2O, CH_4 and H_2) as well as the total weight loss were determined.	Otake & Walker, 1993
Montana lignite (raw and acid washed coal)	Flash pyrolysis	Dilute-phase entrained flow reactor at 800-1000°C at a heating rate of 10^4-10^5K/min kept at that temperature for 10 minutes	Impregnation with Ca, K, Na, Sr and Ba salts as exchangeable cations.	Effect of cations and cations (Ca, Mg, Na, K, Sr and Ba) concentrations on the pyrolysis of lignites in an entrained flow reactor.	Morgan & Jenkins, 1986a
Montana lignite (raw and acid washed coal)	Flash pyrolysis	Dilute-phase entrained flow reactor at 700, 800 and 900°C at a heating rate of 10^4-10^5 K/min kept at that temperature for 10 minutes.	Impregnation with Ca, K, Na, Sr and Ba salts as exchangeable cations.	Effect of ion-exchangeable metal cations on the decomposition of the carboxylic functional groups and tar forming materials.	Morgan & Jenkins, 1986b
Wyodak subbituminous coal	Flash pyrolysis	Two electrodes coupled on two stain less steel mesh plates in a glass pipe or stainless steel pressure vessel for flash pyrolysis at 1000°C at 0.1 and 6.99 MPa in He and H_2 atmospheres respectively at a heating rate of 1000K/s	Na, Ca, K exchanges by acid washing and loading	Increase in tar and water yields after acid washing. Ca-ion exchange led to a decrease in tar yields, increase in CO_2.	Franklin *et al.* 1983
Pittsburgh bituminous Vitrinite-rich coal (raw and acid washed)	Flash pyrolysis	Two electrodes in a glass pipe or stainless steel pressure vessel for flash pyrolysis at 1000°C at 0.1 and 6.9 MPa in He and H_2 atmospheres respectively at a heating rate of 1000K/s	Calcite, montmorillonite, quartz, pyrite, $FeSO_4$	Effect of clays, iron-sulphur compounds and quartz on yields of char, tar and light gaseous volatiles	Franklin *et al.* 1982a
Pittsburgh bituminous Vitrinite-rich coal (raw and acid washed)	Flash pyrolysis	Two electrodes coupled on two stain less steel mesh plates in a glass pipe or stainless steel pressure vessel for flash pyrolysis at 1000°C at 0.1 and 6.99 MPa in He and H_2 atmospheres	Calcite, montmorillonite, quartz, pyrite, $FeSO_4$	Effect of clays, iron-sulphur compounds and quartz on yields of C_3, C_4-C_6 and C_6-C_8 hydrocarbon gases.	Franklin *et al.* 1982b

Coal type	Pyrolysis process	Apparatus / Operating conditions	Minerals studied and effect found	Effect of removal / addition	Authors
		respectively at a heating rate of 1000K/s			
Illinois No. 6 bituminous coal and a 50/50 mixture of Texas lignite and Illinois No. 6	Flash pyrolysis	Fluidized bed reactor at 425-875°C	Calcined dolomite and CaO addition as catalyst	The effect of calcined dolomite on fluidized bed pyrolysis (Analysis of the char and tar fractions, and molecular composition of the gas phase).	Yaw *et al.* 1980
Yallourn brown coal	Very slow pyrolysis	Silica tube reactor at 790/900/1000°C in an N_2 atmosphere over 24 hours.	Impregnation with Mg and Ba acetates as exchangeable cations	Evolution of oxygen during pyrolysis in the form of water and carbon oxides at different pyrolysis temperatures.	Schafer 1980
Yallourn brown coal and Texas Lignite	Slow pyrolysis	Electrically heated setup (silica containers) at 300°C in an N_2 atmosphere over 3 hours	Impregnation with Ca, Mg and Na, acetates as exchangeable cations.	Decomposition of acid groups in coals containing carboxyl groups in the acid and cation forms.	Schafer, 1979a
Yallourn brown coal	Very slow pyrolysis	Electrically heated setup (silica containers with copper tubes) at 100-900°C in an N_2 atmosphere over 12 hours	Impregnation with Ca, Mg, Ba, K and Na acetates as exchangeable cations	Pyrolysis of the Yallourn brown coal in the acid, calcium and barium forms.	Schafer 1979b

Most of the previous studies focussed on flash pyrolysis experimental setups, or setups coupled to TGAs (Reichel *et al.,* 2013; Fei *et al.,* 2012; Ahmad *et al.,* 2009a; Ahmad *et al*., 2009b; Yan *et al.,* 2005; Karaca*,* 2003; Lemaignen *et al.,* 2003; Ôztas & Yürum, 2000; Mondragon *et al.,* 1999; Samaras *et al.,* 1996; Morgan & Jenkins, 1986a and 1986b; Franklin *et al.,* 1982a and 1982b; Yaw *et al.,* 1980). In these experiments very small amounts (< 100 mg) of coal are used and the experimental conditions differ largely from the conditions used in this study. Noting that the heat treatment process is the most prominent factor influencing pyrolysis, it is not unexpected to see deviation from some of these studies (Hu *et al.*, 2004).

The type of coal also plays a role, with various pyrolysis studies reported for low rank coals, i.e. lignites, sub-bituminous or brown coals (Reichel *et al.,* 2013; Fei *et al.,* 2012; Ahmad *et al.,* 2009a; Ahmad *et al*., 2009b; Liu *et al.,* 2004a; Liu *et al.,* 2004b; Karaca*,* 2003; Sciazko & Kubica, 2002; Tsubouchi & Ohtsuka, 2002a; Chen *et al*., 1999; Samaras *et al.,* 1996; Otake & Walker, 1993; Morgan & Jenkins 1986a & 1986b; Franklin *et al.,* 1983; Yaw *et al.,* 1980; Schafer 1980, 1979a and 1979b). Furthermore, South African coal is unique in its composition (Van Niekerk *et al.*, 2008; Kandiyoti *et al*., 2006). Gondwanaland coal, of which the Highveld coalfield is part of, is mostly bituminous in rank, and due to the high inertinite concentrations present, the volatile and tar yields are generally lower (Van Niekerk *et al*., 2008; Kandiyoti *et al*., 2006).

Water yield

The water yield was observed to decrease after acid washing (Ahmad *et al.,* 2009a & 2009b; Tsubouchi & Ohtsuka, 2002; Chen *et al.* 1999; Samaras *et al.,* 1996; Otake & Walker, 1993; Morgan & Jenkins, 1986b; Franklin *et al*., 1982a). Some minerals present in coal, such as kaolinite, contain endothermic water that is released upon decomposition (Ptáček *et al.,* 2010b; Vassilev *et al*., 2009; Heide & Földvari, 2006; Alpern *et al.,* 1983). Removal of these minerals will thus lead to decreased water yields. Some minerals are also associated with carboxylate functional groups (Schobert, 1992; Huffman & Huggins, 1984), as well as some phenolic groups which were also observed to be responsible for water formation (Tsubouchi & Ohtsuka, 2002; Chen *et al.* 1999). Certain minerals also play a role in specific reactions that may take place during pyrolysis. The water-gas shift reaction is one such reaction, and the addition of calcite ($CaCO_3$) to graphite has been observed to lead to increased water yields (McKee, 1980), which might be true in the case of coal as well.

Gas yield

Gas yields were observed to increase after acid washing (Nissar *et al.,* 2011; Ahmad *et al.*, 2009a, Ahmad *et al.,* 2009b). In previous studies, the increase in gas yield due to acid washing was attributed to the fact that the minerals (and particularly their oxides responsible for gas

formation in coal) were non-porous. The removal of mineral matter is believed to alter the softening and swelling behaviour of coal and increase its porosity (Ahmad *et al.,* 2009a; Bexley *et al.,* 1986). Due to higher porosity, increased swelling behaviour and less diffusion limitations, an increase in gas yield is expected (Ahmad *et al.,* 2009a; Reucrofta *et al.,* 1983). Bexley *et al.,* (1986) did however investigate the effect of the addition of various inorganic compounds on dilatometry parameters of coal, and found that $CaCO_3$, Al_2O_3, SiO_2 and FeS_2 showed effects that could only be attributed to dilution by inert material regarding the change in dilatometry parameters. Some authors, however, reported that the porosity seemed to change to no significant extent after the acid washing process (Lee *et al.,* 2014; Klopper *et al.,* 2012; Rivera-Utrilla *et al.,* 1996). Little change in surface area for acid washed bituminous coal chars compared to parent coal chars, derived during pyrolysis was however reported (Klopper *et al.,* 2012; Rivera-Utella *et al.,* 1996).

Tar yield

With regard to the tar yield, various authors reported conflicting results. The tar yield seems to be the pyrolysis product yield most severely influenced by acid washing and the presence of minerals. It was observed that the tar yield increased markedly after acid washing (Reichel *et al.,* 2013; Tsubouchi & Ohtsuka, 2002; Chen *et al.* 1999; Samaras *et al.,* 1996; Otake & Walker, 1993; Morgan & Jenkins, 1986b; Franklin *et al.*, 1982a and 1982b). In contrast, a significant decrease in tar yield was observed for bituminous and subbituminous Pakistani coals and Turkish asphaltites (Sert *et al.,* 2011, Nisar *et al.,* 2011, Ahmad *et al.*, 2009a; Ahmad *et al.,* 2009b). The difference in behaviour is probably due to difference in coal rank, experimental conditions, basis of reporting and coal-type behaviour during pyrolysis.

The reduction in tar yield after acid washing is attributed to hydrogen transfer occurring between the liquid and solid phases during pyrolysis. The liquid yields (tar and water) produced during pyrolysis, are highly dependent on hydrogen transfer. Inorganic matter, (such as minerals), ensure higher hydrogen transfer, thus stabilizing the free radicals formed during thermal shock, causing increased product release and the minimization of re-solidification to char, thus forming more liquid products (Ahmad *et al.,* 2009a; Ishihara *et al.,* 2004; Solomon *et al.,* 1990; Solomon *et al.,* 1988). In the absence of inorganic matter, the free radicals are not effectively capped, disproportionated and stabilised, i.e. the free radicals recombine retrogressively and form char (Ahmad *et al.,* 2009a; Ishihara *et al.,* 2004; McMillen *et al.,* 1989). Sert *et al.* (2011) determined that the negative effect on the amount of liquid product and increase in gas yields after acid treatment with HCl could be attributed to the cracking of liquid products.

A change in the physical appearance of the tar was observed after pyrolysis of acid washed coal – tars from raw coal samples were black and gummy, whilst tars from coal without the minerals present were light to dark brown and powdery (Morgan & Jenkins, 1986b). With regard to groups present in the tar, the methyl, phenol and carboxyl groups were consistent, but the carbon-hydrogen aliphatic groups occur in quantities three times higher for the raw coal (Morgan & Jenkins, 1986b).

The changes in water and tar yields are explained by the fact that water in coal is mostly formed from the phenolic and carboxyl groups in coal, through esterification and dehydration reactions. The combination of tar precursors is another source of water. Acid washing can suppress the repolymerisation of tar (Tsubouchi & Ohtsuka, 2002; Chen *et al.* 1999).

Char yield

Contrasting results were also reported for the char yields. Some authors reported increased pyrolysis conversion after acid washing, i.e. lower char yield (Ôztas & Yürüm, 2000). Others reported no significant change in char yield after acid washing (Nisar *et al.,* 2011; Ahmad *et al.,* 2009b), whilst still others reported increased char yields (Reichel *et al.,* 2013; Ahmad *et al.,* 2009a; Samaras *et al.,* 1996; Solomon *et al.,* 1990; Solomon *et al.,* 1988, Hippo & Walker, 1975).

The increased char yields were attributed to the retrogressive recombination of free radicals due to the absence of inorganic elements, accompanied by char formation (Ahmad *et al.,* 2009a; Samaras *et al.,* 1996; Solomon *et al.,* 1990; Solomon *et al.,* 1988, Hippo & Walker, 1975). Ahmad *et al.* (2009a) did however not compare their coal samples on a dry, mineral-matter-free basis, but simply reported the results (as determined yields) from the pyrolyser furnace used during flash pyrolysis. The basis on which results are reported has a large effect on the trends observed, but unfortunately results from previous studies are often difficult to compare within the context of this study because the basis on which the earlier results were reported is not always clear.

Franklin *et al.* (1982a) observed no structural differences in the pyrolysis yield of raw and acid washed bituminous coal. This implies that the acid washing process had no significant effect on the subsequent pyrolysis behaviour of this coal, although the yields were affected.

2.3.2. Minerals as catalysts

Minerals affect pyrolysis products, but quantifying this effect is a difficult task. During the heat treatment of coal, various interactions between minerals and the coal organic fraction occur; i.e. they can no longer be regarded as separate entities (Pusz *et al.*, 1997). Catalytic effects of inorganic minerals are dependent on their concentration, dispersion and chemical form

within the coal structure (Samaras *et al.*, 1996). The mode of occurrence and the association of an element can be just as important as the concentration in determining its behaviour during coal utilization processes (Huggins, 2002). Due to the differences in composition and properties of different coals there are many discrepancies reported in the literature regarding the effect of minerals on pyrolysis products, as well as the fact that different coal samples and different methods were used. Little has been reported on the kinetics of coal pyrolysis (Liu *et al.*, 2004a). The prediction of catalytic activity from the amount and composition of particular inorganic components appears unlikely to be feasible (Lemaignen *et al.*, 1999). Whilst mineral matter contents clearly affect conversions during gasification, it is difficult to find systematic patterns, regarding the effect of specific inorganic components in different coals. This investigation aims to estimate the catalytic activity of minerals regarding the effect on pyrolysis product yield and composition. These effects will also be related to specific inorganic components.

Tar yield was observed to decrease in the presence of metal cations from minerals, through catalytic cracking, gasification of primary volatiles and secondary tar forming reactions (Chen *et al.* 1999, Samaras *et al.,* 1996; Otake & Walker, 1993; Morgan & Jenkins, 1986b; Franklin *et al.*, 1982). A decrease of 30-94%, depending on coal type and pyrolysis temperature, was reported (Morgan & Jenkins, 1986b). Different minerals also affect pyrolysis product yields differently. For example, Yu *et al.* (2009) found that tar yields were reduced from most effective to least effective in the following order: calcined dolomite (30.9% CaO, 20.9% MgO, 45,4% CO_2) > calcined calcite (53.0% CaO, 0.6% MgO, 41,9% CO_2) > calcined magnesite (0.7% CaO, 47.1% MgO, 52.0% CO_2) >> silica sand. Calcium, iron and magnesium cations were found to have a positive catalytic effect, whilst silicates inhibited the pyrolysis conversion process (Ôztas & Yürüm, 2000). It was observed that metal cations lower the apparent activation energy needed for pyrolysis, and therefore less volatile matter was formed (Morgan & Jenkins, 1986a).

The composition of pyrolysis products is also affected by the presence of minerals. Tars were found to be more aliphatic in the presence of metal cations, whilst the decomposition of the carboxyl functional groups and the tar fraction were strongly decreased by the presence of metal cations as found in studies with fixed bed and fluidized bed reactors (Morgan and Jenkins, 1986b). The sulphur and nitrogen distributions between volatiles and char were also reported to be affected (Yan *et al.*, 2005; Tsubouchi & Ohtsuka, 2002a; Chen *et al.,* 1999). Hydrodesulphurization is affected by clays, dolomite, quartz and calcite (Tsubouchi & Ohtsuka, 2002a; Chen *et al.,* 1999). N_2 formation is promoted with catalyst addition in the following order from largest increase, to smallest increase: Fe>Ca>K>Ti>>Na>>Si = Al. The

char-N ratio decreased correspondingly (Yan *et al.* 2005; Chen *et al.,* 1999). The conversion of coal-N to NH_3 was observed to increase with the addition of minerals and compounds containing the following components, in sequence: Fe>Ca>K=Na>>Si=Al. The tar-N decreased slightly (Yan *et al.* 2005).

Dispersed alkali and alkaline earth metal compounds containing potassium, sodium, calcium and magnesium compounds act as catalysts for gasification (Liu *et al.,* 2004a, Lemaignen *et al.*, 2003; Miura *et al.,* 1989). It is however clear that the manner in which the effect is studied is of importance. Sodium, potassium and calcium compounds were deemed inactive when studying selective acid washed coal, but when loaded on the coal matrix, they were found to be chemically active (Liu *et al.,* 2004a, Lemaignen *et al.*, 2003). This indicates that the form in which the mineral matter is present, plays a role in the way it reacts.

The effect of mineral matter on coal conversion has been studied since the 1920s (Padrick, 1984), but these works are limited with regard to the aspect of pyrolysis yield and composition (Franklin, 1980). For reviews on work done mostly prior to 1980, refer to the works of Padrick (1984), Katzer & Gates (1976), Cox (1975) and Katzman (1974). It is also not within the scope of the current study to discuss the chemistry behind the inherent mineral matter-coal interactions, and therefore the reader is referred to the works of Raask (1985) and Vorres (1986).

The focus will now shift to the specific minerals found to be most abundant in Highveld bituminous coal. The effect of these minerals on the pyrolysis products as reported in the literature will be highlighted. There will also be specifically focused on the thermal behaviour of mineral matter during coal pyrolysis. Table 2-5 provides a summary of the studies previously done to determine the effect of mineral matter on pyrolysis products.

2.3.2.1. Thermal behaviour in general of mineral matter during coal pyrolysis

Thermal decomposition of the minerals present in coal are of importance due to the various interactions taking place between the inorganic and organic fraction, the effect of these minerals on coal properties and compositional changes within the coal, and of the products of heat treatment (Vassileva & Vassilev, 2006). Table 2-6 provides an indication of the physicochemical transformations occurring during heating of coal in air up to 1600°C.

In Table 2-6., it can be observed that various changes occur over a wide temperature range. Changes observed are also difficult to relate to a specific element due to interactions occurring upon heat treatment. It should be noted that the changes observed are based on a study on Bulgarian bituminous coal, subbituminous coal and lignite (Vassileva & Vassilev, 2006).

Table 2-6 Physio-chemical transformations during heating of coal in air up to 1600°C (Adapted from Vassileva & Vassilev, 2006)

Process, Mineral phases and temperature at which it occurs	
Liberation of inorganic matter between 200-700°C (Al, C, Ca, Fe, H, K, Mg, N, Na, O, P, S, Si, Ti, others) associated with organic matter that:	
• **Escape the system as volatile components** **Form discrete inorganic phases**	• React with each other • React with inorganic matter
B.1.1. Dehydration	
• **Kaolinite, illite, montmorillonite (50-200°C)** • **Gypsum and hexahydrite (100-200°C)**	• Bassanite (200-400°C) • Jarosite (300-900°C)
B.1.2. De-hydroxylation	
• **Brucite (400-500°C)** • **Goethite (400-600°C)**	• Portlandite (600-800°C) • Kaolinite, illite, muscovite, montmorillonite, chlorite (600-900°C)
B.1.3. Decarbonisation	
• **Siderite (400-800°C)** • **Ankerite (500-800°C)** • **Calcite and dolomite (500-900°C)**	
B.1.4. Desulphurisation	
• **Jarosite (300-900°C)** • **$MgSO_4$ (>400°C)**	• Anhydrite (900-1300°C) • Barite (1000-1300°C)
B.1.5. Reduction	
• **Hematite (900-1400°C)**	
B.2.1 Destruction of crystal lattice	
• **Kaolinite (300-1100°C)** • **Illite, muscovite (700-1100°C)** • **Montmorillonite, chlorite (800-1100°C)**	
B.2.2. Polymorphic transformation	
• **Marcasite → pyrite (100-400°C)** • **α-quartz → ß-quartz → tridymite → cristobalite (575-1500°C)** • **Orthoclase → sanidine (900-1000°C)**	
B.2.3. Crystallisation-recrystallisation	
• **Opal, chalcedony(<300°C)** • **Amorphous and cryptomere clay minerals (200-300°C)**	
B.2.4. Crystallisation	
• **Amorphous SiO_2 (200-1100°C)** • **Amorphous Al_2O_3 (700-1300°C)** • **K sulphate (1000 - 1100°C)** • **Montmorillonite, illite, muscovite, chlorite (1000 - 1300°C)** • **Acid plagioclases and K-feldspar (1100 - 1200°C)**	• Kaolinite (>1500°C) • Wollastonite (400-1300°C) • Larnite (500-1200°C) • Monticellite (600-1300°C) • Spinel (700-1200°C) • Melilite, rankinite (700-1300°C) • Anorthite (800-1100°C) • Mullite (800-1400°C)
C.2.1. Oxidation	
• **Pyrite, marcasite (100-500°C)** • **Organically bound Fe (200-700°C)** • **Organically bound Ca (300-600°C)**	• Organically bound Mg (400-700°C) • Organically bound Al (500-700°C)
C.2.2. Carbonisation	
Ca, Mg and Fe oxides-hydroxides to: • **Tertiary calcite (Ambient)**	• Secondary calcite (200-500°C) • Secondary dolomite (300-500°C)

• **Secondary ankerite and siderite (200 - 400°C)**	
C.2.3. Sulphurisation	
• **Ca and Ba oxides to: Anhydrite (300 - 1000°C) ; Barite (800-900°C)**	
C.2.4. Hydroxylation	
Lime, periclase and hematite to: • **Tertiary portlandite, brucite, goethite (Ambient)**	• Secondary goethite (100-200°C) • Secondary brucite (300-400°C) • Secondary portlandite (300-600°C)
C.2.5. Hydration	
Anhydrite and bassanite to tertiary gypsum (Ambient)	
C.2.6. Silicate formation with liberation of gas phases	
Reactions between: • **Quartz and calcite to Ca silicates (400 - 800°C)** • **Quartz and anhydrite to Ca silicates (400 - 1300°C)** • **Calcite and wollastonite to larnite (500 - 900°C)**	
D.1. Precipitation from inherent moisture	
Gypsum, bassanite, anhydrite (100 - 200°C)	
D.2. Dissolution of minerals and solid phases in melts	
Quartz, cristobalite, tridymite, Ca and Ca-Mg silicates, spinel, lime, periclase, hematite, magnetite, corundum, others (1100 - 1600°C)	
D.3. Crystallisation of phases in melts	
• **K-feldspar, plagioclase, Ca and Ca-Mg silicates (1100 - 1300°C)** • **Hematite, magnetite, cristobalite (1100 - 1400°C)** • **Tridymite (1100 - 1500°C)** • **Mullite (1100 - 1600°C)**	
D.4. Glass formation	
Glass (1100 - 1600°C)	

2.3.2.2. Calcite ($CaCO_3$)

Calcite is also known as limestone, and is one of the major calcium containing minerals present in coal. It is an effective additive for sulphur removal and a fluxing agent (Li *et al.,* 2007). Calcite decomposition has been found to be independent of atmosphere and is summarized as follows (Liu *et al.,* 2007b; Vassileva & Vassilev, 2006; Tomeczek & Palugniok, 2002; Reifenstein *et al.,* 1999):

- Decomposition to CaO with CO_2 release (600-950°C).
- Reactions with clays and quartz may lead to the formation of Ca-based aluminosilicates such as anorthite and gehlentite (Van Dyk *et al.,* 2009; Mayoral *et al.,* 2001).
- Reactions between the decomposition products of calcite, pyrite and clays may yield low melting point species in the temperature range of 600-760°C (Matjie *et al.,* 2008);
- Formation of polymorphs such as aragonite (orthorhombic) and vaterite (>800°C).

The calcium present in calcite, (especially in the form of CaO) has been reported to affect various pyrolysis product properties (Liu *et al.*, 2004a; Qi *et al.*, 2004; Tsubouchi & Ohtsuka, 2002a, 2002b; Chen *et al*., 1999; Mondragon *et al.*, 1999; Franklin *et al.,* 1982a, 1982b; Yaw

et al. 1980). It was proven to be the most active mineral during the pyrolysis behaviour of coal (Franklin *et al.,* 1982a). It was also observed to promote steam and CO_2 gasification along with potassium carbonate (Ôztas & Yürüm, 2000; Chen *et al*., 1999; Franklin *et al.,* 1982a). In the presence of calcite, the tar yield and the yield of hydrocarbons in the tar fraction were observed to decrease, whilst the char yield increased (Chen *et al*., 1999; Franklin *et al.,* 1982a; Franklin, 1980, Lessing & Banks, 1924), and the yields of CO, CO_2 and H_2O changed (Tsubouchi & Ohtsuka, 2002; Yaw *et al.* 1980; Franklin, 1980; Hippo & Walker, 1975; Forney *et al.,* 1974). Calcite caused decreases in the yields of C_3, C_{4-6} and C_{6-8} tar components, with an increase in molecular weight (Franklin *et al.* 1982b, Solano *et al.,* 1977). Oxygen functional groups were cracked to CO by CaO (Liu *et al.*, 2004a), which explained the shift in gaseous component composition (Karaca, 2003; Tsubouchi & Ohtsuka, 2002). The interaction between alkali carbonates with -COOH and -OH functional groups resulted in the formation of alkali-oxygen surface groups/clusters (Karaca, 2003). Another change observed with the addition of calcite to acid washed coal is that the yields of H_2S and COS decreased significantly (Qi *et al.*, 2004; Chen *et al.*, 1999; Mondragon *et al.*, 1999). With regard to nitrogen distribution, it is believed that CaO particles may react with heterocyclic nitrogen forms in the char (char-N) to form interstitial species such as CaC_xN_y and $CaO_xC_yN_z$. These components undergo further reactions to form N_2 (Tsubouchi & Ohtsuka, 2002a, 2002b). Pan *et al.* (2010) state that calcite hindered the formation of methane from secondary hydrocracking reactions.

2.3.2.3. Dolomite ($CaMgCO_3$)

Dolomite ($CaMgCO_3$) consists of 40-50% magnesium determined as MgO, and the rest as CaO (Liu *et al.*, 2007b). This leads to the decomposition of dolomite as two separate phases (Vassileva & Vassilev, 2006). Decomposition of dolomite may be summarised as follows (Vassileva & Vassilev, 2006; Maitra *et al.,* 2005; Caceres & Attiogbe, 1997):

- Decomposition of dolomite (400-900°C)
    - Decomposition of $MgCO_3$ to MgO (700-800°C)
    - Decomposition of $CaCO_3$ to CaO (800-900°C)

Figure 2-1 indicates the thermal decomposition of dolomite as studied by Caceres and Attiogbe (1997) in an air and CO_2 atmosphere. It can be observed that very little to no mass loss occurs, until a temperature of about 550°C is reached. Some formation of secondary calcite and dolomite is possible due to the presence of Ca-Mg-Fe oxides and C oxides released from organic matter upon heating of coal (Vassileva & Vassilev, 2006). This formation can occur at lower temperatures than that observed for calcite and dolomite decomposition alone.

The presence of dolomite decreases tar yield and increase gas yield during coal pyrolysis (Mun *et al.,* 2012; Pinto *et al.,* 2007; André *et al.,* 2004; Sciazko and Kubica, 2002; Chen *et al*., 1999; Yaw *et al.,* 1980). Dolomite was observed to have little effect on the change in composition of hydrocarbons in the gas phase during co-gasification of coal and olive oil industry wastes (Mun *et al*., 2012; André *et al*., 2004).

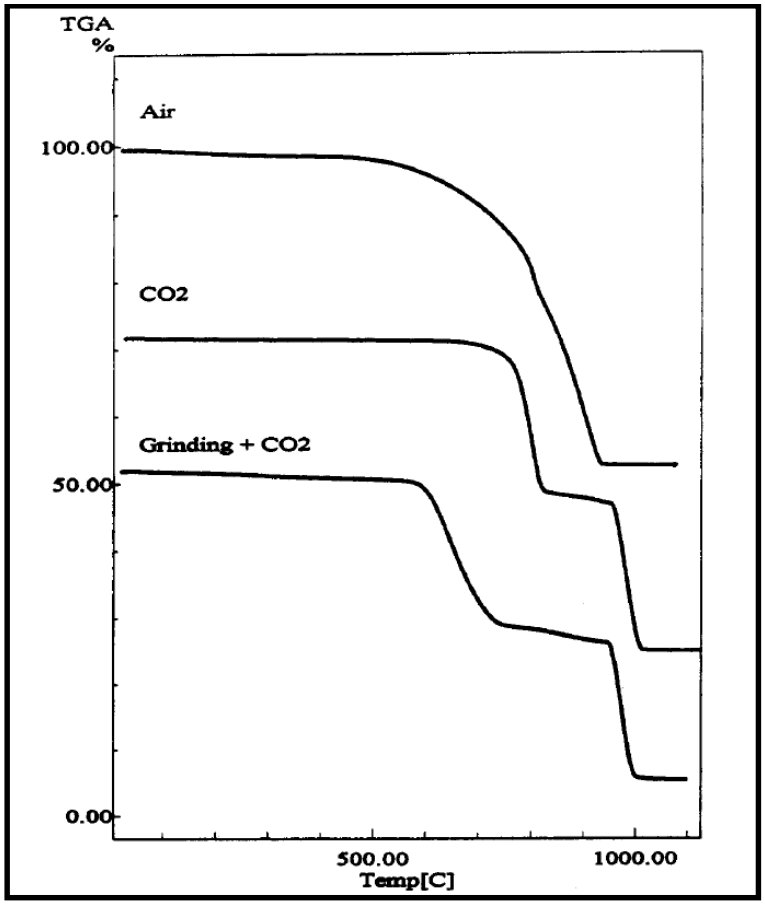

Figure 2-1 Thermal decomposition of dolomite in an air and CO_2 atmosphere.(Adapted from Caceres and Attiogbe, 1997).

An increase in CO release and reduction in CO_2 yield were observed with the addition of dolomite (Pinto *et al.,* 2007). A significant shift in gas composition is difficult to quantify due to the fact that although smaller components form, i.e. H_2, CO and CO_2, more hydrocarbon molecules form as well, which make up those converted to smaller fractions, because of a decrease in tar yield and increase in gas yield (Pinto *et al*., 2007 & 2009).

With regard to tar composition, it was observed that the tar-hydrogen content increased with the addition of calcined dolomite, probably due to the selective pyrolysis of higher boiling point tar compounds. It was also found that H_2S and other low molecular weight sulphur compounds could be effectively removed by calcined dolomite (Sciazko & Kubica, 2002; Yaw *et al.,* 1980). Chlorine compounds could also be captured by dolomite addition, i.e. an increase in the

chlorine content in the char ash, as well as more acidic components in the water fraction, was observed, whilst the yield of poly-aromatic hydrocarbons decreased with the addition of dolomite to acid washed coal (Sciazko & Kubica, 2002).

Different dolomite structures may have different effects during coal pyrolysis. Dolomite with a higher Fe_2O_3 content was reported to be more effective in the reduction of tar (Pinto *et al.,* 2007 and 2009).

2.3.2.4. Kaolinite ($Al_2Si_2O_5(OH)_4$)

Kaolinite ($Al_2Si_2O_5(OH)_4$) is the most common mineral found in coal (Yu *et al.,* 2007; Vassileva & Vassilev, 2006; Franklin, 1980; O'Gorman & Walker, 1972). The decomposition of kaolinite during temperature increase was studied extensively (Tomeczek & Palugniok, 2002; Mayoral *et al.*, 2001; McLennan *et al.,* 2000). The transformation of kaolinite can be described by Equation 2-2 (Ptáček *et al.,* 2010b; Vassilev *et al.*, 2009; Prinsloo, 2008; Van Dyk, 2006; Shirazi *et al.,* 1995; Alpern *et al.*, 1983):

$$3(Al_2O_3.2SiO_2.2H_2O) \xrightarrow{450-800^\circ C} 3(Al_2O_3.2SiO_2) + 6H_2O \xrightarrow{850-1000^\circ C} Al_6O_5(SiO_4)_2 + 6H_2O \quad (2\text{-}2)$$

The decomposition of clay minerals (of which kaolinite forms part) is summarised as follows (Alpern *et al.,* 1983; Vassilev *et al.*, 2009):

- Loss of absorbed water (50 - 200°C)
- Loss of endothermic water (450 - 600°C)
- Formation of metakaolinite (450°C), which is transformed to amorphous silica, mullite, spinel, cristobalite, corundum and aluminosilicate glass (>900°C)
- Dehydroxylation (650-900°C)
- Lattice destruction at 850 - 1000°C

Figure 2-2 indicates the thermal decomposition behaviour (TGA curve) of kaolinite as measured at various heating rates (Ptáček *et al.* 2010b). It can be observed that a higher heating rate leads to slower thermal decomposition. The dehydration and de-hydroxylation temperature range of kaolinite and coal volatile release coincide (Vassilev *et al.,* 2009). This can be responsible for the tar reducing phenomena observed with addition of kaolinite to coal samples in previous studies (Karaca, 2003; Ôztas & Yürüm, 2000; Chen *et al.,* 1999, Franklin *et al.,* 1982a).

The dehydroxylation of kaolinite to form metakaolinite is dependent on various factors, such as the order of the kaolinite structure, impurities (associated minerals, other phyllosilicates,

formation of interstratification structures with smectites, organic matter and even microbial activity), heating rate, pressure and water vapour pressure, sample treatment (grinding, sonification, etc.), particle size, particle shape, surface morphology and other structural characteristics (Ptáček *et al.,* 2010b).

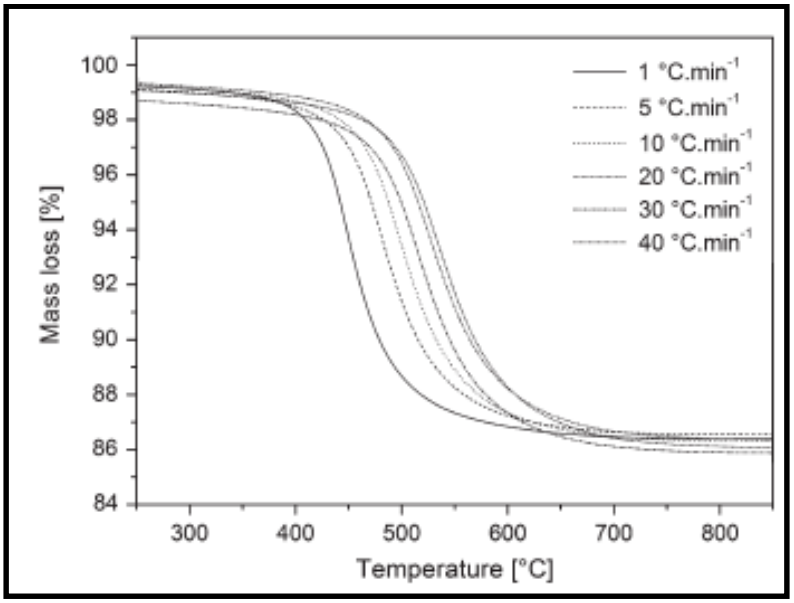

Figure 2-2 Thermal decomposition of kaolinite at different heating rates. (Adapted from Ptáček *et al.,* 2010b)

Natural clay cracking catalysts, consisting of illite, montmorillonite and kaolinite, were used in petroleum refineries in the 1940s and 1950s (Fischer *et al.,* 1975). The sorption and ion-exchange properties of clay minerals are well-known, and therefore a great deal of capture and retention of volatile matter may be possible (Vassilev *et al.*, 2009). This is confirmed by various findings in which the tar yield was observed to decrease in the presence of kaolinite during coal pyrolysis (Karaca, 2003; Ôztas & Yürüm, 2000; Chen *et al.,* 1999, Franklin *et al.,* 1982a; Franklin, 1980; Lessing & Banks, 1924). The effect of kaolinite seems to be on the cracking of hydrocarbons (lower hydrocarbon yield) to char and H_2 (Ôztas & Yürüm, 2000; Chen *et al.* 1999; Franklin *et al.,* 1982a). The effect on tar yield is however less significant when compared to the reduction observed in the C_4-C_8 fractional yield (Franklin *et al.*, 1982a). This change was ascribed to the solid acidity of kaolinite (Chen *et al.*, 1999; Franklin *et al.*, 1982a). The active component in kaolinite is thought to be Al_2O_3. It was reported by Liu *et al.* (2004a) that this component was most effective at higher temperatures, and that it increased pyrolysis conversion of Chinese sub-bituminous lignite by 8-11%.

2.3.2.5. Pyrite (FeS_2)

Pyrite was described as the main inorganic sulphur-containing compound in coal (Qi *et al.*, 2004; Chen *et al.,* 2000; Mondragon *et al.*, 1999, Schobert, 1990; Franklin, 1980; Gluskoter,

1975; O'Gorman & Walker, 1972). It is reduced to ferrous and ferric sulphates at relatively low temperatures (Qi *et al.,* 2004; Mondragon *et al.*, 1999). The effect of pyrite on coal pyrolysis, as well as under oxidizing and reducing conditions was studied extensively (Zhang & Yani, 2011; Yani & Zhang, 2010; Tomeczek & Palugniok, 2002; McLennan *et al.,* 2000a, 2000b; Bool *et al.*, 1995; Slater *et al.*, 1995; Groves *et al.,* 1987). Pyrite decomposition can either occur via excluded or included minerals in coal. The included material comes into contact with aluminosilicates, which can be responsible for the difference in behaviour that follows (McLennan *et al.*, 2000a, 2000b; Bool *et al.,* 1995). Franklin *et al.* (1982a) noticed that included pyrite would lose less than the expected weight. They also remarked that pyrite decomposition depended much on the atmosphere in which it occured. The decomposition of excluded pyrite is summed up as follows (McLennan *et al.*, 2000a, 2000b; Bool *et al.,* 1995; Groves *et al.,* 1987):

- Decomposition to pyrrhotite (330-630°C)
- Oxidation of pyrrhotite to FeO and FeS (>330°C)
- Melting and crystallizing of FeO to Fe_3O_4 (>920°C)

The decomposition of included pyrite is summarized as follows (McLennan *et al.*, 2000a, 2000b; Bool *et al.,* 1995):

- Char decomposition (430-630°C)
- Oxidation of pyrrhotite to FeO, FeS and Fe^{2+} glasses (>330°C)
- FeO melts and crystallizes to Fe_3O_4 (>920°C)
- Fe^{2+} glasses oxidizes to Fe^{3+} glasses (>920°C)

It is important to note that the decomposition of pyrite in a coal matrix occurs different from that of pure pyrite (Borah *et al.,* 2005). Factors such as coal particle size, coal matrix, diffusion resistance, sulphur-containing gases generated, all affect the decomposition of pyrite (Chen *et al.,* 2000). It is noted in various studies that the temperature at which decomposition starts, is about 100°C lower for pyrite included in the coal matrix (Borah *et al.,* 2005; Chen *et al.,* 2000; Gryglewicz *et al.,* 1996; Gryglewicz, 1995).

Borah *et al.* (2005) proposed the following reaction for the decomposition of pyrite above 420°C under reducing conditions:

$$FeS_2 + xH_2 \rightarrow FeS_{2-x} + xH_2S \quad (2\text{-}3)$$

It was stated that this reaction is most likely due to the presence of hydrogen. It was however noted that decomposition of pyrite was more severe under hydropyrolysis, than pyrolysis with

nitrogen (Garcia *et al.*, 1991). In a hydrogen-deficient atmosphere, elemental sulphur will also form during pyrite-pyrrhotite transformation:

$$FeS_2 \rightarrow FeS + S \quad (2\text{-}4)$$

This reaction initiates the generation of some of the free radical reactions and is supposed to be the catalytic influence of pyrite during pyrolysis (Borah *et al.*, 2005). The released elemental sulphur may also stabilise some of the free radicals generated during pyrolysis and enhance depolymerisation by functioning as a cross-linking agent (Borah *et al.,* 2005; Gryglewicz *et al.,* 1996). The most reactive iron disulphide compounds are those formed first, i.e. studies have shown that pyrrhotite is the most active phase (Borah *et al.,* 2005). By formation of activated hydrogen on the surface of the iron sulphide and iron disulphide compounds, (through dynamic equilibrium by the sulphurising and desulphurising reactions), catalytic hydrocracking and hydrogenation are enhanced (Borah *et al.,* 2005; Gryglewicz *et al.,* 1996).

Pyrite was found to be an effective catalyst for the hydro-liquefaction of coal (Grigore *et al.*, 2010; Borah *et al.,* 2005; Ôztas & Yürüm, 2000; Chen *et al.,* 1999; Franklin *et al.,* 1982a). Borah *et al.* (2005) and Franklin *et al.,* (1982a, 1982b) stated that pyrite had a large effect on pyrolysis behaviour and reduced the total volatile yield. This decrease in yield might have been as a result of a decrease in methane yields and reduced yields of C_4-C_6 hydrocarbons and C_6-C_8 volatiles, whilst no other light hydrocarbon yields were affected (Franklin *et al.,* 1982a, 1982b; Franklin, 1980; Cypres & Souden-Moinet, 1980). The temperature range in which pyrite affects pyrolysis yields is limited to 220-650°C (Borah *et al.,* 2005). The decomposition product, pyrrhotite, seems to have the largest effect on pyrolysis (Borah *et al.,* 2005; Franklin, 1980). Pyrite was also found to promote N_2 formation during coal pyrolysis (Wu *et al.,* 2003).

Investigation of the electronic structure of pyrite reveals that the sulphur atom can expand its valency due to the availability of the vacant d-orbital; thus pyrite develops an acidic nature. If the pyrite molecule accepts electrons from electron-rich centres that may be present in the coal matrix, it can weaken the bonds adjacent to the donating elements, thus resulting in product release and devolatilisation (Borah *et al.,* 2005). Surface acidity and acid catalysed reactions of inorganic substances on organic matter have large effects on bond cleavage processes below 500°C (Matsuhashi *et al.*, 2001 and 1997). Pyrite may also capture free electrons from free radicals released during pyrolysis, thus stabilizing the coal structure and effecting volatile release as such (Borah *et al.*, 2005).

2.3.2.6. Quartz (SiO_2)

Quartz is stable up to 1400-1500°C, but the quantity of this mineral reduces significantly above 1000°C upon thermal treatment of coal (Vassileva & Vassilev, 2006). Low quartz (α-quartz)

transforms to high quartz (ß-quartz) at 573°C (Klein, 2002; Reifenstein *et al.,* 1999). The ß-quartz is in turn stable up to 876°C at which temperature it transforms to tridymite via an unstable cristobalite formation (Matjie *et al.,* 2008; Reifenstein *et al.*, 1999). Quartz is less reactive than kaolinite, and at the temperatures that will be used in this study (520 – 900°C) it is expected to remain in its original form or transform to high quartz.

Quartz, irrespective of its chemical inert nature, may act as diluting agent in agglomeration (Ôztas & Yürüm, 2000; Chen *et al.*, 1999; Franklin *et al.,* 1982a). The only influence observed during pyrolysis was on the thermo-plasticity of the coal (Ôztas & Yürüm, 2000). Quartz does not soften during pyrolysis, but it affects the thermoplastic nature of the bed of coal particles. This inhibits the physical contact between particles, and therefore alters the overall agglomerating nature of the coal bed (Ôztas & Yürüm, 2000).

2.3.2.7. Other minerals

The effect of other minerals on pyrolysis products has been evaluated in some studies and the findings can be summarized as such:

- Montmorillonite has been found to reduce tar yield by a small extent, by repolymerisation of pyrolysis products to char rather than cracked gas (Franklin *et al.,* 1982a).
- Montmorillonite has been found to only affect the C_6-C_8 hydrocarbon yields, no other volatile yields (Franklin *et al.,* 1982b).
- Iron sulphate ($FeSO_4$) reduces C_3 hydrocarbons yield in hydro-pyrolysis, while enhancing the yield of C_4-C_6 hydrocarbons in a He atmosphere. (Franklin *et al.,* 1982b).
- Liu *et al.* (2004a) found that the addition of K_2CO_3 led to interactions with the -COOH and -OH functional groups which resulted in the formation of K-oxygen surface groups.
- Tsubouchi *et al.* (2004) found that loading of an acid washed low rank Indonesian coal with Ca, Sr, Ba compounds led to an increase in N_2 formation at temperatures higher than 850°C. They also found that CaO, SrO an BaO promoted the formation of crystallized carbon, H_2 and CO. This suggests that the conversion of char-N to N_2 is by the process of carbon crystallization (Tsubouchi & Ohtsuka, 2002a).

2.4. Chapter Summary

This chapter provided background with regard to the inorganic (mineral) matter present within coal, the way in which this matter decomposes, and the pyrolysis process. Specific focus was given to the effect of inorganic matter on the products derived during pyrolysis.

Coal pyrolysis forms the basis of most coal conversion processes. The understanding thereof is thus of utmost importance for optimum utilisation of coal and coal-derived products. Mineral matter present in coal has a large effect on the pyrolysis product yield and composition. Research with regard to the effect of coal mineral matter on the pyrolysis products has been conducted by numerous researchers. Although most of these studies refer to the effect of mineral matter on the composition of the pyrolysis products, the methods of addition and / or removal of these minerals are sometimes unclear. There is also a lack in detailed characterisation of the effect of the individual minerals on pyrolysis products. The current investigation will make use of a Fischer Assay setup for pyrolysis product preparation of a South African, Highveld bituminous coal. The pyrolysis products will be analysed by various analytical techniques in order to quantify the effect of minerals on the pyrolysis product yield and composition.

There is discrepancy reported in the literature in the trends observed regarding the pyrolysis product yield after acid washing, and it is inconclusive as to what trend can be expected in the current study. Considering that kaolinite, dolomite, quartz, calcite and pyrite are the most abundant minerals found in Highveld coal, focus will be on the effect of these minerals on coal pyrolysis products. Calcite was found to be the most active mineral during the pyrolysis behaviour of coal, and was reported to reduce tar yield by cracking of hydrocarbons present in the tar, whilst the char yield increased. Dolomite decreases tar yield and increases gas yield during coal pyrolysis. Calcite and dolomite were also observed to affect the relative yields of CO, CO_2 and water. Kaolinite reduces tar yield and promotes char forming reactions. Pyrite reduces the total volatile yield. This decrease in yield may be as a result of a decrease in methane yields and reduced yields of C_4-C_6 hydrocarbons and C_6-C_8 volatiles, whilst no other light hydrocarbon yields are affected. It was also found to promote N_2 formation during coal pyrolysis. Quartz is said to act as diluting agent in agglomeration, but has little to no effect on pyrolysis.

Part 2 – Coal and mineral characterisation

Chapter 3: Coal and mineral characterisation

“The element of chance in basic research is overrated. Chance is a lady who smiles only upon those few who know how to make her smile.”

— Hans Selye

Chapter 3: Coal and mineral characterisation

3.1. Introduction

Coal properties such as rank, chemical structure, maceral composition, etc., affect the pyrolysis process. This chapter provides the characterisation results obtained by conventional coal analysis techniques for the coal used in this study, as well as mineralogical characterisation techniques applied, such as XRD and QEMSCAN. It also provides results with regard to the thermal breakdown of the given coal sample and the associated minerals by thermogravimetric analysis. The chapter layout is as follows:

- Choice and origin of coal sample (Section 3.2)
- Coal and mineral sampling (Section 3.3)
- Overview of conventional coal analysis (Section 3.4)
- Chemical coal analyses results and discussion (Section 3.5)
- Mineralogical analyses results and discussion (Section 3.6)
- Petrographic analyses results and discussion (Section 3.7)
- Structural analyses results and discussion (Section 3.8)
- Thermogravimetric analyses results and discussion (Section 3.9).

Further discussion will be dealt with in various sub-sections within the text. This chapter will be summarised in Section 3.10.

3.2. Choice and origin of coal sample

The coal sample used in this study was selected on the following basis:

(1) A bituminous South African coal was identified from a region that produces coal for the synthetic fuel industry, where tar is produced.

(2) The coal should differ in ash content, based on its washability characteristics, i.e. the coal should have a relatively low ash content (< 15 wt% d.b.) on a washed basis, and a relatively high ash content (> 20 wt% d.b.) in its raw form.

A coal sample from the Highveld coalfield was selected. The selected coal was a beneficiated product, with a low ash content (< 15 wt% d.b.).

3.3. Coal and mineral sampling

3.3.1. Coal sample preparation

3.3.1.1. Crushing and milling

A washed and air dried Highveld coal sample (<38 mm) was obtained and prepared by coning and quartering according to the procedure given by Wills and Napier-Munn (2006). A final representative sample mass of 6 kg was prepared to a sieve size of <75 µm by use of a series of crushers and mills. The primary crusher used was a jaw crusher (Samuel Osborne (SA) LTD, Model: 66YROLL) to prepare a sample of particle size <10 mm. A hammer mill (Usborn Coalequip Engineering (PTY) LTD; Speed: 425 rpm; Size: 4x6 macro crusher; Model no.: 46-126) was used for further reduction in size. The sample particle size was further reduced by means of a rotary mill (Wenman Williams & Co. (PTY) LTD. 503A). The crushed sample was sieved thereafter using a Fritsch Analysette (Type 03.5025, no.: 4822) Spartan vibratory sieve-shaker. After the sample had been prepared it was hermetically sealed in a container (SANS, 1974) under N_2 atmosphere to prevent oxidation and uptake / loss of moisture.

3.3.1.2. Acid washing

A part of the sample prepared to <75 µm was acid washed with hydrochloric acid (HCl) and hydrofluoric acid (HF). The method followed was in accordance with the procedure used by Okolo (2010), Van Niekerk, (2008), Maity and Mukherjee, (2006), Liu *et al.*, (2001) and Steel and Patrick, (2001). Five hundred grams (500 g) of the coal sample was added to four litres (4 L) 5 M (32 wt%) concentrated HCl in a glass beaker and stirred for 24 hours using a polyethylene coated magnetic stirrer at 450 revolutions per minute (rpm). The liquor was removed by filtration with the use of a vacuum pump. The insoluble solid fraction from the filtration stage was added to two and a half litres (2.5 L) 29 M (48 wt%) HF in a poly-ethylene beaker. The mixture was agitated for 24 hours at 450 rpm, after which the liquor was once again removed by filtration, and the HF-insoluble fraction further leached in HCl using the method described above. The liquor was once more separated by filtration and the insoluble fraction was thoroughly washed using ultrapure water until the pH of the filtrate was close to 7.0. The acid-insoluble solid was then dried in a vacuum oven at 80°C until a constant weight was obtained. The acid washed coal sample was stored in a hermetically sealed container under N_2.

3.3.2. Mineral samples

Mineral samples were obtained from various industries. Table 3-1 indicates the minerals as well as the suppliers / origin. All mineral samples were prepared to a size of < 45 µm using a hand grinder.

Table 3-1 Minerals obtained for investigation

Mineral	Supplier/Origin	Composition
Calcite [$CaCO_3$]	Sigma Aldrich®	99.999% trace element basis
Dolomite [$CaMg(CO_3)_2$]	Karoo Supergroup dolomite from Klerksdorp region	96% dolomite, 4% muscovite
Kaolinite [$Al_2Si_2O_5(OH)_4$]	Associated Chemical Enterprises®	99.995% trace element basis
Pyrite [FeS_2]	Strem® Chemicals USA	95% pure pyrite
Quartz [SiO_2]	Sigma Aldrich®	99.995% trace element basis

The calcite (MW = 100.09 g/mole) is specified to contain less than 10 ppm impurities, density of 2.93 g/mL at 25°C, and refractive index *n20*/D16584. Dolomite was sourced from dolomite ridges in the Klerksdorp region. These dolomite ridges are part of the Karoo Supergroup which correlates with the dolomite found in the Highveld area. The sample was analysed using XRD (X-ray diffraction) at Sasol Research and Development, Sasolburg. It was found that the sample contained 96% dolomite and 4% muscovite [$KAl_2(AlSi_3O_{10})(F,OH)_2$]. The kaolinite (MW = 258.16 g/mol) is specified to be 99.9% pure, containing arsenic (0.0002%), calcium (0.025%), chloride (0.03%) and lead (0.002%) impurities, with a density of 2.3 g/mL at 25°C and 1.5% mass loss on drying at 105°C and 15% mass loss on ignition. Pyrite (MW = 119.97 g/mol) with a purity of 95% was imported from Strem Chemicals®. The sample is certified to contain 44 wt% Fe and 52.5 wt% S, with the rest being made-up of impurities. The quartz (MW = 60.08 g/mol) is specified to contain less than 50 ppm impurities, with a mass loss on ignition of 2.00% at 1000°C with a holding time of 1 hour, a melting point of 1610°C, density of 2.6 g/mL at 25°C and refractive index *n20*/D of 1.544.

3.4. Overview of conventional coal and thermogravimetric analyses

Conventional analytical techniques such as proximate, ultimate, calorific value and total sulphur analyses were done on the beneficiated coal fraction (TWD) and the acid washed coal fraction (AW TWD). Coal characterisation was also done on both fractions. Table 3-2 indicates the analyses, the laboratories used and the standards according to which the analyses were done. All analyses were conducted by Bureaus Veritas in Pretoria, except for the mineral XRD analysis which was conducted at Sasol Technology R & D based in Sasolburg, South Africa; and the QEMSCAN analysis was done at Eskom in Germiston, South Africa. Refer to Appendix A-1 for a full list of standards used.

Table 3-2 Coal characterisation analyses

Analysis	Property	Laboratory / Standard used
Chemical & Mineralogical	***Proximate***	***Bureaus Veritas***
	Inherent moisture content (%)	ISO 11722: 1999
	Ash content (%)	ISO 1171: 2010
	Volatile matter content (%)	ISO 562: 2010
	Fixed carbon content (%)	By difference
	Ultimate	***Bureaus Veritas***
	Carbon (%)	ISO 29541: 2010
	Hydrogen (%)	ISO 29541: 2010
	Nitrogen (%)	ISO 29541: 2010
	Oxygen (%)	By difference
	Calorific value	***Bureaus Veritas***
		ISO 1928: 2009
	Total sulphur (IR Spectroscopy) (%)	***Bureaus Veritas***
		ISO 19759: 2006
	Ash (XRF)	***Bureaus Veritas***
		ASTM D4326
	Mineral (XRD)	***Sasol Research and Development***
	QEMSCAN	***Eskom***
Petrographic	***Maceral composition***	***Bureaus Veritas***
	Vitrinite reflectance	***Bureaus Veritas***
		ISO 7404 (1 to 5): 1994
Structural	***BET adsorption***	***NWU***
	FTIR	***NWU***

3.4.1. Chemical and mineralogical analyses

These analytical methods provide information regarding the fundamental chemical and elemental composition that comprises the coal matrix. The coal sample was prepared to a size of <3 mm for the chemical analyses. Table 3-2 also indicates the standard methods used in these analyses.

For the XRD analyses, the coal sample was prepared to < 75 µm. The samples were dried overnight in a vacuum oven at 80°C to remove any surface absorbed moisture. The samples were prepared prior to analyses by a back loading preparation method. A McCrone micronising mill was used along with addition of 20% Si to determine the amorphous content. A Phillips X'Pert PW1830 powder diffractometer was used for XRD analysis. X' Pert

Highscone software was used for phase identification. The Rietveld method (Siroquant software) was used for estimation of phase amounts (Bunt *et al.,* 2012a).

QEMSCAN (Quantitative Evaluation of Minerals by Scanning Electron Microscopy) is a combination of scanning electron microscopy (SEM) and electron probe micro-analyser (EPMA); the combination thereof produces an image of individual coal particles and their chemical associations (Klopper, 2011; Ward 2002). A representative sample was mixed with graphite and mounted in Araldite epoxy-resin. After the sample had cured it was carefully polished to a diamond finish of 1 µm and prepared by use of Carnauba wax. These samples were then analysed by use of a configured scanning electron microscope (SEM) to automatically determine the mineralogical composition (Klopper, 2011; Matjie *et al.,* 2011).

3.4.2. Petrographic analyses

The microscopic examination of coals and the information obtained from this analytical technique is known as coal petrography. It provides deeper insight into the organic composition, maturity and carbon-mineral associations contained within coal (Hattingh, 2012). For petrographic analysis, a petrographic block of the coal sample was prepared in accordance with ISO 7404-2. (1994) and examined under an optical reflectance microscope.

Coal samples having a particle size <1 mm were selected for petrographic analyses of the TWD coal. A 500 maceral point-count analysis was used to determine the maceral composition of the coal sample, in accordance with ISO 7404-3 (1994) (ISO, 1994a). Vitrinite reflectance measurements, done according to ISO 7404-5 (1994), were used to determine the rank of the coal (ISO 7404, 1994b). 100 measurements were taken on the vitrinite parts of each sample. Maceral composition is of importance for classification of the coal and the effect the different macerals have on the reactivity and chemical behaviour (Schobert, 1990).

3.4.3. Structural analyses

3.4.3.1. BET adsorption

Physical analyses of both the TWD and the AW TWD coal fractions were done by BET gas CO_2 adsorption analyses. It was conducted on a Micrometics ASAP 2010 Analyser, which is capable of determining pore sizes in the range of 4 Å to 5000 Å (Bunt *et al.,* 2012b; Maphala & Wagner, 2012). The coal samples analysed were all smaller than 75 µm, consistent with the sample sized used for the pyrolysis experiments. The method used is similar to that described by Hattingh (2012). The samples were dried overnight at 80°C in a vacuum oven to remove any excess moisture on the surface of the coal particles. 0.2 g of sample was loaded into the sample tube and connected to the degassing port of the analyser. The sample was degassed for 48 hours at a temperature of 25°C to a final pressure of 4 µmHg. A temperature of 25°C

was used to prevent the formation of low temperature char (Kutchko *et al.,* 2013; Hattingh, 2009). Adsorption analysis commenced after the degassing process. For this adsorption analysis the short coal method, which includes measuring techniques such as Langmuir, Dubinin-Radushkevich, Hovarth-Kawazoe, etc., was used (Hattingh, 2009). A constant analysis temperature (273.15K) was maintained with the use of ice (Bunt *et al.,* 2012b).

3.4.3.2. Diffuse reflectance infrared Fourier transform spectroscopy (DRIFT)

Diffuse reflectance infrared Fourier transform spectroscopy (DRIFT) has been used by various researchers to study coal structures and identify functional groups (Xin *et al.,* 2014; Van Niekerk *et al.,* 2008; Li *et al.,* 2003; Miura *et al.,* 2001; Chen *et al.,* 1998a; Chen *et al.,* 1998b; Christy *et al.,* 1995; Sobkowiak & Painter, 1995; Cai & Smart, 1994, Painter *et al.,* 1987). TWD and AW TWD coals (20 mg) were mixed with 200 mg potassium bromide (KBr) and left overnight in a vacuum oven at 80°C. This is consistent with methods used in previous studies (Bona & Andrés, 2008; Van Niekerk *et al.,* 2008; Sobkowiak & Painter, 1995). For Diffuse reflectance infrared Fourier transform spectroscopy (DRIFT) analyses of the two coal fractions, a Bruker alpha-P FTIR (Vertex 70) spectrometer in the 370-4000 cm^{-1} range was used (Onwudiwe *et al.,* 2013). Spectra were obtained using 400 scans (interferograms) at a resolution of 4 cm^{-1}. A KBr spectrum taken under the same conditions was used as background. The Kubelka-Munk method was used for transformation and further processing (Van Niekerk *et al.,* 2008; Christy *et al.,* 1995). Baseline correction was done in order to indicate only the useful absorption bands (Machnikowka *et al.,* 2002).

3.4.4. Thermogravimetric analyses

A SDT Q600 TGA system with Universal TA Analysis 2000 software was used for thermogravimetric analysis of the coal and mineral samples to be used in this study. Approximately 20 to 70 mg of sample was heated from 25°C to 1 100°C using a heating rate of 6.2°C/min in nitrogen (N_2) gas flow of 120 mL/min.

3.5. Chemical coal analyses results and discussion

3.5.1. Proximate analysis

Proximate analysis provides information with regard to the fraction of moisture, volatile matter (gases and vapours generated during pyrolysis), fixed carbon (the non-volatile fraction of coal), and ash (the residue remaining after combustion) (Probstein & Hicks, 2006). The TWD sample was characterized as a low ash yielding coal, with an ash yield (ISO 1171: 2010) of 14.9 wt% (d.b.), and 2.0 wt% (d.b.) ash yield for the AW TWD fraction (Table 3-3). This result also confirms that the acid washing process was successful, with the XRF, XRD and

QEMSCAN analyses (Section 3.6) providing more insight regarding the minerals present in the coal fractions.

Table 3-3 Proximate analysis results

			TWD			AW TWD		
	Standard	*Unit*	*a.d[a]*	*d.b.[b]*	*d.a.f.[c]*	*a.d.[a]*	*d.b.[b]*	*d.a.f.[c]*
Inherent moisture	ISO 11722:1999	wt%	4.2	0.0	0.0	2.3	0.0	0.0
Ash	ISO 1171:2010	wt%	14.3	14.9	0.0	2.0	2.0	0.0
Volatile matter (VM)	ISO 562:2010	wt%	31.4	32.8	38.5	32.7	33.4	34.1
Fixed carbon (FC)*	-	wt%	50.1	52.3	61.5	63.0	64.6	65.9
TOTAL	**-**	wt%	**100.0**	**100.0**	**100.0**	**100.0**	**100.0**	**100.0**

*[a]a.d = air dry basis; [b]d.b. = dry basis; [c]d.a.f. = dry, ash free basis; [d]d.m.m.f. = dry, mineral matter free basis; * determined by difference*

The decrease in inherent moisture content (ISO 11722: 1999), from 4.2 wt% to 2.3 wt% for the AW TWD fraction, is consistent with findings in other studies (Tsubouchi & Ohtsuka, 2002a; Chen *et al.* 1999). This difference can be attributed to the process followed during acid washing, and the drying of the coal sample at 80°C, that may drive off some moisture. Changes in the coal matrix regarding the porosity may also influence this yield (Suelves *et al.,* 2000). A decrease in volatile matter (ISO 562: 2010), from 38.5 wt% to 34.1 wt% (d.a.f.) was observed with acid washing. This observation is consistent with observations made from the proximate analysis of other acid washed South African coal (Klopper *et al.*, 2012). It is however contrary to the observations made in other studies on coals of different rank from other world regions (Tsubouchi & Ohtsuka, 2002a; Chen *et al.* 1999).

3.5.2. Ultimate analysis

Ultimate analysis refers to a coal analysis which identifies the elemental weight percentages of nitrogen, hydrogen, sulphur and carbon directly, whilst the oxygen content is determined by difference (Probstein & Hicks, 2006). Results for other conventional coal analyses are indicated in Table 3-4. Comparing the ultimate analysis results for the TWD and AW TWD fractions indicate no significant difference with regard to H and N. There is a slight increase observed in the elemental C amount for the AW TWD fraction (79.1 wt% d.b. vs. 80.3 wt% d.b.), as well as a decrease in the elemental O (11.5 wt% d.b. vs. 12.7 wt% d.b.). This difference can be attributed to the removal of the other elemental components which may contain some of the elemental O identified, by the acid washing process. Minerals such as calcite and dolomite contain some oxygen functionalities, which would have been removed off during the acid washing procedure. According to Hashimoto *et al.* (1986) oxygen content is

an indication of the occurrence of active sites after pyrolysis. The total sulphur content of the TWD fraction was 1.4 wt% (d.b.), whilst that of the AW TWD fraction was 1.3 wt% (d.b.). Only a small decrease in sulphur content was observed as the sulphide minerals were the most difficult to remove by conventional acid washing processes (Wu & Steel, 2007; Bolat *et al.*, 1998). Regarding the atomic ratio of H/C and O/C no significant differences were observed.

Table 3-4 Other conventional coal analyses results

			TWD		AW TWD	
	Unit	***Standard***	***a.d.[a]***	***d.b.[b]***	***a.d.[a]***	***d.b.[b]***
Gross Calorific Value (CV)	$MJ.kg^{-1}$	ISO 1928:2009		28.36		30.82
Ultimate analysis						
Carbon	wt%	ISO 29541:2010	70.4	79.1	76.9	80.3
Hydrogen	wt%		4.2	4.7	4.5	4.7
Nitrogen	wt%		1.9	2.1	2.1	2.2
Oxygen (by difference)	wt%		11.3	12.7	11.0	11.5
Sulphur (IR spectroscopy)	wt%	ISO 19579:2006	1.2	1.4	1.2	1.3
TOTAL		**-**	**89.0**	**100.0**	**95.7**	**100.0**
Atomic H/C			**-**	**0.71**	**-**	**0.7**
Atomic O/C		**-**	**-**	**0.12**	**-**	**0.11**

[a]a.d = air dry basis; [b]d.b. = dry basis

3.5.3. Calorific value (C.V.)

Calorific value is defined as the measure of a coal sample to generate heat during combustion (Koekemoer, 2009). The gross calorific value of the TWD fraction was 28.36 $MJ.kg^{-1}$ (d.b.), whilst the AW TWD fraction had a value of 30.82 $MJ.kg^{-1}$(d.b.). This can be attributed to the higher fixed carbon content of the AW TWD coal (64.6 wt% d.b.) versus that of the TWD fraction (59.0 wt% d.b.) due to mineral matter removal. According to the CKS 561-1982 standard, TWD coal can be classified as a grade A coal as the CV is between 27.5 MJ.kg-1 (a.d.b.) and 28.5 $MJ.kg^{-1}$ (a.d.b.). The higher calorific value is also evident from the higher fuel ratio (FC/VM) for the AW TWD fraction (1.9) compared to that of the TWD fraction (1.6).

3.6. Mineralogical analyses results and discussion

3.6.1. X-ray fluorescence (XRF) and Induced coupled plasma (ICP) ash analysis

XRF analysis is used to determine the elemental composition of the ash derived from the coal fractions. It is used for the identification of an element by measurement of its characteristic X-ray emission wavelength or energy (Günzler & Williams, 2002). This is a quantitative method which compares the intensities from “unknowns” to that of primary or secondary standards. Ashing of the coal sample was performed by Bureaveritas, and the XRF analyses were reported on a loss on ignition (L.O.I.) free basis according to ASTM D4326 (1997) in a fusion bead apparatus. ICP analysis had to be carried out on the AW TWD derived ash due to the low ash content

Table 3-5 XRF/ICP results

Ash species	TWD wt% *(d.b.*)*	AW TWD wt% *(d.b.*)*	Removal efficiency (%)
Al_2O_3	25.3	14.9	92.1
CaO	11.5	8.8	89.7
Cr_2O_3	0.1	0.2	55.3
Fe_2O_3	9.6	39.0	45.3
K_2O	0.6	0.4	91.2
MgO	3.7	5.1	81.7
MnO	0.1	0.1	96.3
Na_2O	0.6	1.2	75.0
P_2O_5	1.5	0.3	97.7
SiO_2	35.9	5.1	98.1
TiO_2	1.7	5.7	55.5
V_2O_5	0.1	0.2	59.7
ZrO_2	0.1	0.5	45.2
Ba	0.6	2.5	43.1
Sr	0.7	1.7	68.0
SO_3	8.2	14.3	76.5
Total / Overall efficiency	**100**	**100**	**86.6**

* *d.b. = dry basis*

Table 3-5 indicates the ash analysis results as obtained by XRF/ICP analysis on a loss of ignition (L.O.I) free basis. XRF analysis reports all identified elements as oxides, but in reality the ash from coal is comprised of a complex mixture of alumino-silicates. It can be observed that the ash from the TWD fraction contained significant amounts of SiO_2, Al_2O_3, CaO, Fe_2O_3, SO_3, MgO, TIO_2 and P_2O_5. These are the dominant species that are formed from the minerals present in the raw coal sample. For the AW TWD fraction, the species present in decreasing abundance were Fe_2O_3, Al_2O_3, CaO and TiO_2. Evaluating the species present in the ash of the TWD and the AW TWD fractions, it can be observed that there is a significant decrease in the Al_2O_3 species. This can be attributed to effective removal of minerals such as kaolinite, which contain a lot of the alumina species. It was expected that the leaching process would be effective in removal of the aluminium, carbonate and silicate compounds as it would confirm findings in previous studies (Yan *et al.,* 2005; Liu *et al.*, 2004a; Ôztas & Yürüm, 2000; Bolat *et al.,* 1998; Adanez & De Diego, 1993).

The mineral matter removal efficiency of the acid leaching method, as calculated from the XRF ash analysis, was determined by using the values of the ash percentages (d.b) obtained in the proximate analysis as total ash percentage. This relates to an 86.6% overall removal efficiency. The Fe_2O_3 removal efficiency is very low, indicating the inefficient removal of pyrite

(Bolat *et al.*, 1998), the main iron containing mineral present in the coal samples. The low efficiency values obtained for other species such as Cr_2O_3, ZrO_2, TiO_2, Ba, V_2O_5 relate to trace elements present in the coal sample.

3.6.2. Mineral X-ray diffraction (XRD) analysis

Mineral XRD analysis is used for the identification of mineral crystalline compounds and amorphous carbon forms (Huggins, 2002; Ward, 2002; Hutton & Mandile, 1996). XRD identifies the crystalline mineral matter in Highveld coals (Pinetown *et al.,* 2007). The analysis is based on a calibration procedure that compares the height or area ratios of diffraction peaks of different minerals relative to those of the internal standard (such as CaF_2) (Huggins, 2002, Ward, 2002). Optimum circumstances will provide results for individual minerals in a ± 5-10% error range. XRD provides information on crystalline components and amorphous carbon forms.

Mineral XRD analysis of the TWD fraction (Table 3-6) indicated that kaolinite (4.9 wt%), dolomite (1.6 wt%) and quartz (1.4 wt%) were the most common mineral species. The aragonite species also present in the raw coal sample has the same chemical formula as dolomite, ($CaMgCO_3$), but differs with regard to crystal structure. Aragonite has an orthorhombic crystal structure with acicular crystals (Ward, 2002). Fluorapatite or calcium fluorophosphate ($Ca_5(PO_4)_3OH$) was also present in very low concentration. It has a hexagonal crystal structure and is the most common phosphate mineral.

Table 3-6 XRD Results

	Weight %		Removal efficiency (%)
	TWD	***AW TWD***	
Amorphous Content	90.3	99.3	-
Quartz	1.4	-	100.0
Kaolinite	4.9	-	100.0
Calcite	0.4	-	100.0
Dolomite	1.6	0.1	93.8
Pyrite	0.9	0.6	33.3
Aragonite	0.2	-	100.0
Apatite, F-,	0.1	-	100.0
TOTAL / *OVERALL*	**100.0**	**100.0**	***92.8***

Comparing the TWD fraction XRD results with that of the AW TWD fraction (Table 3-6) it can be observed that most of the crystalline minerals were effectively removed by acid washing. The only minerals still present, as identified in the crystalline phase, were 0.1 wt% dolomite ($CaMg(CO_3)_2$) and 0.6 wt% pyrite (FeS_2). Pyrite is part of the larger sulphide mineral group

and is difficult to remove by the conventional acid washing techniques used in this study (Bolat *et al.*, 1998). The removal efficiency of 33.3% (Table 3-6) relates to the observations from the XRF ash analysis regarding the Fe_2O_3 species being present in the ash.

3.6.3. QEMSCAN results

Quantitative evaluation of minerals by scanning electron microscopy (QEMSCAN) refers to an integrated automated system used to identify mineral matter (Golab *et al.,* 2013; Matjie *et al.,* 2011; Van Alphen, 2007; Liu *et al.,* 2005). It was first used in the precious metal mining industry, but its application has been extended to mineral matter identification in coal and fly ash (Van Alphen. 2007).

In Table 3-7 the QEMSCAN results are summarised. The main minerals (> 1 area %) identified in the TWD fraction were: kaolinite, dolomite, pyrite, quartz and calcite being most abundant. This confirms the XRD observations (Table 3-6) as well as results found in previous studies (Pinetown *et al.*, 2007; Buhmann, 1991). The AW TWD fraction contains very small amounts of minerals, with only pyrite being present in a significant quantity (Table 3-7). TWD coal was reported to contain 17.4 wt% mineral matter, whilst the AW TWD coal fraction contained 3.2 wt% mineral matter.

The QEMSCAN images are indicated in Figure 3-1 (TWD) and Figure 3-2 (AW TWD). In Figure 3-1a wide dispersion of minerals can be observed, whilst Figure 3-2 indicates little dispersion, with mostly coal present. The extent of mineral removal obtained by the acid washing process is visibly noticeable. It can be observed that the pyrite content was not effectively reduced, as expected (Bolat *et al.*, 1998). Small amounts of quartz, kaolinite, calcite and muscovite can also be observed in Figure 3-2. Some particle segregation, especially of pyrite should have occurred. A high proportion of pyrite, calcite and dolomite cleats are observed in Figure 3-2, which is expected of a bright export quality vitrinite-rich coal. The minerals in these cleats are liberated during crushing and milling, forming extraneous fragments.

The removal efficiency of minerals determined from the QEMSCAN results (Table 3-7) indicates 76.9% of mineral matter present in the TWD fraction was effectively removed by acid washing. The acid washing process does not seem to have affected the pyrite, other trace minerals, and to a lesser extent the quartz (carbominerite-group) and rutile content. The XRF ash analysis supports this observation when comparing the Fe_2O_3, Ba, Cr_2O_3, Ba, Sr, V_2O_5, ZrO_2 and TiO_2 removal efficiency obtained (Table 3-5). The XRF (Table 3-5) and XRD (Table 3-6) analysis do however indicate that quartz was removed effectively, 98.1% and 100.0%, respectively. It can be concluded that the remaining quartz mineral matter was present in the amorphous phase, or sampling for the various analyses played a role.

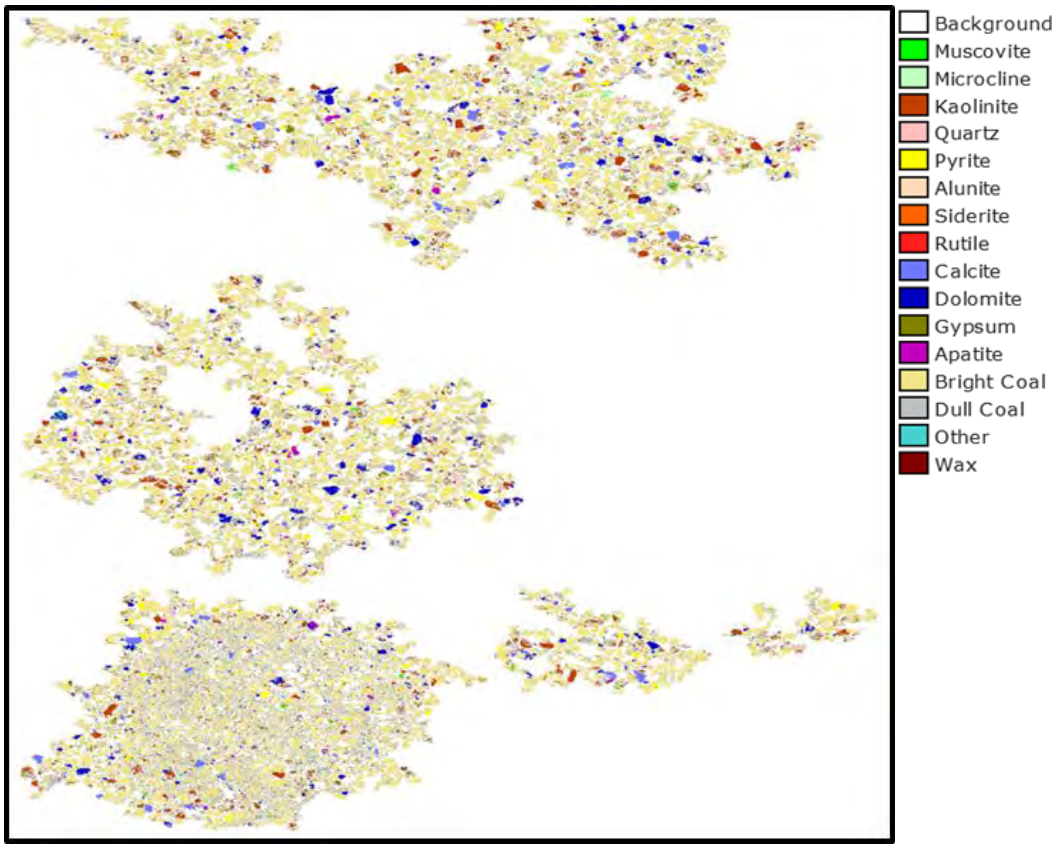

Figure 3-1 Electron microscopy image of TWD coal

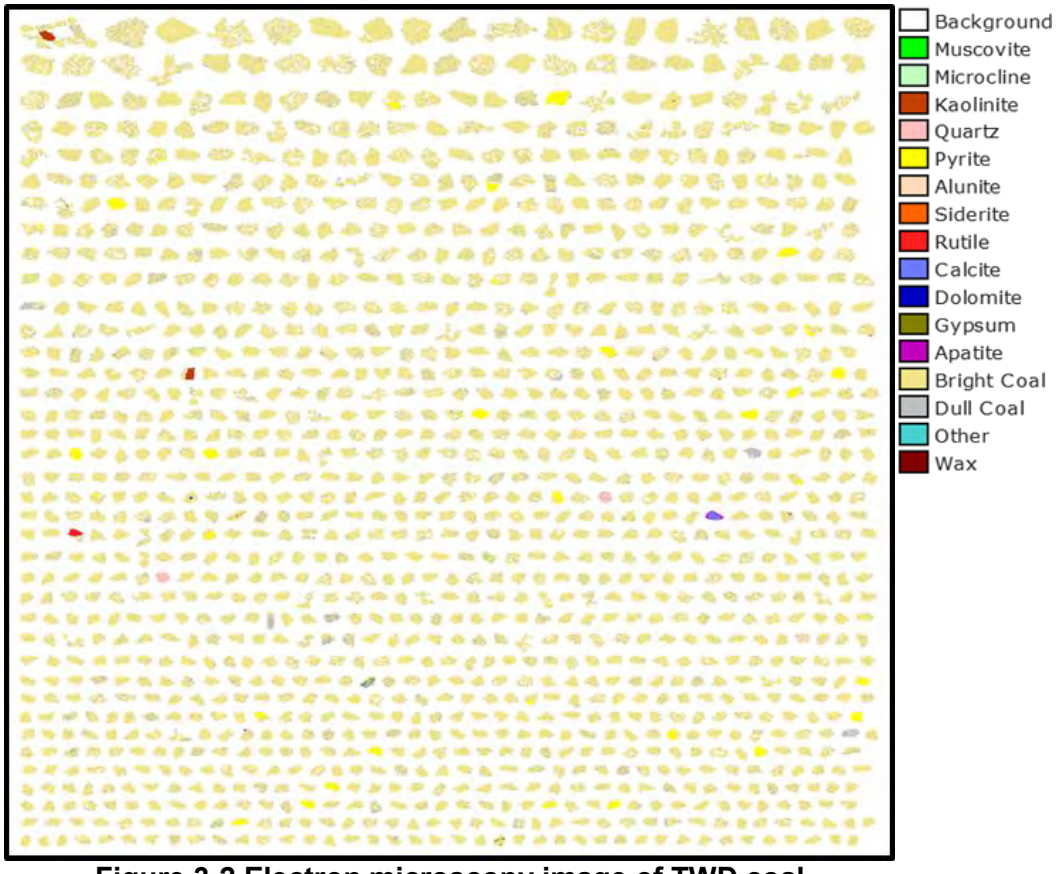

Figure 3-2 Electron microscopy image of TWD coal

Table 3-7 QEMSCAN results

	Area %		Removal efficiency (%)
	TWD	*AW TWD*	
Sulphates/Gibbsite	0.81	0.08	90.1
Pyrite	3.92	4.40	-
Siderite	0.16	0.00	100.0
Calcite	2.28	0.02	99.1
Dolomite	4.75	0.02	99.6
Apatite	0.68	0.03	95.6
Kaolinite	8.63	0.05	99.4
Quartz	1.5	0.18	88.0
Illite/Muscovite	0.76	0.01	98.7
Microcline	0.33	0.00	100.0
Rutile	0.08	0.04	50.0
Other	0.5	0.78	-
TOTAL	**24.4**	**5.63**	**76.9**

Comparison of XRF, XRD and QEMSCAN analyses highlights the need for various methods to analyse coal mineral matter, as well as the limitations and developments needed to obtain a “clear picture” of the mineralogical content of coal (Klopper *et al.,* 2012; Ward 2002).

3.3.7. Relating XRF, XRD and QEMSCAN results

In order to relate the XRF, XRD and QEMSCAN results a method was followed as used by Liu *et al.* (2007a). The QEMSCAN area % values were first transformed to weight % values by density calculations. Then the oxides identified by XRF were determined as fractions of the minerals identified by XRD / QEMSCAN. See Appendix A.2 for detailed discussion of the calculations.

In Figure 3-3 the XRF wt% results are plotted as function of the calculated XRD / QEMSCAN wt% values for the TWD (Figure 3-2a) and AW TWD (Figure 3-2b) fractions. It can be observed that the correlation between the XRD and XRF data (r^2=0.953) is much stronger than that between the QEMSCAN and XRF data (r^2=0.741) for the TWD coal. It is however not possible to predict various oxides, of which no relation can be found in the XRD analyses, for example Na_2O, K_2O etc.. For the AW TWD coal there is very weak correlation between the XRF data and the values estimated from XRD and QEMSCAN data.

Table 3-8 indicates the calculated values for the various components identified by XRF as estimated from the XRD and QEMSCAN data. For the TWD fraction it can be observed that

XRD analysis seems to overcompensate for the SiO_2 component, (relating to quartz and kaolinite), whilst QEMSCAN underestimates this component.

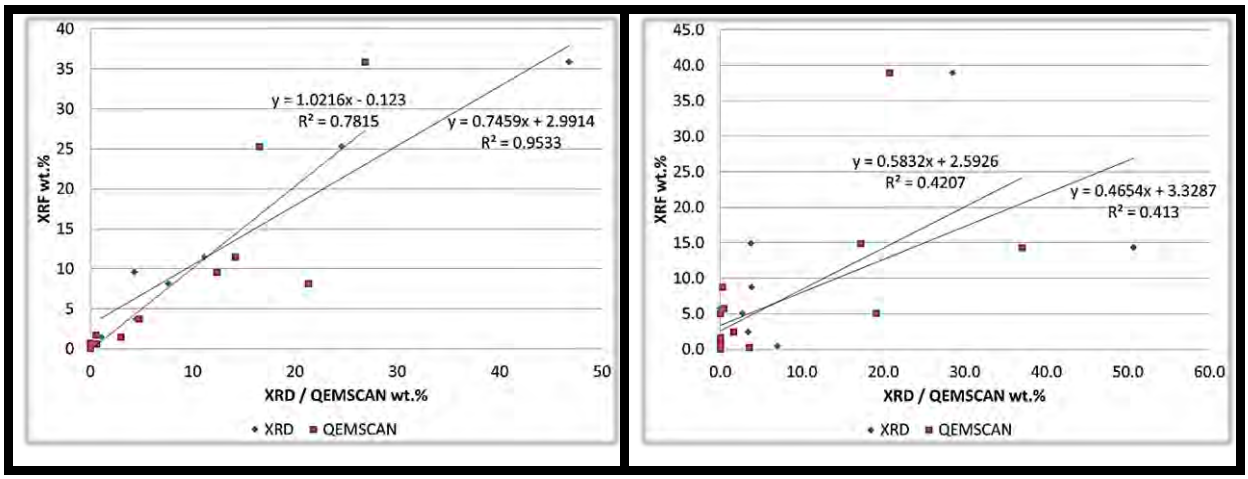

Figure 3-3 Correlation between XRF and XRD/QEMSCAN results for a) TWD and b) AW TWD.

Table 3-8 Estimated XRF oxides from XRD and QEMSCAN results

	TWD			AW TWD		
	wt%					
	XRF	***Pred. XRD***	***Pred. QEMSCAN***	***XRF***	***Pred. XRD***	***Pred. QEMSCAN***
SiO_2	35.9	46.8	26.8	5.1	0.0	19.1
Al_2O_3	25.3	24.6	16.5	14.9	3.8	17.2
Fe_2O_3	9.6	4.3	12.3	39.0	28.5	20.8
CaO	11.5	11.2	14.2	8.8	3.8	0.3
MgO	3.7	4.4	4.7	5.1	2.8	0.0
SO_3	8.2	7.6	21.3	14.3	50.7	37.0
P_2O_5	1.5	1.1	3.0	0.3	0.0	3.6
Na_2O	0.6	0.0	0.0	1.2	0.0	0.0
K_2O	0.6	0.0	0.6	0.4	7.0	0.0
TiO_2	1.7	0.0	0.5	5.7	0.0	0.4
ZrO_2	0.1	0.0	0.0	0.5	0.0	0.0
V_2O_5	0.1	0.0	0.0	0.2	0.0	0.0
Ba	0.6	0.0	0.0	2.5	3.4	1.6
Sr	0.7	0.0	0.0	1.7	0.0	0.0
MnO	0.1	0.0	0.0	0.0	0.0	0.0
Cr_2O_3	0.1	0.0	0.0	0.2	0.0	0.0

Fe_2O_3, relating to pyrite, is underestimated by XRD, whilst it is overestimated by QEMSCAN analysis. The overestimation of pyrite content is specifically observed in the very high estimated SO_3 content determined from the QEMSCAN results. QEMSCAN analysis underestimates the Al_2O_3 component relating to kaolinite, whilst CaO is overestimated. The Al_2O_3, CaO, MgO, SO_3 and P_2O_5 components between XRD and XRF analyses indicate very good correlation. The results for the AW TWD coal fraction are less promising. A decrease in

the various types of minerals identified by an analysis method will lead to a decrease in possible predicted oxides, thus yielding a lower correlation. Both XRD and QEMSCAN do not identify trace minerals/elements, thus limiting the prediction of all oxides as reported by XRF analyses.

3.7. Petrographic analyses results and discussion

For petrographic analysis, a petrographic sample (coal-resin block) was prepared in accordance with ISO 7404-2 (1994). The petrographic sample was then examined under an optical reflectance microscope using an oil immersion lens. Coal samples having a particle size <3 mm were selected for petrographic analyses of the TWD coal.

3.7.1. Vitrinite reflectance

Vitrinite reflectance measurements, done according to ISO 7404-5 (1994), were used to determine the rank of the coals (ISO 7404, 1994b). 100 measurements were taken on the vitrinite parts of each sample. Vitrinite reflectance offers a measure to determine the degree of maturity of rank of a particular coal (Günzler & Williams, 2002). The vitrinite maceral was selected for this purpose due to its linear increase in reflectance during the progression of the coalification process, the higher the reflectance value, the higher the coal rank / maturity (Günzler & Williams, 2002; Schobert, 1990).

The reflectance analysis is usually presented as a vitrinite reflectance distribution grouped according to reflectance V-type classes. For example, a V-type of 7 contains vitrinites having reflectance values from 0.70 to 0.79 %. The mean reflectance is calculated by averaging the 100 reflectance measurements. The mean reflectance is either presented at mean-max reflectance (RoV max). Determination and calculation of reflectance are described in detail in ASTM D2798-11a and ISO 7404-5 (2009).

Table 3-9 Vitrinite reflectance distribution

Vitrinite reflectance distribution	R_r % distribution
V5 (0.50-0.59)	3
V6 (0.60-0.69)	54
V7 (0.70-0.79)	38
V8 (0.80-0.89)	4
V9 (0.90-0.99)	1
V10 (1.00-1.09)	-
RoV max	0.70
Total reactives	76.5
Total inerts	23.5

The vitrinite reflectance range for TWD coal was in the 0.5% to 1.0% distribution range. The mean-maximum random reflectance value (RoV max) was calculated as 0.7% which classifies the TWD coal as a Medium Rank C bituminous coal. Coal rank is known to play a major role in the pyrolysis behaviour of coal, as well as in the product spectrum of tar, char and gases generated (Kandiyoti *et al.,* 2006; Iglesias *et al.,* 2001, Smith *et al.,* 1994). Table 3-9 indicates the obtained vitrinite reflectance distribution results for the TWD coal. The petrographic analysis was only done on the TWD fraction and not on the AW TWD fraction, because acid washing will not affect the coal rank, only the grade of coal.

3.7.2. Organic maceral composition

A 500 maceral point-count analysis was used to determine the petrographic composition of the coal sample, in accordance with ISO 7404-3 (1994) (ISO, 1994a). Maceral composition is of importance for classification of the coal and the effect that the different macerals has on the reactivity and chemical behaviour (Schobert, 1990). From the results in Table 3-10 it can be observed that the TWD coal is a vitrinite rich (50.0 vol.% m.m.b.) coal, with a large inertinite (34.6 vol.% m.m.b.) fraction. The vitrinite found in the medium rank bituminous coals, (such as found in TWD), pyrolyses upon heating and forms porous carbon chars (Hattingh, 2012), the inertinite fraction tends to form denser, inert chars during the pyrolysis process (Falcon & Snyman, 1986).

Liptinite content is low (7.0 vol.% m.m.b) and typical for South African Permian-aged Gondwana land coals. The inertinite consisted mainly of reactive semifusinite and inert semifusinite, with small amounts of fusinite, secretinite and micrinite. The semifusinites are referred to as "tissue type" inertinites, with the smaller fractions coming from the "detrital" inertodetrinites (Hattingh, 2012).

Table 3-10 Maceral composition

Maceral	% by Volume (m.m.b[a])	% by Volume (m.m.f.b.[b])
Vitrinite	**50.0**	**54.6**
Liptinite	**7.0**	**7.6**
Inertinite	**34.6**	**37.8**
- Reactive semifusinite	19.5	21.3
- Inert Semifusinite	14.0	15.3
- Fusinite + Secretinite	0.9	1.0
- Micrinite	0.2	0.2
Mineral matter (calculated)	**8.4**	**-**
TOTAL	**100**	**100**

[a] m.m.b. = mineral matter basis; [b]m.m.f.b. = mineral matter free basis.

3.8. Structural analyses results and discussion

3.8.1. BET Adsorption results and discussion

BET CO_2 adsorption analyses provide insight with regard to the microporous properties in the micropore range pore sizes smaller than 12 Á (Sing *et al.,* 1985). Figure 3-4 indicates the isotherm data obtained for the TWD and AW TWD fractions from CO_2 adsorption.

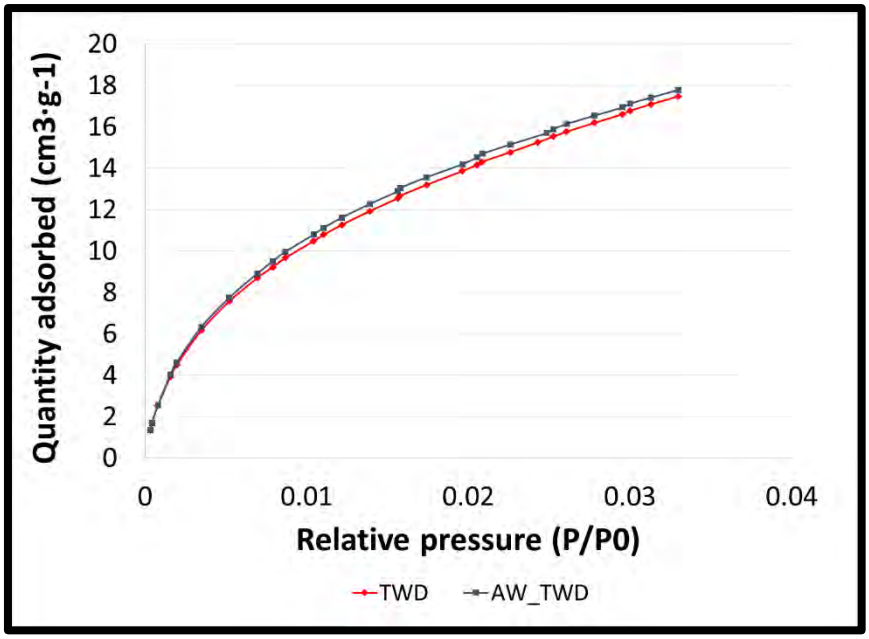

Figure 3-4 CO_2 adsorption isotherms for TWD and AW TWD coal.

Type I behaviour can be identified for both fractions. This behaviour is characteristic of all microporous materials (Hattingh, 2012). The relative low pressures (as observed in Figure 3-4) are typical of narrow micropore widths with high adsorption potential (Hattingh, 2012). Little variance is observed between the TWD and AW TWD coal fractions. Table 3-11 summarises the structural parameters obtained from CO_2 adsorption by application of the Dubinin-Radushkevich (D-R) equation. The error associated with determination of the various parameters from CO_2 adsorption was found to be less than 5% for both fractions.

From Table 3-11 it can be observed that the micropore surface area decreased after acid washing from 162.1 $m^2 \cdot g^{-1}$ for TWD to 142.9 $m^2 \cdot g^{-1}$ for AW TWD. The monolayer capacity indicates a small decrease for AW TWD (31.3 $cm^3 \cdot g^{-1}$ vs. 35.3 $cm^3 \cdot g^{-1}$). The Langmuir and BET surface areas were also somewhat smaller for AW TWD. The Horvath-Kawazoe average micropore diameter was found to be the same for both fractions, 3.9 Å. The CO_2 adsorption parameters reported in Table 3-13 were found to be consistent in order with the same parameters reported for other South African coals (Hattingh, 2012; Maphala and Wagner, 2012).

Table 3-11 CO_2 adsorption parameters (d.m.m.f.)

Physical property	TWD	AW TWD
Micropore surface area ($m^2 \cdot g^{-1}$)	162.1	142.9
Monolayer capacity ($cm^3 \cdot g^{-1}$)	35.5	31.3
Langmuir surface area ($m^2 \cdot g^{-1}$)	114.5	100.1
BET surface area ($m^2 \cdot g^{-1}$)	107.3	93.5
Average micropore diameter (Å)	3.9	3.9

In general, the acid washing process does not seem to affect the CO_2 adsorption parameters to such a great extent. This is consistent with findings in other studies (Lee *et al.,* 2014; Klopper *et al.,* 2012; Rivera-Utrilla *et al.,* 1996). The fact that the surface area for the AW TWD coal fraction was smaller than that of the TWD coal fraction is interesting, and more investigation and attention can be given to this observation in future work. It is possible that the basis on which the data is reported may play a role. Another possibility is that the acid washing process has the same effect as has been observed for pre-oxidation of coals. Pre-oxidation has been seen to lead to the densification of carbonaceous matter. The densification has been attributed to: i) the elimination of less organised surface components such as CO_2 and CO, which is the result of low temperature pyrolysis; ii) the opening of closed pores; and iii) the addition of oxygen to the coal, i.e. less other gases will be adsorbed during studies such as BET (Ruiz *et al.,* 2001)

TWD coal has an ash percentage of 14.9% which can be considered as a low ash content for a South African coal sample; thus further removal of mineral matter from this low ash coal will not have such a large effect on the porosity of the coal. The surface areas of various low ranking coal chars have however been observed to increase to a larger extent when compared to the parent coal chars derived during pyrolysis (Lee *et al.,* 2014; Kuznetsov *et al.,* 2013; Samaras *et al.,* 1991). Little change in surface area for acid washed bituminous coal chars compared to parent coal chars, derived during pyrolysis, has however been reported (Klopper *et al.,* 2012; Rivera-Utella *et al.,* 1996).

3.8.2. Diffuse reflectance infrared Fourier transform spectroscopy (DRIFT) results and discussion

DRIFT spectra are preferred for qualitative analysis of coals due to flat baselines and well-resolved bands (Sobkowiak & Painter, 1995). Results can, however, be at best only semi-quantitative with regard to the contribution of various functional groups present within the coal structure (Machnikowska *et al.* 2002).

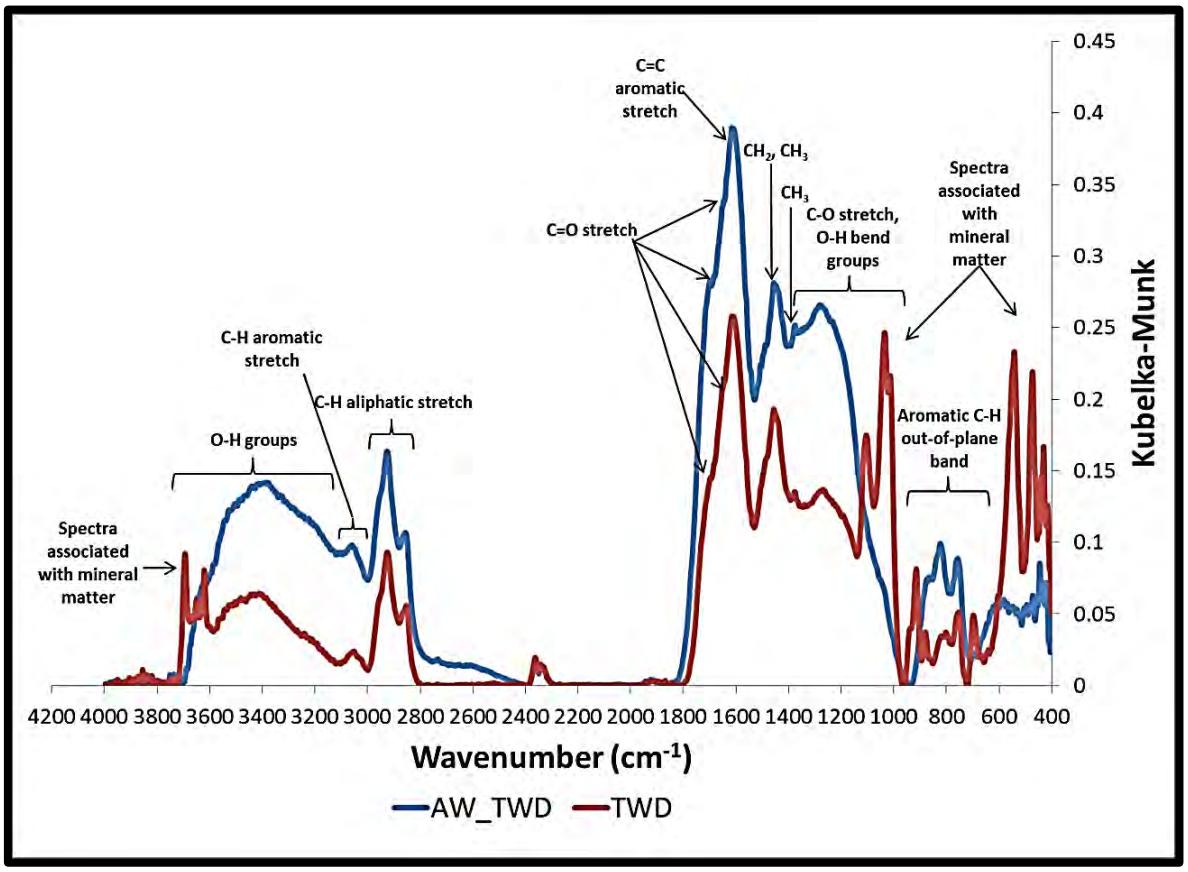

Figure 3-5 DRIFT spectra for TWD and AW TWD coals

Appendix A-3 indicates the experimental reproducibility of the DRIFT analyses for both coal fractions. Based on spectra interpretation of previous studies, spectra were identified as indicated in Figure 3-5 (Xin *et al.,* 2014; Malumbazo *et al.,* 2011; Strydom *et al.,* 2011; Bona & Andrés; 2008b; Van Niekerk *et al.,* 2008; Li *et al.,* 2004; Li *et al.,* 2003; Machnikowska *et al.,* 2002; Miura *et al.,* 2001 Chen *et al.,*1998a; Barth *et al.,* 1994; Cai & Smart, 1994; Painter *et al.,* 1987; Painter *et al.,* 1985; Painter *et al.,* 1981). It can be observed that the obtained spectra are consistent with DRIFT analyses of other South African coals (Malumbazo *et al.,* 2011; Strydom *et al.,* 2011; Van Niekerk *et al.,* 2008). The spectra identified in Figure 3-5 were divided into three sub sections which will be discussed separately: (1) the range 4000 to 2600 cm^{-1} (Figure 3-6 and Table 3-12), (2) the range 1900 to 900 cm^{-1} (Figure 3-7 and Table 3-13), and (3) the range 900 to 370 cm^{-1} (Figure 3-8 and Table 3-14).

3.8.2.1. DRIFT spectra range 4000 – 2400 cm^{-1}

The DRIFT spectra of the range 4000 – 2400 cm^{-1} are presented in Figure 3-6, with identification of the peaks thereof given in Table 3-12. The first peaks observed in this range relate to mineral matter vibrations in the range 3800 – 3600 cm^{-1} (Bona & Andrés; 2008b; Li *et al.,* 2004; Cai & Smart, 1994). It has been identified to relate to kaolinite, with the peaks identified as indicated in Table 3-14 (Frost *et al.,* 2003; Ming & Spark, 2003; Makó *et al.,* 2001;

Madejová & Komadel, 2001; Farmer, 1974). The peaks in the range 3653 – 3595 cm^{-1} can also be identified as free hydroxyl groups. (Xin *et al.,* 2014; Van Niekerk *et al.,* 2008; Li *et al.,* 2004; Li *et al.,* 2003; Machnikowska *et al.,* 2002; Miura *et al.,* 2001; Chen *et al.,*1998b; Painter *et al.,* 1987; Painter *et al.,* 1985). Comparison of the spectra of the TWD and AW TWD fractions indicates that the spectra of AW TWD do not indicate these peaks. This is consistent with results from XRD and QEMSCAN analyses which indicated that kaolinite was effectively removed by the acid washing process. TWD and AW TWD fractions show good comparison for the rest of the OH stretch region.

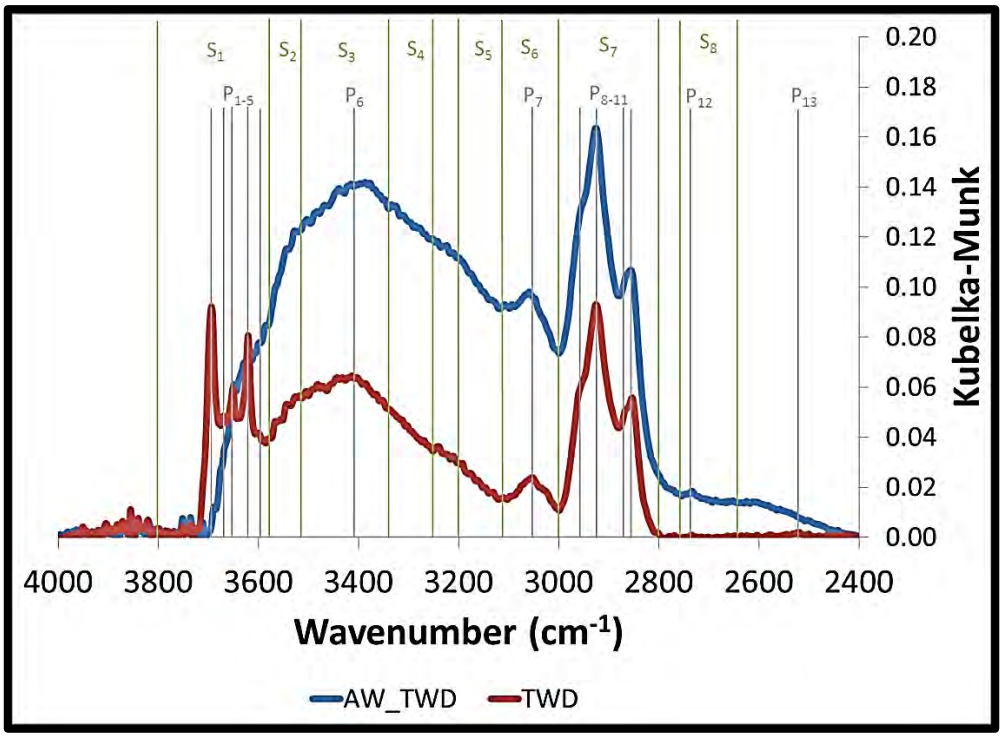

Figure 3-6 DRIFT spectra for TWD and AW TWD coals, 4000 – 2400 cm^{-1}.

The different OH groups have been identified based on research regarding the type of hydrogen bond in previous studies (Xin *et al.,* 2014; Van Niekerk *et al.,* 2008; Li *et al.,* 2004; Li *et al.,* 2003; Machnikowska *et al.,* 2002; Miura *et al.,* 2001 Chen *et al.,*1998a; Painter *et al.,* 1987; Painter *et al.,* 1985).

The aromatic C-H stretch has been identified in the range 3120 to 3000 cm^{-1} for both fractions (Xin *et al.,* 2014; Van Niekerk *et al.,* 2008; Machnikowska *et al.,* 2002; Miura *et al.,* 2001; Nomura & Thomas, 1997; Cai & Smart, 1994; Painter *et al.,* 1981). The TWD coal indicates a broader peak in this region. This stretch is of importance for water formation during the pyrolysis process. OH-groups in the region of 3000 cm^{-1} are associated with the carboxyl groups. The close proximity of protons ensures that water forms easily (Cai and Smart, 1994).

Table 3-12 DRIFT spectra identification (4000 – 2600 cm^{-1})

Peak / Vibrations	Wavenumber (cm^{-1})		Identification	
	TWD	*AW TWD*		
S_1	3800 - 3600	3800 - 3600	Mineral matter	
P_1	3695	-	In-phase inner surface hydroxyl stretching vibration relating to kaolinite	
P_2	3672	-	Out-of-phase vibrations of the inner surface hydroxyl relating to kaolinite	
P_3	3653	-	Out-of-phase vibrations of the inner surface hydroxyl relating to kaolinite	Free OH groups
P_4	3620	-	Hydroxyl stretching vibration of the inner hydroxyl relating to kaolinite	
P_5	3595	-	Water hydroxyl stretching vibration of weakly hydrogen bonded interstitial water relating to kaolinite	
S_2	3574 - 3510	3574 - 3510	OH-π	
S_3	3510 - 3332	3510 - 3332	Various OH bonds	
P_6	3410	3383	Self-associated OH-OH bonds	
S_4	3332 - 3248	3332 - 3248	OH-ether	
S_5	3200 - 3120	3200 - 3120	Cyclic OH	
S_6	3120 - 3000	3120 - 3000	Aromatic C-H stretch	
P_7	3061	3065	Aromatic C-H stretch	
S_7	3000 - 2800	3000 - 2800	Aliphatic C-H stretch	
P_8	2954	2954	Asymmetric CH_3 vibrations	
P_9	2930	2928	Asymmetric CH_2 vibrations	
P_{10}	2866	2866	Symmetric CH_2 and CH_3 vibrations	
P_{11}	2856	2864	Symmetric CH_2 and CH_3 vibrations	
S_8	2756 - 2636	2756 - 2636	-COOH dimers	
P_{12}	-	2731	-COOH dimers	
P_{13}	2515	-	-SH in thiophenols and mercaptans	

Acid washing was observed to decrease the amount of OH-groups for bituminous coals (Chen *et al.,* 1998b).The OH-groups at 3400 cm^{-1} are phenolic groups and more difficult to hydrolyse (Painter *et al.,* 1987). The OH-π type hydrogen bonds are associated with aromatic rings and form weak bonds (Painter *et al.,* 1987; Li *et al.,* 2011). They are difficult to protonate due to shortage of available protons.

The aliphatic C-H stretch was found to be in the region of 3000 to 2800 cm^{-1} (Xin *et al.,* 2014; Van Niekerk *et al.,* 2008; Machnikowska *et al.,* 2002; Miura *et al.,*2001; Nomura & Thomas, 1997; Cai & Smart, 1994; Painter *et al.,* 1981). Asymmetric and symmetric methyl and methylene vibrations were observed at the various peaks as indicated in Table 3-14 for both fractions (Xin *et al.,* 2014; Van Niekerk *et al.*, 2008; Nomura & Thomas, 1997; Painter *et al.,* 1981). The –COOH dimer range was found to be from 2756 to 2636 cm^{-1} (Li *et al.,* 2004; Li *et al.,* 2003). TWD coal does not contain –COOH groups corresponding with this spectra; however, the AW TWD fraction indicates an additional peak in this spectra range at 2731 cm^{-1}. This observation has been attributed to the effect of acid treatment (HCl) of coals in previous studies (Strydom *et al.,* 2011; Geng *et al.,* 2009). A very small vibration was observed at 2515 cm^{-1} for TWD, but not for AW TWD which is identified as an –SH vibration associated with thiophenols and mercaptans (Li *et al.,* 2004; Li *et al.,* 2003).

3.8.2.2. DRIFT spectra range 1900 – 900 cm^{-1}

The DRIFT spectral range of 1900 to 900 cm^{-1} indicates the various aromatic structures of the coal fractions. Figure 3-7 and Table 3-13 summarise the results for this spectra range.

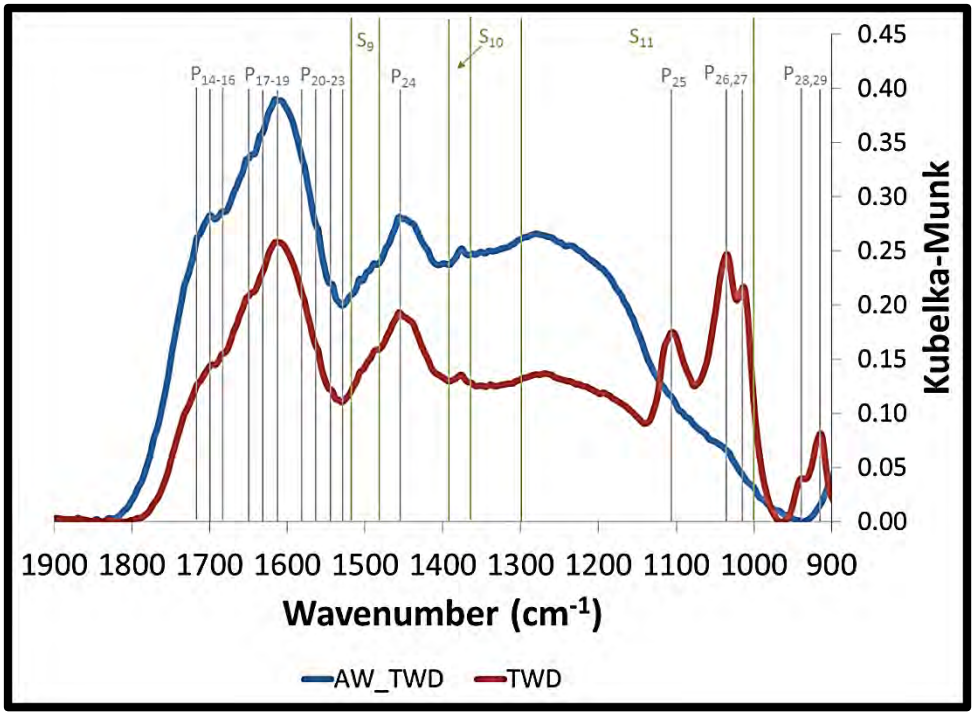

Figure 3-7 DRIFT spectra for TWD and AW TWD coals, 1900 – 900 cm^{-1}.

Table 3-13 DRIFT spectra identification (1900 – 900 cm^{-1})

Peak / Vibrations	Wavenumber (cm^{-1})		Identification
	TWD	*AW TWD*	
P_{14}	1718	1716	Esters
P_{15}	1695	1697	COOH
P_{16}	1685	1685	Conjugated C=O
P_{17}	1647	1647	Highly conjugated C=O
P_{18}	-	1633	Aromatic C=C
P_{19}	1610	1610	Aromatic C=C
P_{20}	1582	1582	Aromatic ring stretching
P_{21}	1560	1562	Aromatic ring stretching
P_{22}	1541	1541	Aromatic ring stretching
P_{23}	1528	1528	Nitrogen functionalities (amine or amide – negative loading)
S_9	1508 - 1487	1508 - 1485	Aromatic C=C
P_{24}	1452	1452	CH_2, CH_3 bend vibrations
S_{10}	1388 - 1369	1384 – 1364	CH_3
S_{11}	1300 - 1000	1300 - 1000	C-O stretch, O-H bending vibrations in phenoxy structures
P_{25}	1105	-	Si-O-Si and Al-O-Al vibrations associated with aluminates and silicates such as kaolinite and quartz
P_{26}	1039	-	
P_{27}	1016	-	
P_{28}	934	-	
P_{29}	912	-	

In the region 1710 to 1540 nine distinct peaks have been identified as indicated in Table 3-13. The identified groups consist of esters, -COOH, C=O, aromatic C=C and aromatic ring stretching vibrations (Xin *et al.,* 2014; Strydom *et al.,* 2011; Geng *et al.,* 2009; Van Niekerk *et al.,* 2008; Machnikowska *et al.,* 2002; Cai & Smart, 1994; Painter *et al.,* 1981). Comparison between TWD and AW TWD fractions indicates that there is only one aromatic C=C shoulder observed for the TWD fraction. Van Niekerk *et al.* (2008) also observed two aromatic C=C shoulders with acid washed bituminous Highveld coal. Barth *et al.,* (1994) attributed the negative inflection point at 1528 cm^{-1} to nitrogen functionalities, either amines or amides. Various CH_2 and CH_3 bend vibrations were identified in the range 1450 to 1360 cm^{-1} (Xin *et al.,* 2014; Van Niekerk *et al.,* 2008; Machnikowska *et al.,* 2002; Barth *et al.,* 1994; Cai and Smart, 1994; Painter *et al.,* 1981).

In the range 1300 to 1000 cm^{-1} various C-O stretch and O-H bending vibrations have been identified (Xin *et al.,* 2014; Van Niekerk *et al.,* 2008; Machnikowska *et al.,* 2002; Barth *et al.,* 1994; Painter *et al.,* 1981). Comparison of TWD and AW TWD fractions indicates the absence

of several peaks in the latter part of this range. These vibrations were attributed to aluminates (O-Al-O vibrations) and silicates (Si-O-Si) (Strydom *et al.,* 2011; Thomas & Kelley, 2009; Breen *et al.,* 2008; Carmody *et al.,* 2005, Frost *et al.,* 2003, Ming & Spark 2003; Martens *et al.*, 2002; Madejová & Komadel, 2001; Matteson & Herron, 1993; Povarennykh, 1978; Farmer, 1974). The removal of these minerals by acid washing is responsible for the absence of these peaks in the AW TW fraction.

3.8.2.3. DRIFT spectra range 900 – 370 cm^{-1}

DRIFT spectra in the range 900 to 370 cm^{-1} contain the aromatic C-H out-of-plane stretch and various spectra attributed to different mineral constituents. Figure 3-8 and Table 3-14 summarise the results for this spectra range. The first peak observed in this region is due to the aromatic C-H out-of-plane vibrations (Xin *et al.,* 2014; Van Niekerk *et al.,* 2008; Machnikowska *et al.,* 2002; Painter *et al.,* 1981). This range also includes C-O out-of-plane bending associated with calcite and dolomite, 878 and 858 cm^{-1} for TWD coal (De Lorenzi Pezollo, 2012; Breen *et al.,* 2008; Pokrovsky *et al.,* 2000; Krivácsy & Hlavay, 1995; Povarennykh, 1978). The peak intensities observed for the AW TWD fraction in this region are much lower, in agreement with the XRD and QEMSCAN results.

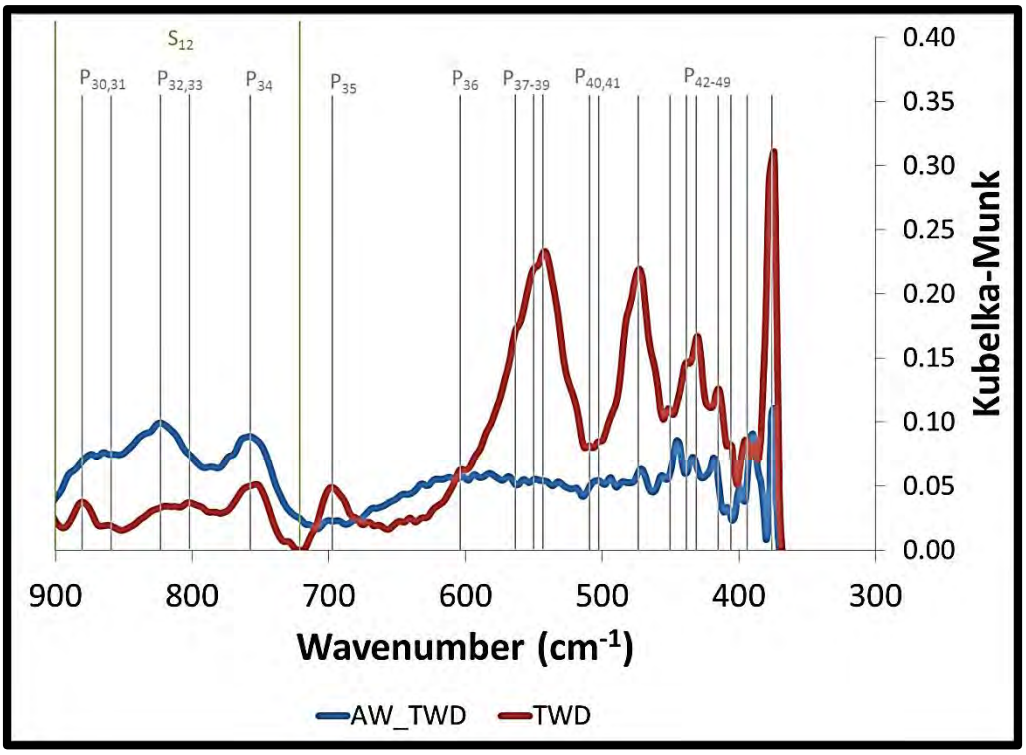

Figure 3-8 DRIFT spectra for TWD and AW TWD coal, 900 – 370 cm^{-1}.

Table 3-14 DRIFT spectra identification (900 – 370 cm^{-1}).

Peak / Band	Wavenumber (cm^{-1})		Identification
	TWD	*AW TWD*	
B_{12}	900 - 720	900 – 700	Out-of-plane aromatic C-H vibrations
P_{30}	878	872	C-O out-of-plane bending associated with calcite and dolomite
P_{31}	858	866	
P_{32}	-	823	
P_{33}	800	-	O-Si-O vibration associated with quartz
P_{34}	754	754	C-O out-of-plane bending, O-Al-O and Si-O vibrations associated with calcite, dolomite, kaolinite and quartz
P_{35}	698	706	
P_{36}	599	-	Si-O vibrations associated with kaolinite and quartz
P_{37}	561	-	Si-O and Si-O-Si deformation associated with kaolinite and quartz
P_{38}	548	-	
P_{39}	540	-	
P_{40}	507	-	
P_{41}	499	500	
P_{42}	473	473	
P_{43}	449	457	S-S vibrations associated with pyrite
P_{44}	436	445	
P_{45}	432	434	
P_{46}	413	417	
P_{47}	407	409	
P_{48}	397	393	
P_{49}	374	371	

At 800 cm^{-1} a peak is observed for the TWD fraction, which is not observed for the AW TWD fraction. This peak is attributed to O-Si-O vibrations associated with quartz in the TWD coal (Carmody *et al.,* 2005, Madejová & Komadel, 2001; Matteson & Herron, 1993; Povarennykh, 1978). Various other peaks associated with mineral matter are observed between 800 and 500 cm^{-1} associated with the respective minerals as indicated in Table 3-14 (Thomas & Kelley, 2009; Breen *et al.,* 2008; Carmody *et al.,* 2005, Frost *et al.,* 2003, Ming & Spark 2003; Martens *et al.,* 2002; Madejová & Komadel, 2001; Matteson & Herron, 1993; Povarennykh, 1978; Farmer, 1974). Below 450 cm^{-1} vibrations attributed to the S-S vibrations of pyrite were observed (Derycke *et al.,* 2013; Strydom *et al.,* 2011; Güler 2005; Hicyilmaz *et al.,* 2004; Matteson & Herron, 1993). The increased peak intensities for the AW TWD fraction in this region is in agreement with the fact that the acid washing process removes only a fraction of the overall pyrite content present.

3.9. Thermogravimetric analyses (TGA) results and discussion

Thermogravimetric analysis (TGA) was carried out as discussed in Section 3.4.4. Duplicate samples were analysed for each sample to ensure good repeatability, error percentages varied between 0.05 – 0.85% for the respective samples (See Appendix A-4).

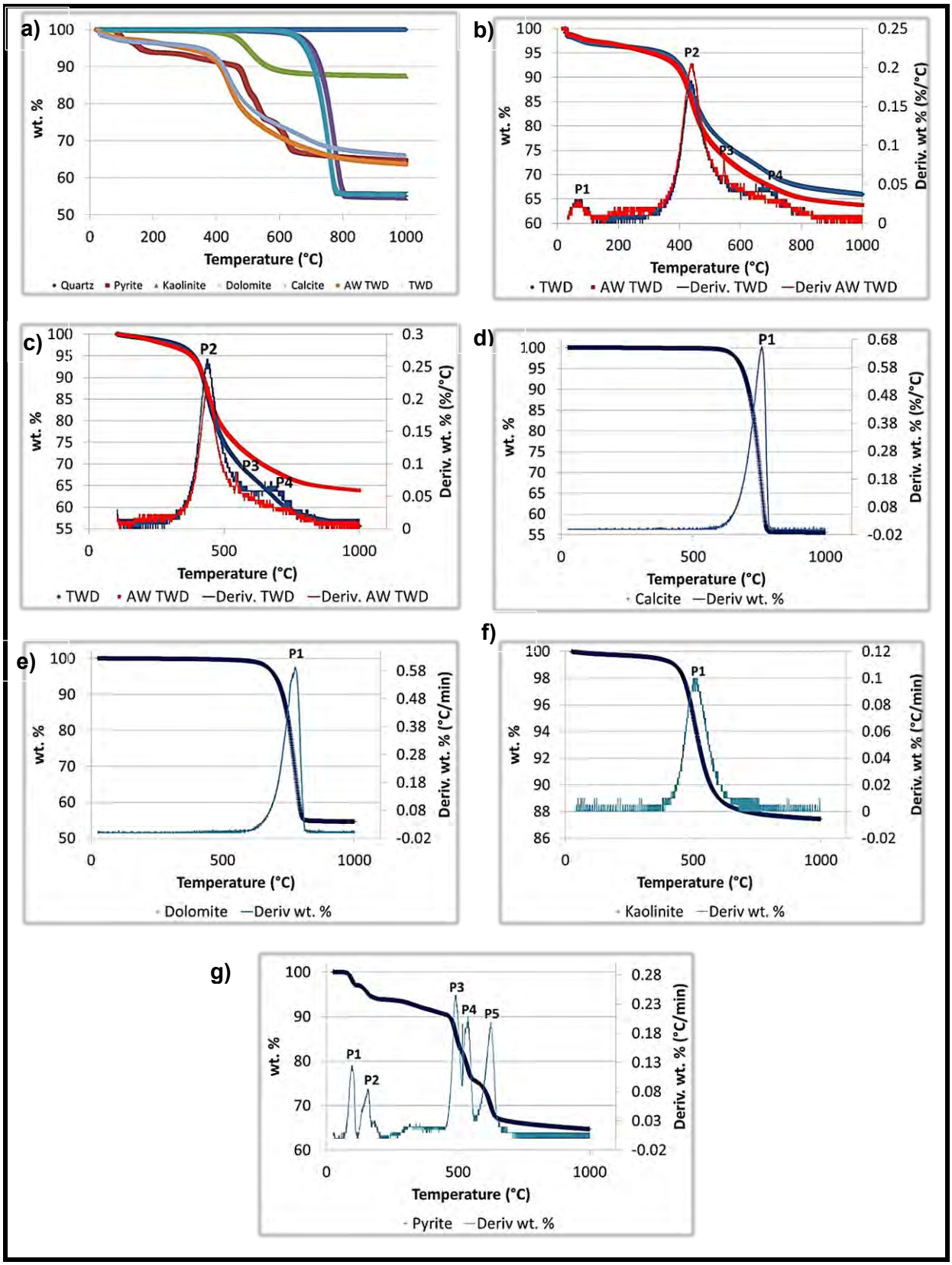

Figure 3-9 a) Mass loss curves for all samples; Mass loss and differential mass loss curves for b) TWD and AW TWD; c) TWD and AW TWD (d.a.f.); d) $CaCO_3$; e) Dolomite; f) Kaolinite and g) Pyrite.

Table 3-15 Summary of characteristic parameters derived from DTG results

Sample	T_i[a] (°C)	T_{P1}[b] (°C)	MR_{P1}[c] (min^{-1})	T_{P2}[b] (°C)	MR_{P2}[c] (min^{-1})	T_{P3}[b] (°C)	MR_{P3}[c] (min^{-1})	T_{P4}[b] (°C)	MR_{P4}[c] (min^{-1})	T_{P5}[b] (°C)	MR_{P5}[c] (min^{-1})
TWD	345 ± 1	61	3.39×10^{-3}	436	2.44×10^{-2}	542	8.12×10^{-3}	671	6.77×10^{-3}	N/A	N/A
TWD *(d.a.f.)*	388 ± 1	434	2.84×10^{-2}	532	1.16×10^{-2}	665	8.70×10^{-3}	N/A	N/A	N/A	N/A
AW TWD	308 ± 1	66	4.09×10^{-3}	437	2.73×10^{-2}	546	9.42×10^{-3}	N/A	N/A	N/A	N/A
AW TWD (*d.a.f.*)	380 ± 1	434	2.84×10^{-2}	546	1.09E-02	N/A	N/A	N/A	N/A	N/A	N/A
Calcite	691 ± 1	755	8.60×10^{-2}	N/A	N/A	N/A	N/A	N/A	N/A	N/A	N/A
Dolomite	700 ± 1	773	7.78×10^{-2}	N/A	N/A	N/A	N/A	N/A	N/A	N/A	N/A
Kaolinite	502 ± 1	504	1.33×10^{-2}	N/A	N/A	N/A	N/A	N/A	N/A	N/A	N/A
Pyrite	159 ± 1	93	1.53×10^{-2}	154	1.07×10^{-2}	489	3.20×10^{-2}	534	2.65×10^{-2}	624.2	2.65×10^{-2}
Quartz	N/A	N/A	N/A	N/A	N/A	N/A	N/A	N/A	N/A	N/A	N/A

[a] Temperature observed at 5% fractional conversion. [b] Temperature observed as well-defined points of local maxima. [c] Corresponding mass loss rates at temperatures of local maxima.

Table 3-16 Retained mass (wt%) for samples at 520, 750 and 900°C

Temp. (°C)	TWD		AW TWD		Calcite	Dolomite	Kaolinite	Pyrite	Quartz
	wt%								
		***d.a.f.*[d]**		***d.a.f.*[d]**					
520	78.1 ± 0.1	72.9 ± 0.2	75.4 ± 0.5	76.4 ± 0.5	99.9 ± 0.1	99.6 ± 0.4	93.3 ± 0.3	81.5 ± 0.4	100.1 ± 0.1
750	68.5 ± 0.3	59.2 ± 0.4	66.1 ± 0.7	66.4 ± 0.7	72.1 ± 0.4	82.4 ± 0.9	87.8 ± 0.1	65.9 ± 0.4	100.1 ± 0.1
900	66.6 ± 0.4	56.6 ± 0.4	64.3 ± 0.8	64.4 ± 0.8	55.6 ± 0.9	54.7 ± 1.0	87.5 ± 0.1	65.1 ± 0.5	100.1 ± 0.1

[d] d.a.f. = dry, ash free basis.

The differential thermogravimetric (DTG) curves were determined by the first order derivative of the temperature versus the mass loss by aid of Origin 9.1 software. These curves are used in addition to the TGA curves to amplify changes in mass loss (Caballero and Conesa, 2005). Some characteristic parameters, which have been derived from the respective DTG curves, are summarised in Table 3-15. These parameters include: initial weight loss temperature (T_i) which is defined as the temperature at 5% fractional conversion, temperatures at which local maxima occurs (T_P) and their corresponding mass loss rates (MR). Similar parameters were reported by Hattingh (2012) and Cai *et al.* (2008).

3.9.1. TWD and AW TWD coal fractions

The averaged curves for all samples are shown in Figure 3-9a. TWD and AW TWD coal fractions are observed to produce a constant weight decrease with increasing temperature (Figure 3-9a, b and c). These profiles are similar to those found in previous studies on similar coals (Hattingh *et al.,* 2014; Shi *et al.,* 2013; Seo *et al.,* 2011; Wang *et al.,* 2010; Liu, 2009; Saikia *et al.,* 2009; Cai *et al.,* 2008; Cui *et al.,* 2002). The first noticeable mass loss (below 150°C) can be attributed to the loss of absorbed moisture and occluded gas (Hattingh *et al.,* 2014; Seo *et al.,* 2011; Wang *et al.,* 2010; Wang*,* 2007).

Comparison in Figure 3-9b between the TWD and AW TWD fractions indicated that the TWD fraction lost more mass below 200°C. This can be related to the lower inherent moisture content for the AW TWD as presented in the proximate results (Table 3-3), but could also be due to the lower oxygen content observed from the ultimate analysis results (Table 3-4) for the AW TWD fraction. Wang (2007) states that monolayer water in coal is strongly hydrogen bonded to oxygen containing functionalities on the coal particle surface, which can be responsible for the lower mass loss observed for the AW TWD fraction due to acid washing. Increased sample weight loss can be observed in the region of 350 – 400°C which is attributed to the scission of covalent bonds to produce a larger volume of hydrocarbons and other gases to form tar and gas (Li *et al.,* 2014; Ahmad *et al.,* 2009a; Kandiyoti *et al.,* 2006; Ôztas and Yürüm, 2000; Chen *et al.,* 1999; Taupitz, 1977). Above 400°C cleavage of aryl-alkyl-ether and ethylene bridges occurs, and above 500°C the breaking of anhydrite groups and aryl-aryl etheric and methylene bridges increases (Ahmad *et al.,* 2009a; Kandiyoti *et al.,* 2006; Ôztas & Yürüm, 2000; Chen *et al.,* 1999; Taupitz, 1977).

Decomposition of coal can be divided into two regions i.e.: i) primary decomposition which leads to the formation of tars, oils and gases below 690°C; and ii) secondary decomposition, which leads to increases in the evolution of CO, CO_2, H_2 and CH_4 (Singh *et al.,* 2012; Saikia *et al.,* 2009; Cai *et al.,* 2008; Kabe *et al.,* 2004).

From the DTG curves for the TWD and AW TWD fractions in Figure 3-9b and Figure 3-9c various peaks were identified. The peaks in Figure 3-9b can be characterized as due to loss of inherent moisture (P_1), primary degradation (P_2) and further degradation (P_3 and P_4), which are in agreement with studies on other South African coals (Hattingh *et al.,* 2014). The absence or decrease in size of the fourth peak (P_4) for the AW coal indicates a change in the pyrolysis behaviour of the AW TWD fractions towards the end of the temperature range studied. It is attributed to the depletion of aliphatic structures, oxygen-containing functionalities, as well as other thermally unstable molecular functionalities (Hattingh *et al.,* 2014, Cai *et al.,* 2008). This is consistent with results found by ultimate analysis regarding the presence of elemental O, which decreases for the AW TWD coal from 12.5 wt% to 11.9 wt% d.a.f. Peak four (P_4) is also attributed to carbonates present in coal, as it always goes along with the release of CO_2 (Shi *et al.,* 2014; Shi *et al.,* 2013). Comparison of the dolomite and calcite minerals (Figure 3-5d and Figure 3-5e) indicates that the decomposition of these species starts within that temperature range. From Table 3-15 it can be observed that the temperatures at which maximum mass loss (P_1) occurs for these mineral species (calcite – 755°C; dolomite – 773°C) are a bit higher than the temperature of the peak observed for the TWD decomposition (671°C). It has however been proven in previous studies that mineral-mineral and mineral-coal interactions may lead to the decomposition of the mineral species at lower temperatures than observed for pure minerals (Nath *et al.,* 2011; Vassileva & Vassilev, 2006).

The peaks in Figure 3-9c correspond with those identified in Figure 3-9b, except that no peak for mass loss of inherent moisture was identified, noting that results were reported on a dry ash-free basis.

In Table 3-15 it can be seen that the mass loss rates at the peak of local maxima (P_1) for the d.a.f. DTG curves, occur at a temperature of 434°C for both fractions. This temperature is found to be in line with the finding by Shi *et al.*, (2013), i.e. that this temperature will be within the 400 – 500°C temperature range for bituminous coals. It can however be observed from Figure 3-9c that at temperatures exceeding 425°C the mass loss rate of the TWD fraction is higher than that of the AW TWD fraction. This result is consistent with findings made with regard to the total volatile matter for the two coal fractions in the proximate analysis - 38.5 wt% (d.a.f.) for the TWD fraction and 34.1 wt% (d.a.f.) for the AW TWD fraction. This is however in contrast to findings made by Bai *et al.* (2014) on a Chinese bituminous coal, although the TGA curves do indicate the same trend as observed by comparing the DTG curves in Figure 3-9c with those obtained by Bai *et al.* (2014). There is also a temperature shift observed for the second peak (P_2) suggesting a change in the pyrolysis process for the acid-washed coal.

Table 3-16 indicates the retained mass (wt%) values at the three temperatures of importance in this study (520, 750 and 900°C). The TWD fraction can be observed to lose more mass when compared to the AW TWD fraction on a dry, ash free basis at all three temperatures, 72.9 wt% vs. 76.6 wt% (520°C); 59.2 wt% vs. 66.4 wt% (750°C) and 56.6 wt% vs. 64.4 wt% (900°C). This is consistent with the proximate results (Table 3-3), indicating a higher volatile matter content (38.5 wt% d.a.f. to 34.1 wt% d.a.f.) for the TWD fraction; thus a higher mass loss is expected.

3.9.2. Calcite

Figure 3-9a also indicates the TGA curves for the minerals under study. Calcite is observed to lose mass at temperatures exceeding 450°C. The decomposition between 450 – 600°C is very slow, which is consistent with findings by Nath *et al.* (2011), whilst it starts to gain momentum at temperatures exceeding 600°C (Liu *et al.,* 2007b; Vassileva & Vassilev, 2006; Tomeczek & Palugniok, 2002). The TG curve produced is consistent with previous studies (Nath *et al.,* 2011; Tabrizy *et al.,* 2011; Tomeczek & Palugniok, 2002). Table 3-15 indicates that very little mass loss has occurred at 520°C. However, under the experimental conditions, at 750°C, 72.1 wt% of the original mass is still present, which further depletes to 55.6 wt% of the original mass at 900°C. The maximum mass loss (P_1 – Figure 3-9d) occurs at 755°C after which all of the calcite has been transformed to CaO. During this mass loss, calcite decomposes to periclase (CaO) between 600 – 950°C with the release of CO_2 (Rodriguez-Navarro & Ortega-Huertas, 2009; Escardino *et al.,* 2008; Vassileva & Vassilev, 2006; Maitra *et al.,* 2005; Caceres & Attiogbe, 1997; Wang & Thomson, 1995). Polymorphs of calcite such as aragonite may form at temperatures exceeding 800°C (Escardino *et al.,* 2008; Liu *et al.,* 2007b; Vassileva & Vassilev, 2006; Tomeczek & Palugniok, 2002; Reifenstein *et al.,* 1999).

3.9.3. Dolomite

From Figure 3-9a it can be observed that the decomposition of dolomite commences around 500°C; at 520°C 99.6 wt% of the original dolomite mass is still present (Table 3-18). Decomposition gains momentum at temperatures exceeding 650°C, with 82.4 wt% original mass remaining at 750°C (Table 3-16), and reaching the maximum mass loss at 773°C (Figure 3-9e; P_1 – Table 3-15) to decompose to a value of 54.6 wt% of the original mass present at 900°C (Table 3-16). The weight loss curve obtained is consistent with previous TGA studies on dolomite (De Souza & Bragança, 2013; Vassileva & Vassilev, 2006; Maitra *et al.,* 2005; Caceres & Attiogbe, 1997). For dolomite, magnesia (MgO) is believed to form between 700 – 800°C, whilst $CaCO_3$ decomposes to CO_2 (Vassileva & Vassilev, 2006; Maitra *et al.,* 2005; Caceres & Attiogbe, 1997). The sharp peaks observed in the DTG curves for the formation of

calcite and dolomite (Figure 3-9d and Figure 3-9e) are an indication of the purity of the minerals (Nath *et al.,* 2011).

3.9.4. Kaolinite

The transformation observed for kaolinite (Figure 3-9a and Figure 3-9f) is consistent with previous studies (Matusik and Klapyta, 2013; Tabrizy *et al.,* 2011; Ptáček *et al.,* 2010b). The transformation of kaolinite to form metakaolinite with the release of endothermic water is believed to occur between 450 and 700°C, with maximum weight loss found to occur at 504°C (P_1) under the conditions used in this study (Ptáček *et al.,* 2010b; Vassilev *et al.*, 2009; Heide and Földvari, 2006; Alpern *et al.,* 1983;). At this temperature, mass loss is said to range between 11.2 and 14.2 wt%, with a theoretical value of 13.96 wt% (Ptáček *et al.,* 2010b). In this study it was found to be 12.03 wt% (Figure 3-9f), which is within the limits provided. Some remnant water may remain present in well crystallised kaolinite up to temperatures of 950°C (Grim & Bradley, 1948). Dehydroxylation of metakaolinite is said to take place between 650 and 900°C, with lattice destruction between 850 and 1000°C; however little further mass loss occurs in this region. From Table 3-16 it can be observed that at 750°C, 87.8 wt% of the original mass is still present, and at 900°C, 87.5 wt% original mass is present. The dehydration and dehydroxylation of kaolinite coincide with coal volatiles release as can be observed from Figure 3-9a (Vassilev *et al.,* 2009). Exothermic reactions will lead to the formation of cubic spinel and amorphous silica at temperatures up to 950°C (Ptáček *et al.,* 2010a). Findings for the mineral transformations that occur will be verified with literature based on XRD and XRF analyses of the chars derived during the pyrolysis process (Chapter 5 – 7).

3.9.5. Pyrite

The TG curves obtained for the thermal decomposition of pyrite in Figure 3-9a and 3-9g are consistent with findings in previous studies (Cheng *et al.,* 2013; Hu *et al.,* 2003; Hu *et al.,* 2002). From Figure 3-9g and Table 3-15 it can be observed that pyrite loses adsorbed water at 92.5°C (P_1) and interparticle water at 154°C (P_2) (Cheng *et al.,* 2013). The third mass loss range is between 200 and 300°C. In this temperature range the evolution of sulphur from the pyrite surface occurs. P_3 – P_5 are assigned to the thermal reaction process that pyrite undergoes and the different transition phases with different Fe/S values (Cheng *et al.,* 2013; Yan *et al.,* 2008). This transformation has been observed to take place in the temperature range of 330 – 630°C (McLennan *et al.*, 2000; Bool *et al.,* 1995; Groves *et al.,* 1987). This process is represented by the following reactions (Cheng *et al.,* 2013):

$$FeS_2 + O_2 \rightarrow FeS + SO_2 \quad (3\text{-}1)$$

$$FeS_2 \rightarrow FeS + S \quad (3\text{-}2)$$

$$S + O_2 \rightarrow SO_2 \quad (3\text{-}3)$$

Oxidation of the sample particle surface occurs in the absence of oxygen in accordance with equation 3-1 and 3-2 below 512°C (before P_4) (Cheng *et al.,* 2013). Between 512 – 556°C (P_4) the thermal process is characterised by the evolution of oxidised sulphur (equation 3-2) due to pyrite decomposition without oxygen (3-3). The oxidation of pyrrhotite is observed as the last step, at 624°C (P_5). Under inert conditions the release of sulphur gas to form pyrrhotite will be the dominant reaction. Pyrrhotite will further transform to troilite (Hu *et al.,* 2006; Vassileva & Vassilev, 2006; Hong & Fegley, 1997; Gryglewicz *et al.,* 1996). Transformation to pyrrhotite occurs especially in a hydrogen-sufficient atmosphere (Borah *et al.,* 2005). Hematite was concluded to be the most prominent phase present after completion of thermal decomposition of coal-derived pyrite in an atmosphere with oxygen by Jorgensen and Moyle (1986). If sufficient oxygen is available, pyrrhotite may also transform to FeO (McLennan *et al.*, 2000; Bool *et al.,* 1995; Groves *et al.,* 1987). The crystallisation of FeO occurs at temperatures exceeding 900°C to form Fe_3O_4 (McLennan *et al.*, 2000a, 2000b; Bool *et al.,* 1995).

Previous researchers found that pyrite reacted differently under pyrolysis conditions, dependent on its presence within the coal matrix or as excluded mineral (Borah *et al,* 2005). It was found that included pyrite decomposes at temperatures almost 100°C lower than that observed for excluded pyrite (Cheng *et al.,* 2013; Borah *et al.,* 2005; Gryglewicz *et al.,* 1996). The maximum mass loss was found to occur at a temperature of 444°C in the study of coal-derived pyrite by Cheng *et al.* (2013). In this study the maximum mass loss peak identified from Figure 3-9g and Table 3-15, is P_3 at 489°C. The difference in the decomposition temperature is attributed to the hydrocarbon with hydrogen donor ability present in coal, which can promote the reduction of pyrite, though the overall shortage of hydrogen ensures the thermal decomposition of pyrite present in coal during pyrolysis (Cheng *et al.,* 2013).

From Figure 3-9g it is evident that little mass loss occurs at temperatures above 700°C (Boyabat *et al.,* 2003). At 520°C, 81.5 wt% of the original mass is still present, at 750°C 65.9 wt%, and at 900°C 65.1 wt% (Table 3-16). According to Yani and Zhang (2010) 73.3 wt% of the initial mass should be retained for complete conversion from pyrite to troilite (FeS) to have occurred. In this current study 6.4 wt% was lost due to mass loss from inherent moisture, i.e. taking this into account the temperature at which total conversion would have taken place was around 658°C. This result is consistent with previous findings which state that the decomposition of pyrite is complete at around 700°C (Cheng *et al.,* 2013; Yan & Zhang, 2010; Saikia *et al.,* 2009; Boyabat *et al.,* 2003).

3.9.6. Quartz

From Figure 3-9a it can be observed that no mass loss occurs for quartz in the temperature range studied. Quartz is stable up to temperatures of 1600°C, and no mass loss is expected (Tabrizy *et al.,* 2011; Vassileva and Vassilev, 2006). The only conversion expected is the formation of β-quartz, also known as high-quartz around the temperature of 573°C (Klein, 2002; Reifenstein *et al.,* 1999). The high-quartz is believed to further transform to tridymite via the unstable cristobalite form at 876°C (Matjie *et al.,* 2008; Reifenstein *et al.*, 1999). These transformations cannot be observed from the TGA data.

3.10. Summary

The TWD fraction and the AW TWD fraction were analysed by means of conventional coal analytical techniques. Proximate analysis revealed a reduction in ash yield from 14.0 wt% (d.b). to 2.0 wt% (d.b). The volatile yield decreased from 38.5 wt% (d.a.f.) to 34.1 wt% (d.a.f.) after acid washing. From the ultimate analysis it was observed that no significant changes were found with regard to H and N content, whilst the C content increased slightly (79.1 wt% d.b. vs. 80.3 wt% d.b.), and the O content decreased from 11.5 wt% d.b. vs. 12.7 wt% d.b. for the AW TWD coal. The mineralogical analyses in the form of XRF, XRD and QEMSCAN analyses revealed that the major minerals present in the TWD coal were kaolinite, dolomite, calcite, quartz and pyrite. As expected, pyrite was not removed effectively by HCl and HF washing. The overall mineral matter removal efficiency as determined based on the analyses was 86.6% (XRF), 92.8% (XRD) and 76.9% (QEMSCAN). The difference in these results is dependent on the analytical method and equipment, i.e. XRF analysis relates components after ashing of the coal sample, XRD can only identify crystalline components, and whilst QEMSCAN identifies most of the components (crystalline and amorphous content), it quantifies the observed area percentages and not the weight percentages. The correlation coefficient between XRD and XRF analyses was found to be 0.953, whilst that of QEMSCAN and XRF analyses was found to be 0.741 for the TWD coal.

Petrographic analysis of the TWD coal sample revealed a vitrinite-rich coal sample (54.6 vol.% m.m.f.b. vitrinite, 7.6 vol.% m.m.f.b. liptinite, 37.8 vol.% m.m.f.b. inertinite) with a random reflectance of 0.77. The inertinite fraction is mostly semifusinite (21.3 vol.% m.m.f.b. reactive, 15.3 vol.% m.m.f.b. inert). Based on the vitrinite reflectance results the coal sample can be classified as a medium rank C coal.

BET CO_2 adsorption results indicated small variations between the adsorption parameters for the respective coal fractions. The AW TWD fraction was found to be slightly less porous than the TWD fraction, which is believed to be related to densification due to pre-oxidation caused

by the acid washing process. The removal of minerals by acid washing does not seem to affect the porosity to a great extent.

The DRIFT spectra for the TWD and AW TWD fractions indicated that the acid washing process removed some of the OH groups, specifically those related to the spectra 3800 to 3600 cm^{-1}, as well as vibrations identified as part of the C-O, O-H bend and aromatic C-H out-of-plane vibrations (1200 – 400 cm^{-1}). TWD coal was observed to show no spectra in the range 2756 to 2636 cm^{-1} associated with –COOH dimers. These differences can be attributed to the acid washing process which removes various minerals, specifically kaolinite (OH groups), calcite and dolomite (C-O stretch) and calcite, dolomite, kaolinite and quartz in the aromatic C-H out-of-plane band (900 – 370 cm^{-1}). Pyrite was observed to be affected less by acid washing, and therefore definite peaks were observed, identified as the S-S band for both fractions (<440 cm^{-1}). An important observation was made in the region of 3000 cm^{-1}, the spectrum of TWD is broader than that of AW TWD. In a previous study OH groups in this range have been found to contribute to water yields.

TG analyses on the various coal and mineral samples were done in order to determine the mass loss with increase in temperature. Comparison between the TWD and AW TWD coal fractions indicated that the acid washed sample lost mass faster in the temperature range below 400°C, which could be associated with loss of aliphatic and carboxylic acid groups. No fourth peak (P_4), was observed on the DTG curve for the AW TWD coal fraction; this confirms that acid washing changes the thermal decomposition behaviour of coal. The AW TWD fraction showed a decrease in mass loss when compared to TWD coal on a dry, ash free basis at all three temperatures, 76.6 wt% vs. 72.9 wt% (520°C); 66.4 wt% vs. 59.2 wt% (750°C) and 64.4 wt% vs. 56.6 wt% (900°C). The temperature at maximum rate of mass loss was however found to be consistent (434°C) for both TWD and AW TWD coal fractions. Calcite ($CaCO_3$) decomposition was found to reach the maximum rate of mass loss at 755°C, which is within the temperature range of 600 – 950°C during which transformation to periclase (CaO) occurs with the release of CO_2. The maximum rate of mass loss for dolomite decomposition was found to be at 773°C, during which decomposition to magnesia (MgO) and calcite ($CaCO_3$) occurs, and that further decomposes to periclase (CaO) with the release of CO_2. Kaolinite decomposes to metakaolinite in the region of 450 – 750°C with the release of H_2O, with maximum mass loss rate occurring at 504°C. Pyrite was found to lose 6.4 wt% mass below 200°C (impurities present), whilst decomposition with the release of sulphur to pyrrhotite occurred in the temperature range 330 – 630°C. Three distinct peaks were identified on the DTG curve for this decomposition, with maximum mass loss rate at 489°C. The peaks were ascribed to the various transition states the pyrrhotite goes through to complete transformation

to troilite (FeS) at 658°C. Quartz was observed to undergo no mass loss in the temperature range studied.

Chapter 4 to Chapter 7 will focus on the pyrolysis experiments and characterisation of theses yields. Specific focus will be given as such:

- Experimental method and analytical techniques (Chapter 4)
- The effect of acid washing (Chapter 5)
- The effect of mineral addition (Chapter 6)
- Model coal-mineral mixtures (Chapter 7)

Part 3 – Pyrolysis product yields and composition

Chapter 4: Experimental methods and analytical techniques

Chapter 5: The effect of acid washing

Chapter 6: The effect of mineral addition

Chapter 7: Model coal-mineral mixtures

Chapter 8: Statistical model

"The way to do research is to attack the facts at the point of greatest astonishment."

— Celia Green

Chapter 4: Experimental methods and analytical techniques

4.1. Introduction

Chapter 4 will deal with the experimental equipment used and the –methodology followed during the course of this investigation. Specific reference will be made to the various experimental techniques, assumptions made and calculations used to assess the experimental data obtained. An experimental plan is provided to indicate the scope of the investigation. This chapter serves as the experimental background to Chapters 5 to 7, where the obtained results will be discussed. The chapter layout is as follows:

- Pyrolysis setup and operating conditions (Section 4.2)
- Pyrolysis product analyses (Section 4.3)
- Experimental plan (Section 4.4)

4.2. Pyrolysis setup and operating conditions

Pyrolysis product preparation was done using the modified NWU Fischer Assay setup (Roets *et al.,* 2014; Bean, 2013). The NWU Fischer Assay setup (Figure 4-1) is a setup containing two modified stainless steel retorts, manufactured according to ISO 647 dimensions (SANS, 1974). The setup has the ability to capture gas, condensable volatiles and char fractions in order to quantify these pyrolysis products.

The NWU Fischer Assay setup (Figure 4-1) consists of an oven and control system using pre-programmed heat curves. The Fischer tar oven was built by Lenton and is specified with a 22 amp - 48 kW rating over 220 V (Roets *et al.,* 2014). The coal bed temperature is measured, as well as the oven chamber temperature. The pyrolysis temperature used in this study will be based on the coal bed temperature. The apparatus was used in a previous study (Roets *et al.,* 2014; Bean, 2013), but under different conditions and without the modifications made for application in this study. See Table 4-1 for the operating conditions of the NWU Fischer Assay setup.

The system is fitted with a TOHO TTM-P4 temperature controller for the oven and TOHO CN-40 temperature sensors connected to K-type thermocouples, providing temperature readings for the bed temperatures within the two retorts. Pressure in the retorts is determined by WIKA

IPT-1* pressure transmitters with an operating range of 0 – 10 bar, reporting pressure differences as small as 0.1 mbar.

Table 4-1 NWU Fischer Assay Setup operating conditions

Variable	Range specification or composition
Coal feedstock	Washed (TWD) and acid washed (AW TWD) Highveld coal
Coal particle size	< 75 µm
Operating temperature	520, 750, 900°C
Pressure	0.855 – 0.953 Bar
Heating rate	6.2 - 6.3°C/min
Holding time	10 minutes
Atmosphere	N_2

4.2.1. Operating temperature, heating rate and heating curve

In this study, pyrolysis yields at 520°C, 750°C and 900°C will be compared. The 520°C operating temperature is motivated by the temperature specified for regular Fischer Assay preparation (SANS, 1974). The temperatures of 750°C and 900°C were selected as temperatures within the range of previous research regarding the effect of mineral matter on pyrolysis products and composition (Fei *et al.,* 2012; Yan *et al.,* 2005; Tscubouchi *et al.,* 2004; Sciazko & Kubica, 2002; Samaras *et al.,* 1996; Morgan & Jenkins, 1986a & 1986b; Schafer, 1980; Yaw *et al.,*1980). A temperature of 750°C was used as high operating temperature in a study by Hattingh (2012), that investigated the devolatilisation behaviour of South African coal. A temperature of 900°C is generally considered to be at the end of the pyrolysis stage of coal, and therefore a good indication of the last pyrolysis product yields and composition (Ladner, 1988; Xu & Tomita, 1987; Jüngten & Van Heek, 1979). This temperature has also been used in pyrolysis studies regarding the effect of mineral matter in various other studies (Fei *et al.,* 2012; Yan *et al.,* 2005; Sciazko & Kubica, 2002; Samaras *et al.,* 1996; Morgan & Jenkins 1986b, Schafer 1980; Schafer 1979b). The study of pyrolysis products at different temperatures is motivated by the fact that some of the mineral matter only starts to decompose at temperatures in excess of 600°C (Table 2-6). A constant heating rate of 6.2 – 6.3°C/min was used for all of the pyrolysis experiments. A holding time of 10 minutes was used at all final pyrolysis temperatures.

Figure 4-2a indicates the heating curves as noted for the three operating temperatures. It can be observed that the final heating rate increases slowly in the experiments done at higher operating temperatures (6.2 vs 6.3°C/min).

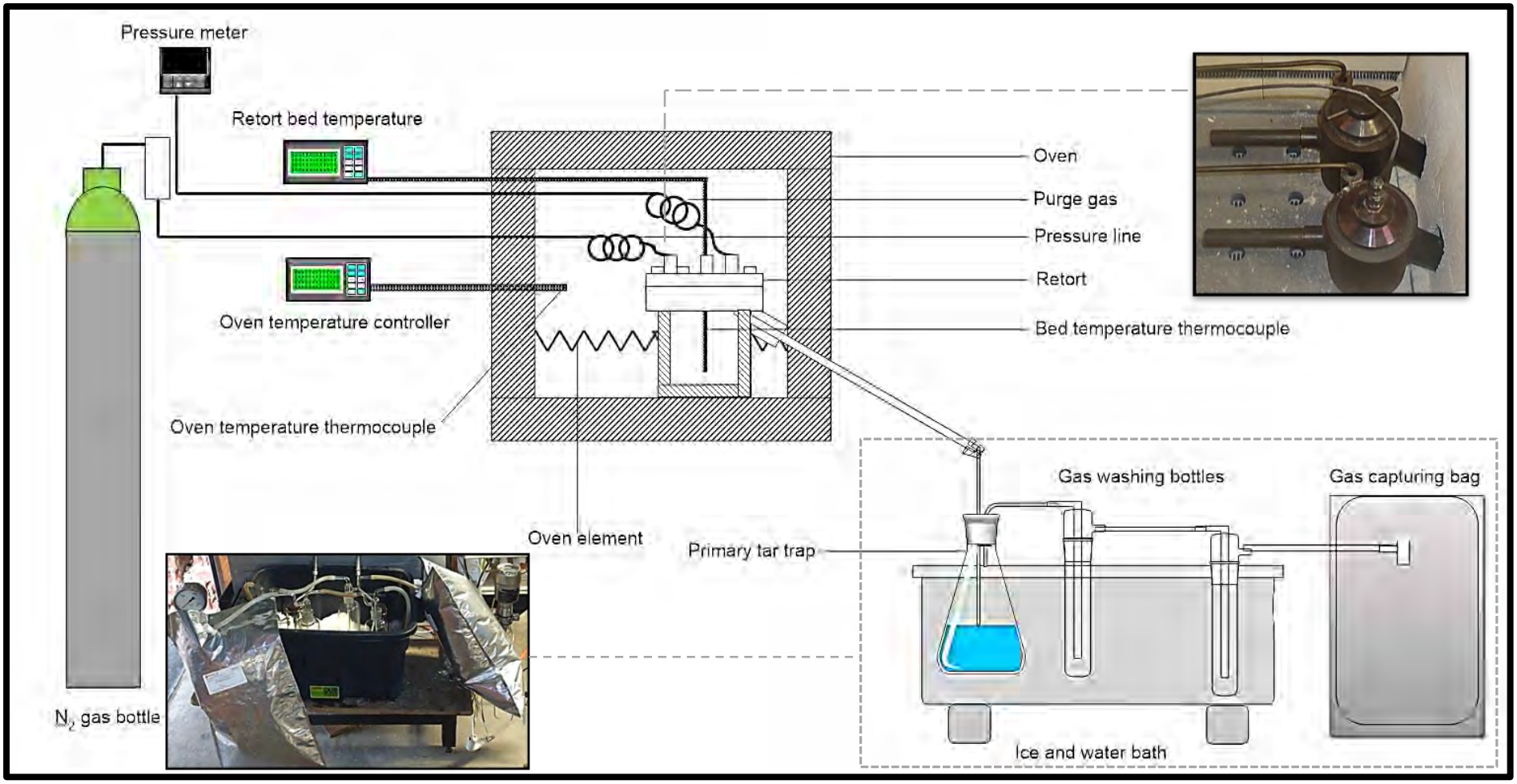

Figure 4-1 The NWU Fischer Assay setup

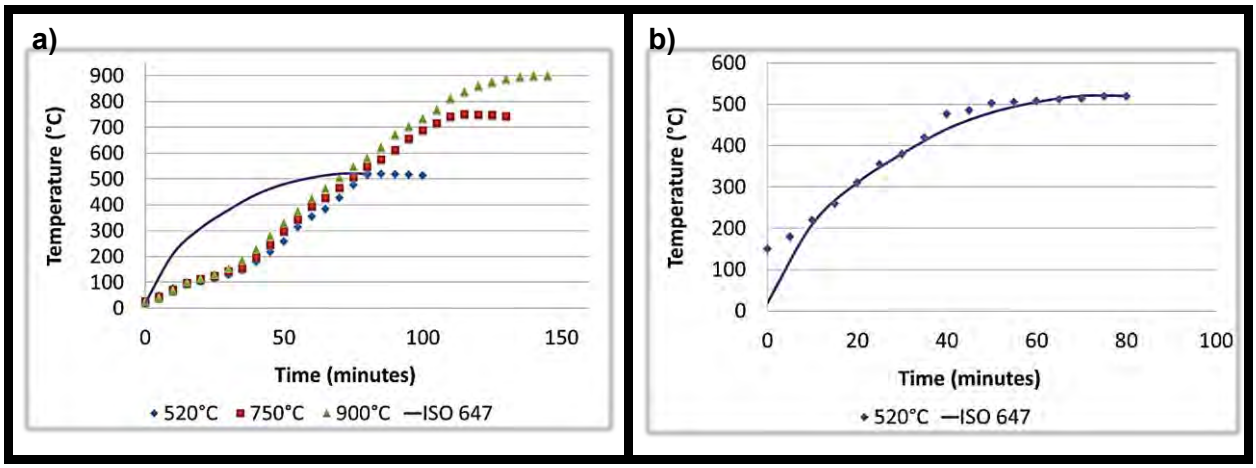

Figure 4-2 Heating curves a) At 520, 750 and 900°C, b) Heating curve at 520°C vs. ISO 647 heating curve after pre-heating up to 150°C for 35 minutes.

This change is however deemed insignificant over the temperature range studied, and considering that pyrolysis products will not be captured at incremental periods, this minimal increase in heating rate at higher operating temperature does not need to be taken into account. Comparison with the ISO 647 curve indicates that the heating rate is much lower. The temperature of 520°C is however reached after the period of 80 minutes as specified by ISO 647. If the system is allowed to heat up to a temperature of 200°C and the curves evaluated from then onwards, a much better correlation is observed. ISO 647 (SANS, 1974) allows for pre-heating of the retorts to ensure that it reaches the temperature of 220°C within 10 minutes after the run commences. In the case of this study, preheating up to 150°C within 35 minutes was done, after which the run commenced (Figure 4-2b).

4.2.2. Operating pressure and atmosphere

An inert (N_2) atmosphere was used to limit the effect of oxidizing reactions. N_2 gas (ultra high purity grade: 99.999%; product no.: 511204_SE-C), as supplied by African Oxygen (AFROX), at a flow rate of 10 NL/min for 10 minutes was admitted before the pyrolysis runs commenced to purge the system. Ambient operating pressure was used, and varied between 0.855 – 0.953 bar depending on the amount of gas evolved within the closed system. Pressure inside the retort was determined by use of the WIKA IPT-1* pressure transmitter.

4.2.3. Receivers, gas washing and sampling

The retort outlet pipes enter sealed receivers in an ice and water bath. Liquid products in the entering vapour condense, whilst the gas undergoes washing, using toluene (analytical standard purity ≥ 99.5% supplied by ACE chemicals) in three stages to remove all liquid products from the gas fraction. The first gas washing stage consists of a sealed round bottomed flask, whilst the latter stage consists of two gas washing bottles with tapered lids as

supplied by Rochelle Glass (Figure 5-3). Each gas washing stage contains 50 mL toluene. The last receiver in the gas washing system is coupled to a 10 L Tedlar gas sampling bag. The final gas composition is analysed by GC analysis, whilst the tar and moisture fractions are further separated by the Dean-Stark method and rotary evaporation. The moisture and toluene free tar fraction is analysed by analytical techniques such as Simdis, GC-MS and SEC-UV analyses.

4.2.4. Quantification of pyrolysis product yields

The pyrolysis product yields were determined by modification of the method described by SANS (1974) and as done in previous studies (Govender, 2005; Stanton et al., 2005; Slaghuis & Raijmakers, 2004). Results will be reported to the nearest 0.1% (SANS, 1974). Yields will be determined based on Equations (4-1 to 4-4) Table 4-2.

Table 4-2 Equations used to determine the percentage of tar, water, char and gas obtained (SANS, 1974).

Parameter	Equation	Equation number
Water,%	$= \frac{m_1 \times 100}{m_0} - M$	(4-1)
Tar,%	$= \frac{m_2 \times 100}{m_0}$; $m_2 = m_{RV,f} - m_{RV,i}$	(4-2)
Char residue,%	$= \frac{m_3 \times 100}{m_0}$	(4-3)
Gas (plus errors),%	$= 100 - (char + tar + total\ water)$ $= \frac{(m_0 - m_1 - m_2) \times 100}{m_0}$	(4-4)
m_0 is the sample mass; m_1 is the mass of water determined by entrainment after subtraction of the inherent moisture as found in the Proximate analysis; m_2 is the mass of tar as determined by subtracting the mass of the empty rotary evaporation flask ($m_{RV,i}$) from the mass of the rotary evaporation flask after toluene removal ($m_{RV,f}$); m_3 is the mass of the char residue and M is the inherent moisture, in percentage, originally present in the sample.		

4.2.4.1. Water yield

The inherent and pyrolytic water present in the condensed volatile fraction (water, tar and liquor) is removed by means of Dean-Stark distillation at medium temperature (ASTM D95, ISO 3733) (ASTM, 2010; ISO, 1999; Dean & Stark, 1920). A schematic diagram of the Dean-Stark setup is shown in Figure 4-3. A Seta MTop 5 heating mantle and a Dean Stark setup with reflux condenser are used for the removal of the water from the tar . The water fraction is decanted and weighed by use of the Radwag PS 200/C/4 balance. The water yield is then determined by use of Equation (4-1).

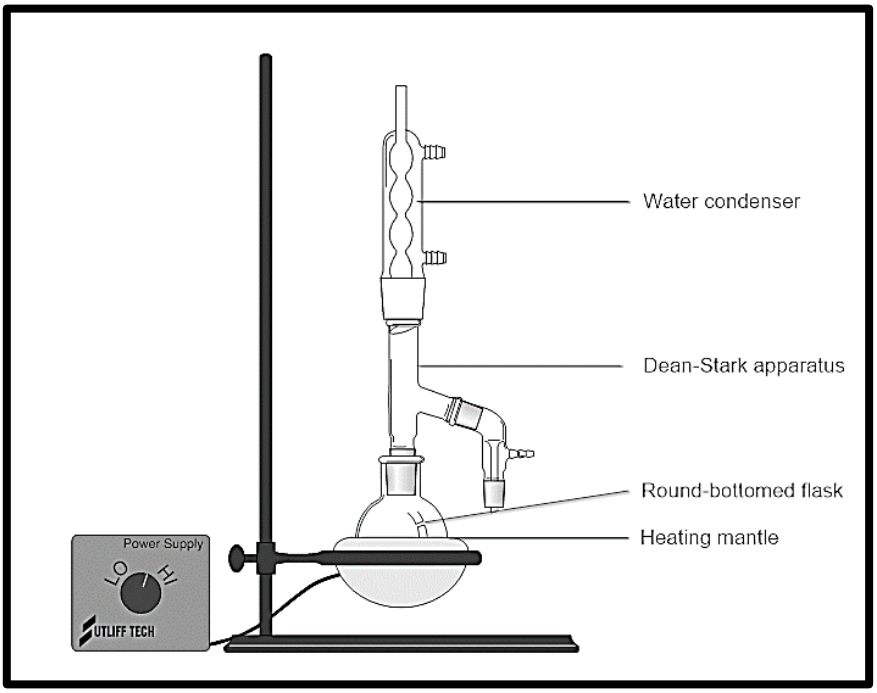

Figure 4-3: Dean-Stark setup.

4.2.4.2. Tar yield

After water removal the round bottomed flask contained toluene, tar and light oils. The toluene was removed by rotary evaporation to achieve the tar fraction. The rotary evaporation setup consisted of a Büchi vacuum controller V-850, Büchi vacuum pump V700 and Büchi Rotavapor R II. The setup is shown in Figure 4-4.

A water bath temperature of 60°C and the sequential lowering of the internal pressure to 27 mbar were used to ensure the removal of toluene from the tar-toluene mixture (Hattingh, 2012). The tar was kept at a constant temperature of 60°C and 27 mbar pressure for 5 minutes, thus ensuring complete removal of toluene. The mass of derived tar was determined by subtracting the mass of the empty rotary evaporation flask from the mass of the flask after toluene removal, with the tar fraction present in the flask. This was done by use of the Radwag PS 200/C/4 balance and the tar yield determined by using Equation (4-2). This procedure

differed from that used in ISO 647 (SANS, 1974), but the gas washing phase necessitated the procedure to be done in this manner.

Figure 4-4 The rotary evaporation setup used (Anon, 2014)

4.2.4.3. Char yield

The char residue in the retort was left to cool to ambient temperature before removal. The char sample was then weighed by means of a Radwag PS 750/C/4 balance and the char yield determined by use of Equation 4-3. After weighing, the char sample was placed in a hermetically sealed container, under N_2, to prevent oxidation, for further analysis.

4.2.4.4. Gas yield

During conventional Fischer Assay determination (SANS, 1974) gas yield is determined by difference after quantification of the char, tar and water yields (Equation 4-4). In this study, the gas yield was determined by using volume calculations along with compositional data for the derived gases. The gas yields were sampled in 10 L Tedlar gas sampling bags for the duration of the experiment. After completion of the experiment, the outline of the sampling bag was drawn up in order to calculate the volume occupied by gas in the bag. The pressure for the system was noted, and by use of the ideal gas law, the GC results and the volume calculations, the weight of the produced gases was calculated. Appendix B-1 gives full detail on the method applied to determine the gas yield. Mass balance closure for all the reported yields was found to be between 98.0 and 99.8%.

4.2.5. Repeatability of pyrolysis experiments

Repeatability of the experimental method was evaluated in two ways:

i. ISO 647 (SANS, 1974) provides maximum allowable differences (indicated in Table 4-3) for repeat runs by the same operator on the same equipment. This was the first evaluation conducted to determine if the runs were repeatable.
ii. A confidence interval of 95% was used to determine the deviation of runs and set up a confidence interval (Table 4-4).

Both the TWD and AW TWD coal fractions were evaluated in this manner. Four experiments were done for each coal at each temperature (520, 750 and 900°C) in order to evaluate repeatability of the experimental method. All experiments were found to be within these limits.

Table 4-3 Average percentage (%) difference between replicate experiments

	520°C			750°C		900°C	
	ISO 647	TWD	AW TWD	TWD	AW TWD	TWD	AW TWD
	% difference between replicate experiments						
Water	0.4	0.2	0.4	0.1	0.3	0.3	0.1
Tar	0.5	0.2	0.2	0.2	0.2	0.1	0.1
Char	0.7	0.3	0.3	0.1	0.2	0.4	0.1

Table 4-3 indicates the average percentage difference between replicate experiments for the TWD and AW TWD coal fractions. These values are all within the limits as determined by ISO 647 (SANS, 1974) and are consistent with previous work on the same setup (Roets *et al.*, 2014).

Table 4-4 Error% on repeatability of TWD and AW TWD experiments, based on 95% confidence intervals

	520°C		750°C		900°C	
	TWD	AW TWD	TWD	AW TWD	TWD	AW TWD
	% error on repeatability (95% confidence)					
Water	5.1	14.4	3.2	10.6	7.3	4.2
Tar	4.0	10.2	5.5	7.9	3.9	4.9
Char	0.7	0.4	0.2	0.5	1.1	0.4
Gas	8.7	2.4	4.6	3.9	4.0	1.9

Table 4-4 indicates the 95% confidence interval error% values for the TWD and AW TWD repeat experiments. Typical error values of between 0.2 – 14.4% were obtained for the respective pyrolysis product yields. All error bars indicated in the Figures following on from this section of the dissertation will be reported within a 95% confidence interval.

4.3. Pyrolysis product analyses

The compositions of the tar, char and gas fractions obtained from the pyrolysis experiments were analysed by various analytical techniques. These analyses provide more insight into the effect of the different operating conditions, the acid washing process, and the mineral addition. A summary of the analytical techniques used are provided in Table 4-5.

Table 4-5 Analytical techniques conducted on the derived pyrolysis products

Product to be analysed	Analyses	Characteristic property	Laboratory responsible
Gas	GC (-TCD and –FID)	Molecular	North-West University
Tar	GC-MS and GC-FID	Molecular	Sasol R & D
	Simdis	Molecular	Sasol R & D
	SEC-UV	Molecular	Sasol R & D
	Ultimate	Molecular	North-West University
Char	Proximate	Chemical	Bureau Veritas
	Ultimate	Chemical	Bureau Veritas
	XRF	Mineralogical	Bureau Veritas
	XRD	Mineralogical	XRD Analytical and Consulting
	DRIFT	Structural	North-West University
	BET CO_2 adsorption	Structural	North-West University

4.3.1. Gas analyses

The gases derived from the pyrolysis experiments were captured using 10 L Tedlar gas sampling bags and were analysed by means of gas chromatographic (GC) analysis with the aid of a SRI 8610C multiple gas chromatograph as previously used by Hattingh (2012). Table 4-9 lists the relevant instrument information, oven programme, carrier gas flow rate and detector temperatures.

Gaseous products are separated by the aid of three packed columns i.e.: 6’ HayeSep D, 6’ 13X molecular sieve and 3’ 5 Å molecular sieve (all with an outer diameter of 1/8’). Gaseous products are quantified by a flame ionization detector (FID) and two thermal conductivity detectors (TCD1 and TCD2). Peak-382 acquisition software logs and stores the chromatographs from the manually injected gaseous sample. Calibration of the equipment was done using a refinery gas standard and by evaluating the typical elution time frames for the expected gas product constituents, which include O_2, N_2, CH_4, CO, CO_2, ethylene, ethane,

C_3s (propylene, propane, propadiene, cyclopropane, methyl-acetylene), C_4s (isobutene, n-butane, isobutylene, 1,3-butadiene, cis-2-butene, trans-2-butene, butane-1), C_5s (isopentane, n-pentane), C_6s (n-hexane, 4-vinyl-1-cyclohexene).

Table 4-6: GC analysis instrument information

GC Conditions	Specification
Inlet temperature	25 ºC
Injection volume	0.5 µL
Detector cell temperatures	TCD1: 300 ºC TCD2: 150 ºC
Carrier gases and gas flow rates	FID: He (25 psi and 20 mL/min) Methaniser: H_2 (20 psi and 25 mL/min) and Air (5 psi and 250 mL/min) TCD1: He (25 psi and 20 mL/min) TCD2: Ar (7 psi and 10 mL/min)
Oven programme	Hold for 7 min at 60ºC, 60ºC to 280ºC at 15ºC/min, and hold for 20 min at 280 ºC.
Calibration standard and unit measure	Refinery gas #1 and mol.%

GC results were further converted to a g gas species / g coal (d.m.m.f.) basis with aid of Equation 4-8.

$$g_{i,j}/g_{coal,d.m.m.f.} = \frac{\left(\frac{wt.\%_i}{100}\right)(G_j)}{C_{g,d.m.m.f.}} \quad (4\text{-}8)$$

Where i is the gas species, G_j refers to the amount (g) gas derived from the coal at temperature j and C_g refers to the amount of coal tar derived on a dry, mineral-matter-free basis. The obtained values are reported as fractions 1000 larger than the true calculated values.

4.3.2. Tar analyses

The light oil and tar fraction is of specific importance. Not only does it constitute 50-80% of the mass loss that occurs during pyrolysis in the form of volatiles (Gavalas, 1982), and provides much useful information regarding the thermal breakdown of coal (Casal *et al.,* 2008; Kandiyoti *et al.,* 2006; Ibarra *et al.,* 1989), but it is also a valuable source of high value chemicals (Jiang *et al.,* 2007; Menéndez *et al*., 2000, Schobert, 1990). Tar analyses consisted of: gas chromatography, mass spectrometry (GC-MS), simulated distillation (Simdis) and size exclusion chromatography with UV column (SEC-UV), all done at Sasol Research and Development in Sasolburg.

4.3.2.1. Simulated distillation (Simdis)

Simulated distillation (Simdis) is a standard test to classify coal tar into a manageable number of components (Li, *et al.*, 2010; Ukwuoma, 2002). The method is said to have good

reproducibility for coal tars, but poor accuracy (Li *et al.,* 2010). Simulated distillation analysis was conducted according to the ASTM D2887 standard using a high-temperature GC-FID fitted with an ARX 2887 Restek column (10m x 0.53 mm x 0.53 µm) (Roets *et al.,* 2014). A sample consisting of 0.2 µL tar dissolved in dichloromethane was injected into the GC column per analysis. The initial temperature of the GC column was 40°C, with a ramp of 15°C per minute, and hold time of 10 minutes at the final temperature of 540°C.

The Simdis results in this study were analysed based on weight average boiling point (WABP) calculation and evaluation of the mass loss curves, as used previously (Roets *et al.,* 2014; Rafenomanantsoa *et al.,* 1998; Bakr, *et al.,* 1996; Gray, 1988). The weight average boiling point is calculated by use of the following equation (Roets *et al.,* 2014; Bean, 2013; Hattingh, 2012; Rafenomanantsoa e*t al.*, 1998; Bakr, *et al.,* 1996; Gibbins-Matham and Kandiyoti, 1988):

$$WABP = \frac{T_{10}+T_{30}+T_{50}+T_{70}+T_{90}}{5} \quad (4\text{-}5)$$

where T_{10}, T_{30}, T_{50}, T_{70} and T_{90} are the temperatures at which 10, 30, 50, 70 and 90% mass losses occur.

This method has been used in various studies (Roets *et al.,* 2014; Li *et al.,* 2007; Ukwuoma, 2002; Mastral *et al.,* 2000; Rafenomanantsoa *et al,* 1998; Sakuneka *et al.,* 1998; Seshadri and Shamsi, 1998, Bakr *et al.,* 1996).

Further analyses of simulated distillation results were done based on division of the boiling point distributions into crude oil distillation fractions based on the work by Rand (2003) and as used by Hattingh (2012). Table 4-6 indicates the cut fractions as identified from crude oil refining.

Table 4-7 Cut fractions of boiling point ranges based on crude oil distillation (Rand, 2003)

Identification	Boiling point range (°C)
Medium naphtha	79-121
Heavy naphtha	121-191
Kerosene	191-277
Distillate fuel oil	277-343
Light vacuum gas oil	343-455
Heavy vacuum gas oil	455-566

4.3.2.2. Gas chromatography-mass spectrometry and–flame ionization detection (GC-MS and GC-FID)

All tar samples were analysed using a GC-MS instrument (peak identification) and a GC-FID instrument (quantification) fitted with PONA column (50m x 0.2 mm x 0.33 µm) (Roets *et al.,* 2014; Bean, 2013; Hattingh, 2012). Samples for GC-MS analysis were prepared by dissolving 200 mg tar in 2 ml dichloromethane in PTFE vials. Approximately 1 µL of prepared sample was injected into the GC column with a split of 200. The GC oven program was as follows: Initial temperature of 60°C held for 5 min., ramp at 6°C/min to 240°C and hold for 30 minutes (until all compounds have eluted). Gas flow through the column was 1.2 ml per minute (helium in GC-MS and hydrogen in GC-FID) (Roets *et al.,* 2014; Bean, 2013; Hattingh, 2012). Only species present in quantities higher than 0.005 wt% were taken into consideration for quantification of the tar components. GC-MS provides semi-quantitative data for the detected peaks as identified by FID. The results were normalised on a solvent free basis to a 100 wt% of the sample analysed.

GC-MS uses one GC column and the effluent passes through a mass spectrometer through an interface held at an elevated temperature (Kandiyoti *et al.*, 2006). GC-MS provides molecular level data and the mass spectrum gives structural information of the separated compounds (Wang *et al.,* 2013, Herod & Stokes, 1988). These studies provide insight into the formation process and composition of the tars. GC-MS has the disadvantage that compounds with a boiling point higher than 300°C are hard to volatilize, and detection of components with a lower boiling point than the solvent may be overlaid by the solvent peaks in the chromatogram (Wang *et al.,* 2013, Kandiyoti *et al.*, 2006; Herod & Stokes, 1988). Another problem is that the range of GC-MS is up to about m/z 500-600 (Herod *et al.,* 2003), and it has even been suggested that it is only accurate up to m/z 300-350 (Menéndez *et al.* 2002). The majority of heavy hydrocarbon liquids cannot be observed by GC and GC-MS, therefore other analytical methods such as size exclusion chromatography (SEC) and matrix-assisted laser desorption/ionization mass spectrometry (MALDI-MS) have to be used, and have been successful at up to 3 000 g/mol (Karaca *et al.*, 2009; Trejo *et al.* 2007). In the case of this study, SEC will be used for further characterisation of the larger molecular weight tar fraction not identified by GC-MS.

GC-MS identifies various components and comparison can be difficult. Therefore, the detected species were classified into molecular families constituting: aliphatics, alkyl-benzenes, alkyl-phenols, aromatic ethers and esters, alkyl indenes, alkyl-naphthalenes, poly-aromatic hydrocarbons, nitrogen heteroatoms and mixed aliphatics and aromatics. Typical compounds identified in each molecular family are indicated in Table 4-7.

The GC-MS analysis of the derived tars will provide insight with regard to the low molecular weight hydrocarbon species present, with boiling points below 300°C.

Table 4-8 Typical compounds identified by GC-MS and classification based on molecular families

Family (Abbreviation)	Typical compounds
Aliphatic compounds (Aliph.)	Normal- and iso-paraffins, olefins and acetylenes. Acyclic compounds.
Alkyl-benzenes (A-B)	Benzene and its derivatives, i.e. toluene, xylene, higher substituted benzenes
Alkyl-phenols (A-P)	Phenol, cresol, xylenol
Aromatic ethers and esters (Arom. E & E)	Dibenzofuran
Alkyl-indenes (A-I)	Indene, Methyl-indene
Alkyl-naphthalenes (A-N)	Naphthalene, methyl-napthalene and other derivatives
Poly-aromatic hydrocarbons (PAH's)	Fluorene, anthracene, phenanthrene, fluoranthene and other aromatics
Nitrogen heteroatoms (N-)	Pyridine, methyl-pyridine, benzene-amine etc.
Mixed aliphatic and aromatic compounds (Mixed)	Co-elution of iso-aliphatics and aromatics

4.3.2.3. Size exclusion chromatography (SEC-UV)

Size exclusion chromatography (SEC) is a useful analytical technique that has been used extensively in a number of studies to clarify the distribution of heteroatoms over a wide molecular size range (Trejo *et al.*, 2007; Kandiyoti *et al.,* 2006; Millan *et al.*, 2005; Herod *et al.,* 2003). SEC is accurate for detection of components within a factor 2 to masses of 3000 u, because no surface interactions are involved between sample and packing, such as observed in other HPLC based methods. SEC indicates consistency with regard to its permeation (lower molecular mass) limit (Kandiyoti *et al*., 2006, Karaca *et al.,* 2005; Herod *et al.*, 2003; Islas *et al.,* 2003).

SEC uses a polymer standard for calibration of known mass to determine molecular mass distributions of samples by comparison (George *et al.*, 2010). In SEC, the largest molecules elute first due to the fact that penetration through the inter-particulate voids within the column is not possible. The smallest particles that penetrate the smallest porosity elute last, and form the permeation limit. After the permeation limit is reached, no other particles should elute in true SEC. SEC functions under the assumption that there is a relation between the molecular mass of the hydrocarbons and polymers used for calibration; but the difficulty with this

assumption is that molecular structures of tar components with mass greater than 500 u is not known (George *et al.*, 2010; Trejo *et al.*, 2007).

Various solvents can be used for SEC analysis. Toluene, chloroform, dichloromethane, benzonitrile and dimethylformamide will however not dissolve tar completely, and results with these eluents will only show the more soluble parts (Herod *et al.*, 2003; Herod *et al.*, 2007; Johnson *et al.,* 1998). Lafleur and Nakagawa (1989) suggested the use of 1-methyl-2-pyrrolidinone (NMP) due to its ability to dissolve most of the coal tar liquids, even a coal tar pitch, which is a solid at room temperature. Due to the powerful nature of NMP, aggregates do not form with large molecules, and this is an added advantage that is not observed with THF or pyridine, due to the adsorption tendency between solute and column packing (Morgan, 2008; Trejo *et al.*, 2007; Herod *et al.*, 2003 & 2007).

The samples for SEC-UV analysis were prepared by dissolving a small amount of tar in 1 ml 1-methyl-2-pyrollidone (NMP) and mixing it thoroughly. The prepared samples were diluted in NMP (100 µl tar and 1400 µl NMP) prior to the SEC-UV analyses. An Agilent 1100 high-performance liquid chromatograph (HPLC) was set at 80°C using a 300 mm long, 7,5 mm internal diameter PLgel mixed-E (Varian) GPC column for separation. HPLC grade 1-methyl-2-pyrollidone (NMP) from Merck Chemicals at a flow rate of 0.5 ml/min was used as eluent (Roets *et al.,* 2014). All chromatograms were collected using an ultra-violet (UV) detector with wavelengths of 280, 300, 350 and 370 nm (Roets *et al.,* 2014). According to Alvarez *et al.,* (2008) and Trejo *et al.,* (2007), NMP is known to be opaque at a wavelength of 254 nm, but becomes partially transparent at wavelengths higher than 270 nm. In this current study a wavelength of 300 nm was selected to obtain results.

Integration of the SEC-UV data was done using the HP 1100 Data Analysis software. The data was peak-normalised and divided into lighter and heavier components, by determining the areas under the heavier and lighter component peaks as identified by the UV-column. The results were normalised to 100 area%. Figure 4-5 indicates a typical SEC chromatogram. The peak identified between ~ 7 and ~ 10 minutes corresponds to material of molecular size and/or molecular composition unable to penetrate the porosity of the column packing (Fidalgo *et al.*, 2014). This peak was excluded in further calculations. A shoulder is observed as part of the peak identified with the heavy components, this is consistent with previous observations (Hattingh, 2012).

Calibration was done by dissolving SEC polystyrene standards (purchased from Varian) with molecular weights ranging from 162 - 19 640 g/mol in NMP (George *et al.,* 2010). Calibration was done at a wavelength of 260 nm, due to the transparency of NMP (Trejo *et al.,* 2007). The calibration data (see Figure 4-6a) was used to derive an equation (see Figure 4-6b) from which

the molecular weight of the molecules passing through the SEC columns could be determined by intra- and extrapolation. The equation derived for this purpose is therefore defined as:

$$log(M_P) = -0.2335 \cdot t_E + 6.5474 \quad (4\text{-}7)$$

Size exclusion chromatography (SEC) results can be area and peak normalised according to the method described in previous studies (Roets *et al.,* 2014; George *et al.,* 2010; Trejo *et al.,* 2007); however comparison based on the evaluation of the heavy and light component areas as indicated in Figure 4-5 is adequate.

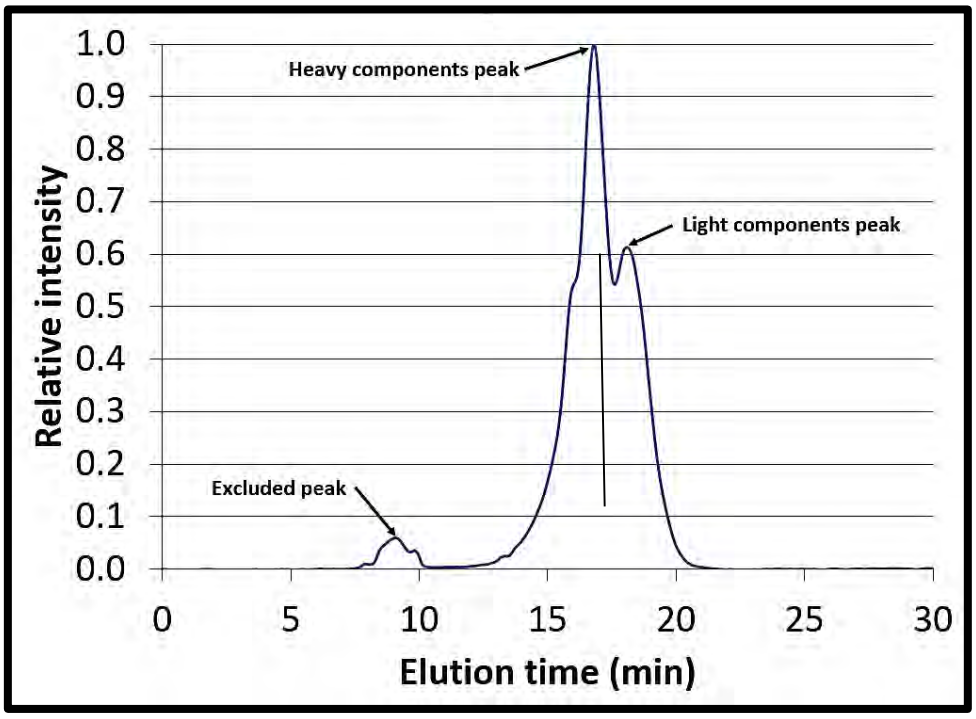

Figure 4-5 Typical SEC Chromatogram for derived tars

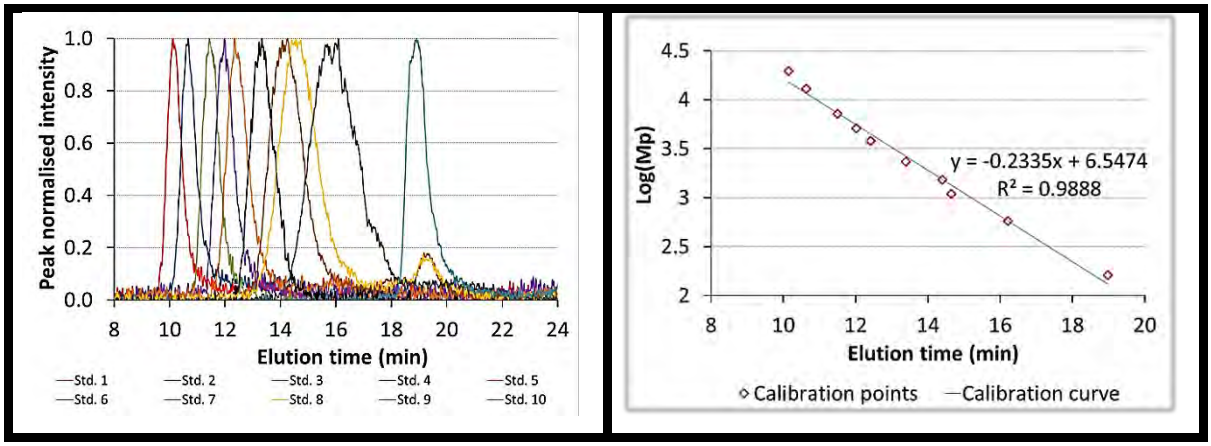

Figure 4-6 SEC chromatogram of the 10 calibration standards used a) and b) calibration curve determined from the elution times of the different calibration standards.

4.3.3. Char analyses

The various chars prepared under the same experimental conditions were combined for analyses. Char analyses consisted of proximate, ultimate, XRF, XRD, BET CO_2 adsorption and DRIFT analyses.

4.3.3.1. Proximate, ultimate and XRF analyses

Proximate, ultimate and XRF analyses were done by Bureaus Veritas after sample preparation according to ISO 13909-4 (2001). Table 4-8 indicates the standards used. These analyses are discussed in Section 3.4.1.

Table 4-9 Char analyses and laboratory/standards used

Analyses	Standard used
Proximate	
Inherent moisture content (%)	ISO 11722: 1999
Ash content (%)	ISO 1171: 2010
Volatile matter content (%)	ISO 562: 2010
Fixed carbon content (%)	By difference
Ultimate	
Carbon (%)	ISO 29541: 2010
Hydrogen (%)	ISO 29541: 2010
Nitrogen (%)	ISO 29541: 2010
Oxygen (%)	By difference
Total sulphur **(IR Spectroscopy) (%)**	ISO 19759: 2006
Ash (XRF)	ASTM D4326

4.3.3.2. XRD analysis

XRD Analytical and Consulting conducted XRD analyses to provide insight regarding the crystalline mineral phases present within the chars. Samples were prepared using a back loading preparation method. A PANalytical Empyrean diffractometer with PIXcel detector and fixed slits with Fe-filtered Co-Kα radiation was used. Phases were identified using X'Pert Highscore plus software.

4.3.3.3. BET CO_2 adsorption

BET CO_2 adsorption analyses were carried out as discussed in Section 3.4.3.

4.3.3.4. DRIFT analysis

Diffuse reflectance infrared Fourier transform spectroscopy (DRIFT) analysis was carried out as discussed in Section 3.4.3.

4.4. Experimental plan

Various pyrolysis experiments were carried out on the two coal fractions that were characterised in Chapter 3. Five cases were examined in this study:

I. 50.0 g Highveld washed coal, referred to as TWD
II. 50.0 g Acid washed Highveld washed coal, referred to as AW TWD
III. 50.0 g Acid washed Highveld coal (AW TWD) with addition of 5 wt% mineral compound additional to the 50.0 g coal sample, i.e. 52.5 g, based on its mineral additive AW-Cal (calcite addition), AW-Dol (dolomite addition), AW-Kao (kaolinite addition), AW-Pyr (pyrite addition) or AW-QZ (quartz addition), depending on the mineral added
IV. Acid washed Highveld coal with addition of a mineral mixture similar to the mineral constituents originally present in the coal sample, referred to as LM (low wt% mineral mixture)
V. Acid washed Highveld coal with addition of a mineral mixture similar to the mineral constituents originally present in the run of mine Highveld coal, before any beneficiation, referred to as HM (high wt% mineral mixture).

Table 4-10 provides more detail with regard to the pyrolysis experiments done. In cases I and II (Chapter 5) four experiments were done at each temperature. This was done in order to ensure good reproducibility of results, as well as to obtain a repeatable base case to which the addition of mineral experiments (cases III to V – Chapter 6 and Chapter 7) could be compared. For cases III -V duplicate experiments were done. A duplicate experiment was only regarded as successful if it was found to be within the maximum allowable difference (Table 4-10) for duplicate experiments conducted by the same operator, on the same apparatus as specified by ISO 647, (SANS, 1974).

In case III, the 5 wt% mineral addition experiments were done using the 50.0 g coal sample, so as to ensure that the same amount of carbonaceous material was present in the retort, thereby ensuring that differences observed were due to the addition of mineral matter. The addition of 5 wt% mineral matter was further motivated by the desire to ensure that quantification of the effect on the pyrolysis product yields of the specific mineral was possible. Nel (2009) followed the same rationale in her study with regard to the effect of trace minerals on ash fusion temperature by use of a 4 wt% mineral addition. For Cases V and VI, the mineral mixtures were set up, based on QEMSCAN and CCSEM data available. The discussion of this procedure will be handled in Chapter 7 of this dissertation.

Table 4-10 Pyrolysis experiments done during this study

Case	Exp. #*	Code	Coal sample weight (g)	Mineral addition	Final weight (g)	Pyrolysis temperature (°C)
I	1-12	TWD01 – TWD12	49.95 - 50.05	-	49.95 - 50.05	520, 750, 900
II	13-24	AW TWD01 – AW TWD12		-		520, 750, 900
III	25-26	AW-CAL01 – AW-CAL06		5 wt% $CaCO_3$	52.45 - 52.55	520, 750, 900
	31-36	AW-DOL01 – AW-DOL06		5 wt% $CaMg(CO_3)_2$		520, 750, 900
	37-32	AWKAO01 – AW-KAO06		5 wt% $Al_2Si_2O_5(OH)_4$		520, 750, 900
	43-48	AW-PYR01 – AW-PYR06		5 wt% FeS_2		520, 750, 900
	49-54	AW-QZ01 – AW-QZ06		5 wt% SiO_2		520, 750, 900
V	55-60	LM01 – LM06	41.85 - 41.95	1.10 g $CaCO_3$; 2.38 g $CaMg(CO_3)_2$; 4.00 g $Al_2Si_2O_5(OH)_4$; 0.15 g FeS_2; 0.62 g SiO_2	49.95 - 50.05	520, 750, 900
VI	61-66	HM01 – HM06	34.28 - 34.38	1.90 g $CaCO_3$; 1,00 g $CaMg(CO_3)_2$; 7.00 g $Al_2Si_2O_5(OH)_4$; 2.80 g FeS_2; 2.90 g SiO_2		520, 750, 900

Chapter 5: Effect of acid washing

5.1. Introduction

In order to determine the effect of minerals on coal pyrolysis products, one needs to consider how coal behaves without these minerals present. In order to achieve this goal, acid washing, (also referred to as demineralisation, acid leaching or acid treatment), of the coal was done. In this chapter the pyrolysis product yields and composition derived from the TWD and AW TWD fractions will be evaluated as follows:

- Pyrolysis product yields (Section 5.2)
- Gas composition (Section 5.3)
- Tar composition (Section 5.4)
- Char composition (Section 5.5)

The gas composition was analysed by GC analyses, the tar composition as analysed by Simdis, GC-MS and -FID, and SEC-UV, and the char composition as analysed by proximate, ultimate, XRF, XRD, DRIFT and BET CO_2 adsorption analyses. In Section 5.6 a summary of the most relevant findings will be reported.

** It should be noted that in cases where there is referred to, for example, chars derived at 520°C, the author implies that these chars were derived upto a final pyrolysis temperature of 520°C, i.e. over the temperature range 25°C to 520°C.*

5.2. Pyrolysis product yields

The effect of acid washing will be discussed by comparison of the pyrolysis product yields at the respective temperatures (520, 750 and 900°C). Figure 5-1 indicates the pyrolysis product yields obtained for TWD and AW TWD fractions on an as determined basis at the three temperatures studied. Line graphs have been included to guide the reader's eye through the experimental data points.

The gas yields are observed to increase with an increase in final pyrolysis temperature, with quite a large difference between the yields at 520°C and 750°C. This is consistent with previous findings in which the secondary pyrolysis stage (>450°C) was found to be dominated by increasing gas yields (Sert *et al.,* 2011; Kandiyoti *et al.,* 2006, Mill, 2000; Ladner, 1988; Nelson *et al.,* 1988).

The water yields are observed to remain constant for the AW TWD fraction, whilst a small increase is observed with an increase in final pyrolysis temperature for the TWD fraction. This

different behaviour can be related to the removed minerals, such as kaolinite which contains endothermic water that is released in the temperature range of 450°C to 650°C (Ptáček *et al.,* 2010b; Vassilev *et al.*, 2009; Heide & Földvari, 2006; Alpern *et al.,* 1983). Other minerals, such as dolomite and calcite, also influence water yields due to the water-gas shift reaction that may take place (Abu El-Rub, 2004; McKee, 1980), whilst tar precursors are also thought to be a source of water (Tsubouchi & Ohtsuka, 2002; Chen *et al.* 1999).

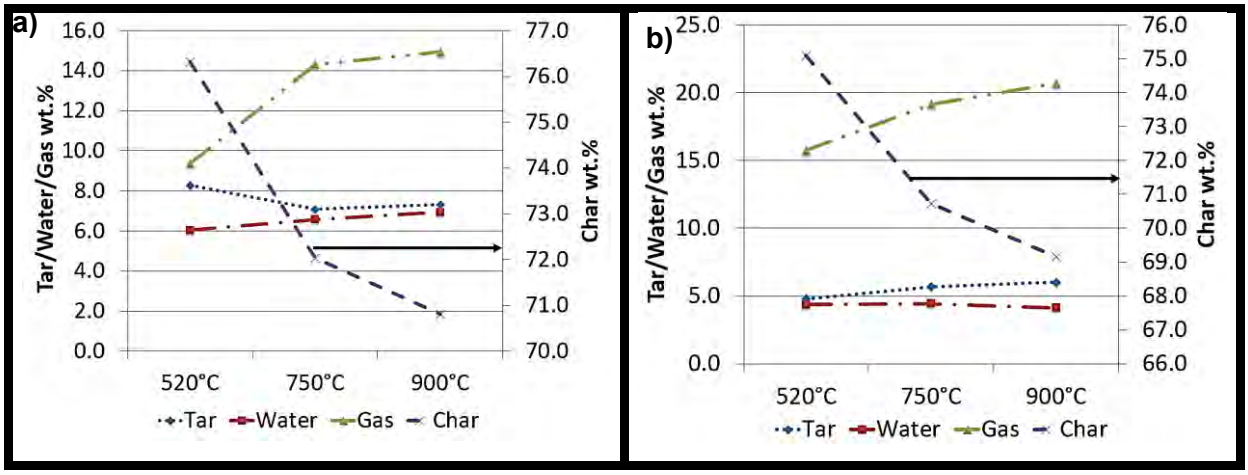

Figure 5-1 Pyrolysis product yields at 520°C, 750°C and 900°C for a) TWD, b) AW TWD.

The tar yield from the TWD fraction is observed to decrease with an increase in final pyrolysis temperature between 520°C and 750°C, in accordance with previous findings (Fei *et al.*, 2012; Hattingh, 2012; Ahmad *et al.,* 2009a). The tar yield of the AW TWD fraction is observed to increase for the same temperature range. The maximum tar yield would have been reached at 600°C (Liu *et al.*, 2004a; Ôztas & Yürüm, 2000, Yaw *et al.*, 1980), and therefore no significant change in tar yield is observed between 750°C and 900°C for both coal fractions. The difference in tar-forming behaviour of the two coals suggests that either the pyrolysis range for the acid washed coal is at higher temperatures, as has been suggested by previous authors (Smith *et al.,* 1994), or the removal of minerals inhibits secondary tar cracking reactions said to take place at higher pyrolysis temperatures (Ahmad *et al.,* 2009; Yaw *et al.,* 1980). Minerals such as calcite and dolomite have been observed to be effective tar cracking catalysts (Mun *et al.,* 2012; Pinto *et al.,* 2007; André *et al.,* 2004; Liu *et al.*, 2004a; Sciazko & Kubica, 2002; Chen *et al*., 1999; Yaw *et al.,* 1980). Decomposition of these minerals only start at temperatures in excess of 500°C (Liu *et al.,* 2007a; Vassileva & Vassilev, 2006; Tomeczek & Palugniok, 2002; Reifenstein *et al.,* 1999), thus possibly explaining the decrease in tar yield at the higher final pyrolysis temperatures.

The char yields for both coal fractions are observed to decrease with an increase in final pyrolysis temperature in accordance with previous studies (Reichel *et al.,* 2013; Fei *et al.,*

2012; Ahmad *et al.,* 2009a and 2009b; Kandiyoti *et al.,* 2006; Hu *et al.,* 2004; Smith *et al.,* 1994; Ladner, 1988; Franklin *et al.,* 1982a, 1982b, Yaw *et al.,* 1980).

Comparison of the pyrolysis product yields from the TWD and AW TWD fractions will be discussed next. The water yields (Figure 5-2a) are reported on a mineral matter free basis (m.m.f.b.), whilst the other pyrolysis product yields (Figure 5-2b to Figure 5-2d) are reported on a dry, mineral matter free basis (d.m.m.f). The correction for mineral matter was done by use of the QEMSCAN results. It was previously reported that the TWD fraction contained 17.4 wt% mineral matter, whilst the AW TWD fraction contained 3.2 wt% mineral matter (Section 3.6.3). Refer to Appendix C-1 for all the pyrolysis product yields, reported on an as determined basis, mineral matter free basis, and on a dry, mineral matter free basis, along with the calculated error on repeatability values at a 95% confidence interval.

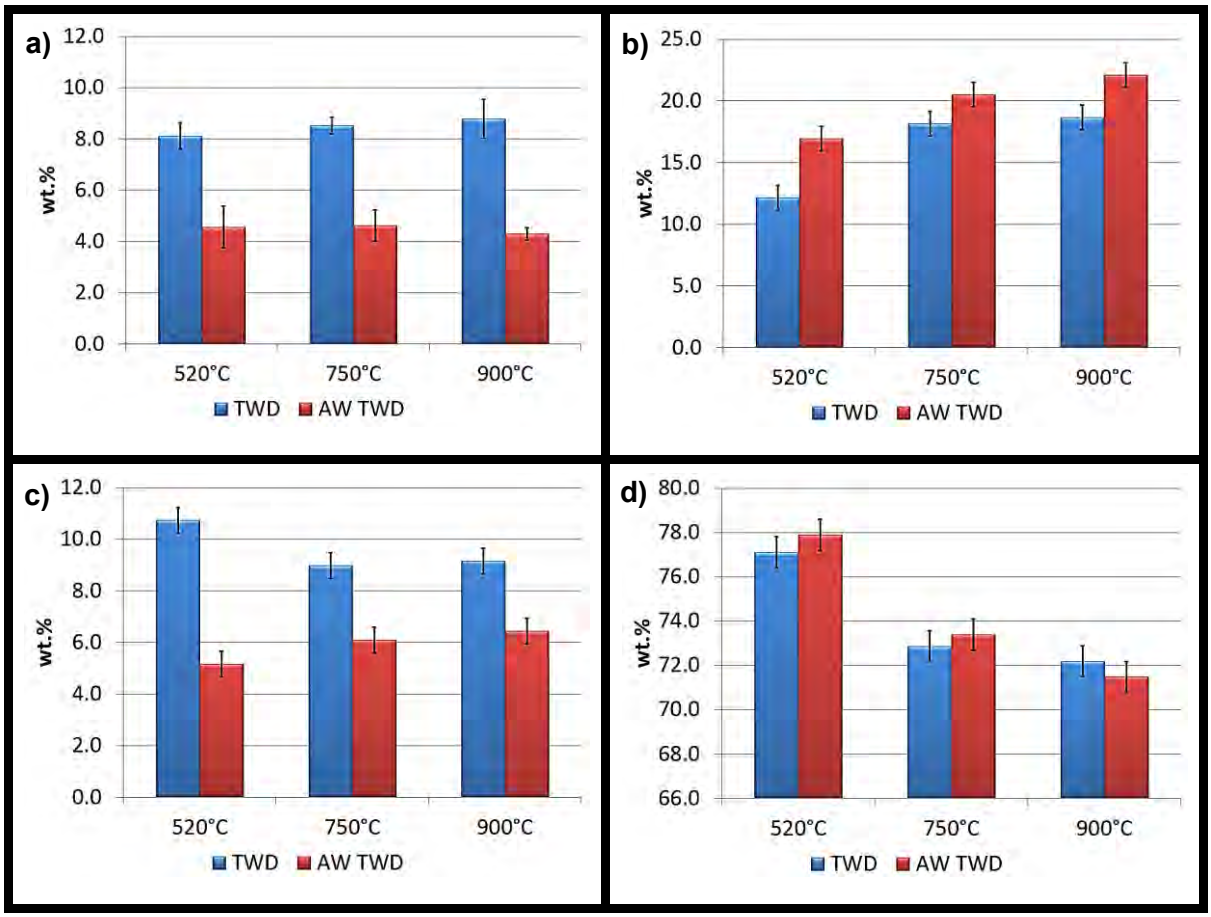

Figure 5-2 a) Water yields (m.m.f.); b) Gas yields (d.m.m.f.); c) Tar yields (d.m.m.f.) and d) Char yields (d.m.m.f.) for TWD and AW TWD coal at 520°C, 750°C and 900°C.

5.2.1. Water yields

Figure 5-2a indicates the water yields on a mineral-matter-free basis for the TWD and AW TWD fractions. It can be observed that the water yields from the AW TWD fraction were markedly lower, i.e. ranging between 8.1 and 8.8 wt% for the TWD fraction vs. 4.3 to 4.6 wt%

for the AW TWD fraction. The decrease observed in water yields after acid washing has been observed by various authors (Ahmad *et al.,* 2009a and 2009b; Tsubouchi & Ohtsuka, 2002; Chen *et al.* 1999; Samaras *et al.,* 1996; Otake & Walker, 1993; Morgan & Jenkins, 1986b; Franklin *et al.*, 1982a).

Both coal fractions were dried at 80°C until a constant weight was obtained and hermetically sealed in an N_2 atmosphere, to ensure that the coal fractions underwent the same processes. It should also be remembered with reference to Equation 4-1 that the difference in inherent moisture content, as determined by proximate analysis, is accounted for. Thus, the decrease observed in water yield can be attributed to the effect of the removal of mineral matter by acid washing.

Minerals such as kaolinite produce endothermic water upon transformation at increased temperature (Ptáček *et al.,* 2010b; Vassilev *et al.*, 2009; Heide & Földvari, 2006; Alpern *et al.,* 1983). From the DRIFT results (Section 3.8.2) it was observed that the free hydroxyl groups and OH groups associated with kaolinite were not present in the AW TWD fraction. Reference was also made to the OH-groups in the region of 3000 cm^{-1} which are said to be associated with the carboxyl groups, and that the close proximity of protons ensures that water forms easily (Cai & Smart, 1994). The stretch width in this area was less for the AW TWD fraction, and thus this is believed to influence the total water yield. Previous authors who studied the pyrolysis yields from acid washed coals also attributed the decreased water yield to be associated with the phenolic and carboxylic groups (Tsubouchi & Ohtsuka, 2002; Chen *et al.* 1999). Tar precursors were also identified as a possible source of water (Tsubouchi & Ohtsuka, 2002; Chen *et al.* 1999), and as will be observed in the next section, the tar yield from the AW TWD coal was also remarkably lower than that of the TWD fraction. There is also a case that some minerals, (such as dolomite and calcite), present in the TWD fraction, may accelerate the reactions of solid carbon with gaseous oxygen, water vapour and carbon dioxide (water-gas shift reaction). Studies on graphite-H_2O reactions showed that the addition of $CaCO_3$ led to an increased water yield (McKee, 1980).

5.2.2. Gas yield

Comparison of the gas yields (Figure 5-2b) indicates that for the experiments carried out up to 520°C, (12.1 wt% vs 16.9 wt. %), for the experiments carried out up to 750°C, (18.2 wt% vs. 20.5 wt%), and for the experiments carried out up to 900°C, (18.7 wt% vs. 22.1 wt%) gas is produced for the TWD fraction and AW TWD fraction, respectively. The gas yields from the AW TWD fraction are thus significantly higher; consistent with previous findings (Nissar *et al.,* 2011; Ahmad *et al.*, 2009a, Ahmad *et al.,* 2009b).

In previous studies the increase in gas yield due to acid washing was attributed to the fact that the minerals (and particularly their oxides responsible for gas formation in coal), were non-porous, thus the removal of mineral matter was believed to alter the softening and swelling behaviour of coal and increase its porosity (Ahmad *et al.,* 2009; Bexley *et al.,* 1986). Due to higher porosity, increased swelling behaviour and less diffusion limitations, an increase in gas yield was expected (Ahmad *et al.,* 2009; Reucrofta *et al.,* 1983). Bexley *et al.,* (1986) did however investigate the effect of the addition of various inorganic compounds on dilatometry parameters of coal, and found that $CaCO_3$, Al_2O_3, SiO_2 and FeS_2 showed effects that could only be attributed to dilution by inert material regarding the change in dilatometry parameters. Thus a change in swelling behaviour is believed to be unlikely in the current study, knowing that these compounds (which showed little effect) are the most prominent mineral constituents in TWD coal. In Section 3.8.1, BET CO_2 adsorption analyses revealed very little increase in porosity for the AW TWD fraction. Further BET CO_2 adsorption results of the chars derived at the 3 different temperatures will be discussed in Section 5.5.4.. From the BET CO_2 adsorption results (to be discussed in Section 5.5.4), it was observed that the AW TWD chars had a significantly higher porosity, thus confirming this hypothesis.

The increase in gas yield obtained for the TWD fraction between 520°C and 750°C is 6.1 wt%, and only 3.6 wt% for the AW TWD fraction, whilst between 750°C and 900°C the difference is 0.5 wt% vs. 1.6 wt% for the respective coals. The larger increase in gas yield observed between 520°C and 750°C for the TWD fraction may be related to decomposition of some of the mineral species, whilst the difference between 750°C and 900°C might be related to a shift in pyrolysis range (Smith *et al.,* 1994), or increased porosity of the acid washed coal (Ahmad *et al.*, 2009a). It was reported in previous studies that some minerals decompose at lower temperatures due to coal-mineral interactions, than when they were analysed individually by TG analysis (Nath *et al.,* 2011; Vassileva & Vassilev, 2006). This may also be attributed to the fact that primary pyrolysis continues up until temperatures of 690°C (Singh *et al.,* 2012; Saikia *et al.,* 2009; Cai *et al.,* 2008; Kabe *et al.,* 2004), during which the TWD fraction shows a greater mass loss than observed for the AW TWD fraction (TG analyses, Section 3.8.1), and as observed for the char yields (Section 5.2.4).

5.2.3. Tar yield

A change in the physical appearance of the derived tars was observed after acid washing, i.e. tars derived from the TWD fraction were black and gummy in appearance, whilst tars derived from the AW TWD fraction were light to dark brown and powdery (Morgan and Jenkins, 1986b). The tar yields were markedly lower after acid washing (Figure 5-2c), i.e. 50% lower for the experiments carried out up to 520°C, 30% lower for the experiments carried out up to

750°C, and 25% lower for the experiments carried out up to 900°C. This result is consistent with previous findings (Sert *et al.,* 2011; Nisar *et al.*, 2011; Ahmad *et al.,* 2009a; Ahmad *et al.,* 2009b).

The reduction in tar yield after acid washing is attributed to hydrogen transfer occurring between the liquid and solid phases during pyrolysis. The liquid yields (tar and water) produced during pyrolysis, are highly dependent on hydrogen transfer. Inorganic matter, (such as minerals), ensures higher hydrogen transfer, thus stabilizing the free radicals formed during thermal shock, causing increased product release and the minimization of re-solidification to char, thus forming more liquid products (Ahmad *et al.,* 2009a; Ishihara *et al.,* 2004; Solomon *et al.,* 1990; Solomon *et al.,* 1988). In the absence of inorganic matter, the free radicals are not effectively capped, disproportionated and stabilised, i.e. the free radicals recombine retrogressively and form char (Ahmad *et al.,* 2009a; Ishihara *et al.,* 2004; McMillen *et al.,*1989). Sert *et al.* (2011) determined that the negative effect on amounts of liquid products and increase in gas yields after acid treatment with HCl could be attributed to the cracking of liquid products.

5.2.4. Char yield

From Figure 5-2d it can be observed that for the experiments carried out up to 520°C that the char yields were 77.1 wt% vs. 77.9 wt%, for the experiments carried out up to 750°C 72.9 wt% vs. 73.4 wt%, and for the experiments carried out up to 900°C 72.2 wt% vs. 71.5 wt%, for the TWD and AW TWD fractions, respectively. There is thus no significant difference in char yields between the two fractions, consistent with previous results (Nisar *et al.,* 2011; Ahmad *et al.,* 2009b). However, the differences observed between the char yields at the various temperatures were larger for the TWD fraction between 520°C and 750°C than for the AW TWD fraction (4.2 wt% vs. 3.5 wt%), whilst between 750°C and 900°C, the difference was only 1.9 wt% for AW TWD, and only 0.7 wt% for the TWD fraction. This is in accordance with observations made from the TG analyses (Section 3.9) and other authors, who stated that a shift in pyrolysis range was observed after acid washing (Smith *et al.,* 1994).

Other previous studies found an increase in char yields during pyrolysis of acid washed coals. This was attributed to the retrogressive recombination of free radicals due to the absence of inorganic elements, accompanied by char formation (Ahmad *et al.,* 2009a; Samaras *et al.,* 1996; Solomon *et al.,* 1990; Solomon *et al.,* 1988, Hippo & Walker, 1975). Ahmad *et al.* (2009a) did however not compare their coal samples on a dry, mineral-matter-free basis, but simply reported the results (as determined yields) from the pyrolyser furnace used during flash pyrolysis. The basis on which results are reported has a large effect on the trends observed, but unfortunately results from previous studies are often difficult to relate to in the context of

this study, because the basis on which the earlier results are reported is not always clear. The char yields are reported on a mineral-matter-free basis in Table C-3, Appendix C-1, for the TWD fraction, the yield for the 520°C experiments is 70.9 wt% for the 750°C experiments it is 66.7 wt%, and for the 900°C experiments it is 65.8 wt%, whilst for the AW TWD fraction the yields at the same temperatures are 74.3 wt%, 70.0 wt% and 68.4 wt% respectively. Thus, the AW TWD fraction indicates larger char yields than observed for the TWD coal when compared on a mineral-matter-free basis, consistent with previous findings (Ahmad *et al.,* 2009a; Solomon *et al.,* 1990; Solomon *et al.,* 1988).

5.3. Gas composition

Gas chromatography (GC) analyses were carried out on the captured gas fractions for the various pyrolysis experiments. All results reported were normalised on a N_2 and O_2 free basis. The most common gases evolved at all temperatures for both fractions included H_2, CO, CO_2, CH_4, C_2s and C_3s (Fuentes-Cano *et al.,* 2013; Reichel *et al.*, 2013; Neves *et al.,* 2011; Gómez-Barea *et al.*, 2010; Zhang *et al.,* 2010; Wang et al., 2013; Wen *et al.,* 2009, Mill, 2000; Hayashi *et al.,* 1992; Xu & Tomita, 1989; Nelson *et al.,* 1988). The C_2s and C_3s identified included: ethane (C_2H_6), ethylene (C_2H_4), propane (C_3H_6) and propylene (C_3H_4) as well as C_4s which included gases such as butane, iso-butane, n-butane, butadiene, etc. Of the other gases ethylene and ethane were most prominent in that order. The C_4s was only identified in small amounts in some cases. At elevated temperatures, the dominant gas species is H_2 in all cases. Appendix C-2 provides the full set of GC results. For the sake of brevity, the focus will be on the most dominant gas species and the yields of the various gas species on a [g gas species] / [g coal (d.m.m.f.)] as determined by the use of Equation (4-6).

Table 5-1 Molar composition of most dominant gas species evolved at 520°C, 750°C and 900°C

	TWD			AW TWD		
	mol. %					
	520°C	**750°C**	**900°C**	**520°C**	**750°C**	**900°C**
H_2	17.7 - 20.4	29.0 - 34.0	37.7 - 38.6	20.9 - 25.3	37.7 - 38.6	43.8 - 46.8
CH_4	30.5 - 32.8	25.2 - 27.3	19.6 - 21.9	35.3 - 38.8	26.8 - 27.1	27.6 - 29.7
CO	21.0 - 25.3	25.2 - 26.2	26.8 - 27.1	13.3 - 14.9	13.6 - 15.6	11.3 - 13.8
CO_2	19.8 - 20.0	11.6 - 12.7	10.2 - 11.8	17.4 - 19.4	10.2 - 11.8	8.1 - 11.2

Table 5-1 presents the results (mol.%) of the dominant evolved gases (H_2, CO, CO_2 and CH_4) at the respective pyrolysis temperatures, consistent with previous findings (Fuentes-Cano *et al.,* 2013; Neves *et al.,* 2011; Zhang *et al.,* 2010; Wang et al., 2013; Wen *et al.,* 2009; Mill, 2000; Xu & Tomita, 1989; Nelson *et al.,* 1988). For the TWD fraction, the dominant gases in order of amounts observed were found to be: CH_4>CO>CO_2>H_2 for the 520°C experiments;

H_2> CH_4>CO >CO_2 for the 750°C experiments, and H_2>CO>CH_4 >CO_2 for the 900°C experiments. The change in order of most prominent dominant gases observed for the TWD fraction was consistent with observations made with other raw coals (Fuentes-Cano *et al.,* 2013; Neves *et al.,* 2011; Chen *et al.,* 2010; Wen *et al.,* 2009; Cui *et al.,* 2006; Smith *et al.,* 1994; Xu & Tomita, 1989; Khan, 1989). For the AW TWD fraction, the order of most abundant gases was CH_4>H_2>CO_2>CO for the 520°C experiments, and H_2>CH_4>CO>CO_2 for the 750°C and 900°C experiments. The yields of ethane (C_2H_6) and ethylene (C_2H_4) decreased with an increase in temperature, whilst the other gases showed no significant changes with an increase in final pyrolysis temperature for both the TWD and AW TWD derived gases (not shown here). The gas yields for the TWD and AW TWD fractions with regard to the various gas species will now be discussed on a quantitative basis.

5.3.1. H_2 yield

Both the TWD and AW TWD fractions show an increase in H_2 yield with an increase in final pyrolysis temperature (Fuentes-Cano *et al.,* 2013; Reichel *et al.*, 2013; Neves *et al.,* 2011; Gómez-Barea *et al.*, 2010; Zhang *et al.,* 2010; Wang et al., 2013; Wen *et al.,* 2009, Mill, 2000; Hayashi *et al.,* 1992; Xu & Tomita, 1989; Nelson *et al.,* 1988, Franklin, 1980; Anthony, 1974). The increased yield of H_2 at higher temperatures is related to the cracking of CH_4 at temperatures in excess of 725°C, where it is unstable (Siva *et al.,* 2013; Khan, 1989).

From Table 5-1 it is evident that evolved gases at the higher temperatures consist predominantly of H_2 (mol.%). From Figure 5-3a it can be observed that the H_2 yield of the AW TWD fraction was higher at all temperatures when compared to that of the TWD fraction, in accordance with previous studies (Sert *et al.,* 2011). With an increase in final pyrolysis temperature, the difference in H_2 yield between the two samples increases even further. This result is in disagreement with findings reported by Solomon *et al.,* (1990) and Franklin *et al.* (1983). These authors did however report increased tar yields, with either a decrease or no significant change in the overall gas yield; thus it can be assumed that the reaction mechanism for the coals studied differed from this study.

The difference in H_2 yield between the TWD and AW TWD coal fractions can possibly be attributed to four causes: i) the cracking of heavier hydrocarbons (Fuentes-Cano *et al.,* 2013; Khan, 1989); ii) the re-arrangement and condensing of aromatic structures and the direct de-hydrogenation of the formed chars (Siva *et al.,* 2013; Uzun *et al.,* 2007; Williams & Taylor, 1993; Cypress & Bettens, 1989); iii) the bond stabilisation after scission of very weak aliphatic (C-H) bonds (Smith *et al.* 1994; Abbot and Wojciechowski, 1988); and, iv) lower hydrogen

transfer (Ahmad *et al.,* 2009a; Ishihara *et al.,* 2004; Solomon *et al.,* 1990; Solomon *et al.,* 1988).

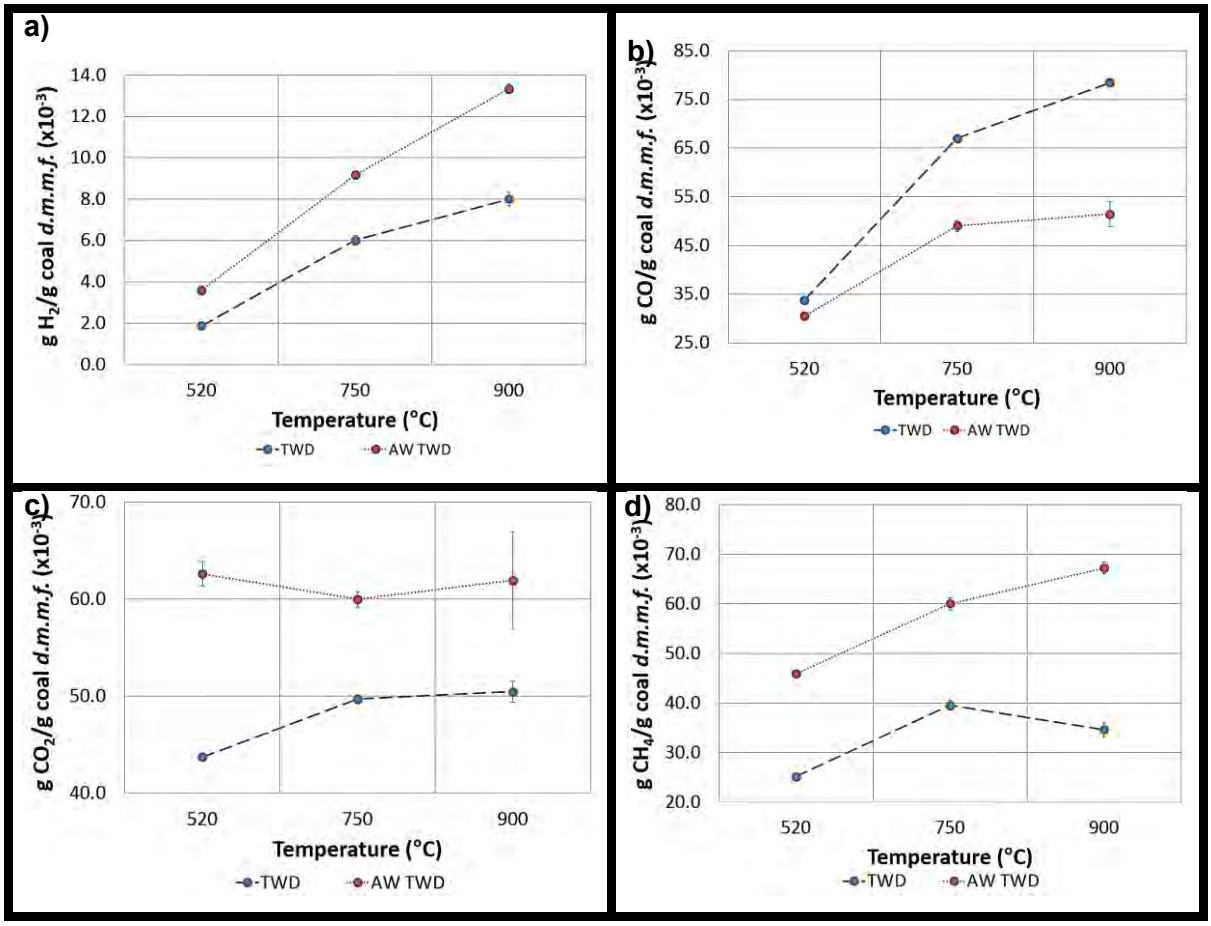

Figure 5-3 a) H_2, b) CO, c) CO_2 and d) CH_4 yields for TWD and AW TWD coals.

5.3.2. CO yield

CO formation has been attributed to various routes which include: the decomposition of carbonyl groups at temperatures below 400°C (Zhu *et al.,* 1998); in excess of 500°C the rupture of oxygen heterocycles (Zhu *et al.,* 2000); the de-hydrogenation of hydroxyl groups (Zhu *et al.,* 2000); and at temperatures exceeding 700°C, the initiation of CO_2 gasification (Wang *et al.,* 2005; Smith *et al.,* 1994). In Figure 5-3b both the TWD and AW TWD fractions show an increase in CO yield with an increase in final pyrolysis temperature (Fuentes-Cano *et al.,*2013). The increase between 750°C and 900°C for the AW TWD can however be regarded as insignificant; thus it indicates that the maximum CO yield has already been formed for the 750°C experiments, i.e. no significant amounts of CO is evolved between 750°C and 900°C. The higher yield of CO observed for the TWD fraction can be regarded as significant at all final pyrolysis temperatures.

The higher CO yields observed for the TWD fraction is indicative of the presence of more oxygen functionalities within the coal (Chen *et al.,* 2010) and is consistent with findings by

Franklin *et al.* (1983) and Solomon *et al.* (1990). This is consistent with the DRIFT analyses results (Section 3.8.1) which showed a decrease in oxygen functionalities after acid washing, specifically in the range 1300 to 1000 cm^{-1}, which are attributed to C-O stretching vibrations, of which some are related to minerals such as calcite and dolomite (Xin *et al.,* 2014; Van Niekerk *et al.,* 2008; Machnikowska *et al.,* 2002; Barth *et al.,* 1994; Painter *et al.,* 1981). The AW TWD fraction has also been shown to contain less hydroxyl groups, i.e. the derivation of CO by de-hydrogenation of these groups are less likely. The removal of minerals such as calcite and dolomite minerals, which form CO_2 upon decomposition, will also make the chance of CO_2 gasification, if possible, taking place less likely.

5.3.3. CO_2 yield

Figure 5-3c indicates an increase in CO_2 yield for the TWD fraction with an increase in pyrolysis temperature up to 750°C, but no significant difference between the yields produced for the 750°C and 900°C experiments (Fuentes-Cano *et al.,* 2013; Mill, 2000). This initial increase in CO_2 yield can be attributed to the decomposition of carboxyl functionalities (Ziong *et al.,* 2010; Cui *et al.,* 2006; Wang *et al.,* 2005; Zhu *et al.,* 2000; Murakami *et al.,* 1997), as well as the decomposition of the carbonate mineral species, calcite and dolomite (Campbell & Stephens, 1976). For the AW TWD fraction, the yields at all final pyrolysis temperatures are within repeatability limits.

Comparison of the CO_2 yields obtained from the TWD coal and that of the AW TWD coal indicates that the CO_2 yield of the AW TWD fraction is higher than that of TWD fraction at all temperatures. This is in contrast with previous findings (Solomon *et al.,* 1990; Franklin *et al.,* 1983). However, in previous studies, acid washed coals showed less crosslinking, to which the increased tar yield and decrease in CO_2 yield was attributed (Ibarra *et al.,* 1991; Deshpande *et al.,* 1988). This may explain the anomalies in the current investigation. The cracking and reforming of light hydrocarbons present in the tar will also attribute to the CO_2 and CO yield (Fuentes-Cano *et al.,* 2013). In the case of the AW TWD fraction, it seems as if most of this cracking and reforming of light hydrocarbons in the tar may be due to CO_2, which may explain this discrepancy.

The focus needs to be placed on the water-gas shift reaction, Equation 5-1:

$$CO(g) + H_2O(g) \rightleftharpoons CO_2(g) + H_2(g) \quad (5\text{-}1)$$

For the TWD coal fraction higher water and CO yields were observed, whilst for the AW TWD coal fraction increased CO_2 and H_2 yields were observed. This possibly suggests that a shift in equilibrium took place after acid washing, thus favouring the right hand-side of the equation, causing shifts in product yields.

5.3.4. CH_4 yield

An increase in CH_4 yield is observed for the AW TWD fraction at all final pyrolysis temperatures (Figure 5-3d) (Fuentes-Cano *et al.,* 2013). For the TWD fraction, an increase in CH_4 yield is observed up to 750°C after which the CH_4 yield decreases significantly. The CH_4 yield of the AW TWD coal is also observed to be much higher than that of the TWD fraction at all temperatures, in accordance with previous studies (Reichel *et al.,* 2013; Sert *et al.,* 2011).

The decomposition of hydro-aromatic and/or methyl groups are mainly responsible for the formation of CH_4 (Charpenay *et al.,* 1996). The presence of CH_4 as the dominant gas at an experimental temperature of up to 520°C is indicative of the decomposition and/or hydrogenation of the methyl side chains on the parent coal or formed tars (Cui *et al.*, 2006). The formation of CH_4 at increased temperatures is attributed to the cross-linking reactions of coal macromolecules and/or the cracking of saturated hydrocarbons (Cui *et al.,* 2006). This was observed for the AW TWD coal sample in the 750°C and 900°C experiments. De-alkylation reactions due to decomposition of primary tars above 600°C have been found to be a source of CH_4 (Fuentes-Cano *et al.,* 2013; Milne *et al.,* 1998), thus suggesting that the lower tar yields observed for the TWD coal at increased final pyrolysis temperature, may be due to this reaction. The overall higher CH_4 content observed for the AW TWD coal when compared to the yield of the TWD fraction can also be related to this process.

5.3.5. Other gas species

The gas species C_2H_4, C_2H_6, C_3H_4, C_3H_6 and the C_4s constitute a small fraction of the total gas composition. Of these gases, the saturated alkane species, C_2H_6 is the most prominent. The yields of these gases and the formation of light oil compounds during pyrolysis were also observed to be related (Franklin *et al.,* 1982b). The formation of these compounds are attributed to the cracking of tars and long-chain aliphatic hydrocarbons to produce short chain alkenes (Fuentes-Cano *et al.,* 2013; Cui *et al.,* 2006; Gavalas, 1982). Short alkene gases, such as C_2H_4 and C_3H_4 were observed to increase in yield with an increase in temperature, with a maximum yield being obtained at 650°C (Cui *et al.,* 2006). The decomposition of the alkane compounds is said to form alkene and H_2 due to the thermal stability of the olefins (Cui *et al.,* 2006; Gavalas, 1982). The saturated hydrocarbon species (ethane and C_3) form due to dealkylation of substituted aromatic molecules and the breakage of long chain tars, whilst the unsaturated hydrocarbon species (ethylene and acetylene) are due to dehydrogenation reactions of small saturated hydrocarbons and the decomposition of primary tars at increased temperatures (Fuentes-Cano *et al.,* 2013; Hayashi *et al.,* 1992).

With regard to the C_2H_4 and C_2H_6 yields obtained in this study (Figure 5-4a and Figure 5-4b), it was observed that both samples showed no significant change in yields with an increase in

final pyrolysis temperature when the 95% confidence intervals were taken into account. Thus the maximum amounts of C_2H_4 and of C_2H_6 were formed up to 520°C, as a decrease between 750°C and 900°C was observed.

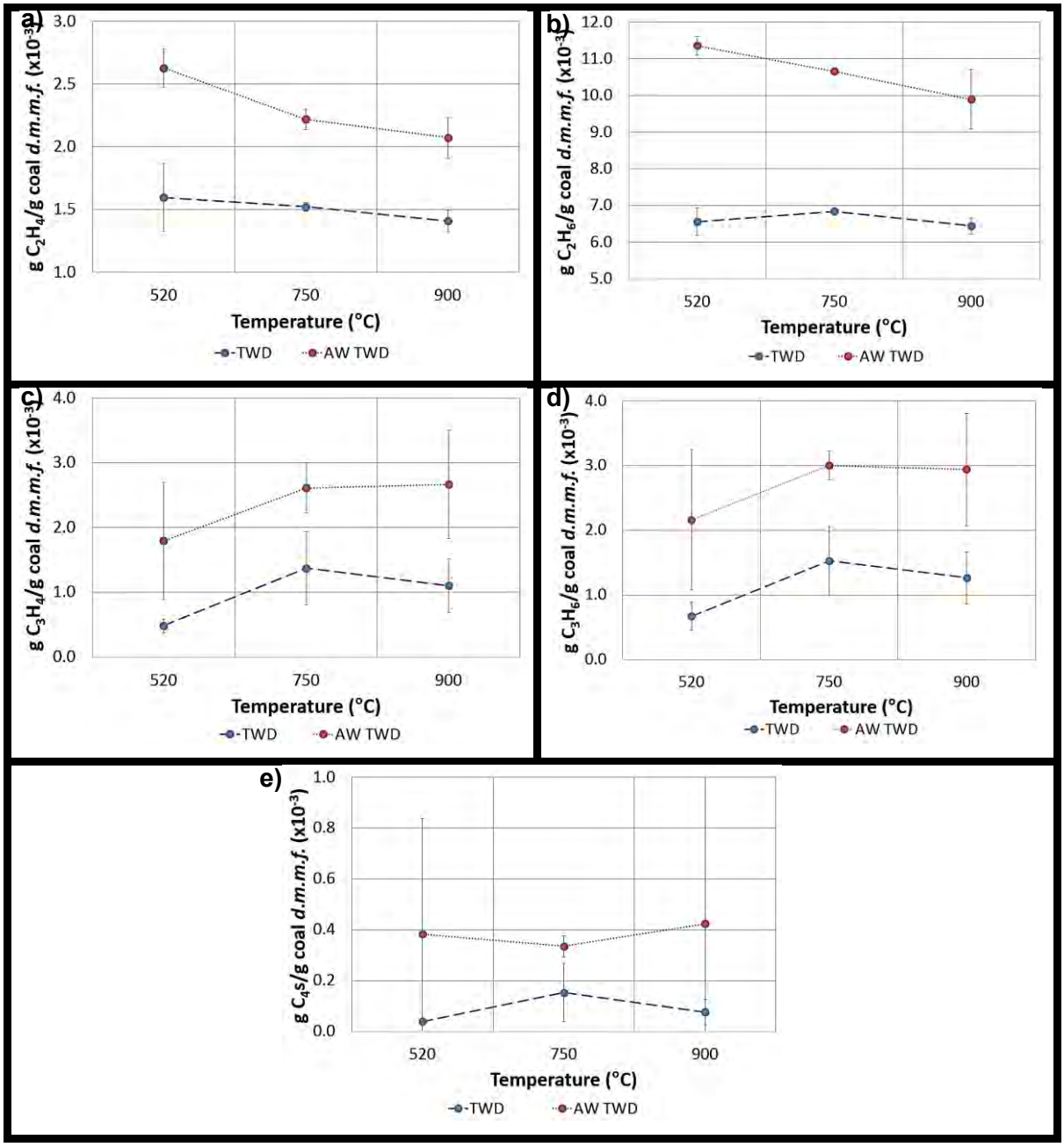

Figure 5-4 a) C_2H_4, b) C_2H_6, c) C_3H_4, d) C_3H_6 and e) C_4s yields for TWD and AW TWD coals.

With regard to the C_3H_4 yield (Figure 5-4c), the AW TWD fraction indicates no significant change in yield with an increase in final pyrolysis temperature, thus the maximum amount of C_3H_4 was formed up to 520°C. The TWD fraction however indicates an increase in the yield of C_3H_4 and C_3H_6 with an increase in final pyrolysis temperature between 520°C and 750°C. With regard to the C_3H_6 yields, the same trend is observed as for the C_3H_4 species. The AW

TWD fraction indicates no significant change in C_3H_6 yield with an increase in final pyrolysis temperature when the 95% confidence interval limits are taken into account. These results are in agreement with the findings of Fuentes-Cano *et al.* (2013) regarding C_3 and C_2 gases.

The C_4s species constitute a very small part of the gas yield for both fractions. Yields are observed to vary between 0.0 and 0.2 x 10^{-3} g C_4s per gram coal (d.m.m.f.) for the TWD fraction; and between 0.3 and 0.4 x 10^{-3} g C_4s per gram coal (d.m.m.f.) for the AW TWD fraction. No significant change is observed with an increase in temperature for the AW TWD fraction, but the TWD fraction indicates a significant increase in these compounds between 520°C and 750°C (Figure 5-4e). The yield of these gases is higher for the AW TWD fraction in all the cases, except for the C_4s, when compared to that of the TWD fraction. The higher yields of these gases for the AW TWD coal fraction are possibly related to the cracking of primary tars (Fuentes-Cano *et al.,* 2013; Cui *et al.,* 2006; Gavalas, 1982)

5.4. Tar composition

The tar composition was analysed by Simdis, GC-MS and FID and SEC-UV analyses.

5.4.1. Simulated distillation (Simdis)

Simulated distillation (Simdis) is a standard test to classify coal tar into a manageable number of components based on boiling point distribution (Li, *et al.*, 2010; Ukwuoma, 2002). The derived tars of the various pyrolysis experiments were each analysed and the averages of the results determined, the WABP is reported within a 95% confidence interval. Refer to Appendix C-3 for repeatability curves. The boiling points of the derived tars were confined to the region 112.2°C – 525°C.

The boiling point distributions for the derived tars of the TWD and AW TWD fractions are indicated in Figure 5-5. The boiling point distribution curves indicate that no compounds were identified with boiling points below 100°C. These compounds were already removed by the water and tar removal processes prior to analysis. The tars derived from the TWD fraction (Figure 5-5a) indicates more consistency in composition than that observed for the tars derived from the AW TWD fraction (Figure 5-5b). For the TWD tar it can be observed that the yields derived at a final pyrolysis temperature of 520°C and 750°C correspond very well.

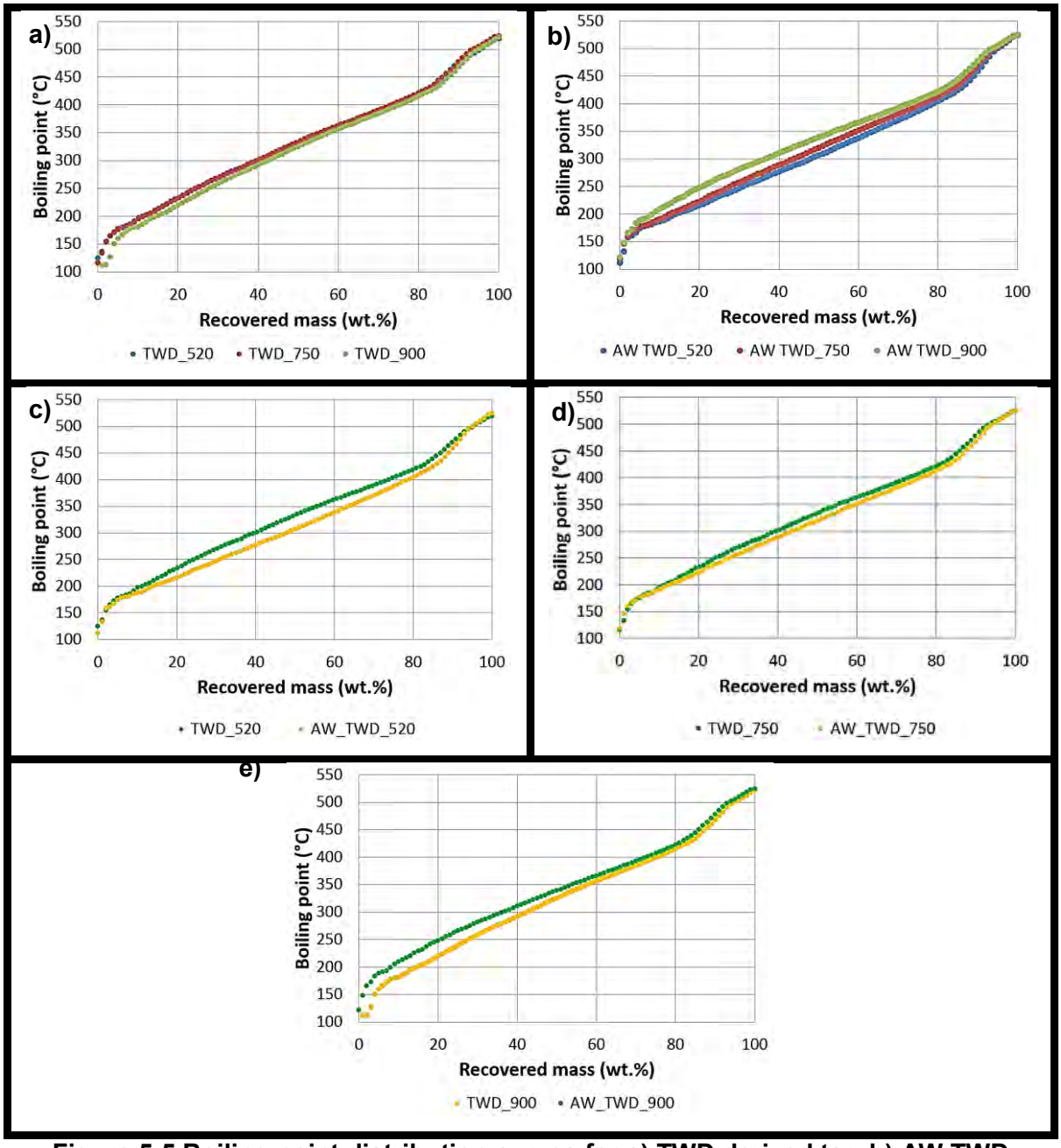

Figure 5-5 Boiling point distribution curves for a) TWD derived tar; b) AW TWD derived tar; TWD vs. AW TWD tars at c) 520°C; d) 750°C and e) 900°C.

The tar derived up to a final pyrolysis temperature of 900°C seems to contain more material boiling off at lower temperatures (the variation is however small), and the tars derived at all three temperatures seem consistent in composition. On the other hand, for the AW TWD fraction, the tars derived up until the higher final pyrolysis temperatures consist of higher boiling point compounds, especially for the tar derived up to a final pyrolysis temperature of 900°C. The boiling point distributions observed are in accordance with typical fossil fuel and waste-derived tars and oils as observed in previous studies (Roets *et al.,* 2014; Bean 2013; Hattingh, 2012; Lee, 2009; Karayildirim *et al.,* 2006; Shie *et al.,* 2003; Li *et al.,* 2001; Bunger 1976). Further comparison of Simdis results is done according to the weight, average boiling

point calculation as mentioned in Section 4.2.3.1, and as used in previous studies (Roets *et al.,* 2014; Bean, 2013; Siva *et al.,* 2013; Hattingh, 2012; Rafenomanantsoa e*t al.*, 1998; Bakr, *et al.,* 1996; Gibbins-Matham & Kandiyoti, 1988).

Table 5-2 Boiling point distributions for tars based on crude oil fractions

Boiling point range (°C)		TWD	TWD	AW TWD	AW TWD
		wt%/°C	g/100 g coal (d.m.m.f)	wt%/°C	g/100 g coal (d.m.m.f)
520°C					
Medium naphtha	79-121	0.5	0.10	1.0	0.10
Heavy naphtha	121-191	7.6	0.80	10.2	0.50
Kerosene	191-277	23.2	2.50	29.6	1.50
Distillate fuel oil	277-343	21.2	2.30	21.4	1.10
Light vacuum gas oil	343-455	34.4	3.70	28.6	1.50
Heavy vacuum gas oil	455-566	13.1	1.40	9.2	0.50
IBP	-	112.2	-	112.2	-
WABP	100 - 550	326 - 336	-	302 - 326	-
FBP	-	519.4	-	524.3	-
750°C					
Medium naphtha	79-121	1.0	0.10	1.0	0.10
Heavy naphtha	121-191	8.1	0.70	8.0	0.50
Kerosene	191-277	22.2	2.00	26.0	1.60
Distillate fuel oil	277-343	21.2	1.90	20.0	1.20
Light vacuum gas oil	343-455	33.4	3.00	31.0	1.90
Heavy vacuum gas oil	455-566	14.1	1.30	14.0	0.90
IBP	-	112.2	-	112.2	-
WABP	100 - 550	327 - 341	-	318 -330	-
FBP	-	524.7	-	524.7	-
900°C					
Medium naphtha	79-121	1.7	0.20	0.8	0.10
Heavy naphtha	121-191	9.3	0.80	5.2	0.30
Kerosene	191-277	28.0	2.50	22.0	1.40
Distillate fuel oil	277-343	22.0	2.00	23.0	1.50
Light vacuum gas oil	343-455	28.0	2.50	35.0	2.20
Heavy vacuum gas oil	455-566	11.0	1.00	14.0	0.90
IBP	-	112.2	-	112.2	-
WABP	100 - 550	329 - 336	-	326 - 354	-
FBP	-	524.3	-	524.8	-

Table 5-2 indicates these results as well as the division of the boiling point distributions into cut fractions. The cut fractions were developed based on crude oil refining (Rand, 2003). The initial and final boiling point temperatures are also indicated in Table 5-2. The initial and final boiling point temperatures for all tars, (both TWD and AW TWD), correspond well with an initial boiling point of 112.2°C and final boiling point of around 524°C, except for the AW TWD tar derived at a final pyrolysis temperature of 520°C (519.4°C). Table 5-2 indicates that the heavy naphtha and kerosene crude fractions for this tar were significantly higher than that observed for the TWD fraction, i.e.10.2 vs 7.6 wt% and 29.6 vs. 23.2 wt%, respectively. With regard to

the WABP calculations, it can be observed that these values overlap for all derived tars. It can thus be observed that this parameter is highly influenced by the most prominent crude fractions, being distillate fuel oil and light vacuum gas oil.

It is evident from Table 5-2 that all derived tars contain considerable amounts of the higher boiling point fraction such as kerosene, heavy distillate oil, light- and heavy vacuum gas oil. The largest fraction (28.0 – 35.0 wt%) consisted of light vacuum gas oil, i.e. components having boiling points in the range 343 to 455°C. Comparison of the tars derived for the TWD fraction indicate that with an increase in final pyrolysis temperature more lighter components such as kerosene and heavy naphtha are present.

Thermal cracking is responsible for this shift to lighter fractions (Hattingh, 2012; King *et al.,* 1978; Bunger, 1976). For the AW TWD tar the inverse is observed, i.e. a decrease in the lighter fractions (heavy naphtha and kerosene) is observed with an increase in temperature. It was suggested that the pyrolysis range shifts to higher temperature ranges for acid washed coal (Smith *et al.,* 1994), as was observed from the pyrolysis product yield results obtained in this study. To obtain further insight, the boiling point distributions as indicated in Table 4-6 (Section 4.3.2.1) were used to calculate the amount of tar in a specific crude oil fraction per 100 g coal on a dry, mineral-matter-free basis.

From Table 5-2 it is evident that the TWD fraction yields more tar in every crude tar fraction, and it is also clear that the AW TWD fraction yields more components with a higher boiling point with increasing final pyrolysis temperature. The increase in tar yield observed with an increase in final pyrolysis temperature for the AW TWD fraction can almost wholly be attributed to the light vacuum gas oil fraction (343 – 455°C), with a small increase also in the distillate fuel (277 – 343°C) fraction. The shift to lower boiling point components for the TWD fraction is mainly due to a reduction in the light and heavy vacuum gas oil fractions, whilst the kerosene fraction indicates an increase at a final pyrolysis temperature of 900°C.

5.4.2. Gas chromatography-mass spectrometry and flame ionization detection (GC-MS and GC-FID)

The GC-MS analysis of the derived tars is expected to provide insight into the low molecular weight hydrocarbon species present, with boiling points below 300°C. From the Simdis results it is evident that a large fraction of the tar (~60 %) will not be identified by GC-MS, in accordance with previous findings (Bean, 2013; Hattingh, 2012; Sun *et al.,* 2012; Ledesma *et al.,* 2000; Nelson *et al.,* 1988).

Table 5-3 GC-MS and –FID results summarised

	TWD		AW TWD	
	wt%			
	Full spectrum	Aromatic spectrum	Full spectrum	Aromatic spectrum
520°C				
Aliphatic compounds	5.1 - 5.4	- - -	4.9 - 5.6	- - -
Alkyl-Benzenes	0.8 - 1.1	1.5 - 2.4	0.5 - 1.5	1.0 - 3.0
Alkyl-Phenols	36.6 - 39.4	75.2 - 79.5	39.3 - 40.5	77.1 - 80.0
Aromatic ethers and esters	0.4 - 2.1	0.9 - 4.1	1.1 - 1.7	2.3 - 3.3
Alkyl-Indenes	0.1 - 0.1	0.1 - 0.1	0.0 - 0.1	0.1 - 0.2
Alkyl-Naphthalenes	2.5 - 2.6	5.0 - 5.5	2.8 - 3.3	5.5 - 6.6
Poly-aromatic hydrocarbons	0.2 - 0.2	0.3 - 0.5	0.1 - 0.2	0.2 - 0.5
Nitrogen heteroatoms	5.7 - 6.5	12.1 - 12.8	4.6 - 5.7	9.2 - 11.0
Mixed aliphatic and aromatic compounds	43.6 - 47.5	- - -	42.1 - 45.7	- - -
750°C				
Aliphatic compounds	4.8 - 5.0	- - -	4.9 - 5.9	- - -
Alkyl-Benzenes	0.9 - 1.5	1.6 - 2.9	0.3 - 1.0	0.6 - 2.1
Alkyl-Phenols	40.5 - 45.1	78.4 - 79.6	37.0 - 39.0	77.5 - 80.0
Aromatic ethers and esters	0.5 - 1.1	1.0 - 1.9	0.3 - 1.1	0.7 - 2.3
Alkyl-Indenes	0.0 - 0.1	0.0 - 0.2	0.0 - 0.1	0.0 - 0.2
Alkyl-Naphthalenes	2.9 - 3.1	5.4 - 5.7	2.9 - 3.1	6.0 - 6.4
Poly-aromatic hydrocarbons	0.0 - 0.3	0.1 - 0.5	0.1 - 0.3	0.2 - 0.6
Nitrogen heteroatoms	5.7 - 6.6	11.0 - 11.7	4.8 - 6.6	10.1 - 13.4
Mixed aliphatic and aromatic compounds	38.3 - 43.6	- - -	44.9 - 47.7	- - -
900°C				
Aliphatic compounds	4.7 - 5.2	- - -	5.2 - 6.4	- - -
Alkyl-Benzenes	1.3 - 2.2	2.5 - 4.3	0.3 - 0.5	0.6 - 1.2
Alkyl-Phenols	35.7 - 39.8	72.4 - 76.4	36.4 - 37.2	78.5 - 84.2
Aromatic ethers and esters	1.7 - 3.2	3.2 - 6.4	0.3 - 0.8	0.6 - 1.6
Alkyl-Indenes	0.1 - 0.1	0.2 - 0.3	0.0 - 0.0	0.0 - 0.1
Alkyl-Naphthalenes	2.8 - 2.9	5.4 - 5.9	0.9 - 2.9	2.2 - 6.2
Poly-aromatic hydrocarbons	0.2 - 0.3	0.5 - 0.7	0.1 - 0.2	0.3 - 0.4
Nitrogen heteroatoms	4.9 - 6.3	9.9 - 12.1	5.2 - 5.7	11.6 - 12.5
Mixed aliphatic and aromatic compounds	42.4 - 46.3	- - -	49.0 - 49.9	- - -

GC-MS provides semi-quantitative data for the detected peaks as identified by FID. The results were normalised on a solvent-free basis to a 100 wt% of the sample analysed. Results reported in Table 5-3 were summarised based on the molecular families as identified in Table 4-7 (Section 4.3.2.2).

The aromatic spectrum is reported separately due to the commercial importance of some of the identified groups, such as the alkyl-benzenes, alkyl-phenols and alkyl-naphthalenes (Jiang *et al.,* 2007; Menéndez *et al*., 2000; Schobert & Song, 2002; Speight, 1994; Schobert, 1990). All results are reported within a 95% confidence interval, as calculated from standard deviation values for four repeat experiments. Discussion of full spectrum results will focus on the aliphatic and mixed aliphatic and aromatic compounds, whilst discussion of the aromatic spectrum will focus on the other molecular families identified. Refer to Appendix C-4 for GC-MS and –FID data with indicated confidence intervals.

5.4.2.1. Full spectrum

Table 5-3 indicates the full spectrum results as identified by GC-MS analysis. For the TWD tar, no difference in yields of aliphatic compounds and mixed aliphatic and aromatic compounds are observed with an increase in final pyrolysis temperature. For the AW TWD fraction tar, the yield of aliphatic compounds ranges between 4.9 and 6.4 wt%. The mixed aliphatic and aromatic components do however show a tendency to increase with an increase in final pyrolysis temperature, 42.1 to 45.7 wt% for the 520°C experiments, 44.9 to 47.7 wt% for the 750°C experiments and 49.0 to 49.9 wt% for the 900°C experiments.

Comparison of the derived tars from the TWD and AW TWD fraction indicates that the yield of aliphatic compounds corresponds for both fractions. The yields of mixed aliphatic and aromatic components for the AW TWD fraction are higher than that of the TWD fraction in the 750°C and 900°C experiments, i.e. 44.9 to 47.7 wt% vs. 38.3 to 43.6 wt% and 49.0 to 49.9 wt% vs. 42.4 to 46.3 wt%, respectively. The results of the aliphatic compounds are indicative of these compounds having formed at temperatures below 520°C for both fractions, and therefore no change is observed. This result is consistent with previous findings (Wang *et al.,* 2013; Jones *et al.,* 2005; Nelson & Tyler, 1988).

The tars derived at a temperature below 600°C can be classified as primary tars (Fuentes-Cano *et al.,* 2013; Casal *et al.,* 2008; Solomon *et al.,* 1993; Khan, 1989; Evans & Milne, 1987, Gavalas, 1982; Lowry, 1963), whilst those derived above 600°C can be classified as secondary tars, which will be more aromatic in structure due to decomposition of the thermally unstable primary tar compounds to gas and other tars (Zhang *et al.,* 2010; Casal *et al.,* 2008; Jones *et al.,* 2005; Morf *et al.,* 2002, Jess *et al.,* 1996). No definite conclusions can however be made with regard to the mixed aliphatic and aromatic compounds due to co-elution. It is

suggested that future work should conduct GC-MS analyses in order to prevent co-elution of these molecular compounds.

5.4.2.2. Aromatic spectrum

Increase in final pyrolysis temperature

Conversion of aromatic tar species during pyrolysis is a sequential process involving various reactions (Fuentes-Cano *et al.,* 2013; Ledesma *et al.,* 2002). Primary tars produce mono-aromatic compounds through breakage and decarboxylation of primary tars (Fuentes-Cano *et al.,* 2013; Cypres, 1987), and Diels-Alder reactions with small unsaturated hydrocarbons, followed by dehydrogenation (Fuentes-Cano *et al.,* 2013; Ledesma *et al.,* 2002; Morf *et al.,* 2002; Cypres, 1987). Above 750°C, the mono-aromatic compounds are further converted by direct combination of two aromatic species to produce dimers (Fuentes-Cano *et al.,* 2013; Morf *et al.,* 2002; Ledesma *et al.,* 2000; Bruinsma *et al.,* 1989; Cypres, 1987). The addition of light, unsaturated hydrocarbons to aromatic rings which can lead to PAH formation and growth (Fuentes-Cano *et al.,*2013; Thomas *et al.,* 2007; Morf *et al.,* 2002; Ledesma *et al.,* 2000), thus producing heavy tars, also occurs. Dealkylation and dehydroxylation reactions are another route of conversion which leads to the formation of lower aromatic molecules such as benzene (Fuentes-Cano *et al.,* 2013; Ledesma *et al.,* 2002; Taralas *et al.,* 2003; Jess, 1996).

The increase in alkyl-benzene, alkyl-indene and alkyl-naphthalene families with an increase in final pyrolysis temperature observed for the TWD derived tar, is attributed to the severity of pyrolysis at increased temperatures and the cleavage of more aromatic bridge structures (Tang *et al.*, 2014; Hattingh, 2012; Nelson *et al.,* 1988). The maximum yields of substituted aromatic structures are said to form at around 850°C, where after a significant decrease in these compounds will be observed with an increase in temperature (Nelson *et al.,* 1988). The yields of alkyl-substituted benzenes and naphthalenes could have been larger, but decomposition to CH_4 and parent aromatics, i.e. benzene and naphthalene is probable due to transport limitations (Gräber & Hüttinger, 1982), and this could have attributed to the increase in CH_4 yields observed from the gas analyses (Section 5.3.4.). In the case of the AW TWD fraction tar, this seems likely and therefore explains the higher CH_4 yield observed, whilst the yields of alkyl-benzenes decrease with an increase in final pyrolysis temperature. No significant change is observed in alkyl-indene and alkyl-naphthalene yields with increasing final pyrolysis temperature.

The alkyl-phenol compounds were found to be the most prominent molecular family in the aromatic spectrum, in accordance with previous studies (Roets *et al.,* 2014; Wang *et al.,* 2013; Bean, 2013; Hattingh, 2012; Sun *et al.,* 2012; Casal *et al.,* 2008; Lazaro *et al.,* 2001). The

phenolic nature of the tars is related to the most prominent maceral found in the TWD and AW TWD fractions, namely vitrinite (Iglesias *et al.,* 2001; Hartgers *et al.,* 1994). The alkyl-phenol compounds decrease with an increase in final pyrolysis temperature for the TWD derived tar. This was observed in previous studies as well (Hattingh, 2012; Nelson *et al.,* 1988). It is expected as the oxygen functionalities are eliminated from the coal structure with an increase in pyrolysis temperature (Casal *et al.,* 2008). The AW TWD derived tars do however indicate an increase in these compounds with an increase in final pyrolysis temperature, i.e. this can be related to the difference in CO yields (Section 5.3.2) observed for the two coals. These species were found to decompose via decarbonylation to form CO and cyclopentadiene (C_5H_6) at temperatures ranging between 665°C and 865°C (Fuentes-Cano *et al.,* 2013; Morf *et al.,* 2002; Sharma & Hajaligol, 2003; Nelson *et al.,* 1988; Cypres, 1987; Cypres & Bettens, 1974 and 1975). The cyclopentadiene may further react to produce high molecular weight tars by dimerization (Fuentes-Cano *et al.,* 2013; Morf *et al.,* 2002; Sharma & Hajaligol, 2003), or form low molecular weight hydrocarbons due to decomposition (Fuentes-Cano *et al.,*2013; Scheer *et al.,* 2011 & 2010; Ledesma *et al.,* 2002). Aromatic rings can in turn be produced via Diels Alder reactions at high temperatures from the light unsaturated hydrocarbons. Light hydrocarbon gases such as propene may influence this transformation (Fuentes-Cano *et al.,* 2013; Ledesma *et al.,* 2002, Horne & Williams, 1996; Williams & Taylor, 1993).

TWD coal tar indicates lower yields of alkyl-phenols with an increase in final pyrolysis temperature, thus forming CO due to secondary decomposition reactions, whilst the AW TWD fraction tar shows increased yields, with no significant change in CO yield between 750°C and 900°C. It was also found that CH_4 could take part in the formation of phenols. The presence of free radicals such as CH_3 can lead to cresol and alkyl-substituted phenol formation during the CO_2 reforming methane process, which will lead to a decrease in the ratio of phenols to alkyl-substituted phenols (Wang *et al.,* 2013; Naito *et al.,* 2005; Wei *et al.,* 2004; Hu *et al.,* 1998). Table 5-4 indicates the phenol / alkyl-substituted phenol ratios of the derived tars for the two coals at the different final pyrolysis temperatures. The only significant difference was observed at the final pyrolysis temperature of 900°C, with the AW TWD fraction producing more alkyl-substituted phenols. At this temperature the CH_4 yield for the AW TWD fraction further increased, whilst for the TWD fraction a decrease was observed in the CH_4 yield.

No trend was observed in the amounts of aromatic ethers and esters with an increase in final pyrolysis temperature for the TWD fraction derived tars, but for the AW TWD fraction derived tar a decrease in these compounds was observed with an increase in final pyrolysis temperature between 520°C and 900°C.

Table 5-4 Ratios of phenols to alkyl-substituted phenols for TWD and AW TWD derived tars

	520°C	750°C	900°C
TWD	0.21	0.24	0.22
AW TWD	0.21	0.24	0.20

For the poly-aromatic hydrocarbon (PAH) group, there is an increase observed in these compounds for the tars derived from the TWD fraction at a final temperature of 900°C, i.e. 0.1 – 0.5 wt% vs. 0.5 – 0.7 wt% for the 520°C and 750°C experiments. This increase in PAH yield with an increase in final pyrolysis temperature is in accordance with previous findings (Fuentes-Cano *et al.,* 2013; Hattingh 2012; Nelson & Tyler, 1988; Nelson *et al.,* 1988). The AW TWD derived tars showed no significant change in PAHs with an increase in final pyrolysis temperature. The mechanism for PAH formation is unclear, but it has been found that PAHs can form from aromatic species such as toluene (Bruinsma *et al.,* 1989; Smith 1979; Badger, 1965); flames of acetylene and benzene (Homann & Wagner, 1967); ethylene and acetylene (Bruinsma *et al.,* 1989; Crittenden & Long, 1973); benzene (Bruinsma *et al.,* 1989), and butadiene (Cole *et al.,* 1973). It is also possible that PAHs can form directly from the parent coal structure (Hattingh, 2012).

For the nitrogen heteroatoms group, no significant change can be reported for both coal tars. The identified functionalities consisted mainly of pyridenes, analines and benzene amines (Hattingh, 2012). The nitrogen functionalities found in the tar fraction are related to aromatic structures in the coal such as pyridenes and pyrroles (Smith *et al.,* 1994; Chen *et al.,* 1990). No sulphur functionalities were identified. Most of the sulphur present within the coal structure is probably related to the sulphide minerals such as pyrite, and would mainly form H_2S gas during pyrolysis (Smith *et al.,* 1994). Sulphur functionalities will probably be better identifiable with techniques such as specialised GC-MS and XPS (X-ray photoelectron spectroscopy) (Hattingh, 2012).

TWD tar vs. AW TWD tar

Comparison of the tars derived from the TWD and AW TWD fractions indicates that the tars show good comparison between the 520°C and 750°C experiments for all families except in the case of the alkyl-indenes and nitrogen heteroatoms. For the 900°C experiments, there is variation between most of the groups. In the case of the alkyl benzenes, the AW TWD fraction tar yielded significantly less of these compounds in the 900°C experiments, i.e. 0.6 - 1.2 wt% vs. 2.5 - 4.3 wt% for TWD coal tar. For the alkyl-phenols the AW TWD tar yielded 80.5 - 84.2 wt%, whilst the TWD tar yielded only 72.4 - 76.4 wt%. Comparison of the aromatic ether and ester families indicates that a larger fraction of these compounds was present in tars derived

from the TWD coal, i.e. 3.2 - 6.4 wt% vs. 0.6 - 1.6 wt% for the AW TWD derived tar in the 900°C experiments. The alkyl-indenes are a small fraction of the analysed tar, yet the TWD derived tars do however show higher yields of alkyl-indenes, 0.2 - 0.3 wt% vs. 0.0 to 0.1 wt% for the AW TWD tars. More PAHs were present in the TWD fraction derived tars than in the AW TWD derived tars from the 900°C experiments, i.e. 0.5 - 0.7 wt% vs. 0.3 - 0.4 wt%. This result can be related to the higher gas yields, i.e. gases such as C_2H_4 in the case of the AW TWD coal, which may indicate increased cracking of long-chain hydrocarbons (Ledesma *et al.*, 2000; Calkins and Tyler, 1984; Ledesma *et al.,* 1998). Regarding the alkyl-naphthalene group, the AW TWD derived tars contained more of these components from the 520°C and 750°C experiments, i.e. 5.5 - 5.6 wt% vs. 5.0 - 5.4 wt% and 6.0 to 6.4 wt% vs. 5.4 - 5.7 wt%, respectively, when compared to the TWD derived tars. For the 900°C experiments, there is however no significant difference observed between the tars derived from the two coals with regard to the alkyl-naphthalene molecular family. The AW TWD derived tars produced less nitrogen heteroatom compounds from the 520°C experiments than for the TWD derived tars, i.e. 9.2 - 11.0 wt% vs. 12.1 - 12.8 wt%. In the case of the 750°C and 900°C experiments, no significant difference can be observed for these components between the derived tars.

5.4.3. Size exclusion chromatography (SEC-UV)

Size exclusion chromatography (SEC) is a useful analytical technique that has been used extensively in a number of studies to clarify the distribution of heteroatoms over a wide molecular size range (Trejo *et al.*, 2007; Kandiyoti *et al.,* 2006; Millan *et al.*, 2005; Herod *et al.,* 2003). SEC results will be reported as discussed in Section 4.4.2.3. Appendix C-5 includes all repeatability curves for the duplicate samples.

Table 5-5 summarises the obtained SEC results for the various derived tars. It is clear that the tars consisted of components between the molecular size ranges of 30 – 6000 Da. These observations are in accordance with previous studies (Fidalgo *et al.,* 2014; Hattingh, 2012; Mokoena *et al.,* 2008; Adegoroye *et al.,* 2004; Mill, 2000; John *et al.,* 1994; Li *et al.,* 1993a). With the use of NMP as eluent, the aliphatic species are not included in the observation, due to low solubility. Therefore, eluents such as heptane have been proposed for identification of aliphatic compounds (Herod *et al.,* 2007). Aliphatic compounds can also be better identified by other detection methods such as RID (refractive index detection) (Hattingh, 2012; Herod *et al.,* 2003). The heavy component peak maximum is observed around ~400 Da for all tars, and the light component peak maximum around ~200 Da; consistent with findings for tars derived from coal gasification as investigated by Fidalgo *et al.* (2014). The increase in heavy component peak maxima observed with an increase in final pyrolysis temperature for the TWD derived tars is in agreement with results obtained for gasification and devolatilisation derived

tars in previous studies (Hattingh, 2012; Mokoena *et al.,* 2008; Adegoroye *et al.,* 2004). Tars derived from the AW TWD fraction indicate heavy and light component peak maxima at smaller molecular sizes, indicating a shift to lighter components.

Table 5-5 Summary of SEC results obtained for the various derived tars.

	TWD			AW TWD		
	520°C	***750°C***	***900°C***	***520°C***	***750°C***	***900°C***
Molecular mass range (Da)	46 - 5109	31 - 5839	34 - 5118	36 - 5244	58 - 5719	37 - 5114
Heavy component peak max. (Da)	405	417	426	399	395	402
Light component Peak max. (Da)	197	211	201	193	201	206
Light components (Area %)	31.9	33.9	33.0	38.9	37.5	35.3
Heavy components (Area %)	68.1	66.1	67.0	61.1	62.5	64.7

For the TWD derived tars, it is evident that there is little variance in product composition as observed from SEC-UV analyses at the respective final pyrolysis temperatures, i.e. only a small increase in light components is observed with an increase in temperature, consistent with previous findings (Hattingh, 2012; Mill, 2000; Herod *et al.,* 1996; Li *et al.*, 1993a; Unger & Suuberg, 1984). This result is consistent with the observations made by the Simdis analyses, where it was shown that the crude oil fractions shifted to lower boiling point compounds with an increase in final pyrolysis temperature. It is possible that at increased pyrolysis temperatures the increased H_2 yield assists in the degradation of larger tar molecules through extensive cracking (Fidalgo *et al.,* 2014; Moliner *et al.,* 1989). At lower pyrolysis temperatures it is possible that the molecular mass of the tars may increase due to hydrogenation or chemical recombination reactions, which can alter the molecular form from relatively tight, coiled structures to more linear open ones (Herod *et al.,* 1996).

In the case of the AW TWD derived tars it can be observed that with increasing final pyrolysis temperature there is a shift to the heavy components. These results are in agreement with the Simdis analyses results that indicated a shift to the higher boiling point fractions with an increase in final pyrolysis temperature. No reference could be found in literature related to this observed change, but recombination of the tar molecules is speculated to take place. The secondary reactions taking place, may lead to the formation of heavier hydrocarbon species. Further analyses of the derived tars by analytical techniques such as C^{13}-NMR may provide a better understanding of the overall structure of the tars to explain the observation.

Comparison of the results between the TWD and AW TWD derived tars indicates that the AW TWD tar derived for the 520°C experiments contained more light components, i.e. 39.0 area % vs. 31.9 area % for the TWD tar. In the case of the 750°C experiments, the TWD derived tars contained 33.9 area % light components, whilst the AW TWD tar contained 37.5 area % light components. From the 900°C experiments, the TWD tar contained 33.0 area % light components, whilst the AW TWD derived tar contained 35.3 area % light components. The higher light component fraction as observed for the AW TWD derived tar can possibly be related to the higher H_2 yields, especially at the experimental temperature up to 520°C, where a large difference in H_2 yield is observed between the two coal fractions due to lower hydrogen transfer and increased cracking.

5.5. Char composition

The derived chars were analysed by proximate, ultimate, XRF, XRD, BET CO_2 adsorption and DRIFT analyses.

5.5.1. Proximate and Ultimate analyses

From the proximate analyses (Table 5-6), systematic trends during coal pyrolysis can be observed – i.e. the volatile matter (d.a.f.) decreases, whilst the fixed carbon content increases. This is in accordance with previous findings (Bunt *et al.,* 2012; Hattingh, 2012; Malumbazo *et al.,* 2012; Chabalala *et al.,* 2011; Jones *et al.,* 1999). The increase in fixed carbon content is typical of a pyrolysis process, because if combustion occurred, a decrease in this content should have been observed (Bunt *et al.,* 2012; Malumbazo *et al.,* 2012; Jones *et al.,* 1999).

During the release of volatile matter, structural ordering of aromatic structures will occur (Malumbazo *et al.,* 2012). The decrease in VM is most prominent up to 520°C, with smaller differences observed between 520°C and 750°C, and an even smaller change occurring between 750°C and 900°C for both fractions. The release of volatiles is greatest during the primary pyrolysis stage (Singh *et al.,* 2012; Saikia *et al.,* 2009; Cai *et al.,* 2008; Kabe *et al.,* 2004). At temperatures above 690°C, the char to gas reactions will be the most prominent pyrolysis process.

Both the TWD and AW TWD chars show inherent moisture values ranging between 0.7 and 1.0 wt% after pyrolysis at all temperatures.

The ash content can be observed to increase for the TWD fraction with an increase in final pyrolysis temperature, typical of raw coal under heat treatment (Hattingh, 2012; Malumbazo *et al.,* 2012). For the AW TWD fraction, the ash content stays the same at around 2.0 wt%, which can be related to the type of minerals, (mostly pyrite), present in the coal sample.

Table 5-6 Proximate and ultimate analyses results

	TWD				AW TWD			
	wt%							
	Raw	**520°C**	**750°C**	**900°C**	**Raw**	**520°C**	**750°C**	**900°C**
Proximate analysis (As determined)								
Inherent moisture	4.2	0.8	0.8	1.0	2.3	0.8	0.7	0.8
Ash	14.3	19.3	22.0	22.1	2.0	1.9	2.0	2.0
Volatile matter (VM)	31.4	9.1	3.4	2.1	32.7	7.3	3.0	1.6
Fixed carbon (FC) – by difference	50.1	70.8	73.8	74.8	63.0	89.9	94.2	95.6
TOTAL	**100.0**	**100.0**	**100.0**	**100.0**	**100.0**	**100.0**	**100.0**	**100.0**
Proximate analysis (Dry basis)								
Ash	14.9	19.5	22.2	22.3	2.0	2.0	2.0	2.0
Volatile matter (VM)	32.8	9.2	3.5	2.1	33.4	7.4	3.1	1.6
Fixed carbon (FC) – by difference	52.3	71.4	74.3	75.6	64.6	90.6	94.9	96.4
TOTAL	**100.0**	**100.0**	**100.0**	**100.0**	**100.0**	**100.0**	**100.0**	**100.0**
Proximate analysis (Dry, ash free basis)								
Volatile matter (VM)	38.5	11.4	4.4	2.7	34.1	7.6	3.1	1.7
Fixed carbon (FC) – by difference	61.5	88.6	95.6	97.3	65.9	92.4	96.9	98.3
TOTAL	**100.0**	**100.0**	**100.0**	**100.0**	**100.0**	**100.0**	**100.0**	**100.0**
Ultimate analysis (Dry, ash free basis)								
Carbon	79.1	89.3	95.3	96.6	80.3	90.9	94.5	95.3
Hydrogen	4.7	2.8	1.2	0.1	4.7	2.7	1.2	0.3
Nitrogen	2.1	2.8	2.2	1.8	2.2	2.8	2.6	2.1
Oxygen – by difference	12.7	4.0	0.1	0.1	11.5	2.8	0.9	1.6
Total sulphur (IR spectroscopy)	1.4	1.2	1.2	1.3	1.3	0.8	0.8	0.6
TOTAL	**100.0**	**100.0**	**100.0**	**100.0**	**100.0**	**100.0**	**100.0**	**100.0**
C/H ratio	1.4	2.7	6.6	54.4	1.4	2.9	6.4	28.0
Atomic H/C ratio	0.71	0.38	0.15	0.02	0.70	0.35	0.16	0.04
Atomic O/C ratio	0.12	0.03	0.00	0.00	0.11	0.02	0.01	0.01

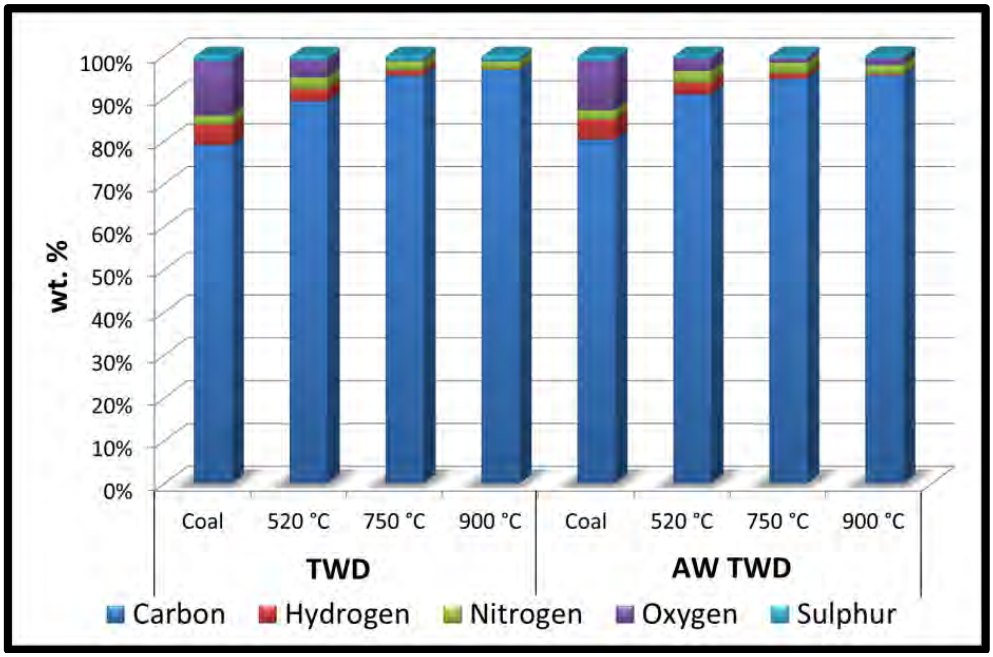

Figure 5-6 Ultimate analyses results

Pyrite will form pyrrhotite, and in the end troilite (FeS) under the current conditions, and thus little change with regard to overall ash weight, irrespective of final pyrolysis temperature is expected.

From Table 5-7 and Figure 5-6 it is clear that the hydrogen, oxygen and nitrogen contents for both fractions decrease with an increase in final pyrolysis temperature, whilst the carbon content increases, analogous to the observation made with regard to the proximate analysis FC content. The sulphur is observed to remain relatively constant at all pyrolysis temperatures for the TWD fraction and chars, with only a small decrease observed. The decrease observed in the sulphur content of the AW TWD derived chars is however much larger. It is possible that the acid washing process liberated some of the sulphur which led to easier removal during pyrolysis than was the case for the TWD coal.

Chen *et al.* (1999) stated that mineral matter present in the coal structure might trap sulphur, and therefore lower sulphur yields were observed after acid washing. Calcite and dolomite were identified to capture sulphur (Sciazko & Kubica, 2002; Yaw *et al.,* 1980). With regard to the oxygen content, the decrease is more significant in the case of the AW TWD fraction when compared to that of the TWD fraction; this relates to the higher CO_2 yield derived from the AW TWD coal. For the TWD derived chars no significant change in oxygen content is observed between 750°C and 900°C. In the case of the AW TWD derived chars, there is some discrepancy in the results as oxygen is determined by difference. No conclusion can be made with regard to this observation, although little change is expected between these two temperatures because the CO and CO_2 yields do not change significantly between these two final pyrolysis temperatures. The carbon content of both coal chars is observed to increase

drastically with an increase in final pyrolysis temperature, and that of the TWD derived chars is higher than that of the AW TWD derived chars up to 750°C and 900°C. The trends observed are in accordance with previous work (Hattingh, 2012; Bai *et al.,* 2010; Wang et al., 2013; Jones *et al.,* 1999; Davis *et al.,* 1995).

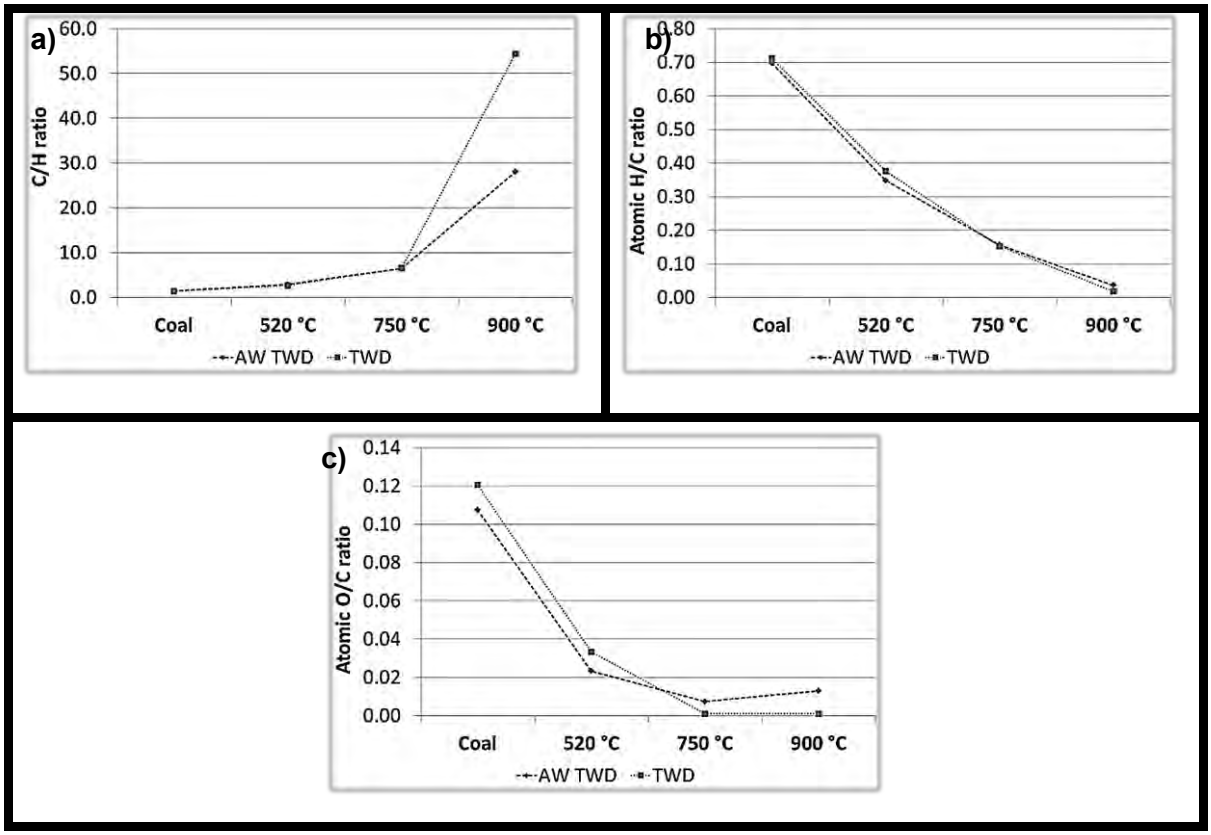

Figure 5-7 a) C/H ratio, b) Atomic H/C ratio and c) Atomic O/C ratio for TWD and AW TWD coals at the various temperatures.

Figure 5-7a indicates the C/H ratio for the respective chars derived at the various final pyrolysis temperatures. An increase in this ratio is observed for both coal chars with an increase in final pyrolysis temperature, as the hydrogen content of the coals is depleted. Good agreement is observed for the derived chars up to 520°C and 750°C for both fractions, but up to 900°C, the C/H ratio of the TWD char is much larger than that of the AW TWD char, due to the higher carbon content and lower hydrogen content. The atomic H/C ratio (Figure 5-7b) indicates the inverse of what was found for the C/H ratio. Good correspondence between the derived chars for both fractions is observed at all final pyrolysis temperatures, indicating structural similarity between the chars with regard to these components. The rapid decrease in atomic H/C ratio was observed in previous studies as well (Hattingh, 2012; Bai *et al.,* 2010; Wang *et al.*, 2013; Jones *et al.,* 1999; Davis *et al.,* 1995).

Figure 5-7c indicates the atomic O/C ratios of the coals and derived chars. Both the TWD and AW TWD derived chars show the same decreasing trend in this ratio with an increase in final

pyrolysis temperature. The AW TWD coal and AW TWD char have lower atomic O/C ratios in the 520°C experiments compared with that of the TWD coal and the TWD char at 520°C. From the 750°C and 900°C experiments, the atomic O/C ratio of AW TWD chars is higher than that of the TWD derived chars. This observation correlates with the CO and CO_2 yields of the AW TWD coal/chars; levelling off at 750°C, whilst the TWD fraction still yields more of these gases at these temperatures. It is possible that the absence of calcite and dolomite minerals which have been found to assist in the production of these gases at these temperatures, causes this difference, i.e. not only do these minerals produce CO_2 through calcination of the minerals itself, but it also cracks oxygen functionalities present within the coal structure (Liu *et al.*, 2004a; Karaca, 2003; Tsubouchi & Ohtsuka, 2002). The decrease observed in atomic ratios with an increase in final pyrolysis temperature is indicative of a more aromatic char structure (Davis *et al.,* 1995; Furimsky & Ripmeester, 1983). The lower atomic O/C and H/C ratios of the TWD chars are indicative of a higher aromaticity. The nitrogen content of the AW TWD chars is higher in the 750°C and 900°C experiments than that of the TWD chars.

5.5.2. X-Ray Fluorescence (XRF) and Inductive coupled plasma (ICP) analysis

Table 5-7 summarizes the XRF results for the ashes derived from the TWD fraction and chars, as well as the ICP results for the AW TWD fraction and chars. ICP analysis had to be carried out on the AW TWD derived ash due to the low ash content. In the case of the TWD coal and char ash, similar composition was observed with regard to most of the identified oxides. The pyrolysis process did however lead to lower Fe_2O_3 compounds, i.e. 5.5 – 6.1 wt% vs. 9.6 wt% for the TWD coal/char ash. Regarding SO_3 identification, the chars yielded higher concentrations than for the coal, i.e. 8.7 – 10.6 wt% vs. 8.2 wt%. Since pyrite is the most prominent iron and sulphur containing mineral present in the coal, these yields are believed to be related. The largest difference was observed at a final pyrolysis temperature of 750°C, i.e. this was the pyrolysis temperature after complete decomposition of the original pyrite had occurred. The SiO_2 yield of the char ash was higher than that of the coal, i.e. 38.3 – 39.3 wt% vs. 35.9 wt%, whilst some minor differences were observed in components comprising a small fraction of the overall ash yield, such as TiO_2, BaO and V_2O_5, all being less prominent in the char ashes.

Comparison of the ICP ash analyses values obtained for the AW TWD derived chars to that of the AW TWD coal ash indicated lower Al_2O_3, CaO, K_2O, MgO, Na_2O, SiO_2, BaO and SO_3 values for the chars, whilst the yields of Fe_2O_3 and TiO_2 increased in the chars. The variation in ash composition for the AW TWD coal ash was much greater than that observed for the TWD derived ash. The Fe_2O_3 and SO_3 content of the AW TWD char derived ash once more indicated large deviation from what was observed from the AW TWD coal ash.

Table 5-7 XRF/ICP results for TWD and AW TWD coals and chars

	TWD				AW TWD			
	wt%							
	Coal	***520°C***	***750°C***	***900°C***	***Coal***	***520°C***	***750°C***	***900°C***
Al_2O_3	25.3	26.1	25.1	26.1	14.9	13.1	11.2	11.7
CaO	11.3	11.2	11.8	11.3	8.8	7.1	6.6	6.6
Cr_2O_3	0.1	0.1	0.1	0.1	0.4	0.7	1.0	1.4
Fe_2O_3	9.6	5.9	5.5	6.1	39.0	52.8	59.3	55.4
K_2O	0.6	0.7	0.7	0.7	0.4	0.2	0.1	0.1
MgO	3.7	3.2	3.5	3.3	5.1	2.2	2.0	2.2
MnO	0.1	0.1	0.1	0.1	0.0	0.1	0.1	0.1
Na_2O	0.6	0.5	0.5	0.5	1.2	0.7	0.5	0.5
P_2O_5	1.5	1.6	1.6	1.6	0.3	0.8	0.6	0.7
SiO_2	35.9	38.9	38.3	39.3	5.1	4.7	2.4	3.4
TiO_2	1.7	1.3	1.2	1.3	5.7	10.4	9.6	10.2
V_2O_5	0.1	0.0	0.0	0.0	0.2	0.4	0.3	0.3
ZrO_2	0.1	0.1	0.1	0.1	0.5	0.7	0.7	0.8
BaO	0.6	0.3	0.3	0.3	2.5	2.1	1.9	2.0
SrO	0.7	0.6	0.6	0.6	1.7	1.6	1.5	1.6
SO_3	8.2	9.5	10.6	8.7	14.3	2.7	2.0	3.0
TOTAL	**100.0**	**100.0**	**100.0**	**100.0**	**100.0**	**100.0**	**100.0**	**100.0**

5.5.3. X-Ray Diffraction (XRD) analysis

XRD analyses were conducted on the derived chars to identify the most prominent crystalline mineral constituents and amorphous carbon forms (Huggins, 2002; Ward, 2002; Hutton and Mandile, 1996). Appendix C-6 includes the XRD spectra graphs. The X-Ray Diffraction (XRD) results for the TWD and AW TWD coals and chars are summarized in Table 5-8. It is evident from the results that the crystalline mineral matter of the TWD coal underwent several transformations with an increase in final pyrolysis temperature, with the amorphous content increasing with increasing final pyrolysis temperature at 750°C and 900°C, due to mineral transformation (Bai *et al.,* 2013; Min *et al.,* 2011). The general trends observed are in line with findings as described by Bai *et al.,* (2013), Matjie (2008) and Tomeczek and Palugniok (2002).

A decrease in aragonite, calcite, dolomite, fluorapatite, kaolinite and pyrite content is observed with an increase in final pyrolysis temperature. Aragonite, calcite and dolomite will transform due to calcination with the release of CO_2 (Vassileva and Vassilev, 2006; Maitra *et al.,* 2005; Caceres & Attiogbe, 1997). At a final pyrolysis temperature of 750°C, all of the dolomite had already calcined, forming calcite and periclase (MgO); the periclase was however not identified by XRD.

Table 5-8 XRD results for TWD and AW TWD coals and chars.

Identification	Molecular formula	TWD				AW TWD			
		Coal	*520°C*	*750°C*	*900°C*	*Coal*	*520°C*	*750°C*	*900°C*
		wt%							
Amorphous content	-	90.5	90.0	93.1	94.5	99.3	99.4	99.8	99.7
Aragonite	$CaCO_3$	0.2	-	-	-	-	-	-	-
Calcite	$CaCO_3$	0.4	2.2	1.0	0.5	-	-	-	-
Dolomite	$CaMg(CO_3)_2$	1.6	1.4	-	-	0.1	-	-	-
Fluorapatite	$Ca_5(PO_4)_3F$	0.1	-	-	-	-	-	-	-
Hematite	Fe_2O_3	-	0.2	0.8	0.8	-	-	-	-
Kaolinite	$Al_2Si_2O_5(OH)_4$	4.9	2.8	1.3	0.7	-	-	-	-
Magnetite	Fe_3O_4	-	-	-	-	-	-	0.1	0.2
Oldhamite	CaS	-	0.1	1.0	1.2	-	-	-	-
Pyrite	FeS_2	0.9	-	-	-	0.6	-	-	-
Pyrrhotite	$Fe_{(1-x)}S$	-	0.3	-	-	-	0.6	0.1	0.1
Quartz	SiO_2	1.4	3.0	2.8	2.3	-	-	-	-
TOTAL	**-**	**100.0**	**100.0**	**100.0**	**100.0**	**100.0**	**100.0**	**100.0**	**100.0**

Kaolinite transforms to the amorphous phase with the release of endothermic water between 450°C to 600°C forming meta-kaolinite (Ptáček *et al.,* 2010b; Vassilev *et al.*, 2009; Heide & Földvari, 2006; Alpern *et al.,* 1983). The pyrite present in the TWD coal completely transformed below 750°C, consistent with previous findings (McLennan *et al.*, 2000; Bool *et al.,* 1995; Groves *et al.,* 1987). Transformation to pyrrhotite and hematite takes place (Hu *et al.,* 2006; Vassileva & Vassilev, 2006; Hong & Fegley, 1997; Gryglewicz *et al.,* 1996). Some of the sulphur, released during the decomposition of pyrite, reacts with the calcium upon calcination of calcite and dolomite to form increased amounts of oldhamite (CaS) with increasing final pyrolysis temperature, in accordance with previous observations (Matjie, 2008; Speight, 2005).

The quartz content increased up to 520°C, where after a decrease in crystalline quartz content was observed as it transforms to the amorphous phase (Klein, 2002; Reifenstein *et al.,* 1999). The increase in quartz content may be due to transformation of kaolinite up to 520°C. The decrease in quartz content at 750°C and 900°C is believed to be related to reaction of some of the minerals, such as kaolinite in reaction with partially-oxidised pyrite and CaO from calcite and dolomite to form amorphous silicate glass (Matjie, 2008; Briggs, 1986). This transformation was observed to take place around 750 – 760°C (Briggs, 1986). At temperatures higher than 800°C, kaolinite was found to transform to reactive aluminosilicate and amorphous quartz (Matjie, 2008; Van Alphen, 2005; Ward & French, 2004; Bryers, 1986).

In the case of the AW TWD coal/char, only some minute dolomite was identified, with the largest mineral fraction present being pyrite. The pyrite present in the AW TWD coal transforms to pyrrhotite at 520°C (Hu *et al.,* 2006; Vassileva & Vassilev, 2006; Hong & Fegley, 1997; Gryglewicz *et al.,* 1996) and then undergoes further transformation to form magnetite (Fe_3O_4) up to 750°C and 900°C. The transformation of pyrrhotite to magnetite at these temperatures is interesting, as previous authors found that this change only occurred in the presence of excessive oxygen, from ferrous oxide at temperatures exceeding 900°C (McLennan *et al.*, 2000a, 2000b; Bool *et al.,* 1995).

5.5.4. BET CO_2 adsorption

BET CO_2 adsorption analyses provides insight with regard to the microporous properties in the micropore range pore sizes smaller than 12 Á (Sing *et al.,* 1985). Figure 5-8 indicates the micropore, Langmuir and BET surface areas for the TWD and AW TWD coal fractions and chars. It can be seen that both coal fractions showed increased micropore, Langmuir and BET surface areas with increasing final pyrolysis temperature up to 750°C. This is consistent with previous findings (Bunt *et al.,* 2012b; Klopper *et al.,* 2012; Bunt & Waanders, 2009; Li *et al.,* 1999). The increased surface area is attributed to the formation of new pores, or the expansion

of existing pores, due to heat treatment. The decrease in surface area above 750°C was attributed to thermal annealing and the increased graphitic nature of coal at higher pyrolysis temperatures (Bunt *et al.,* 2012b; Centeno *et al.,* 2001).

The Horvath-Kawazoe pore diameter was reported as 3.9 Å for the coal (TWD and AW TWD), whilst for the chars it was between 4.2 Å and 3.6 Å for TWD, and 4.02 Å and 3.6 Å for AW TWD. An initial increase in pore diameter is seen between 520°C and 750°C, after which a decrease in pore diameter is seen. This trend is consistent with previous findings (Bunt *et al.,* 2012b).

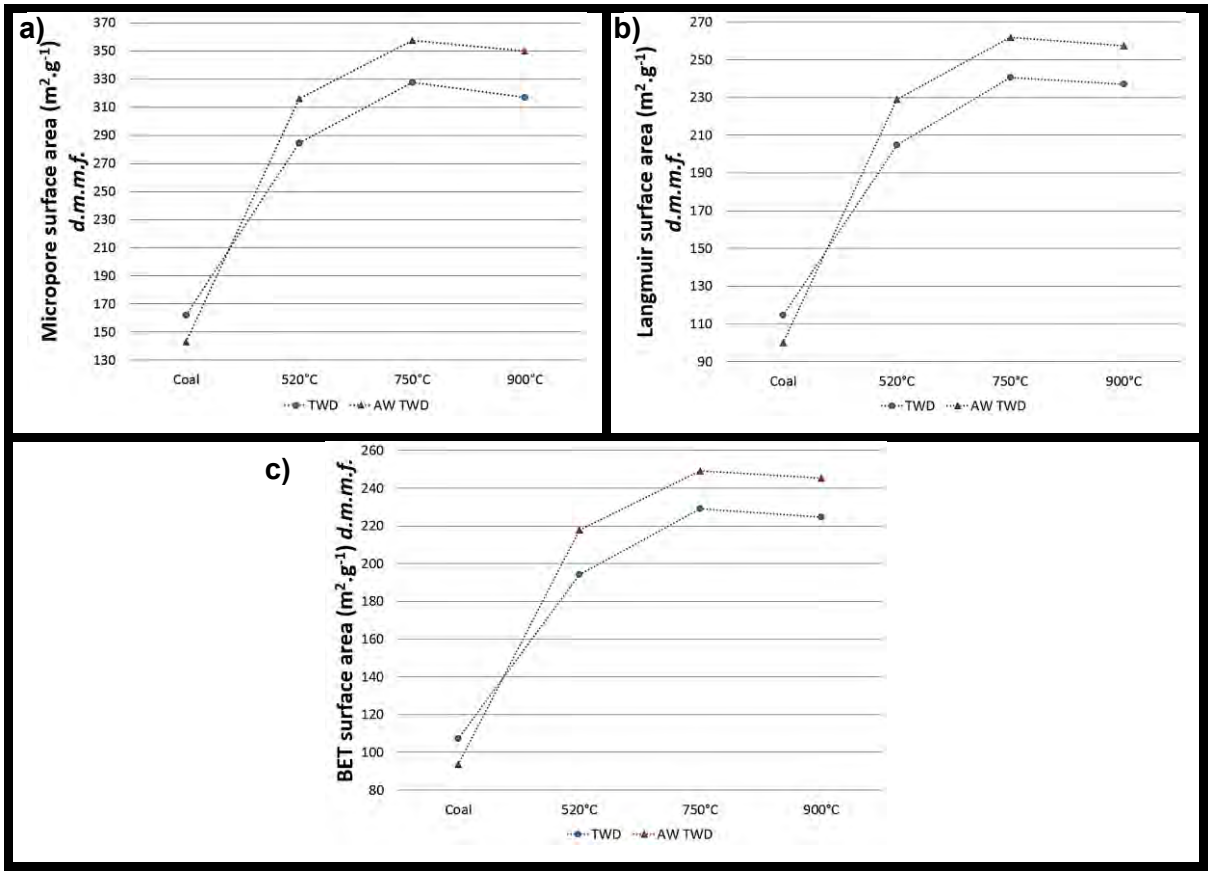

Figure 5-8 a) Micropore- , b) Langmuir- and c) BET surface area for TWD and AW TWD coal fractions and chars.

The AW TWD chars showed significantly higher micropore surface areas for all obtained chars. This indicates higher porosity, and thus explains increased release of volatile gases. In previous studies the increase in gas yield due to acid washing was attributed to the fact that the minerals (and particularly their oxides responsible for gas formation in coal), were non-porous, thus the removal of mineral matter was believed to alter the softening and swelling behaviour of coal and increase its porosity (Ahmad *et al.,* 2009; Bexley *et al.,* 1986). Due to higher porosity, increased swelling behaviour and less diffusion limitations, an increase in gas

yield is expected (Ahmad *et al.,* 2009; Reucrofta *et al.,* 1983). These results thus confirm this hypothesis.

5.5.5. DRIFT analysis

DRIFT analyses of the obtained chars were carried out as discussed in Section 3.4.3.2. In Section 3.8.2 the DRIFT spectra for the coal fractions were compared and discussed based on functional group identification. This section will only focus on changes observed with an increase in final pyrolysis temperature, and all identified functional groups will not be discussed here. Figure 5.9 indicates the DRIFT spectra for both coal fractions and the obtained chars at the three respective pyrolysis temperatures (520, 750 and 900°C).

Regarding the OH-groups (3800 -3200 cm^{-1}), it can be seen that most of these groups had been driven off already at a pyrolysis temperature of 520°C for both coal fractions (Xin *et al.,* 2014; Van Niekerk *et al.,* 2008; Li *et al.,* 2004; Li *et al.,* 2003; Machnikowska *et al.,* 2002; Miura *et al.,* 2001; Chen *et al.,* 1998b; Cai & Smart, 1994; Painter *et al.,* 1987; Painter *et al.,* 1985). The small peak observed around 3400 cm^{-1} for the 520°C chars can be associated with phenolic OH groups which are more difficult to hydrolyse (Chen *et al.,* 1998; Cai & Smart, 1994). The other vibrations seen around 3535 cm^{-1} are related to OH-π type hydrogen bonds. These OH groups can only form weak interactions with aromatic rings As such they are difficult to protonate and remove during pyrolysis (Chen *et al.,* 1998; Cai & Smart, 1994; Painter *et al.,* 1987).

The C-H aromatic stretch (3120 – 3000 cm^{-1}) and the C-H aliphatic stretch (3000 – 2800cm^{-1}) are observed for both the TWD and the AW TWD fractions in the 520°C char, but not in the 750°C and 900°C char (Xin *et al.,* 2014; Van Niekerk *et al.,* 2008; Machnikowska *et al.,* 2002; Miura *et al.,* 2001; Nomura and Thomas, 1997; Cai & Smart, 1994; Painter *et al.,* 1981).

The C=O stretch is observed to have depleted already in the 520°C chars for both coal fractions, whilst the C=C aromatic stretch is still present in decreasing intensity with an increase in final pyrolysis temperature.

Some aromatic ring stretching is seen around 1560 cm^{-1} for both coal fractions in the 520°C, and to some extent in the 750°C char (Xin *et al.,* 2014; Van Niekerk *et al.,* 2008; Machnikowska *et al.,* 2002; Miura *et al.,*2001; Nomura & Thomas, 1997; Cai & Smart, 1994; Painter *et al.,* 1981).

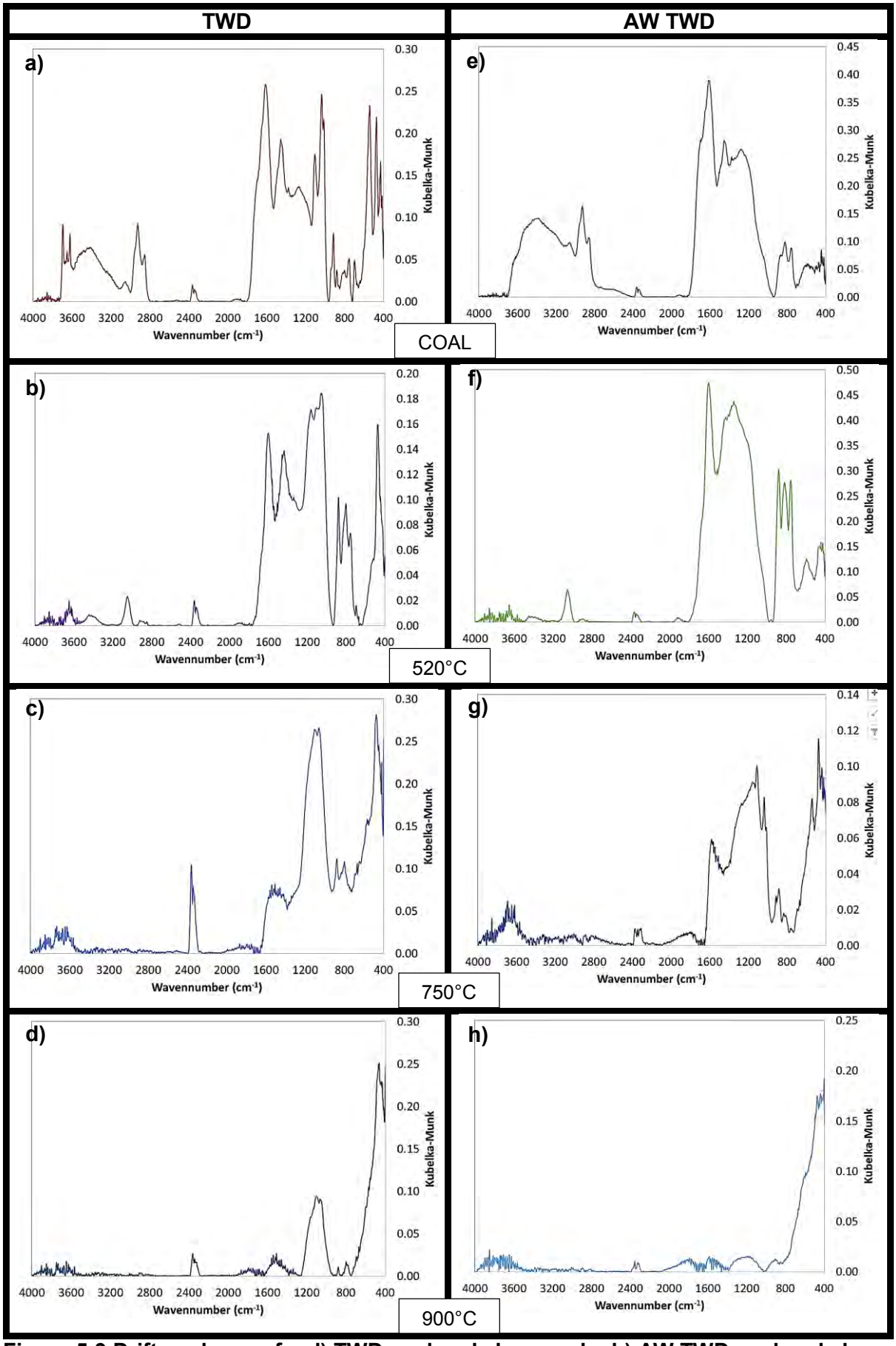

Figure 5-9 Drift analyses of a-d) TWD coal and chars and e-h) AW TWD coal and chars.

The CH_2 and CH_3 bend vibrations observed around 1452 cm^{-1} are seen to be present in the 520°C TWD char, but not in the AW TWD char at the same temperature (Xin *et al.,* 2014; Van Niekerk *et al.,* 2008; Machnikowska *et al.,* 2002; Miura *et al.,* 2001; Nomura & Thomas, 1997; Cai & Smart, 1994; Painter *et al.,* 1981). This difference indicates a dehydrogenation process occurring for the AW TWD coal fraction, which is only seen in the higher temperature chars for the TWD chars. This can be related to the higher H_2 yield seen for the AW TWD. The C-O stretch and O-H bending vibrations in phenoxy structures are observed around 1300 – 1000 cm^{-1} for both coal fractions (Xin *et al.,* 2014; Van Niekerk *et al.,* 2008; Machnikowska *et al.,* 2002; Barth *et al.,* 1994; Painter *et al.,* 1981). The amount of these functional groups is seen to decrease with an increase in final pyrolysis temperature. This decrease is of greater significance in the AW TWD char. At 900°C, the AW TWD obtained char shows very low intensity in this range. These groups are believed to be associated with the water yields as well, and might

The AW TWD chars show no significant peaks in the range 1100 – 900 cm^{-1}. In this range peaks associated with Si-O-Si and Al-O-Al vibrations related to kaolinite and quartz minerals are expected (Strydom *et al.,* 2011; Thomas & Kelley, 2009; Breen *et al.,* 2008; Carmody *et al.,* 2005, Frost *et al.,* 2003, Ming & Spark 2003; Martens *et al.,* 2002; Madejová and Komadel, 2001; Matteson & Herron, 1993; Povarennykh, 1978; Farmer, 1974). Between 900 – 700 cm^{-1} out-of-plane aromatic C-H vibrations are seen for both coals and chars (De Lorenzi Pezollo, 2012; Breen *et al.,* 2008; Pokrovsky *et al.,* 2000; Krivácsy & Hlavay, 1995; Povarennykh, 1978). These vibrations are also seen to become less significant with an increase in final pyrolysis temperature. The absence of some of the peaks identified for TWD coal, (but not in the chars) can be related to C-O out-of-plane bending associated with calcite and dolomite. These peaks are not observed in the chars due to decomposition of these minerals, especially in the 750°C and 900°C chars.

The peak observed at 473 cm^{-1} for the TWD derived chars can be related to Si-O and Si-O deformation associated specifically with quartz, which does not decompose at the temperatures of this study (Carmody *et al.,* 2005, Madejová & Komadel, 2001; Matteson & Herron, 1993; Povarennykh, 1978). This peak is however not observed for the AW TWD chars due to acid washing. S-S vibrations (<450 cm^{-1}) are not observed in the chars due to decomposition/transformation of the pyrite responsible for these vibrations (Derycke *et al.,* 2013; Strydom *et al.,* 2011; Güler 2005; Hicyilmaz *et al.,* 2004; Matteson & Herron, 1993).

The decrease in aliphatic stretches, whilst aromatic vibrations are still observed, is consistent with findings by Cai and Smart (1994). Solid state NMR (nuclear magnetic resonance) analysis

may provide more quantitative data regarding the changes seen with regard to the functional groups present in the coal fractions and the derived chars.

5.6. Chapter summary

Chapter 5 presented and discussed the yield and compositional data as analysed by various analytical techniques for the pyrolysis products derived from the TWD and AW TWD coal fractions. The water (m.m.f.) and tar (d.m.m.f.) yields from the AW TWD fraction were found to be lower, whilst the gas yields (d.m.m.f.) were found to be much larger than that from the TWD fraction. The char yields (d.m.m.f) were unaffected by acid washing.

The decreases in water yields were attributed to difference in the carboxylic and phenolic functional groups caused by the acid washing procedure. DRIFT analyses of the derived chars did indicate the absence of some C-O and O-H bending vibrations in phenoxy structures, but solid-state NMR analysis is recommended for future studies in order to confirm this hypothesis. Some of the removed mineral matter may also be responsible for the difference in the water yield, and also play a role in some reactions taking place, especially with respect to the water-gas shift reaction.

The H_2 and CO_2 yields were significantly higher from the AW TWD coal fraction, whilst the CO yield was lower than that from the TWD coal fraction. This suggests that some shift in equilibrium in the water-gas shift reaction could have occurred due to the acid washing procedure. The increased CO_2 yields from the AW TWD fraction can be related to more tar cracking. The lower CO yields after acid washing can be related to more oxygen functionalities being available from the TWD fraction. Calcite and dolomite minerals may also assist in CO_2 gasification, whilst the de-hydrogenation of OH groups can also produce more CO. It was seen from the DRIFT results that less OH-vibrations were present in the case of the AW TWD coal fraction. The GC-MS analysis of the tar also revealed that the AW TWD tars at 750°C and 900°C contained more compounds that form part of the alkyl-phenol family. The cracking of these components at these temperatures would have been catalysed by the decomposition products of calcite and dolomite minerals, forming amongst others CO.

The higher H_2 yield from the AW TWD coal fraction can also be related to the lower tar yield. The cracking of the tar, as well as lower hydrogen transfer, due to less stabilisation of free radicals, is believed to be related. The direct de-hydrogenation of the acid washed chars is also more significant, leading to higher H_2 yields. This was confirmed by the DRIFT analyses, as no CH_2 and CH_3 bend vibrations were seen round 1452 cm^{-1}. The absence of some C-O and O-H bending vibrations in phenoxy structures also attributes to the increased H_2 yield seen for the AW TWD coal fraction.

The CH_4 yields from the AW TWD fraction were also significantly higher and are likely related to the de-alkylation of the AW TWD derived tar and cross-linking reactions of the coal macro molecules. The AW TWD fraction also produced higher yields of C_2H_4, C_2H_6, C_3H_4, C_3H_6 and C_4s due to the cracking of long-chain aliphatics, making the AW TWD tars more aromatic in nature.

The simdis analysis revealed that the TWD tars consisted of increased lower boiling point compounds with increasing final pyrolysis temperature, whilst the inverse was true for the AW TWD tars. GC-MS analyses revealed that the TWD tars contained more alkyl-benzene, aromatic ether and esters, alkyl-indenes, PAHs and N-heteroatom related compounds than the AW TWD tars derived at 900°C. The AW TWD tars in turn contained more alkyl phenolic compounds at 750°C and 900°C, as well as more alkyl-naphthalene compounds at 520°C and 750°C. The increase in alkyl-naphthalene compounds is related to increased cleavage of aromatic bridges, explaining the increase in higher boiling point compounds as identified by Simdis, whilst the SEC-UV analyses revealed a decrease in light components with increase in final pyrolysis temperature. In general the TWD tars were more aliphatic in nature, due to more catalytic cracking.

The higher gas yields from the AW TWD coal fraction are likely due to increased char porosity due to mineral removal. The acid washed chars thus have less diffusion limitations, producing more gas. This was confirmed by BET CO_2 adsorption analyses, which indicated significant higher micropore surface areas for the AW TWD chars.

Proximate analysis of the derived chars revealed trends consistent with previous pyrolysis studies. Ultimate analyses indicated that the AW TWD chars derived up to 750°C and 900°C had higher oxygen and nitrogen contents, whilst more sulphur was removed from these chars than that from the TWD derived chars. This can be related to the sulphur capturing ability attributed to minerals such as calcite and dolomite. Ash analyses (by XRF and/or ICP) and XRD analysis of the chars revealed little more than what was seen from the same analyses of the respective coal fractions.

Chapter 6 will now focus on the changes seen in pyrolysis products with addition of the main removed minerals (calcite, dolomite, kaolinite, pyrite and quartz). Focus will once more be placed on pyrolysis product yields and analyses of the pyrolysis products.

Chapter 6: Effect of mineral addition

6.1. Introduction

Chapter 6 examines the effect of the addition of the most prominent minerals present in TWD coal, (as observed from XRD and QEMSCAN analyses), i.e. calcite, dolomite, kaolinite, pyrite and quartz, to the AW TWD fraction on the pyrolysis product yields and composition. All additions were done on a 5 wt% basis upon 50.0 g of AW TWD coal. Duplicate experiments were conducted for each mineral added at each of the final pyrolysis temperatures (520, 750 and 900°C). In this chapter the derived pyrolysis products with mineral addition will be evaluated as follows: Section 6.2 will deal with the pyrolysis product yields, in Section 6.3 the gas composition as analysed by GC analyses will be discussed, Section 6.4 will deal with the tar composition as analysed by Simdis, GC-MS and –FID and SEC-UV. Section 6.5 will deal with the char composition as analysed by proximate, ultimate, XRF and XRD analyses. In Section 6.6 a summary of the most relevant findings will be reported.

Table 6-1 Mass loss percentage of original added mass of the various minerals at the respective temperatures under experimental conditions.

Mass loss percentage of original mass (wt%)				
	200°C	**520°C**	**750°C**	**900°C**
Calcite	0.0	0.1	24.9	44.0
Dolomite	0.0	0.0	16.9	45.3
Kaolinite	0.3	6.7	12.1	12.4
Pyrite	6.1	18.1	33.7	34.6
Quartz	0.0	0.0	0.0	0.0

The different additions will be referred to as AW-Cal, AW-Dol, AW-Kao, AW-Pyr and AW-Qz respectively as indicated in Section 4.2.3. All additions were done on a 5 wt% basis. Water, gas and tar yields will be compared on a g water/gas/tar per 50 g coal basis. Char yields will be compared on a mineral matter free basis. Comparisons of the gas and water yields will be shown on a gram gas or water produced per 50 g coal basis, after corrections have been made for the “believed / true” values of gas or inherent moisture evolved from the respective minerals added. Table 6-1 indicates the amount of decomposition that should have taken place at the specific pyrolysis temperature for the given mineral, based on the TG analyses results (Section 3.9). Values reported at 200°C were related to inherent moisture loss from the

minerals, and the water yields were corrected based on these values. The gas yield was corrected for pyrite, calcite and dolomite addition. Calcite and dolomite are believed to release CO_2, whilst pyrite is believed to release H_2S and some SO_2.

** It should be noted that in cases where there is referred to, for example, chars derived up to 520°C, the author implies that these chars were derived up to a final pyrolysis temperature of 520°C, i.e. over the temperature range 25°C to 520°C.*

6.2. Pyrolysis product yields

Figure 6-1 indicates the various pyrolysis yields (expressed on an as determined basis) for the addition of the various minerals. It can be observed that in all cases the char yield decreased, whilst the gas yield increased, with an increase in final pyrolysis temperature. Water yields were mostly consistent, with only small changes observed for the respective mineral additions (Ptáček *et al.,* 2010b; Vassilev *et al.*, 2009; Heide & Földvari, 2006; Alpern *et al.,* 1983). With regard to the tar yields, AW-Cal and AW-Dol showed a definite decrease in tar yield with an increase in pyrolysis temperature. AW-Kao indicated no change. AW-Pyr indicates an increase in tar yield for experiments conducted at 520°C, but little change in tar yield value is observed between 750°C and 900°C. AW-Qz indicates an increase in tar yield both at 750°C and 900°C, which is consistent with the trend observed for the AW TWD fraction, without any mineral addition (Figure 5-1b, Section 5.2). The char yields are observed to decrease with an increase in final pyrolysis temperature (Reichel *et al.,* 2013; Fei *et al.,* 2012; Ahmad *et al.,* 2009a and 2009b; Kandiyoti *et al.,* 2006; Hu *et al.,* 2004; Smith *et al.,* 1994; Ladner, 1988; Franklin *et al.,* 1982a, 1982b, Yaw *et al.,* 1980), whilst the gas yields increase in all cases (Sert *et al.,* 2011; Kandiyoti *et al.,* 2006, Mill, 2000; Ladner, 1988; Nelson *et al.,* 1988). The differences observed in the yields of water, tar, char and gas will be discussed separately.

6.2.1. Water yields

Figure 6-2 indicates the amount of water produced (g) per 50 g coal for the various mineral additions. It should be noted that the amount of inherent moisture due to mineral addition has been corrected for. The water produced for the AW-TWD coal fraction varies between 3.2 – 3.3 g per 50 g coal at the respective temperatures. For the AW-Cal, the amount of water produced varies between 4.0 – 4.3 g per 50 g coal, whilst for AW-Dol it varies between 4.1 – 4.4 g per 50 g coal. For AW-Kao it varies between 3.2 – 3.4 g per 50 g coal, whilst for AW-Pyr an AW-Qz the ranges vary between 3.8 – 3.9 g per 50 g coal and 3.2 – 3.4 g per 50 g coal, respectively.

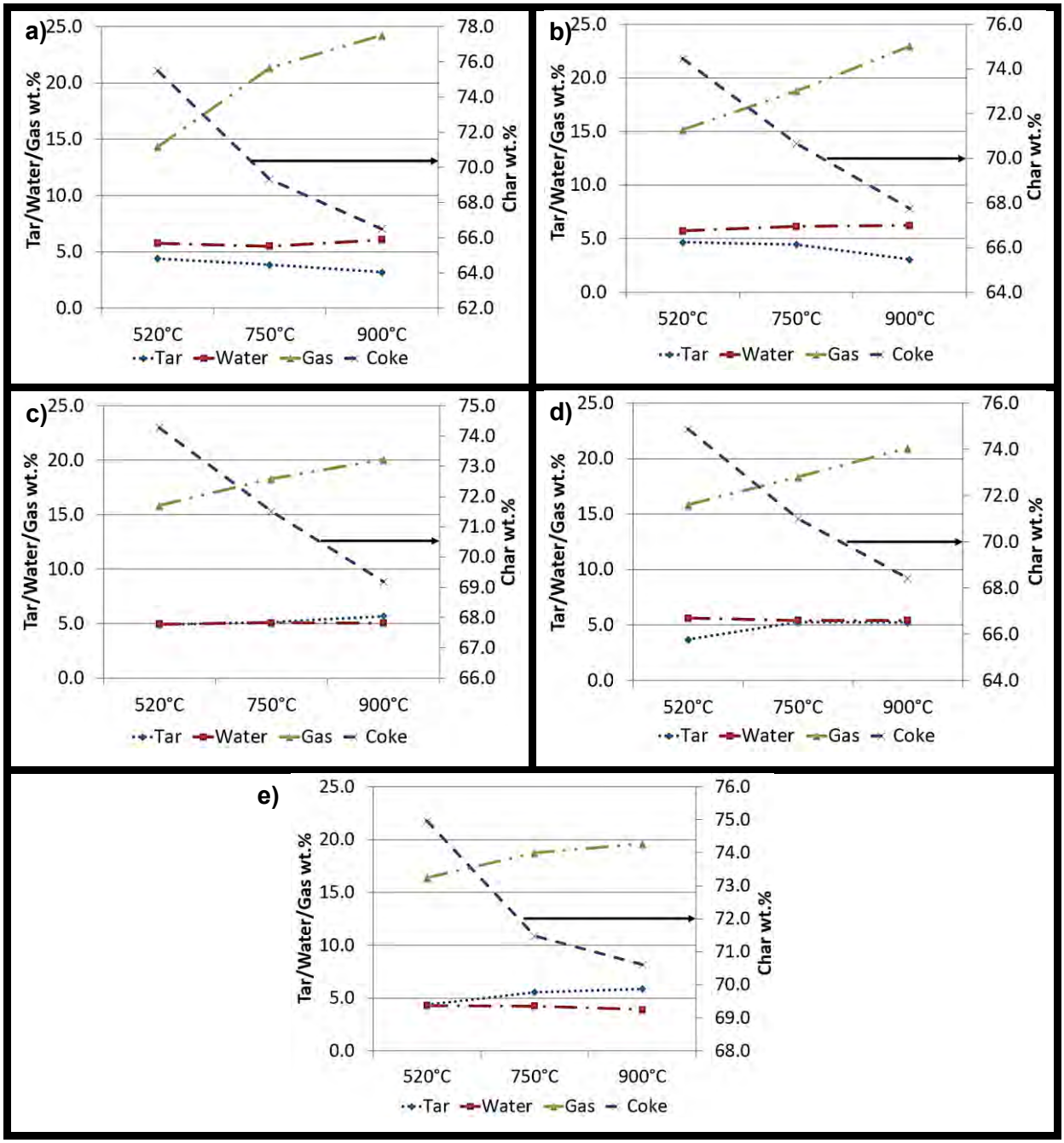

Figure 6-1 Pyrolysis product yields on an "as determined basis" for a) AW-Cal; b) AW-Dol; c) AW-Kao; d) AW-Pyr and e) AW-Qz.

The difference in water yield for AW-Kao and AW-Qz cannot be regarded as significant, but for the AW-Cal, AW-Dol and AW-Pyr experiments, further investigation is needed. The small variation in water yield observed between the different final pyrolysis temperatures indicates that most of the water has been driven off up to 520°C as can be expected, considering that water forming reactions are predominantly related to the primary pyrolysis stage (Solomon *et al.,* 1988). The increase in water yield obtained in the experiments designed to measure the effects of the addition of minerals, i.e. calcite (AW-Cal), dolomite (AW-Dol) and pyrite (AW-Pyr) is very interesting. Two postulations are made: i) the addition of these minerals leads to

the formation of more light fraction components, which are driven off during the water and tar removal processes; ii) these minerals have possible effects on the release of certain volatiles which are coupled with the release and or formation of water.

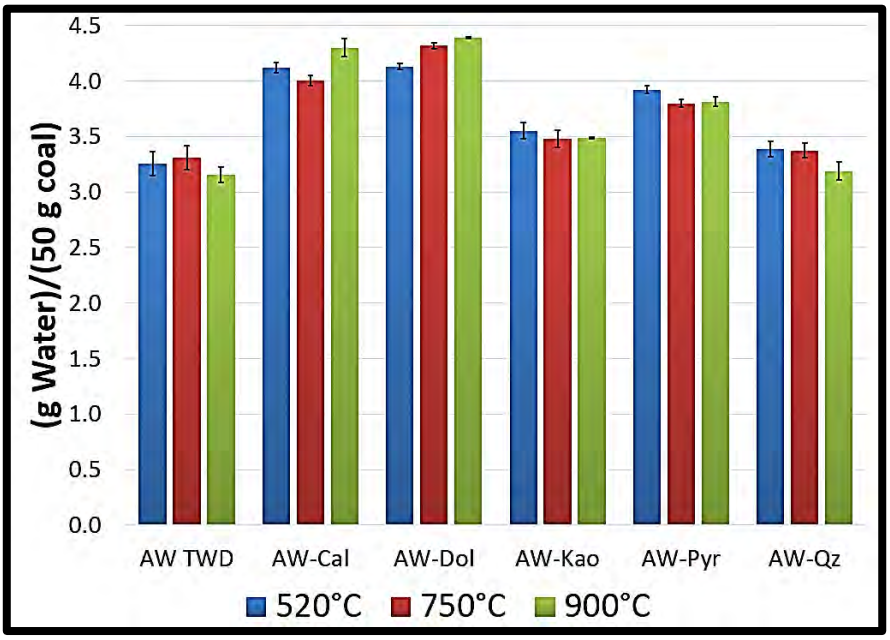

Figure 6-2 Water yields for AW TWD and the various mineral additions after corrections for mineral addition.

The first postulation can only be confirmed by more studies in which all of the volatiles in the liquid phase are not forced to the organic phase by the water and tar removal steps, such as used in this current study. A quantitative study can however be done making use of GC-MS, with free fatty acids phase (FFAP) column, to determine the polar compounds present in the liquid fraction. However, toluene cannot be used as solvent. A solvent such as dichloromethane can be used, but the water and tar fractions need to be separated by decantation. The quantification of pyrolysis liquid fractions (tar and water) will however not be possible, and thus it will only give an indication of the type of compounds present. If more polar compounds are found where calcite, dolomite and pyrite have been added, it can serve as proof that more compounds with a boiling point < 110°C are formed, and thus the higher 'water' yield observed in these experiments can be explained.

Previous pyrolysis studies also found increased water/liquid (excluding tar) yields with the addition or pre-treatment using $CaCO_3$ and $MgCO_3$ (Ahmad *et al.,* 2009a). McKee (1980) found that alkaline earth carbonates, (such as calcite and dolomite), might accelerate the reactions of solid carbon with gaseous oxygen, water vapour and carbon dioxide. Studies on graphite-H_2O reactions reported that the addition of $CaCO_3$ to graphite led to an increased

water yield (McKee, 1980). The formation of tar, CO_2 and water was found to be inter-related due to the water-gas shift reaction (Abu El-Rub, 2004; McKee, 1980).

6.2.2. Gas yield

Figure 6-3 indicates the gas yields as produced from the coal fraction after corrections have been made for gas being expelled from the added minerals, as determined from the TG analyses (Section 3-9). If the 95% confidence intervals are taken into account it can be observed that the change in the gas yield is regarded as significant for the addition of calcite (AW-Cal), kaolinite (AW-Kao) and quartz (AW-Qz). The addition of calcite (AW-Cal) led to lower gas yields, whilst AW-Kao and AW-Qz produced more gas at 520°C. In the case of the 750°C experiments, the AW-Cal experiment produced more gas, whilst AW-Pyr produced less gas, and all other gas yields were within repeatability limits. From the 900°C experiments AW-Cal, AW-Dol and AW-Kao produced more gas than the AW TWD experiment, whilst the addition of pyrite (AW-Pyr) and quartz (AW-Qz) had no significant effect.

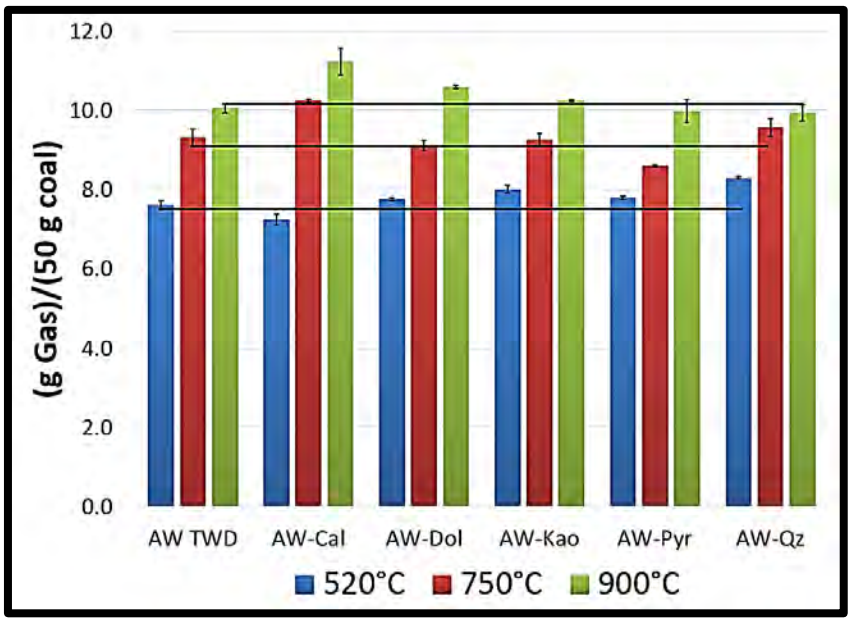

Figure 6-3 Gas yields for AW TWD and the various mineral additions

The increase in gas yield observed with the addition of calcite (AW-Cal) and dolomite (AW-Dol) is consistent with previous findings (Mun *et al.,* 2012; Pinto *et al.,* 2007; André *et al.,* 2004; Liu *et al.*, 2004a; Qi *et al.*, 2004; Sciazko & Kubica, 2002; Tsubouchi & Ohtsuka, 2002a, 2002b; Chen *et al.*, 1999; Mondragon *et al.*, 1999; Franklin *et al.,* 1982a, 1982b; Yaw *et al.,* 1980). In most cases the increased gas yield was attributed to tar cracking reactions. In this current study, it seems as if these additions might catalyse char to gas reactions as well. Ahmad *et al.* (2009b) attributed the increased gas yield to secondary decomposition of tar molecules to lower molecular weight hydrocarbons. It was previously stated that the increased

gas yield indicated that the minerals stayed external to coal organic matter, and thus acted as catalysts for tar cracking reactions (Ahmad *et al.,* 2009a).

The addition of kaolinite was associated with the cracking of tar to form increased yields of H_2 (Ôztas & Yürüm, 2000; Chen *et al.* 1999; Franklin *et al.,* 1982a), and it was reported in previous studies that the overall gas yield could be increased by kaolinite addition (Sert *et al.,* 2011). This can explain the higher gas yields at 520°C and 900°C, although the bulk of H_2 is only formed at temperatures exceeding 690°C (Fuentes-Cano *et al.,* 2013; Khan, 1989), but it was reported (Chapter 5) that the AW TWD gas was characterised by exceptionally high H_2 yields already for the 520°C experiments. The higher yield for the 520°C experiments also coincided with the temperature range wherein kaolinite transforms to metakaolinite, 450°C to 600°C (Ptáček *et al.,* 2010b; Vassilev *et al.*, 2009; Heide & Földvari, 2006; Alpern *et al.,* 1983).

The lower gas yield of the AW-Pyr run for the 750°C experiments is interesting to note, if it is taken into account that the decomposition of the added mineral would have been completed at this temperature, yielding H_2S and SO_2 gas (Cheng *et al.,* 2013; Yan and Zhang, 2010; Saikia *et al.,* 2009; Boyabat *et al.,* 2003). The increase in gas yield observed at 520°C from the addition of quartz (AW-Qz) may be related to the effect this mineral has on the thermoplasticity of the coal bed. Due to non-softening of the quartz particles, the thermoplasticity of coal is affected. No decomposition occurs except for the transformation to β-high quartz at around 573°C (Klein, 2002; Reifenstein *et al.,* 1999). This inhibits the physical contact between particles and therefore alters the overall agglomerating nature of the coal bed (Ôztas and Yürüm, 2000). It was observed that quartz might influence the maximum fluidity and the fluidity temperature range (Ryan, 1997), thus ensuring the release of more pyrolysates.

6.2.3. Tar yield

Figure 6-4 indicates the amount of tar produced (g) per 50 g coal for the AW TWD coal and the various mineral additions. Comparison of the 520°C experiments indicates that the AW-Pyr run produced less tar than the AW TWD fraction; all other tar yields are within repeatability limits. In the case of the 750°C experiments, AW-Cal and AW-Dol yielded less tar than for AW TWD, whilst the other additions had no significant effect on tar quantities. In the 900°C experiments, AW-Cal, AW-Dol and AW-Pyr yielded less tar, with AW-Kao and AW-Qz producing yields that corresponded with that of the AW TWD case.

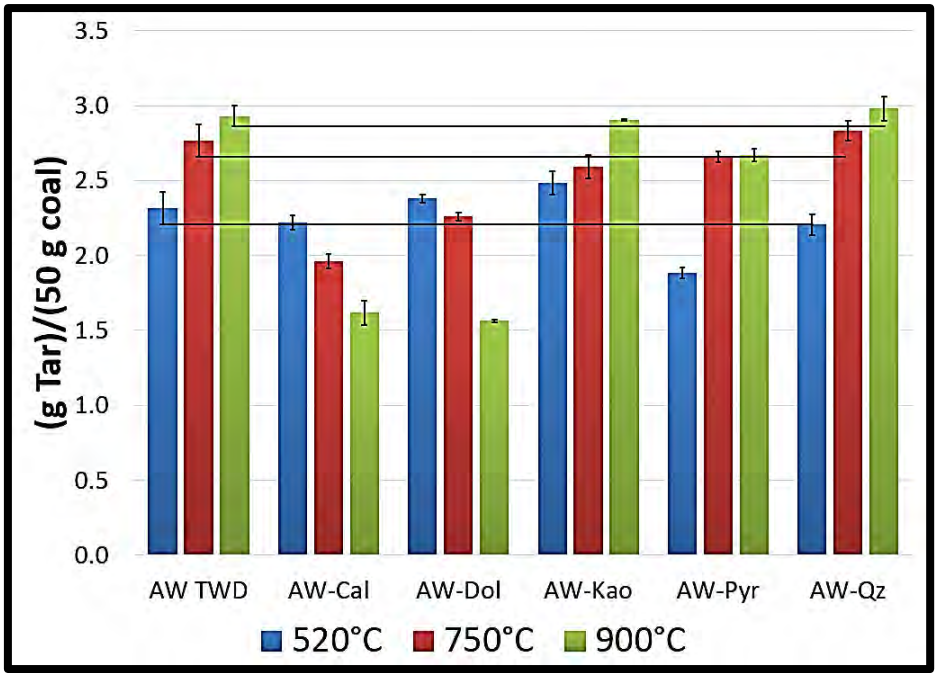

Figure 6-4 Tar produced (g) for various mineral additions to AW TWD

Table 6-2 Important secondary catalytic reactions (Adapted from Abu El-Rub *et al.,* 2004).

Number	Reaction type	Reaction	Reference
6-1	Steam reforming	$C_nH_m + nH_2O \rightleftharpoons nCO + \left(n + \frac{m}{2}\right) H_2$	Abu El Rub *et al.* (2004); Corella *et al.,* (2002); *Orio* et al., (1997)
6-2	Dry reforming	$C_nH_m + nCO_2 \rightleftharpoons 2nCO + \left(\frac{m}{2}\right) H_2$	Abu El Rub *et al.* (2004); Corella *et al.,* (2002); *Orio* et al., (1997)
6-3	Thermal cracking	$C_nH_m \rightarrow C^* + C_xH_y + gas$	Abu El Rub *et al.* (2004); Baker *et al.,* (1987)
6-4	Hydrocracking or hydroreforming of tars	$C_nH_m + H_2 \rightleftharpoons CO + H_2 + CH_4 + \ldots + coke$	Abu El Rub *et al.* (2004); Corella *et al.,* (2002); *Orio* et al., (1997)
6-5	Water-gas shift reaction	$CO(g) + H_2O(g) \rightleftharpoons CO_2(g) + H_2(g)$	Abu El Rub *et al.* (2004); Baker *et al.,* (1987)

C_nH_m hydrocarbons represent tars, C_xH_y hydrocarbons present lighter tars

The decrease in tar yield observed from the addition of calcite and dolomite (AW-Cal and AW-Dol) can be regarded as highly significant. These two minerals have similar structures, thus the same trend is expected. Dolomite does however decompose at higher temperatures than calcite (as observed from TG analyses in Section 3-9), which may explain the reason why the decrease in tar yield with the addition of dolomite was smaller than that observed for calcite for the 750°C experiments, as well as when the basis of mineral addition is taken into account. Mineral addition was done on a weight percentage basis, whilst the molecular weights of the different minerals differed, i.e. addition on a molar basis could be more accurate for quantification and effectivity purposes.

The catalytic effect of calcite and dolomite in tar reduction is well known, and both these minerals are used in the biomass gasification industry for this purpose (Abu El-Rub, 2004). It is the calcined forms of these minerals that are deemed to have a catalytic effect. Calcination occurs due to the loss of carbon dioxide upon heat treatment (Abu El-Rub *et al.*, 2004). In coal studies, the reduction of tar yield by addition or pre-treatment with dolomite was confirmed (Mun *et al.,* 2012; Pinto *et al.,* 2007; André *et al.,* 2004; Liu *et al.*, 2004a; Sciazko & Kubica, 2002; Chen *et al*., 1999; Yaw *et al.,* 1980; Yeboah *et al.,* 1980), as well as for calcite (Liu *et al.*, 2004a; Qi *et al.*, 2004; Tsubouchi & Ohtsuka, 2002a, 2002b; Chen *et al*., 1999; Mondragon *et al.*, 1999; Franklin *et al.,* 1982a, 1982b; Yaw *et al.* 1980). The reactions involved in this reduction is not well known, but Equations 6.1 – 6-4 (indicated in Table 6-2) are all believed to be included in this process, as derived from biomass studies (Abu El-Rub *et al.,* 2004). Tar reduction has been said to take place due to secondary tar cracking and re-polymerization, catalysed by the calcium additive (Ahmad *et al.,* 2009b; Franklin *et al.,* 1982a, Franklin *et al.,*1981, Yeboah *et al.,* 1980). Calcium may provide a nascent crosslink site in coal. This allows for coordination of groups such as carboxyls and hydroxyls which are prone to such reactions. These sites would otherwise coordinate with water, through hydrogen bonds (Ahmad *et al.,* 2009b).

The catalytic activity of calcined dolomite and calcite is further enhanced by large pore sizes and surface areas (Abu El-Rub *et al.,* 2004; Simell *et al.,*1992), as well as relatively high alkaline (K, Na) content that may be present as impurities (Abu El-Rub *et al.,* 2004; Delgado *et al.,* 1996; Klein *et al.*, 1985). The alkaline earth metals (which may be present as impurities) are proposed to enhance the gasification reaction of carbon intermediates deposited on the catalyst surface. Catalytic activity is observed to be improved by an increase in the CaO/Mg ratio, decreasing the grain size and increasing the active metal content such as iron (Abu El-Rub *et al.,* 2004).

The CaO/MgO ratio for limestone (CaO), to which calcite ($CaCO_3$) decomposes, is reported to be greater than 50 in most natural rocks, whilst that of dolomite is around 1.5 (Simell *et al.,*1992). However, at 900°C the added dolomite should have decomposed, thus forming calcined dolomite (decomposition products CaO and MgO), which is deemed as the most effective catalyst for tar reduction (Abu El-Rub *et al.,* 2004; Delgado *et al.,* 1996). If the molar amounts of added calcite and dolomite are taken into account, the current study confirms that calcined dolomite is the most effective catalyst for tar reduction. An additional observation from the literature reported that calcium oxide decreased the fluid temperature range, thereby inhibiting release of pyrolysates (Ryan, 1997).

The initial increase observed in tar yield with the addition of 5 wt% kaolinite (AW-Kao) for the 520°C experiments is in contrast with previous findings (Abu El-Rub *et al.,* 2004; Karaca, 2003; Ôztas & Yürüm, 2000; Chen *et al.,* 1999; Wen & Cain., 1984; Franklin *et al.,* 1981). The initial increase in tar yield may be attributed to the fact that the additional sites provided by kaolinite addition might assist the tar precursors to leave the coal structure and form tar, stabilising the formed free radicals to yield tar at 520°C. Kaolinite has been observed to decrease the maximum fluidity temperature of coal, as well as increase the fluidity by up to 5%; this thus may cause higher tar yields (Ryan, 1997). The dehydration and de-hydroxylation temperature range of kaolinite and coal volatile release coincide (Vassilev *et al.,* 2009). In previous studies, this was attributed to assist the decrease in tar yield (Karaca, 2003; Ôztas & Yürüm, 2000; Chen *et al.,* 1999, Franklin *et al.,* 1982a).

The effect of kaolinite in tar reduction is attributed to the acidity of the mineral, thus providing protonates for increased pyrolysis conversion (Chen *et al.*, 1999; Wen & Cain, 1984; Franklin *et al.*, 1982a). Kaolinite is however less active than dolomite and calcite in tar reduction (Abu El Rub *et al.,* 2004; Franklin *et al.,* 1982a; Franklin *et al.,* 1981). This was attributed to the loss of pore structure at increased temperatures and a small surface area of 15-20 m^2/g (Abu El-Rub *et al.,*1984*;* Wen & Cain , 1984). The active component in kaolinite is thought to be Al_2O_3. It was reported by Liu *et al.* (2004a) that this component was most effective at higher temperatures, and that it increased pyrolysis conversion of Chinese sub-bituminous lignite by 8-11%. The small difference observed in tar yield at 900°C is also consistent with some previous findings (Franklin *et al.,* 1981).

The addition of pyrite (AW-Pyr) was observed to decrease the tar yield in the 520°C experiments. The effect of pyrite on the tar yield was previously observed (Borah *et al.,* 2005; Franklin *et al.,* 1982a & 1982b). The temperature range in which pyrite affects pyrolysis yield is limited to 220-650°C (Borah *et al.,* 2005). This explains why the tar yield of the 750°C experiments was not affected. The decrease observed in the 900°C experiments, could be

attributed to the decrease in yield at the lower temperature range. Investigation of the electronic structure of pyrite reveals that the sulphur atom can expand its valency due to the availability of the vacant d-orbital; thus pyrite develops an acidic nature. If the pyrite molecule accepts electrons from electron-rich centres that may be present in the coal matrix, it could weaken the bonds adjacent to the donating elements, thus resulting in product release and pyrolysis (Borah *et al.,* 2005). Surface acidity and acid catalysed reactions of inorganic substances on organic matter have a large effect on bond cleavage processes below 500°C (Matsuhashi *et al.*, 2001 & 1997). The decomposition products of pyrite may also capture free electrons from free radicals released during pyrolysis, thus stabilizing the coal structure and effecting volatile release (Borah *et al.*, 2005). The decomposition products, such as magnetite (Fe_3O_4) and hematite (Fe_2O_3), have the largest effect on pyrolysis (Borah *et al.,* 2005; Abu El-Rub *et al.,* 2004). The oxides however have less active sites than calcite and dolomite, and are therefore deemed to be less active during catalytic cracking (Abu El-Rub *et al.*, 2004). Metallic iron is more effective in tar reduction than the oxides or sulphides. Iron was reported to catalyse the reactions of the main components of fuel gas, H_2, CO, CO_2. H_2O, such as the water-gas shift reaction (Abu El-Rub, *et al.,* 2004).

The addition of 5 wt% quartz (AW-Qz) did not have any effect on the tar yield. This was to be expected due to the inert chemical nature of this mineral (Ôztas and Yürüm, 2000; Chen *et al.*, 1999; Franklin *et al.,* 1982a, Franklin *et al.,* 1981).

A hypothesis explaining the addition of solid compounds to facilitate tar reduction was provided by Greensfelder *et al.*, (1949) which stated that the surfaces of the compounds enhance the formation of free radicals, which in turn accelerates the kinetic rate. Howard (1981) accepted this explanation in their tar pyrolysis studies. Wen and Cain (1984) went further, stating that the surface-assisted reactions due to solid mineral additions, transform part of the large hydrocarbons into free radicals and/or carbenium ions. Polymerisation occurs when the immobilised species react with the colliding hydrocarbons to form char, releasing hydrogen and other gases such as CH_4, C_2H_4 etc.

6.2.4. Char yield

The char yields for the AW TWD coal and the various mineral addition runs are shown in Figure 6-5. From the 520°C and 750°C experiments, the char yields of AW-Cal, AW-Dol, AW-Kao and AW-Qz were lower, whilst that of AW-Pyr and AW TWD corresponded. In the case of the 900°C experiments, all the mineral additions led to lower char yields, with calcite addition (AW-Cal) being most effective in reducing the char yield. The yields with the addition of other minerals were all in the same range.

In general, it can be said that the addition of mineral matter increased the overall pyrolysis conversion, with pyrite showing the least activity, especially in the 520°C and 750°C experiments. From the 900°C experiments, all the minerals showed increased pyrolysis conversion. The decrease in char yield observed with the addition of calcite (AW-Cal) and dolomite (AW-Dol) is in contrast with previous findings (Ahmad *et al.,* 2009b; Chen *et al*., 1999; Franklin *et al.,* 1982a; Franklin *et al.,* 1981). In the current study it was found that the addition of minerals assisted the conversion to pyrolysis products. Little effect was observed with the addition of clay, iron and silica minerals (Franklin *et al.,* 1981).

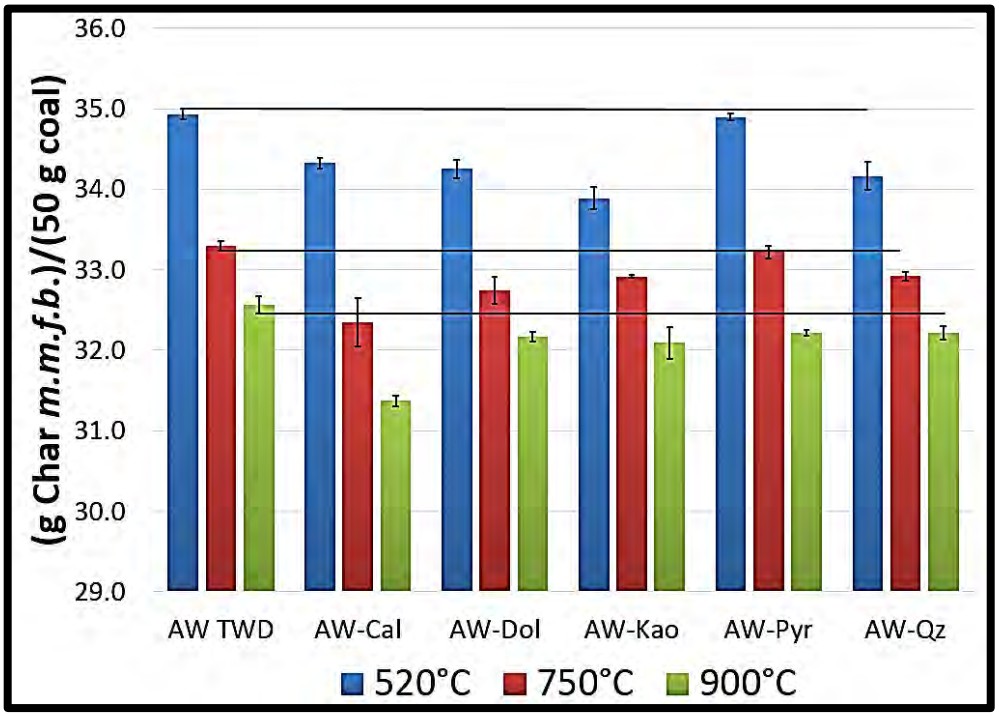

Figure 6-5 Char yield m.m.f.b. (g) for AW TWD coal and the various mineral additions.

6.2.1. Qualifying experiments

Qualifying experiments were carried out with the minerals (calcite, dolomite, kaolinite, pyrite and quartz) to confirm that the trends observed could be expected when addition of these minerals to the washed TWD coal was done as well. Figure 6-6 indicates the obtained results on an “as determined” weight percentage yield of the pyrolysis products, whilst Figure 6-7 compares the different yields with that of TWD coal. Only one experiment for each mineral added was conducted at 900°C.

Reference will be made based on the addition, i.e. calcite addition will be referred to as TWD-Cal, dolomite addition as TWD-Dol, kaolinite addition as TWD-Kao, pyrite addition as TWD-Pyr and quartz addition as TWD-Qz. Comparison of the yields with that of TWD coal will now be discussed. Appendix C-7 indicates all the detailed results obtained for these experiments.

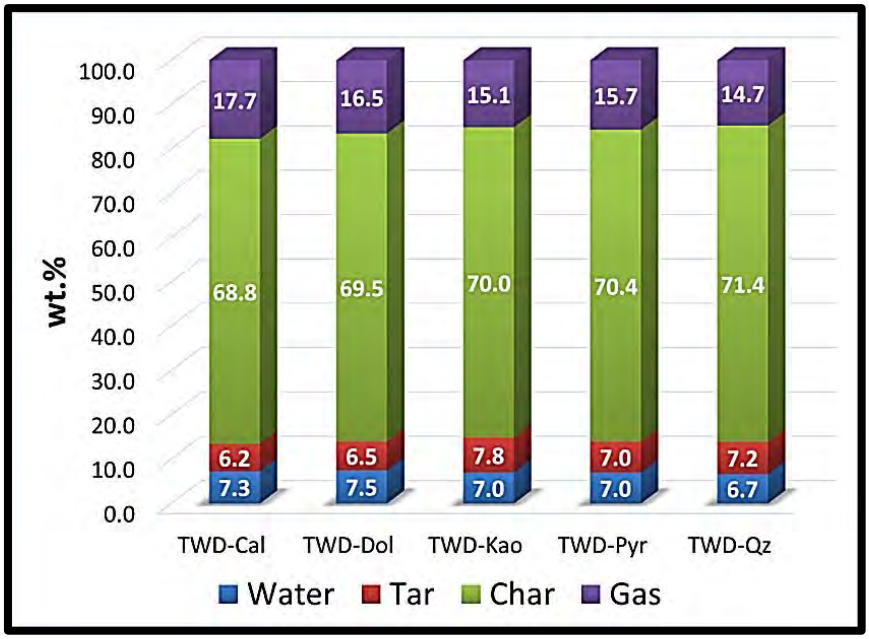

Figure 6-6 Pyrolysis product yields at 900°C for mineral addition to TWD coal.

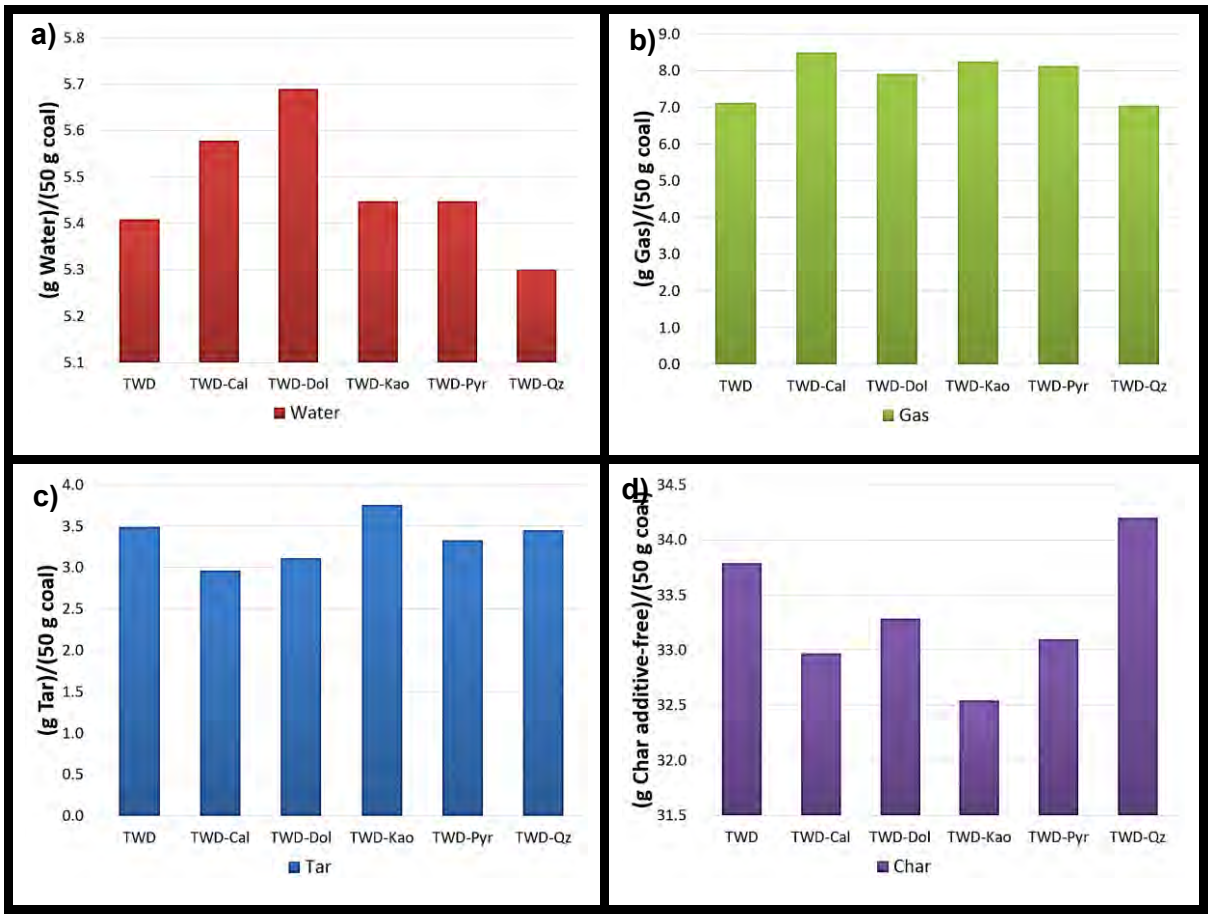

Figure 6-7 Pyrolysis product yields at 900°C for TWD coal and various mineral additions a) Water from coal (g); b) Tar produced (g); c) Gas from coal (g) and d) Char produced, *additive-free* (g).

With regard to water yield (Figure 6-7a), only TWD-Cal and TWD-Dol show a significant difference, (outside of the 95% confidence interval of TWD coal), with both mineral additions increasing the water yield. This result is consistent with the finding made for addition of these minerals to the AW TWD coal.

Comparison of the tar and gas yields (Figure 6-7b and Figure 6-7c), indicated that the addition of calcite (TWD-Cal) and dolomite (TWD-Dol) led to a decrease in tar yield, whilst the gas yield increased. This was attributed to the secondary tar cracking reactions to gas (Ahmad *et al.,* 2009b; Franklin *et al.,* 1982a, Franklin *et al.,*1981, Yeboah *et al.,* 1980). Kaolinite addition (TWD-Kao) had no significant effect on the tar and gas yields. Pyrite addition (TWD-Pyr) led to a small decrease in tar yield, with little change in the gas yield being observed. Pyrite is however believed to be more active at lower pyrolysis temperatures, during which it decomposes (Botah *et al.,* 2005; Franklin *et al.,* 1982a & 1982b). The addition of quartz, TWD-Qz, showed no significant differences for any of the pyrolysis product yields.

The char yield was reduced by the addition of calcite and dolomite, unaffected by kaolinite and pyrite addition, whilst quartz addition led to an increase in char yield. Calcite and dolomite addition showed the same trends than observed with the addition of these minerals to the AW TWD coal, whilst kaolinite, pyrite and quartz addition showed different trends. The effect of quartz addition can possibly be related to the limiting effect of quartz on the thermo-plasticity of the coal during heat treatment (Ôztas & Yürüm, 2000). The fact that no significant change in char yield was observed with the addition of kaolinite and pyrite may be related to the non-availability of minerals in the case of the AW TWD coal; thus addition thereof had a catalytic effect providing more active sites. In Chapter 5 it was also noted that little change in pyrolysis product yield took place between 750°C and 900°C for the TWD coal, which might limit the effect of these minerals in that reaction region, thus reducing the change observed. Kaolinite for example is deemed more active at higher temperatures with the active component being Al_2O_3 (Liu *et al.*, 2004a). In the case of pyrite the decomposition products, such as magnetite (Fe_3O_4) and hematite (Fe_2O_3), had the largest effect on pyrolysis (Borah *et al.,* 2005; Abu El-Rub *et al.,* 2004). These decomposition products formed at higher temperatures (>650°C). However, TWD coal indicated little pyrolysis activity at these temperatures.

6.3. Gas composition

The evolved gases were analysed by GC analyses. General trends are in agreement with the findings from Section 5.3. Appendix C-2 provides the full set of GC results, but for the sake of brevity, focus will be given to the most dominant gas species and the yields of the various gas species on a [g gas species] / [g coal (d.m.m.f.)] as determined by the use of Equation (4-6).

With regard to the order of the most prominent gases, good correspondence is observed to that of the AW TWD experiments up to 520°C and 900°C. The orders of decreasing amounts of gases evolved up to 520°C and 900°C were: CH_4>H_2>CO_2>CO and H_2>CH_4>CO>CO_2, respectively. In the case of the 750°C experiments, a change in order was however observed for the AW-Cal and AW-Dol runs, i.e. H_2>CH_4>CO_2>CO. The order for AW-Pyr is H_2>CH_4>CO_2=CO. The shift in composition in the case of AW-Cal and AW-Dol can be related to the decomposition of the calcite and dolomite minerals due to calcination, and thus release of CO_2, which will be most prominent for the 750°C experiments. The change observed for AW-Pyr at this temperature may be related to other gases that form that are not analysed using the current calibration gas, such as COS, SO_2 and H_2S. These gas species are however believed not to constitute such a large amount to bring about this large observed change, but the decomposition of the added pyrite must certainly play a role. In order to discuss the changes quantitatively, the discussion will now focus on the yield of the various gas species on a [g gas species] / [g coal (d.m.m.f.)] basis. Corrections for CO_2 produced due to calcination of the added minerals were made as discussed in Section 6.1.

6.3.1. H_2 yield

Figure 6-8a gives the H_2 gas yield obtained for the various mineral addition cases and the AW TWD coal. Up to 520°C, AW-Cal, AW-Dol and AW-Pyr showed a significant decrease in the H_2 gas yield. Up to 750°C, AW-Cal indicated a significant increase in H_2 yield, whilst AW-Dol caused a significant decrease in H_2 yield. At 900°C, all added minerals caused a significant decrease in the in H_2 yield, i.e. in the order of increasing significant change it is AW-Qz, AW-Pyr, AW-Cal, AW-Kao and AW-Dol. The decrease in H_2 yields with the addition of minerals were in accordance with the trends observed for the TWD fraction and AW TWD fraction (Chapter 5). As discussed in Chapter 5, addition of the removed minerals reduces the H_2 yield in accordance with what was observed for the raw coal (TWD). This trend was however most prominent at the higher pyrolysis temperatures.

The increased H_2 yield observed from the AW TWD fraction was based on four hypotheses:: i) the cracking of heavier hydrocarbons (Fuentes-Cano *et al.,* 2013; Khan, 1989); ii) the re-arrangement and condensing of aromatic structures and the direct de-hydrogenation of the formed chars (Siva *et al.,* 2013; Uzun *et al.,* 2007; Williams & Taylor, 1993; Cypress & Bettens, 1989); iii) the bond stabilisation after scission of very weak aliphatic (C-H) bonds (Smith *et al.* 1994; Abbot and Wojciechowski, 1988); and, iv) lower hydrogen transfer (Ahmad *et al.,* 2009a; Ishihara *et al.,* 2004; Solomon *et al.,* 1990; Solomon *et al.,* 1988).

Table 6-3 Molar composition of gas species evolved at 520°C, 750°C and 900°C

	AW TWD	AW-Cal	AW-Dol	AW-Kao	AW-Pyr	AW-Qz
			mol. %			
			520°C			
H_2	22.0 - 24.2	21.2 - 22.9	20.4 - 21.9	20.8 - 23.5	20.9 - 22.3	22.3 - 22.3
CH_4	36.1 - 37.9	33.8 - 34.3	33.5 - 34.2	36.2 - 37.1	36.5 - 37.1	36.6 - 37.8
CO	13.7 - 14.5	13.2 - 14.0	16.7 - 16.9	14.1 - 14.5	12.6 - 14.2	14.4 - 14.5
CO_2	17.9 - 18.9	23.2 - 24.8	20.8 - 21.2	18.4 - 19.9	21.0 - 22.6	18.7 - 19.3
			750°C			
H_2	38.0 - 38.4	37.2 - 38.2	36.2 - 38.7	37.8 - 39.3	37.6 - 38.8	38.0 - 38.3
CH_4	20.2 - 21.4	27.5 - 28.5	26.4 - 27.9	31.1 - 31.4	30.9 - 31.0	31.4 - 31.5
CO	26.9 - 27	14.5 - 15.0	14.3 - 15.4	14.4 - 14.6	12.8 - 13.2	14.2 - 14.3
CO_2	10.6 - 11.4	15.8 - 16.0	15.7 - 17.4	11.0 - 11.3	12.9 - 13.8	11.2 - 11.3
			900°C			
H_2	44.5 - 46.1	35.8 - 38.8	34.9 - 37.0	38.7 - 39.9	38.7 - 43.3	42 - 45.2
CH_4	28.2 - 29.2	24.2 - 25.2	24.0 - 24.6	27.5 - 28.4	25.3 - 27.3	28.9 - 30.3
CO	11.9 - 13.2	19.6 - 22.0	20.5 - 22.6	19.7 - 21.7	18.5 - 20.2	13.0 - 13.4
CO_2	8.8 - 10.4	13.1 - 14.5	14.1 - 15.4	8.6 - 9.0	9.6 - 10.7	8.9 - 9.9

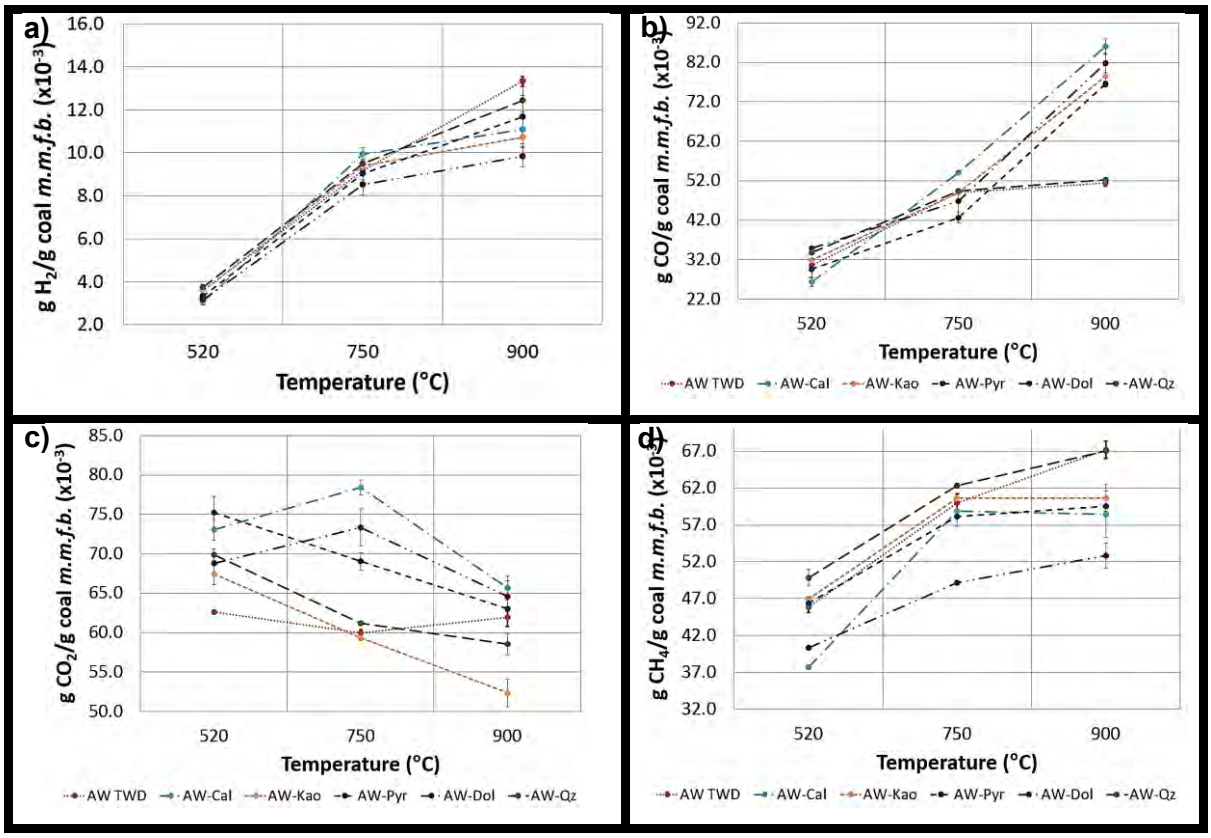

Figure 6-8 a) H_2, b) CO, c) CO_2 and d) CH_4 yields for the various mineral additions.

It is clear from Figure 6-8a that the added minerals were observed to influence the H_2 yields to such an extent that these reactions [hypothesis (i)-(iv)] were inhibited by their presence.

Calcite and dolomite are known to increase H_2 yields in gas clean-up systems (Ortiz & Harrison, 2001; Balasubramanian *et al.,* 1999), and kaolinite was observed to increase H_2 yields during pyrolysis (Ôztas & Yürüm, 2000; Chen *et al.* 1999; Franklin *et al.,* 1982a, Howard 1963). The increased H_2 yield observed for AW-Cal up to 750°C could be related to the reduced tar yield at the same temperature due to tar cracking taking place (Orio *et al.,* 1997). The tar cracking capabilities of calcite (Liu *et al.*, 2004a; Qi *et al.*, 2004; Tsubouchi & Ohtsuka, 2002a, 2002b; Chen *et al*., 1999; Mondragon *et al.*, 1999; Franklin *et al.,* 1982a, 1982b; Yaw *et al.* 1980) and dolomite (Mun *et al.,* 2012; Pinto *et al.,* 2007; André *et al.,* 2004; Liu *et al.*, 2004a; Sciazko & Kubica, 2002; Chen *et al*., 1999; Yaw *et al.,* 1980) are well documented. The decrease observed with the addition of minerals in the 900°C experiments seems somewhat odd if this is taken into account, i.e. it suggests that the minerals present in TWD coal play a different role during pyrolysis than is expected at first sight. At the higher pyrolysis temperatures it is possible that the minerals assist in increasing the hydrogen transfer of the coal structure (and subsequently reducing the H_2 yield) as the hydrogen transfer rate for acid washed coals was found to be lower than that of the raw coal (Ahmad *et al.,* 2009a; Ishihara

et al., 2004; Solomon *et al.,* 1990; Solomon *et al.,* 1988). Clay minerals such as kaolinite were found to catalyze H_2 transfer to coal and coal model compounds (Franklin *et al.*, 1981; Mukherjee & Choudry, 1976; Given, 1974).

6.3.2. CO yield

From Figure 6-8b it can be observed that for all the mineral addition experiments an increase in CO yield was observed together with an increase in final pyrolysis temperature, except with the addition of quartz (AW-Qz) for which the difference in CO yield between 750°C and 900°C could not be regarded as significant. The CO yield profile of AW-Qz did however indicate a significant increase in CO yield in the 520°C experiments. AW-Dol and AW-Kao also showed a significant increase in CO yield at 520°C, whilst AW-Cal showed a significant decrease in CO yield. The 750°C AW-Cal experiments are observed to have produced an increased yield of CO, whilst AW-Dol and AW-Pyr showed significant decreases. In the case of the 900°C experiments, all the mineral additions are observed to have caused a significant increase in CO yield, except for AW-Qz. The CO yield of the mineral addition cases corresponded to the CO yield of the TWD coal up to 900°C (Chapter 5).

The increased CO yield obtained with the addition of calcite and dolomite is attributed to the cracking of oxygen functional groups on the parent coal by CaO (Pinto *et al.,* 2007; Liu *et al.*, 2004a; Karaca, 2003; Tsubouchi *et al.*, 2004; Tsubouchi and Ohtsuka, 2002, Delgado *et al.,* 1996, Franklin, 1980). CaO is a decomposition product of calcite and dolomite and starts to form at temperatures in excess of 500°C. This explains the larger difference observed with an increase in final pyrolysis temperature. It is known from the ultimate and DRIFT analyses of the TWD and AW TWD chars, that the AW TWD chars had a higher oxygen content or functionalities present in the chars for the 750°C and 900°C experiments, thus ultimate and DRIFT analyses of the chars derived from the mineral added cases (Section 6.5.1.), may provide more insight with regard to this hypothesis.

6.3.3. CO_2 yield

Figure 6-8c indicates the CO_2 yields obtained for the various mineral additions. It can be observed that the CO_2 yields up to 520°C with mineral addition is higher than that of the AW TWD coal for all minerals, with an increase in significance in the order of AW-Kao, AW-Dol, AW-Qz, AW-Dol and AW-Pyr. Up to 750°C, the CO_2 yields of AW-Kao and AW-Qz showed no significant difference to that of AW TWD. At the same temperature, AW-Cal, AW-Dol and AW-Pyr (in decreasing order of significance), showed higher yields of CO_2. At the final pyrolysis temperature of 900°C a decrease in CO_2 yields was observed with the addition of kaolinite and quartz. The CO_2 yield from AW-Cal and AW-Dol were still higher than that of the AW TWD coal fraction, but not as significant as at 750°C. The CO_2 yield of AW-Pyr corresponded to that

of AW TWD up to 900°C. Between 750°C and 900°C, a dramatic decrease in CO_2 yield of AW-Cal and AW-Dol was observed. The addition of kaolinite clearly reduced the CO_2 yield to showed better correspondence with the lower CO_2 yield of the TWD coal (Chapter 5).

The increased yield of CO_2 with the addition of calcite (Yongbin *et al.,* 2004; Aznar *et al.,* 1996; Franklin *et al.,* 1981; Franklin, 1980) and dolomite was expected. In this study it was not observed to be active in reduction of CO_2 yields in the temperature range 400 – 800°C (Yeboah *et al.,* 1980; Vestal *et al.,* 1970; Dedman & Owen, 1962). Calcite and dolomite, which decomposes to CaO, were found to decrease CO_2 yields in previous work in the temperature range 800 – 900°C. The current study confirms this observation, noting that the CO_2 yield was greatly reduced between 750°C and 900°C (Sert *et al.,* 2011; Yeboah *et al.,* 1980). CO_2 could also be produced from the tar cracking reactions where carboxyl functional groups in the tar were cracked; this would have completed at 650°C (Yongbin *et al.,* 2004). The CO_2 peak observed up to 750°C was characteristic of this behaviour. Decomposition of calcite related to coal was observed at lower temperatures than was the case for calcite in the absence of coal (Franklin, 1980), which could explain the earlier peak in CO_2.

The focus needs to be placed on the water-gas shift reaction, Equation 6-5, as indicated in Table 6-2 (Section 6.2.3):

$$CO(g) + H_2O(g) \rightleftharpoons CO_2(g) + H_2(g) \quad (6\text{-}5)$$

The importance of this equation with regard to product yields and composition with the addition of dolomite or calcite was confirmed (Abu El-Rub, 2004; McKee, 1980). With the addition of calcite and dolomite, increased CO and water yields were reported, whilst the CO_2 and H_2 yields were lower. When observing the water-gas shift reaction it is clear that under the current experimental conditions the left hand side of this equation must be favoured, thus explaining the shift observed in composition. If the gas yields of the AW TWD coal are taken into account, it can be observed that a relatively high H_2 and CO_2 yield was already present at the lower pyrolysis temperature (520°C). The amount of CO and H_2O produced was thus lower than that of the TWD coal, i.e. the reaction products present are thus in favour of the water-gas shift reaction going to the left hand side.

6.3.4. CH_4 yield

Up to 520°C, the CH_4 yield (Figure 6-8d) of AW-Qz is higher than that of the AW TWD run, whilst it is lower for AW-Cal and AW-Dol, and AW-Kao and AW-Pyr show no significant difference. Up to 750°C, the CH_4 yields of AW-Pyr and AW-Dol are significantly lower, whilst that of AW-Qz is significantly higher, with AW-Kao and AW-Cal showing no significant difference. Up to 900°C, all the minerals are observed to have a significant effect in decreasing

the CH_4 yield, except for the addition of quartz (AW-Qz). The CH_4 yields of AW-Cal, AW-Kao and AW-Pyr does not show any differences between 750°C and 900°C, which indicates that no CH_4 was formed at temperatures higher than 750°C. Dolomite addition had the most profound effect on the CH_4 yield, decreasing the CH_4 yield similar to the trend observed for TWD coal (Section 5.3.4).

The decrease in CH_4 yield observed with the addition of dolomite is in agreement with what was observed from gasification experiments by Mun *et al.* (2012) and Pinto *et al.* (2007) as well as in some biomass gasification experiments (Gerber, 2007; Asadulla *et al.,* 2002; Sutton *et al.,* 2001; Perez *et al.,* 1997, Yeboah *et al.,*1980; Solano *et al.,* 1977). The reduction of CH_4 yield with the addition of pyrite was confirmed in this study in accordance with findings by Franklin *et al.,* (1982a and 1982b).

The complexity of the reactions taking place during coal pyrolysis and varying experimental conditions may be responsible for these differences. A significant shift in gas composition is difficult to quantify due to the fact that although smaller components form, i.e. H_2, CO and CO_2, more hydrocarbon molecules form as well, which make up those converted to smaller fractions, because of a decrease in tar yield and increase in gas yield (Pinto *et al.*, 2007 and 2009). The fact that the addition of these minerals shows trends that correlate with the TWD coal is a positive indication, indicating that these minerals have a definite effect in the pyrolysis behaviour of coals, and that the synergistic effect of the interactions taking place cannot be underestimated. Discrepancy in gas yields with the addition of dolomite as catalyst in biomass gasification can also be observed in various reports (Sutton *et al.,* 2001; Perez *et al.,* 1997; Aznar *et al.,*1996).

6.3.5. Other gas species

The effect of the addition of the various minerals on the respective gas yields is indicated in Figure 6-9. The C_2H_4 yields (Figure 6-9a) for the various mineral addition runs show no significant difference with an increase in final pyrolysis temperature for AW-Cal. A significant decrease with increase in final pyrolysis temperature is observed for AW-Dol between 520°C and 750°C, but the change to 900°C cannot be regarded as significant. AW-Kao, AW-Pyr and AW-Qz all show significant decreases in C_2H_4 yield with increasing final pyrolysis temperature.

Comparison of the influence of various mineral additions to the C_2H_4 yield as observed for AW TWD indicates that AW-Dol and AW-Pyr show no significant difference in the yield of C_2H_4 up to 520°C, whilst AW-Cal indicates a definite decrease in yield, with AW-Kao and AW-Qz indicating an increase in C_2H_4 yield. In the case of the 750°C experiments, only AW-Dol indicates a significant decrease in C_2H_4 yield, with no other mineral addition causing any

significant change. From the 900°C experiments, no significant difference in C_2H_4 yield is observed.

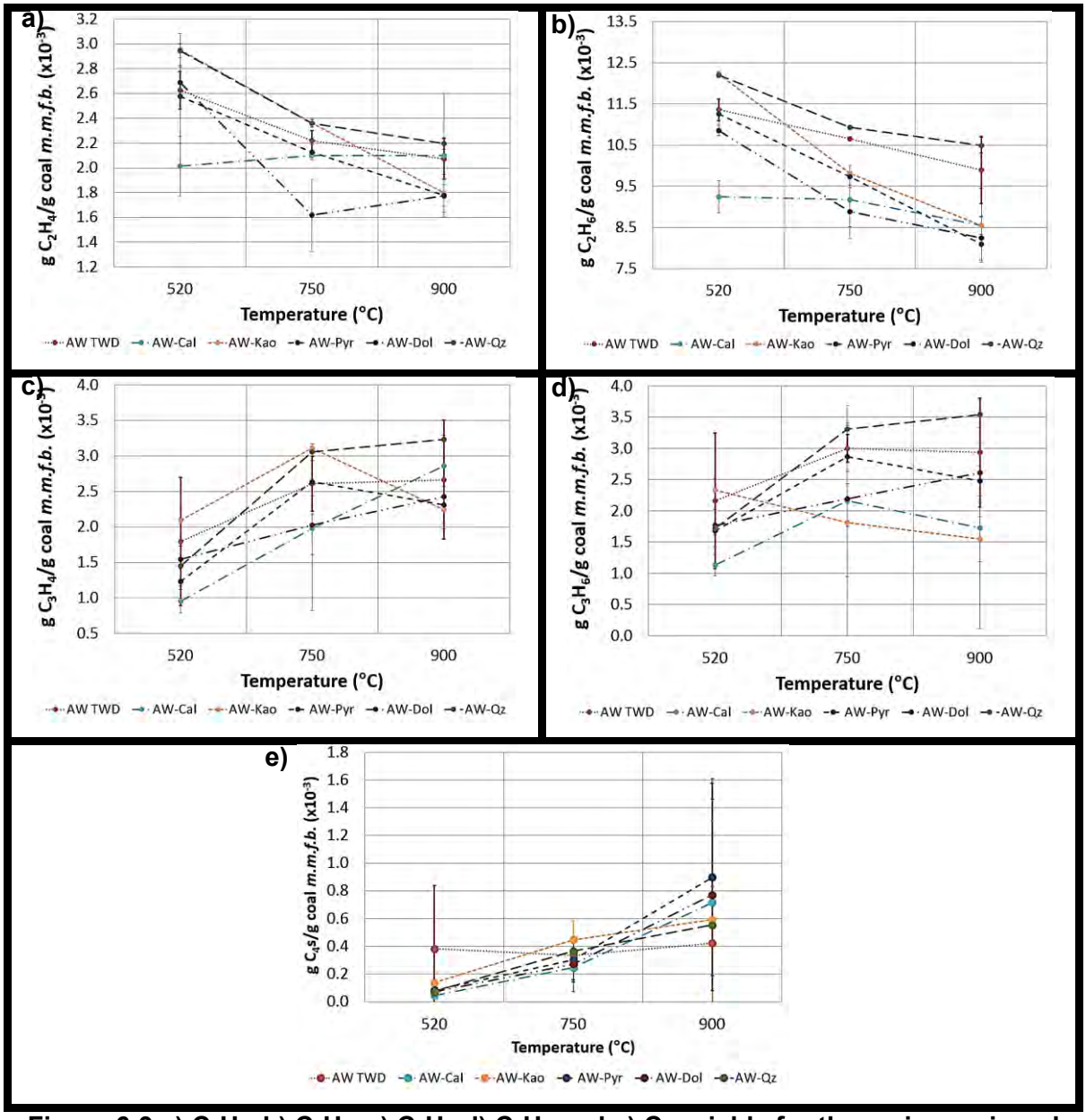

Figure 6-9 a) C_2H_4, b) C_2H_6, c) C_3H_4, d) C_3H_6 and e) C_4s yields for the various mineral addition cases.

Figure 6-9b indicates the C_2H_6 yields obtained. It can be observed that for all mineral addition cases a significant decrease in C_2H_6 yield is evident, except for AW-Cal. Comparison with the C_2H_6 yield of the AW TWD run indicates that for the 520°C experiments that the AW-Cal significantly decreases the C_2H_6 yield, whilst AW-Kao and AW-Pyr showed significant increases. From the 750 and 900°C experiments, all the mineral additions [except for the addition of quartz (AW-Qz)], all show significant decreases in C_2H_6 yield.

Figure 6-9c to Figure 6-9e indicate the yields of C_3H_4, C_3H_6 and C_4s, respectively. No significant difference is observed in any of these yields when compared to that of the AW TWD coal.

In general, it can be observed that the addition of minerals led to the reduction of gases of the form C_nH_m. Quartz addition was most inactive in changes in gas yields, whilst kaolinite addition showed varying trends. The changes caused by pyrite addition were also less significant, except in the reduction of the C_2s at higher temperatures, and increases in C_4s up to 900°C. The cracking of gases (of the form C_nH_m) by calcite and dolomite was confirmed previously and is related to the tar cracking capabilities, mainly attributed to the decomposition product CaO (Mun *et al.,* 2012; Pinto *et al.,* 2007; Yongbin *et al.,* 2004; Xu & Tomita, 1989; Franklin *et al.* 1982b; Yeboah *et al.,* 1980). Kaolinite was observed to cause shifts in pyrolysis product composition due to cracking of hydrocarbons (Ôztas and Yürüm, 2000; Chen *et al.* 1999; Franklin *et al.,* 1982a). The active component is however believed to be Al_2O_3 and is more active at higher temperatures (Liu *et al.*, 2004a). This is confirmed by the current results. Literature reports little change in the C_2 – C_4s (Franklin *et al.,* 1982a, 1982b). Experimental conditions do however differ, i.e. slow pyrolysis vs. flash pyrolysis. Another factor is that the decomposition products of pyrite are believed to be most active and effect pyrolysis products to the greatest extent (Borah *et al.,* 2005). This explains why the changes are only observed at the elevated final pyrolysis temperatures. The inactive nature of quartz on the pyrolysis yield was also expected.

6.4. Tar composition

The tar composition was analysed by ultimate, Simdis, GC-MS and –FID and SEC-UV analyses.

6.4.2. Simulated distillation (Simdis)

The boiling point distributions obtained for the derived tars produced are indicated in Figure 6-10. The tar boiling points were confined in the region 112.2°C – 550°C. All injected tar (100%) was recovered at temperatures below 550°C. Refer to Appendix C.3.2 for repeatability curves.

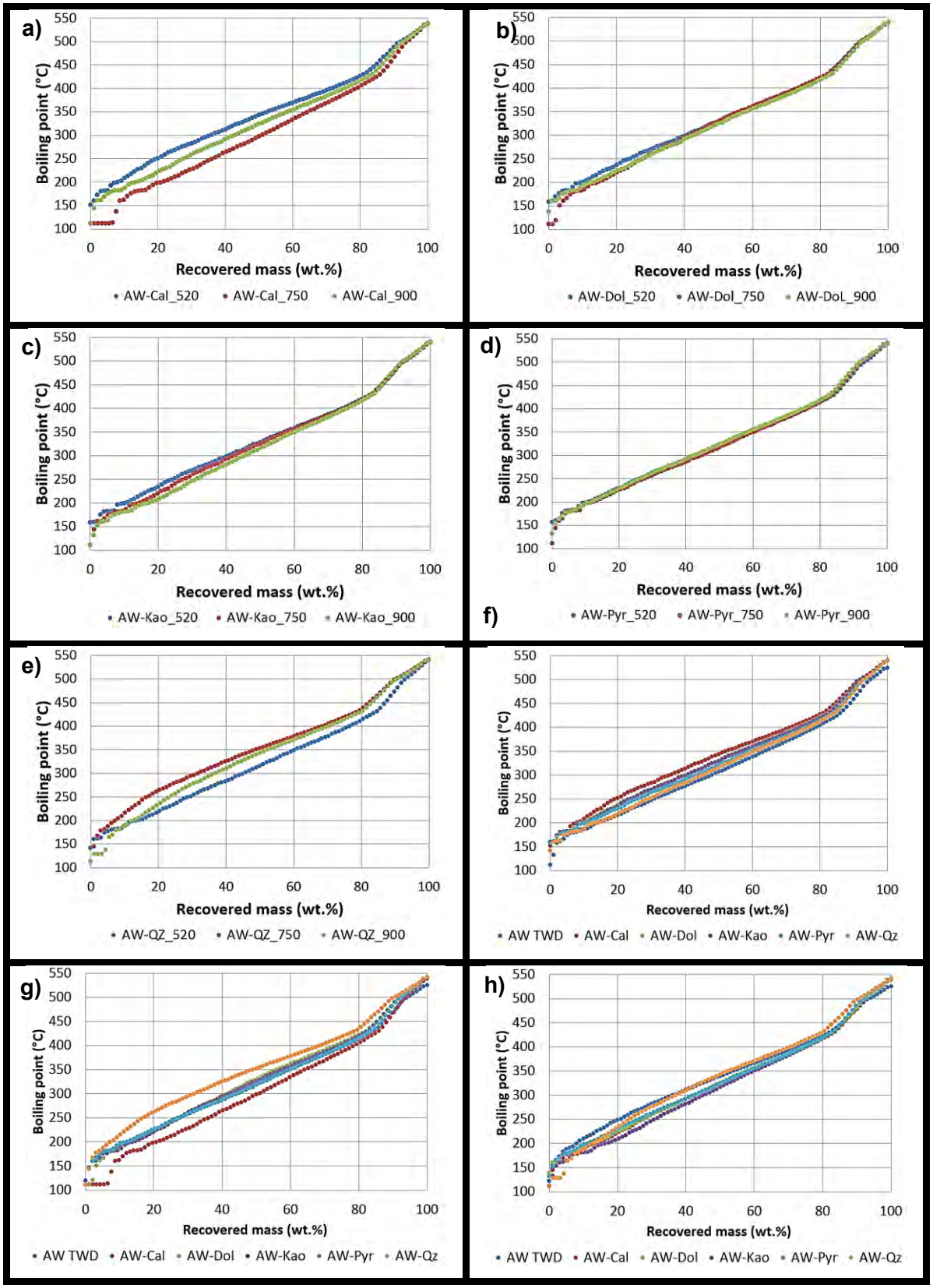

Figure 6-10 Boiling point distribution curves for a) AW-Cal; b) AW-Dol; c) AW-Kao; d) AW-Pyr; e) AW-Qz; f) Mineral additions at 520°C; g) Mineral additions at 750°C and h) Mineral additions at 900°C.

Table 6-4 Boiling point distributions for tars based on crude oil fractions

Boiling point range (°C)		AW TWD		AW-Cal		AW-Dol		AW-Kao		AW-Pyr		AW-Qz	
		wt% /°C	g/100 g coal	wt% /°C	g/100 g coal	wt% /°C	g/100 g coal	wt% /°C	g/100 g coal	wt% /°C	g/100 g coal	wt% /°C	g/100 g coal
520°C													
Medium naphtha	79-121	1.0	0.1	1.0	0.1	1.0	0.1	1.0	0.1	1.0	0.0	1.0	0.1
Heavy naphtha	121-191	10.2	0.5	4.0	0.2	6.0	0.3	6.0	0.3	7.0	0.3	9.2	0.5
Kerosene	191-277	29.6	1.5	22.0	1.1	25.0	1.4	25.0	1.4	27.0	1.1	26.5	1.3
Distillate fuel oil	277-343	21.4	1.1	22.0	1.1	21.0	1.1	22.0	1.2	23.0	1.0	21.5	1.1
Light vacuum gas oil	343-455	28.6	1.5	36.0	1.8	33.0	1.8	32.0	1.8	30.0	1.3	29.6	1.5
Heavy vacuum gas oil	455-566	9.2	0.5	15.0	0.8	14.0	0.8	14.0	0.8	13.0	0.6	12.2	0.6
IBP	-	112.2		112.2		112.2		112.2		112.2		112.2	
WABP	100 - 550	302 - 326		342 - 346		330 - 336		330 - 334		327 - 331		319 - 321	
FBP	-	524.3		539.8		539.8		539.8		539.8		539.8	
750°C													
Medium naphtha	79-121	1.0	0.1	5.4	0.2	3.2	0.2	1.0	0.1	1.0	0.1	1.0	0.1
Heavy naphtha	121-191	8.0	0.5	10.9	0.5	7.3	0.4	9.4	0.6	7.2	0.4	4.1	0.3
Kerosene	191-277	26.0	1.6	27.2	1.2	23.2	1.2	24.0	1.4	28.5	1.7	18.4	1.2
Distillate fuel oil	277-343	20.0	1.2	18.5	0.8	20.0	1.0	19.8	1.2	21.4	1.3	22.4	1.4
Light vacuum gas oil	343-455	31.0	1.9	26.0	1.1	31.6	1.6	31.2	1.8	29.6	1.8	36.8	2.3
Heavy vacuum gas oil	455-566	14.0	0.9	12.0	0.5	14.7	0.8	14.6	0.9	13.3	0.8	17.3	1.1
IBP	-	112.2		112.2		112.2		112.2		112.2		112.2	
WABP	100 - 550	318 -330		304 - 308		329 - 333		327 - 328		327 -329		347 - 354	
FBP	-	524.7		538.8		540.1		540		540.8		541.2	
900°C													
Medium naphtha	79-121	0.8	0.1	1.0	0.0	1.0	0.0	1.0	0.1	1.0	0.1	1.1	0.1
Heavy naphtha	121-191	5.2	0.3	9.2	0.3	8.2	0.3	12.3	0.8	7.2	0.4	9.8	0.7
Kerosene	191-277	22.0	1.4	24.5	0.9	25.5	0.9	24.5	1.6	26.5	1.6	18.4	1.2
Distillate fuel oil	277-343	23.0	1.5	20.4	0.8	20.4	0.7	19.3	1.2	21.4	1.3	20.7	1.4
Light vacuum gas oil	343-455	35.0	2.2	31.3	1.2	31.6	1.1	28.6	1.8	30.6	1.8	33.7	2.2
Heavy vacuum gas oil	455-566	14.0	0.9	13.3	0.5	13.3	0.5	14.3	0.9	14.3	0.9	16.3	1.1
IBP	-	112.2		112.2		112.2		112.2		112.2		112.2	
WABP	100 - 550	326 - 354		326 - 328		328 - 331		320 - 324		329 - 333		340 - 348	
FBP	-	524.8		539.8		540.4		540.8		541.2		541	

6.4.2.1. Effect of temperature

The tars derived from the AW-Pyr experiment (Figure 6-10d) indicate the most consistency with regard to composition, whilst the AW-Dol (Figure 6-10b) and AW-Kao (Figure 6-10c) derived tars also indicate good consistency at the different pyrolysis temperatures, but the AW-Cal (Figure 6-10a) and AW-Qz (Figure 6-10e) derived tars show quite a lot of variation. In the case of the AW-Cal, AW-Dol and AW-Kao experiments (Figure 6-10a, 6-10b and 6-10c respectively), increased lighter boiling point compounds are formed with increasing pyrolysis temperature, which can be attributed to thermal cracking (Hattingh, 2012; King *et al.,* 1978; Bunger, 1976). On the other hand, with the addition of quartz (Figure 6-10e – AW-Qz) increased higher boiling compounds are formed with an increase in final pyrolysis temperature, consistent with the observations made for the AW TWD case, i.e. thus indicating that this mineral is inactive during the pyrolysis process. The AW-Pyr derived tars (Figure 6-10d) showed no significant change in boiling point distribution of the derived tars with increasing final pyrolysis temperature, but must however suppress the formation of higher boiling point compounds that were observed for the AW TWD derived tar without any mineral addition. The boiling point distributions observed are in accordance with typical fossil fuel and waste-derived tars and oils as observed in previous studies (Roets *et al.,* 2014; Bean 2013; Hattingh, 2012; Lee, 2009; Karayildirim *et al.,* 2006; Shie *et al.,* 2003; Li *et al.,* 2001; Bunger 1976).

Table 6-4 indicates the IBP, FBP, and WABP for the various mineral addition cases and the AW TWD base case derived tars. The IBP of all the mineral addition experiments are in agreement with that of the AW TWD coal tar. Regarding the FBP, it can be observed that the FBP for the mineral addition derived tars is higher in all cases (in the area of 539°C – 541°C). Comparison of the WABPs for the various mineral addition cases indicates that the WABP decreased with increasing final pyrolysis temperature for the derived tars of the AW-Cal, AW-Dol and AW-Kao experiments. This is in agreement with the observations made from the boiling point distribution graphs (Figure 6-10a – Figure 6-10c). The WABPs of AW-Pyr indicate no difference with increasing final pyrolysis temperature, consistent with what was observed from the boiling point distribution graphs (Figure 6-10d). The WABP of the AW-Qz tar is observed to increase with an increase in final pyrolysis temperature, in accordance with the boiling point distribution graphs (Figure 6-10e).

6.4.2.2. Effect of mineral addition

Comparison of the boiling point distributions of the derived tars for the various mineral additions to that of the AW TWD derived tar, at the various pyrolysis temperatures, is shown in Figure 6-10f – Figure 6-10h. From the 520°C experiments (Figure 6-10f), the addition of all

mineral compounds are observed to lead to the formation of more compounds having higher boiling points, consistent with the derived tar of the TWD coal.

Comparison of the yields of the different cut fractions on a quantitative basis between the AW TWD tar and the tars derived from the respective mineral addition cases produced at 520°C (Table 6-4) indicates that the medium, heavy naphtha and kerosene derived compounds decreased for all additions. The addition of quartz had very little effect on the heavy naphtha fraction. The distillate fuel oil cut fraction derived compounds are observed to be unaffected by the addition of calcite and dolomite, whilst the addition of pyrite led to an increase in these compounds, and the addition of kaolinite and quartz led to decreases. The light vacuum gas oil cut fraction compounds were observed to increase with the addition of calcite, dolomite and kaolinite, whilst pyrite decreased these compounds, and quartz showed no effect. The heavy vacuum gas oil cut fraction compounds were observed to increase with the addition of all the minerals, except pyrite, which showed no effect.

In the case of the 750°C experiments (Figure 6-10g), the addition of calcite (AW-Cal) led to the formation of more lighter boiling compounds; this can be attributed to the tar cracking properties previously confirmed (Liu *et al.*, 2004a; Qi *et al.*, 2004; Tsubouchi & Ohtsuka, 2002a, 2002b; Chen *et al*., 1999; Mondragon *et al.*, 1999; Franklin *et al.,* 1982a, 1982b; Yaw *et al.* 1980). The fact that dolomite showed no significant change at this temperature may be related to the fact that calcination was still in process and had not fully taken place yet. From the TG analyses (Section 3.9) it is known that dolomite starts decomposition at a slightly higher temperature than for calcite. From Table 6-4 it can be observed that in the case of the 750°C tars, the medium naphtha fraction was increased only by the addition of calcite. The heavy naphtha fraction was decreased by the addition of dolomite and quartz, and unaffected by the other minerals. The kerosene fraction compounds were decreased by the addition of calcite, dolomite and kaolinite, whilst the addition of pyrite and quartz led to an increase in these compounds. The compounds derived as part of the distillate fuel oil were decreased by the addition of calcite and dolomite, unaffected by the addition of kaolinite, and increased by the addition of pyrite and quartz. The light and heavy vacuum gas oil derived compounds are observed to be decreased by the addition of calcite, dolomite and pyrite, unaffected by the addition of kaolinite, and increased by the addition of quartz.

At a final pyrolysis temperature of 900°C (Figure 6-10h), all the mineral matter, except for the addition of quartz (AW-Qz), seem to lead to the formation of increased lighter boiling point compounds, in the temperature range up to 400°C; consistent with the trend observed for the TWD derived tar. The tar cracking capabilities of calcite (Liu *et al.*, 2004a; Qi *et al.*, 2004; Tsubouchi & Ohtsuka, 2002a, 2002b; Chen *et al*., 1999; Mondragon *et al.*, 1999; Franklin *et*

al., 1982a, 1982b; Yaw *et al.* 1980), dolomite (Mun *et al.,* 2012; Pinto *et al.,* 2007; André *et al.,* 2004; Liu *et al.*, 2004a; Sciazko& Kubica, 2002; Chen *et al.*, 1999; Yaw *et al.,* 1980; Yeboah *et al.,* 1980), kaolinite (Karaca, 2003; Ôztas & Yürüm, 2000; Chen *et al.,* 1999, Franklin *et al.,* 1982a) and pyrite (Borah *et al.,* 2005; Franklin *et al.,* 1982a and 1982b) are known, whilst the inactivity of quartz on pyrolysis product yields and composition was to be expected due to the chemical inert nature of this mineral (Ôztas & Yürüm, 2000; Chen *et al.*, 1999; Franklin *et al.,* 1982a, Franklin *et al.,* 1981). From Table 6-4 it can be observed that at 900°C the addition of calcite and dolomite led to a decrease in medium naphtha compounds, whilst the other additions had little effect. The heavy naphtha compounds were increased by the addition of kaolinite, pyrite and quartz, but unaffected by calcite and dolomite addition. The addition of calcite, dolomite and quartz led to a decrease in the kerosene fraction, whilst kaolinite and pyrite increased within this fraction. On the other hand the distillate fuel oil fraction is observed to be decreased by all mineral additions. The light vacuum gas oil fraction was decreased by the addition of all minerals, except quartz. The addition of calcite and dolomite led to an increase in heavy vacuum gas oil cut fraction compounds, whilst kaolinite and pyrite addition had no effect, and the addition of quartz led to an increase in these compounds.

Comparison of the WABPs of the mineral addition runs to that of the AW-TWD run indicates that the WABP of the AW-Cal, AW-Dol, AW-Kao and AW-Pyr derived tars were significantly higher in the case of the 520°C experiments, whilst the WABP of AW-Qz derived tar corresponded to that of AW TWD. The WABP of AW-Cal tar indicated the largest increase in WABP (342°C – 346°C). This result is in agreement with the conclusions made from the boiling point distribution graphs (Figure 6-10e). In the 750°C experiments, the WABP of AW-Cal tar was significantly lower than that of AW-TWD tar, while that of AW-Qz tar was significantly higher; the WABP of all the other minerals was in agreement with that of the AW TWD tar. At a final pyrolysis temperature of 900°C, the WABP of AW-Kao tar was lower than that of AW TWD tar, whilst all other mineral additions derived tar WABPs, showed good agreement with that of the AW TWD tar.

6.4.3. Gas chromatography-mass spectrometry and -flame ionization detection (GC-MS and -FID)

The GC-MS analyses of the derived tars are indicated in Figure 6-11. All results are reported within a 95% confidence interval, as calculated from standard deviation values for four repeat experiments. Refer to Appendix C-4 for GC-MS and –FID data with indicated confidence intervals.

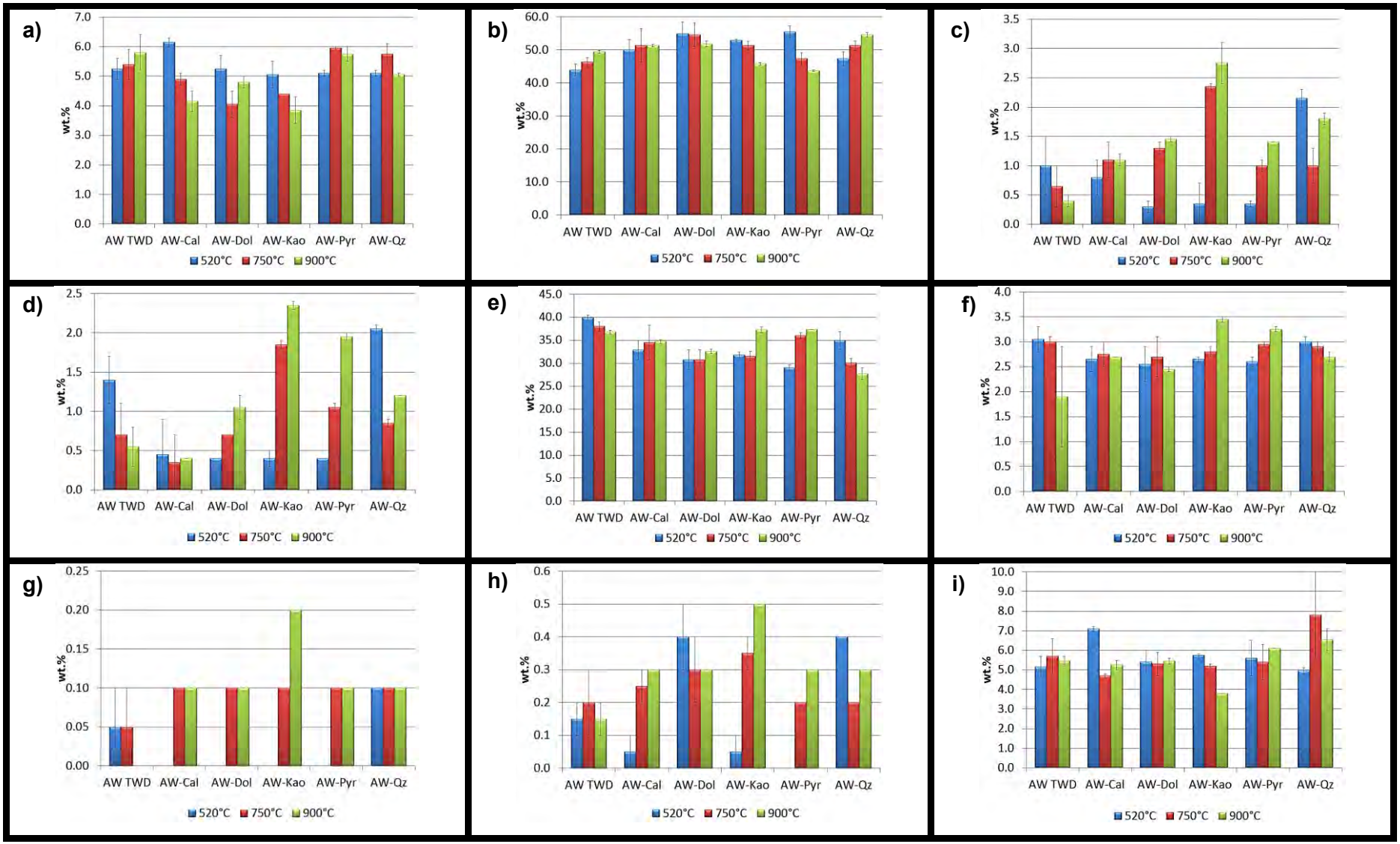

Figure 6-11 a) Aliphatic compounds; b) Mixed aromatics and aliphatics; c) Alkyl-benzenes; d) Aromatic ethers and esters; e) Alkyl-phenols; f) Alkyl-naphthalenes; g) Alkyl-Indenes; h) PAHs and i) N-heteroatoms.

6.4.3.1. Full spectrum

Effect of temperature

Figure 6-11a indicates the results obtained for the aliphatic compounds. The AW TWD derived tars showed no significant difference in aliphatic compounds with increasing final pyrolysis temperature. For the AW-Cal and AW-Kao derived tars, it can be observed that the aliphatic compounds decreased with an increase in final pyrolysis temperature. In the case of the AW-Dol tars, a decrease in aliphatic compounds was observed between 520°C and 750°C, whilst between 750°C and 900°C the aliphatic content increased again. AW-Pyr derived tars showed an increase in aliphatic compounds between 520°C and 750°C, with no significant difference between 750°C and 900°C. For the AW-Qz derived tars, no significant difference in aliphatic compound yield was observed between 520°C and 900°C, but at 750°C the aliphatic compounds were however slighly higher.

A decrease in aliphatic compounds with increasing final pyrolysis temperature is in agreement with previous findings (Wang *et al.,* 2013; Jones *et al.,* 2005; Nelson & Tyler, 1988). In the case of the TWD derived tars, the decrease in aliphatic compounds was related to thermal cracking of the aliphatic compounds, which were predominantly formed during primary pyrolysis (Zhang *et al.,* 2010; Casal *et al.,* 2008; Jones *et al.,* 2005; Morf *et al.,* 2002, Jess *et al,* 1996). From the obtained results it can be stated that this cracking is catalysed by the calcite, dolomite and kaolinite minerals present in the coal.

Comparison of the mixed aliphatic and aromatic compounds (Figure 6-11b) for the AW-Cal and AW-Dol derived tars at the various pyrolysis temperatures indicate no significant change with increasing final pyrolysis temperature. In the case of the AW-Kao derived tar, no significant change was observed between 520°C and 750°C, but at a final pyrolysis temperature of 900°C the yield of these compounds decreased significantly. The AW-Pyr derived tars show a significant decrease in the mixed compounds with increasing final pyrolysis temperature.

The AW-Qz derived tars showed a significant increase in mixed components with increasing final pyrolysis temperature; consistent with the trend observed for the AW TWD derived tar. The little variance observed with regard to these compounds with an increase in final pyrolysis temperature is indicative of the possibility that bulk of these compounds had already formed up to 520°C, i.e. changes observed were only indicative of secondary reactions taking place (Wang *et al.,* 2013; Zhang *et al.,* 2010; Casal *et al.,* 2008; Jones *et al.,* 2005; Morf *et al.,* 2002, Jess *et al,* 1996; Nelson & Tyler, 1988).

Effect of mineral addition

Comparison of the various mineral addition yields of the aliphatic compounds (Figure 6-11a) to that of the AW TWD derived tar indicates no significant difference in the 520°C experiments, except for the addition of 5 wt% calcite (AW-Cal), which led to an increase in these compounds, and is consistent with an observation made at 600°C for biomass tars by Dickerson and Serio (2013). This is probably due to increased cracking of larger ring structures and heavier tar molecules of aromatic nature, such as the aromatic ethers and esters (Figure 6-11c), alkyl-phenols (Figure 6-11d), alkyl-naphthalenes (Figure 6-11e) and PAHs (Figure 6-11h) (Yongbin *et al.,* 2004; Franklin, 1980; Mead, 1979).

In the case of the 750°C experiments, lower yields of aliphatic compounds can be reported with the addition of 5 wt% dolomite (AW-Dol), with no other significant differences observed for the other minerals. This reduction in aliphatic compounds can be related to MgO, one of the decomposition products of dolomite, which would have formed in the 750°C experiments, and was observed to reduce long chain alkanes and alkenes to lower molecular weight hydrocarbons in biomass tar cracking studies (Dickerson & Serio, 2013; Putun, 2010).

From the 900°C tars, lower aliphatic compound yields are observed with the addition of kaolinite (AW-Kao), calcite (AW-Cal), dolomite (AW-Dol) and quartz (AW-Qz), in decreasing order of significant effect. The addition of minerals clearly catalyses the cracking of tars to other components, i.e.calcite and dolomite are active even at the lower pyrolysis temperatures, whilst kaolinite and quartz are only active at higher temperatures, and pyrite seems to have no effect on the aliphatic content of the tars. Franklin *et al.,* (1982a), and (1982b) found that pyrite was only active in cracking the short chain light hydrocarbons C_4-C_8, and it thus explains why no definite influence was observed for the aliphatic compounds in the current study, as they comprised longer chains. These compounds (C_4-C_8) cannot be identified in the liquid/tar state in the current study due to the water removal method used. The cracking by calcite and dolomite is related to CaO, which was observed to be active in the production of lighter hydrocarbons and hydrocarbon gases (Abu El-Rub *et al.,* 2004; Yongbin *et al.,* 2004; Simell *et al.,*1992).The cracking of the aliphatic content by quartz is somewhat unexpected due to the chemically inert nature of this mineral, but some minor changes were observed in previous studies (Wen & Cain, 1984), and clay minerals (such as kaolinite), were however found to play some role in tar cracking due to its solid acidity (Abu El-Rub, 2004; Schobert, 1992; Ross *et al.,* 1987, Wen & Cain, 1984).

Comparison of the various mineral addition yields of mixed aliphatic and aromatic compounds (Figure 6-11b) to that of the AW TWD derived tar indicates a significant increase up to 520°C with the addition of all the minerals [except for quartz (AW-Qz)], which indicates no effect. Up

to 750°C, the addition of dolomite (AW-Dol), kaolinite (AW-Kao) and quartz (AW-Qz) led to increased yields, whilst the addition of pyrite (AW-Pyr) and calcite (AW-Cal) had no significant effect. Up to 900°C, the addition of calcite (AW-Cal), dolomite (AW-Dol) and quartz (AW-Qz) led to an increase in the amount of mixed compounds produced, whilst the addition of kaolinite (AW-Kao) and pyrite (AW-Pyr) led to significant decreases in these compounds. No definite conclusions can be made with regard to the mixed aliphatic and aromatic compounds due to co-elution; it is suggested that future work be conducted using GC-GC-MS analyses in order to prevent co-elution of these molecular compounds.

6.4.3.2. Aromatic spectrum

Effect of temperature

The alkyl-benzene compounds (Figure 6-11c) and aromatic ethers and esters (Figure 6-11d) show significant increase in yield with increasing final pyrolysis temperature for the AW-Dol, AW-Kao and AW-Pyr derived tars. Tars derived from the AW TWD and AW-Cal runs showed no significant change, whilst that of AW-Qz indicated a decrease in both of these molecular families with increases in final pyrolysis temperature, most prominent for the 750°C experiments.

Regarding alkyl-phenols (Figure 6-11e) and alkyl-naphthalenes (Figure 6-11f), no significant change in the yield of these molecular families is observed with increasing final pyrolysis temperature for AW-Cal and AW-Dol derived tars. AW-Kao derived tars show a significant increase in these compounds between 750°C and 900°C, whilst AW-Pyr derived tars indicate an increase in both these molecular families with increasing final pyrolysis temperature. AW-Qz derived tars indicated decreases in both these molecular families with an increase in final pyrolysis temperature, similar to the trend observed for the AW TWD derived tars.

Regarding alkyl-indenes (Figure 6-11g), no significant change is observed with increasing final pyrolysis temperature for AW-Cal, AW-Dol and AW-Pyr derived tars between 750°C and 900°C. This is an indication that in these cases that the alkyl-indenes were derived between 520°C and 750°C, as no traces of these compounds were observed for the 520°C experiments. AW-Kao derived tar also indicated a significant increase in these compounds between 750 ° and 900°C, whilst none of these components were present up to 520°C. AW-Qz derived tar showed constant yields of these components with increasing final pyrolysis temperatures.

The increases observed in alkyl-substituted compounds with increasing final pyrolysis temperature are related to the severity of the pyrolysis process which leads to increased cleavage of aromatic bridges (Tang *et al.*, 2014; Hattingh, 2012; Nelson *et al.,* 1988). This

behaviour is consistent with observations made for the TWD derived tar, but not observed for the AW TWD tar.

Regarding PAHs yields (Figure 6-11h), no significant change is observed with increasing final pyrolysis temperature for the AW TWD and AW-Dol runs. AW-Cal derived tars indicated significant increases in PAHs between 520°C and 750°C, but no change up to 900°C. AW-Kao and AW-Pyr derived tars indicated significant increases in these compounds with increasing final pyrolysis temperature, whilst AW-Qz derived tars showed significant decreases in these compounds with increasing final pyrolysis temperature. This behaviour is consistent to that of the AW TWD derived tar, and thus indicative of the inactivity of quartz in the derivation of these compounds. The increase in PAH yield with increasing final pyrolysis temperature is in accordance with previous findings (Fuentes-Cano *et al.,* 2013; Hattingh 2012; Nelson and Tyler, 1988; Nelson *et al.,* 1988).

Regarding the nitrogen heteroatom yields (Figure 6-11i), no significant change is observed with increasing final pyrolysis temperature for the AW TWD, AW-Dol and AW-Pyr runs. The AW-Cal derived tars indicated significant decreases in these compounds between 520°C and 750°C, and a significant increase between 750°C and 900°C. AW-Kao derived tars indicated significant decreases in these compounds with increasing final pyrolysis temperature, whilst AW-Qz derived tar indicated significant increases in these compounds between 520°C and 750°C, but no significant change between 750°C and 900°C. The nitrogen functionalities found in the tar fraction are related to aromatic structures in the coal such as pyridenes and pyrroles (Smith *et al.,* 1994; Chen *et al.,* 1990).

Effect of mineral addition

Comparison of the AW TWD derived tar to that of the various mineral addition derived tars indicates with regard to the alkyl benzene compounds (Figure 6-11c), that calcite addition (AW-Cal) led to higher yields up to 900°C. Dolomite (AW-Dol) and pyrite (AW-Pyr) addition decreased the yield up to 520°C and increased it up to 750°C and 900°C; wheras kaolinite addition (AW-Kao) led to higher yields at 750°C and 900°C, whilst quartz addition (AW-Qz) led to higher yields at 520°C and 900°C. An increase in alkyl-benzenes had been previously observed in coal tar cracking studies at 900°C with the addition of CaO, which is one of the decomposition products of calcite and/or dolomite (Wang *et al.,* 2014). The increase in these compounds with increasing final pyrolysis temperature is characteristic of the TWD coal, and therefore the minerals clearly catalyse the formation of these species.

Comparison of the aromatic ethers and esters yield at 520°C (Figure 6-11d) indicates a decrease in yield for the 520°C experiments with the addition of calcite (AW-Cal). Dolomite

addition (AW-Dol) also led to lower yields from the 520°C experiments, whilst the yield up to 900°C was higher. Kaolinite addition (AW-Kao) led to lower yields for the 520°C experiments, whilst the yields up to 750°C and 900°C were significantly higher. Pyrite addition (AW-Pyr) led to lower yields in the 520°C experiments, whilst the yields at 900°C were significantly higher. Quartz addition (AW-Qz) led to higher yields at 520 ° and 900°C. Increased yields of these compounds after mineral addition relate to the trend observed for the TWD derived tar (Section 5.4.3), thus indicating that the minerals play an active role in the production of these compounds, as they provide additional oxygen functionalities which can assist in the formation of these compounds.

Comparison with regard to the alkyl phenols yield (Figure 6-11e) indicate lower yields for AW-Cal for the 520°C and 900°C experiments, lower yields for AW-Dol and AW-Qz at all three temperatures, whilst AW-Kao and AW-Pyr produce lower yields in the 520°C and 750°C experiments. Previous authors also reported a decrease in phenols with the addition of CaO, i.e. one of the decomposition products of calcite and/or dolomite (Dickerson and Serio, 2013). The lower alkyl-phenolic compounds obtained with the addition of the various minerals is related to the higher CO yield observed in these cases. The cracking of phenolic compounds was found to contribute to CO yields (Yongbin *et al.,* 2004*;* Li *et al.,* 1998; Xu and Tomita, 1989). The TWD tar (Section 5.4.3) was also observed to have a lower alkyl phenolic content, thus supporting the argument that the minerals were responsible for these observed changes.

The alkyl naphthalene yield (Figure 6-11f) was unaffected by calcite, dolomite and quartz addition. Addition of kaolinite (AW-Kao) leds to lower yields up to 520°C and 750°C, whilst the yield up to 900°C was higher. With regard to pyrite addition (AW-Pyr), a lower yield was observed up to 520°C, whilst up to 900°C the alkyl-naphthalene yield was higher than that of the AW TWD case. This is once more in agreement with the TWD derived tar results, in which lower alkyl-naphthalene content was observed (Section 5.4.3).

Comparison of the alkyl-indenes yield (Figure 6-11g) shows no significant change with addition of any minerals at any final pyrolysis temperature, except with the addition of kaolinite at a final pyrolysis temperature of 900°C, which led to a higher yield of alkyl-indenes.

With regard to the PAHs (Figure 6-11h), calcite addition (AW-Cal) led to a decrease in these components up to 520°C, whilst a higher yield was observed at 900°C in PAHs when compared to the AW TWD case. Dolomite addition (AW-Dol) and quartz addition (AW-Qz) led to increased yields in the case of the 520°C and 900°C experiments, whilst kaolinite (AW-Kao) addition led to a higher yield at 900°C. Pyrite addition (AW-Pyr) suppressed the formation of PAHs up to 520°C, thereafter an increase in PAHs was observed up to 900°C. The increase in PAHs up to 900°C is consistent with the trend observed for the TWD coal tar, thus

suggesting that the minerals play a role in the formation of PAHs. The higher yields of PAHs up to 900°C can be related to the lower H_2 and CH_4 yields at the same temperature for the mineral addition cases, as the decomposition of PAHs is a source of a large number of H_2 and CH_4 (Yongbin *et al.,* 2004). It was found previously that this tends to occur at temperatures exceeding 700°C due to the dehydrogenation of CaO (Yongbin *et al.,* 2004; Kinoshita *et al.,* 1995). Fe_2O_3, which is a probable decomposition product of pyrite, was reported to increase PAHs in biomass tars produced by catalytic fast pyrolysis (Dickerson & Soria, 2013). The inverse effect of CaO, (a decomposition product of calcite and/or dolomite), on PAH cracking was previously noticed; i.e. cracking the components at medium-low temperatures, (as observed at 520°C) and increasing the PAHs yield at higher temperatures, (as observed at 900°C). The increase at higher temperature is attributed to more macromolecular PAH split (Wang *et al.,* 2014; Yongbin *et al.,* 2004; Kinoshita *et al.,* 1995). The same trend in PAHs formation was observed for the TWD derived tar at 900°C (Section 5.4.3).

In the case of the 520°C experiments, AW-Cal produced more nitrogen heteroatoms (Figure 6-11i), whilst the addition of other minerals had no effect. Up to 750°C, the nitrogen heteroatoms yield of all the runs was in agreement, whilst at a final pyrolysis temperature of 900°C, kaolinite addition (AW-Kao) led to lower nitrogen heteroatom production, whilst quartz addition (AW-Qz) led to increased yields of these compounds. Little variation was observed in nitrogen heteroatom yields between the TWD and AW TWD derived tars earlier (Section 5.4.3). It seems as if the derivation of these compounds is independent of mineral presence within the coal structure, and is related to the aromatic structure in the coal such as pyridenes and pyrroles (Smith *et al.,* 1994; Chen *et al.,* 1990). The nitrogen found in coal is also mainly associated with the organic matter (Speight, 2005).

6.4.4. Size exclusion chromatography (SEC-UV)

The SEC-UV results (Table 6-5) will be reported as discussed in Section 4.4.2.3. Appendix C-5 includes all repeatability curves for the duplicate samples. The mineral addition derived tars consisted of components between the molecular size ranges of 30 – 6000 Da, consistent with the findings made for the TWD and AW TWD derived tars. Table 6-5 summarises the obtained SEC results for the various derived mineral addition derived tars.

Table 6-5 SEC results (Light / Heavy component areas) for the various derived tars.

	AW TWD	AW-Cal	AW-Dol	AW-Kao	AW-Pyr	AW-Qz
520°C						
Heavy component peak max. (Da)	399	424	430	402	404	404
Light component Peak max. (Da)	193	201	213	198	200	200
Light components (Area %)	38.9	36.1	39.1	38.3	38.8	38.8
Heavy components (Area %)	61.1	63.9	60.9	61.7	61.2	61.2
750°C						
Heavy component peak max. (Da)	395	404	399	430	418	427
Light component Peak max. (Da)	201	217	195	198	211	200
Light components	37.5	35.4	36.6	36.2	36.0	36.1
Heavy components	62.5	64.6	63.4	63.8	64.0	63.9
900°C						
Heavy component peak max. (Da)	402	412	399	399	404	410
Light component Peak max. (Da)	206	199	197	193	211	220
Light components	35.3	35.0	35.1	39.2	37.2	35.6
Heavy components	64.7	65.0	64.9	60.8	62.8	64.4

These observations are in accordance with previous studies (Fidalgo *et al.,* 2014; Hattingh, 2012; Mokoena *et al.,* 2008; Adegoroye *et al.,* 2004; Mill, 2000; John *et al.,* 1994; Li *et al.,* 1993a). The heavy component peak maximum is observed around ~400 Da for all tars and the light component peak maximum around ~200 Da, consistent with findings for tars derived from coal gasification as investigated by Fidalgo *et al.,* (2014). The variances in peak maxima show no specific trend, and therefore the discussion of results will focus on the determined area percentages for light and heavy components.

6.4.4.1. Effect of temperature

From Table 6-5 it can be observed that the AW-Cal derived tars showed little difference with reference to the light vs. heavy component fractions with increasing final pyrolysis temperature; a small increase in the heavy component fraction was observed, but can be regarded as negligible. For the AW-Dol derived tars, a definite increase in the heavy component fraction is observed with an increase in final pyrolysis temperature. AW-Kao and AW-Pyr derived tars showed a decrease in heavy component fraction up to 750°C, but an increase between a final pyrolysis temperature of 750°C and 900°C.

The AW-Qz derived tars indicate a decrease in heavy components with increasing final pyrolysis temperature between 520°C and 750°C, with the difference between 750°C and 900°C regarded as negligible. The decrease in lighter component fraction is typical of the AW TWD derived tars, but not of the TWD derived tar. No reference in literature could be found related to this change, but recombination of the tar molecules is believed to take place, and due to the secondary reactions taking place, may lead to the formation of heavier hydrocarbon species. Further analyses of the derived tars by analytical techniques such as C^{13}-NMR may provide a better understanding of the overall structure of the tars to explain this interesting change observed.

6.4.4.2. Effect of mineral addition

Comparison of the mineral addition derived tars, to that of the AW TWD tar, indicates that up to 520°C only the addition of calcite (AW-Cal) influenced the composition, showing a shift to heavier components. This is consistent with the observations made by Simdis analyses (Section 6.4.2). The TWD derived tar also had a larger heavy component fraction at this temperature, which is indicative that the minerals had some effect with regard to this composition. Up to 750°C, all mineral additions led to a small increase in heavier components when compared to the AW TWD derived tars, but this is contrary to the observation made for the TWD derived tar. In the case of the 900°C tars, the composition of AW-Cal, AW-Dol and AW-Qz was in agreement with that of the AW TWD derived tar, whilst larger yields of light components were observed for AW-Kao and AW-Pyr, in agreement with the trend observed

for the TWD tar at this temperature. The variation observed with SEC-UV analyses was not that significant as observed with the Simdis and GC-MS analyses. Further analyses of the derived tars by analytical techniques such as C^{13}-NMR may provide more insight with regard to overall structural differences.

6.5. Char composition

The derived chars were analysed by proximate, ultimate, XRF, XRD, and DRIFT analyses.

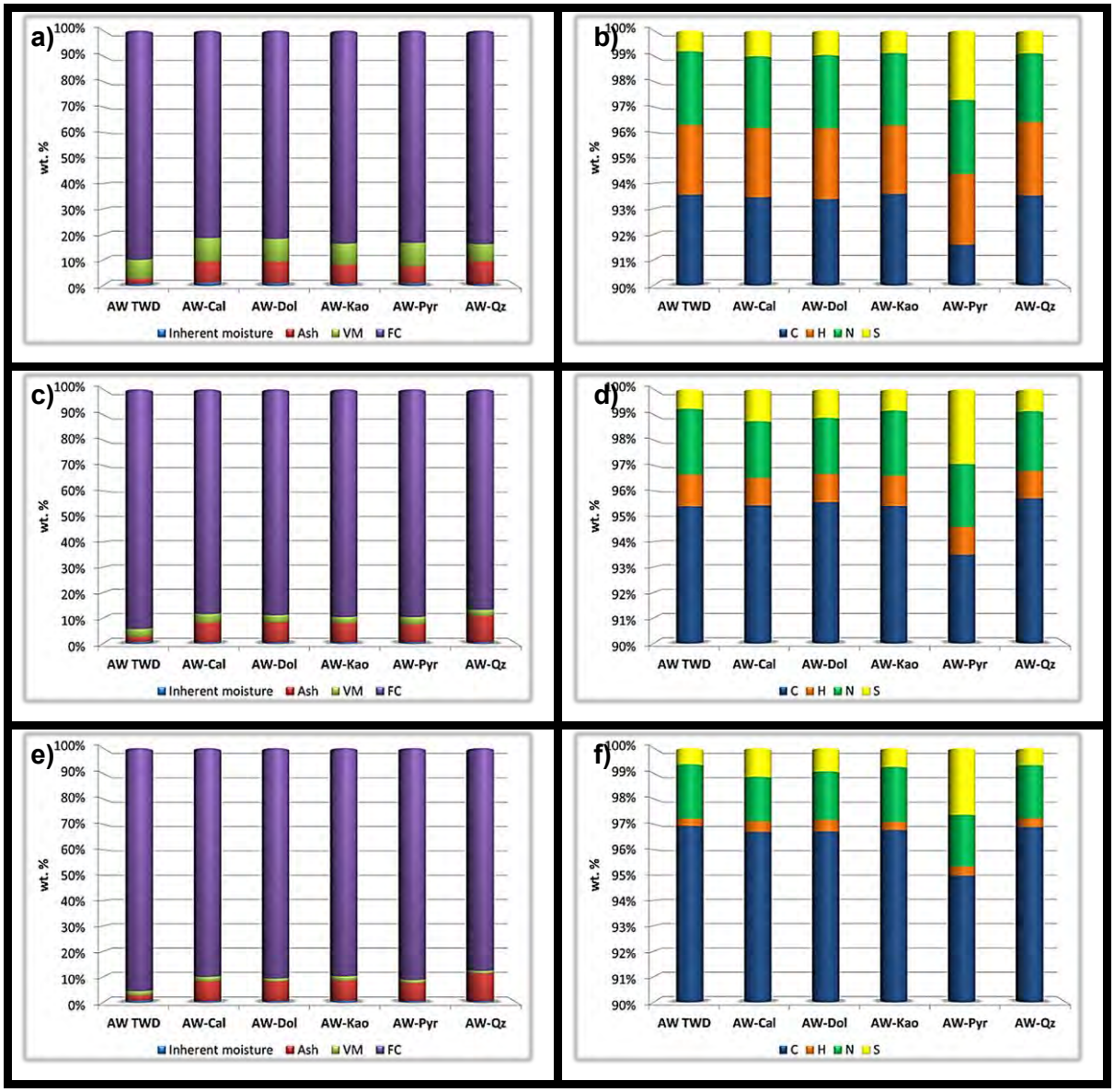

Figure 6-12 Proximate and ultimate analyses results at 520°C (a & b); 750°C (c & d) and 900°C (e and f).

6.5.1. Proximate and Ultimate analyses

The proximate analysis results are presented in Figure 6-12a, Figure 6-12c and Figure 6-12e, whilst the ultimate analysis results for C, H, N and S are presented in Figure 6-12b, Figure 6-

12d and Figure 6-12f. The ultimate analysis results are only represented for C, H, N and S due to the oxygen content (which is calculated by difference), and for which negative values were obtained in some instances (Table 6-7), due to the summation of errors. Table 6-6 presents the proximate analysis results, VM and FC, on a dry, additive free, ash free basis. This was done by use of Equation 6-6, 6-7 and 6-8.

$$VM = {(VM_{reported} - m_d)}/{(VM_{reported} - m_d + FC_{reported})} \times 100 \quad 6\text{-}6$$

$$FC = {(FC_{reported})}/{(VM_{reported} - m_d + FC_{reported})} \times 100 \quad 6\text{-}7$$

$$m_d = {(m_{m\,@\,X^\circ C} \cdot \%\, m_{d\,X^\circ C - 900^\circ C})}/{100} \quad 6\text{-}8$$

Where $VM_{reported}$ and $FC_{reported}$ refer to the respective volatile matter and fixed carbon values, on a dry, ash free basis as determined from the received proximate analysis results, and m_d refers to the amount of mineral additive that would have decomposed at temperature X°C, which can be either 520°C or 750°C. The value m_d is determined by determining the amount of original mass of mineral still present at temperature X°C from the TG analyses, and multiplying this value by the percentage mass loss that would have occurred between temperature X°C and 900°C, the condition under which the ultimate analyses values are determined.

Table 6-6 Proximate analysis results on a dry, additive free, ash free basis.

	AW TWD	AW-Cal	AW-Dol	AW-Kao	AW-Pyr	AW-Qz
wt%						
520°C						
Volatile matter (VM)	7.6	8.1	7.7	8.9	9.3	7.4
Fixed carbon (FC)	92.4	91.9	92.3	91.1	90.7	92.6
TOTAL	**100.0**	**100.0**	**100.0**	**100.0**	**100.0**	**100.0**
750°C						
Volatile matter (VM)	3.1	2.9	1.8	2.7	3.2	2.6
Fixed carbon (FC)	96.9	97.1	98.2	97.3	96.8	97.4
TOTAL	**100.0**	**100.0**	**100.0**	**100.0**	**100.0**	**100.0**
900°C						
Volatile matter (VM)	1.7	1.9	1.2	1.9	1.3	1.0
Fixed carbon (FC)	98.3	98.1	98.8	98.1	98.7	99.0
TOTAL	**100.0**	**100.0**	**100.0**	**100.0**	**100.0**	**100.0**

From Figure 6-12a, 6-12c and 6-12e the systematic trends that occured during coal pyrolysis is clearly visible, in accordance to what was seen in Section 5.5.1 for the TWD and AW TWD

coal fractions. Comparison of the volatile matter and fixed carbon values obtained for the various mineral addition experiments given in Table 6-6 indicate that more volatile matter was derived from the 520°C chars for AW-Cal, AW-Kao and AW-Pyr. Of the 750°C chars, AW-Cal, AW-Dol, AW-Kao and AW-Qz derived chars had lower VM content, whilst for the 900°C experiments, AW-Dol, AW-Pyr and AW-Qz derived chars produced less volatile matter, and AW-Cal and AW-Kao derived chars produced more volatile matter. A systematic trend in this data is difficult to identify and the differences in the values are in most cases not very significant.

Table 6-7 Ultimate analysis results, as received.

	AW TWD	AW-Cal	AW-Dol	AW-Kao	AW-Pyr	AW-Qz
wt%						
520°C						
Carbon	88.4	83.3	84.2	83.1	82.9	81.8
Hydrogen	2.6	2.4	2.5	2.4	2.5	2.5
Nitrogen	2.7	2.5	2.6	2.5	2.6	2.4
Oxygen – by difference	2.7	1.8	2.2	3.2	2.0	3.0
Total sulphur (IR Spectroscopy)	0.8	0.9	0.9	0.8	2.5	0.8
TOTAL	**97.3**	**91.0**	**92.3**	**91.9**	**92.5**	**90.4**
750°C						
Carbon	91.9	86.9	87.8	87.4	87.3	83.2
Hydrogen	1.2	1.0	1.0	1.1	1.0	0.9
Nitrogen	2.5	2.0	2.0	2.3	2.3	2.0
Oxygen – by difference	0.9	0.7	-0.4	0.4	-0.8	2.1
Total sulphur (IR Spectroscopy)	0.8	1.1	1.0	0.8	2.8	0.8
TOTAL	**97.3**	**91.7**	**91.6**	**92.0**	**92.5**	**89.0**
900°C						
Carbon	92.6	89.3	90.5	87.4	89.0	85.9
Hydrogen	0.3	0.4	0.4	0.3	0.3	0.3
Nitrogen	2.0	1.6	1.8	1.9	1.9	1.9
Oxygen – by difference	1.6	0.0	0.0	1.2	0.0	0.0
Total sulphur (IR Spectroscopy)	0.6	1.0	0.9	0.7	2.5	0.6
TOTAL	**97.2**	**92.3**	**93.6**	**91.5**	**93.8**	**88.6**

Table 6-7 presents the ultimate analysis results on an as received basis. It should be noted that in some cases negative values are reported for the oxygen content, due to the summation of experimental errors, as this value is determined by difference. In most cases the oxygen is observed to decrease with increasing final pyrolysis temperature, consistent with previous observations (Bai *et al.,* 2010; Chen *et al.*, 1999; Jones *et al.,* 1999). Although some of the values are negative, there is some relevance in them, i.e. it was observed that at higher

pyrolysis temperatures, (750°C and 900°C), the TWD derived chars had lower oxygen content when compared to that of the AW TWD char (Section 5.5.1). This was attributed to assisted break up of oxygen functionalities by the minerals present in the coal structure. It can be clearly observed from the values calculated for oxygen that the mineral added runs had a lower oxygen content in most of the cases for the 750°C and 900°C experiments, except in the case of AW-Qz for the 750°C experiments, and AW-Kao for the 900°C experiments.

For better comparison of the C, H, N and S values, refer to Figure 6-12b, 6-12d and 6-12f and Table 6-8, which present the obtained values on a dry, ash free basis, excluding oxygen. It can be observed that the hydrogen and nitrogen contents decreased with increasing final pyrolysis temperature, whilst the carbon content increased, typical of the observation made with regard to the proximate analysis FC content; i.e. these trends were also observed for other coals (Bai *et al.,* 2010; Chen *et al.*, 1999; Jones *et al.,* 1999), and were also observed for the TWD coal (Section 5.5.1). The carbon content in all cases is identical, and the lower carbon content in the case of AW-Pyr is only due to the higher sulphur content due to pyrite addition.

Table 6-8 Ultimate analysis (C, H, N, S) results (d.a.f.)

	AW TWD	AW-Cal	AW-Dol	AW-Kao	AW-Pyr	AW-Qz
wt%						
520°C						
C	93.6	93.5	93.4	93.6	91.6	93.5
H	2.7	2.7	2.8	2.7	2.8	2.9
N	2.9	2.8	2.9	2.8	2.9	2.7
S	0.8	1.0	1.0	0.9	2.7	0.9
TOTAL	**100.0**	**100.0**	**100.0**	**100.0**	**100.0**	**100.0**
750°C						
C	95.4	95.4	95.6	95.4	93.5	95.7
H	1.2	1.1	1.1	1.2	1.1	1.1
N	2.6	2.2	2.2	2.6	2.5	2.3
S	0.8	1.3	1.1	0.9	2.9	0.9
TOTAL	**100.0**	**100.0**	**100.0**	**100.0**	**100.0**	**100.0**
900°C						
C	96.9	96.7	96.7	96.8	95.0	96.9
H	0.3	0.4	0.5	0.3	0.4	0.3
N	2.1	1.7	1.9	2.2	2.0	2.1
S	0.6	1.1	0.9	0.8	2.6	0.7
TOTAL	**100.0**	**100.0**	**100.0**	**100.0**	**100.0**	**100.0**

With regard to the nitrogen content, no significant difference is observed in the 520°C chars. In the case of the 750°C and 900°C chars, the calcite and dolomite added derived chars have lower nitrogen content. This decrease in char-N was observed previously (Tsubouchi &

Ohtsuka, 2002a, 2002b) and related to CaO, a decomposition product of calcite and dolomite. The CaO particles may react with heterocyclic nitrogen forms in the char (char-N) to form interstitial species such as CaC_xN_y and $CaO_xC_yN_z$. These components underwent further reactions to form N_2 (Tsubouchi & Ohtsuka, 2002a, 2002b), and subsequently the char-N decreased. Little variance is observed in nitrogen content with the addition of other minerals; the exception being quartz addition of the 750°C chars, but this is not believed to be related to any specific change during pyrolysis.

Regarding the sulphur content, it can be observed that AW-Cal and AW-Dol derived chars had a higher sulphur content, which was consistent around 0.9 – 1.1 wt%. This change is believed to be related to the desulphurisation characteristic previously identified for calcite and dolomite (Sciazko & Kubica, 2002; Yaw *et al.,* 1980). These minerals are used as a scrubber in fuel gas applications, especially in the gasification of biomass for the removal of sulphur, as well as tar cracking (Meng *et al.,* 2010; Adanez *et al.,* 2005; Abu El-Rub, 2004). Identified gases that were removed included H_2S, COS and CS_2, which were also expected to be present in the current gas composition, as it is typically derived from the pyrite mineral, present in the coal structure. The desulphurisation trend of these minerals was observed in calcined and un-calcinated form (Adanez *et al.,* 2005), and thus the values obtained in the 520°C experiments are not unexpected. The higher sulphur content identified in the case of AW-Pyr is typical of the added pyrite (FeS_2), and is observed to vary little with increasing final pyrolysis temperature. This higher S value (due to the addition of pyrite), is also responsible for the seemingly lower carbon content. The addition of kaolinite (AW-Kao) and quartz (AW-Qz) did not affect the sulphur content of the derived chars, thus further backing the evidence that calcite and dolomite captured some of the sulphur that would have been released during pyrolysis. A higher sulphur content was also noticed for the TWD derived chars, in which calcite and dolomite were present. Thus the hypothesis that some of the mineral matter blocks the release of sulphur, and the acid washing process liberates the sulphur, so as to be released during pyrolysis can be reverted, and replaced with a confirmed hypothesis that it is the calcite and dolomite minerals that are responsible for the higher sulphur content due to sulphur capturing from the released gases such as H_2S and COS.

6.5.2. X-Ray Fluorescence (XRF) and Inductive Coupled Plasma (ICP) analysis

Table 6-9 indicates the XRF / ICP results for the derived chars, (only the AW TWD and AW-Cal derived chars' ash content was determined by ICP). The results are presented on a g ash species per 100 g char basis, for better comparison.

Table 6-9 XRF/ICP results for the derived chars on a g/species per 100 g char basis

	AW TWD	AW-Cal	AW-Dol	AW-Kao	AW-Pyr	AW-Qz
g ash species / 100 g char						
520°C						
Al_2O_3	0.26	0.40	0.48	2.51	0.38	0.33
CaO	0.14	4.07	2.26	0.25	0.22	0.21
Cr_2O_3	0.01	0.02	0.01	0.01	0.01	0.01
Fe_2O_3	1.03	1.05	1.32	1.13	5.06	0.97
K_2O	0.00	0.00	0.02	0.10	0.01	0.01
MgO	0.04	0.14	1.49	0.14	0.12	0.10
MnO	0.00	0.00	0.03	0.00	0.01	0.00
Na_2O	0.01	0.01	0.03	0.03	0.02	0.02
P_2O_5	0.02	0.01	0.01	0.01	0.01	0.01
SiO_2	0.09	0.21	0.23	2.75	0.14	6.83
TiO_2	0.20	0.16	0.18	0.16	0.15	0.14
V_2O_5	0.01	0.01	0.01	0.01	0.01	0.01
ZrO_2	0.01	0.02	0.02	0.01	0.01	0.01
BaO	0.04	0.06	0.07	0.06	0.06	0.05
SrO	0.03	0.04	0.04	0.04	0.03	0.04
SO_3	0.05	2.12	2.18	0.09	0.36	0.21
750°C						
Al_2O_3	0.22	0.31	0.44	2.55	0.36	0.34
CaO	0.13	3.62	2.22	0.25	0.23	0.22
Cr_2O_3	0.02	0.01	0.01	0.01	0.01	0.01
Fe_2O_3	1.19	0.94	1.21	1.15	5.38	1.05
K_2O	0.00	0.00	0.03	0.10	0.01	0.01
MgO	0.04	0.11	1.45	0.13	0.11	0.10
MnO	0.00	0.00	0.03	0.00	0.01	0.00
Na_2O	0.01	0.01	0.02	0.02	0.01	0.02
P_2O_5	0.01	0.01	0.01	0.01	0.01	0.01
SiO_2	0.05	0.12	0.21	2.82	0.09	8.08
TiO_2	0.19	0.13	0.17	0.16	0.17	0.15
V_2O_5	0.01	0.01	0.01	0.01	0.01	0.01
ZrO_2	0.01	0.02	0.02	0.01	0.01	0.01
BaO	0.04	0.05	0.06	0.06	0.06	0.05
SrO	0.03	0.04	0.04	0.04	0.04	0.04
SO_3	0.04	2.39	1.97	0.08	0.38	0.29
900°C						
Al_2O_3	0.24	0.24	0.45	2.69	0.39	0.61
CaO	0.13	3.60	2.06	0.26	0.23	0.24
Cr_2O_3	0.03	0.05	0.01	0.01	0.01	0.01
Fe_2O_3	1.12	1.04	1.23	1.28	5.50	1.14
K_2O	0.00	0.00	0.03	0.11	0.01	0.04
MgO	0.04	0.07	1.31	0.15	0.13	0.11
MnO	0.00	0.00	0.03	0.00	0.01	0.00
Na_2O	0.01	0.00	0.02	0.02	0.03	0.02
P_2O_5	0.01	0.01	0.01	0.02	0.01	0.01
SiO_2	0.07	0.09	0.23	2.94	0.13	8.32
TiO_2	0.21	0.14	0.16	0.16	0.16	0.15
V_2O_5	0.01	0.01	0.01	0.01	0.01	0.00
ZrO_2	0.02	0.01	0.02	0.02	0.01	0.01
BaO	0.04	0.04	0.06	0.06	0.06	0.05
SrO	0.03	0.03	0.04	0.04	0.04	0.03
SO_3	0.06	2.42	2.10	0.07	0.35	0.16

Comparison of the ash composition at the various pyrolysis temperatures for the different cases reveals similar composition at all temperatures for most of the components. The only truly significant changes observed were in the composition of the AW-Cal ash, for which a decrease in CaO, MgO and SiO_2 is observed with increasing final pyrolysis temperature, whilst the SO_3 content increases. The increase in SO_3 content can be due to the sulphur capturing as discussed. The values of the AW-Dol ash for this component is also higher in the case of the 900°C experiments, compared to the values of the 520°C and 750°C experiments. The variances may be related to experimental error.

Comparisons of the ash composition of the various mineral addition cases to that of the AW TWD char ash composition reveal that the largest variances are observed with regard to the added minerals. However, some other ash species also increased, probably due to impurities within the added mineral, or retention of some ash species due to the presence of other minerals. In general, it is observed that the Al_2O_3, CaO and SiO_2 content in the ash increased with the addition of all minerals, accept for the SiO_2 content of AW-Pyr. The Cr_2O_3, TiO_2, V_2O_5, P_2O_5, ZrO_2,, BaO and SrO ash yields are unaffected by mineral addition. The Fe_2O_3 and MnO content of the AW-Dol case are observed to be higher than that of AW TWD. This can be related to impurities within the added dolomite, i.e. dolomites with a higher Fe_2O_3 content were reported to be more effective in the reduction of tar (Pinto *et al.,* 2007 and 2009).

The higher SO_3 content, specifically observed for the AW-Cal and AW-Dol cases, is related to the sulphur capture as discussed in the ultimate analysis results (Table 6-8). It can also be observed that most of the added pyrite (AW-Pyr) converted to Fe_2O_3, and probably formed sulphur-containing gases upon decomposition, as the SO_3 content in the ash was not observed to change to such a great extent. The SO_3 content of the AW-Qz run was also higher, which can be related to a small increase in sulphur content, as observed from the ultimate analysis as well (Table 6-8).

6.5.3. X-Ray Diffraction (XRD) analysis

In general, it can be said that for all the derived chars the crystalline mineral matter underwent several transformations with increasing final pyrolysis temperature, with the amorphous content increasing with an increase in final pyrolysis temperature particularly at 750°C and 900°C, due to mineral transformation (Bai *et al.,* 2013; Min *et al.,* 2011). The general trends observed are in line with findings as described by Bai *et al.,* (2013), Matjie (2008) and Tomeczek and Palugniok (2002), and in accordance with observations made for the AW TWD and TWD derived chars reported in Section 5.5.3. Table 6-10 indicates the XRD results for the AW TWD derived chars, without any mineral addition, as discussed in Section 5.5.3. The

major phases identified were related to the initial pyrite content which transformed to pyrrhotite and magnetite under the experimental conditions of this study. Appendix C-6 includes the XRD spectra graphs.

Table 6-10 XRD results for AW-TWD derived chars

Identification	Molecular formula	AW TWD			
		Coal	*520°C*	*750°C*	*900°C*
Amorphous content	-	99.3	99.4	99.8	99.7
Dolomite	$CaMg(CO_3)_2$	0.1	-	-	-
Magnetite	Fe_3O_4	-	-	0.1	0.2
Pyrite	FeS_2	0.6	-	-	-
Pyrrhotite	$Fe_{(1-x)}S$	-	0.6	0.1	0.1
TOTAL	**-**	**100.0**	**100.0**	**100.0**	**100.0**

6.5.3.1. Calcite (AW-Cal) and dolomite (AW-Dol) addition

The XRD results for the AW-Cal and AW-Dol derived chars are indicated in Table 6-11. It can be observed that the amorphous content increased consistently with increasing final pyrolysis temperature. Calcite/dolomite composition decreased with an increase in final pyrolysis temperature due to calcination, and the subsequent release of CO_2. For calcite, CaO formed upon calcination, whilst dolomite formed CaO and MgO (Vassileva & Vassilev, 2006; Maitra *et al.,* 2005; Caceres & Attiogbe, 1997). It is interesting to note the presence of fluorite, (CaF_2), which is related to the capture of fluoride from the coal structure and was present due to the acid washing process using HF. It appears as if the HF was not totally successfully removed by the second HCl washing step, and then reacted with the calcite upon calcination to form calcium fluorite (Doymaz *et al.,* 2007; Fauerstenau *et al.,* 1983). The fluorite content is observed to decrease with increasing final pyrolysis temperature, as further transformation occured. The higher fluoride yields obtained for the AW-Cal runs at 520°C and 750°C are related to the fact that decomposition of calcite starts at an earlier stage than observed from the TG analyses (Section 3.9).

The magnetite content was also observed to increase with final pyrolysis temperature, as transformation of the pyrite (not removed by the acid washing process) continued to form pyrrhotite at 520°C, which in turn formed magnetite (Hu *et al.,* 2006; Vassileva & Vassilev, 2006; Hong & Fegley, 1997; Gryglewicz *et al.,* 1996). Under reducing conditions, magnetite was identified as one of the major mineral forms in coal char (Ma *et al.* 2013). The presence of oldhamite, CaS, could be related to the sulphur capturing observed in the ultimate analysis and XRF analysis results. As was the case for sulphur identified by ultimate analysis, the addition of calcite led to higher sulphur capture, as can be observed from the higher oldhamite values for the chars derived from this addition. The increase in oldhamite with an increase in

final pyrolysis temperature was previously observed (Ma *et al.,* 2013), and it was observed to be one of the major mineral forms that formed under reducing conditions.

Table 6-11 XRD results for AW-Cal and AW-Dol derived chars

	AW-Cal			AW-Dol		
	wt%					
	520°C	**750°C**	**900°C**	**520°C**	**750°C**	**900°C**
Amorphous content	92.6	95.8	95.8	94.9	95.9	96.6
Calcite ($CaCO_3$)	4.7	0.6	0.3	1.1	0.5	0.0
Dolomite $CaMg(CO_3)_2$	0.0	0.0	0.0	1.5	0.0	0.0
Fluorite (CaF_2)	2.0	1.7	1.1	1.0	1.1	0.9
Magnetite (Fe_3O_4)	0.0	0.3	0.4	0.1	0.1	0.4
Oldhamite (CaS)	0.2	1.5	1.4	0.1	0.8	1.0
Periclase (MgO)	0.0	0.0	0.2	0.8	1.3	1.1
Pyrrhotite ($Fe_{(1-x)}S$)	0.5	0.0	0.0	0.5	0.2	0.0
Quartz (SiO_2)	0.0	0.0	0.8	0.0	0.0	0.0
TOTAL	**100.0**	**100.0**	**100.0**	**100.0**	**100.0**	**100.0**

The presence of periclase (MgO) at 900°C (in the AW-Cal char) is probably related to impurities in the added calcite, and the quartz content can probably be related to remnant SiO_2 not removed by the acid washing process, as was identified by QEMSCAN analysis (Section 3.6.3). It is also possible that these species were in the amorphous phase, and upon interaction with CaO (a decomposition product of calcite) and SiO_2 were formed (Ma *et al.,* 2013). The increase in periclase content with an increase in final pyrolysis temperature as observed for AW-Dol derived chars can be related to the fact that decomposition of dolomite first needs to take place (and from the TG analyses). This is known to occur at a maximum rate at around 773°C. The fact that decomposition of both of these minerals is already observed to have occurred in the 520°C chars, can be related to previous observations in which it was stated that minerals tended to decompose at lower temperatures during interaction within a coal matrix (Cheng *et al.,* 2013; Borah *et al.,* 2005; Gryglewicz *et al.,* 1996).

6.5.3.3. Kaolinite addition (AW-Kao)

The XRD results for the AW-Kao derived chars are shown in Table 6-12. The major mineral phases identified include: kaolinite, muscovite, mullite, pyrrhotite and quartz. The kaolinite content is observed to decrease between 520°C and 750°C, but remains constant thereafter. Transformation from kaolinite to metakaolinite would have taken place between 450°C – 700°C due to dehydration and dehydroxylation (Ptáček *et al.,* 2010b; Vassilev *et al.*, 2009; Heide & Földvari, 2006; Alpern *et al.,* 1983). Further transformation to mullite starts around 750°C, which increases even further up to 900°C. Some of the kaolinite forms muscovite, which decreases in yield with increasing final pyrolysis temperature, probably due to mullite. The pyrrhotite content is observed to decrease with an increase in final pyrolysis temperature,

but no other identifiable iron compounds are observed, thus suggesting another reaction route that differs from the interactions observed with the addition of calcite and dolomite. With the addition of dolomite and calcite magnetite forms, which is not the case with kaolinite addition. The quartz content is observed to decrease with an increase in final pyrolysis temperature, and is most likely transformed to amorphous silica (Ptáček *et al.,* 2010a), which cannot be identified by XRD.

Table 6-12 XRD results for AW-Cal derived char

AW-Kao	520°C	750°C	900°C
	wt%		
Amorphous content	96.1	97.6	97.2
Kaolinite [$Al_2Si_2O_5(OH)_4$]	2.4	1.2	1.2
Mullite ($3Al_2O_3.2SiO_2$)	0.0	0.1	1.1
Muscovite [$KAl_2(AlSi_3O_{10})(F,OH)_2$]	0.9	0.6	0.4
Pyrrhotite ($Fe_{(1-x)}S$)	0.3	0.2	0.0
Quartz (SiO_2)	0.4	0.3	0.2
TOTAL	**100.0**	**100.0**	**100.0**

6.5.3.4. Pyrite addition (AW-Pyr)

The XRD results for the AW-Pyr derived chars are indicated in Table 6-13. The major mineral phases identified include hematite, magnetite, pyrrhotite and quartz.

Table 6-13 XRD results for AW-Pyr derived char

AW-Pyr	520°C	750°C	900°C
	wt%		
Amorphous content	96.0	96.1	97.8
Hematite	0.9	0.1	0.1
Magnetite	0.5	0.4	0.4
Pyrrhotite	2.3	3.4	1.8
Quartz	0.4	0.0	0.0
TOTAL	**100.0**	**100.0**	**100.0**

Pyrrhotite is observed to be the most prominent of all mineral phases at all temperatures, indicating that the conversion of pyrite was incomplete in the current setup, as pyrrhotite is of the formula $Fe_{(1-x)}S$, and would generally transform to troilite (FeS) which is more stable. Hematite was concluded by Jorgensen and Moyle (1986) to be the most prominent phase present after completion of thermal decomposition of coal-derived pyrite in an atmosphere with oxygen, and was observed to decrease with increasing final pyrolysis temperature. The magnetite content was relatively constant at all final pyrolysis temperatures, and was identified

as a major mineral present under reducing conditions (Ma *et al.,* 2013). Quartz was only identified to be present in the 520°C char.

6.5.3.5. Quartz addition (AW-Qz)

The XRD results for the AW-Qz derived chars are indicated in Table 6-14. The major mineral phases identified include pyrrhotite and quartz. It can be observed that the pyrrhotite content is relatively constant, whilst the quartz content is observed to decrease with increasing final pyrolysis temperature, as transformation to amorphous silica takes place. Low quartz (α-quartz) transforms to high quartz (ß-quartz) at 573°C (Klein, 2002; Reifenstein *et al.,* 1999). The ß-quartz is in turn stable up to a temperature of 876°C, at which it transforms to tridymite via an unstable cristobalite formation (Matjie *et al.,* 2007; Reifenstein *et al.*, 1999).

Table 6-14 XRD results for AW-Cal derived char

AW-Qz	520°C	750°C	900°C
	wt%		
Amorphous content	91.7	95.1	96.0
Pyrrhotite	0.6	0.5	0.5
Quartz	7.7	4.4	3.5
TOTAL	**100.0**	**100.0**	**100.0**

6.6. Chapter summary

The effect of mineral addition to the AW TWD coal fraction indicates that the various minerals play a definite role during pyrolysis. The addition of 5 wt.% calcite and dolomite led to a decrease in tar yield in the 750°C and 900°C experiments, whilst the gas yields increased. Markedly, increased water yields were also observed with the addition of these minerals and is consistent with previous studies. The decrease observed in char yields (at all experimental temperatures) with the addition of calcite and dolomite, is in contrast with previous findings, but the same observation was made with the addition of these minerals to the raw TWD coal. The minerals seemed to assist in the conversion of char to gas and tar to gas reactions during the pyrolysis process. The H_2 and CH_4 gas yields decreased with the addition of calcite and dolomite, whilst the CO and CO_2 yields were higher.

A lot of variance was observed in tar composition in the case of the various mineral addition runs. In general, the tars produced with the added minerals were more aliphatic in nature and consisted of lighter boiling point compounds in the 750°C and 900°C experiments, whilst in the 520°C experiments, the tars were heavier, consisting of higher boiling point compounds. Various components identified by GC-MS were cracked by the added minerals, or the formation of these compounds was catalysed by the presence of certain minerals. Proximate

analyses of the chars provided little insight. Ultimate, XRF and XRD analyses confirmed the sulphur capturing occurrence by calcite and dolomite as more SO_3 components were observed in the ash from the XRF analysis, whilst XRD revealed the presence of oldhamite (CaS). Another observation from the XRD analysis was the presence of fluorite (CaF_2) with the addition of calcite and dolomite, probably due to inefficient removal of fluoride by HCl after HF washing of the coal.

The addition of 5 wt% kaolinite led to an increase in tar, char and gas yields for the 520°C experiments, whilst for the 750°C experiments, a decrease in tar yield was observed, with other yields in agreement with that of the raw AW TWD coal. The increase in tar yield produced from the 520° experiments might be attributed to the fact that the additional sites provided by kaolinite addition might assist the tar precursors to leave the coal structure and form tar, stabilizing the formed free radicals to yield tar. The effect of kaolinite in tar reduction is attributed to the solid acidity of the mineral, thus providing protonates for increased pyrolysis conversion. Kaolinite is however less active than dolomite and calcite in tar reduction. Kaolinite addition also led to lower H_2 yields, whilst the CO yields were higher. The CO_2 yield for the 520°C experiments was higher, whilst decreasing to below the value of AW TWD for the 900°C experiments. The most prominent mineral forms identified by XRD were mullite and muscovite.

The addition of pyrite led to increased water yields at all temperatures. The tar yield was observed to be lower than that of the AW TWD case for the 520°C and 900°C experiments. The temperature range in which pyrite affects pyrolysis yield was limited to 220-650°C, therefore the difference observed in the 900°C experiments was attributed to the changes occurring in the lower pyrolysis range. The only significant effect observed with the addition of pyrite with regard to the gas yield, was in a decrease in gas yield in the case of the 750°C experiments; thus it is believed there is some relationship between the gas and tar phases in this region. The H_2 yield was decreased by pyrite addition, whilst CO yield was higher at all final pyrolysis temperatures, and that of CO_2 was higher from the 520°C and 750°C experiments. The CH_4 yield decreased for the 900°C experiments. The most prominent crystalline mineral forms identified due to pyrite addition by XRD included: hematite, magnetite and pyrrhotite.

The addition of quartz showed no significant effects on most of the pyrolysis yields, except in the showing of increased conversion, lower char yields, and an increase in gas yield in the 520°C experiments, which might be related to changes in the thermo-plastic nature and fluidity of the coal. Quartz was the most inactive of all added minerals regarding pyrolysis compositional changes. A reduction in H_2 yield was observed in the 900°C experiments with

quartz addition, whilst the CO_2 yield for the 520°C experiments was higher. The tar composition was affected to a small degree.

The synergism of minerals during coal pyrolysis cannot be underestimated, and therefore Chapter 7 will focus on the synergistic effect of different mineral mixtures added to the AW TWD coal in an attempt to mimic the original mineral constituents present in the TWD coal, prior to acid washing.

Chapter 7: Model coal-mineral mixtures

7.1. Introduction

Up to now the effect of acid washing of TWD coal (Chapter 5), and individual addition of the most prominent minerals found in TWD coal to the AW TWD coal on the pyrolysis products (Chapter 6), have been investigated. In Chapter 7, the pyrolysis product yields and composition results for model coal-mineral mixtures set up to mimic the original coal-mineral mixture found in TWD coal are discussed. Two cases are examined as indicated in the experimental plan, (1) a low percentage mineral matter mixture, related to the TWD coal by means of FactSage modelling and use of the QEMSCAN results, and (2) a high percentage mineral matter mixture set up to mimic a TWD run of mine (ROM) coal, based on characterisation as done by Govender (2005). Section 7.2 will discuss the manner in which the composition of the coal-mineral mixture was determined. Section 7.3 will deal with the pyrolysis product yields. In Section 7.4, the gas composition as analysed by GC analyses will be discussed. Section 7.5 will deal with the tar composition as analysed by Simdis, GC-MS and –FID and SEC-UV analyses. Section 7.6 will deal with the char composition as analysed by proximate, ultimate, XRF, XRD and DRIFT analyses. In Section 7.7, a summary of the most relevant findings will be reported.

** It should be noted that in cases where there is referred to, for example, chars derived up to 520°C, the author implies that these chars were derived up to a final pyrolysis temperature of 520°C, i.e. over the temperature range 25°C to 520°C.*

7.2. Evaluation of model coal-mineral mixtures

Appendix C-8 provides detailed results obtained by the use of FactSage simulation software for different coal-mineral mixtures to determine which method of mineral addition provides results closest to that observed for the TWD coal. Based on these results it was decided to add the minerals based on the QEMSCAN results as reported in Section 3.6.3.

Two model mineral mixtures were made up:

i. Low ash percentage mineral mixture, referred to as LM. This mineral mixture is typical of the washed TWD coal, and the composition was based on the QEMSCAN analyses as reported in Section 3.6.3 for the TWD coal, and the remaining mineral matter present in the AW TWD coal taken into account.

ii. High ash percentage mineral mixture, referred to as HM. This mineral mixture is typical of the ROM TWD coal. The composition is based on CCSEM results as reported by Govender (2005) for this coal. Appendix C-9 provides all of the analytical results as reported by Govender (2005).

The theory behind the FactSage models was to use constant carbon content (as reported from ultimate analyses) for all model mineral-coal mixtures. Thus, the overall mineral content might be higher than originally present in the parent coal, but with regard to the gas yields and composition, it corresponded much better with the original coal mixture, than observed when using constant ash (mineral matter) content.

Table 7-1 indicates the two mineral mixtures as determined from the respective QEMSCAN (Section 3.6.3) and CCSEM results as reported by Govender (2005) (Appendix C-9.2).

Table 7-1 Model mineral mixtures

	LM[a] MODEL	HM[b] MODEL
	mass (g)	
Calcite	1.10	1.73
Dolomite	2.38	0.97
Kaolinite	4.01	6.46
Pyrite	0.15	1.59
Quartz	0.62	2.70
Coal	41.75	36.56
TOTAL	**50.00**	**50.00**

[a]LM = Low ash percentage mineral mixture (TWD Model); [b]HM = High ash percentage mineral mixture (TWD ROM model)

Model mineral mixtures were set up based on the QEMSCAN analysis results as indicated in Section 4.3, with the assistance of FactSage thermodynamic software. The philosophy was to obtain a mineral mixture in which the ratios of minerals corresponded to the QEMSCAN results, but added in an amount to the AW TWD coal that would ensure a fixed carbon value consistent with that of TWD coal.

7.3. Pyrolysis product yields

The synergistic effect of minerals on the pyrolysis product yields will now be assessed at the respective experimental temperatures, 520, 750 and 900°C. Figure 7-1 indicates the pyrolysis product yields obtained for the LM and HM coal-mineral mixtures on an as determined basis at the three temperatures studied. Line graphs were included to guide the reader's eye through

the experimental data points. The graphs indicate the evolved pyrolysis products at the three temperatures studied. The gas yields are observed to increase with an increase in final pyrolysis temperature (Sert *et al.,* 2011; Kandiyoti *et al.,* 2006, Mill, 2000; Ladner, 1988; Nelson *et al.,* 1988). The gas evolution rate seems to remain quite constant between the final pyrolysis temperatures for the HM coal-mineral mixture, whilst for the LM coal-mineral mixture, an accelerated gas evolution rate is observed between 750°C and 900°C. This can be related to the higher concentration of calcite and dolomite minerals present in this minerals mixture, which achieves maximum decomposition rate above 750°C, as has been identified in Section 3.9.

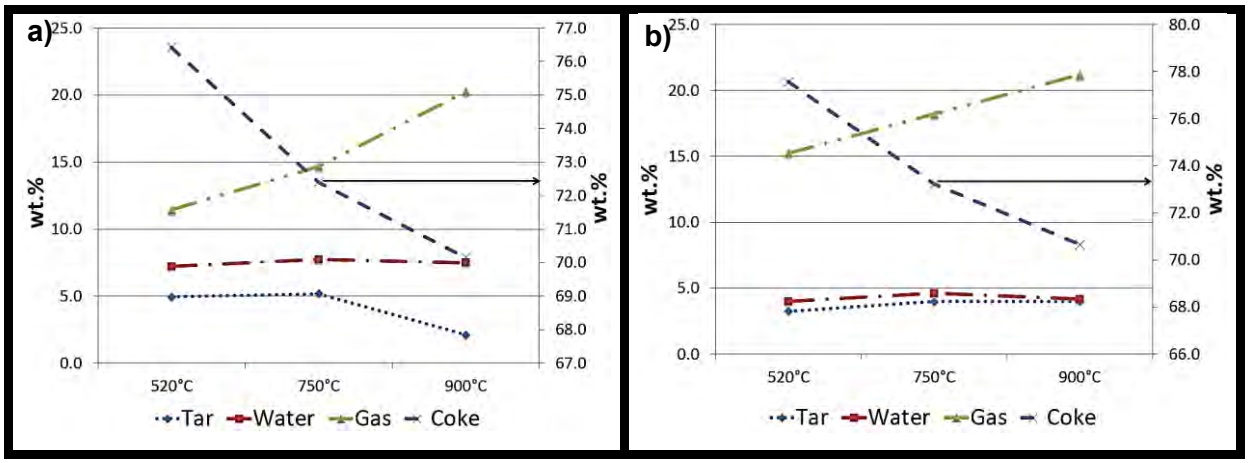

Figure 7-1 Pyrolysis product yields at 520°C, 750°C and 900°C for a) LM, b) HM

The water yield is observed to remain constant for both coal-mineral mixtures. The tar yield from the LM coal-mineral mixture is observed to decrease with increasing final pyrolysis temperature between 750°C and 900°C, whilst that of the HM coal-mineral mixture is observed to increase only to a small extent with an increase in final pyrolysis temperature. The maximum tar yield would have been reached at 600°C (Liu *et al.*, 2004a; Ôztas & Yürüm, 2000, Yaw *et al.*, 1980), and therefore no significant change in tar yield is observed between 750°C and 900°C for both fractions. Minerals such as calcite and dolomite have been shown to be effective tar cracking catalysts (Mun *et al.,* 2012; Pinto *et al.,* 2007; André *et al.,* 2004; Liu *et al.*, 2004a; Sciazko & Kubica, 2002; Chen *et al*., 1999; Yaw *et al.,* 1980), and decomposition of these minerals only started at temperatures in excess of 500°C (Liu *et al.,* 2007a; Vassileva & Vassilev, 2006; Tomeczek & Palugniok, 2002; Reifenstein *et al.,* 1999). Therefore the higher concentration of these minerals present in the LM coal-mineral mixture can probably be responsible for the large decrease observed in tar yield between 750°C and 900°C.

The char yield for both fractions is observed to decrease with an increase in final pyrolysis temperature, whilst the gas yield is in accordance with previous studies (Reichel *et al.,* 2013;

Fei *et al.,* 2012; Ahmad *et al.,* 2009a & 2009b; Kandiyoti *et al.,* 2006; Hu *et al.,* 2004; Smith *et al.,* 1994; Ladner, 1988; Franklin *et al.,* 1982a, 1982b, Yaw *et al.,* 1980).

Table 7-2 TWD ROM Fischer assay values as reported by Govender (2005).

	Char	Tar	Water	Gas
Fischer assay (as determined)	83.7	5.2	7.4	3.7
Fischer assay d.b.	90.4	5.6	-	4.0
Fischer assay d.m.m.f.	88.3	7.5	-	4.2

Comparison of the as determined values of the HM coal-mineral mixture from the 520°C experiments to that of the TWD ROM coal indicates that the char, tar and water yield for the HM coal-mineral mixture was much lower, whilst the gas yield was much larger. The lower water yield is expected due to the lower inherent moisture content of the AW TWD coal. The lower tar yield can be related to the experimental setup used. It has been observed that the tar yield produced from the NWU Fischer assay setup is lower than that observed for the conventional ISO 647 method (Roets *et al.,* 2014). The difference in other product yields can also be due to differences in the experimental method, such as the use of an N_2 atmosphere, different heating rates (Figure 4-2a), and differences related to the coal structure, although the coals were produced from the same coal seam.

Comparison of the pyrolysis product yields obtained from the LM and HM coal-mineral mixtures will now be compared and evaluated against the yields obtained from the TWD and AW TWD coals. The water yields (Figure 7-2a) are reported on a mineral matter free basis (m.m.f.b.), whilst the other pyrolysis product yields (Figure 7-2b to Figure 7-2d) are reported on a dry, mineral matter free basis (d.m.m.f). Correction for mineral matter was done by use of the QEMSCAN results of the coals, whilst the results obtained from the TG analyses (Section 3.9) were used to determine the weight of added minerals still present at a given final pyrolysis temperature as outlined in Section 6.1. Refer to Appendix B-X for all the pyrolysis product yields, reported on an as determined basis, mineral matter free basis and on a dry, mineral matter free basis, along with the calculated error on repeatability values for a 95% confidence interval.

7.3.1. Water yield

Figure 7-2a indicates the water yield values for TWD (8.1 – 8.8 wt%), LM (8.5 – 8.7 wt%), HM (3.8 – 4.7 wt%) and AW TWD (4.3 – 4.6 wt%) on a mineral-matter-free basis. The water yields of the TWD coal and LM coal-mineral mixture correspond very well, whilst the addition of minerals to the AW TWD coal for the HM coal-mineral mixture seems to have influenced the water yield to no great extent. The higher dolomite and calcite content may be responsible for

the increased water yield of the LM coal-mineral mixture, as addition of these minerals was observed to lead to increased water yields. Ahmad *et al.,* 2009a; McKee (1980) found that alkaline earth carbonates, (such as calcite and dolomite), may accelerate the reactions of solid carbon with gaseous oxygen, water vapour and carbon dioxide. The increase observed in the water yields with the addition of the LM mineral mixture is consistent with findings in Section 6.2.1.

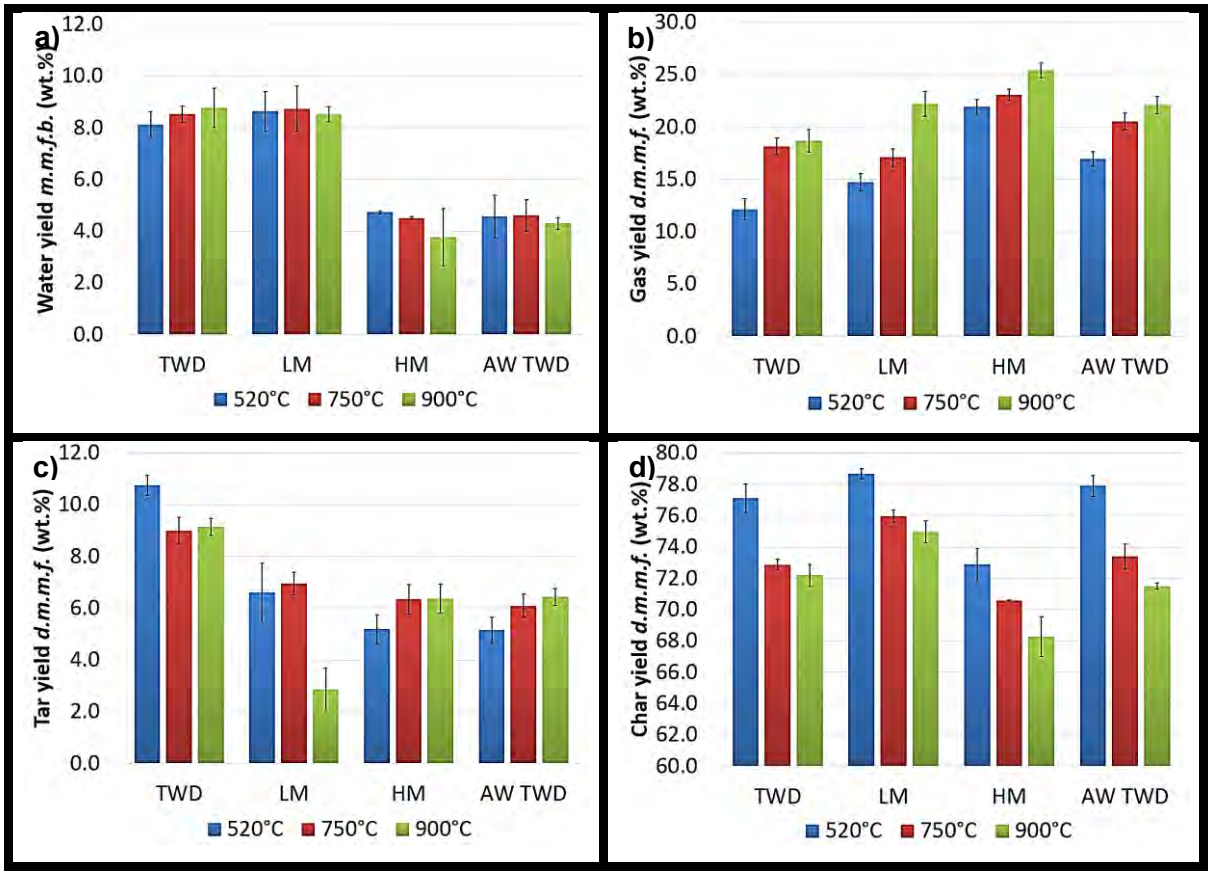

Figure 7-2 a) Water yield m.m.f.b.; b) Gas yield d.m.m.f.; c) Tar yield d.m.m.f. and d) Char yield d.m.m.f. for the LM and HM coal-mineral mixtures and TWD and AW TWD coals.

7.3.2. Gas yield

The gas yields (d.m.m.f) are indicated in Figure 7-2b. It was reported in Section 5.2.2. that the AW TWD coal fraction produced gas yields larger than that of the TWD coal fraction. In Figure 7-2b, it can be observed that the gas yields of the LM coal-mineral mixture indicate a significant decrease from the yields observed for the AW TWD coal fraction, in the 520°C experiments (14.7 vs. 16.9 wt%) and for the 750°C experiments (17.1 vs. 20.5 wt%). In the case of the 900°C experiments, the gas yields of the AW TWD and LM experiments do however correspond (22.1 vs. 22.2 wt%). The gas yield of the HM coal-mineral mixture is higher than

that of the AW TWD at all three final pyrolysis temperatures, similar to the observations observed when minerals were added individually.

The decrease in gas yield observed for the LM coal-mineral mixture runs at 520°C and 750°C indicated that at these temperatures the tar and char forming reactions were favoured; thus increased yields of these products were observed, whilst the gas yield decreased. At the final pyrolysis temperature of 900°C, the gas-forming reactions were favoured, which led to an increase in overall gas yield. In the case of the 520°C and 750°C experiments, better consistency with the TWD coal was observed than for any of the individual mineral additions (Section 6.2.2.); at 900°C, the correspondence was not good, however. The gas yields did however not reach the values observed with the individual addition of some of the minerals such as the calcite and dolomite (Section 6.2.2), thus indicating that there was some synergism involved in the evolution of the gas species. The HM coal-mineral mixture however indicated resemblance to the trends observed with the addition of the minerals individually. At all three temperatures increased gas yields were observed.

7.3.3. Tar yield

Figure 7-2c indicates the tar yield values for the different temperatures. From the LM coal-mineral mixture, it can be observed that the tar yields increased when compared to the AW TWD coal (6.6 wt% for the 520°C and 6.9 wt% for the 750°C experiments). At 900°C, a significant decrease in tar yield was observed for the LM coal-mineral mixture. This result may indicate that the added mineral mixture could increase the tar yield, up until a temperature at which the tar cracking capabilities of the added calcite and dolomite became evident. In the case of the HM coal-mineral mixture, no significant changes in the tar yield were observed when compared to the tar yields of the AW TWD coal fraction. At all temperatures, the tar yields for the TWD coal fraction were much greater, i.e. 10.7, 9.0 and 9.1 wt% at 520°C, 750°C and 900°C respectively.

The reduction in tar yield observed in the 900°C experiments of the LM coal-mineral mixture is consistent with previous results reported in Section 6.6.3, i.e. if the large amount of dolomite and calcite present in this coal-mineral mixture is taken into account. In previous coal studies, the reduction of tar yield by addition / pre-treatment with dolomite was confirmed (Mun *et al.,* 2012; Pinto *et al.,* 2007; André *et al.,* 2004; Liu *et al.*, 2004a; Sciazko & Kubica, 2002; Chen *et al*., 1999; Yaw *et al.,* 1980; Yeboah *et al.,* 1980) as well as for calcite (Liu *et al.*, 2004a; Qi *et al.*, 2004; Tsubouchi & Ohtsuka, 2002a, 2002b; Chen *et al*., 1999; Mondragon *et al.*, 1999; Franklin *et al.,* 1982a, 1982b; Yaw *et al.* 1980).

The HM mineral mixture indicates no significant change in tar yields at any of the temperatures when compared to that of the AW TWD fraction. The most prominent mineral in the HM coal-mineral mixture was kaolinite, followed by quartz. These minerals, (especially quartz), showed very little activity when added individually to the AW TWD fraction, but it is interesting that the tar reducing phenomena observed with the addition of calcite and dolomite individually is not observed. The inactivity of these minerals in the 750°C experiments (present in the LM coal-mineral mixture), might suggest that there was some suppression of catalytic activity of minerals when various minerals, such as calcite, dolomite, kaolinite and pyrite, were present, thus not influencing the pyrolysis yield. In the case of the LM coal-mineral mixture, the other mineral matter might only be effective up to a certain temperature, noting that the calcite and dolomite minerals constituted a much larger fraction than was the case for the HM mineral mixture. This is however only speculation as no other studies could be found exploring these phenomena.

7.3.4. Char yield

The char yields obtained for the TWD, AW TWD fractions and LM and HM coal-mineral mixtures are indicated in Figure 7-2d. As discussed in section 5.2.4, there was no significant difference observed between the char yields for the TWD and AW TWD coal on a dry, mineral-matter-free basis. The values for these two coal ranged between 77.1 and 77.9 wt% in the 520°C experiments, 72.9 and 73.4 wt% in the 750°C experiments, and 71.5 and 72.2 wt% in the 900°C experiments. From Figure 7-2d, it can be observed that the LM coal-mineral mixture showed an increase in char yield in the 750°C and 900°C experiments, whilst the HM coal-mineral mixture indicated the inverse effect, i.e. with a decrease in char yield observed at all three final pyrolysis temperatures. It was observed in previous studies that some minerals such as calcite and dolomite, could lead to increased char-forming reactions (Ahmad *et al.,* 2009b; Chen *et al*., 1999; Franklin *et al.,* 1982a; Franklin *et al.,* 1981). This trend was not observed for the individual additions, but synergism between the various minerals might play a role. Another possibility is that the corrections made for the obtained results based on the TG analyses (Section 3.9) were not accurate. These results are difficult to explain, but the synergism between minerals and coal-mineral mixtures seem to be unique, and it is difficult to observe a definite trend. The decrease in char yield observed for the HM coal-mineral mixture is in agreement with the findings made with the individual addition of the various minerals.

7.4. Gas composition

The derived gases were analysed by GC analyses and the results of the most prominent gases are indicated in Table 7-3. General trends are in agreement with the findings from Section 5.3. Appendix C-2 provides the full set of GC results; for the sake of brevity focus will be given to

the most dominant gas species and the yields of the various gas species on a [g gas species] / [g coal (d.m.m.f.)] as determined by the use of Equation (4-6). The true values are a factor 10^3 smaller than reported. The errors on repeatability within a 95% confidence limit are indicated in Appendix C-2.2.

The composition of the LM coal-mineral mixture indicates good comparison to that of the TWD coal. The order of dominant gases produced by the LM coal-mineral mixture is $CH_4>CO_2>CO>H_2$ at 520°C, $H_2>CO>CH_4>CO_2$ at 750°C and 900°C. It can be observed that the added minerals definitely caused a shift between the CO and CH_4 gas species. On the other hand the HM mineral mixture showed a different trend, with the dominant gases being in the order: $CO_2=CH_4>CO>H_2$ at 520°C, $H_2>CH_4>CO_2=CO$ at 750°C, and $H_2>CH_4=CO, CO_2$ at 900°C.

Table 7-3 GC results of most prominent gas species evolved

	TWD	AW TWD	LM	HM
		mol. %		
		520°C		
H_2	18.6 - 18.7	22 - 24.2	16.8 - 18.9	14.6 - 16.7
CH_4	31.2 - 31.4	36.1 - 37.9	28.8 - 29.2	28.8 - 30.9
CO	23.9 - 24.3	13.7 - 14.5	21.8 - 21.9	17.7 - 19.3
CO_2	19.8 - 19.9	17.9 - 18.9	24.7 - 26.1	28.4 - 32.0
		750°C		
H_2	31.5 - 32.5	38 - 38.4	31.2 - 35.0	26.6 - 29.4
CH_4	26.1 - 26.8	20.2 - 21.4	22.7 - 23.0	23 - 24.1
CO	25.5 - 25.9	26.9 - 27.0	26.4 - 26.7	21.4 - 22.8
CO_2	11.8 - 12.4	10.6 - 11.4	12.9 - 16.5	21.4 - 24.1
		900°C		
H_2	38 - 38.4	44.5 - 46.1	39.3 - 40.6	35.2 - 38
CH_4	20.2 - 21.4	28.2 - 29.2	20.5 - 21.6	20.7 - 21.3
CO	26.9 - 27.0	11.9 - 13.2	24.9 - 26.1	20.7 - 22.6
CO_2	10.6 - 11.4	8.8 - 10.4	9.9 - 12.1	17.8 - 17.9

7.4.1. H_2 yield

Figure 7-3a indicates the H_2 yields of the TWD, AW TWD coals and LM and HM coal-mineral mixtures. It can be observed that in the case of the 520°C and 750°C experiments that the addition of the LM mineral mixture decreased the yield of H_2 content to values consistent with those of the TWD coal, whilst at 900°C a significant decrease in H_2 yield was observed, but not in accordance with the yield of the TWD coal. The HM coal-mineral mixture produced a lower H_2 yield from the 520°C experiments, but not as significant as the change observed with the addition of the LM mineral mixture. The greater change observed in the LM mineral mixture

addition in the yield of H_2 is attributed to the larger fraction of calcite and dolomite minerals present. At 750°C, the H_2 yields of the LM and HM mineral mixtures were both within the 95% confidence limits of the TWD coal. This change could be related to the synergism of the minerals, as well as increased activation of the dolomite mineral at elevated temperatures. At 900°C, the mineral mixtures produced a H_2 yield between that of the AW TWD and TWD coal. At this temperature all of the added dolomite and calcite would have been calcined and decomposition thereof had seized, thus reducing the catalytic effect observed during calcination. This result is also consistent with what was observed from the overall pyrolysis product yields at 900°C, with the addition of the respective mineral mixtures (Section 7.3). In the case of this study the reduction in H_2 yield with the addition of the mineral mixture can thus either be attributed to less cracking of heavy hydrocarbons and/or inhibiting of the dehydrogenation of the formed chars by the condensing of aromatic structures.

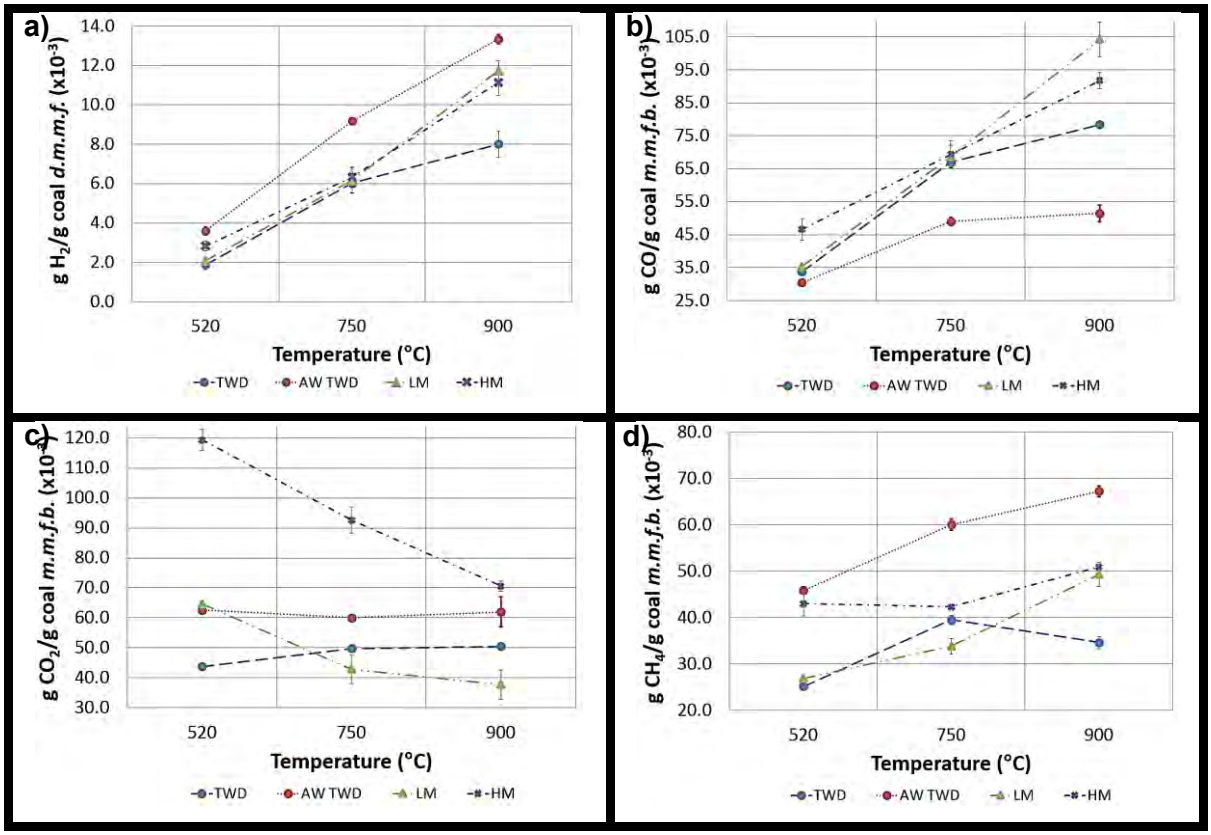

Figure 7-3 a) H_2, b) CO, c) CO_2 and d) CH_4 yields for TWD and AW TWD coals.

7.4.2. CO yield

Figure 7-3b indicates the CO yields obtained with the addition of the model coal-mineral mixtures. At 520°C and 750°C, the LM coal-mineral mixture indicated good correspondence with the CO yield of the TWD coal. This trend proved the importance of the synergism of minerals during coal pyrolysis. In the case of the 900°C experiments, the LM mineral mixture did however seem to over-compensate in terms of CO production. The HM mineral mixture

produced increased CO yields with an increase in final pyrolysis temperature. The difference in LM and HM CO yields could probably be attributed to the lower calcite and dolomite content present, which was observed to affect the CO yield the greatest (Section 6.3.2).

The synergistic effect of the mineral mixture was once more confirmed with all the minerals except for the addition of quartz, which was confirmed to affect the CO yield (Section 6.3.2). The increased CO yield with the addition of calcite and dolomite is attributed to the cracking of oxygen functional groups on the parent coal by CaO (Pinto *et al.,* 2007; Liu *et al.*, 2004a; Karaca, 2003; Tsubouchi *et al.*, 2004; Tsubouchi & Ohtsuka, 2002, Delgado *et al.,* 1996), a decomposition product of these minerals, which started to form at temperatures in excess of 500°C, thus explaining the larger difference observed with an increase in final pyrolysis temperature.

7.4.3. CO_2 yield

Figure 7-3c indicates that the CO_2 yield of the LM coal-mineral mixture decreased with an increase in final pyrolysis temperature. In the case of the 520°C experiments, the addition of the LM mineral mixture seems to have no effect on the CO_2 yield. However, for the 750°C and 900°C experiments, the CO_2 yield is much lower than that of the AW TWD, but also significantly lower than that of the TWD coal. In the case of the HM coal-mineral mixture, the CO_2 yield is significantly higher than that of the AW TWD coal at all temperatures, with a decrease in significance prevalent with increasing final pyrolysis temperature. The decrease observed with increasing pyrolysis temperature for the HM coal-mineral mixture is consistent with the behaviour of AW-Kao and AW-Pyr (Section 6.3.3). The much higher CO_2 yield of the HM coal-mineral mixture for the 520°C experiments can probably be related to the large amount of pyrite added in this mineral mixture, whilst a much smaller amount of pyrite was added to the LM coal-mineral mixture. The trend of the CO_2 yield of the LM mineral mixture once again indicates that the synergism between minerals plays a vital role in the composition and yields produced from pyrolysis.

The decreased yields of CO_2 obtained from the addition of calcite (Yongbin *et al.,* 2004; Aznar *et al.,* 1996; Franklin *et al.,* 1981) and dolomite was expected. Calcite and dolomite which decomposes to CaO were found to decrease CO_2 yields in previous work (Yeboah *et al.,* 1980; Vestal *et al.,* 1970; Dedman & Owen, 1962). The current study confirms this observation, noting that the CO_2 yield is greatly reduced between 750°C and 900°C, which are within the temperature range of previous studies where reduction in CO_2 yields was reported (Sert *et al.,* 2011; Yeboah *et al.,* 1980). The focus needs to be placed on the water-gas shift reaction, Equation 6-5, as indicated in Table 6-2 (Section 6.2.3) :

$$CO(g) + H_2O(g) \rightleftharpoons CO_2(g) + H_2(g) \quad (6\text{-}5)$$

The importance of this equation with regard to product yields and composition with the addition of dolomite / calcite was confirmed (Abu El-Rub, 2004; McKee, 1980). With the addition of calcite and dolomite, increased CO and water yields were reported, whilst the CO_2 and H_2 yields were lower. When observing the water-gas shift reaction, it is clear that under the current experimental conditions the left hand side of this equation must be favoured, thus explaining the shift observed in composition. If the gas yields of the AW TWD coal are taken into account, it was shown that a relatively high H_2 and CO_2 yield was already present at the lower pyrolysis temperature range of 520°C, whilst the amount of CO and H_2O produced was lower than that of the TWD coal, i.e. the reaction products present are thus in favour of the water-gas shift reaction going to the left hand side.

7.4.4. CH_4 yield

In Figure 7-.3d, the CH_4 yields of the coal-mineral mixtures are indicated. In the case of the LM mineral mixture, a significant decrease in CH_4 yield was observed at all temperatures when compared to the yield of the AW TWD coal. At 520°C, good correspondence was observed between the CH_4 yields of the TWD and the LM coal-mineral mixture, whereas at 750°C the CH_4 yield of the LM mineral mixture was significantly lower than that of TWD, and at 900°C, an increase in CH_4 yield was observed. The HM coal-mineral mixture did not show any change in CH_4 yield between 520°C and 750°C, whilst between 750 ° C and 900°C, an increase was observed in the CH_4 yield.

The effect of calcite, dolomite and pyrite addition on the CH_4 yield was confirmed in Section 7.3.4. The fact that the addition of the mineral mixtures produces yields that correlate with the yields from the TWD coal fraction is a very positive indication. It also highlights the need to determine the synergistic effect between various minerals.

7.4.5. Other gas species

Figure 7-4a indicates the C_2H_4 yields for the coal-mineral mixtures. It can be observed that the C_2H_4 yield of the LM coal-mineral mixture corresponded with that of the TWD coal at all pyrolysis temperatures. The LM coal mineral mixture C_2H_4 yield decreased with increasing pyrolysis temperature up to 750°C, after which it remained constant. The addition of the HM mineral mixture did not affect the C_2H_4 yield of the 520°C experiments, but for the 750°C and 900°C experiments a decrease in C_2H_4 yield was observed when compared to the AW TWD coal. There is no significant difference observed between the yields of LM and HM, between 750°C and 900°C. The decrease in LM C_2H_4 yield for the 520°C experiments is attributed to

the addition of calcite; at 750°C to dolomite, and at 900°C due to the addition of dolomite, pyrite and kaolinite.

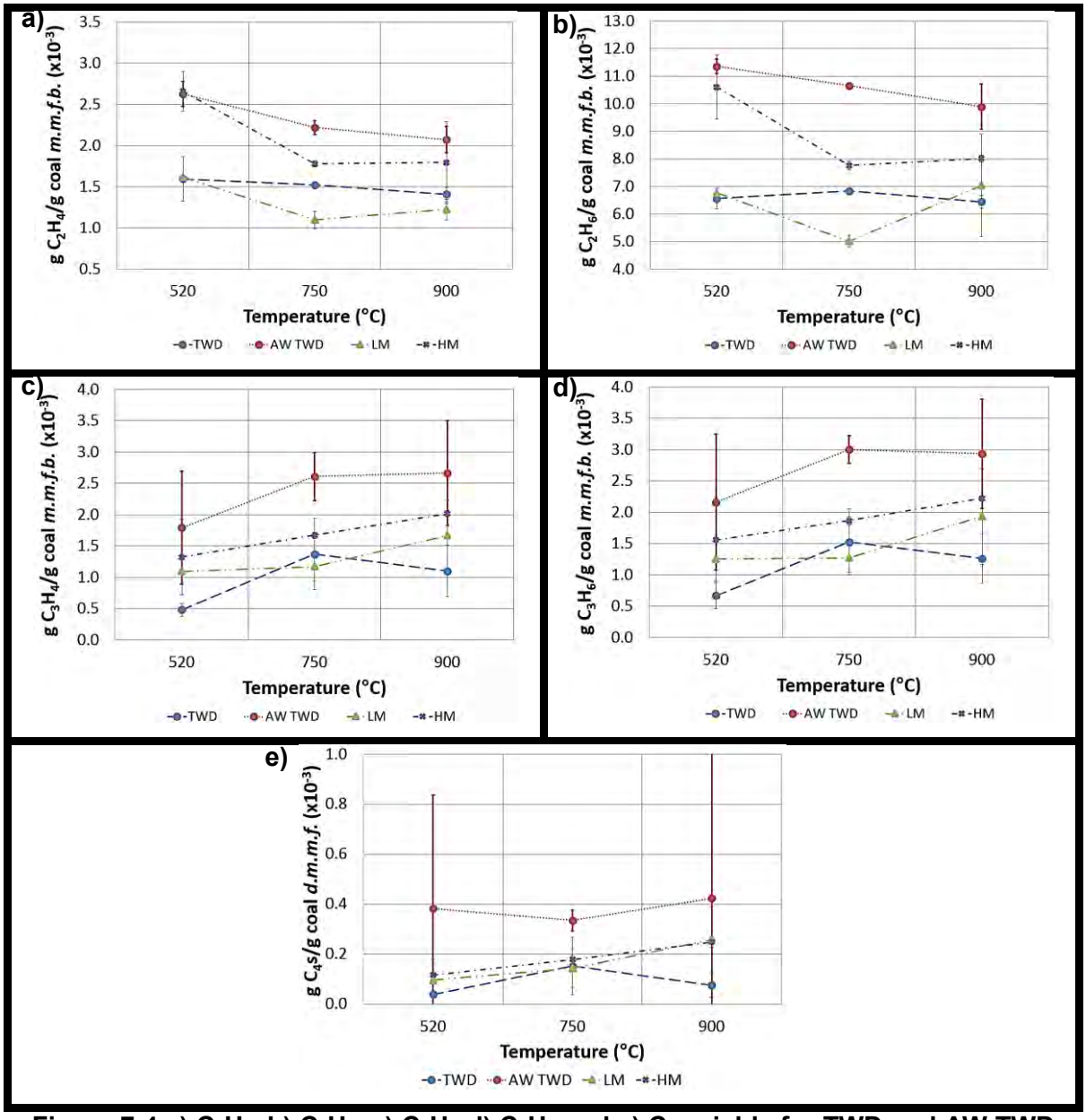

Figure 7-4 a) C_2H_4, b) C_2H_6, c) C_3H_4, d) C_3H_6 and e) C_4s yields for TWD and AW TWD coals and LM and HM coal-mineral mixtures.

Figure 7-4b indicates the C_2H_6 yields of the coal-mineral mixtures. It can be observed that the C_2H_6 yield of the LM coal-mineral mixture corresponded with that of the TWD coal at 520°C and 900°C. The large decrease in C_2H_6 yield below the values of TWD coal for the 750°C experiments is attributed to the addition of calcite and dolomite and the cumulative effect of this addition on the C_2H_6 yield.

The addition of the HM mineral mixture did not affect the C_2H_4 yield of the 520°C experiments, but at 750°C and 900°C a decrease in C_2H_6 yield was observed when compared with the AW

TWD case. There was no significant difference between the HM C_2H_6, yields between 750°C and 900°C, but the LM mineral mixture did however indicate an increase in C_2H_6 yield between 750°C and 900°C. The decrease in LM C_2H_6 yield at 520°C is attributed to the addition of calcite, at 750°C and at 900°C to calcite, dolomite, kaolinite and pyrite addition.

In Figure 7-4c the LM and HM mineral mixtures are observed to have decreased the C_3H_4 values at all final pyrolysis temperatures, with an increase in C_3H_4 yield occurring with increasing final pyrolysis temperature. At 750°C, good agreement was observed in the C_3H_4 yield of the TWD coal and the LM coal-mineral mixture. At 900°C, the C_3H_4 yield of the LM coal-mineral mixture was however larger than that of the TWD coal, following the same trend as observed than that of the AW TWD case. There was however still a significant decrease in this component. The HM coal-mineral mixture is observed to have produced C_3H_4 yields lower than that of the AW TWD coal, but the yields did not decrease to such a great extent as observed for the the LM coal-mineral mixture. The decrease in yield is attributed mainly to the addition of calcite and dolomite, but also to the overall interaction of the various mineral mixtures.

C_3H_6 yields given in Figure 7-4d also indicate the same trends than identified in Figure 7-4c, i.e. thus indicating that the respective mineral mixtures had the same effect on both these product yields.

Figure 7-4e indicates the C_4s yield which constitutes a very small fraction of the overall gas yield. Good correspondence between the C_4s yield of the LM and HM mineral mixture is observed at all pyrolysis temperatures. No significant differences can be reported with increasing final pyrolysis temperature.

In general, it can be observed that the addition of minerals led to the reduction of gases of the form C_nH_m. From Section 6.3.5 it was shown that quartz addition was most inactive in changing gas yields, whilst kaolinite addition showed varying trends, and the changes caused by pyrite addition were also less significant (except in the reduction of the C_2s at higher temperatures), and an increase in C_4s at 900°C. The cracking of gases of the form C_nH_m by calcite and dolomite was confirmed previously and is related to the tar cracking capabilities, mainly attributed to the decomposition product CaO (Mun *et al.,* 2012; Pinto *et al.,* 2007; Yongbin *et al.,* 2004; Xu & Tomita, 1989; Franklin *et al.* 1982b; Yeboah *et al.,* 1980). Kaolinite has been observed to cause shifts in pyrolysis product composition due to cracking of hydrocarbons (Ôztas and Yürüm, 2000; Chen *et al.* 1999; Franklin *et al.,* 1982a). The active component is however believed to be Al_2O_3 and is more active at higher temperatures (Liu *et al.*, 2004a), which can be confirmed from the current results. Little change in the C_2 – C_4s was expected, based on previous findings (Franklin *et al.,* 1982a, 1982b); however, experimental conditions

differed, slow pyrolysis vs. flash pyrolysis, and the decomposition products of pyrite are believed to be most active and effect pyrolysis products to the greatest extent (Borah *et al.,* 2005). This explains why the changes are only observed at the elevated final pyrolysis temperatures.

7.5. Tar composition

The tar composition was analysed by Simdis, GC-MS and –FID and SEC-UV analyses.

7.5.1. Simulated distillation (Simdis)

The boiling point distributions for the derived tars of the LM and HM coal-mineral mixtures are indicated in Figure 7-5. The tar boiling points were confined in the region 112.2°C – 550°C. All injected tar (100%) was recovered at temperatures below 550°C. Refer to Appendix C-3 for repeatability curves. The tars derived from the HM coal-mineral mixture (Figure 7-5b) indicated more consistency than observed for the tars derived from the LM coal-mineral mixture (Figure 7-5a).

Figure 7-5a indicates that the tar derived at 900°C for the LM coal-mineral mixture contained more higher boiling point compounds than the tars derived at 520°C and 750°C. From Figure 7-5b it can be observed that there was little variation between the derived tars for the HM coal-mineral mixture, with small deviations indicating that the tars derived at the higher final pyrolysis temperature also contained more higher boiling point compounds.The boiling point distributions observed are in accordance with typical fossil fuel and waste-derived tars and oils as observed in previous studies (Roets *et al.,* 2014; Bean 2013; Hattingh, 2012; Lee, 2009; Karayildirim *et al.,* 2006; Shie *et al.,* 2003; Li *et al.,* 2001; Bunger 1976).

Comparison between the coal-mineral mixture derived tars and the tars derived from the TWD and AW TWD coal in the case of the 520°C experiments (Figure 7-5c) indicate that the tars derived from the LM coal-mineral mixture and the TWD coal tar corresponded very well, whilst the HM mineral mixture seemed to have changed the composition of the tar very little, showing good correspondence with that of the AW TWD tar.

At 750°C, the LM coal-mineral mixture contained more lighter boiling compounds than for any of the other derived tars; this is consistent with what was observed for the tars derived from AW-Cal and AW-Dol (Section 6.4.2). The LM coal-mineral mixture also showed good correspondence with the TWD derived tar components with boiling point distribution between 230°C and 450°C.

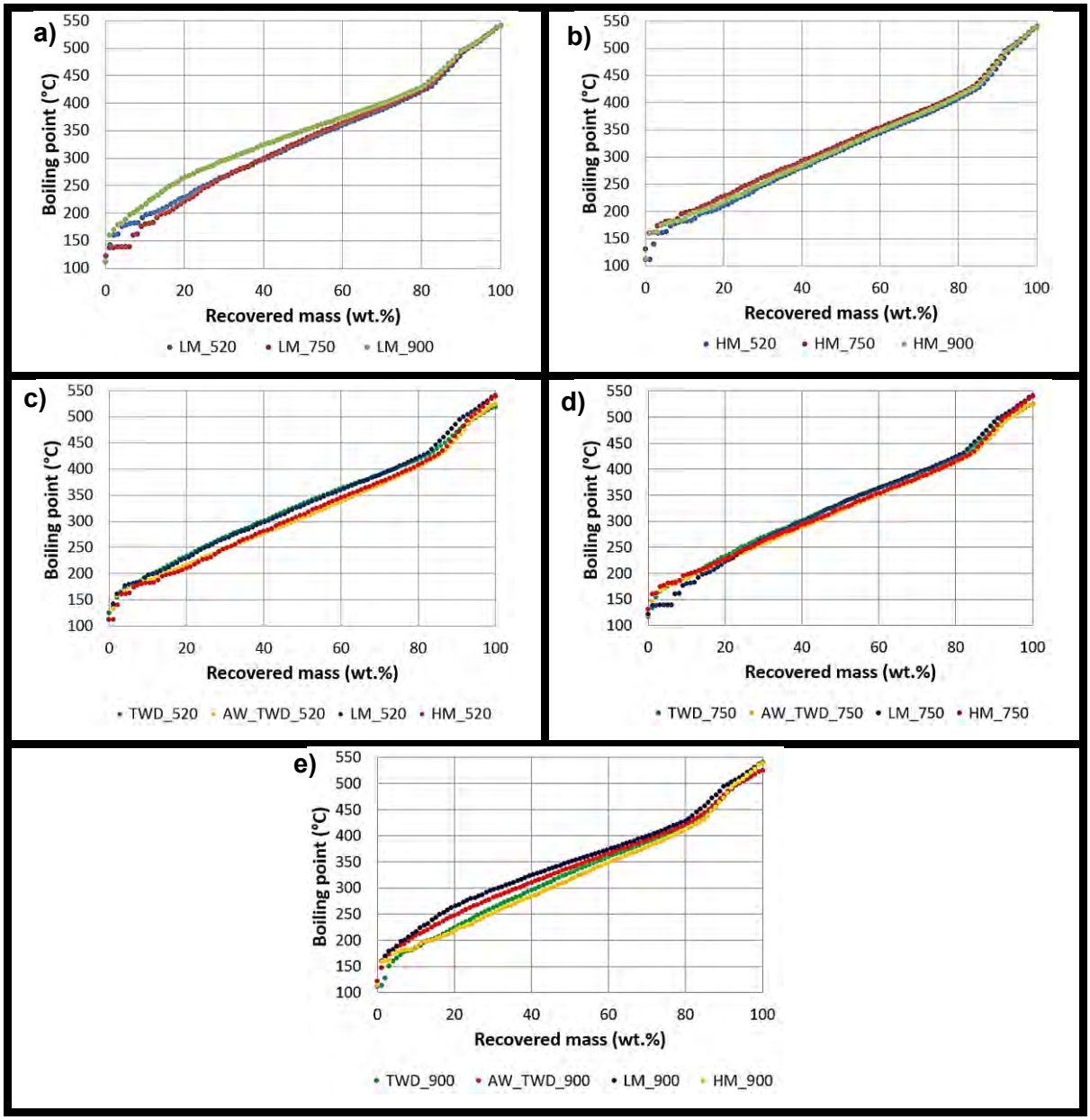

Figure 7-5 Boiling point distribution curves for a) LM derived tar; b) HM derived tar; TWD, AW TWD, LM and HM tars at c) 520°C; d) 750°C and e) 900°C.

Little variation is observed between the various derived tars for the 750°C experiments; this is consistent with the other results as observed for the TWD and AW TWD derived tars, as well as for the various mineral additions. At 900°C, the correspondence between the TWD tar and LM tar was once more very good. The HM tar indicates increased higher boiling point temperature compounds at this final pyrolysis temperature, in contrast with the observations made with the individual addition of minerals.

Table 7-4 Boiling point distributions for tars based on crude oil fractions

	Boiling point range (°C)	TWD		AW TWD		LM		HM	
		wt% /°C	*g/100 g coal*	*wt% /°C*	*g/100 g coal*	*wt% /°C*	*g/100 g coal*	*wt% /°C*	*g/100 g coal*
520°C									
Medium naphtha	79-121	0.5	0.1	1.0	0.1	1.0	0.1	2.1	0.1
Heavy naphtha	121-191	7.6	0.8	10.2	0.5	7.2	0.5	10.5	0.4
Kerosene	191-277	23.2	2.5	29.6	1.5	24.8	1.6	25.3	1.0
Distillate fuel oil	277-343	21.2	2.3	21.4	1.1	20.6	1.4	21.0	0.8
Light vacuum gas oil	343-455	34.4	3.7	28.6	1.5	32.0	2.1	29.5	1.1
Heavy vacuum gas oil	455-566	13.1	1.4	9.2	0.5	14.4	1.0	11.6	0.4
IBP	-	112.2		112.2		112.2		112.2	
WABP	100 - 550	326 - 336		302 - 326		333 - 334		317.0 - 319.0	
FBP	-	519.4		524.3		540.8		539	
750°C									
Medium naphtha	79-121	1.0	0.1	1.0	0.1	1.0	0.1	1.0	0.1
Heavy naphtha	121-191	8.1	0.7	8.0	0.5	12.0	0.8	7.2	0.5
Kerosene	191-277	22.2	2.0	26.0	1.6	20.0	1.4	25.5	1.6
Distillate fuel oil	277-343	21.2	1.9	20.0	1.2	20.0	1.4	22.4	1.4
Light vacuum gas oil	343-455	33.4	3.0	31.0	1.9	33.0	2.3	30.6	1.9
Heavy vacuum gas oil	455-566	14.1	1.3	14.0	0.9	15.0	1.0	13.3	0.8
IBP	-	112.2		112.2		112.2		112.2	
WABP	100 - 550	327 - 341		318 -330		335 - 336		328 - 330	
FBP	-	524.7		524.7		541.2		540.4	
900°C									
Medium naphtha	79-121	1.7	0.2	0.8	0.1	1.0	0.0	1.1	0.1
Heavy naphtha	121-191	9.3	0.8	5.2	0.3	9.2	0.3	4.1	0.3
Kerosene	191-277	28.0	2.5	22.0	1.4	26.5	0.8	18.1	1.2
Distillate fuel oil	277-343	22.0	2.0	23.0	1.5	20.4	0.6	23.2	1.5
Light vacuum gas oil	343-455	28.0	2.5	35.0	2.2	30.7	0.9	37.3	2.4
Heavy vacuum gas oil	455-566	11.0	1.0	14.0	0.9	12.2	0.4	16.2	1.0
IBP	-	112.2		112.2		113.5		112.8	
WABP	100 - 550	329 - 336		326 - 354		320 - 322		351 - 355	
FBP	-	524.3		524.8		539.6		540.8	

Comparison of the IBP (Table 7-4) indicates good correspondence with the TWD and AW TWD derived tars, i.e. the FBP was once more higher with mineral addition. With regard to the WABP's, it can be observed from Table 7-4 that the WABPs of the LM and HM tar was in accordance with the WABP of the TWD tar for the 520°C and 750°C experiments. At 900°C, the HM tar was however in agreement with the AW TWD derived tar, and the LM tar had a lower WABP than for any of the other coal tars, 320°C – 322°C.

Comparison of the cut fraction composition of the LM coal-mineral mixture with increasing final pyrolysis temperature indicates that the medium naphtha and distillate fuel oil compounds showed no significant change with an increase in final pyrolysis temperature. The light- and heavy vacuum gas oil fractions were observed to decrease between 750°C and 900°C. The heavy naphtha cut fraction compounds increased up to 750°C, and decreased thereafter in relation to the final pyrolysis temperature of 900°C. The kerosene fraction in turn decreased up to 750°C, and thereafter increased in relation to the final pyrolysis temperature of 900°C. The HM-coal mineral mixture tars are observed to consist of less medium and heavy naphtha for the 750°C experiments, whilst the light vacuum gas oil fraction increased, and the other fractions were unaffected. Between 750°C and 900°C, the HM tar consisted of less heavy naphtha and kerosene cut fraction compounds, whilst the light and heavy vacuum gas oil fraction compounds increased, and the other compounds were unaffected.

Comparison of the coal-mineral mixture tars to that of the TWD and AW TWD coal based on cut fractions indicates that there was good comparison between the compositions of the LM mineral mixture tars at all final pyrolysis temperatures with that of the TWD coal. The only exceptions were that of the heavy naphtha fraction obtained at 750°C (which can be attributed to the addition of calcite), which is known for its tar cracking propensity previously confirmed (Liu *et al.*, 2004a; Qi *et al.*, 2004; Tsubouchi & Ohtsuka, 2002a, 2002b; Chen *et al*., 1999; Mondragon *et al.*, 1999; Franklin *et al.,* 1982a, 1982b; Yaw *et al.* 1980). All the yields were not necessarily exactly the same in quantity, but based on the comparison between the TWD and AW TWD derived tars, it is clear that the added mineral mixtures changed the tar composition in such a manner that it much better resembled the composition of the TWD tar. The tar cracking capabilities of calcite (Liu *et al.*, 2004a; Qi *et al.*, 2004; Tsubouchi & Ohtsuka, 2002a, 2002b; Chen *et al*., 1999; Mondragon *et al.*, 1999; Franklin *et al.,* 1982a, 1982b; Yaw *et al.* 1980), dolomite (Mun *et al.,* 2012; Pinto *et al.,* 2007; André *et al.,* 2004; Liu *et al.*, 2004a; Sciazko & Kubica, 2002; Chen *et al*., 1999; Yaw *et al.,* 1980; Yeboah *et al.,* 1980), kaolinite (Karaca, 2003; Ôztas & Yürüm, 2000; Chen *et al.,* 1999, Franklin *et al.,* 1982a) and pyrite (Borah *et al.,* 2005; Franklin *et al.,* 1982a & 1982b) are known, whilst the inactivity of quartz on pyrolysis product yields and composition was to be expected due to the chemical inert nature of this mineral (Ôztas & Yürüm, 2000; Chen *et al.*, 1999; Franklin *et al.,* 1982a, Franklin

et al., 1981). The HM coal mineral mixture indicated better comparison to the composition of the AW TWD coal tar; i.e. this was related to the lower calcite and dolomite concentration, which are the most active minerals during the pyrolysis of coal.

7.5.3. Gas chromatography-mass spectrometry and flame ionization detection (GC-MS and -FID)

The GC-MS analysis results (Figure 7-6) are reported within a 95% confidence interval, as calculated from standard deviation values for two replicate experiments. Refer to Appendix C-4 for GC-MS and –FID data with indicated confidence intervals.

7.5.3.1. Full spectrum

The LM and HM derived tars did not portray any significant change in the yield of aliphatic compounds (Figure 7-6a) with increasing final pyrolysis temperature. The aliphatic compounds yield of the LM derived tar agreed with that of the TWD and AW TWD derived tars at all final pyrolysis temperatures. On the other hand, the yield of these compounds is observed to be lower at all final pyrolysis temperatures in the case of the HM derived tars, which may be related to the synergistic cracking effects of the present minerals. This is possibly due to increased cracking of larger ring structures and heavier tar molecules, such as the aromatic ethers and esters (Figure 7-6c), alkyl-phenols (Figure 7-6d), alkyl-naphthalenes (Figure 7-6e) and PAHs (Figure 7-6h) (Yongbin *et al.,* 2004). Kaolinite was observed to affect the aliphatic compound yield to the greatest extent in Section 6.4.3, which might explain why the change observed with the addition of the HM mineral mixture was more significant. The cracking capability of kaolinite is related to the solid acidity of this mineral (Abu El-Rub, 2004; Schobert, 1992; Ross *et al.,* 1987, Wen & Cain, 1984).

With regard to the mixed aliphatic and aromatic compound yields (Figure 7-6b), a significant increase was observed with increasing final pyrolysis temperature between 750°C and 900°C for both the LM and HM derived tars. This change is indicative of secondary cracking reactions taking place (Wang *et al.,* 2013; Zhang *et al.,* 2010; Casal *et al.,* 2008; Jones *et al.,* 2005; Morf *et al.,* 2002, Jess *et al,* 1996; Nelson & Tyler, 1988).The yield of these compounds was significantly higher for both coal-mineral model mixtures (LM and HM) at all pyrolysis temperatures when compared to the yields of the TWD and AW TWD derived tars.

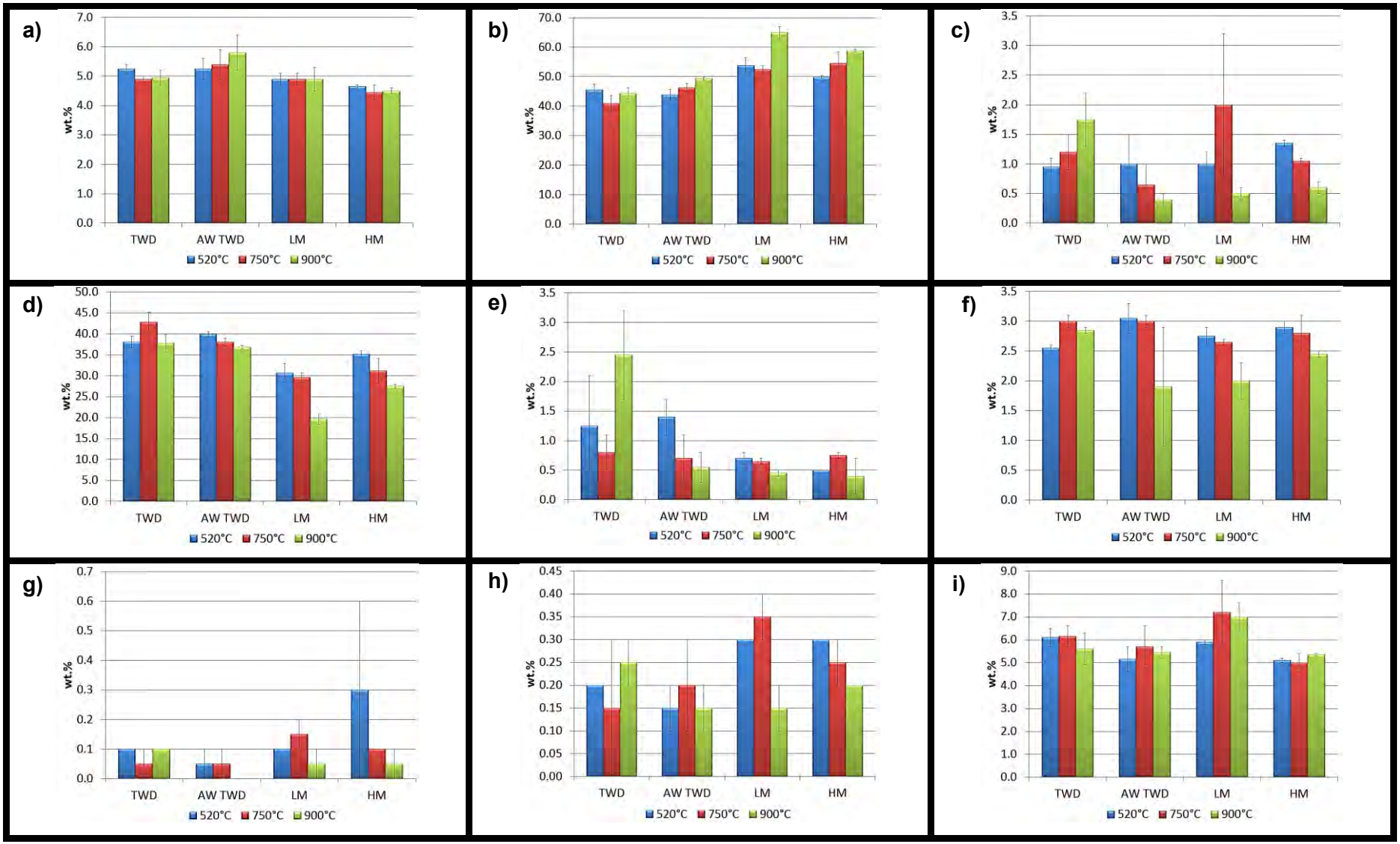

Figure 7-6 a) Aliphatic compounds; b) Mixed aromatics and aliphatics; c) Alkyl-benzenes; d) Alkyl-phenols; e) Aromatic ethers and esters; f) Alkyl-naphthalenes; g) Alkyl-Indenes; h) PAHs and i) N-heteroatoms.

The significantly higher mixed aliphatic and aromatic component yield of the LM coal-mineral mixture (especially for the 900°C experiments), can be related to the higher calcite and dolomite content present, although quartz was also shown to have a positive catalytic effect when added individually (Section 6.4.3). Kaolinite and pyrite showed negative effects on this yield at 900°C.

7.5.3.2. Aromatic spectrum

For both coal-mineral mixtures' derived tars, no significant difference in alkyl benzene yield (Figure 7-6c) is observed with increasing final pyrolysis temperature. The alkyl-phenols yield (Figure 7-6d) is observed to decrease with an increase in final pyrolysis temperature, whilst the aromatic ethers and esters yield (Figure 7-6e) increases; but a decrease is observed between 750°C and 900°C for the LM coal-mineral mixture derived tars. The alkyl-indenes yield (Figure 7-6f) is observed to increase between 520°C and 750°C, with no change observed in the 900°C experiments for the LM coal-mineral mixture. The alkyl-naphthalenes yield (Figure 7-6g) for the 750°C experiments is higher than that produced for the 520°C experiments, but no significant difference is observed at 900°C, with overlap occurring for values reported at 520°C and 750°C in the case of the LM coal-mineral mixture derived tars. No significant difference in alkyl phenol, aromatic ether and ester, alkyl indene and alkyl naphthalene yield is observed with increasing final pyrolysis temperature of the HM coal-mineral mixture derived tars. The increase observed in alkyl-substituted compounds with an increase in final pyrolysis temperature is related to the severity of the pyrolysis process, which leads to increased cleavage of aromatic bridges (Tang *et al.*, 2014; Hattingh, 2012; Nelson *et al.,* 1988). This behaviour is consistent with observations made for the TWD derived tar, but not observed for the AW TWD tar. It once more fixes the attention on the activity of the calcite and dolomite minerals, and might explain why the variance for the HM derived tar was not significant.

No significant change is observed in PAH yield (Figure 7-6h) with increasing final pyrolysis temperature for both coal-mineral mixtures' derived tars. The nitrogen heteroatoms yield (Figure 7-6i) increases significantly between 750°C and 900°C for both coal-mineral mixture derived tars. The nitrogen functionalities found in the tar fraction are related to aromatic structures in the coal such as pyridenes and pyrroles (Smith *et al.,* 1994; Chen *et al.,* 1990). No sulphur functionalities were identified; i.e. most of the sulphur present within the coal structure is probably related to the sulphide minerals such as pyrite, and would mainly form H_2S gas during pyrolysis (Smith *et al.,* 1994). Sulphur functionalities will probably be better identifiable with techniques such as specialised GC-MS and XPS (X-ray photoelectron spectroscopy) (Hattingh, 2012).

Comparison with the TWD and AW TWD derived tars indicate that the LM coal-mineral mixture derived tars produced alkyl-benzene yields (Figure 7-6c), in agreement with both the TWD and AW TWD derived tars at 520°C and 750°C, but slightly lower at 900°C than for the TWD derived tar, but in agreement with the AW TWD derived tar. The alkyl-benzene yield of the HM coal-mineral mixture derived tar is in agreement with that of the AW-TWD case at 520°C and 900°C, whilst being slightly higher for the 750°C run. An increase in alkyl-benzenes was previously observed in coal tar cracking studies at 900°C with the addition of CaO, which is one of the decomposition products of calcite and/or dolomite (Wang *et al.,* 2014).

With regard to the alkyl-phenols yield (Figure 7-6d) for the 520°C experiments, all four (TWD, AW TWD, LM and HM) derived tars were in accordance. At 750°C, the yields of the LM and HM coal-mineral mixtures were significantly lower, as well as for the 900°C experiments. The alkyl-phenol yield of the HM derived tar was however larger than that of the LM derived tar; but this difference is attributed to the difference in mineral mixture make-up. The decrease in alkyl-phenols with the addition of minerals, is consistent with observations for individual addition of minerals (Section 6.4.3.2). Previous authors also reported a decrease in phenols with the addition of CaO, one of the decomposition products of calcite and/or dolomite (Dickerson and Serio, 2013). The lower alkyl-phenolic compounds observed with the addition of the various minerals are related to the higher CO yields observed in these cases. The cracking of phenolic compounds was found to contribute to CO yields (Yongbin *et al.,* 2004*;* Li *et al.,* 1998; Xu & Tomita, 1989).

At 520°C, the aromatic ethers and esters yields (Figure 7-6e) of both the LM and HM derived tars were in agreement with the TWD derived tars. At 750°C, the yields were in accordance with the TWD and AW TWD derived tars, and at 900°C, they were only consistent with the AW TWD derived tar. The alkyl-indene yields (Figure 7-6f) of all four cases (TWD, AW TWD, LM and HM) were all in accordance, at all final pyrolysis temperatures.

The alkyl-naphthalenes yields (Figure 7-6g) of the AW TWD, LM and HM derived tars were in agreement at 520°C. At 750°C, the alkyl-naphthalenes yields of both the LM and HM cases were larger than that of the TWD and AW TWD derived tar. At 900°C, the yields of the TWD and LM tar were in agreement, but that of HM derived tar was much larger than the corresponding yield of the TWD and AW TWD derived tars. This can be related to the higher kaolinite and pyrite content present in the HM coal-mineral mixture, which was observed to show the same trend for individual addition of these respective minerals (Section 6.4.3.2).

The PAH yield (Figure 7-6h) at 520°C was in agreement for the TWD, AW TWD and LM derived tars, whilst the yield is larger for the HM derived tar. The increased yield in PAHs for the 520°C experiments could be related to the presence of dolomite and quartz (Section

6.4.3.2). At 750°C, the PAH yield for the TWD, AW TWD and LM derived tars were all in agreement, whilst the yield of the HM derived tar agreed with that of the AW TWD derived tar. At 900°C, the PAH yield of the LM and HM derived tar was larger than that of the AW TWD derived tar, in agreement with the TWD derived tar. The higher yields of the 900°C experiments could be attributed to the presence of all of the minerals. The higher yields of PAH for the 900°C experiments could be related to the lower H_2 and CH_4 yields at the same temperature for the mineral addition cases, as the decomposition of PAHs was a great source of a large number of H_2 and CH_4 (Yongbin *et al.,* 2004). It was found previously that this tends to occur at temperatures exceeding 700°C due to the dehydrogenation of CaO (Yongbin *et al.,* 2004; Kinoshita *et al.,* 1995). Fe_2O_3, which is a probable decomposition product of pyrite, and was reported to increase PAHs in biomass tars produced by catalytic fast pyrolysis (Dickerson & Soria, 2013).

With regard to nitrogen heteroatom yields from the 520°C experiments, good agreement is observed for the LM derived tar with both the TWD and AW TWD derived tars, whilst the yield of the HM derived tar corresponded to that of the AW TWD derived tar. At 750°C, the yields of the LM and HM derived tars were larger than that of the TWD derived tar, in agreement with the AW TWD derived tar. At 900°C, the nitrogen heteroatoms yield of the LM and HM derived tars were much larger than that of the TWD and AW TWD derived tars. The LM derived tar indicated exceptionally higher yields of nitrogen heteroatoms. The increased nitrogen heteroatoms yield for the 900°C experiments is attributed to the presence of quartz in the mineral mixtures (Section 6.4.3.2). Derivation of the nitrogen heteroatom compounds is mostly independent of mineral presence within the coal structure and is related to the aromatic structures in the coal such as pyridenes and pyrroles (Smith *et al.,* 1994; Chen *et al.,* 1990). The nitrogen found in coal is also mainly associated with the organic matter (Speight, 2005).

7.5.4. Size exclusion chromatography (SEC-UV)

SEC results will be reported as discussed in Section 4.4.2.3. Appendix C-5 includes all repeatability curves for the duplicate samples. The coal-mineral mixture derived tars consisted of components between the molecular size ranges of 30 – 6000 Da, consistent with the findings made for the TWD and AW TWD derived tars (Section 5.4.4). Table 7-5 summarises the obtained SEC results for the various mineral addition derived tars. These observations are in accordance with previous studies (Fidalgo *et al.,* 2014; Hattingh, 2012; Mokoena *et al.,* 2008; Adegoroye *et al.,* 2004; Mill, 2000; John *et al.,* 1994; Li *et al.,* 1993a). With the use of NMP as eluent, the aliphatic species were not included in the observation, due to low solubility, and therefore eluents such as heptane should be used for identification of aliphatic compounds in future studies (Herod *et al.,* 2007). Aliphatic compounds can also be better identified by

other detection methods such as RID (refractive index detection) (Hattingh, 2012; Herod *et al.,* 2003). The heavy component peak maximum is observed around ~400 Da for all tars, and the light component peak maximum around ~200 Da, consistent with findings for tars derived from coal gasification as investigated by Fidalgo *et al.,* (2014). The variances in peak maxima show no specific trend, and therefore the discussion of results will focus on the determined area percentages for light and heavy components.

Table 7-5 Summary of SEC-UV results for the various derived tars.

	TWD	AW TWD	LM	HM
520°C				
Heavy component peak max. (Da)	405	399	400	398
Light component Peak max. (Da)	197	193	202	186
Light components (Area %)	31.9	38.9	36.6	37.4
Heavy components (Area %)	68.1	61.1	63.4	62.6
750°C				
Heavy component peak max. (Da)	417	395	399	404
Light component Peak max. (Da)	211	201	215	197
Light components (Area %)	33.9	37.5	36.5	36.4
Heavy components (Area %)	66.1	62.5	63.5	63.6
900°C				
Heavy component peak max. (Da)	426	402	404	401
Light component Peak max. (Da)	201	206	203	200
Light components (Area %)	33.0	35.3	38.6	37.2
Heavy components (Area %)	67.0	64.7	61.4	62.8

Comparison of the tar composition of the LM coal-mineral mixture derived tars at the various pyrolysis temperatures given in Table 7-5 indicates no significant change in composition between a final pyrolysis temperature of 520°C and 750°C, but for the 900°C experiments an increase in light components was observed. In the case of the HM derived tars, little variation with increasing final pyrolysis temperature was observed, with a slight decrease in light components evident from the 750°C experiments.

Comparison of the coal-mineral mixture derived tars and that of the TWD and AW TWD coal indicates lower light components produced at 520°C and 750°C, but higher light component yields for the 900°C experiments when compared to the composition of the AW TWD derived tar at the same temperatures. There was however little correspondence between the coal-mineral mixture tar composition and the composition of the TWD derived tars as identified by SEC-UV. The observations made are in accordance with the observations made from the Simdis analyses. Heavy and light peak maxima values are in agreement with the values as observed for AW TWD derived tars (Table 6-5, Section 6.4.4).

7.6. Char composition

The derived chars were analysed by proximate, ultimate, XRF and XRD analyses.

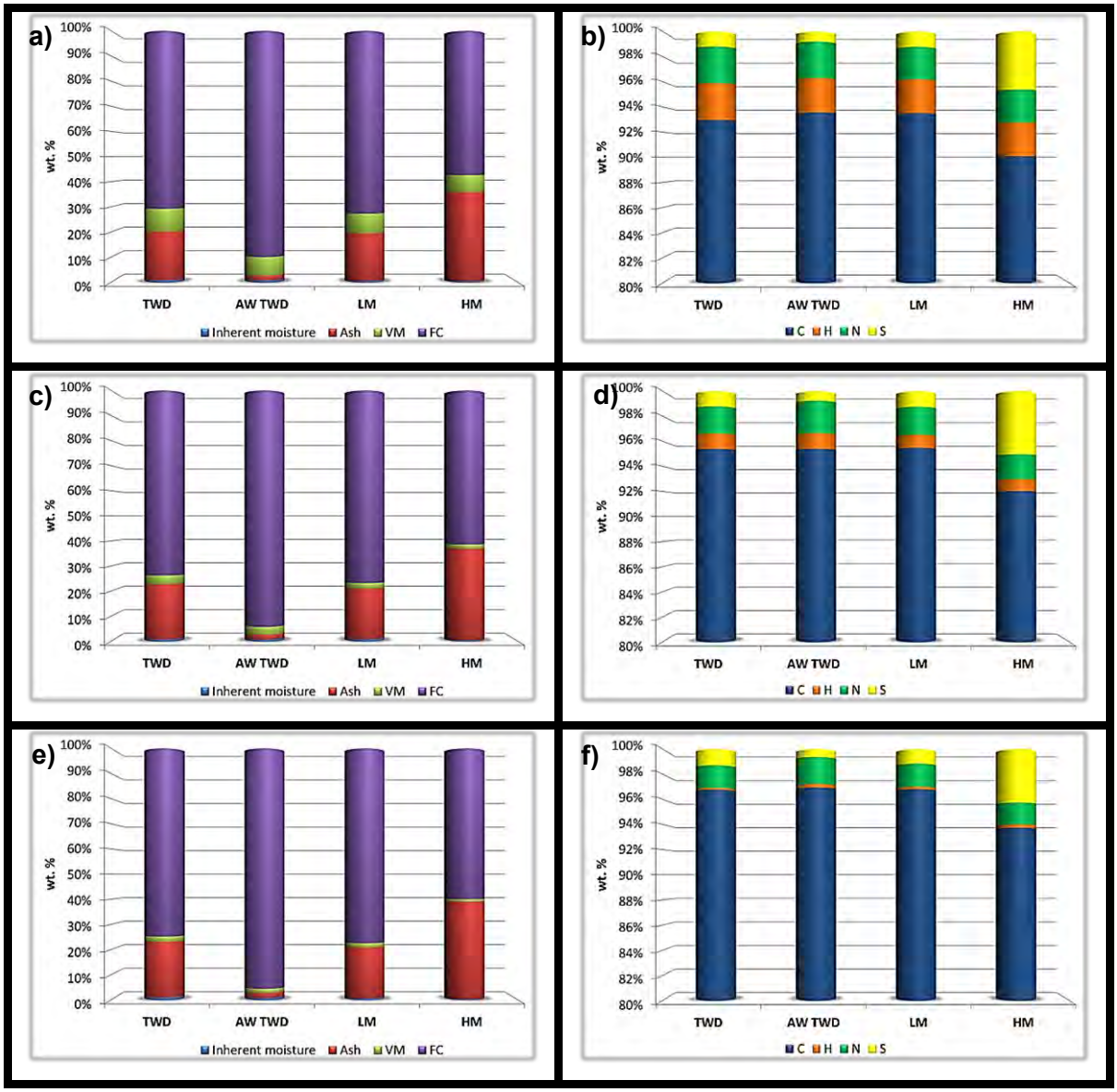

Figure 7-7 Proximate and ultimate analyses results at 520°C (a & b); 750°C (c & d) and 900°C (e and f).

7.6.1. Proximate and Ultimate analyses

The proximate analysis results are presented in Figure 7-7a, Figure 7-7c and Figure 7-7e, whilst the ultimate analysis results for C, H, N and S is depicted in Figure 7-7b, Figure 7-7d and Figure 7-7f. The reason why the ultimate analysis results are only represented by C, H, N and S, is due to the oxygen content which is calculated by difference (Table 7-7) due to the summation of errors (and for which negative values were obtained in some of the cases). Table 7-6 presents the proximate analysis results, VM and FC, on a dry, ash free basis. The results in Table 7-6 will not be corrected for addition of minerals, because the aim of the

respective coal-mineral mixtures was to mimic the composition of the TWD coal, in order to obtain similar pyrolysis products (yields and composition).

From Figures 7-7a, 7-7c and 7-7e the systematic trends that occur during coal pyrolysis are clearly visible and in agreement with the trends seen for the TWD and AW TWD coal fractions (Section 5.5.1). The decrease in VM is most prominent up to 520°C, with smaller differences occurring between 520°C and 750°C, and even smaller changes observed between 750°C and 900°C for both coal-mineral mixtures. It can be observed that the inherent moisture values ranged between 0.4 and 1.0 wt% after pyrolysis at all temperatures for all mineral additions.

The proximate analysis results as presented in Figure 7-7a, 7-7c and 7-7e indicate that the TWD derived chars and the LM coal-mineral mixture derived chars show good comparison at all final pyrolysis temperatures. The ash and volatile matter contents of the LM coal-mineral mixture are a bit lower, and subsequently the fixed carbon is higher, than that of the TWD chars.

Table 7-6 Proximate analysis results, dry, ash free basis.

	TWD	AW TWD	LM	HM
wt%				
520°C				
Volatile matter	11.4	7.6	9.8	10.5
Fixed carbon (by calculation)	88.6	92.4	90.2	89.5
Total	**100.0**	**100.0**	**100.0**	**100.0**
750°C				
Volatile matter	4.4	3.1	2.8	2.6
Fixed carbon (by calculation)	95.6	96.9	97.2	97.4
Total	**100.0**	**100.0**	**100.0**	**100.0**
900°C				
Volatile matter	2.7	1.7	2.2	1.6
Fixed carbon (by calculation)	97.3	98.3	97.8	98.4
Total	**100.0**	**100.0**	**100.0**	**100.0**

Comparison of the FC and VM values for the various derived chars indicate that The VM content of the LM and HM chars of the 520°C experiments is larger than that of the AW TWD case, however, not in accordance with that of the TWD derived char. At 750°C, the VM content of both coal-mineral mixture derived chars are lower than that of the AW TWD derived char, whilst for the 900°C experiments, the LM char had a higher VM content than that of the AW TWD char, but the HM derived char VM content is in accordance with that of AW TWD derived char. In the case of the individual mineral additions (Section 6.5.1), it was difficult to identify systematic trends, from the present results. It can be stated that the addition of minerals led to increased VM content of the 520°C and 900°C experiments in the case of the LM coal-mineral mixture. The difference in VM content between the two coal-mineral mixtures at the

different temperatures can be related to the composition of the added minerals. In the case of the HM coal-mineral mixture, a higher VM content can be expected for the 520°C chars due to the larger kaolinite and pyrite content which decomposes in the lower temperature range (<650°C), whilst the same holds true at 900°C; i.e. in which case of the LM coal-mineral mixture it contains more minerals that decompose at higher temperatures, such as calcite and dolomite.

Table 7-7 Ultimate analysis results, as received.

	TWD	AW TWD	LM	HM
wt%				
520°C				
Carbon	71.3	88.4	74.4	58.2
Hydrogen	2.2	2.6	2.1	1.7
Nitrogen	2.2	2.7	2.0	1.7
Oxygen (by calculation)	3.2	2.7	1.0	-0.5
Total sulphur	0.9	0.8	1.0	3.0
TOTAL	**79.8**	**97.3**	**80.5**	**64.1**
750°C				
Carbon	73.5	91.9	76.8	59.3
Hydrogen	0.9	1.2	0.8	0.6
Nitrogen	1.7	2.5	1.8	1.3
Oxygen (by calculation)	0.1	0.9	-1.2	-3.4
Total sulphur	0.9	0.8	1.0	3.3
TOTAL	**77.2**	**97.3**	**79.2**	**61.0**
900°C				
Carbon	74.3	92.6	76.9	60.5
Hydrogen	0.1	0.3	0.2	0.2
Nitrogen	1.4	2.0	1.4	1.1
Oxygen (by calculation)	0.1	1.6	-0.4	-1.5
Total sulphur	1.0	0.6	0.9	2.8
TOTAL	**76.9**	**97.2**	**79.0**	**63.1**

Table 7-7 presents the ultimate analysis results on an as received basis. In most cases the oxygen is observed to decrease with an increase in final pyrolysis temperature, consistent with previous observations (Bai *et al.,* 2010; Chen *et al.*, 1999; Jones *et al.,* 1999). Although some of the values are negative, (there is still some relevance in them), as it was observed that at higher pyrolysis temperatures, (750°C and 900°C), the TWD and mineral addition derived chars had lower oxygen content when compared to that of the AW TWD case (Section 5.5.1 and Section 6.5.5.1). This was attributed to assisted break up of oxygen functionalities by the minerals present in the coal structure. It can be clearly observed from the values calculated for oxygen that the coal-mineral mixture runs had lower oxygen content when compared to the TWD and AW TWD derived chars.

For better comparison of the C, H, N and S values, refer to Figure 7-7b, 7-7d and 7-7f and Table 7-8, which present the obtained values on a dry, ash free basis, without oxygen content. As expected, the hydrogen and nitrogen content decreased with an increase in final pyrolysis temperature, whilst the carbon content increased (typical to the observation made with regard to the proximate analysis FC content); these trends have been observed in numerous coals (Bai *et al.,* 2010; Chen *et al.*, 1999; Jones *et al.,* 1999), and was also shown to be in agreement for the TWD and AW TWD coals (Section 5.5.1), and for the various mineral additions (Section 6.5.1) used in this study.

Table 7-8 Ultimate analysis (C, H, N, S) results (d.a.f.)

	TWD	AW TWD	LM	HM
wt%				
520°C				
C	93.0	93.6	93.5	90.1
H	2.9	2.7	2.7	2.7
N	2.9	2.9	2.6	2.6
S	1.2	0.8	1.2	4.6
TOTAL	**100.0**	**100.0**	**100.0**	**100.0**
750°C				
C	95.4	95.4	95.5	92.0
H	1.2	1.2	1.1	1.0
N	2.2	2.6	2.2	2.0
S	1.2	0.8	1.3	5.0
TOTAL	**100.0**	**100.0**	**100.0**	**100.0**
900°C				
C	96.8	96.9	96.8	93.7
H	0.1	0.3	0.2	0.3
N	1.8	2.1	1.8	1.7
S	1.3	0.6	1.2	4.3
TOTAL	**100.0**	**100.0**	**100.0**	**100.0**

Comparison of the ultimate analysis results for the TWD coal and the LM coal-mineral mixture derived chars in Figure 7-7b, 7-7d and 7-7f and Table 7-8 indicates very good comparison. The increase in sulphur content when compared to that of the AW TWD char is probably due to the sulphur capturing capability of the calcite and dolomite minerals - as has been observed in Section 6.5.1 for the individual mineral additions, and as observed in previous studies (Sciazko & Kubica, 2002; Yaw *et al.,* 1980). The desulphurisation trend of these minerals has been observed in calcined and uncalcinated form (Adanez *et al.,* 2005), and therefore the trend is observed at all final pyrolysis temperatures. The much larger sulphur content of the HM derived chars can be related to the high pyrite content present in the mineral mixture.

The lower nitrogen content of the LM derived chars at 750°C and 900°C when compared to that of the AW TWD case is also related to the presence of calcite and dolomite, which has

been previously observed (Tsubouchi & Ohtsuka, 2002a, 2002b), and is related to CaO, a decomposition product of calcite and dolomite. The CaO particles may react with heterocyclic nitrogen forms in the char (char-N) to form interstitial species such as CaC_xN_y and $CaO_xC_yN_z$. These components undergo further reactions to form N_2 (Tsubouchi & Ohtsuka, 2002a, 2002b), and subsequently the char-N decreases.

7.6.2. X-Ray Fluorescence (XRF) and Inductive coupled plasma (ICP) analysis

Table 7-9 indicates the XRF / ICP results for the derived chars. Only the AW TWD derived chars' ash content was determined by ICP; whilst the other chars ash contents were all determined by XRF analyses. The major changes observed with an increase in final pyrolysis temperature for both the LM and HM derived chars were in an increase in Al_2O_3, Fe_2O_3 and SiO_2 species, whilst the SO_3 species decreased.

Comparison of the LM char ash with that of the TWD ash indicates that the mineral mixture probably over-compensated for the presence of dolomite, as the MgO and CaO ash species identified was higher for the LM mixture. The kaolinite content, and to some extent the quartz content, may have been underestimated as the Al_2O_3 and SiO_2 content of the LM char ash is lower than that of the TWD char ash. The higher Fe_2O_3 content can also indicate that the pyrite content was overestimated, but then the SO_3 content of the LM char is lower than that of the TWD char, thus indicating some difference in composition between the added pyrite and pyrite present in the TWD coal. The higher concentrations of Al_2O_3, SiO_2, Fe_2O_3 (at all final pyrolysis temperatures) and SO_3 (for the 520°C and 750°C experiments) species in the HM char is related to the difference in composition of the coal-mineral mixtures. The higher SO_3 value observed for the LM char for the 900°C experiments can be related to the sulphur capturing capabilities of the calcite and dolomite minerals, which was more abundant in the LM mineral mixture. At 520°C and 750°C, the sulphur release due to decomposition of pyrite was probably still in progress, explaining the higher SO_3 concentrations.

7.6.3. X-Ray Diffraction (XRD) analysis

Table 7-10 indicates the XRD results for the TWD, AW TWD, LM and HM derived chars. Appendix C-6 includes the XRD spectra graphs. In general, it can be said that for all the derived chars the crystalline mineral matter underwent several transformations with increasing final pyrolysis temperature, i.e. with the amorphous content increasing with an increase in final pyrolysis temperature at 750°C and 900°C due to mineral transformation (Bai *et al.,* 2013; Min *et al.,* 2011).

Table 7-9 XRF/ICP results for the derived chars on a g/species per 100 g char basis

	TWD	AW TWD	LM	HM
g ash species / 100 g char				
520°C				
Al_2O_3	5.08	0.26	3.86	6.27
CaO	2.18	0.14	3.76	3.68
Cr_2O_3	0.01	0.01	0.01	0.03
Fe_2O_3	1.15	1.03	1.28	5.02
K_2O	0.13	0.00	0.18	0.28
MgO	0.62	0.04	1.34	0.54
MnO	0.02	0.00	0.03	0.02
Na_2O	0.10	0.01	0.01	0.05
P_2O_5	0.31	0.01	0.01	0.02
SiO_2	7.58	0.09	6.54	16.22
TiO_2	0.25	0.20	0.14	0.13
V_2O_5	0.01	0.01	0.01	0.00
ZrO_2	0.01	0.01	0.01	0.01
BaO	0.06	0.04	0.05	0.02
SrO	0.12	0.03	0.04	0.02
SO_3	1.85	0.05	1.72	3.23
TOTAL	**19.48**	**1.95**	**18.99**	**35.54**
750°C				
Al_2O_3	5.58	0.22	4.14	6.57
CaO	2.61	0.13	3.82	3.72
Cr_2O_3	0.01	0.02	0.01	0.03
Fe_2O_3	1.21	1.19	1.39	5.38
K_2O	0.15	0.00	0.20	0.29
MgO	0.78	0.04	1.37	0.55
MnO	0.02	0.00	0.03	0.02
Na_2O	0.12	0.01	0.01	0.05
P_2O_5	0.36	0.01	0.02	0.02
SiO_2	8.50	0.05	7.06	16.95
TiO_2	0.27	0.19	0.15	0.13
V_2O_5	0.01	0.01	0.01	0.01
ZrO_2	0.02	0.01	0.01	0.01
BaO	0.07	0.04	0.06	0.02
SrO	0.14	0.03	0.04	0.02
SO_3	2.36	0.04	2.04	2.84
TOTAL	**22.20**	**2.00**	**20.37**	**36.61**
900°C				
Al_2O_3	5.83	0.24	4.30	6.72
CaO	2.51	0.13	3.75	3.66
Cr_2O_3	0.02	0.03	0.02	0.04
Fe_2O_3	1.36	1.12	1.60	6.34
K_2O	0.15	0.00	0.21	0.31
MgO	0.74	0.04	1.30	0.53
MnO	0.02	0.00	0.03	0.02
Na_2O	0.11	0.01	0.02	0.05
P_2O_5	0.35	0.01	0.02	0.02
SiO_2	8.76	0.07	7.31	19.69
TiO_2	0.28	0.21	0.15	0.15
V_2O_5	0.01	0.01	0.01	0.00
ZrO_2	0.02	0.02	0.01	0.01
BaO	0.07	0.04	0.05	0.02
SrO	0.14	0.03	0.04	0.02
SO_3	1.94	0.06	1.48	1.17
TOTAL	**22.31**	**2.03**	**20.29**	**38.78**

In the case of the LM and HM coal-mineral mixtures, lower amorphous content is observed for the 900°C experiments, in contrast to the previous findings (Section 5.5.3 and 6.5.3).This may be related to the fact that a large amount of pure crystalline minerals are added initially as extraneous minerals, (whilst inherent coal minerals differ in form), being more amorphous as observed from the higher amorphous content of the TWD chars. Varying experimental conditions may also be responsible for this difference.

The general trends observed are in line with findings as described by Bai *et al.,* (2013), Matjie (2008) and Tomeczek and Palugniok (2002), and in accordance with observations made for the AW TWD and TWD derived chars in Section 5.5.3 and the mineral additions in Section 6.5.3. With increasing final pyrolysis temperature it is observed for the LM chars that the crystalline calcite, dolomite, fluorite, kaolinite, pyrrhotite and quartz species decrease, whilst the hematite and plagioclase species increase.

It can be seen that he muscovite species remain relatively constant at all three temperatures, whilst the periclase species indicate a spike at 750°C, which is related to the decomposition of dolomite (Vassileva & Vassilev, 2006; Maitra *et al.,* 2005; Caceres & Attiogbe, 1997), whereafter other mineral species are formed. For the HM chars, a decrease is observed in crystalline calcite, dolomite, fluorite, kaolinite and pyrrhotite species, whilst the hematite, quartz, muscovite and plagioclase species increase. The oldhamite species are observed to be most prominent in the 750°C chars; this is probably related to the sulphur capturing capabilities of calcite and dolomite, which are most prominent during decomposition.

Comparison of the chars derived from the coal-mineral mixtures and the TWD char indicates the presence of fluorite which has been observed to be present due to remnant fluoride in the coal structure after the acid washing process with HF (Doymaz *et al.,* 2007; Fauerstenau *et al.,* 1983).

Transformation to other mineral forms due to mineral – mineral interactions are also more likely to occur with the added minerals that do not form part of the coal structure, and thus quite a high yield of plagioclase is observed in the 900°C chars of both the LM and HM chars. The formation of such aluminosilicates has been observed previously (Alpern *et al.,* 1983; Vassilev *et al.*, 2009). Mineral forms identified in the LM char, but not identified in the TWD char are: fluorite, muscovite, plagioclase and periclase.

Table 7-10 XRD results for TWD, AW TWD, LM and HM derived chars

Identification	Molecular formula	TWD	AW TWD	LM	HM
	wt%				
	520°C				
Amorphous content	-	90.0	99.4	86.7	84.5
Calcite	$CaCO_3$	2.2		3.4	2.0
Dolomite	$CaMg(CO_3)_2$	1.4		0.9	0.3
Fluorite	CaF2			1.3	1.0
Hematite	Fe_2O_3	0.2			0.0
Kaolinite	$Al_2Si_2O_5(OH)_4$	2.8		1.7	2.7
Magnetite	Fe_3O_4				
Mullite	$3Al_2O_3..2SiO_2$				
Muscovite	$KAl_2(AlSi_3O_{10})(F,OH)_2$			1.3	1.0
Oldhamite	CaS	0.1		0.3	0.6
Periclase	MgO			0.7	
Plagioclase	$NaAlSi_3O_8 – CaAl_2Si_2O_8$			1.0	0.9
Pyrrhotite	$Fe_{(1-x)}S$	0.3	0.6	0.7	3.4
Quartz	SiO_2	3.0		2.0	3.8
TOTAL	-	**100.0**	**100.0**	**100.0**	**100.0**
	750°C				
Amorphous content	-	93.1	99.8	91.3	85.9
Calcite	$CaCO_3$	1.0		0.3	0.5
Dolomite	$CaMg(CO_3)_2$			0.1	
Fluorite	CaF2			1.4	0.9
Hematite	Fe_2O_3	0.8		0.1	0.2
Kaolinite	$Al_2Si_2O_5(OH)_4$	1.3		1.6	1.4
Magnetite	Fe_3O_4		0.1		
Muscovite	$KAl_2(AlSi_3O_{10})(F,OH)_2$			1.0	1.5
Oldhamite	CaS	1.0		1.0	1.4
Periclase	MgO			1.0	
Plagioclase	$NaAlSi_3O_8 – CaAl_2Si_2O_8$			1.0	0.8
Pyrrhotite	$Fe_{(1-x)}S$		0.1		3.0
Quartz	SiO_2	2.8		1.1	4.5
TOTAL	-	**100.0**	**100.0**	**100.0**	**100.0**
	900°C				
Amorphous content	-	94.5	99.7	89.4	82.8
Calcite	$CaCO_3$	0.5		0.4	0.2
Dolomite	$CaMg(CO_3)_2$			0.2	0.2
Fluorite	CaF2			0.9	0.2
Hematite	Fe_2O_3	0.8		0.2	0.6
Kaolinite	$Al_2Si_2O_5(OH)_4$	0.7		1.5	1.0
Magnetite	Fe_3O_4		0.2		
Mullite	$3Al_2O_3..2SiO_2$				0.2
Muscovite	$KAl_2(AlSi_3O_{10})(F,OH)_2$			1.3	1.7
Oldhamite	CaS	1.2		0.2	0.4
Periclase	MgO			0.1	
Plagioclase	$NaAlSi_3O_8 – CaAl_2Si_2O_8$			3.8	5.1
Pyrrhotite	$Fe_{(1-x)}S$		0.1	0.1	2.1
Quartz	SiO_2	2.3		1.8	5.4
TOTAL	-	**100.0**	**100.0**	**100.0**	**100.0**

7.7. Chapter summary

Chapter 7 presented and discussed the yield and compositional data as analysed by various analytical techniques for the pyrolysis products derived from the TWD, AW TWD coal fractions and the LM and HM coal-mineral mixtures. With regard to pyrolysis product yields, it was found that the water yields from the LM coal-mineral mixture were in agreement with that of the TWD coal, whilst the tar yields were lower, and the char and gas yields increased. GC analyses of the derived gases indicated that good consistency was observed with regard to the H_2, CO and CH_4 yields for the 520°C and 750°C experiments. At 900°C, the LM coal-mineral mixture produced a yield of these gases intermittent between that of the TWD and AW TWD coals. The CO_2 yield was lower than that of the TWD coal for the 750°C and 900°C experiments. The C_2H_4, C_3H_4, C_3H_6 and C_4s gas yields were observed to be affected in such a manner that it was better related to the yields from the TWD coal.

The analyses of the tar fraction by Simdis revealed similar boiling point distributions for the derived tars of the 520°C and 900°C experiments, whilst the derived tar for the 750°C experiments for the LM coal-mineral mixture contained increased lighter boiling point compounds, indicative of more extensive catalytic cracking. The GC-MS analysis revealed that the LM derived tars were compositionally in accordance with that of TWD coal regarding the aliphatic, alkyl-phenols, alkyl-benzenes and PAHs at all final pyrolysis temperatures. The mixed aromatic and aliphatic component contents were higher in the LM derived tars, whilst variance was observed in the nitrogen heteroatoms and aromatic ester and ether yields. SEC-UV analyses revealed that the LM derived tars consisted of lower molecular weight compounds.

Proximate and ultimate analyses of the derived chars revealed good similarity between the TWD and LM chars. The TWD chars did however indicate a higher ash content and more volatile matter. XRF ash analyses revealed that the LM mineral mixture probably overcompensated for calcite and dolomite content, whilst pyrite and kaolinite contents were underestimated. This probably led to the increased lower boiling point / lower molecular weight tar species that were identified for the LM derived tars. XRD analyses of the derived chars showed that the LM chars were more crystalline in nature, and more species were identified. This was probably due to the fact that the added minerals did not form part of the coal structure as they were added extraneously, in contrast to the case for the TWD derived char.

The HM coal-mineral mixture showed much less variance than observed for the LM coal-mineral mixture, and trends observed were much more consistent with that of the AW TWD coal. This difference was attributed to the difference in mineral composition. Calcite and dolomite were identified as most active minerals in Chapter 6, and thus this was clearly

observed to be true in the case of the mineral mixtures as well. There is unfortunately no external reference to compare the HM coal-mineral mixture yields and composition to, and the reader is referred to the specific sections of this chapter (if more information is required) regarding the HM coal-mineral mixture. The differences observed between the LM and HM pyrolysis yields and product compositions confirm that synergism between minerals is an important factor to take into account when the effect of minerals on pyrolysis product yields and composition needs to be researched.

Chapter 8: Statistical models

8.1. Introduction

Thus far the effect of acid washing, effect of mineral addition to acid washed coal, and the make-up of coal-mineral mixtures have been examined. The effect of the removal/addition of minerals on the pyrolysis product yields and composition has been studied by various analytical techniques. The aim of this chapter is to provide models that can predict the expected yields, as well as the composition of some of the pyrolysis products using the obtained data as input. These models will by no means be universal in application, and is limited by the following:

- The models will only apply to the coal used in this study, i.e. TWD.
- The models will only apply to the product yields derived under the same conditions, i.e. heating rate, setup, pressure etc.
- The models will be limited to the temperature range studied, i.e. 520°C to 900°C. Although the tar yield for example can probably be determined as low as 450°C, it is suggested that this is not done as intra- and extrapolation may not be accurate, as no experimental values exist outside the temperature range studied.

These models provide a foundation to motivate more research in this field, and also prove that the prediction of catalytic activity from amounts and compositions of particular inorganic components appears to be feasible, in contrast with previous opinions (Lemaignen *et al.*, 1999).

8.2. Deriviation of statistical models

Models have been used extensively in scientific applications as it can reduce costs and provide means that are much easier than experimental work to predict the outcomes of certain experiments. Different models can be derived depending on the accuracy required, as well as the type of prediction needed (Lopez-Urionabarranechea *et al.,* 2012). In thermal sciences, such as pyrolysis, the following model types have been applied: (i) Empiric models – these models use a collection of experimental data which is computationally optimised in order to obtain a general model which explains the obtained experimental results, whilst also predicting possible future ones (Ateş & Erginel, 2012; Lopez-Urionabarranechea *et al.,* 2012; Xiao *et al.,* 2009; Miranda *et al.,* 2009; Guo *et al.,* 2001); (ii) Kinetic models – TGA analyses are usually used to obtain global kinetic behaviour of the process (Lopez-Urionabarranechea *et al.,* 2012; Hattingh, 2012; Saha *et al.,* 2008; Saha & Goshal, 2005; Faravelli *et al.,* 2001; Pant & Kunzru,

1997); (iii) Chemical equilibrium based models – the proximate and ultimate analysis of the sample, as well as some species which will form during the process, is taken into account to predict the concentration of some process products. The representative reactions are not considered (Lopez-Urionabarranechea *et al.,* 2012; Prins *et al.,* 2007); (iv) Mechanistic models – A set of differential equations is mathematically solved based on input with regard to all species and concentrations in order to predict product concentrations (Lopez-Urionabarranechea *et al.,* 2012; Levine & Broadbelt, 2009; Mastral *et al.,*2007).

Table 8-1 highlights the advantages and disadvantages of each of these models. Although the chemical equilibrium and mechanistic models seem to provide the most detailed outputs, they can lead to big errors due to the assumption of chemical equilibrium state conditions. These conditions are difficult to fulfil at low temperatures, and when kinetic constraints come into play (Lopez-Urionabarranechea *et al.,* 2012; Lee *et al.,* 2007). The number of reactions taking place during pyrolysis will also limit the use of the mechanistic model. Consequently, an empirical model seems to be the best option to use in this study due to its simplicity and accuracy in the specific application. The amount of experimental work carried out in this study is deemed sufficient for such a model, and the limitations of the applicability of the model are noted, but believed to provide a foundation for similar future studies.

Table 8-1 Major advantages and drawbacks of different types of models (Adapted from Lopez-Urionabarrenechea *et al.,* 2012).

Model type	Major advantages	Major drawbacks
Empiric	• Model simplicity • Accuracy in specific application	• Need of lots of experimental work • Limited validity
Kinetic	• Low experimental requirements	• Description of a complex system using a global kinetic scheme
Chemical equilibrium	• Simple experimental input • Independent of reactor design	• Errors derived from assuming equilibrium state • Kinetics are not considered
Mechanistic	• Detailed and accurate compounds prediction	• Computational and theoretical difficulties

The essence of regression analysis is a model fitted to data and used to predict values of the dependent variable (DV) from one or more independent variables (IVs). Regression analysis is a way of predicting an outcome variable from one or more predictor variables in order to best fit a set of data observations (Ateş & Erginel, 2012, Field, 2009). It is a statistical technique used to determine the relationship between variables (Ateş & Erginel, 2012). In models such

as these developed in this investigation, regression analysis is used to develop a model that expresses the yield as a function of independent variables such as temperature. The regression analysis also defines the degree of the explanation of total variability accounted for by use of a coefficient of determination, known as R^2 (Ateş & Erginel, 2012).

Linear regression models have been used in various pyrolysis studies, and it is specifically the field of biomass pyrolysis that has made use of these models to a large extent (Ateş & Erginel, 2012; Lopez-Urionabarranechea *et al.,* 2012).

The statistical software SPSS was used to assess the data. Independent variables were removed if they correlated highly with each other (i.e., if two independent variables exhibited a high correlation only one was kept in the model), or when they were not statistically significant. The high correlation manifested for example in a case where minerals like calcite and dolomite showed the same trend and were found to be dependent. From the experimental work it is known that this is related to similar chemical structures upon decomposition of these minerals. Selection was done automatically by the statistical data software. The method used for the models is referred to as 'Enter', where the program basically "enters" the determined values into a model until a suitable correlation is found.

The objective of the derived model is to predict the different pyrolysis product yield as a function of the mineral composition as obtained from QEMSCAN analyses. To the best of the author's knowledge there is no published information in the literature about a prediction tool of this type. Models derived include:

- Gas yield (d.m.m.f.)
- Tar yield (d.m.m.f.)
- Char yield (d.m.m.f.)
- H_2 yield
- CO yield
- CO_2 yield
- CH_4 yield.

Models for tar composition based on the cut fractions (as determined from Simdis data), were also developed; but the results were unsatisfactory with R^2 values ranging between 0.2 and 0.3 which is indicative that only between 20% and 30% of the variation in the data is explained by the model.

Table 8-2 Part of the input to SPSS software for statistical model development.

		X_1	X_2	X_3	X_4	X_5	X_6	Y_1	Y_2	Y_3
		wt%								
Group	**Temperature**	**Coal**	**Pyrite**	**Calcite**	**Dolomite**	**Kaolinite**	**Quartz**	**Tar**	**Char**	**Gas**
TWD	520	84.60	2.86	1.67	3.47	6.30	1.10	10.79	76.59	12.62
TWD	520	84.60	2.86	1.67	3.47	6.30	1.10	10.67	76.85	12.48
TWD	520	84.60	2.86	1.67	3.47	6.30	1.10	10.99	77.52	11.49
TWD	520	84.60	2.86	1.67	3.47	6.30	1.10	10.52	77.49	11.99
TWD	750	84.60	2.86	1.67	3.47	6.30	1.10	9.10	72.69	18.22
TWD	750	84.60	2.86	1.67	3.47	6.30	1.10	9.30	73.11	17.59
TWD	750	84.60	2.86	1.67	3.47	6.30	1.10	8.72	72.79	18.49
TWD	750	84.60	2.86	1.67	3.47	6.30	1.10	8.81	72.87	18.32
TWD	900	84.60	2.86	1.67	3.47	6.30	1.10	9.34	72.54	18.13
TWD	900	84.60	2.86	1.67	3.47	6.30	1.10	9.10	72.13	18.76
TWD	900	84.60	2.86	1.67	3.47	6.30	1.10	8.94	72.37	18.69
TWD	900	84.60	2.86	1.67	3.47	6.30	1.10	9.20	71.70	19.10
AW TWD	520	97.33	2.51	0.01	0.01	0.03	0.10	5.30	77.54	17.16
AW TWD	520	97.33	2.51	0.01	0.01	0.03	0.10	5.01	78.11	16.88
AW TWD	520	97.33	2.51	0.01	0.01	0.03	0.10	4.89	78.24	16.87
AW TWD	520	97.33	2.51	0.01	0.01	0.03	0.10	5.44	77.67	16.89
AW TWD	750	97.33	2.51	0.01	0.01	0.03	0.10	6.40	73.38	20.22
AW TWD	750	97.33	2.51	0.01	0.01	0.03	0.10	6.13	72.87	20.99
AW TWD	750	97.33	2.51	0.01	0.01	0.03	0.10	5.95	73.44	20.60
AW TWD	750	97.33	2.51	0.01	0.01	0.03	0.10	5.89	73.86	20.26
AW TWD	900	97.33	2.51	0.01	0.01	0.03	0.10	6.64	71.46	21.90
AW TWD	900	97.33	2.51	0.01	0.01	0.03	0.10	6.50	71.52	21.98
AW TWD	900	97.33	2.51	0.01	0.01	0.03	0.10	6.30	71.60	22.10
AW TWD	900	97.33	2.51	0.01	0.01	0.03	0.10	6.29	71.35	22.36

The input data consisted of variables $X_1 \ldots X_{13}$ which is the coal composition as determined from the QEMSCAN analyses, including the most prominent minerals and a "coal" value. These values are used as input to determine the output Y which is the respective yield examined. Thus the yield is determined as function of the coal composition. Table 8-2 shows part of such an input.

Models derived for pyrolysis product yields (gas, tar and char) were based on dry mineral matter free input data normalised to 100 wt%. Models derived for the most prominent gases (H_2, CO, CO_2 and CH_4) were based on input data normalised to 100 mol.%.

A short coming of linear regression models is that it does not take into account what experimental data describes, but only fits the data with suitable models based on the observed variance and determined correlations. This can lead to models that are inaccurate, and does not describe the real changes observed.

8.3. Evaluation of the derived models

The models are evaluated based on the R^2 value which provides an indication of the correlation obtained with the use of the data obtained from the 66 experiments. R^2 tells us how much variance is explained by the model compared to how much variance there is to explain in the first place. It is the proportion of variance in the outcome variable that is shared by the predictor variable (Field, 2009), as well as normal Q-Q plots of regression standardised residual dependent variables. Refer to Appendix C-10 for all the normal Q-Q plots.

The predicted and average experimental values as obtained from the experimental work will also be compared. Another evaluation of the efficiency of the derived models is the comparison with the yields as determined from the qualifying experiments in Section 6.2.5. These experiments were done in order to qualify the trends seen with the addition of the individual minerals to the TWD coal fraction. The yield data of these experiments did not form part of the input in the SPSS software. As such, this will provide an accurate measure as to evaluate the derived models. The gas composition models were, however, not evaluated by this measure, as no data was available for comparison.

8.4. Models

All models developed are in the form:

$$y_i = B_i + c_i T + c_j X_k + \cdots \quad (8\text{-}1)$$

Where y_i refers to the relevant yield value that is to be predicted, B_i is a general constant, c_i refers to a constant derived for the temperature variation (T in°C) and c_j refers to a constant

derived for the variable X_k (wt%), which is a compositional value of a certain mineral deemed to affect the specific yield significantly.

8.4.1. Gas yield

Equation 8-2 indicates the formula derived for prediction of the gas yield. The prediction gives an R^2 correlation coefficient of 0.837.

$$\text{Gas yield (wt\%)} = 11.415 + 0.015\text{T} + 0.288\text{X}_{calcite} + 0.231\text{X}_{dolomite} - 0.242\text{X}_{quartz} - 102.887\text{X}_{rutile} \quad (8\text{-}2)$$

The R^2 value provides an indication that 83.7% of the data in the data set is included in the model, thus this is an acceptable correlation. The minerals determined to show significant correlation with the gas yield include calcite, dolomite, quartz and rutile. The presence of rutile may highlight an important aspect for future research – some of the less prominent and even trace minerals may also affect pyrolysis yields, and further attention can be given to this matter.

Evaluation of the signs in front of the respective factors of the model shows good consistency with experimental findings. The gas yield was observed to increase with increase in pyrolysis temperature, dolomite addition was observed to lead to increased gas yields. The negative sign for the quartz content, is unexplainable based on experimental findings, but as such it best described the current data set. This highlights one of the short comings of linear regression models.

Comparison of the absolute error % values in Table 8-3 for the experimental vs. predicted gas yields indicates good error values in accordance with the percentage error on repeatability values as reported in Table 4-3 (Section 4.2.5) for the repeatability experiments of TWD and AW TWD coal fractions (% error on repeatability for 95% confidence between 1.9 to 8.7 %). The LM gas yield of the 520°C and 750°C experiments is however grossly overestimated, probably due to the high percentage dolomite and calcite present in this mineral mixture. At 900°C, the correlation does however provide an acceptable gas yield. The gas yield for the HM experiments at 520°C is underestimated, probably due to the high quartz content in this coal-mineral mixture. For the AW-Cal experiments at 520°C, the gas yield is overestimated by the derived model. This can be related to the fact that the addition of calcite attributed to a significant effect to the gas yield, but at 520°C very little decomposition of this mineral would have taken place. In most of the cases the model seems more accurate for prediction of the gas yield at the higher temperatures. This makes sense, as the gas phase reactions are predominantly favoured during secondary pyrolysis, taking place at temperatures exceeding 690°C (Singh *et al.,* 2012; Saikia *et al.,* 2009; Cai *et al.,* 2008; Kabe *et al.,* 2004).

Table 8-3 Experimental vs. predicted gas yield

	Temperature. (°C)	Experimental yield (wt%)	Predicted yield (wt%)	Absolute. error %
TWD	520	12.1	13.3	-9.4
	750	18.2	16.7	7.8
	900	18.7	19.0	-1.7
AW TWD	520	16.9	16.9	0.3
	750	20.5	20.4	0.8
	900	22.1	22.6	-2.3
LM	520	14.7	17.1	-16.2
	750	17.1	20.6	-20.4
	900	22.2	22.8	-2.8
HM	520	21.9	19.4	11.7
	750	23.1	22.8	1.1
	900	25.4	25.1	1.2
AW-Cal	520	16.6	18.4	-11.0
	750	23.0	21.8	5.1
	900	25.4	24.1	5.2
AW-Dol	520	17.5	15.9	-3.4
	750	20.7	19.4	-4.3
	900	23.9	21.6	0.2
AW-Kao	520	17.9	17.0	5.0
	750	20.5	20.5	0.3
	900	22.7	22.7	-0.2
AW-Pyr	520	17.5	17.0	2.7
	750	19.3	20.5	-5.8
	900	22.2	22.7	-2.1
AW-Qz	520	18.6	18.2	2.2
	750	21.1	21.6	-2.4
	900	22.0	23.9	-8.4

Table 8-4 Experimental vs. Predicted gas yields for qualifying experiments

Case	Average experimental yield (wt%)	Predicted yield (wt%)	Error %
TWD Cal	20.8	21.6	3.9
TWD Dol	21.5	21.4	0.8
TWD Kao	21.2	20.3	4.6
TWD Pyr	18.3	19.3	5.1
TWD Qz	18.7	19.1	2.4

Table 8-4 provides the predicted and experimental gas yields for the qualifying experiments.. The average error percentage between the average experimental yield and the predicted yield is 3.4 %. The largest deviation is seen in the cases in which kaolinite and pyrite were added. These error percentages are however well within the repeatability values as reported in Table 4-3, Section 4.2.5. In Chapter 6 it was shown that these minerals did affect the pyrolysis gas yields, but the effects were adverse. As such, the SPSS software could not find a linear

relationship, and the effects of change in yield caused by these minerals were not deemed significant.

8.4.2. Tar yield

Equation 8-3 indicates the formula derived for the prediction of the tar yield. The prediction gives an R^2 correlation coefficient of 0.785.

$$\text{Tar yield (wt\%)} = 5.763 + 17.753X_{microcline} + 0.133X_{kaolinite} - 0.291X_{calcite} - 0.196X_{dolomite} \quad (8\text{-}3)$$

Table 8-5 Experimental vs. predicted tar yield

	Temperature. (°C)	Experimental yield (wt%)	Predicted yield (wt%)	Absolute. error %
TWD	520	10.7	9.6	10.4
	750	9.0	9.6	-7.1
	900	9.1	9.6	-5.2
AW TWD	520	5.2	5.8	-11.7
	750	6.1	5.8	5.5
	900	6.4	5.8	10.4
LM	520	6.6	5.3	20.4
	750	6.9	5.3	24.4
	900	2.9	5.3	-83.9
HM	520	5.2	6.1	-17.6
	750	6.3	6.1	3.8
	900	6.4	6.1	4.2
AW-Cal	520	5.1	4.4	13.7
	750	4.4	4.4	0.7
	900	3.7	4.4	-19.6
AW-Dol	520	5.4	4.8	10.0
	750	5.1	4.8	5.8
	900	3.5	4.8	-36.8
AW-Kao	520	6.3	6.4	-1.0
	750	6.5	6.4	1.5
	900	6.4	6.4	0.4
AW-Pyr	520	4.2	5.8	-36.4
	750	6.0	5.8	3.6
	900	6.0	5.8	3.2
AW-Qz	520	4.9	5.8	-16.6
	750	6.3	5.8	7.8
	900	6.6	5.8	12.8

The R^2 value provides an indication that 78.5% of the data in the data set is included in the model; thus this is an acceptable correlation. The minerals determined to show significant correlation with the gas yield include: microcline, kaolinite, calcite and dolomite. The presence of microcline in the model once more highlights the fact that some less prominent minerals may also affect pyrolysis yields. The SPSS did not find that change in final pyrolysis temperature affected the data significantly to such an extent that a correlation could be established. With an increase in pyrolysis temperature various factors come into play – thermal

cracking of tar, catalytic cracking caused by the decomposition products of certain minerals (such as calcite and dolomite), some cases indicate an increase in tar yield, whilst others indicate no change, and still others indicate a decrease. Thus, this model can be expected to be inaccurate for some cases as the predicted yield would be the same for all three pyrolysis temperatures.

Evaluation of the signs in front of the respective factors of the model shows good consistency with experimental findings. The tar yield was observed to increase with addition of kaolinite (at 520°C), and decrease with the addition of calcite and dolomite due to catalytic cracking.

Comparison of the absolute error % values in Table 8-5 for the experimental vs. predicted tar yields indicate good error values in accordance with the percentage error on repeatability values as reported in Table 4-3 (Section 4.2.5) for the repeatability experiments of TWD and AW TWD coal fractions (% error on repeatabilityfor 95% confidence between 3.9 to 10.2 %) for most of the experimental cases. Evaluation of the model indicates that the tar yield is not successfully predicted for the LM model coal-mineral mixture, the AW-Cal and AW-Qz cases for the 520°C and 900°C experiments, AW-Dol for the 900°C experiments, HM and AW-Pyr for the 520°C experiments.

Table 8-6 provides the predicted and experimental tar yields for the qualifying experiments. The average error percentage between the average experimental yield and the predicted yield is 2.9 %. The largest deviation is seen for the cases in which pyrite and quartz were added. These error percentages are, however, well within the repeatability values as reported in Table 4-3, Section 4.2.5. From Chapter 6 it is however known that pyrite did affect pyrolysis tar yields, but the effects were adverse. As such, the SPSS software could not find a linear relationship and the effects of change in yield caused by these minerals were not deemed significant.

Table 8-6 Experimental vs. Predicted tar yields for qualifying experiments

Case	Average experimental yield (wt%)	Predicted yield (wt%)	Error %
TWD Cal	8.2	8.1	1.4
TWD Dol	8.7	8.5	2.1
TWD Kao	9.8	10.1	2.7
TWD Pyr	9.0	9.4	5.3
TWD Qz	9.1	9.4	3.2

8.4.3. Char yield

Equation 8-4 indicates the formula derived for the prediction of the char yield. The prediction gives an R^2 correlation coefficient of 0.846.

$$\text{Char yield (wt\%)} = 84.697 - 0.014\text{T} + 0.366\text{X}_{dolomite} - 0.148\text{X}_{kaolinite} - 0.288\text{X}_{quartz} \quad (8\text{-}4)$$

The R^2 value provides an indication that 84.6% of the data in the data set is included in the model; thus this is an acceptable correlation. The minerals determined to show significant correlation with the char yield include dolomite, kaolinite and quartz.

Table 8-7 Experimental vs. predicted char yield

	Temperature. (°C)	Experimental yield (wt%)	Predicted yield (wt%)	Absolute. error %
TWD	520	77.1	77.4	-0.4
	750	72.9	74.2	-1.9
	900	72.2	72.1	0.1
AW TWD	520	77.9	77.4	0.6
	750	73.4	74.2	-1.1
	900	71.5	72.1	-0.8
LM	520	78.7	77.6	1.4
	750	76.0	74.4	2.1
	900	75.0	72.3	3.6
HM	520	72.9	74.6	-2.4
	750	70.6	71.4	-1.2
	900	68.3	69.3	-1.6
AW-Cal	520	78.4	77.4	1.3
	750	72.6	74.2	-2.2
	900	70.9	72.1	-1.6
AW-Dol	520	77.2	79.1	-2.5
	750	74.2	75.9	-2.3
	900	72.6	73.8	-1.7
AW-Kao	520	75.8	76.7	-1.2
	750	73.0	73.5	-0.7
	900	70.9	71.4	-0.6
AW-Pyr	520	78.3	77.4	1.1
	750	74.7	74.2	0.7
	900	71.8	72.1	-0.4
AW-Qz	520	76.5	76.0	0.6
	750	72.6	72.8	-0.2
	900	71.4	70.7	1.0

Evaluation of the signs in front of the respective factors of the model shows good consistency with experimental findings. The char yield was observed to decrease with increase in pyrolysis temperature. From literature it is known that dolomite addition has been observed to lead to an increase in char yield (Ahmad *et al.,* 2009b; Chen *et al*., 1999; Franklin *et al.,* 1982a; Franklin *et al.,* 1981). Although this was not seen in the individual addition of dolomite to the AW TWD coal fraction, it may be possible that when the whole data set was taken into account by the SPSS software that this trend was observed. The addition of kaolinite and quartz was observed to lead to decreased char yields.

Comparison of the absolute error % values in Table 8-7 for the experimental vs. predicted char yields indicates good error values in accordance with the percentage error on repeatability values as reported in Table 4-3 (Section 4.2.5) for the repeatability experiments of TWD and AW TWD coal fractions (% error on repeatabilityfor 95% confidence between 0.2 to 1.1 %) for most of the experimental cases. Evaluation of the predicted and experimental yields indicate that the prediction of the LM char yield is first underestimated (520°C and 750°C), and then overestimated (900°C). For the AW-Cal and AW-Dol cases, overestimation of the char yields also seem to be prevalent. However, in general the char yield results are very satisfactory and the model indicates very good fitting.

Table 8-8 Experimental vs. Predicted gas yields for qualifying experiments

Case	Aevrage experimental yield (wt%)	Predicted yield (wt%)	Error %
TWD Cal	71.0	72.1	1.5
TWD Dol	70.1	73.9	5.4
TWD Kao	68.7	71.4	4.0
TWD Pyr	72.7	72.1	0.8
TWD Qz	72.2	70.7	2.0

Table 8-8 provides the predicted and experimental char yields for the qualifying experiments. The average error percentage between the average experimental yield and the predicted yield is 2.7 %. The largest deviation is seen for the case in which dolomite and kaolinite were added. The addition of dolomite was seen to lead to decreased char yields (Chapter 6); however in the model the contrary is observed. This may highlight the fact that there are limiting factors for the presence of certain minerals. This has been observed in previous studies with dolomite addition (Pinto *et al.*, 2007). Previous authors also reported an increase in char yield with an increase in dolomite loading (Ahmad *et al.,* 2009b; Chen *et al*., 1999; Franklin *et al.,* 1982a; Franklin *et al.,* 1981).

8.4.4. Gas composition

8.3.4.1. H_2 yield

Equation 8-5 indicates the formula derived for prediction of the H_2 yield. The prediction gives an R^2 correlation coefficient of 0.917.

$$\mathrm{H_2\ (mol.\%)} = -2.926 + 0.052\mathrm{T} - 0.469\mathrm{X}_{calcite} - 0.441\mathrm{X}_{dolomite} - 0.336\mathrm{X}_{kaolinite} \qquad (8\text{-}5)$$

The R^2 value provides an indication that 91.7% of the data in the data set is included in the model, thus this is an acceptable correlation. The minerals determined to show significant correlation with the H_2 yield include calcite, dolomite and kaolinite.

Evaluation of the signs in front of the respective factors of the model shows good consistency with experimental findings. The H_2 yield was observed to increase with increase in pyrolysis temperature. The addition of calcite, dolomite and kaolinite to the AW TWD coal fraction was observed to lead to a decrease in H_2 yield (Section 6.3.1).

Table 8-9 evaluates the experimental and predicted yield data for the H_2 gas. In general, good correlation is seen between the predicted and experimental data, with the largest error value being 13.8 %. This is an acceptable error value if it is taken into consideration that the experimental data is determined by use of GC analysis. General acceptable error on repeatability values for this instrument is around 10 %.

8.3.4.2. CO yield

Equation 8-6 indicates the formula derived for prediction of the CO yield. The prediction gives an R^2 correlation coefficient of 0.702.

$$\text{CO yield (mol.\%)} = 8.158 + 0.009\text{T} + 1.165\text{X}_{dolomite} + 0.458\text{X}_{kaolinite} \quad (8\text{-}6)$$

The R^2 value provides an indication that 70.2% of the data in the data set is included in the model, thus this is an acceptable correlation. The minerals determined to show significant correlation with the CO yield include dolomite and kaolinite.

Evaluation of the signs in front of the respective factors of the model shows good consistency with experimental findings. The CO yield was observed to increase with increase in pyrolysis temperature. The addition of dolomite and kaolinite to the AW TWD coal fraction was observed to lead to an increase in CO yield (Section 6.3.2).

Table 8-9 evaluates the experimental and predicted yield data for the CO gas. In general good correlation is seen between the predicted and experimental data. The CO yield for the TWD case is, however, not accurately predicted by the model at any temperature, with error values ranging from 16.2 to 17.8%. This large difference may be related to the experimental data. A large difference was seen between CO and CO_2 yield for the TWD and AW TWD coal fractions. Noting that the bulk of the data is made up of data derived from the AW TWD coal fraction with addition of minerals, this might be responsible for the deviation. This suggests that some other factor might have a dominant role in this case. Other variations may be related to the data not necessarily showing a linear trend, i.e. the large difference in yield between 750°C and 900°C. These differences may be related to catalytic activity, and therefore the model is less accurate in predicting these values.

8.3.4.3. CO_2 yield

Equation 8-7 indicates the formula derived for prediction of the CO_2 yield. The prediction gives an R^2 correlation coefficient of 0.869.

$$\mathrm{CO_2\ yield\ (mol.\%)} = 30.430 - 0.028\mathrm{T} + 0.746\mathrm{X}_{pyrite} + 1.152\mathrm{X}_{calcite} + 0.590\mathrm{X}_{dolomite} + 0.450\mathrm{X}_{quartz} \quad (8\text{-}7)$$

The R^2 value provides an indication that 86.9% of the data in the data set is included in the model, thus this is an acceptable correlation. The minerals determined to show significant correlation with the CO_2 yield include calcite, dolomite, quartz and pyrite.

Evaluation of the signs in front of the respective factors of the model shows good consistency with experimental findings. The CO_2 yield was observed to decrease with increase in pyrolysis temperature in some of the examined cases, or either showed very little change with increase in final pyrolysis temperature. The addition of pyrite, calcite, dolomite and quartz to the AW TWD coal fraction was observed to lead to an increase in CO_2 yield, if not at all final pyrolysis temperatures, at least at some (Section 6.3.2).

Table 8-9 evaluates the experimental and predicted yield data for the CO_2 gas. In general good correlation is seen between the predicted and experimental data. The CO_2 yield for some cases is however not accurately predicted by the model due to non-linearity of the data (larger difference between certain data points than other in the same data set). This suggests that some other factor might have a dominant role in this case, such as extensive catalytic cracking. For example, for the AW-Dol case at 900°C, the model overestimates the effect of temperature, whilst the decomposition of dolomite is more active between 750°C and 900°C, thus the value is very inaccurate.

8.3.4.4. CH_4 yield

Equation 8-8 indicates the formula derived for prediction of the CH_4 yield. The prediction gives an R^2 correlation coefficient of 0.978.

$$\mathrm{CH_4\ (mol.\%)} = 50.783 - 0.024\mathrm{T} - 0.267\mathrm{X}_{pyrite} - 0.803\mathrm{X}_{calcite} - 0.976\mathrm{X}_{dolomite} - 0.214\mathrm{X}_{kaolinite} \quad (8\text{-}8)$$

The R^2 value provides an indication that 97.8% of the data in the data set is included in the model, thus this is an acceptable correlation. The minerals determined to show significant correlation with the CH_4 yield include calcite, dolomite, kaolinite and pyrite.

Evaluation of the signs in front of the respective factors of the model shows good consistency with experimental findings. The CH_4 yield was observed to decrease with increase in pyrolysis temperature. The addition of pyrite, calcite, dolomite and kaolinite to the AW TWD coal fraction

was observed to lead to a decrease in CH_4 yield, if not at all final pyrolysis temperatures, at least at some (Section 6.3.2).

Table 8-9 evaluates the experimental and predicted yield data for the CH_4 gas. As can be observed from the very high R^2 value, the model predicts the CH_4 yield very accurately, with the largest error value being 7.0 %.

NORTH-WEST UNIVERSITY
UNIBESITI YA BOKONE-BOPHIRIMA
NOORDWES-UNIVERSITEIT
POTCHEFSTROOMKAMPUS

Table 8-9 Experimental vs. predicted H_2, CO, CO_2 and CH_4 yields

		H_2			CO			CO_2			CH_4		
	Temp. (°C)	Exp. value	Pred. value	Abs. error %	Exp. value	Pred. value	Abs. error %	Exp. value	Pred. value	Abs. error %	Exp. value	Pred. value	Abs. error %
TWD	520	19.1	19.6	2.8	23.2	19.8	-17.3	19.9	22.5	11.4	31.7	31.5	-0.7
	750	31.5	31.6	0.3	25.7	21.8	-17.8	12.1	16.0	24.4	26.3	25.9	-1.3
	900	38.2	39.4	3.1	26.9	23.2	-16.2	11.0	11.8	6.8	20.8	22.3	7.0
AW TWD	520	23.1	24.1	4.2	14.1	12.9	-9.6	18.4	17.8	-3.4	37.0	37.6	1.6
	750	38.0	36.1	-5.5	14.6	14.9	2.1	11.4	11.4	0.0	31.2	32.1	2.7
	900	45.3	43.9	-3.3	12.6	16.3	22.8	9.6	7.2	-34.3	28.7	28.5	-0.7
LM	520	17.9	18.2	1.9	21.8	22.1	1.1	25.4	23.6	-7.6	29.0	29.5	1.6
	750	33.1	30.2	-9.6	26.5	24.1	-9.9	14.7	17.2	14.3	22.8	24.0	4.9
	900	39.9	38.0	-5.1	25.5	25.5	0.0	11.0	13.0	15.1	21.1	20.4	-3.3
HM	520	15.7	17.2	8.9	18.5	21.0	11.9	30.2	27.2	-11.0	29.9	29.5	-1.2
	750	28.0	29.1	3.9	22.1	23.1	4.4	22.8	20.8	-9.7	23.5	24.0	2.0
	900	36.6	36.9	1.0	21.7	24.5	11.3	17.8	16.6	-7.7	21.0	20.4	-3.0
AW-Cal	520	22.1	21.7	-1.7	13.6	12.9	-5.9	24	23.2	-3.5	34.0	33.8	-0.7
	750	37.7	33.7	-11.8	14.7	14.9	1.4	15.9	16.8	5.3	28.0	28.3	0.9
	900	37.3	41.5	10.1	20.8	16.3	-27.9	13.8	12.6	-9.7	24.7	24.7	-0.2
AW_Dol	520	21.1	22.0	3.8	16.8	18.4	8.9	21.0	20.5	-2.4	33.8	33.0	-2.6
	750	37.4	33.9	-10.3	14.8	20.5	27.7	16.5	14.1	-17.4	27.2	27.4	1.0
	900	36.0	41.7	13.8	21.5	21.9	1.4	14.7	9.9	-48.8	24.3	23.8	-1.9
AW-Kao	520	22.2	22.5	1.4	14.3	15.1	5.1	19.2	17.7	-8.3	36.6	36.6	-0.1
	750	38.5	34.4	-11.9	14.5	17.1	15.5	11.2	11.3	1.1	31.3	31.1	-0.6
	900	39.3	42.2	7.0	20.7	18.5	-11.9	8.8	7.1	-24.1	27.9	27.5	-1.6
AW-Pyr	520	21.1	24.1	12.4	13.4	12.9	-4.5	21.8	21.3	-2.4	36.8	36.4	-1.3
	750	38.2	36.1	-5.9	13.0	14.9	13.0	13.4	14.8	10.0	30.9	30.8	-0.2
	900	42.6	43.9	3.0	19.3	16.3	-18.7	10.1	10.6	4.9	26.3	27.2	3.5
AW-Qz	520	22.3	24.1	7.4	14.4	12.9	-12.3	19	19.9	4.3	37.2	37.6	1.1
	750	38.1	36.1	-5.8	14.3	14.9	4.5	11.3	13.4	16.2	31.5	32.1	2.0
	900	43.6	43.9	0.6	13.2	16.3	19.0	9.4	9.2	-2.0	29.6	28.5	-3.8

Part 4 – Conclusions and recommendations

Chapter 9: Conclusions and recommendations

“I think that the thing I most want you to remember is that research is a ceremony. And so is life. Everything that we do shares in the ongoing creation of our universe.”

— Shawn Wilson

Chapter 9: Conclusions and Recommendations

9.1. Introduction

The effect of acid washing and mineral addition on the pyrolysis products derived from typical Highveld (South African) coal was the topic of investigation in this dissertation. This chapter concludes the work by providing an evaluation of the objectives as set out in Chapter 1 (Section 9.2); describing the contribution to the existing knowledge field (Section 9.3), and providing recommendations for future work (Section 9.4).

9.2. Conclusions based on project objectives

i. Characterisation of a typical Highveld (South African) coal by means of chemical, mineralogical, structural and petrographic analyses as to provide detailed information with regard to the make-up of the coal structure and changes seen after acid washing.

The prepared TWD coal fractions were characterised by means of chemical- (proximate and ultimate analyses), mineralogical- (XRF, XRD, QEMSCAN), structural (BET CO_2 adsorption and DRIFT analysis) and petrographic (maceral and vitrinite reflectance – TWD only) analyses. TWD coal was classified as a medium rank C coal consisting of 54.6 vol.% m.m.f.b. vitrinite, 7.6 vol.% m.m.f.b. liptinite and 37.8 vol.% m.m.f.b. inertinite with a random reflectance of 0.77. Proximate analysis revealed a lower inherent moisture content for the AW TWD coal fraction; the ash content decreased from 14.0 wt% (d.b). to 2.0 wt% (d.b), whilst the volatile yield decreased from 38.5 wt% (d.a.f.) to 34.1 wt% (d.a.f.) after acid washing. Ultimate analysis showed an increased C content (80.2 wt% d.b. vs. 81.4 wt% d.b.), whilst the O content slightly decreased (11.6 wt% d.b. vs. 12.9 wt% d.b.) after acid washing. The major minerals identified by XRD and QEMSCAN analyses included: kaolinite, dolomite, calcite, quartz and pyrite. As expected, pyrite was not removed effectively by HCl and HF washing, whilst most of the other major minerals were successfully removed. BET CO_2 adsorption results indicated that the AW TWD fraction was slightly less porous than the TWD fraction, which is believed to be related to densification due to pre-oxidation due to the acid washing process. The DRIFT spectra for the TWD and AW TWD fractions indicated that the acid washing process removed some of the OH-groups, specifically those related to the spectra 3800 to 3600 cm^{-1}, as well as

vibrations identified as part of the C-O, O-H bend and aromatic C-H out-of-plane vibrations (1200 – 400 cm^{-1}). These differences were related to the removed minerals. Additionally, TG analyses revealed a decrease in mass loss when the AW TWD coal fraction was compared to the TWD coal on a dry, ash free basis at all three temperatures; i.e. 76.6 wt% vs. 72.9 wt% (520°C); 66.4 wt% vs. 59.2 wt% (750°C) and 64.4 wt% vs. 56.6 wt% (900°C). This difference in decomposition behaviour can be related to mineral activity.

ii. Determine the effect of acid washing on the pyrolysis product yield and composition by pyrolysis experiments (520, 750 and 900°C), and characterisation of the different pyrolysis products.

The water and tar yields of the AW TWD coal were found to be lower, whilst the gas yield was found to be much larger than that of the TWD coal. The char yields were unaffected by acid washing. GC analyses of the derived pyrolysis gases indicated that the AW TWD derived gas contained higher yields of H_2, CH_4, CO_2, C_2H_4, C_2H_6, C_3H_4, C_3H_6 and C_4s when compared to the gas derived from the TWD coal, whilst the CO yield from the TWD coal was higher at all final pyrolysis temperatures. These differences were related to the increased porosity of the AW TWD chars, thus releasing more volatiles. BET CO_2 adsorption analyses indicated higher micro porous surface areas at all three final pyrolysis temperatures for the AW TWD chars when compared to the TWD chars.

Analyses of the tar fraction by means of Simdis, GC-MS and –FID and SEC-UV indicated that the AW TWD derived tars were more aromatic in nature, containing more heavier boiling point components, which increased with increasing final pyrolysis temperature. On the other hand, the tars derived from the TWD coal contained lighter boiling point components with increasing final pyrolysis temperatures. It can thus be concluded that the presence of minerals assists in catalytic cracking of tar components to smaller entities.

The proximate analyses of the chars indicated an increase in fixed carbon content, with subsequent decrease in volatile matter content with an increase in final pyrolysis temperature for both coal/char fractions. The volatile matter content of the TWD derived char was found to be higher than that of AW TWD derived char at all temperatures, in accordance with the observations made with regard to the tar yields. The ash content of the TWD derived chars increased with an increase in final pyrolysis temperature, whilst that of the AW TWD derived chars remained constant. Ultimate analyses indicated that the AW TWD chars derived at 750°C and 900°C had higher oxygen and nitrogen contents, whilst more sulphur was removed from these chars than from the TWD derived chars. XRF analyses indicated similarity in ash content derived at the various pyrolysis temperatures for both samples. The AW TWD ash

analyses had to be done by ICP due to very low ash content and the derived chars showed greater variation in ash composition derived from the coal than was the case for TWD derived chars and coal ash. XRD analyses identified the most prominent crystalline minerals present in the derived chars, showing good agreement with previous findings. BET CO_2 adsorption analysis indicated that the AW TWD chars had greater micro pore surface areas, thus confirming the hypothesis that the increased gas yields were due to increased porosity. The DRIFT analyses revealed trends consistent with previous studies, with no significant difference in pyrolysis behaviour that could be observed from the char structure with this analytical technique.

iii. ***Determine the effect of the addition of individual minerals, (in significant quantities to ensure measurements above the detection limits of the analysis), to acid washed coal on the pyrolysis product yield and composition by pyrolysis experiments, and characterisation of the different pyrolysis products at the respective pyrolysis temperatures (520, 750 and 900°C).***

Minerals have a definite effect on pyrolysis product yields and composition. Mineral activity decreases in the order calcite/dolomite>pyrite>kaolinite>>>quartz.

Calcite and dolomite addition

The effect of mineral addition to AW TWD coal indicated that the various minerals play a definite role during pyrolysis. The addition of 5 wt.% calcite and dolomite led to a decrease in tar yield at the temperatures of 750°C and 900°C, whilst the gas yield was increased. Markedly, increased water yields were also observed with the addition of these minerals, and is consistent with previous studies. The decrease observed in char yields (at all temperatures studied) with the addition of calcite and dolomite is in contrast with previous findings, but the same observation was made for the addition of these minerals to the raw TWD coal. The minerals seem to assist in the conversion of char to gas and tar to gas reactions during the pyrolysis process.

The H_2 and CH_4 gas yields decreased with the addition of calcite and dolomite, whilst the CO and CO_2 yields were higher. A lot of variance was observed in tar composition for the various mineral additions. In general, the tars produced with the added minerals were more aliphatic in nature and consisted of lighter boiling point compounds for the 750°C and 900°C experiments, whilst for the 520°C experiments, the tars were heavier consisting of higher boiling point compounds. Various components identified by GC-MS were cracked by the added minerals, or it even appeared as if the formation of these compounds were catalysed by the presence of certain minerals. Proximate analyses of the chars provided little insight.

Ultimate, XRF and XRD analyses confirmed sulphur capturing by calcite and dolomite as more SO_3 components were observed in the ash from the XRF analysis, whilst XRD revealed the presence of oldhamite (CaS). Another observation from the XRD results was the presence of fluorite (CaF_2) with the addition of calcite and dolomite, due to inefficient removal of fluoride by HCl after HF washing of the coal.

Kaolinite addition

The addition of 5 wt% kaolinite led to an increase in tar, char and gas yield for the 520°C experiments, whilst at 750°C, a decrease in tar yield was observed, with other yields in agreement with that of the raw AW TWD coal. The initial increase in tar yield might be attributed to the fact that the additional sites provided by kaolinite addition might assist the tar precursors to leave the coal structure and form tar, stabilizing the formed free radicals to yield more tar at 520°C. The effect of kaolinite in tar reduction is attributed to the solid acidity of the mineral, thus providing protonates for increased pyrolysis conversion. Kaolinite is however less active than dolomite and calcite in tar reduction. Kaolinite addition also led to lower H_2 yields, whilst the CO yields were higher. The CO_2 yield at 520°C was higher, whilst decreasing to below the value of the AW TWD case at 900°C. The most prominent mineral forms identified by XRD were mullite and muscovite.

Pyrite addition

The addition of pyrite led to increased water yields at all temperatures. The tar yield was observed to be lower than that of the AW TWD at 520°C and 900°C. The temperature range in which pyrite affects pyrolysis yield is limited to 220-650°C, therefore the difference observed in the 900°C experiments is attributed to the change occurring in the lower pyrolysis range. The only significant effect observed with the addition of pyrite with regard to the gas yield, was in a decrease in gas yield at 750°C; thus it is believed there is some relationship between the gas and tar phases in this region. The H_2 yield was decreased by pyrite addition, whilst CO yield was higher at all final pyrolysis temperatures, and that of CO_2 was higher for the 520°C and 750°C experiments. The CH_4 yield was decreased for the 900°C experiments. The most prominent crystalline mineral forms identified due to pyrite addition by XRD included hematite, magnetite and pyrrhotite.

Quartz addition

The addition of quartz showed no significant effects on most of the pyrolysis yields, except showing increased conversion, lower char yields, and an increase in gas yield for the 520°C experiments, which might be related to changes in the thermo-plastic nature and fluidity of the coal. Quartz was the most inactive of all added minerals regarding pyrolysis compositional

changes. A reduction in H_2 yield was observed for the 900°C experiments with quartz addition, whilst the CO_2 yield of the 520°C experiments was higher. The tar composition was affected to a small degree, affecting the aliphatic content of the 900°C experiments.

iv. The make-up of coal-mineral mixtures similar to the original coal prior to acid washing and evaluation of the pyrolysis product yields and compositions at the respective pyrolysis temperatures (520°C, 750°C, 900°C).

The water yields from the LM coal-mineral mixture were in agreement with that of the TWD coal, whilst the tar yields were lower, and the char and gas yields increased. GC analyses of the derived gases indicated that good consistency was observed with regard to the H_2, CO and CH_4 yields of the 520°C and 750°C experiments. At 900°C, the LM coal-mineral mixture produced a yield of these gases intermittent between that of the TWD and AW TWD coals. The CO_2 yield was lower than that of the TWD coal at 750°C and 900°C. The C_2H_4, C_3H_4, C_3H_6 and C_4s gas yields were observed to be affected in such a manner that it was better related to the yields produced from the TWD coal.

The analyses of the tar fraction by Simdis revealed similar boiling point distributions of the derived tars for the 520°C and 900°C experiments, whilst the derived tar at 750°C for the LM coal-mineral mixture contained increased lighter boiling point compounds, indicative of more extensive catalytic cracking. The GC-MS analysis revealed that the LM derived tars were compositionally in accordance with that of the TWD coal regarding the aliphatic, alkyl-phenols, alkyl-benzenes and PAH's, at all final pyrolysis temperatures. The mixed aromatic and aliphatic component contents were higher in the LM derived tars, whilst variance was observed in the nitrogen heteroatoms and aromatic esters and ethers yields. SEC-UV analyses revealed that the LM derived tars consisted of lighter molecular weight compounds.

Proximate and ultimate analyses of the derived chars revealed good similarity between the TWD and LM chars. The TWD chars did however indicate a higher ash content and more volatile matter. XRF ash analyses revealed that the LM mineral mixture probably overcompensated for calcite and dolomite content, whilst pyrite and kaolinite content was underestimated. This probably led to the increased lower boiling point / lower molecular weight tar species that were identified for the LM derived tars. XRD analyses of the derived chars revealed that the LM chars were more crystalline in nature, and more species were identified. This was probably due to the fact that the added minerals did not form part of the coal structure as they were added extraneously, in contrast to the case for the TWD derived char.

The HM coal-mineral mixture showed much less variance than observed for the LM coal-mineral mixture, and trends observed were much more consistent to that of the AW TWD coal. This difference was attributed to the difference in mineral composition. The differences observed between the LM and HM pyrolysis yields and product compositions confirm that synergism between minerals is an important factor to take into account when the effect of minerals on pyrolysis product yields and composition needs to be researched.

i. Statistical evaluation of the obtained data and derivation of predictive models for char, tar and gas yields at the respective pyrolysis temperatures (520, 750 and 900°C).

SPSS software was used for the development of linear regression models to predict the gas, tar and char yields (d.m.m.f.). The respective R^2 values were found to be 0.837, 0.785 and 0.846. The gas and char models took into account variance in temperature and variance in mineral loading. The tar yield model only took variance in mineral loading into account as no linear correlation could be established for the change in pyrolysis temperature. Linear regression models for prediction of the yields of H_2, CO, CO_2 and CH_4 were also developed with R^2 values of 0.917, 0.702, 0.869 and 0.978, respectively.

9.3. Contribution to existing knowledge field

The following contributions were made to the existing knowledge field:

- Full account of the chemical, mineralogical and structural features of the raw and acid washed coal, thus providing more insight on the probable changes brought about by acid washing. The use of analytical techniques for further characterisation of the molecular properties/characteristics is also regarded as a valuable contribution. It provides much more insight into the changes that occur, as well as assists in ascribing these changes to specific sources.
- Pyrolysis experiments also revealed valuable information. The quantification and analyses of the gas yield derived during ISO 647 / similar experiments are definitely excellent contributions. A simple and cheap solution was provided which can be applied in future studies.
- Quantification of the effect of the removal/addition of minerals on pyrolysis yield provides a solid basis to motivate future studies in this research field. The detailed characterisation of these products provided more insight and revealed that more attention can be given to the study of these effects.
- This is the first laboratory study examining these phenomena done on South African coal as far as the relevant literature was reviewed.

- An exstensive characterisation of pyrolysis products, looking into the effects of mineral removal/addition, is the first of its sort as far as the relevant literature was reviewed.
- The development of statistical models to predict pyrolysis product yields and certain pyrolysis product composition, is also a first of its sort as far as the relevant literature was studied.
- The statistical models will provide a solid base for future work in order to refine the models and develop them for other coals as well.

9.4. Recommendations

This investigation revealed a few aspects that need to be studied further in order to understand the effect of minerals on the pyrolysis products derived from coal better. The following recommendations are made:

- The use of more coals of different rank from different parts of the world in order to determine the effect of acid washing, as well as relate the differences seen to specific sources.
- Better acid washing/mineral removal procedures that will provide a coal structure as close as possible to being “mineral-free”. Ferric ions/HNO_3 washing can for example be used for the removal of pyrite.
- The addition of various loadings of minerals at various temperatures in order to determine if there are limiting effects and maximum limits, after which higher addition of the specific mineral would not have any effect any more.
- More focus on synergism between minerals; i.e. adding two minerals at one time to the acid washed coal to see if the mineral-mineral reactions are of importance.
- Expanding the minerals studied to also include minerals found in lower concentrations such as illite, rutile and trace elements.
- Experimental conditions should be studied closer to the conditions used in industry in order to expand this work, and make it more accurate and relevant for industry-specific use.
- Tars and chars can be further characterised by more advanced methods. Tar characterisation can possibly include solution-state NMR, GC-GC-MS, GC-MS with FFAP column, SEC with RID detection, XPS and MALDI-TOF MS. Char characterisation can possibly include Raman spectroscopy, tomography, FTIR and solid-state NMR. GC-GC-MS can for example assist to separate the mixed aliphatic and aromatic components which co-elute during regular GC-MS. C^{13} NMR, and FTIR can provide more insight into the structural families present and provide a more overall view of tar/char composition than is seen with the methods used in this study.

- Elemental/ultimate analysis of the tar fraction in order to complete elemental balances for the coals studied.
- Better characterisation of the gas fraction with a more advanced GC system which will identify more gas species such as H_2S. COS, SO_2, NH_3 and NO_2 amongst others. This will assist in better describing distributions between the various pyrolysis products.
- Impregnation of large particles with some of these minerals can be researched in order to expand the knowledge to large particles. Another possibility is the make-up of pellets in order to study these effects on a larger scale.
- Addition of minerals on a molar basis as to ensure that comparison is more effective.
- More in-depth studies regarding the chemistry behind changes seen due to the addition/removal of minerals in order to find definite sources and predict expected changes better.
- Expansion of the developed statistical models to be relevant for more coal types, different mineral loadings, and different ranks of coal. These models can also be developed further to describe product composition better, and be more generalised taking into account a variety of aspects such as operating conditions of the pyrolysis setup used.
- Comparison of the yields predicted by the derived empirical models to the yields predicted by software used in the coal industry such as FLASHCHAIN.
- Integration of coal characterisation data and pyrolysis yields and compositions in order to provide more insight with respect to pyrolysis behaviour of coal and the effects of mineral addition/removal.
- Tar producers should note – the mineral composition of coal (particularly dolomite and calcite) may influence tar production to a significant extent.

Bibliography

Abbot, J. & Wojciechowski, B.W. 1988. Catalytic reactions of branched paraffins on HY zeolite. *Journal of Catalysis,* 113:353-366.

Abu El-Rub, Z. Bramer, E.A. & Brem, G. 2004. Review of catalysts for tar elimination in biomass gasification processes. *Industrial and Engineering Chemistry Research,* 43:6911-6919.

Adanez, J. & De Diego, L.F. 1993. Reactivity of lignite chars with CO_2: influence of the mineral matter. *International Chemical Engineering,* 33(4):656-662.

Adegoroye, A., Paterson, N., Li, X., Morgan, T., Herod, A.A., Dugwell, D.R. & Kaniyoti, R. 2004. The characterisation of tars produced during the gasification of sewage sludge in a spouted bed reactor. *Fuel,* 83:1949-1960.

Ahmad, T., Awan, I.A., Nisar, J. & Ahmad, I. 2009a. Influence of inherent minerals and pyrolysis temperature on the yield of pyrolysates of some Pakistani coals. *Energy Conversion and Management,* 50:1163-1171.

Ahmad T., Nisar, J.m Ahmad I.A. & Ahmad, I. 2009b. Effect of solid additives on pyrolysis behaviour of Makerwal coal. *Journal of the Chemistry Society of Pakistan,*31(1): 11-15.

Alpern, B., Nahuys, J., & Martinez, L. 1983. Mineral matter in ashy and non-washable coals - Its influence on chemical properties. *Comunicaçoes dos Serviços Geológicos de Portugal.* Symposium on Gondwana coals, p.299-317, Lisbon.

Alvarez, P., Granda, M., Sutil, J., Menendez, R., Fernandez, J.J., Vina, J.A., Morgan T.J., Milan, M., Herod, A.A. & Kandiyoti, R. 2008. Characterization and Pyrolysis Behaviour of Novel Anthracene Oil Derivatives. *Energy & Fuels,* 22:4077-4086.

André, R.N., Pinto, F., Franco, C., Dias, M., Gulyurtlu, I, Matos, M.A.A. & Cabrita I. 2004. Fluidised bed co-gasification of coal and olive oil industry wastes. *Fuel,* 84:1635-1644.

Anon. 2014 Trade India. http://pimg.tradeindia.com/01602357/b/1/BUCHI-ROTARY-EVAPORATORS.jpg Date of access: 30 June 2014.

Anthony, D.B. 1974. Rapid devolatilisation and hydrogasification of pulverised coal. (PhD Thesis – MIT).

Anthony, D.B. & Howard, J.B. 1976. Coal Devolatilization and hydrogasification. *American Institute of Chemical Engineering Journal,* 22:625-656.

Anthony, D.B., Howard, J.B., Hottel, H.C. & Meissner, H.P. 1976. Rapid devolatilisation and hydrogasification of bituminous coal. *Fuel,* 55:121-128.

Anthony, D.B., Howard, J.B., Hottel, H.C. & Meissner, H.P. 1974. Apparatus for determining high pressure coal-hydrogen reaction kinetics under rapid heating conditions. *Rev. Sco. Instrum.* 45:992-995.

Assadulla, M., Ito, S., Kunimori, K., Yamada, M. & Tomishige, K. 2002. Biomass gasification to hydrogen and syngas at low temperature: novel catalytic system using fluidized-bed reactor. *Journal of Catalysis,* 208: 255-259.

ASTM (American Society for Testing and Materials). 2010. Standard test method for major and minor elements in coal and coke ash by X-Ray Fluorescence. Pennsylvania: ASTM International. (ASTM D4326).

ASTM (American Society for Testing and Materials). 2010. Standard test method for water in petroleum products and bituminous materials by distillation. Pennsylvania: ASTM International. (ASTM D95).

ASTM (American Society for Testing and Materials). 1998. Standard classification of coals by rank. Pennsylvania: ASTM International. (ASTM D388).

Ateş, F. & Erginel, N. 2012. The regression analysis of fast pyrolysis product yields and determination of product quality. *Fuel,* 102:681-690.

Aznar, M.P., Corella, J., Gill, J., Martin, JA., Caballero, M.A., Olivares A. & Francés, E. 1996. In *Proceedings of Conference on Developments in Thermochemical Biomass Conversion*, p.1117, Banff, Canada.

Baggio, P., Baratieri, M., Fiori, L. & Grigiante, M. 2009. Experimental and thermodynamic constraints on the performance of the conversion process. *Bioresources Technology,* 99:7063-7073.

Bai, Y., Yan, L., Li, G., Zhao, R. & Li, F. 2014. Effects of demineralization on phenols distribution and formation during coal pyrolysis. *Fuel,* (In Press).

Bai, Y., Wang, P. Yan, L., Liu, C., Li, F. & Xie, K. 2013. Effects of CO_2 on gas evolution and char structure formation during lump coal pyrolysis at elevated pressures. *Journal of Analytical and Applied Pyrolysis,* 104:202-209.

Bai, J., Li, W., Bai, Z. & Li, B. 2010. Influences of minerals transformation on the reactivity of high temperature char gasification. *Fuel Processing Technology,* 91:404-409.

Baker, E.G., Mudge, L.K. & Brown, M.D. 1987. Steam gasification of biomass with nickel secondary catalysts. *Industial and Engineering Chemistry Research,* 26:1335-1339.

Bakr, M.Y., Thompson, G.E., Burchill, P. & Jones, M.A. 1996. Unusually high extraction yield from the liquefaction of an Egyptian coal from Al Maghara coalfield. *Fuel Processing Technology,* 46:71-76.

Balasubramanian, B., Ortiz, A.L., Kaytakoglu, S. & Harrison, D.P. 1999. Hydrogen from methane in a single-step process. *Chemical Engineering Science,* 54(15-16):3543-3552.

Barth, T., Seim, M., Christy, A.A. & Kvalheim, O.M. 1994. Maturity trends in asphaltenes from pyrolysed source rocks and natural coals – multivariate modelling of diffuse reflectance Fourier-transform infrared spectra. *Organic Geochemistry,* 23(2):139-158.

Bean, N.C. 2013. Influence of additives on devolatilisation products and combustion reactivity of typical South African coals. Potchefstroom – NWU (M.Eng dissertation).

Bell, D.A., Towler, B.F. & Fan, M. 2011. Coal gasification and its applications. Amsterdam: Elsevier. 416p.

Bishop M. & Ward, D.L. 1958. The direct determination of mineral matters in coal. *Fuel,* 37:191.

Bolat, E., Sağlam, S. & Pişkin, S. 1998. Chemical acid washing of a Turkish high ash bituminous coal. *Fuel Processing Technology,* 57:93-99.

Bona, M.T. & Andrés, J.M.. 2008a. Application of chemometric tools for coal classification and multivariate calibration by transmission and drift mid-infrared spectroscopy. *Analytica Chimica Acta,* 624:68-78.

Bona, M.T. & Andrés, J.M.. 2008b. Reflection and transmission mid-infrared spectroscopy for rapid determination of coal properties by multivariate analysis. *Talanta,* 74:998-1007.

Bool, L.E., Peterson, T.W. & Wendt, J.O.L. 1995. The partitioning of iron during combustion of pulverized coal. *Combustion and Flame Journal,* 100:262-270.

Borah, D., Barau, M. & Baruah, M.K. 2005. Dependence of pyrite concentration on kinetics and thermodynamics of coal pyrolysis in non-isothermal systems. *Fuel Processing Technology,* 86:977-993.

Borrego, A.G., Marbán, G., Alonso, M.J.G., Álvarez, D. & Menéndez, R. 2000. Maceral effects in the determination of proximate volatiles in coals. *Energy & Fuels*, 14:117-126.

Boyabat, N., Özer, A.K., Bayarakçen, S. & Gülaboğlu, M.S. 2003. Thermal decomposition of pyrite in nitrogen atmosphere. *Fuel Processing Technology,* 85:179-188.

Bredenberg, J.B.S., Huuska, M., Räty, J. & Korpio, M. 1982. Hydrogenolysis and hydrocracking of the carbon-oxygen bond (I) Hydrocracking of some simple aromatic O-compounds. *Journal of Catalysis*, 77(1):242-247.

Breen, C., Clegg, F., Herron, M.M. Hild, G.P., Hillier, S., Hughes, T.L., Jones, T.G.J., Matteson, A. & Yarwood, J. 2008. Bulk mineralogical characterisation of oilfield reservoir rock and sandstones using Diffuse Reflectance Infrared Fourier Transform Spectroscopy and Partial Least Sqaures analysis. *Journal of Petroleum Science and Engineering,* 60:1-17.

Briggs, D.L. & Lindsay, C.G. 1986. High-temperature interactions among minerals occurring in coal, In: *Mineral matter and ash in coal, Symposium of American Chemical Society,* Vorres K. (Ed). p.128-137.

Bruinsma, O.S.L. & Moulijn, J.A. 1989. The pyrolytic formation of polycyclic aromatic hydrocarbons from benzene, toluene, ethylbenzene, styrene, phenylacetlyne and n-decane in relation to fossil fuels utilization. *Fuel Processing Technology,* 21:25-37.

Bryers, R.W. 1986. Influence of segregated mineral matter in coal. In: *Mineral matter and ash in coal, Symposium of American Chemical Society,* Vorres K. (Ed). p.351-374.

Buhmann, D. 1991. Mineral matter content of the No. 4L coal seam from the Witbank and Highveld coalfields. Abstract in Conference on South Africa's Coal Resources. Geological Society of South Africa.

Bunger, J.W. 1976. Characterization of Utah tar sand bitumen. Chapter 10: in T.F. Yen ed. *Shale oil, tar sands, and related fuel sources,* Washnington: ACS Publications. P.121-136.

Bunt, J.R., Waanders, F.B. and Schobert, H. 2012a. Behaviour of selected major elements during fixed-bed gasification of South African bituminous coal. *Journal of Analytical and Applied Pyrolysis,* 93:85-94.

Bunt, J.R., Waanders, F.B., Nel, A., Dreyer, L. & Van Rensburg, P.W.A. 2012b. An understanding of the porosity of residual coal/char/ash samples from an air-blown packed bed reactor operating on inertinite-rich lump coal. *Journal of Analytical and Applied Pyrolysis,* 95:241-246.

Bunt, J.R. & Waanders, F.B. 2008. An understanding of the behaviour of a number of element phases impacting on a commercial-scale Sasol-Lurgi FBDB gasifier. *Fuel,* 87(10-11):1751-1762.

Bunt, J.B. & Waanders, F.B. 2009. Pipe reactor gasification studies of a South African bituminous coal blend. Part 1 – carbon and volatile matter behaviour as function of feed coal particle size distribution. *Fuel,* 88:585-594.

Caballero, J.A. & Conesa, J.A. 2005. Mathematical considerations for non-isothermal kinetics in thermal decomposition. *Journal of Analytical and Applied Pyrolysis,* 73:85-100.

Caceres, P.G. & Attiogbe, E.K. 1997. Thermal decomposition of dolomite and the extraction of its constituents. *Minerals Engineering,* 10:1165-1176.

Cai, M.F. & Smart, R.B. 1994. Comparison of seven West Virginia coals with their n-methyl-2-pyrrolidinone-soluble extracts and residues. 1. Diffuse reflectance Fourier transform spectroscopy, *Energy & Fuels,* 8:369-374.

Cai, J., Wang, Y., Zhou, L & Huang, Q. 2008. Thermogravimetric analysis and kinetics of coal/plastic blends during co-pyrolysis in nitrogen atmosphere. *Fuel Processing Technology,* 89:21-27.

Cairncross, B. 2001. An overview of the Permian (Karoo) coal deposits of southern Africa. *African Earth Sciences*, 33:529-562.

Cakal, G.Ö., Yücel, H. & Gürüz, A.G. 2007. Physical and chemical properties of selected Turkish lignites and their pyrolysis and gasification rates determined by thermogravymetric analysis. *Journal of Analytical and Applied Pyrolysis,* 80:262-268.

Calkins, W.H. & Tyler, R.J. 1984. Coal flash pyrolysis: 2. Polymenthylene compounds in low temperature flash pyrolysis tars. *Fuel,* 63:1119-1124.

Campbell, J.H. & Stephens, D.R. 1976. Kinetic studies of gas evolution during pyrolysis of subbituminous coal. Paper presented at the American Chemical Society meeting, San Francisco, CA, 29 August. http://web.anl.gov/PCS/acsfuel/preprint%20archive/Files/21_7_SAN%FRANCISCO_08-76_0094.pdf. Date of access: 17 September 2014.

Carmody, O., Kristóf, J., Frost, R.L., Makó, E., Kloprogge, J.T. & Kokot, S. 2005. A spectroscopic study of mechanochemically activated kaolinite with the aid of chemometrics. *Journal of Colloid Interface Science,* 287(1):43-56.

Casal, M.D., Díez, M.A., Alvarez, R. & Barriocanal, C. 2008. Primary tar of different coking coal ranks. *International Journal of Coal Geology,* 76:237-242.

Centeno, T.A., Pis, J.J., Pajares, J.A. & Fuertes, A.B. 2001. Microporous structure of chars produced by pyrolysis of pre-oxidized coals. *Journal of Analytical and Applied Pyrolysis,* 44(2):205-218.

Chabalala, V.P., Wagner, N., & Potgieter-Vermaak, S. 2011. Investigation into the evolution of char structure using Raman spectroscopy in conjunction with coal petrography; Part 1. *Fuel Processing Technology,* 92:750-756.

Chen, J., Castagnoli, C. & Niksa, S. 1990. The effects of secondary reactions on product and elemental distributions from rapid coal pyrolysis. Paper (no. 90-48) presented at the Western States Section of the Combustion Institure, San Diego, CA.

Chen, C., Gao, J. & Yan, Y. 1998a. Observation of the type of hydrogen bonds in coal by FTIR. *Energy & Fuels,* 12:446-449.

Chen, C., Gao, J, & Yan, Y. 1998b. Role of noncovalent bonding in swelling coal. *Energy & Fuels,* 12:1328-1334.

Chen, H., Li, B., Yang, J. & Zhang, B. 1997. Transformation of sulfur during pyrolysis and hydropyrolysis of coal. *Fuel,* 77:487-493.

Chen, H., Li, B. & Zhang, B. 1999. Effects of mineral matter on products and sulfur distributions in hydropyrolysis. *Fuel,*78:713-719.

Chen, H., Li, B. & Zhang, B. 2000. Decomposition of pyrite and the interaction of pyrite with coal organic matrix in pyrolysis and hydropyrolysis. *Fuel,* 79:1627-1631.

Chen, Y., Mastalerz, M. & Schimmelmann, A. 2012. Characterization of chemical functional groups in macerals across different coal ranks via micro-FTIR spectroscopy. *International Journal of Coal Geology,* 104:22-33.

Cheng, H., Liu, Q., Huang, M., Zhang, S. & Frost, R.L. 2013. Application of TG-FTIR to study SO_2 evolved during the thermal decomposition of coal-derived pyrite. *Thermochimica Acta,* 555:1-6.

Christy, A.A., Kvalheim, O.M. & Velapoldi, R.A. 1995. Quantitative analysis in diffuse reflectance spectrometry: A modified Kubelka-Munk equation. *Vibrational Spectroscopy,* 9:19-27.

Coetzer, R.L.J. & Keyser M.J. 2003. Experimental design and statistical evaluation of a full-scale gasification project. *Fuel Processing Technology,* 80:263-278.

Corella, J., Toledo, J.M. & Aznar, M.P. 2002. Improving the modelling of the kinetics of the catalytic tar elimination in biomass gasification. *Industrial and Engineering Chemistry Research,* 41:3351-3356.

Cox, J.L. 1975. Catalysts for coal conversion. Paper presented at the *ICT Symposium – Clean fuels from coal*, Chicago, p.311.

Cui, H., Yang, J., Liu, Z. & Bi, J. 2002. Effects of remained catalysts and enriched coal minerals on devolatilization of residual chars from coal liquefaction. *Fuel,* 81:1525-1531.

Cui, L.-J., Lin, W.-G. & Yao, J.-Z. 2006. Influences of temperature and coal particle size on the flash pyrolysis of coal in a fast-entrained bed. *Chemical Research in Chinese Universities,* 22(1):103-110.

Cypres, R. & Bettens, B. 1974. Mechanismes de fragmentation pyrolytique du phenol et des cresols. *Tetrahedron,* 30:1253-1260.

Cypres, R. & Bettens, B. 1975. La formation de la plupart des composes aromatiques produits lors de la pyrolyse du phenol, ne fait pas intervener le carbone porteur de la function hydroxyle *Tetrahedron,* 31:359-365.

Cypres, R. & Bettens, B. 1989. Production of benzoles and active carbon from waste rubber and plastic materials by means of pyrolysis with simulateous port-cracking. Ferrero, G.L., Maniatis, K., Buekens, A., Bridgwater, A.V. (Eds.) *Pyrolysis and gasification*, Elsevier Applied Science: London, p.209 – 229.

Cypres, R. & Souden-Moinet, C. 1980. Pyrolysis of coal and iron oxide mixtures I, Influence of iron oxides on the pyrolysis of coal. *Fuel,* 59: 48-54.

Davis, K.A., Hurt, R.H., Yang, N.Y.C. & Headley, T.J. 1995. Evolution of char chemistry, crystallinity and ultrafine structure during pulverized-coal combustion. *Combustion and Flame,* 100(1-2):31-40.

Dean, E.W. & Stark, D.D. 1920. A convenient method for the determination of water in petroleum and other organic emulsions. *The Journal of Industrial and Engineering Chemistry,* May:486-490.

Delgado, J., Aznar, M.P. & Corella, J. 1996. Calcined dolomite, magnesite and calcite for cleaning hot gas from a fluidized bed biomass gasifier with steam: Life and Usefulness. *Industrial and Engineering Chemistry Research,* 37:3637-3643.

De Lorenzi Pezzolo, A. 2013. An exercise on calibration: DRIFTS study of binary mixtures of calcite and dolomite with partially overlapping spectral features. *Journal of Chemical Education,* 90:118-122.

Derycke, V., Kongolo, M., Benzaazoua, M., Mallet, M., Barrès, O., De Donato, P., Bussière, B. & Mermillod-Blondin, R. 2013. Surface chemical characterization of different pyrite size fractions for flotation purposes. *International Journal of Mineral Processing,* 118:1-14.

De Souza, F. & Bragança, S.R. 2013. Thermogravimetric analysis of limestones with different contents of MgO and microstructural characterization in oxy-combustion. *Thermochimica Acta,* 561:19-25.

Deshpande, G.V., Solomon, P.R. & Serio, M.A. 1988. Crosslinking reactions in coal pyrolysis. http://web.anl.gov/PCS/acsfuel/preprint%20archive/Files/33_2_TORONTO_06-88_0310.pdf. Date of access: 20 July 2014.

Domínguez, A., Alvarez, R., Blanco, C.G. & Díez, M.A. 1996. Chromatographic evaluation of some selected polycyclic aromatic hydrocarbons of coal tars produced under coking conditions and pitches derived from them. *Journal of Chromatography*, Vol. 719:181-194.

Dedman, A.J. & Owen, A.J. 1962. Calcium cyanimide synthesis. Part 4 – The reaction CaO + CO_2 = $CaCO_3$. *Transactions of the Faraday Society,* 59:2027-2035.

Dickerson, T. & Soria, J. 2013. Catalytic fast pyrolysis: A review. *Energies,* 6:514-538.

Doymaz, I., Gulen, J., Piskin, S. & Toprak, S. 2007. The effects of aqueous caustic and various acid treatments on the removal of mineral matter in asphaltite. *Energy Sources,* 29(4): 337-346.

Edwards, A.H., Daybell, G.N. & Pringle, W.J. 1958. An investigation into methods for the determination of forms of sulphur in coals. *Fuel,* 37:47-50.

Erasmus, H.B.D. & Scholtz, J.H. 2002. Proven coal liquefaction processes: Sasol-Lurgi coal gasification and Sasol Fischer-Tropsch gas conversion. *China International Hi-tech Symposium and Exhibition on Coal Chemical Industry and Conversion.* PRC, Beijing, November 6-9 2002.

Escardino, A., Garcia-Ten, J. & Feliu, C. 2008. Kinetic study of calcite particle (powder) thermal decomposition: Part I. *Journal of the European Ceramic Society,* 28: 3011-3020.

Evans, R.J. & Milne, T.A. 1987. Molecular characterization of the pyrolysis of biomass. 1. Fundamentals. *Energy & Fuels,* 1: 123-137.

Everson, R.C., Neomagus, H.W.J.P., Kaitano, R., Falcon, R., Van Alphen, C. & Du Cann, V.M. 2008. Properties of high ash char particles derived from inertinite-rich coal: 1. Chemical, structural and petrographic characteristics. *Fuel,* 87:3082-3090.

Falcon, R., & Ham, A.J. 1988. The characteristics of Southern African coals. *Journal of the South African Institute of Mining and Metallurgy,* 88(5):145-161.

Falcon, R.M.S. & Snyman, C.P. 1986. An introduction to coal petrography: Atlas of petrographic constituents in the bituminous coals of Southern Africa. Johannesburg: The Geological Society of South Africa. 106 p.

Faravelli, T., Pinciroli, M., Pisano, F., Bozzano, G., Dente, M. and Ranzi, E. 2001. Thermal degradation of polysterene. *Journal of Analytical and Applied Pyrolysis,* 60:103-121.

Farmer, V.C. 1968. Infrared spectroscopy in clay mineral studies. *Clay Minerals,* 7: 373-388.

Farmer, V.C. 1974. Mineral Society Monograph 4: The Infrared Spectra of Minerals. London: Mineral Society.

Fei, J., Zhang, J., Wang, F. & Wang, J. 2012. Synergistic effect on co-pyrolysis of lignite and high-sulphur swelling coal. *Journal of Analytical and Applied Pyrolysis,* 95:61-67.

Field, A. 2009. Discovering statistics using SPSS. 3rd ed. London: Sage Publications.

FFF (Fossil Fuel Foundation). 2013. The South African Coal Roadmap. www.sanedi.org.za/coal-roadmap/ Date of access: 21 March 2014.

Fidalgo, B., Van Niekerk, D. & Millan, M. 2014. The effect of syngas on tar quality and quantity in pyrolysis of a typical South African inertinite-rich coal. *Fuel,* 134: 90-96.

Fischer, J., Che, S., Lo, R., Podolski, W., Nandi, S. & Jonke, A. 1975. Argonne National Laboratory – Chemical Engineering Division – Coal Technology semi-annual report, July – December 1974. Report ANL-8151.

Forney, A.J., Haynes, W.P., Gasior, S.J. & Kenney, R.F. 1974. Effects of additives upon the gasification of coal in the SYNTHANE gasifier. *ACS Division of Fuel Chemistry Preprints,* 19(1): 111.

Franklin, H.D. 1980. Mineral matter effects in coal pyrolysis and hydropyrolysis. USA – MIT (Thesis – PhD).

Franklin, H.D., Peters, W.A. & Howard, J.B. 1981a. Effects of calcium minerals on the rapid pyrolysis of a bituminous coal. *ACS Division of Fuel Chemistry Preprints,* 26(2):121-132.

Franklin, H.D., Peters, W.A. & Howard, J.B. 1981b. Mineral matter effects on the rapid pyrolysis and hydropyrolysis of a bituminous coal. *Preprints of the American Chemical Society Division for Fuel Chemistry,* 26(3): 121-130.

Franklin, H.D., Peters, W.A. & Howard, J.B. 1982a. Mineral matter effect on the rapid pyrolysis and hydropyrolysis of a bituminous coal. 1. Effects on yield of char, tar and light gaseous volatiles. *Fuel,* 61(2):155-160.

Franklin, H.D., Peters, W.A. & Howard, J.B. 1982b. Mineral matter effect on the rapid pyrolysis and hydropyrolysis of a bituminous coal. 2. Effects on yields of C_3-C_8 hydrocarbons. *Fuel,* 61(12):1213-1217.

Franklin, H.D., Cosway, R.G., Peters, W.A. & Howard, J.B. 1983. Effects of cations on the rapid pyrolysis of a Wyodak Subbituminous coal. *Industrial and Engineering Chemical Process Design and Development,* 22:39-42.

Frost, R.L., Kristóf, J., Makó, E. & Horváth, E. 2003. A DRIFT spectroscopic study of potassium acetate intercalated mechanochemically activated kaolinite. *Spectrochimica Acta Part A,* 59:1183-1194.

Fuentes-Cano, D., Gómez-Barea, A., Nilsson, S. & Ollero, P. 2013. The influence of temperature and steam on the yields of tar and light hydrocarbon compounds during devolatilization of dried sewage sludge in a fluidized bed. *Fuel,* 108:341-350.

Fuerstenau, D.W., Rosenbaum, J.M. & Laskowski, J. 1983. Effect of surface functional groups on the flotation of coal. *Colloids and Surfaces,* 8(2): 153-173.

Furimsky, E. & Ripmeester, J. 1983. Characterization of Canadian coals by nuclear magnetic resonance spectroscopy. *Fuel Processing Technology,* 7(3):191-202.

Garcia, R., Moinelo, S.R., Lafferty, C.J. & Shape, C.E. 1991. *Energy & Fuels,* 5:582-

Gavalas, G.R. 1982. Coal Science and Technology 4 - Coal Pyrolysis. Amsterdam: Elsevier.

Geng, W., Nakajima, T., Takanashi, H. & Ohki, A. 2009. Analysis of carboxyl group in coal and coal aromaticity by Fourier transform infrared (FT-IR) spectrometry. *Fuel,* 88:139-144.

George, A., Morgan, T.J., Alvarez, P., Millan, M., Herod, A.A. & Kandiyoti, R. 2010. Fractionation of a coal tar pitch by ultra-filtration and characterisation by size exclusion chromatography, UV-fluorescence and laser desorption-mass spectroscopy. *Fuel,* 89:2953-2970.

Gerber, M.A. 2007. Review of novel catalysts for biomass tar cracking and methane reforming. *Pacific Northwest National Laboratory, PNNL-16950.* Available at: http://www.pnl.gov/main/publications/external/technical_reports/pnnl-16950.pdf Date of access: 3 August 2014.

Gibbins-Matham, J.R. & Kandiyoti, R. 1988. Coal pyrolysis yields from fast and slow heating in a wire- mesh apparatus with a gas sweep. *Energy & Fuels,* 2:505.

Given, P.H. 1974. A research and development program for catalysis in coal conversion processes. *EPRI Report* No. 207-0-0, p. A-122. http://www.fischer-tropsch.org/DOE/DOE_reports/242412/pb242412_sec01.pdf Date of access: 18 September 2014.

Gluskoter, H.J. 1965. Electronic low temperature ashing of bituminous coal. *Fuel,* 44:285.

Golab, A., Ward, C.R., Permana, A., Lennox, P. & Botha, P. 2013. High-resolution three-dimensional imaging of coal using microfocus X-ray computed tomography, with special reference to modes of mineral occurrence. *International Journal of Coal Gology,* 113:97-108.

Gómez-Barea, A., Nilsson, S., Barrero, F.V. & Campoy, M. 2010. Devolatilization of wood and wastes in fluidized bed. *Fuel,* 91:1624-1631.

Gornostayev, S., Härkki, J. & Kerkkonen, O. 2009. Transformations of pyrite during formation of metallurgical coke. *Fuel,* 88:2032-2036.

Gosiewska, A., Drelich, J., Laskowski, J.S. & Pawlik, M. 2002. Mineral matter distribution on coal surface and its effect on coal wettability. *Journal of colloid and Interface Science,* 247:107-116.

Govender, A. 2005. Determination and statistical evaluation of the effect of minerals and mineral associations in specific dense medium fractions on ash fusion temperature. Potchefstroom: NWU. (Dissertation: MSc).

Gräber, W.D. & and Hüttinger, K.J. 1982. Chemistry of methane formation in hydrogasification of aromatics. 2. Aromatics with aliphatic groups. *Fuel,* 61:-

Gray, V.R. 1988. The role of explosive ejection in the pyrolysis of coal. *Fuel,* 67:1298.

Greensfelder, B.S., Voge, H.H. & Good, G.M. 1949. Catalytic activity and cracking by carbenium ion mechanism. *Industrial Engineering and Chemistry,* 41:2573-2584.

Grigore, M., Sakurovs, R., French, D. & Sahajwalla, V. 2010. Mineral matter in coals and their reactions during coking. *International Journal of Coal Geology,* 76:301-308.

Grim, R.E. & Bradley, W.F. 1948. Rehydration and dehydration of clay minerals. *American Mineralogist,* 33:50-59.

Groves, S.J., Williamson, J. & Sanyal, A. 1987. Decomposition of pyrite during pulverized coal combustion. *Fuel,* 66:461-466.

Gryglewicz, G. 1995. Sulfur transformations during pyrolysis of a high sulfur Polish coking coal. *Fuel,* 74(3):356-361.

Gryglewicz, G., Wilk, P., Yperman, J., Franco, D.V., Maes, I.I., Mullens, J. & Van Poucke, L.C. 1996. Interaction of the organic matrix with pyrite during pyrolysis of a high-sulfur bituminous coal. *Fuel,* 75(13):1499-1504.

Güler, T. 2005. Dithiophosphinate-pyrite interaction: Voltammetry and DRIFT spectroscopy investigations at oxidizing potentials. *Journal of Colloid and Interface Science,* 288: 319-324.

Günzler, H. & Williams, A. 2002. Handbook of Analytical Techniques, Vol. 1. Weinheim: Wiley-VCH.

Guo, B., Li, D., Cheng, C., Lü, Z. & Shen, Y. 2001. Simulation of biomass gasification with a hybrid neural network model, *Bioresources Technology,* 76:77-83.

Hartgers, W.A., Damsté, J.S.S., de Leeuw, J.W., Ling, Y. & Dyrkacz, G.R. 1994. Molecular characterization of flash pyrolysates of two carboniferous coals and their constituting maceral fractions. *Energy & Fuels*, 8:1055-1067.

Hashimoto, K., Miura, K. & Ueda, T. 1986. Correlation of gasification rates of various coals measured by a rapid heating method in a steam atmosphere at relatively low temperatures. *Fuel*, 65:1516-1523.

Hattingh, B.B. 2009. The determination of the reaction mechanisms involved in the CO_2 gasification of inertinite-rich, high ash coals. Potchefstroom – NWU (Dissertation – M.Eng).

Hattingh, B.B. 2012. Product evaluation and reaction modelling for the devolatilizaton of large coal particles. Potchefstroom – NWU (Thesis - PhD).

Hattingh, B.B., Everson, R.C., Neomagus, H.W.J.P. & Bunt, J.R. 2011. Assessing the catalytic effect of coal ash constituents on the CO_2 gasification rate of high ash South African coal. *Fuel Processing Technology,* 92:2048-2054.

Hattingh, B.B., Everson, R.C., Neomagus, H.W.J.P., Bunt, J.R., Van Niekerk, D., Jordaan, J.H.L. and Mathews, J.P. 2013. Elucidation of the structural and molecular properties of typical South African coals. *Energy & Fuels,* 27:3161-3172.

Hayashi, J.I., Nakagwa, K., Kusakabe, K., Morooka, S. & Yumura, M. 1992. Change in molecular structure of flash pyrolysis tar by secondary reaction in a fluidized bed reactor. *Fuel Processing Technlogy,* 30:237-248.

Heide, K. & Földvari. 2006. High temperature mass spectrometric gas-release studies of kaolinite $Al_2[Si_2O_5(OH)_4]$ decomposition. *Thermochimica Acta,* 446:106-112.

Herod, A.A. & Stokes, B.J. 1988. Liquid chromatographic mass spectrometric analysis of coal tar fractions. *Analyst*, 113:797-805.

Herod, A.A., Bartle, K.D. & Kandiyoti, R. 2007. Characterisation of heavy hydrocarbons by chromatographic and mass spectrometric methods: An Overview. *Energy & Fuels,* 21:2176-2203.

Herod, A.A., Lazaro, M.J., Domin, M., Islas, C.A. & Kandiyoti, R. 2000. Molecular mass distributions and structural characterisation of coal derived liquids. *Fuel,* 79:323-337.

Herod, A.A., Zhang, S.-F, Johnson, B.R., Bartle, K.D. & Kandiyoti, R. 1996. Solubility limitations in the determination of molecular mass distributions of coal liquefaction and hydrocracking products: 1-methyl-2-pyrrolidinone as mobile phase in size exclusion chromatography. *Energy & Fuels,* 10:743-750.

Herod, A.A., Zhuo, Y. & Kandiyoti, R. 2003. Size-exclusion chromatography of large molecules from coal liquids, petroleum residues, soots, biomass tars and humic substances. *Journal of Biochemical and Biophysical Methods,* 56:335-361.

Hicyilmaz, C., Altun, N.E., Ekmekci, Z. & Gokagac, G. 2004. Pyrite-DTPI interaction as a function of pulp potential and pH. *Colloids and Surfaces A: Physiochemical and Engineering Aspects,* 233:11-24.

Hippo, E. & Walker, P.L. 1975. Reactivity of heat-treated coals in carbon dioxide at 900°C. *Fuel*, 54(4):245-248.

Homann, K.H. & Wagner, H.G. 1967. New aspects of the mechanism of carbon formation in premixed flames. *Proceedings of the Combustion Institute,* 11:371-379.

Hong, Y. & Fegley, B. 1997. The kinetics and mechanism of pyrite thermal decomposition. *Berichte der Bunsengesellschaft für Physikalische Chemie*, 101:1870-1881.

Horne, P.A. & Williams, P.T. 1996. Influence of temperature on the products from the flash pyrolysis of biomass. *Fuel,* 75:1051-1059.

Howard, H.C. 1963. Pyrolytic reactions of coal, contained in Chemistry of coal utilization Lowry, H.H., Ed. Suppl. Vol. Wiley: NY.

Howard, J.B. 1980. Fundamentals of coal Pyrolysis in Chemistry of Coal utilization Elliot, M.A. ed. 2nd Suppl. ed. Wiley

Howard, J.B. 1981. Fundamentals of coal pyrolysis and hydropyrolysis In *Chemistry of Coal Utilization,* Elliot, M.A. Ed. Wiley: New York. p. 665.

Hu, H., Chen, Q., Yin, Z., Zhang, P, Zou, J. & Che, H. 2002. Study on the kinetics of thermal decomposition of mechanically activated pyrites. *Thermochimica Acta,* 389:79-83.

Hu, H., Chen, Q., Yin, Z. & Zhang, P. 2003. Thermal behaviors of mechanically activated pyrites by thermogravimetry (TG). *Thermochimica Acta,* 398:233-240.

Hu, H., Zhou, Q., Zhu, S., Meyer, B. Krzack, S. & Chen, G. 2004. Product distribution and sulphur behaviour in coal pyrolysis. *Fuel Processing Technology,* 85:849-861.

Hu, Y.H. & Ruckenstein, E. 1998. Isotopic GC-MS study of the mechanism of methane partial oxidation to synthesis gas. *Journal of Physical Chemistry A,* 102:10568-10571.

Huffman, G.P. & Huggins, F.E. 1984. Analysis of the inorganic constituents of low-rank coals, in H.H. Schobert (ed.) The Chemistry of Low-Rank coals, American Chemical Society: Washington, Chapter 10.

Huggins, F.E. 2002. Overview of analytical methods for inorganic constituents in coal. *Coal Geology,* 50:169-214.

Hutton, A.C. & Mandile, A.J. 1996. Quantitative XRD measurement of mineral matter in Gondwana coals using the Rietveld method. *Journal of African Earth Sciences,* 23:61-72.

Ibarra, J., Cervero, I. & Moliner, R. 1989. Structural characterisation of low temperature pyrolysis tars and their relation with parent coals. *Fuel Processing Technology*, 22(2):135-149.

Ibarra, J., Moliner, R. & Gavilan, M.P. 1991. Functional group dependence of cross-linking reactions during pyrolysis of coal. *Fuel,* 70(3):406-413.

Iglesias, M.J., Cuesta, M.J. & Suárez-Ruiz, I. 2001. Structure of tars derived from low-temperature pyrolysis of pure vitrinites: influence of rank and composition of vitrinites. *Journal of Analytical and Applied Pyrolysis,* 58-59(2001):255-284.

Ishihara, A., Sutrisna, I.P., Finahari, I., Qian, E.W. & Kabe, T. 2004. Effect of demineralization on hydrogen transfer of coal with tritiated gaseous hydrogen. *Fuel Processing Technology,* 85:887-901.

Islas, C.A., Suelves, I., Li, W., Morgan, T.J., Herod, A.A. and Kandiyoti, R. 2003. The unusual properties of high mass materials form coal-derived liquids. *Fuel,* 82:1813-1823.

ISO (International Organization for Standardization). 1981. Solid mineral fuels - Determination of phosphorus content -- Reduced molybdophosphate photometric method. Geneva: ISO Standards. (ISO 622).

ISO (International Organization for Standardization). 1994a. Methods for the petrographic analysis of bituminous coal and anthracite-Part 2: Preparation of coal samples. Geneva: ISO Standards. (ISO 7404-2).

ISO (International Organization for Standardization). 1994b. Methods for the petrographic analysis of bituminous coal and anthracite-Part 3: Method of determining maceral group composition. Geneva: ISO Standards. (ISO 7404-3).

ISO (International Organization for Standardization). 1994c. Methods for the petrographic analysis of bituminous coal and anthracite-Part 5: Method of determining microscopically the reflectance of vitrinite. Geneva: ISO Standards. (ISO 7404-5).

ISO (International Organization for Standardization). 1999. Solid mineral fuels - Hard coal - Determination of moisture in the general analysis test sample by drying in nitrogen. Geneva: ISO Standards. (ISO 11722).

ISO (International Organisation for Standardisation). 1999. Petroleum products and bituminous materials-determination of water-distillation method. Geneva: ISO Standards. (ISO 3733).

ISO (International Organization for Standardization). 2001. Hard coal and coke – Mechanical sampling – Part 4: Coal – Preparation of test samples. Geneva: ISO Standards. (ISO 13909-4).

ISO (International Organization for Standardization). 2006. Determination of total sulphur through IR spectroscopy. Geneva: ISO Standards. (ISO 19579).

ISO (International Organization for Standardization). 2009. Solid mineral fuels - Determination of gross calorific value by the bomb calorimetric method and calculation of net calorific value. Geneva: ISO Standards. (ISO 1928).

ISO (International Organization for Standardization). 2010. Hard coal and coke - Determination of volatile matter. Geneva: ISO Standards. (ISO 562)

ISO (International Organization for Standardization). 2010. Solid mineral fuels - Determination of ash. Geneva: ISO Standards. (ISO 1171).

ISO (International Organization for Standardization). 2010. Solid mineral fuels - Determination of total carbon, hydrogen and nitrogen-instrumental method. Geneva: ISO Standards. (ISO 29541).

Jeffrey, L.S. 2005. Characterisation of the coal resources of South Africa. *The Journal of The South African Institute of Mining and Metallurgy,* February:95-102.

Jess, A. 1996. Mechanisms and kinetics of thermal reactions of aromatic hydrocarbons from pyrolysis of solid fuels. *Fuel,* 75:1441-1448.

Jiang, J., \Wang, Q., Wang, Y., Weicheng, T. & Xiao, B. 2007. GC-MS analysis of coal tar composition produced from coal pyrolysis. *Bulletin of the Chemical Society of Ethiopia*, 21(2):229-240.

John, P., Johnson C.A.F., Parker, J.E., Smith, G.P., Herod, A.A., Li, C.-Z., Humphery, P., Chapman, J.R. & Kandiyoti, R. 1994. Molecular masses up to 270, 000u in coal and coal-derived products by matrix assisted laser desorption ionization mass spectrometry (MALDI-m.s.). *Fuel,* 73(10):1606-1616.

Johnson, B.R., Bartle, K.D., Domin, M., Herod, A.A. & Kandiyoti, R. 1998. Absolute calibration of size exclusion chromatography for coal derivatives through MALDI-MS. *Fuel,* 77(9/10):933-945.

Jones, J.M., Kubacki, M., Kubica, K., Ross, A.B. & Williams, A. 2005. Devolatilisation characteristics of coal and biomass blends. *Journal of Analytical and Applied Pyrolysis,* 74:502-511.

Jones, J.M., Pourkashanian, M., Rena, C.D. & Williams, A. 1999. Modelling the relationship of coal structure to char porosity. *Fuel,* 78(14):1737-1744.

Jorgensen, F.R.A. & Moyle, F.J. 1986. Gas diffusion during the thermal analyis of pyrite. *Journal of Thermal Analysis and Calorimetry,* 31:145-156.

Jüngten, H. & Van Heek, K.H. 1979. An update of German non-isothermal pyrolysis work. *Fuel Processing Technology,* 2(4):261-293.

Kabe, T., Ishihara, A., Qain, E.W., Sutrisna, I.P & Kabe, Y. 2004. Coal and coal related compounds: Structures, reactivity and catalytic reactions. Amsterdam: Elsevier. 362p.

Kandiyoti, R. Herod, A. & Bartle, K. 2006. Solid fuels and heavy hydrocarbon liquids. Thermal characterisation and analysis. Amsterdam: Elsevier. 353p.

Karaca, S. 2003. Desulfurization of a Turkish lignite at various gas atmospheres by pyrolysis. Effect of mineral matter. *Fuel,* 82:1509-1516.

Karaca, F., Morgan, T.J., George, A., Bull, I.D., Herod, A.A., Millan, M. & Kandiyoti, R. 2009. Molecular mass ranges of coal tar pitch fractions by mass spectrometry and size-exclusion chromatography. *Rapid Communications in Mass Spectrometry,* 23:2087-2098.

Karayildirim, T., Yanik, J., Yuksel, M. & Bockhorn, H. 2006. Characterization of products from pyrolysis of waste sludges. *Fuel,* 85:1498-1508.

Katzer, J.R. & Gates, B.C. 1976. Catalytic processes in fossil fuel conversion – Coal gasification. *AIChE Today Series,* Chicago ITT. Section I-C, December.

Katzman, H. 1974. A research and development program for catalysis in coal conversion processes. *EPRI Report* no. 207-0-0. http://www.fischer-tropsch.org/DOE/DOE_reports/242412/pb242412_sec01.pdf Date of access: 18 September 2014.

Khan, M.R. 1989. A literature survey and an experimental study of coal devolatilization at mild and severe conditions: influences of heating rate, temperature, and reactor type on products yield and composition. *Fuel,* 68:1522-1530.

Kinoshita, C.M., Wang, Y. & Zhou, J.C.. 1995. *Industrial and Engineering Chemistry Resources,* 34: 2949-2954.

Klein, C. 2002. The 22nd edition of the manual of mineral science. 22nd Edition. John Wiley & Sons Inc., USA.

Klein, C. & Hurlbut, H. 1985. Manual of Mineralogy, 21st ed. Wiley: New York.

Klopper, L. 2011. The behaviour of potassium and sodium species during the thermal treatment of a demineralised Highveld coal. Potchefstroom: NWU (Dissertation – MSc.)

Klopper, L., Strydom, C.A. & Bunt, J.R. 2012. Influence of added potassium and sodium carbonates on CO2 reactivity of the char from a demineralized inertinite rich bituminous coal. *Journal of Analytical and Applied Pyrolysis,* 96:188-195.

Koekemoer, A.F. 2009. The influence of minerals content and petrographic composition on the gasification of inertinite-rich, high ash coal. Potchefstroom: NWU. RSA. (Dissertation – M.Eng).

Krivácsy, Z. & Hlavay, J. 1995. Comparison of calibration methods in quantitative diffuse reflectance infrared spectroscopy. *Talanta,* 42(4):613-620.

Kutchko, B.G., Goodman, A.L., Rosenbaum, E., Natesakhawat, S. & Wagner, K. 2013. Characterization of coal before and after supercritical CO_2 exposure via feature relocation using field-emission scanning electron microscopy. *Fuel,* 107:777-786.

Kuznetsov, P.N., Kolesnikova, S.M. & Kuznetsova, L.I. 2013. Steam gasification of different brown coal catalysed by the naturally occurring calcium species. *International Journal of Clean Coal and Energy,* 2:1-11.

Ladner, W.R. 1988. The products of coal pyrolysis: properties, conversion and reactivity. *Fuel Processing Technology,* 20:207-222.

Lafleur A.L., & Nakagawa Y. 1989. Multimode size exclusion chromatography with poly(divinylbenzene) columns and n-methylpyrrolidinone for the characterisation of coal-derived mixtures. *Fuel*, 68:741–52.

Lazaro, M.J., Moliner, R., Suelves, I, Herod, A.A. & Kandiyoti, R. 2001. Characterisation of tars from the co-pyrolysis of waste lubricating oils with coal. *Fuel,* 80(2):179-194.

Leckel, D. 2006. Catalytic hydroprocessing of coal-derived gasification residues to fuel blending stocks: effect of reaction variables and catalyst on hydrodeoxygenation (HDO), hydrodenitrogenation (HDN) and hydrodesulphurization (HDS). *Energy & Fuels*, 20:1761-1766.

Leckel, D. 2008. Hydrodeoxygenation of heavy oils derived from low-temperature coal gasification over NiW catalysts - effect of pore structure. *Energy & Fuels,* 22:231-236.

Leckel, D. 2011. Diesel production in coal-based high-temperature Fischer-Tropsch plants using fixed bed dry bottom gasification technology. *Fuel Processing Technology*, 92:959-969.

Ledesma, E.B., Kalish, M.A., Nelson, P.F., Wornat, M.J. & Mackie, J.C. 2000. Formation and fate of PAH during the pyrolysis and fuel-rich combustion of coal primary tar. *Fuel,* 79:1801-1814.

Ledesma, E.B., Marsh, N.D., Sandrowitz, A. & Wornat, M.J. 2002. An experimental study on the thermal decomposition of cathecol. *Proceedings of the Combustion Institute,* 29: 2299-2306.

Ledesma E.B., Nelson, P.F. & Mackie J.C. 1998. In: *Twenty-Seventh Symposium (International) on Combustion.* The Combustion Institute, Pittsburgh, P.A., p.1687.

Lee, D.H., Yang, H., Yan, R. & Liang, D. 2007. Prediction of gaseous products from biomass pyrolysis through combined kinetic and thermodynamic simulations. *Fuel,* 86:410-417.

Lee, I., Jin, S., Chun, D., Choi, H., Lee, S., Lee, K. & Yoo, J. 2014. Ash-free coal as fuel for direct carbon fuel cell. *Science China, Chemistry,* 57(7):1010-1018.

Lee K.K.-H. 2009. Thermal and catalytic degradation of pyrolytic oil from pyrolysis of municipal plastic wastes. *Journal of Analytical and Applied Pyrolysis,* 85:372-379.

Lemaignen, L., Zhuo, Y., Reed, G.P., Dugwell, D.R. & Kandiyoti, R. 2002. Factors governing reactivity in low temperature coal gasification. Part II. An attempt to correlate conversions with inorganic and mineral constituents. *Fuel,* 81:315-326.

Lessing, R. & Banks, M.A. 1924. The influence of catalysts on carbonization. *Journal of the Chemical Society, London,* 125:2344-2354. http://www.rsc.org/Publishing/Journals/ct/Article.asp?Journal=CT28372&VolumeYear=1924125&Volume=125&JournalCode=CT&MasterJournalCode=CT&Subyear=1924&Issue=0&Type=Issue&Page=290 Date of access: 5 May 2014.

Lessing, R. 1925. The inorganic constituents of coal. *Journal of the Society of Chemical Industry.* 44:227-233.

Levine, S.E. & Broadbelt, L.J. 2009. Detailed mechanistic modelling of high-density polyethylene pyrolysis: Low molecular weight product evolution. *Polymere Degradation & Stability,* 94:810-822.

Li, D., Li, W. & Li, B. 2003. A new hydrogen bond in coal. *Energy & Fuels,* 17: 791-793.

Li, B., Chen, G, Zhang, H. & Sheng, C. 2014. Development of non-isothermal TGA-DSC for kinetics analysis of low temperature coal oxidation prior to ignition. *Fuel,* 118:385-391.

Li, C.Z. 2007. Some recent advances in the understanding of the pyrolysis and gasification behaviour of Victorian brown coal. *Fuel,* 86:1664-1683.

Li, C.Z., Bartle, K.D., Kandiyoti, R. 1993. Vacuum pyrolysis of maceral concentrates in a wire-mesh reactor. *Fuel,* 72(11):1459-1468.

Li, D., Li, W., Chen, H. & Li, B. 2004. The adjustment of hydrogen bonds and its effect on pyrolysis property of coal. *Fuel Processing Technology,* 85:815-825.

Li, F., Chang, L.-P., Wen, P. & Xie, K.C. 2001. Simulated distillation of coal tar. *Energy Sources,* 23:189-199.

Li, H.B., Yang, Z.Y., Lv, H., Wang, Y & Zhang, B. 1998. *Journal of Fuel Chemistry and Technology,* 26:389-394.

Li, W., Bai, Z., Bai, J. & Guo, Z. 2011. Decomposition kinetics of hydrogen bonds in coal by a new method of in-situ diffuse reflectance FT-IR. *Journal of Fuel Chemistry and Technology,* 39(5):321-327.

Li, Y., Lu, G.Q. & Rudolph, V. 1999. Compressibility and fractal dimension of fine coal particles in relation to pore structure characterisation using mercury porosimetry. *Particle and Particle Systems Characterization,* 16:25-31.

Liu, G., Benyon, P., Benfell, K.E., Bryant, G.W., Tate, A.G., Boyd, R.K., Harris, D.J. & Wall, T.F. 2001. The porous structure of bituminous coal chars and its influence on combustion and gasification under chemically controlled conditions. Fuel, 79:617-626.

Liu, H. 2009. Combustion of Coal chars in O_2/CO_2 and O_2/N_2 mixtures: A comparative study with non-isothermal thermogravimetric analyzer (TGA) tests. *Energy & Fuels,* 23:4278-4285.

Liu, Y., Gupta, R. & Wall, T. 2007a. A comparison of CCSEM and QEMSCAN analysis of pulverized coal. *Cooperative Research Centre for Coal in Sustainable Development,* Research report 71. Available at: http://trove.nla.gov.au/work/33533327?selectedversion= NBD43194403 Accessed on: 4 April 2014.

Liu, Y., Gupta, R., Sharma, A., Wall, T., Butcher, A., Miller, G., Gottlieb & French, D. 2005. Mineral matter- organic matter association characterisation by QEMSCAN and applications in coal utilisation. *Fuel,* 84:1259-1267.

Liu, Q., Hu, H., Zhou, Q., Zhu, S. & Chen, G. 2004a. Effect of inorganic matter on reactivity and kinetics of coal pyrolysis. *Fuel,* 83:713-718.

Liu, Q., Hu, H., Zhou, Q., Zhu, S. & Chen, G. 2004b. Effect of mineral on sulphur behaviour during coal pyrolysis. *Fuel,* 85:863-871.

Liu, F., Li, W., Chen, H. & Li, B. 2007b. Uneven distribution of sulphurs and their transformation during coal pyrolysis. *Fuel*, 86:360-366.

Longwell, J.P., Rubin, E.S. & Wilson, J. 1995. Coal: Energy for the future. *Progressive Energy Combustion Science*, 21:269-360.

Lopez-Urionabarrenechea, A., De Marco, I., Caballero, B.M., Adrados, A & Laresgoiti, M.F. 2012. Empiric model for te prediction of packaging waste pyrolysis yields. *Applied Energy,* 98:524-532.

Lowry, H.H. (Ed.) 1945. Chemistry of Coal Utilization Vol. II. Committee on Chemical utilization of Coal, National Research Council. New York: Wiley.

Lowry, H.H. (Ed.) 1963. Chemistry of coal utilization. 2nd Supplementary Volume. Wiley, New York. pp. 983-1002, Chapter 16.

Lu, M. & Mulholland, J.A. 2004. PAH growth from the pyrolysis of CPD, indene and naphthalene mixture. *Chemosphere,* 55:605-610.

Lu, Q, Zhang, Z.-F., Dong, C.-Q., & Zhu, X.-F. 2010. Catalytic upgrading of biomass fast pyrolysis vapors with nano metal oxides: An analytical Py-GC-MS study. *Energies,* 3:1805-1820.

Ma, Z., Bai, J., Li, W., Bai, Z. & Kong, L. 2013. Mineral transformation in char and its effect on coal char gasification reactivity at high temperatures, Part 1: Mineral transformation in char. *Energy & Fuels,* 27: 4545-4554.

Machnikowska, H., Krztoń, A. & Machnikowski, J. 2002. The characterization of coal macerals by diffuse reflectance infrared spectroscopy. *Fuel,* 81:245-252.

Madejová, J. & Komadel, P. 2001. Baseline studies of the clay minerals society source clays: Infrared models. *Clays and Clay Minerals,* 49(5):410-432.

Mahlaba, J.S., Kearsley, E.P. & Kruger, R.A. 2011. Physical, chemical and mineralogical characterisation of hydraulically disposed fine coal ash from Sasol Synfuels. *Fuel,* 90:2491-2500.

Maitra, S., Choudry, A., Das, H.S. & Pramanik, MS. J. 2005. Effect of compactation on the kinetics of thermal decomposition of dolomite under non-isothermal condition. *Journal of Materials Science,* 40:4749-4751.

Maity, S. & Mukherjee, P. 2006. X-ray structural parameters of some Indian coals. Current Science, 91:337-340.

Makó, E., Frost, R.L., Kristóf, J. & Horváth, E. 2001. The effect of quartz content on the mechanochemical activation of kaolinite. *Journal of Colloid and Interface Science,* 244:359-364.

Malumbazo, N., Wagner, N.J. & Bunt, J.R. 2012. The petrographic determination of reactivity differences of two South African inertinite-rich lump coals. Journal of Analytical and Applied Pyrolysis, 93:139-146.

Malumbazo, N., Wagner, N.J., Bunt, J.R., Van Niekerk, D. & Assumption, H. 2011. Structural analysis of chars generated from South African inertinite coals in a pipe-reatcor combustion unit. *Fuel Processing Technology,* 92:743-749.

Maphala, T. & Wagner, N.J. 2012. Effects of CO_2 storage in coal on coal properties. *6th Trondheim Carbon Capture and Storage Conference (TCCS-6), Energy Procedia,* 23:426-438.

Martens, W.N., Frost, R.L., Kristof, J. & Horvath, E. 2002. Modification of kaolinite surfaces through intercalation with deuterated dimethylsulfoxide. *Journal of Physical Chemistry B,* 106:4162-4171.

Marzec, A. 2002. Towards an understanding of the coal structure: a review. *Fuel Processing Technology,* 77-78:25-32.

Mastral, A.M., Callen, M.S., Garcia, T. & Navarro, M.V. 2000. Improvement of liquids from coal - tire co-thermolysis. Characterisation of the obtained oils. *Fuel Processing Technology,* 64:135-140.

Mastral, J.F., Berrueco, C. and Ceamanos, J. 2007. Modelling of the pyrolysis of high density polyethylene. Product distribution in a fluidized bed reactor. *Journal of Analytical and Applied Pyrolysis,* 79:313-322.

Matjie, R.H., French, D., Ward, C.R., Pistorius, P.C. & Li, Z. 2011. Behaviour of coal mineral matter in sintering and slagging of ash during the gasification process. *Fuel Processing Technology,* 92:1426-1433.

Matjie, R.H., Li, Z., Ward, C.R. & French, D. 2008. Chemical composition of glass and crystalline phases in coarse coal gasification ash. *Fuel,* 87:857-869.

Matjie, R.H. & Van Alphen, C. 2008. Mineralogical features of size and density fractions in Sasol coal gasification ash, South Africa and potential by-products. *Fuel,* 87:1439-1445.

Matjie, R.H., Van Alphen, C. & Pistorius, P.C. 2006. Mineralogical characterisation of Secunda gasifier feedstock and coarse ash. *Minerals Engineering,* 19:256-261.

Matshuhashi, H., Asari, K. and Arata, K. 2001. Catalytic activities of calcined iron sulfates for hydrocracking of model compounds of coal. *Energy & Fuels,* 15:1523-1527.

Matshuhashi, H., Nakamura, K., Arata, K., Yoshida, R. and Maekawa, Y. 1997. Catalytic activities of metal oxides containing iron for hydrocracking coal model compounds and Taiheiyo coal. *Fuel,* 76:913-918.

Matteson, A. & Herron, M.M. 1993. Quantitative mineral analysis by Fourier transform infrared spectroscopy, *SCA Conference paper*, 9308. http://www.scaweb.org/assets/papers /1993_papers/1-SCA1993-08.pdf Date of access: 14 July 2014.

Matusik, J. & Klapyta, Z. 2013. Characterization of kaolinite intercalation compounds with benzylalkylammonium chlorides using XRD, TGA/DTA and CHNS elemental analysis. *Applied Clay Science,* 83-84:433-440

Mayoral, M.C., Izquierdo, M.T., Andrés, J.M. & Rubio, B. 2001. Different approaches to proximate analysis by thermogravimetric analysis. *Thermochimica Acta,* 370:91-97.

McKee, D.W. 1980. Catalytic effects of alkaline earth carbonates in the carbon-carbon dioxide reaction. *Fuel,* 59:308-315.

McLennan, A.R., Bryant, G.W., Stanmore, B.R. & Wall, T.F. 2000. Ash formation mechanisms during pf combustion in reducing conditions. *Energy & Fuels,* 14:150-159.

McMillen, D.F., Malhorta, R. & Nigenda, S.E. 1989. The case for induced bond scission during coal pyrolysis. *Fuel,* 68(3):380-386.

Mead, D.W. 1979. Thermal cracking of aromatic and heteroaromatic compounds over lime. *(S.M. Thesis* – MIT).

Menéndez, R., Blanco, C., Santamaría, R., Domínguez, A., Blanco, C.G., Suelves, I., Herod, A.A., Morgan, T.G. & Kandiyoti, R. 2002. Effects of air-blowing on the molecular size and structure of coal-tar pitch components. *Energy & Fuels,* 16:1540-1549.

Meng, X, De Jong, W., Pal, R. & Verkooijen, A.H.M. 2010. In bed and downstream hot gas desulphurization during solid fuel gasification: A review. *Fuel Processing Technology,* 91(8): 964-981.

Mill, C. 2000. Pyrolysis of fine coal particles at high heating rate and pressure. Sydney (PhD thesis – University of New South Wales).

Milne, T.A., Evans, R.J. & Abatzouglou, N. 1998. Biomass gasifier "tars": Their nature, formation and conversion [NREL/TP-570-25357]. www.nrel.gov/docs/fy99osti/25357.pdf Date of access: 27 July 2014.

Min, F.F., Zhang, M.X., Zhang, Y., Cao, Y. & Pan, W.P. 2011. An experimental investigation into gasification reactivity and structure of agricultural waste chars. *Journal of Analytical and Applied Pyrolysis,* 92:250-257.

Mindat. 2012a. Gibbsite. www.mindat.org/min-1689.html. Date of access: 3 April 2014.

Mindat. 2012b. Pyrite. www.mindat.org/min-3314.html. Date of access: 3 April 2014.

Mindat. 2012c. Siderite. www.mindat.org/min-3647.html. Date of access: 3 April 2014.

Mindat. 2012d. Calcite. www.mindat.org/min-859.html. Date of access: 3 April 2014.

Mindat. 2012e. Dolomite. www.mindat.org/min-1304.html. Date of access: 3 April 2014.

Mindat. 2012f. Apatite. www.mindat.org/min-29229.html. Date of access: 3 April 2014.

Mindat. 2012g. Kaolinite. www.mindat.org/min-2156.html. Date of access: 3 April 2014.

Mindat. 2012h. Quartz. www.mindat.org/min-3337.html. Date of access: 3 April 2014.

Mindat. 2012i. Illite. www.mindat.org/min-2815.html. Date of access: 3 April 2014.

Mindat. 2012j. Microcline. www.mindat.org/min-2704.html. Date of access: 3 April 2014.

Mindat. 2012j. Rutile. www.mindat.org/min-3486.html. Date of access: 3 April 2014.

Mindat. 2012l. Gorceixite. www.mindat.org/min-1727.html. Date of access: 3 April 2014.

Ming, H. & Spark, K.M. 2003. Radio frequency plasma-induced hydrogen bonding on kaolinite. *Journal of Physical Chemistry B,* 107:694-702.

Miranda, M., Pinto, F., Gulyurtlu, I., Cabrita, I., Nogueira, C.A. and Matos, A. 2010. Response surface methodology optimization applied to rubber tyre and plastic wastes thermal conversion. *Fuel,* 89:2217-2229.

Miura, K., Hashimoto, K. & Silveston, P.L. 1989. Factors affecting the reactivity of coal chars during gasification, and indices representing reactivity. *Fuel,* 68:1461-1475.

Miura, K., Mae, K., Li, W., Kusakawa, T., Morozumi, F. & Kumano, A. 2001. Estimation of hydrogen bond distribution in coal through the analysis of OH stretching bands in diffuse reflectance infrared spectrum measured by in-situ technique. *Energy & Fuels,* 15:599-610.

Mokoena, K., Van der Walt, T.J., Morgan, T.J., Herod, A.A. & Kandiyoti, R. 2008. Heat treatment of medium-temperature Sasol-Lurgi gasifier coal-tar pitch for polymerising to higher value products. *Fuel,* 87:751-760.

Moliner, R., Ibarra, J. & Lagarma, M.D. 1989. Size exclusion chromatography of pyrolysis and gydropyrolysis tars from Spanish low rank coal. *Fuel,* 68:1487-1488.

Mondragon, F., Jaramillo, A, Saldarriaga, F., Quintero, G., Fernandez, J., Ruiz, W. & Hall, P.J. 1999. The effects of morphological changes and mineral matter on H_2S evolution during coal pyrolysis. *Fuel,* 78:1841-1846.

Morf, P.O., Hasler, P. & Nussbaumer, T. 2002. Mechanisms and kinetics of homogeneous secondary reactions of tar from continuous pyrolysis of wood chips. *Fuel,* 81:843-851.

Morgan, M.E. & Jenkins, R.G. 1986a. Pyrolysis of a lignite in an entrained flow reactor. 1. Effect of metal cations on decarboxylation and tar yield. *Fuel,* 65:764-768.

Morgan, M.E. & Jenkins, R.G. 1986b. Pyrolysis of a lignite in an entrained flow reactor. 1. Effect of cations on total weight loss. *Fuel,* 65:757-763.

Morgan, T.J. 2008. Molecular mass of structural characterisation of heavy hydrocarbon materials. London: Imperial College (Dissertation - PhD).

Mukherjee. D.K. & Choudhury, P.B. 1976. Catalytic effect of mineral matter in North Assam coal on hydrogenation. *Fuel,* 55: 4-8.

Mun, T.Y., Kim, J-W. & Kim, J-S. 2012. Air gasification of railroad wood ties treated with creosote: Effects of additives and their combination on the removal of tar in a two-stage gasifier. *Fuel,* 102:326-332.

Murakami, K., Shirato, H. & Nishiyamat, Y. 1997. In-situ infrared spectroscopic study of the effects of exchanged cations on thermal decomposition of a brown coal. *Fuel,* 76:655-661.

Naito, S., Takada, A. Tokizawa, S. & Miyao, T. 2005. Mechanistic study on the methane activation of various supported molybdenum carbide caralysts with isotopic tracer methods. *Applied Catalysis A,* 289:22-27.

Nath, S.K., Bordoloi, S. & Dutta, R.K. 2011. Effect of acid on morphology of calcite during acid enhanced deflouridation. *Journal of Fluorine Chemistry,* 132:19-26.

Nel, M.V. 2009. The influence of coal-associated trace elements on sintering and agglomeration of a model coal mineral mixture. Potchefstroom: NWU. (Dissertation - PhD).

Nel, M.V., Strydom, C.A., Schobert, H.H.. Beukes, J.P. & Bunt, J.R. 2014. Reducing atmosphere ash fusion temperatures of a mixture of coal-associated minerals – The effect of inorganic additives and ashing temperature. *Fuel Processing Technology,* 124:78-86.

Nelson, J.B. 1953. Assessment of the mineral species associated with coal. *BCURA Monthly Bulletin,* 17:41.

Nelson, P.F. & Tyler, R.J. 1988. Formation of light gases and aromatic species during the rapid pyrolysis of coal. *Proceedings of the Combustion institute,* 21(1):427-453.

Nelson, P.F., Smith, I.W., Tyler, R.J. & Mackie, J.C. 1988. Pyrolysis of coal at high temperatures. *Energy & Fuels,* 2(4):391-400.

Neves D., Thunman, H, Matos, A., Tarelho, L. & Gómez-Barea, A. 2011. Characterization and prediction of biomass pyrolysis products. *Progress in Energy and Combustion Science,* 37:611-630.

Nisar, J., Niamat, U., Awan, I.A., Khan, K. & Ahamd, I. 2011. Characterization of the products obtained in coal pyrolysis: A case study of some Pakistani coals. *Iranian Journal of Chemistry and Chemical Engineering,* 30(3):53-56.

Nomura, S. & Thomas, K.M. 1997. Fundamental aspects of coal structural changes in the thermoplastic phase. *Fuel,* 77(8):829-836.

Nosyrev, I.E., Gruber, R., Cagniant, D., Krzton, A., Pajak, J., Stefanova, M.D. & Grishchuk, S. 1996. DRIFT spectroscopic characterization of coal samples modified by chemical treatments. *Fuel,* 75(13):1549-1556.

Oboirien, B.O., Engelbrecht, A.D., North, B.C., Du Cann, V.M., Verryn, S. & Falcon, R. 2011. Study on the structure and gasification characteristics of selected South African bituminous coals in fluidised bed gasification. *Fuel Processing Technology,* 92:735-742.

Ode, W.H. 1963. Coal analysis and mineral matter contained in Chemistry of coal utilization Lowry, H.H., Ed. Suppl. Vol. Wiley: NY.

O'Gorman, J.V. & Walker, P.L. 1972. Mineral matter and trace elements in US coals. OCR R&D Report 61, Interim Report 2.

Okolo, G.N. 2010. The effects of chemical and physical properties of chars derived from inertinite-rich, high ash coal on gasification reaction kinetics. Potchefstroom – NWU (Dissertation - M.Eng).

Onwudiwe, D.C., Arfin, T., Strydom, C.A. & Kriek, R.J. 2013. Synthesis, spectroscopic characterization and behaviour

of AC impedance spectroscopy of Cd (II) bis(N-para-methylphenyl dithiocarbamate). *Electrochimica Acta,* 104:19-25.

Orio, A., Corella, J.. & Narvaz, I. 1997. Performance of different dolomites on hot raw gas cleanining from biomass gasificaqtion with air. *Industrial and Engineering Chemistry Research,* 36:3800-3808.

Orrego-Ruiz, J.A., Cabanzo, R. & Mejía-Ospino, E. 2011. Study of Colombian coals using photoacoustic Fourier transform infrared spectroscopy. *Internation Journal of Coal Geology,* 85:307-310.

Ortiz, A.L. & Harrison, D.P. 2001. Hydrogen production using sorption enhanced reaction. *Industrial Engineering and Chemistry Research,* 40:5102-5109.

Otake, Y. & Walker Jr, P.L. 1993. Pyrolysis of acid washed and metal cation loaded lignites. *Fuel,* 72:139-149.

Öztas, N.A. & Yürüm, Y. 2000. Pyrolysis of Turkish Zonguldak bituminous coal. Part 1. Effect of mineral matter. *Fuel,* 79:1221-1227.

Padrick, T.D. 1984. An overview of mineral matter catalysis of coal conversion. *ACS Fuel Chemistry Preprints,* 29(4): 270-273. https://web.anl.gov/PCS/acsfuel/preprint%20archive/Files/29_4_PHILADELPHIA_08-84_0270.pdf. Date of access: 2014/08/31.

Painter, P.D., Sobkowiak, M. & Youtcheff, J. 1987. Study of hydrogen bonding in coal. *Fuel,* 66: 973-978.

Painter, P.C., Snyder, R.W., Starsinic, M., Coleman, M.M., Kuehn, D.W. & Davis, A. 1981. Concerning the application of FT-IR to the study of coal: a critical assessment of band

assignments and the application of spectral analysis programs. *Applied Spectroscopy,* 35(5):475-485.

Painter, P.C., Starsinic, M. & Coleman, M. 1985. Fourier Transform Infrared Spectroscopy – Applications to Chemical Systems; Ferraro J.R. and Rasile, L.J., Eds.; Academic Press, Inc.: New York, Vol 4, p.196.

Pan, C., Jiang, L., Liu, J., Zhang, S. & Zhu, G. 2010. The effects of calcite and montmorillonite on oil cracking in confined pyrolysis experiments. *Organic Geochemistry,* 41:611-626.

Pant, K.K. & Kunru, D. 1997. Pyrolysis of methylcyclohexane: kinetics and modelling. *Chemical Engineering Journal,* 67:123-129.

Pérez, P., Aznar, P.M., Caballero, M.A., Gill, J., Martin J.A. & Corella, J. 1997. Hot gas cleaning and upgrading with a calcined dolomite located downstream a biomass fluidized bed gasifier operating with steam-oxygen mixtures. *Energy & Fuels,* 11: 1194-1203.

Pinetown, K.L., Ward, C.R. & Van der Westhuizen, W.A. 2007. Quantitative evaluation of minerals in coal deposits in the Witbank and Highveld coalfields, and the potential impact on acid mine drainage. *Coal Geology,* 70:166-183.

Pinheiro, H.J. 1999. A techno-economic and historical review of the South African coal industry in the 19th and 20th centuries AND analyses of coal product samples of South African collieries 1998-1999. (In Bulletin 113. SABS: Pretoria. 97p.) SANS.

Pinto, F., André, R.N., Franco, C., Lopes, H., Gulyurtlu, I & Cabrita, I. 2009. Co-gasification of coal and wastes in a pilot-scale installation 1: Effect of catalysts in syngas treatment to achieve tar abatement. *Fuel,* 88:2392-2402.

Pinto, F, Lopes, H., André, R.N., Gulyurtlu, I & Cabrita, I. 2007. Effect of catalysts in the quality of syngas and by-products obtained by co-gasification of coal and wastes. 1. Tars and nitrogen compounds abatement. *Fuel,* 86:2052 - 2063.

Pokrovsky, O.S., Mielczarski, J.A., Barres, O. & Schott, J. 2000. Surface speciation models of calcite and dolomite/aqueous solution interfaces and their spectroscopic evaluation. *Langmuir,* 16:2677-2688.

Povarennykh, A.S. 1978. The use of infrared spectra for the determination of minerals. *American Mineralogist,* 63:956-959.

Prins, M.J., Ptasinki, K.J. and Janssen, F.J.J.G. 2007. From coal to biomass gasification: comparison of thermodynamic efficiency. *Energy,* 32:1249-1259.

Prinsloo, C.B. 2008. A study into the fundamental understanding of iron-transformations and the effect of iron as fluxing agent on Highveld fine coal sources during gasification. Potchefstroom: NWU. (Dissertation - MSc)

Probstein, R.F. & Hicks, R.E. 2006. Synthetic Fuels. New York: McGraw-Hill.

Ptáček, P., Kubátová, D., Havlica, J., Brandštetr, J., Šoukal, F. & Opravil, T. 2010a. The isothermal kinetic analysis of the thermal decomposition of kaolinite: The thermogravimetric study. *Thermochimica Acta,* 501:24-29.

Ptáček, P., Kubátová, D., Havlica, J, Brandštetr, J., Šoukal, F. & Opravil, T. 2010b. The non-isothermal kinetic analysis of the thermal decomposition of kaolinite by thermogravimetric analysis. *Powder Technology,* 204:222-227.

Pusz, S., Krzton, A., Komraus, J.L., Martinez-Tarazona, M.R., Martinez-Alonso, A. & Tascon, J.M.D. 1997. Interactions between organic matter and minerals in two bituminous coals of different rank. *Coal Geology,* 33:369-386.

Putun, E. 2010. Catalytic pyrolysis of biomass: Effect of pyrolysis temperature, sweping gas flow rate and MgO catalyst. *Energy,* 35: 2761-2766.

Qi, Y., Li, W., Chen, H. & Li, B. 2004. Desulfurization of coal through pyrolysis in a fluidized-bed reactor under nitrogen and 0.6% O_2-N_2 atmosphere. *Fuel,* 83:705-712.

Raask, E. 1985. Mineral impurities in coal combustion. Hemisphere Publishing Corporation, Washington.

Rafenomanantsoa, A., Nicole, D., Rubini, P. & Lauer, J.C. NMR and FIMS structural analysis of the oil obtained from the pyrolysis of Bemolanga tar-sand bitumen (Madagascar) according to a post combustion process. *Fuel,* 77(1/2):33-41.

Rand, S.J. 2003. Significance of tests for petroleum products. 7th ed. Bridgeport: ASTM International. 262p.

Reichel, D., Klinger, M., Krzack, S. & Meyer, B. 2013. Effect of ash components on devolatilization behaviour of coal in comparison with biomass – Product yields, composition, and heating values. *Fuel,* 114:64-70.

Reifenstein, A.P., Kahraman, H., Coin, C.D.A., Calos, N.J., Miller, G. & Uwins, P. 1999. Behaviour of selected minerals ~ in an improved ash fusion test: quartz, potassium feldspar, kaolinite, illite, calcite, dolomite, siderite, pyrite and apatite. *Fuel*, 78:1449-1461.

Reucrofta, P.J., Patel, K.B. 1983. Surface area and swellability of coal. *Fuel,* 62(3):279-284.

Rivera-Utella, J., López-Ramón, M.V., Carrasco-Marìn, Maldonado-Hódar, F.J. & Moreno-Castilla, C. 1996. Demineralization of a bituminous coal by froth flotation before obtaining acitvated carbons. *Carbon,* 34(7):917-921.

Rodriguez-Navarro, A. & Ortega-Huertas, M. 2009. Thermal decomposition of calcite: Mechanisms of formation and textural evolution of CaO nanocrystals. *American Mineralogist,* 94:578-593.

Roets, L., Bunt, J.R., Neomagus, H.W.J.P. & Van Niekerk, D. 2014. An evaluation of a new automated duplicate-sample Fischer Assay setup according to ISO/ASTM standard and analysis of the tar fraction. *Journal of Analytical and Applied Pyrolysis,* 106:190-196.

Ross, D.S., Green, T.K., Mansani, R. & Hum, G.P.. 1987. Coal conversion in water: 1. Conversion Mechanism. *Energy & Fuels,* 1:287-291.

Ruiz, B., Parra, J.B., Pajares, J.A. & Pis, J.J. 2001. Study of porous devolpment in pyrolysis chars obtained from a low-volatile coal. *Journal of Analytical and Applied Pyrolysis,* 58-59:873-886.

Ryan, B. 1997. Fluidity of western Canadian coals and its relationship to other coal and coke properties. *British Columbia Geological Survey Geological Fieldwork,* 27:1-17.

Saghafi, A., Pinetown, K.L., Grobler, P.G. & Van Heerden, J.H.P. 2008. CO_2 storage potential of South African coals and gas entrapment enhancement due to igneous intrusions. *Coal Geology,* 73:74-87.

Saha, B. & Ghoshal, A.K. 2005. Thermal degradation kinetics of poly(ethylene terephthalate) from waste soft drink bottles. *Chemical Engineering Journal,* 111:39-43.

Saha, B., Karthik Reddy, P. & Ghoshal, A.K. Hybrid genetic algorithm to find the best model and the globally optimized overall kinetics parameters for themal decomposition of plastics. *Chemical Engineering Journal,* 138:20-29.

Saikia, B.K., Boruah, R.K., Gogoi, P.K. & Baruah, B.P. 2009. A thermal investigation on coals from Assam (India). *Fuel Processing Technology,*90:196-203.

Sakuneka, T.M., Nel, R.J.J. & De Klerk, A. 2008. Benzene reduction by alkylation in a solid phosphoric acid catalyzed olefin oligomerization process. *Industrial and Engineering Chemistry Research,* 47:7178-7183.

Samaras, P., Diamadopoulos, E. & Sakellaropoulos, P. 1991. The effect of demineralization on lignite activation. *Carbon,* 29(8):1181-1190.

Samaras, P., Diamadopoulos, E. & Sakellaropoulos, G.P. 1996. The effect of mineral matter and pyrolysis conditions on the gasification of Greek lignite by carbon dioxide. *Fuel,* 75:1108-1114.

SANS (South African National Standards). 1974. Brown coals and lignites - Determination of the yields of tar, water, gas and coke residue by low temperature distillation. Pretoria: SABS, Standards Division. (SANS 647:1974)

Schafer, H.N.S. 1979a. Pyrolysis of brown coals. 1. Decomposition of acid groups in coal containing carboxyl groups in the acid and cation forms. *Fuel,* 58:667-6772

Schafer, H.N.S. 1979b. Pyrolysis of brown coals. 1. Decomposition of acidic groups on heating in the range 100-900°. *Fuel,* 58:673-679.

Schafer, H.N.S. 1980. Pyrolysis of brown coals. 3. Effect of cation content on the gaseous products containing oxygen from Yallourn coal. *Fuel,* 59:295-301.

Scheer, A.M., Mukarate, C., Robichaud, D.J., Ellison, B. & Nimlos, M.R. 2010. Radical chemistry in the thermal decomposition of anisole and deuterated anisoles: an investigation of aromatic growth. *Journal of Physical Chemistry,* 114:9043-9050.

Scheer, A.M., Mukarate, C., Robichaud, D.J., Ellison, B. & Nimlos, M.R. 2011. Thermal decomposition mechanism of the metoxyphenols: formation of phenol, cyclopentadiene, vinylacetylene and acetylene. *Journal of Physical Chemistry,* 115:13381-1389

Schlosberg, R.H. 1985. Chemistry of coal conversion. Ney York: Plenum Press. 336p.

Schobert, H.H. 1990. The chemistry of hydrocarbon fuels. Cornwall: Butterworths. 352p.

Schobert, H.H. 1992. Catalytic and chemical behaviour of coal mineral matter in the coal conversion process. In *Clean Utilization of coal,* Y. Yürüm (ed.), Kluwer Academic publishers: Dordrecht, Netherlands. p. 65 – 73.

Sciazko, M. & Kubica, K. 2002. The effect of dolomite addition on sulphur, chlorine and hydrocarbon distribution in a fluid-bed mild gasification of coal. *Fuel Processing Technology,* 77-78:95-102.

Seo, D.K., Park, S.S., Kim, Y.T., Hwang, J. & Yu, T-.U. 2011. Study of coal pyrolysis by thermo-gravimetric analysis (TGA) and concentration measurements of the evolved species. *Journal of Analytical and Applied Pyrolysis,* 92: 209-216.

Sert, M., Ballice, L., Yüksel, M. & Sağlam, M. 2011. Effect of demineralization on product yield and composition at isothermal pyrolysis of Eynez lignites. *Industrial and Engineering Chemistry Resources,* 50:10400-10406.

Seshadri, K.S. & Shamsi, A. 1998. Effect of temperature, pressure and carrier gas on the cracking of coal tar over a char-dolomite mixture and calcined dolomite in a fixed-bed reactor. *Industrial and Engineering Chemistry Research,* 37:3830-3837.

Sharma, R.K. & Hajaligol, M.R. 2003. Effect of pyrolysis conditions on the formation of polycyclic aromatic hydrocarbons (PAHs) from polyphenolic compounds. *Journal of Analytical and Applied Pyrolysis,* 66:123-144.

Shen, C., Lin, W., Wu, S., Tong, X. & Song, W. 2009. Experimental study of the combustion characteristics of bituminous char derived under mild pyrolysis conditions. *Energy & Fuels,* 23:5322-5330.

Shi, L., Liu, Q., Guo, X., Wu, W. & Liu, Z. 2013. Pyrolysis behaviour and bonding information of coal – A TGA study. *Fuel Processing Technology,* 108:125-132.

Shi, L., Liu, Q., Guo, X., He, W. & Liu, Z. 2014. Pyrolysis of coal in TGA: Extent of volatile condensation in crucible. *Fuel Processing Technology,* 121:91-95.

Shirazi, A.R., Börtin, O., Eklund, L. & Lindqvist, O. 1995. The impact of mineral matter in coal on its combustion, and a new approach to the determination of the calorific value of coal. *Fuel,* 74:247-251.

Simell, P.A., Leppälahti, J.K. & Bredenberg, J.B. 1992. Catalytic purification of tarry fuel gas with carbonate rocks and ferrous materials. *Fuel,* 71:211-218.

Sing, K.S.W., Everett, D.H., Haul, R.A.W., Moscou, L., Pierrotti, R.A., Rouquerol, J. & Siemieniewska, T. 1985. Reporting physisorption data for gas/solid systems; with special reference to the determination of surface are and porosity. *Pure Applied Chemistry,* 57:603-619.

Singh, S., Wu, C. & Williams, P.T. 2012. Pyrolysis of waste materials using TGA-MS and GA-FTIR as complementary characterisation techniques. *Journal of Analytical and Applied Pyrolysis,* 94:99-107.

Siva, M., Onenc, S., Uçar, S. & Yanik, J. 2013. Influence of oily wastes on the pyrolysis of scrap tire. *Energy Conversion and Management,* 75: 474-481.

Slaghuis, J.H. & Raijmakers, N. 2004. The use of thermogravimetry in establishing the Fischer tar of a series of South African coal types. *Fuel,* 83:533-536.

Slaghuis, J.H., Ferreira, L.C. & Judd, M.R. 1991. Volatile matter in coal: effect of inherent mineral matter. *Fuel,* 70:471-473.

Slater, P.N., Richards, G.H. & Harb, J.N. 1995. Pyrite and illite associations in two eastern US bituminous coals. *Fuel Processing Technology,* 44:55-69.

Smith, K.L., Smoot, L.D., Fletcher, T.H. & Pugmire, R.J. 1994. The structure and reaction processes of coal. New York: Plenum Press. 473p.

Solomon, P.R. & Hamblen, D.G. 1985. Chapter 5: Pyrolysis. In *Chemistry of coal conversion.* Schlosberg, R.H., ed. New York: Plenum press. p. 121-251.

Solano, A.L., Mahajan, O.P. & Walker, P.L. 1977. Carbon decomposition from methane over minerals. *Fuel,* 56:452-455.

Solomon, P.R., Fletcher, T.H. & Pugmire, R.J. 1993. Progress in coal pyrolysis. *Fuel,* 72:587-597.

Solomon P.R., Hamblen D.G. & Yu, Z.Z.. 1990. Network models of coal thermal decomposition. *Fuel,* 68(3):754-763.

Solomon, P.R., Hamblen, D.G. & Carangelo, RM. 1988. General model of coal devolatilisation. *Energy & Fuels*, 2(4):405-422.

Song, C. & Moffat. 1994. Zeolite-catalysed ring-shift isomerisation of sym-octahydrophenanthrene and conformational isomerisation of sym-decahydronaphthalene. *Microporous Materials,* 2:459-466.

Song, C. & Schobert, H.H. 1993. Opportunities for developing speciality chemicals and advanced materials from coal. *Fuel Processing Technology,* 34(2):157-196.

Sobkowiak, M. & Painter, P. 1995. A comparison of Drift and KBr pellet methodologies for the quantitative analysis of functional groups in coal by infrared spectroscopy. *Energy & Fuels,* 9:359-363.

South Africa. Department of Mineral Resources. 2009. Developments in the economic contribution of hydrocarbons, natural gas and coal. Pretoria.

Speight, J.G. 1994. The chemistry and technology of coal. 2nd Ed. New York: Marcel Dekker. 642p.

Speight, J.G. 2005. Handbook of coal analysis. Vol. 166. USA: John Wiley & Sons Ltd. 238p.

Stanton, R.W., Warwick, P.D. & Swanson, S.M. 2005. Tar yields from low-temperature carbonization of coal facies from the Powder River Basin, Wyoming, USA. *International Journal of Coal Geology,* 63:13-26.

Steel, K.M. & Patrick, J.W. 2001. The production of ultra clean coal by chemical demineralisation. Fuel, 80:2019-2023.

Strydom, C.A., Bunt, J.R., Schobert, H.H. & Raghoo, M. 2011. Changes to the organic functional groups of an inertinite rich medium rank bituminous coal during acid treatment processes. *Fuel Processing Technology,* 92:764-770.

Su, S., Pohl, J.H., Holcombe, D. & Hart, J.A. 2001. Techniques to determine ignition, flame stability and burnout of blended coals in p.f. power station boilers. *Progress in Energy and Combustion Science,* 27(1):75-98.

Suelves, I., Moliner, R. & Lázaro, M.J. 2000. Synergetic effects in the co-pyrolysis of coal and petroleum residues: Influences of coal mineral matter and petroleum ratio. *Journal of Analytical and Applied Pyrolysis,* 55:29-41.

Sun, Y., Jiang, J., Kantarelis, E., Xu, J. Li. L., Zhao, S. & Yang, W. 2012a. Development of a bimetallic dolomite based tar cracking catalyst. *Catalysis Communications,* 20:36-40.

Sun, M., Ma, X.X., Cao, W., Du, P.-P., Yang, Y.-H. & Xu, L. 2012b. Effect of polymerization with paraformaldehyde on thermal reactivity of >300°C fraction from low temperature coal tar. *Thermochimica Acta,* 538:48-54.

Sutton, D., Kelleher, B. & Ross, J.R.H. 2001. Review of literature on catalysts for biomass gasification. *Fuel Processing Technology,* 73: 155-173.

Suuberg, E.M. 1977. Rapid pyrolysis and hydropyrolysis of coal. USA: Massachusetts Institute of technology. (Thesis – PhD)

Suuberg, E.M., Peters, W.A. & Howard, J.B. 1978a. Product composition and kinetics of lignite pyrolysis. *Industrial and Engineering Chemistry Process Design and Development,* 17:37-46.

Suuberg, E.M., Peters, W.A. & Howard, J.B. 1978b. Product compositions and formation kinetics in rapid pyrolysis of pulverised coal. *17th International Symposium on Combustion,* Leeds.

Suuberg, E.M., Peters, W.A. & Howard, J.B. 1979. A comparison of the rapid pyrolysis of a lignite and bituminous coal. *ACS Advances in Chemical Ser.,* 183:239.

Suuberg, E.M., Peters, W.A. & Howard, J.B. 1980. Product compositions in rapid pyrolysis of coal. *Fuel,* 59:405.

Tabrizy, V.A., Denoyel, R. & Hamouda, A.A. 2011. Characterizatrion of wttability alteration of calcite, quartz and kaolinite: Surface energy analysis. *Colloids and Surfaces A: Physicochemical and Engineering Aspects,* 384:98-108.

Tang, W., Fang, M., Wang, H., Yu, P., Wang, Q. & Luo, Z. 2014. Mild hydrotreatment of low temperature coal tar distillate: Product composition. *Chemical Engineering,* 236:529-537.

Taralas, G., Kontominas, M.G. & Kakatsios, X. 2003. Modelling the thermal destruction of toluene (C_7H_8) as tar-related species for fuel-gas cleanup. *Energy & Fuels,* 17:329-337.

Taupitz, K.C. 1977. Making liquids from solid fuels. *Hydrocarbon Processing,* 56(9):219-225.

Thomas, J.E. & Kelley, M.J. 2009. The adsorption of salicylic acid onto γ-alumina and kaolinite from solution in hexane studied using diffuse reflectance infrared Fourier transforms spectroscopy (DRIFT). *Journal of Colloid and Interface Science,* 338:389-394.

Thomas, J.E. & Kelley, M.J. 2010. A study of competitive adsorption of organic molecules onto mineral oxides using DRIFTS. *Journal of Colloid and Interface Science,* 342:474-478.

Thomas, S., Ledesma, E. & Wornat, M. 2007. The effects of oxygen on the yields of the thermal decomposition products of cathecol under pyrolysis and fuel-rich oxidation conditions. *Fuel,* 86:2581-2595.

Tomeczek, J. & Palugniok, H. 2002. Kinetics of mineral matter transformation during coal combustion. *Fuel,* 81:1251-1258.

Trejo, F., Ancheyta, J., Morgan, T.J., Herod, A.A. & Kandiyoti, R. 2007. Characterization of Asphaltenes from Hydrotreated Products by SEC, LDMS, MALDI, NMR and XRD. *Energy & Fuels,* 21:2121-2128.

Tsubouchi, N. & Ohtsuka, Y. 2002a. Formation of N_2 during pyrolysis of Ca-loaded coals. *Fuel,* 83:1423-1431.

Tsubouchi, N. & Ohtsuka, Y. 2002b. Nitrogen release during high temperature pyrolysis of coals and catalytic role of calcium in N_2 formation. *Fuel,* 81:2335-2342.

Tsubouchi, N. Xu, C. & Ohtsuka, Y. 2004. Effect of alkaline earth metals on N_2 formation during fixed bed pyrolysis of a low rank coal. *Fuel Processing Technology,* 85:1039-1052.

Ukwuoma, O. 2002. Comparative study of the compositional characteristics of liquids derived by hydrotreating of Nigerian tar sand bitumen. i. Simulated distillation. *Petroleum Science and Technology,* 20(5 & 6):525-534.

Unger, P.E. & Suuberg, E.M. 1984. Molecular weight distributions of tar produced by flash pyrolysis of coals. *Fuel,* 63(5): 606-611.

Uzun, B.B., Pütün, A.E. & Pütün, E. 2007. Composition of products obtained via fast pyrolysis of olive-oil residue: Effect of pyrolysis temperature. *Journal of Analytical and Applied Pyrolysis,* 79:147-153.

Van Alphen, C. 2005. Factors influencing fly ash formation and slag deposit formation (slagging) on combusting a South African pulverised fuel in a 200 MWe boiler. Johannesburg – University of the Witwatersrand (Thesis – PhD).

Van Alphen, C. 2007. Automated mineralogical analysis of coal and ash products – Challenges and requirements. *Minerals Engineering,* 20: 496-505.

Van Dyk, J.C. 2006. Understanding the influence of acidic components (Si, Al and Ti) on ash flow temperature of South African coal sources. *Minerals Engineering,* 19:280-286.

Van Dyk, J.C., Benson, S.A., Lomb, M.L. & Waanders, F.B. 2009. Coal and coal ash characteristics to understand mineral transformations and slag formation. *Fuel,* 88:1057-1063.

Van Dyk, J.C., Melzer, S. & Sobiecki, A. 2006. Mineral matter transformation during Sasol-Lurgi fixed bed dry bottom gasification - utilization of HT-XRD and FactSage modelling. *Minerals Engineering,* 19:1126-1135.

Van Heek, K.H. & Kodek, W. 1994. Structure and pyrolysis behaviour of different coals and model substances. *Fuel,* 73(6):886-896.

Van Niekerk, D. 2008. Structural elucidation, molecular representation and solvent interactions of vitrinite-rich and inertinite-rich South African coals. Pennsylvania: Pennsylvania State University. USA. (Thesis-PhD).

Van Niekerk, D., Mitchell, G.D. & Mathews, J.P. 2010. Petrographic and reflectance analysis of solvent-swelled and solvent-extracted South African vitrinite-rich and inertinite-rich coals. *International Journal of Coal Geology,* 81:45-52.

Van Niekerk, D., Pugmire, R.J., Solum, M.S., Painter, P.C. & Mathews, P. 2008. Structural characterisation of vitrinite-rich and inertinite rich Permian-aged South African bituminous coals. *International Journal of Coal Geology,* 76:290-300.

Vassilev, S.V. & Vassileva, C.G. 1996. Occurrence, abundance and origin of minerals in coals and coal ashes. *Fuel Processing Technology,* 48:85-106.

Vassilev, S.V., Kitano, K., Takeda, S. & Tsurue, T. 1995. Influence of mineral and chemical composition of coal ashes on their fusibility. *Fuel Processing Technology,* 45(1):27-51.

Vassilev, S.V., Vassileva, C.G., Baxter, D. & Andersen, L.K. 2009. A new approach for the combined chemical and mineral classification of the inorganic matter in coal. 2. Potential applications of the classification systems. *Fuel,* 88:246-254.

Vassileva, C.G. & Vassilev S.V. 2006. Behaviour of inorganic matter during heating of Bulgarian coals 2. Subbituminous and bituminous coals. *Fuel Processing Technology,* 87:1095-1116.

Velegol, D. Gautam, M. & Shamsi, A. 1997. Catalytic cracking of a coal tar in a fluid bed reactor. *Powder Technology,* 93(2):93-100.

Vestal, M.L., Essenhigh, R.H. & Johnston, W.H. 1970. *American Chemical Society, Division of Petroleum Chemistry,* 15(4): A153.

Vorres, K.S. 1986. Mineral matter and ash in coal. American Chemical Society, Washington.

Wagner, N.J. & Hlatshwayo, B. 2005. The occurrence of potentially hazardous trace elements in five Highveld coals, South Africa. *Coal Geology,* 63:228-246.

Wang, H.-H. 2007. Kinetic analysis of dehydration of a bituminous coal using the TGA technique. *Energy & Fuels,* 21:3070-3075.

Wang, J., Jiang, M., Yao, Y., Zhang, Y. & Cao, J. 2009. Steam gasification of coal char catalyzed by K_2CO_3 for enhanced production of hydrogen without formation of methane. *Fuel,* 88:1572-1579.

Wang, J., Takaya, A. & Tomita, A. 2004. Leaching of ashes and chars for examining transformations of trace elements during coal combustion and pyrolysis. *Fuel,* 83:651-660.

Wang P., Jin L., Liu J., Zhu S. & Hu H. 2013. Analysis of coal tar derived from pyrolysis at different atmospheres. *Fuel* 104:14-21.

Wang, S., Tang, Y., Schobert, H.H., Mitchell, G.D., Liao, F. & Liu, Z. 2010. A thermal behaviour study of Chinese coals with high hydrogen content. *International Journal of Coal Geology,* 81:37-44.

Wang, Y. & Thomson, W.J. 1995. The effect of sample preparation on the thermal decomposition of $CaCO_3$. *Thermochimica Acta,* 25:383-390.

Wang, Y., Zhao, R., Zhang, C., Li, G., Zhang, J, & Li, F. 2014. The investigation of reducing PAHs emission from coal pyrolysis by gaseous catalytic cracking. *The Scientific World Journal,* 2014: 528413. Available at: http://dx.doi.org/10.1155/2014/528413, Date of access: 3 August, 2014.

Ward, C.R. 2002. Analysis and significance of mineral matter in coal seams. *International Journal of Coal Geology,* 50:135-168.

Ward, C.R. & French, D. 2004. Analysis and significance of mineral matter in coal. *The Society of organic petrology, short course notes.* Sydney – University of New South Wales, 2-68.

Watt, J.D. 1968. The physical and chemical behaviour of the mineral matter in coal under th conditions met in the combustion plant: Part 1 – The occurrence, origin, identity, distribution and estimation of the mineral species in British coals. *BCURA Monthly Bulletin Literature survey*.

WCA (World Coal Association). 2012. Coal Matters 1: Coal in the global energy supply. www.worldcoal.org/publications. Date of access: 21 March 2014.

WCI (World Coal Institution). 2005. The Coal Resource: A Comprehensive Overview of Coal. www.worldcoal.org. Date of Access: 21 March 2014.

WCI (World Coal Institution). 2009. Coal: Liquid fuels. www.worldcoal.org/publications. Date of Access: 21 March 2014.

Wei, J.M. & Iglesia, E. 2004. Isotopic and kinetic assessment of the mechanism of reactions of CH_4 with CO_2 or H_2O to form synthesis gas and carbon on nickel catalysts. *Journal of Catalysis,* 224:370-383.

Wen, Y.W. & Cain, E. 1984. Catalytic pyrolysis of a coal tar in a fixed-bed reactor. *Industrial Engineering and Chemical Process Design,* 23(4):627-637.

Williams, P.T. & Taylor, D.T. 1993. Aromatization of tyre pyrolysis oil to yield polycyclic aromatic hydrocarbons. *Fuel,* 72:1469-1474.

Wills, B.A. & Napier-Munn, T. 2006. Wills' Mineral Processing Technology. An introduction to the practical aspects of ore treatment and mineral recovery. 7th ed. Oxford: Elsevier.

Wu, Z. & Steel, K.M. 2007. Acid washing of a UK bituminous coal using HF and ferric ions. *Fuel,* 86:2194-2200.

Wu, Z., Sugimoto, Y. & Kawashima, H. 2003. Effect of acid washing and catalyst addition on N_2 formation during coal pyrolysis and on char gasification. *Fuel,* 82:2057-2064.

Xiao, G., Ni, M., Chi, Y., Jim, B., Xiao, R., & Zhong, Z. 2009. Gasification characteristics of MSW and an ANN prediction model. *Waste Management,* 29:240-244.

Xin, H., Wang, D., Qi, X., Qi, G. & Duo, G. 2014. Structural characteristics of coal functional groups using quantum chemistry for quantification of infrared spectra. *Fuel Processing Technology,* 118:287-295.

Xu, W. & Tomita, A. 1987. Effect of temperature on the flash pyrolysis of various coals. *Fuel,* 66(5):632-636.

Xu, W. & Tomita, A. 1989. The effects of temperature and residence time on the secondary reactions of volatiles from coal pyrolysis. *Fuel Processing Technology,* 21:25-37.

Yaman, S., Yavuz, R., Küçükbayrak, S. & Taptik, Y. 2001. Stepwise acid washing and chemical isolation of the mineral matter in Göynük lignite. *Energy Conversion and Management,* 42:2119-2127.

Yan, J., Xu, L. & Yang, J. 2008. A study on the thermal decomposition of coal-derived pyrite. *Journal of Analytical and Applied Pyrolysis,* 82:229-234.

Yan, X. Che, D. & Xu, T. 2005. Effect of rank, temperatures and inherent minerals on nitrogen emissions during coal pyrolysis in a fixed be reactor. *Fuel Processing Technology,* 86:739-756.

Yani, S. & Zhang, D. 2009. Transformation of organic and inorganic sulphur in a lignite during pyrolysis: Influence of inherent and added inorganic matter. *Proceeding of the Combustion Institute,* 32:2083-2089.

Yani, S. & Zhang, D. 2010. An experimental study into pyrite transformation during pyrolysis of Australian lignite samples. *Fuel,* 89:1700-1708.

Yaw, D., Longwell, J.P., Howard, J.B. & Peters, W.A. 1980. Effect of calcined dolomite on the fluidized bed pyrolysis of coal. *Industrial and Engineering Chemical Process Design and Development,* 19(4):645-653.

Ye, D.P., Agnew, J.B. & Zhang, D.K. 1998. Gasification of a South Australian low-rank coal with carbon dioxide and steam: kinetics and reactivity studies. *Fuel,* 77(11):1209-1219.

Yeboah Y.D., Longwell, J,.P., Howard, J.B. & Peters W.A. 1980. Effect of calcined dolomite on the fluidized bed pyrolysis of coal. *Industrial and Engineering Chemistry Research,* 19:646-653.

Yongbin, J., Jiejie, H. & Yang, W. 2004. Effects of calcium oxide on the cracking of coal tar in the freeboard of a fluidized bed. *Energy & Fuels,* 18:1625-1632.

Yu, J., Zhang, M., Chen, M., Song, Y., Fan, W. & Zhou, Y. 2001. TGA study on humified activation and desulfurization performance of high-CaO coal ash at low temperature. *Industrial and Engineering Chemistry Research,* 40:3634-3638.

Yu, L.E., Hildemann, L.M., DaDamio, J. & Niksa, S. 1998. Characterisation of coal tar organics via gravity flow column chromatography. *Fuel,* 77(5):437-445.

Yu, Q.Z., Brage, C., Nordgreen, T. & Sjöström, K. 2009. Effects of Chinese dolomites on tar cracking in gasification of birch. *Fuel,* 88:1922-1926.

Zhang, D. & Yani, S. 2011. Sulphur transformations during pyrolysis of an Australian lignite. *Proceedings of the Combustion Institute,* 33:1747-1753.

Zhang, Y., Kajitani, S., Ashizawa, M. & Oki, Y. 2010. Tar destruction and coke formation during rapid pyrolysis and gasification of biomass in a drop-tube furnace. *Fuel,* 89:302-309.

Zhao, Y., Hu, H., Jin, L, He, X. & Wu, B. 2011. Pyrolysis behaviour of vitrinite and inertinite from Chinese Pingshuo coal by TG-MS and in a fixed bed reactor. *Fuel Processing Technology,* 92:780-786.

Appendix A: Coal characterisation

A-1 Description of standard methods used

Table A-1 provides a description of the standard methods used for the characterisation of the TWD coal sample (Chapter 3).

Table A-1 Description of standard methods used

Standard	Description
ASTM D4326	Standard test method for major and minor elements in coal and coke ash by X-ray fluorescence. Pennsylvania: ASTM International. (ASTM, 1997)
ISO 562	Hard coal and coke - Determination of volatile matter. Geneva: ISO Standards. (ISO, 2010)
ISO 1171	Solid mineral fuels - Determination of ash. Geneva: ISO Standards. (ISO, 2010)
ISO 29541	Solid mineral fuels - Determination of total carbon, hydrogen and nitrogen-instrumental method. Geneva: ISO Standards. (ISO, 2010)
ISO 1928	Solid mineral fuels - Determination of gross calorific value by the bomb calorimetric method and calculation of net calorific value. Geneva: ISO Standards. (ISO, 2009)
ISO 19579	Determination of total sulphur through IR spectroscopy. Geneva: ISO Standards. (ISO, 2006).
ISO 11722	Solid mineral fuels - Hard coal - Determination of moisture in the general analysis test sample by drying in nitrogen. Geneva: ISO Standards. (ISO, 1999).
ISO 7404-2	Methods for the petrographic analysis of bituminous coal and anthracite-Part 2: Preparation of coal samples. Geneva: ISO Standards. (ISO, 1994a).
ISO 7404-3	Methods for the petrographic analysis of bituminous coal and anthracite-Part 3: Method of determining maceral group composition. Geneva: ISO Standards. (ISO, 1994b).
ISO 7404-5	Methods for the petrographic analysis of bituminous coal and anthracite-Part 5: Method of determining microscopically the reflectance of vitrinite. Geneva: ISO Standards. (ISO, 1994c).

ISO 622	Solid mineral fuels - Determination of phosphorus content -- Reduced molybdophosphate photometric method. Geneva: ISO Standards. (ISO, 1981).
SANS 647	Brown coals and lignites - Determination of the yields of tar, water, gas and coke residue by low temperature distillation. Pretoria: SABS, Standards Division. (SANS, 1974)

A-2 Relating XRF, XRD and QEMSCAN results

The received QEMSCAN results (area %, Table 3-7) were transformed to a wt% basis (Table A-3) by means of density calculations. The assumed densities are indicated in Table A-2. The following formula was used:

$$\rho = \frac{m}{V} \tag{A-1}$$

Where ρ is the density of the mineral, V is the volume %, and m the determined "mass" of the mineral. This calculation was done for all minerals, and then normalised to obtain a wt% value for the identified minerals. Table A-3 indicates the determined wt% values.

The components identified by XRF analysis were determined as fractions of the original minerals identified by QEMSCAN and/or XRD. The molecular weight of the XRF oxide ($MW_{XRF,i}$) was divided by the molecular weight of the mineral identified by QEMSCAN and/or XRD ($MW_{QS/XRD,i}$). Equation (A-2) indicates this calculation:

$$x_i = \frac{MW_{XRF,i}}{MW_{QS,i}} \tag{A-2}$$

The molecular weights of the oxides are indicated in Table A-4. The determined fractions are indicated in Table A-4. These fractions are in turn multiplied with the wt% values in Table A-3 (Equation A-3). These values are then normalised to obtain a wt% value for the identified minerals in terms of the identified XRF oxides. The normalised values are indicated in Table 3-8 (Section 3.3.7.).

$$wt.\%_{\,XRF-QS,i} = x_i \cdot wt.\%_{QS} \tag{A-3}$$

Table A-2 Assumed chemical formula, molecular weight and density of QEMSCAN / XRD minerals

	Chemical formula	Molecular weight	Density (g/cm^3)	Reference
Sulphates/Gibbsite	$Al(OH)_3$	78	2.4	Mindat, 2012a
Pyrite	FeS_2	119.98	5	Mindat, 2012b
Siderite	$FeCO_3$	115.86	3.9	Mindat, 2012c
Calcite	$CaCO_3$	100.09	2.7	Mindat, 2012d
Dolomite	$CaMg(CO_3)_2$	184.4	2.8	Mindat, 2012e
Apatite	$Ca_5(PO_4)_3F$	504.1	3.2	Mindat, 2012f
Kaolinite	$Al_2Si_2O_5(OH)_4$	258.16	2.6	Mindat, 2012g
Quartz	SiO_2	60.08	2.6	Mindat, 2012h
Illite/Muscovite	$KAl_2(AlSi_3O_{10})(OH)_2$	398.71	2.8	Mindat, 2012i
Microcline	$KAlSi_3O_8$	278.33	2.5	Mindat, 2012j
Rutile	TiO_2	79.88	4.2	Mindat, 2012k
Gorceixite	$BaAl_3(PO_4)_2(OH)_5 \cdot H_2O$	511.27	3.1	Mindat, 2012l
Other			2.7	Liu, 2007a

Table A-3 QEMSCAN wt% results

Mineral	wt%	
	TWD	AW TWD
Sulphates/Gibbsite	2.6	0.8
Pyrite	26.2	87.0
Siderite	0.8	0.0
Calcite	8.2	0.2
Dolomite	17.8	0.2
Apatite	2.9	0.4
Kaolinite	30	0.5
Quartz	5.2	1.8
Illite/Muscovite	2.8	0.1
Microcline	1.1	0.0
Rutile	0.4	0.7
Gorceixite	0.0	0.0
Other	1.8	8.3
TOTAL	**100**	**100**

Table A-4 Molecular weights of XRF oxides

XRF Oxide	MW (g/mol)
SiO_2	60.08
Al_2O_3	101.96
Fe_2O_3	159.96
CaO	56.08
MgO	40.30
Na_2O	61.98
K_2O	94.20
TiO_2	79.87
SO_3	80.07
P_2O_5	283.89
ZrO_2	123.22
V_2O_5	181.88
Ba	137.33
Sr	87.62
MnO	70.94

A-3 Experimental repeatability of DRIFT analyses

The absolute peak strength of the spectra obtained from analyses of the same coal in different experiments may vary, although the shape of the spectra are almost exactly the same (Li *et al.,* 2004). The density of the sample, depending in the varied forces to press the sample in the sample holder, affects the peak strength. Thus variation of the peak strength is not indicative of differences in results. These are the DRIFT analyses results as reported in Section 3.8.2, Chapter 3.

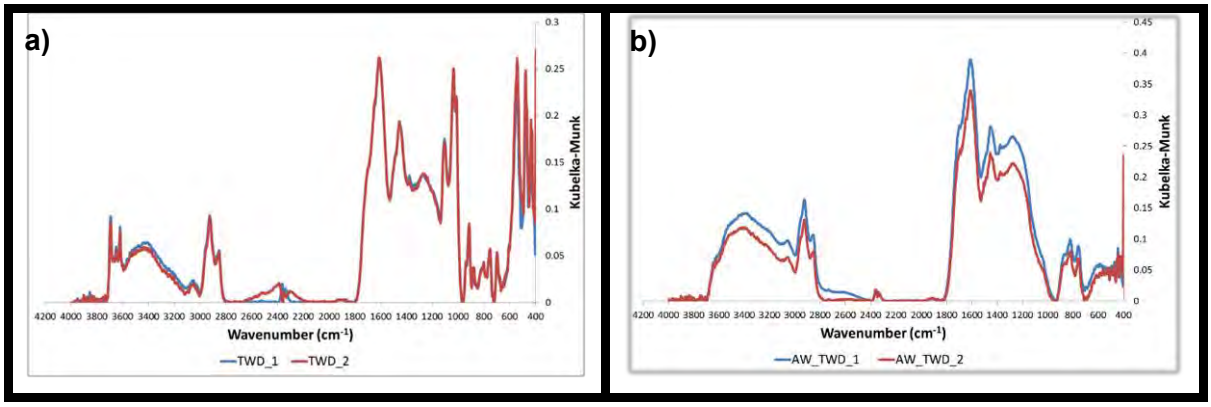

Figure A-1 DRIFT spectra of duplicate analyses of a) TWD and b) AW TWD.

A-4 Experimental repeatability of thermogravimetric analyses

A summary of the results obtained for the thermogravimetric analysis experiments (Section 3.9, Chapter 3) done is indicated in Figure A-2.

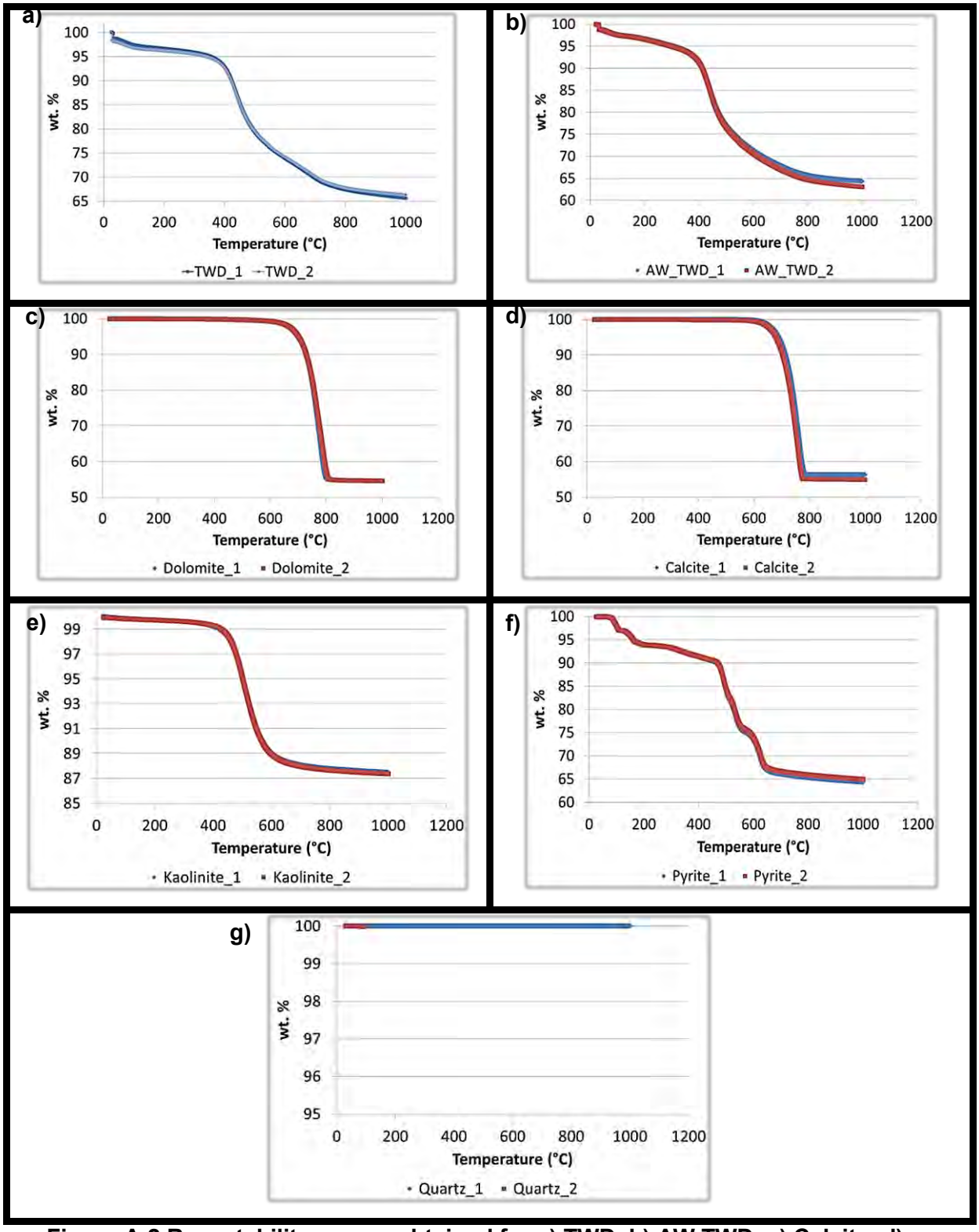

Figure A-2 Repeatability curves obtained for a) TWD, b) AW TWD, c) Calcite, d) Dolomite, e) Kaolinite, f) Pyrite and g) Quartz.

Appendix B: Experimental methods and –analyses techniques

B-1 Determination of gas yields derived during pyrolysis experiments

The gas yields derived during pyrolysis were determined by a graphical method. The outline of the gas bag profile was drawn up in length and width. Figure B-1 indicates this procedure for the length profile. Figure B-1a, b and c indicates the drawing procedure followed. The gas bag was placed in front of an A1 poster that was stuck to the wall (Figure B-1a). The profile was drawn up by use of a pencil, placed horizontally on the gas bag, without applying pressure to the bag that will lead to deformation (Figure B-1b).

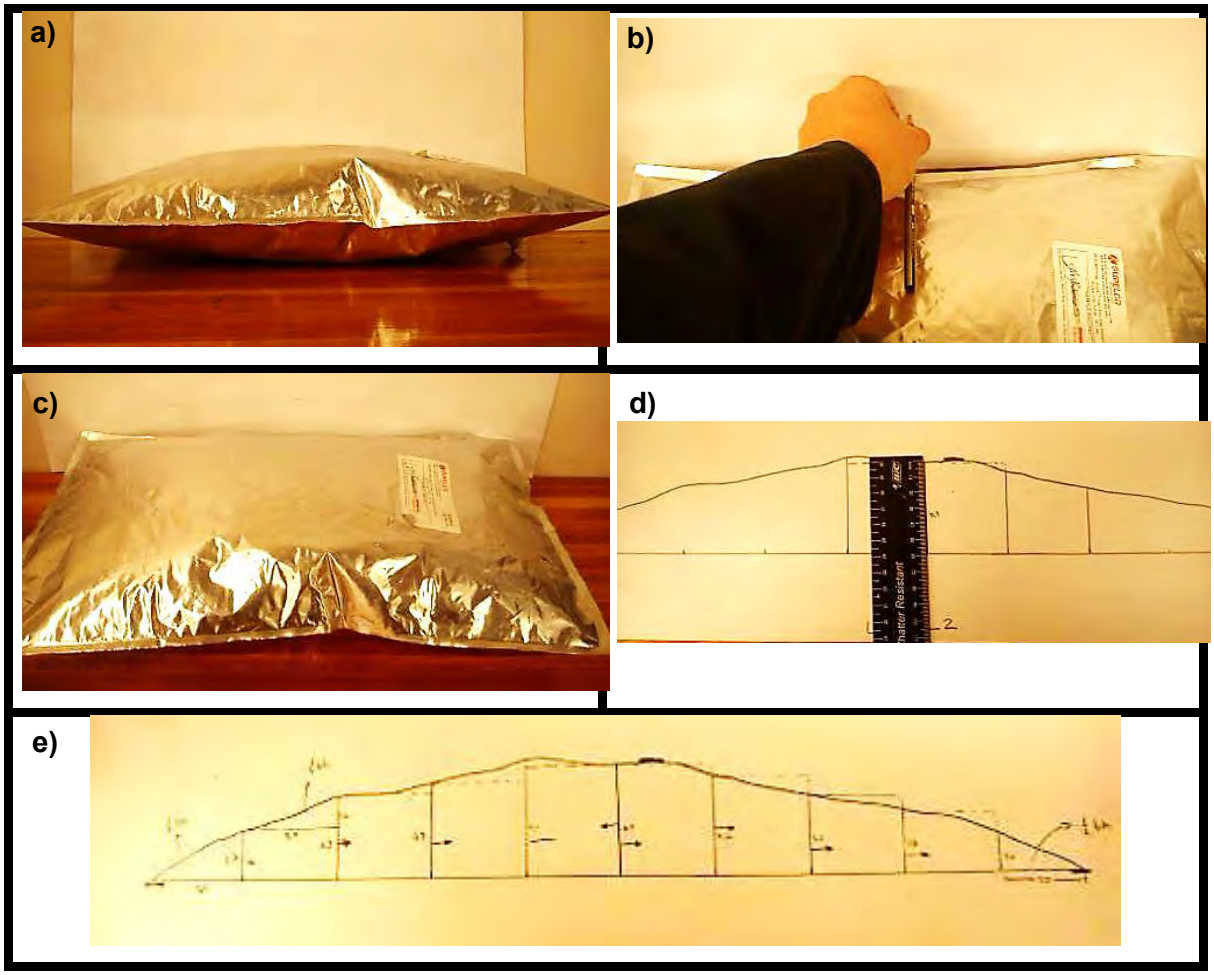

Figure B-1 Determination of gas bag volume a) Gas bag placed in front of A1 poster; b) Drawing of the gas bag length profile; c) Gas bag profile after drawing; d) Measurement of height from mid-line to curve; d) Gas bag profile with the identified lengths and geometries for the length of the gas bag.

Figure B-1c indicates the profile which was used to determine the volume. A horizontal line was drawn from which the height from the mid-line to the curve was determined (Figure B-1d). The height to the curve was determined at intervals of 5 cm and by use of various geometrical formulas, the area under the curve was determined (Figure B-1e). This was done for the width profile of the gas bag as well, thus obtaining geometries that could be used for a 3D volume determination. Geometric similarity was assumed and half of the length profile and the full width profile were used for the final volume calculation. The length and width of the gas bags were determined to be 30 and 50 cm respectively. Equation B-1 was derived for these calculations.

$$V_B(m^3) = \frac{[200(B_1+2(B_2+B_3+B_4+B_5))+500(B_6+B_7)]}{10\,000} \quad \text{(B-1)}$$

Where V_B is the volume of the gas bag, B_1 to B_7 refers to the different parameters as determined from the gas bag profile. B_1 is the parameter calculated according to the formula for the area of a triangle for the length profile, thus the first parameters, B_2 to B_5 are parameters of which the area of a normal rectangular is assumed. B_6 and B_7 are the parameters determined from the width profile for which areas are calculated according to the triangle area formula. The unit of the length B_1 to B_7 is in cm, thus division by 10 000 gives the final gas bag volume in m^3. Figure B-2 indicates the length (a) and width (b) profiles for a typical gas bag and the parameters as measured.

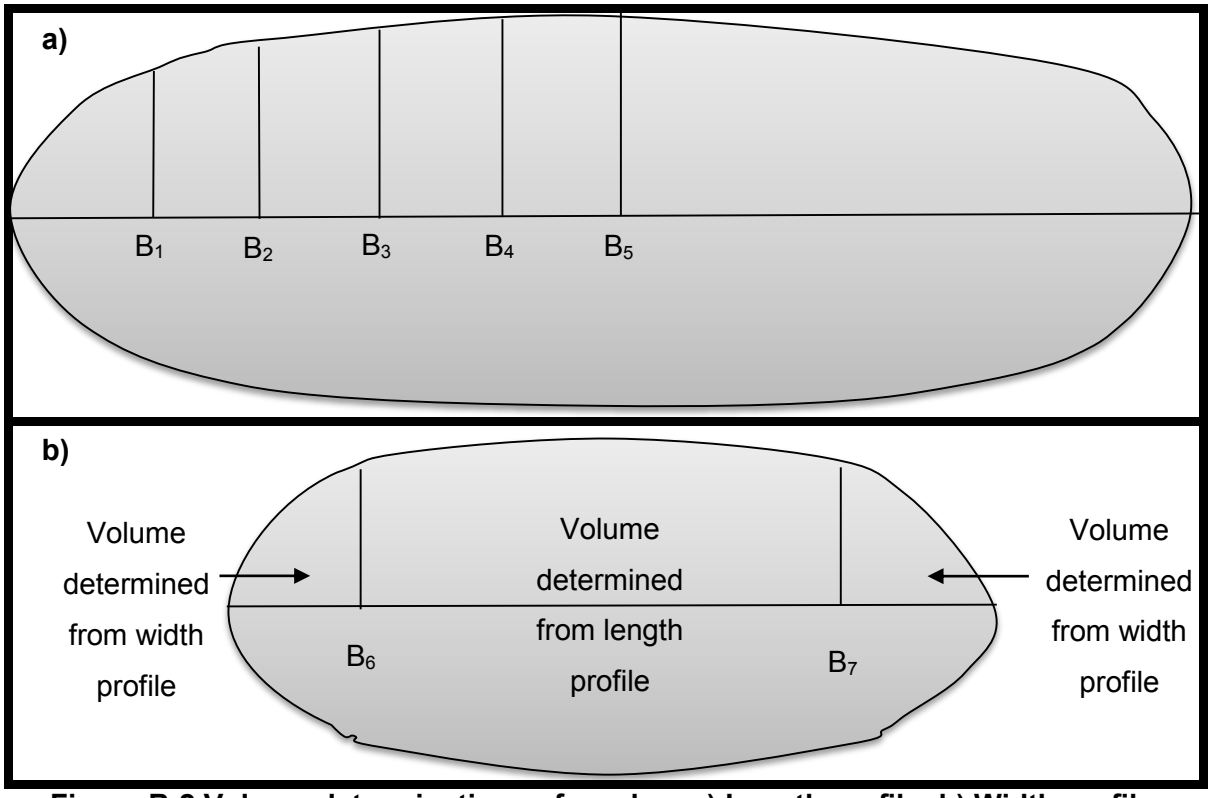

Figure B-2 Volume determinations of gas bag a) Length profile; b) Width profile.

The volume of the system was determined by determining the volumes of the retort, piping and gas washing bottles. This volume along with the volume determined for the gas bag was used as the final volume. By use of the ideal gas law, and the temperature and pressure as indicated by the pressure meter, the initial and final number of moles of gas present were determined. The gas composition inside the gas bag was analysed by the GC as described in Chapter 5, Section 5.2.1. Compositional similarity between the gas in the system (retort, receiver flask, gas washing bottle and piping) and the gas in the gas bag were assumed. The compositional data, provided on a mol% basis, were converted to a molar basis by multiplication with the final mole value. Table B-1 indicates the various molecular weights used to transform the gas data, on a molar basis to a mass basis. The initial molar value was used to determine the initial N_2 and O_2 mass present, subtracting these amounts the final gas weight, as produced from the coal sample during pyrolysis, was determined

Table B-1 Molecular weights for gas species identified by GC analysis

	MW (g/mole)
H_2	2.02
O_2	32.00
N_2	28.01
CH_4	16.04
CO	28.01
CO_2	44.01
C_2H_4	28.05
C_2H_6	30.07
C_3H_6	42.08
C_3H_8	44.10
C_4s	56.11

Appendix C: Pyrolysis product yields and composition

C-1 Pyrolysis experiments

The results for the pyrolysis product yields as discussed in Chapter 5 to Chapter 7 are reported here. The pyrolysis product results are indicated in Table C-1, as determined, Table C-3, mineral-matter-free basis, and Table C-5, dry, mineral-matter-free basis. Table C-2, C-4 and C-6 indicates the error on repeatability values within a 95% confidence interval for the respective basis of representation.

Table C-1 Pyrolysis product yields as determined

	TWD	LM	HM	AW TWD	AW-Cal	AW-Dol	AW-Kao	AW-Pyr	AW-Qz
					Wt%				
					520°C				
Water	6.0	7.2	4.0	4.4	5.8	5.7	4.9	5.6	4.3
Tar	8.3	4.9	3.2	4.8	4.4	4.7	5.6	3.7	4.4
Char	76.3	76.4	77.6	75.1	75.5	74.5	73.8	74.9	75.0
Gas	9.4	11.4	15.2	15.7	14.4	15.2	15.7	15.8	16.4
TOTAL	**100.0**	**100.0**	**100.0**	**100.0**	**100.0**	**100.0**	**100.0**	**100.0**	**100.0**
					750°C				
Water	6.6	7.7	4.6	4.4	5.5	6.1	5.0	5.4	4.2
Tar	7.1	5.2	4.0	5.7	3.9	4.4	5.7	5.2	5.5
Char	72.0	72.4	73.2	70.7	69.3	70.7	71.0	71.0	71.5
Gas	14.3	14.7	18.2	19.1	21.3	18.8	18.2	18.3	18.7
TOTAL	**100.0**	**100.0**	**100.0**	**100.0**	**100.0**	**100.0**	**100.0**	**100.0**	**100.0**
					900°C				
Water	6.9	7.5	4.2	4.1	6.1	6.2	5.1	5.4	3.9
Tar	7.3	2.1	4.0	6.0	3.2	3.1	5.7	5.2	5.9
Char	70.8	70.2	70.6	69.2	66.5	67.7	69.2	68.4	70.6
Gas	14.9	20.2	21.2	20.7	24.2	23.0	20.1	20.9	19.6
TOTAL	**100.0**	**100.0**	**100.0**	**100.0**	**100.0**	**100.0**	**100.0**	**100.0**	**100.0**

Table C-2 Error on repeatability values for 95% confidence (Pyrolysis product yields as determined)

	TWD	LM	HM	AW TWD	AW-Cal	AW-Dol	AW-Kao	AW-Pyr	AW-Qz
					wt%				
520°C									
Water	0.4	0.6	0.0	0.8	0.3	0.6	0.2	0.4	0.8
Tar	0.3	0.9	0.3	0.5	0.3	0.1	0.2	0.4	0.0
Char	0.5	0.3	0.5	0.3	0.2	0.8	0.9	0.3	0.6
Gas	0.8	0.5	0.3	0.7	0.6	0.8	0.5	0.5	0.1
750°C									
Water	0.3	0.7	0.0	0.6	0.2	0.2	0.0	0.4	0.6
Tar	0.4	0.3	0.4	0.4	0.2	0.2	0.1	0.2	0.4
Char	0.2	0.3	0.0	0.4	0.3	0.0	0.6	0.0	0.1
Gas	0.7	0.7	0.4	0.7	0.6	0.4	0.8	0.7	1.1
900°C									
Water	0.7	0.2	0.7	0.2	0.4	0.7	0.3	0.7	0.2
Tar	0.3	0.6	0.4	0.3	0.5	0.0	0.0	0.2	0.4
Char	0.8	0.4	0.4	0.3	0.8	0.6	0.0	0.7	0.5
Gas	0.6	0.9	0.7	0.4	1.7	0.1	0.2	1.3	1.1

Table C-3 Pyrolysis product yields (m.m.f.b.)

	TWD	LM	HM	AW TWD	AW-Cal	AW-Dol	AW-Kao	AW-Pyr	AW-Qz
					wt%				
					520°C				
Water	8.1	7.4	3.5	4.6	6.4	6.4	5.2	5.9	4.8
Tar	9.9	5.2	3.7	4.9	4.7	5.0	6.0	4.0	4.7
Char	70.9	75.8	77.1	74.3	73.3	72.3	71.8	73.6	72.8
Gas	11.2	11.6	15.6	16.2	15.5	16.4	17.0	16.5	17.7
TOTAL	100.0	100.0	100.0	100.0	100.0	100.0	100.0	100.0	100.0
					750°C				
Water	8.5	7.8	3.6	4.6	6.1	6.8	5.0	5.7	4.8
Tar	8.2	5.7	4.8	5.8	4.1	4.8	6.2	5.6	6.0
Char	66.7	72.7	73.9	70.0	68.2	69.2	69.3	70.4	69.2
Gas	16.6	13.9	17.6	19.6	21.6	19.3	19.5	18.2	20.1
TOTAL	100.0	100.0	100.0	100.0	100.0	100.0	100.0	100.0	100.0
					900°C				
Water	8.8	7.8	3.1	4.3	6.7	6.9	5.0	5.7	4.4
Tar	8.3	2.4	5.1	6.2	3.4	3.3	6.1	5.6	6.3
Char	65.8	71.2	71.6	68.4	66.2	67.6	67.4	67.7	68.2
Gas	17.0	18.6	20.2	21.1	23.7	22.3	21.5	21.0	21.0
TOTAL	100.0	100.0	100.0	100.0	100.0	100.0	100.0	100.0	100.0

Table C-4 Error on repeatability values for 95% confidence (Pyrolysis product yields m.m.f.b.)

	TWD	LM	HM	AW TWD	AW-Cal	AW-Dol	AW-Kao	AW-Pyr	AW-Qz
					wt%				
520°C									
Water	0.5	0.8	0.1	0.8	0.3	0.6	0.2	0.4	0.9
Tar	0.4	1.1	0.5	0.5	0.3	0.5	0.2	0.5	0.0
Char	0.6	0.3	0.9	0.3	0.2	0.9	0.9	0.3	0.7
Gas	1.0	0.6	0.4	0.7	0.6	0.8	0.5	0.5	0.1
750°C									
Water	0.3	0.9	0.1	0.6	0.2	0.2	0.0	0.5	0.6
Tar	0.5	0.3	0.6	0.5	0.2	0.2	0.1	0.3	0.4
Char	0.2	0.3	0.0	0.4	0.3	0.0	0.6	0.0	0.1
Gas	0.8	0.9	0.5	0.8	0.7	0.4	0.8	0.7	1.2
900°C									
Water	0.8	0.3	1.1	0.2	0.5	0.7	0.3	0.8	0.2
Tar	0.3	0.8	0.6	0.3	0.5	0.0	0.1	0.2	0.5
Char	0.9	0.4	0.5	0.3	0.8	0.6	0.0	0.7	0.5
Gas	0.7	0.0	1.0	0.4	1.8	0.1	0.2	1.4	1.2

Table C-5 Pyrolysis product yields (d.m.m.f.)

	TWD	LM	HM	AW TWD	AW-Cal	AW-Dol	AW-Kao	AW-Pyr	AW-Qz
520°C									
Tar	10.7	5.6	3.8	5.2	5.1	5.4	6.3	4.2	4.9
Char	77.1	81.9	80.0	77.9	78.4	77.2	75.8	78.3	76.5
Gas	12.1	12.5	16.2	16.9	16.6	17.5	17.9	17.5	18.6
TOTAL	100.0	100.0	100.0	100.0	100.0	100.0	100.0	100.0	100.0
750°C									
Tar	9.0	6.1	5.0	6.1	4.4	5.1	6.5	6.0	6.3
Char	72.9	78.8	76.7	73.4	72.6	74.2	73.0	74.7	72.6
Gas	18.2	15.1	18.3	20.5	23.0	20.7	20.5	19.3	21.1
TOTAL	100.0	100.0	100.0	100.0	100.0	100.0	100.0	100.0	100.0
900°C									
Tar	9.1	2.6	5.2	6.4	3.7	3.5	6.4	6.0	6.6
Char	72.2	77.2	73.9	71.5	70.9	72.6	70.9	71.8	71.4
Gas	18.7	20.2	20.9	22.1	25.4	23.9	22.7	22.2	22.0
TOTAL	100.0	100.0	100.0	100.0	100.0	100.0	100.0	100.0	100.0

Table C-6 Error on repeatability values for 95% confidence (Pyrolysis product yields d.m.m.f.)

	TWD	LM	HM	AW TWD	AW-Cal	AW-Dol	AW-Kao	AW-Pyr	AW-Qz
					wt%				
					520°C				
Tar	0.4	1.1	0.6	0.5	0.4	0.1	0.2	0.4	0.0
Char	0.9	0.3	1.0	0.7	0.5	0.4	0.8	0.6	0.0
Gas	1.0	0.8	0.7	0.7	0.5	0.7	0.6	0.5	0.0
					750°C				
Tar	0.5	0.4	0.6	0.5	0.2	0.3	0.1	0.2	0.5
Char	0.4	0.4	0.0	0.8	0.5	0.2	0.7	0.4	0.6
Gas	0.8	0.8	0.6	0.8	0.7	0.4	0.5	0.8	1.1
					900°C				
Tar	0.3	0.8	0.6	0.3	0.6	0.0	0.0	0.1	0.5
Char	0.7	0.7	1.3	0.2	1.2	0.1	0.2	1.4	0.7
Gas	1.1	1.2	0.7	0.8	1.8	0.1	0.2	1.3	1.2

C-2 Gas analysis

C-2.1 Gas yields as identified by GC (molar composition)

Table C-7 and Table C-8 indicate the molar composition results of the evolved gas species at 520°C and 750°C, and 900°C, respectively.

Table C-7 Molar composition of gas species evolved at 520°C and 750°C and 900°C

	TWD	AW TWD	LM	HM	AW-Cal	AW-Dol	AW-Kao	AW-Pyr	AW-Qz
				mol. %					
				520°C					
H_2	18.6 - 18.7	22.0 - 24.2	16.8 - 18.9	14.6 - 16.7	21.2 - 22.9	20.4 - 21.9	20.8 - 23.5	20.9 - 21.3	22.3 - 22.3
CH_4	31.2 - 31.4	36.1 - 37.9	28.8 - 29.2	28.8 - 30.9	33.8 - 34.3	33.5 - 34.2	36.2 - 37.1	36.5 - 37.1	36.6 - 37.8
CO	23.9 - 24.3	13.7 - 14.5	21.8 - 21.9	17.7 - 19.3	13.2 - 14.0	16.7 - 16.9	14.1 - 14.5	12.6 - 14.2	14.4 - 14.5
CO_2	19.8 - 19.9	17.9 - 18.9	24.7 - 26.1	28.4 - 32.0	23.2 - 24.8	20.8 - 21.2	18.4 - 19.9	21.0 - 22.6	18.7 - 19.3
C_2H_4	0.9 - 1.3	1.1 - 1.3	1.0 - 1.0	0.9 - 1.2	0.9 - 1.2	1.2 - 1.3	1.3 - 1.4	1.0 - 1.4	1.2 - 1.3
C_2H_6	4.1 - 4.6	4.8 - 5.0	3.8 - 4.0	3.4 - 4.5	4.3 - 4.6	4.8 - 5.0	5.0 - 5.2	4.6 - 5.0	4.8 - 4.9
C_3H_4	0.2 - 0.3	0.3 - 0.8	0.4 - 0.5	0.2 - 0.5	0.3 - 0.4	0.5 - 0.5	0.6 - 0.7	0.3 - 0.4	0.3 - 0.5
C_3H_6	0.2 - 0.4	0.3 - 1.0	0.5 - 0.5	0.2 - 0.6	0.3 - 0.4	0.5 - 0.6	0.6 - 0.7	0.5 - 0.5	0.4 - 0.6
C_4s	0.0 - 0.0	0.0 - 0.2	0.0 - 0.0	0.0 - 0.0	0.0 - 0.0	0.0 - 0.0	0.0 - 0.0	0.0 - 0.0	0.0 - 0.0
				750°C					
H_2	31.5 - 32.5	38.0 - 38.4	31.2 - 35.0	26.6 - 29.4	37.2 - 38.2	36.2 - 38.7	37.8 - 39.3	37.6 - 38.8	38.0 - 38.3
CH_4	26.1 - 26.8	20.2 - 21.4	22.7 - 23.0	23.0 - 24.1	27.5 - 28.5	26.4 - 27.9	31.1 - 31.4	30.9 - 31.0	31.4 - 31.5
CO	25.5 - 25.9	26.9 - 27.0	26.4 - 26.7	21.4 - 22.8	14.5 - 15.0	14.3 - 15.4	14.4 - 14.6	12.8 - 13.2	14.2 - 14.3
CO_2	11.8 - 12.4	10.6 - 11.4	12.9 - 16.5	21.4 - 24.1	15.8 - 16.0	15.7 - 17.4	11.0 - 11.3	12.9 - 13.8	11.2 - 11.3
C_2H_4	0.6 - 0.6	0.4 - 0.5	0.4 - 0.5	0.5 - 0.6	0.6 - 0.6	0.4 - 0.6	2.9 - 2.9	0.6 - 0.7	0.7 - 0.7
C_2H_6	2.4 - 2.5	2.0 - 2.2	1.6 - 2.0	2.2 - 2.4	2.1 - 2.5	2.5 - 2.8	0.6 - 0.7	2.6 - 2.9	2.9 - 3.0
C_3H_4	0.2 - 0.5	0.1 - 0.4	0.2 - 0.4	0.3 - 0.4	0.1 - 0.6	0.3 - 0.5	0.5 - 0.7	0.4 - 0.6	0.6 - 0.6
C_3H_6	0.2 - 0.5	0.2 - 0.4	0.2 - 0.4	0.4 - 0.4	0.2 - 0.6	0.3 - 0.5	0.0 - 0.7	0.5 - 0.6	0.6 - 0.6
C_4s	0.0 - 0.1	0.0 - 0.0	0.0 - 0.0	0.0 - 0.0	0.0 - 0.1	0.0 - 0.1	0.0 - 0.1	0.0 - 0.1	0.0 - 0.1

Table C-8 Molar composition of gas species evolved at 900°C

	TWD	AW TWD	LM	HM	AW-Cal	AW-Dol	AW-Kao	AW-Pyr	AW-Qz
	mol. %								
	900°C								
H_2	38.0 - 38.4	44.5 - 46.1	39.3 - 40.6	35.2 - 38.0	35.8 - 38.8	34.9 - 37.0	38.7 - 39.9	38.7 - 43.3	42.0 - 45.2
CH_4	20.2 - 21.4	28.2 - 29.2	20.5 - 21.6	20.7 - 21.3	24.2 - 25.2	24.0 - 24.6	27.5 - 28.4	25.3 - 27.3	28.9 - 30.3
CO	26.9 - 27.0	11.9 - 13.2	24.9 - 26.1	20.7 - 22.6	19.6 - 22.0	20.5 - 22.6	19.7 - 21.7	18.5 - 20.2	13.0 - 13.4
CO_2	10.6 - 11.4	8.8 - 10.4	9.9 - 12.1	17.8 - 17.9	13.1 - 14.5	14.1 - 15.4	8.6 - 9.0	9.6 - 10.7	8.9 - 9.9
C_2H_4	0.4 - 0.5	0.5 - 0.5	0.3 - 0.3	0.4 - 0.4	2.0 - 2.1	0.5 - 0.5	0.4 - 0.5	0.4 - 0.5	0.5 - 0.6
C_2H_6	2.0 - 2.2	2.1 - 2.4	1.1 - 2.1	1.7 - 1.8	0.4 - 0.5	1.9 - 2.1	1.9 - 2.3	1.8 - 2.0	2.4 - 2.6
C_3H_4	0.1 - 0.4	0.3 - 0.6	0.2 - 0.4	0.3 - 0.3	0.4 - 0.5	0.4 - 0.5	0.1 - 0.5	0.4 - 0.4	0.5 - 0.6
C_3H_6	0.2 - 0.4	0.3 - 0.6	0.2 - 0.4	0.3 - 0.3	0.0 - 0.5	0.4 - 0.5	0.3 - 0.4	0.4 - 0.4	0.5 - 0.6
C_4s	0.0 - 0.0	0.1 - 0.1	0.0 - 0.0	0.0 - 0.0	0.1 - 0.1	0.0 - 0.2	0.0 - 0.2	0.0 - 0.2	0.1 - 0.1

C-2.2 Gas yields as identified by GC (mass produced)

Table C-9 and Table C-10 indicate the amount (g) of each gas species formed as identified by GC analyses for the various experimental cases.

Table C-9 Gas yields of the various species identified by GC analyses (g)

	Amount of gas formed (g)									
	520°C	*520-750°C*	*750°C*	*750-900°C*	*900°C*	*520°C*	*520-750°C*	*750°C*	*750-900°C*	*900°C*
	TWD					*AW TWD*				
H_2	0.07	0.16	0.24	0.08	0.31	0.17	0.26	0.43	0.20	0.63
CH_4	0.99	0.56	1.55	-0.19	1.36	2.17	0.67	2.84	0.35	3.19
CO	1.32	1.30	2.63	0.45	3.07	1.44	0.88	2.32	0.12	2.44
CO_2	1.71	0.23	1.95	0.03	1.98	2.96	-0.12	2.83	0.10	2.94
C_2H_4	0.06	0.00	0.06	0.00	0.06	0.12	-0.02	0.10	-0.01	0.10
C_2H_6	0.26	0.01	0.27	-0.02	0.25	0.54	-0.03	0.50	-0.03	0.47
C_3H_4	0.02	0.03	0.05	-0.01	0.04	0.08	0.04	0.12	0.00	0.13
C_3H_6	0.03	0.03	0.06	-0.01	0.05	0.10	0.04	0.14	0.00	0.14
C_4s	0.00	0.00	0.01	0.00	0.00	0.02	0.00	0.02	0.01	0.03
Total	**4.46**	**2.34**	**6.81**	**0.55**	**7.13**	**7.60**	**1.88**	**9.31**	**0.79**	**10.06**
	LM					**HM**				
H_2	0.08	0.16	0.24	0.22	0.46	0.09	0.12	0.21	0.16	0.36
CH_4	1.06	0.27	1.34	0.61	1.95	1.30	0.07	1.37	0.28	1.65
CO	1.40	1.32	2.71	1.40	4.12	1.41	0.84	2.25	0.73	2.98
CO_2	2.55	-0.19	2.36	0.43	2.79	3.61	0.03	3.64	0.20	3.85
C_2H_4	0.06	-0.02	0.04	0.01	0.05	0.08	-0.02	0.06	0.00	0.06
C_2H_6	0.27	-0.07	0.20	0.08	0.28	0.32	-0.07	0.25	0.01	0.26
C_3H_4	0.04	0.00	0.05	0.02	0.07	0.04	0.01	0.05	0.01	0.07
C_3H_6	0.05	0.00	0.05	0.03	0.08	0.05	0.01	0.06	0.01	0.07
C_4s	0.00	0.00	0.01	0.00	0.01	0.00	0.00	0.01	0.00	0.01
Total	**5.52**	**1.75**	**7.00**	**2.80**	**9.80**	**6.90**	**1.14**	**7.90**	**1.40**	**9.30**
	AW-Cal					**AW-Dol**				
H_2	0.15	0.32	0.47	0.05	0.52	0.15	0.25	0.40	0.06	0.46
CH_4	1.78	1.00	2.78	-0.02	2.76	1.90	0.42	2.32	0.17	2.50
CO	1.24	1.31	2.55	1.51	4.06	1.65	0.56	2.22	1.65	3.87
CO_2	3.45	0.88	4.33	-0.10	4.23	3.25	0.63	3.89	0.27	4.15
C_2H_4	0.10	0.00	0.10	0.30	0.40	0.13	-0.05	0.08	0.01	0.08
C_2H_6	0.44	0.00	0.43	-0.33	0.10	0.51	-0.09	0.42	-0.03	0.39
C_3H_4	0.05	0.05	0.09	0.04	0.13	0.07	0.02	0.10	0.02	0.11
C_3H_6	0.05	0.05	0.10	-0.02	0.08	0.08	0.02	0.10	0.02	0.12
C_4s	0.00	0.01	0.01	0.02	0.03	0.00	0.01	0.01	0.02	0.04
Total	**7.25**	**3.62**	**10.87**	**1.93**	**12.33**	**7.76**	**1.92**	**9.54**	**2.22**	**11.73**

Table C-10 Gas yields of the various species identified by GC analyses (g)

	Amount of gas formed (g)									
	520 °C	*520-750°C*	*750° C*	*750-900°C*	*900° C*	*520° C*	*520-750°C*	*750° C*	*750-900°C*	*900° C*
	AW-Kao					**AW-Pyr**				
H_2	0.17	0.28	0.44	0.06	0.51	0.15	0.24	0.40	0.12	0.52
CH_4	2.22	0.65	2.86	0.00	2.87	2.11	0.43	2.54	0.09	2.63
CO	1.51	0.81	2.32	1.39	3.71	1.34	0.52	1.87	1.51	3.38
CO_2	3.19	-0.38	2.80	-0.33	2.47	3.43	-0.41	3.02	-0.24	2.78
C_2H_4	0.14	0.32	0.46	-0.38	0.08	0.12	-0.02	0.09	-0.01	0.08
C_2H_6	0.58	-0.47	0.11	0.29	0.40	0.51	-0.09	0.43	-0.07	0.36
C_3H_4	0.10	0.05	0.15	-0.07	0.07	0.06	0.06	0.12	-0.01	0.10
C_3H_6	0.11	-0.02	0.09	0.02	0.11	0.08	0.05	0.13	-0.02	0.11
C_4s	0.01	0.01	0.02	0.01	0.03	0.00	0.01	0.01	0.03	0.04
Total	**8.01**	**2.12**	**9.26**	**1.78**	**10.25**	**7.80**	**1.32**	**8.60**	**1.75**	**10.00**
	AW-Qz									
H_2	0.18	0.27	0.45	0.14	0.59					
CH_4	2.36	0.59	2.95	0.22	3.17					
CO	1.60	0.74	2.33	0.13	2.47					
CO_2	3.30	-0.41	2.89	-0.12	2.77					
C_2H_4	0.14	-0.03	0.11	-0.01	0.10					
C_2H_6	0.58	-0.06	0.52	-0.02	0.50					
C_3H_4	0.07	0.08	0.14	0.01	0.15					
C_3H_6	0.08	0.08	0.16	0.01	0.17					
C_4s	0.00	0.01	0.02	0.01	0.03					
Total	**8.30**	**1.76**	**9.56**	**0.52**	**9.93**					

C-2.3 Error on repeatability for GC Analyses results (Section 5.3.2)

Table C-11 and Table C-12 indicate the error on repeatability values within a 95% confidence interval for the results in Section 5.3.2. Relating the gas yields of the respective species on a g gas / g coal (d.m.m.f.) (x 10^{-3}).

Table C-11 Error on repeatability within a 95% confidence interval for TWD, AW TWD, LM and HM derived gases

	TWD			AW TWD			LM			HM		
	520°C	*750°C*	*900°C*	*520°C*	*750°C*	*900°C*	*520°C*	*750°C*	*900°C*	*520°C*	*750°C*	*900°C*
H_2	0.0	0.2	0.1	0.2	0.1	0.2	0.2	0.6	0.5	0.3	0.5	0.7
CH_4	0.1	1.0	1.3	0.8	1.2	1.2	0.2	1.7	2.5	2.7	0.0	0.2
CO	0.3	0.5	0.8	0.7	1.2	2.6	0.4	3.4	5.3	3.3	4.1	2.5
CO_2	0.1	0.4	1.1	1.3	0.8	5.0	0.8	4.8	4.9	3.5	4.3	1.7
C_2H_4	0.3	0.0	0.1	0.2	0.1	0.2	0.0	0.1	0.1	0.3	0.0	0.0
C_2H_6	0.4	0.0	0.2	0.3	0.0	0.8	0.0	0.2	1.9	1.2	0.2	0.1
C_3H_4	0.1	0.6	0.4	0.9	0.4	0.8	0.0	0.2	0.6	0.6	0.1	0.0
C_3H_6	0.2	0.5	0.4	1.1	0.2	0.9	0.0	0.2	0.8	0.7	0.1	0.0
C_4s	0.0	0.1	0.0	0.5	0.0	1.2	0.0	0.1	0.1	0.1	0.0	0.0

Table C-12 Error on repeatability within a 95% confidence interval for AW-Cal, AW-Dol, AW-Kao, AW-Pyr and AW-Qz

	AW-Cal			AW-Dol			AW-Kao			AW-Pyr			AW-Qz		
	520°C	*750°C*	*900°C*	*520°C*	*750°C*	*900°C*	*520°C*	*750°C*	*900°C*	*520°C*	*750°C*	*900°C*	*520°C*	*750°C*	*900°C*
H_2	0.2	0.3	0.8	0.1	0.5	0.5	0.3	0.3	0.3	0.1	0.3	1.0	0.0	0.1	0.8
CH_4	0.2	2.0	3.2	0.1	0.2	1.7	0.3	0.6	1.8	0.8	0.8	0.2	1.1	0.3	0.2
CO	1.1	0.1	1.9	0.1	2.7	2.5	0.1	0.4	2.7	2.0	1.4	0.7	0.1	0.2	0.6
CO_2	1.3	1.0	1.5	0.1	2.4	1.9	1.3	0.1	1.7	2.0	1.1	1.2	0.7	0.2	1.3
C_2H_4	0.2	0.0	0.5	0.1	0.3	0.1	0.1	0.0	0.2	0.4	0.1	0.0	0.1	0.0	0.0
C_2H_6	0.4	0.6	0.2	0.1	0.7	0.5	0.1	0.0	0.9	0.4	0.3	0.0	0.0	0.0	0.2
C_3H_4	0.2	1.2	0.4	0.0	0.4	0.5	0.2	0.4	1.1	0.2	0.5	0.3	0.3	0.1	0.0
C_3H_6	0.2	1.2	1.6	0.0	0.4	0.5	0.2	1.9	0.4	0.1	0.4	0.2	0.3	0.1	0.0
C_4s	0.0	0.2	0.1	0.0	0.1	0.7	0.0	0.1	0.7	0.0	0.2	0.7	0.0	0.1	0.0

C-3 Simdis analyses (Repeatability)

Figure C-1 to Figure C-3 indicates the repeatability curves of the analysed tars.

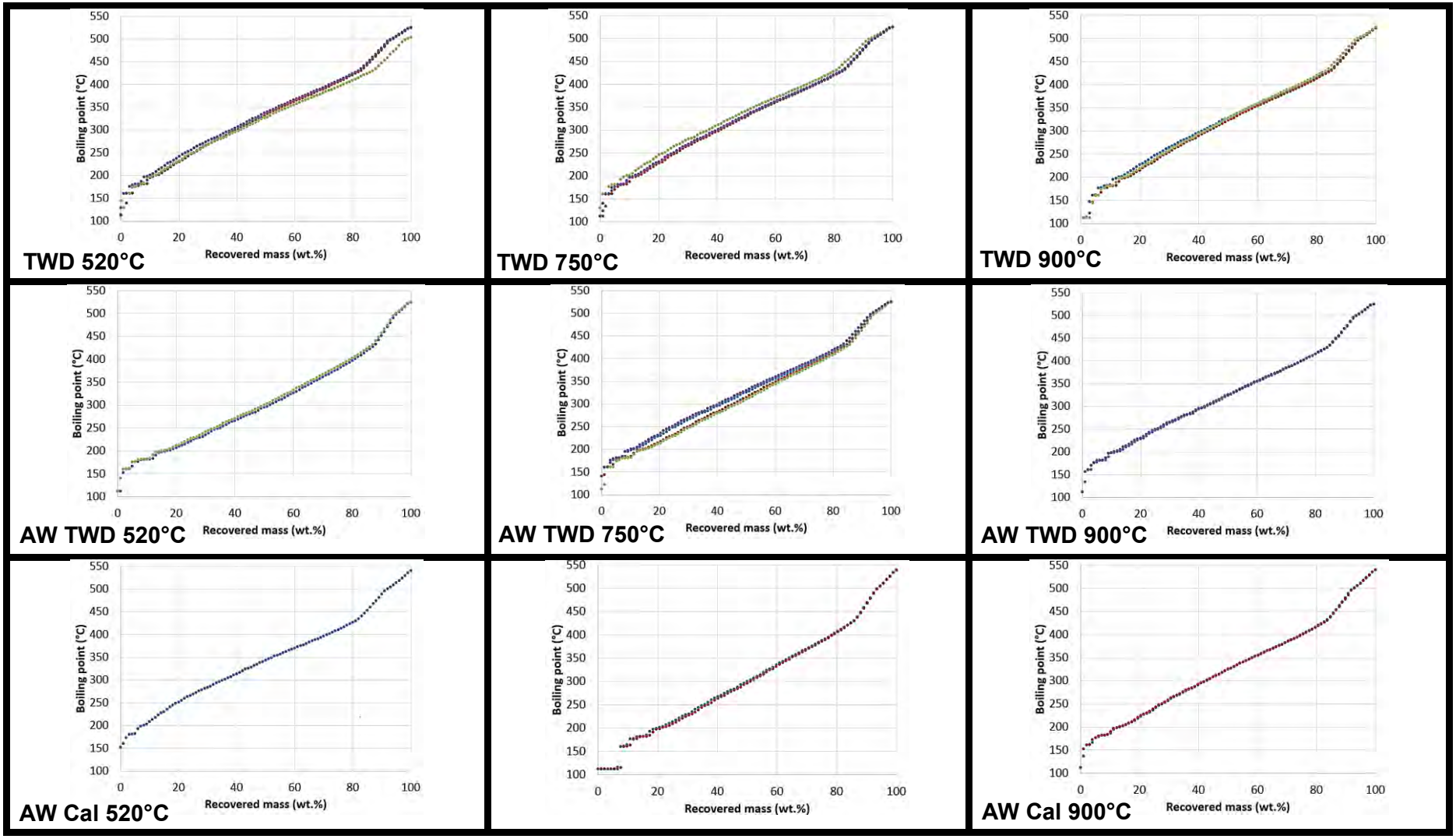

Figure C-1 Simdis repeatability curves I

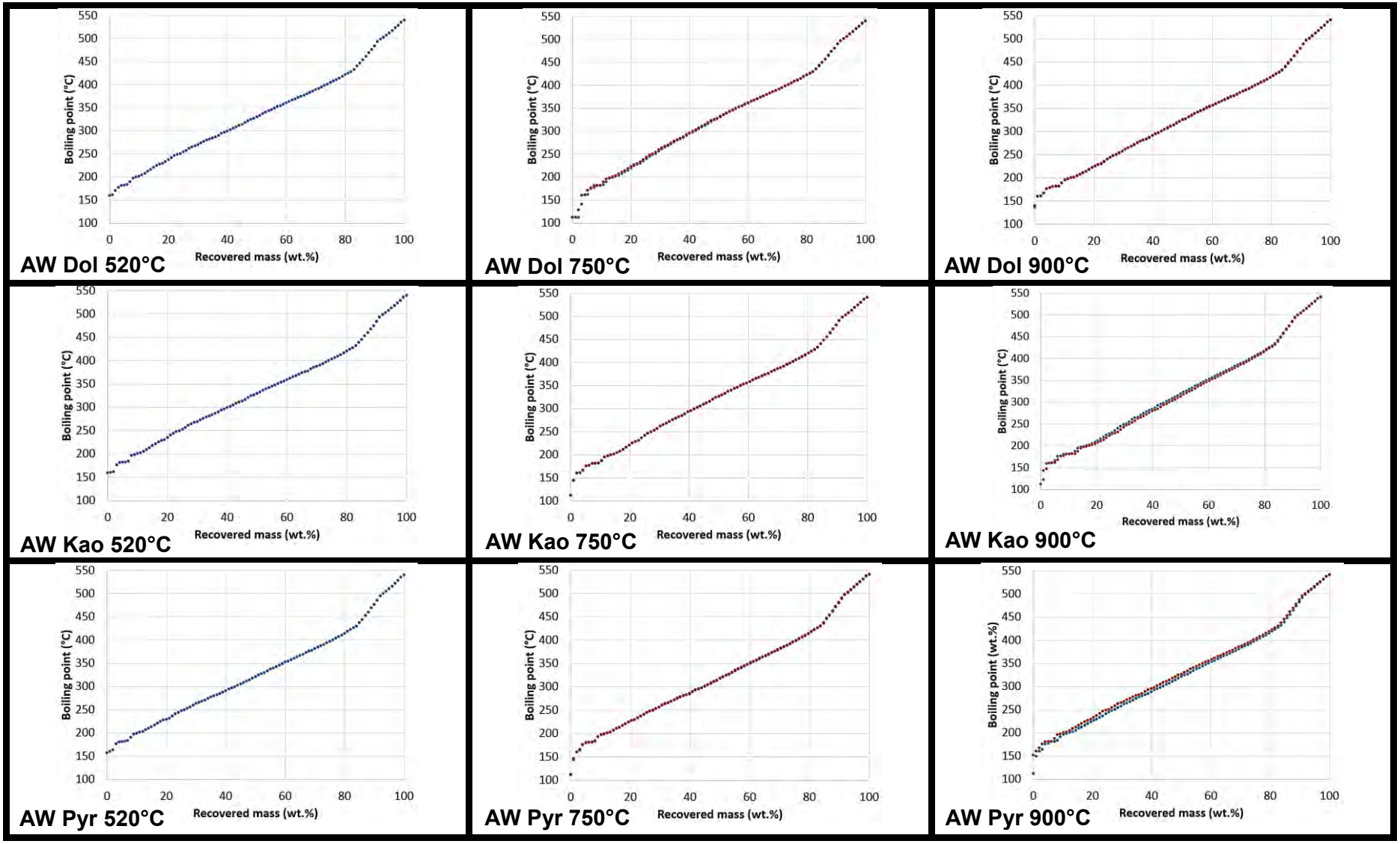

Figure C-2 Simdis repeatability curves II

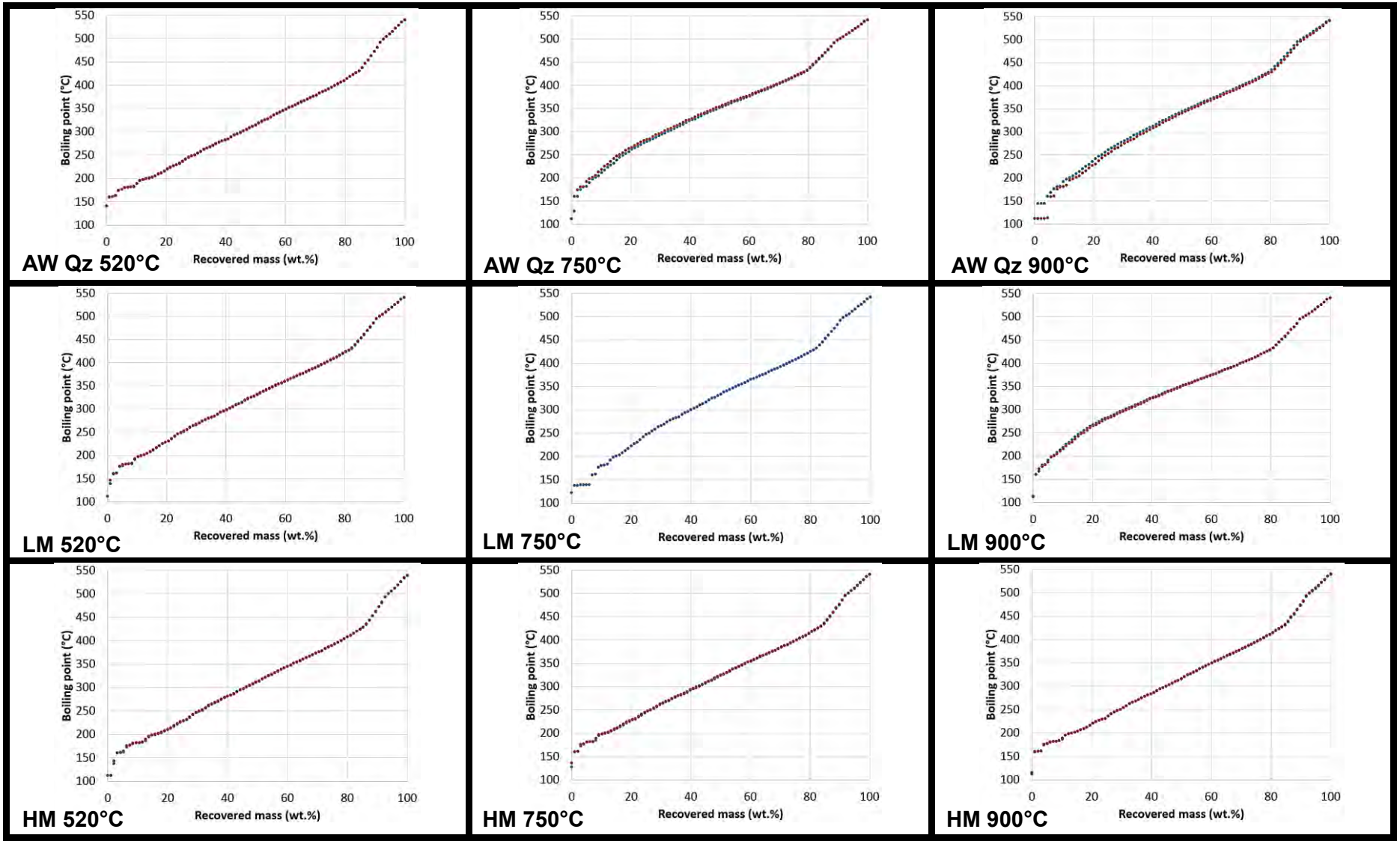

Figure C-3 Simdis repeatability curves III

C-4 GC-MS and -FID analyses

The full set of GC-MS and –FID results of the analysed tars are indicated in Table C-13. The confidence interval (C.I.) is also provided.

Table C-13 GC-MS and -FID analyses results for the derived tars on a g molecular family / g coal (d.m.m.f.) x 10^{-3} basis.

	TWD		AW TWD		AW-Cal		AW-Dol		AW-Kao		AW-Pyr		AW-Qz		LM		HM	
	wt%	C.I.*	wt%	C.I.*	wt%	C.I.*	wt%	C.I.*	wt%	C.I.*	wt%	C.I.*	wt%	C.I.*	wt%	C.I.*	wt%	C.I.*
520°C																		
Aliph.	2.12	0.09	1.23	0.15	1.02	0.09	1.08	0.22	1.08	0.25	0.89	0.04	1.08	0.02	1.22	0.22	1.05	0.01
A-B	0.39	0.14	0.24	0.24	0.13	0.15	0.07	0.07	0.07	0.18	0.06	0.04	0.45	0.03	0.18	0.13	0.30	0.01
A-P	15.28	1.12	9.33	0.27	5.44	1.91	6.34	1.09	6.81	0.31	5.08	0.32	7.39	0.40	9.21	1.74	7.93	0.35
Arom. E & E	0.51	0.65	0.33	0.14	0.07	0.23	0.08	0.02	0.09	0.03	0.07	0.01	0.43	0.01	0.11	0.02	0.11	0.01
A-I	0.03	0.01	0.02	0.02	0.00	0.01	0.00	0.02	0.00	0.00	0.00	0.00	0.03	0.00	0.01	0.00	0.07	0.11
A-N	1.02	0.05	0.72	0.13	0.44	0.14	0.52	0.19	0.56	0.03	0.46	0.03	0.64	0.03	0.67	0.11	0.66	0.04
PAH's	0.08	0.03	0.04	0.03	0.00	0.03	0.09	0.06	0.01	0.01	0.00	0.00	0.08	0.00	0.05	0.01	0.07	0.01
N-	2.46	0.31	1.20	0.25	1.17	0.06	1.11	0.32	1.23	0.01	0.98	0.46	1.04	0.03	1.33	0.05	1.15	0.04
Mixed	18.33	1.53	10.25	0.81	8.26	2.61	11.28	1.87	11.32	0.19	9.70	0.89	10.00	0.47	11.95	2.18	11.27	0.23
750°C																		
Aliph.	1.67	0.07	1.39	0.25	1.05	0.04	0.82	0.09	1.02	0.00	1.51	0.02	1.10	0.07	1.26	0.09	1.10	0.12
A-B	0.42	0.21	0.17	0.17	0.23	0.06	0.27	0.03	0.55	0.01	0.25	0.02	0.19	0.06	0.26	0.10	0.26	0.03
A-P	14.67	1.53	9.78	0.50	7.38	0.80	6.23	0.43	7.34	0.24	9.13	0.16	5.72	0.18	7.86	1.13	7.73	1.43
Arom. E & E	0.27	0.17	0.18	0.20	0.06	0.10	0.14	0.01	0.43	0.02	0.27	0.01	0.16	0.00	0.18	0.03	0.19	0.02
A-I	0.02	0.03	0.01	0.02	0.02	0.00	0.02	0.01	0.03	0.00	0.02	0.00	0.01	0.00	0.02	0.00	0.02	0.00
A-N	1.03	0.07	0.77	0.04	0.58	0.06	0.55	0.07	0.65	0.02	0.76	0.01	0.55	0.02	0.70	0.07	0.69	0.14
PAH's	0.06	0.08	0.05	0.05	0.05	0.01	0.05	0.02	0.09	0.01	0.06	0.00	0.04	0.00	0.07	0.01	0.06	0.01
N-	2.11	0.31	1.46	0.44	1.00	0.02	1.07	0.13	1.21	0.02	1.37	0.23	1.49	0.42	1.51	0.05	1.24	0.20
Mixed	14.06	1.78	11.90	0.72	10.99	1.10	11.04	0.74	11.92	0.29	12.00	0.44	9.76	0.27	13.79	1.37	13.51	1.91
900°C																		
Aliph.	1.84	0.18	1.30	0.26	0.59	0.05	0.69	0.03	1.08	0.13	1.40	0.06	1.01	0.01	0.56	0.09	0.82	0.03
A-B	0.64	0.33	0.09	0.06	0.16	0.01	0.21	0.00	0.77	0.10	0.35	0.00	0.35	0.02	0.05	0.02	0.11	0.04
A-P	13.99	1.50	8.24	0.18	4.98	0.04	4.66	0.07	10.38	0.17	9.02	0.00	5.52	0.24	2.24	0.29	5.04	0.16
Arom. E & E	0.89	0.55	0.11	0.11	0.06	0.00	0.15	0.02	0.66	0.02	0.47	0.00	0.24	0.00	0.05	0.01	0.08	0.11
A-I	0.04	0.02	0.01	0.01	0.01	0.00	0.02	0.00	0.04	0.00	0.03	0.00	0.02	0.00	0.01	0.00	0.01	0.00
A-N	1.05	0.05	0.43	0.42	0.38	0.00	0.35	0.01	0.96	0.02	0.79	0.00	0.54	0.02	0.22	0.07	0.46	0.02
PAH's	0.11	0.04	0.03	0.02	0.04	0.00	0.05	0.00	0.14	0.00	0.08	0.00	0.06	0.01	0.02	0.00	0.04	0.00
N-	2.07	0.49	1.22	0.13	0.75	0.04	0.78	0.02	1.06	0.01	1.47	0.00	1.31	0.11	0.79	0.13	0.98	0.02
Mixed	16.44	1.43	11.08	0.21	7.35	0.06	7.42	0.13	12.75	0.10	10.57	0.05	10.84	0.13	7.41	0.45	10.80	0.17

C-5 SEC-UV analyses (Repeatability)

The repatability curves of the SEC-UV analyses of the derived tars are indicated in Figures C-4 to Figure C-6.

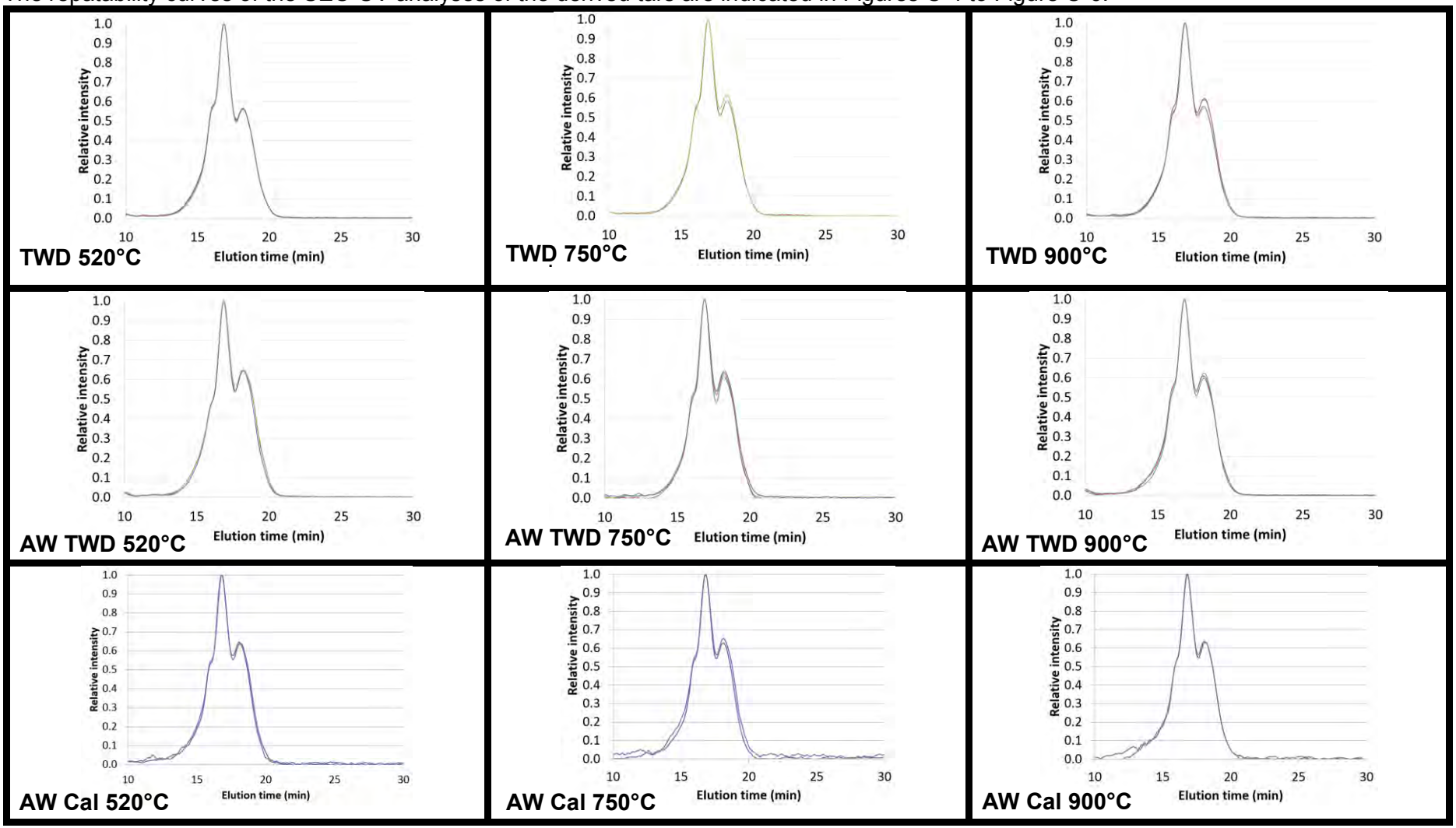

Figure C-4 SEC-UV repeatability curves I

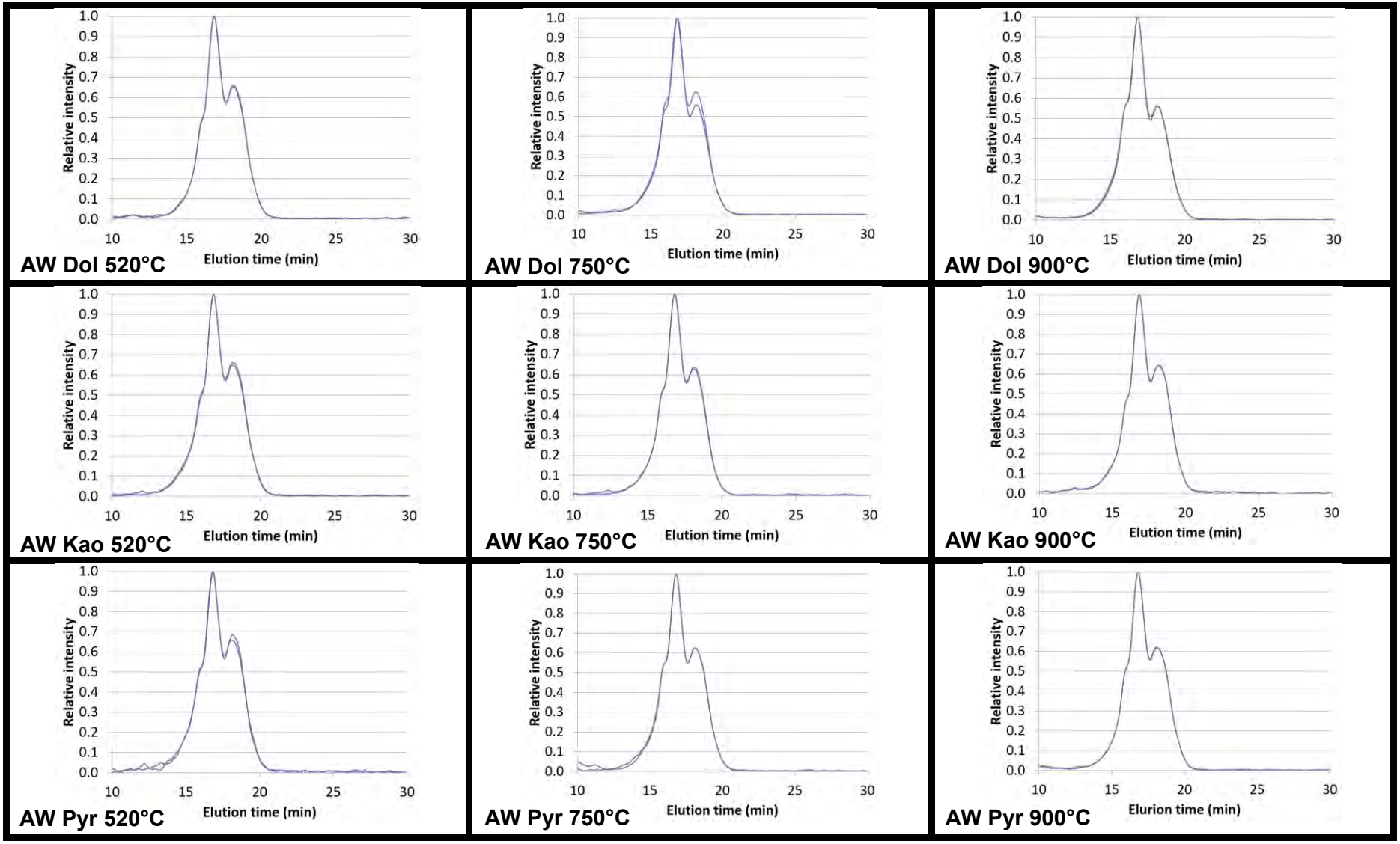

Figure C-5 SEC-UV repeatability curves II

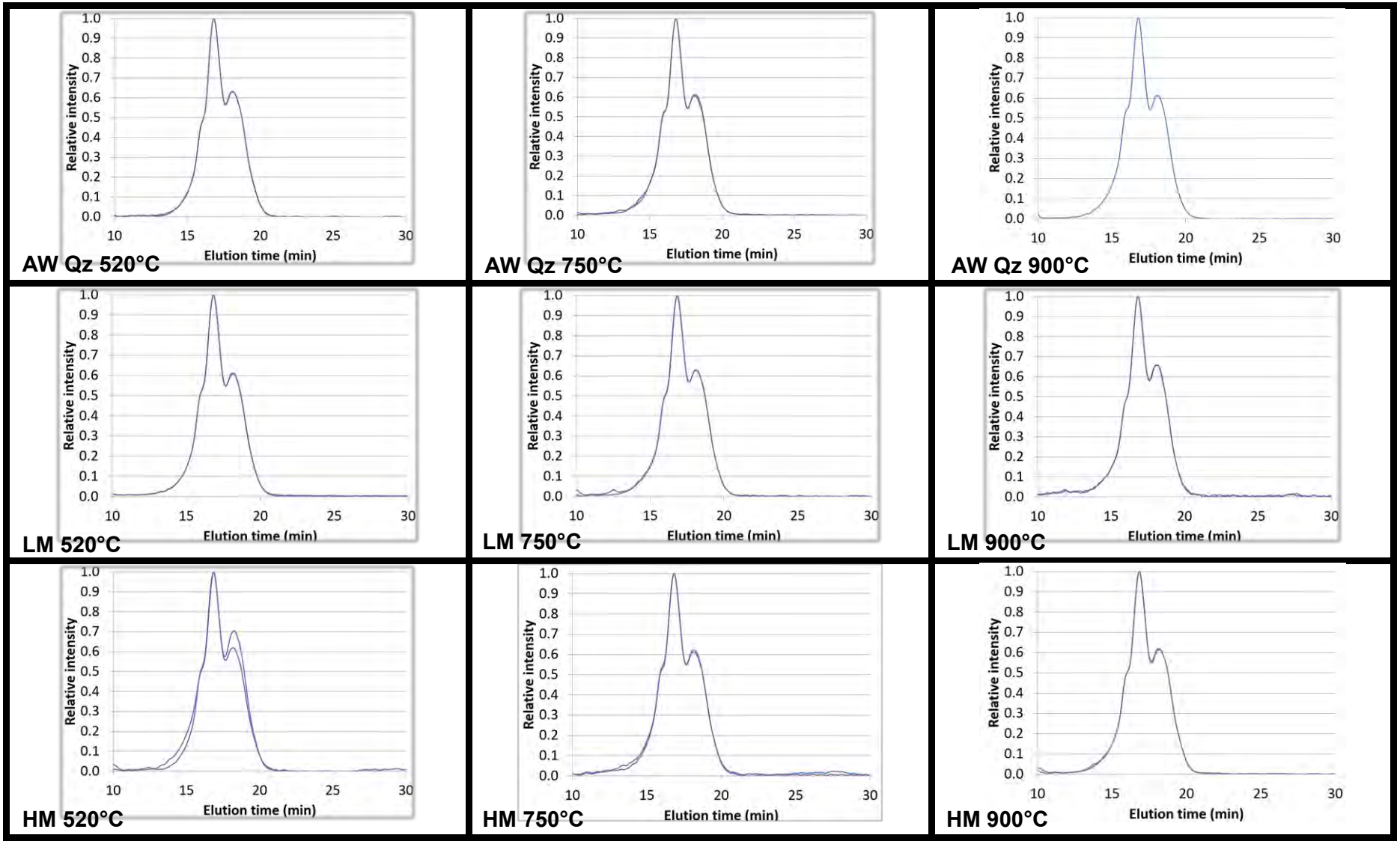

Figure C-6 SEC-UV repeatability curves III

C-6 XRD Spectra

The XRD spectra of the analysed chars are indicated in Figure C-7 to Figure C-15.

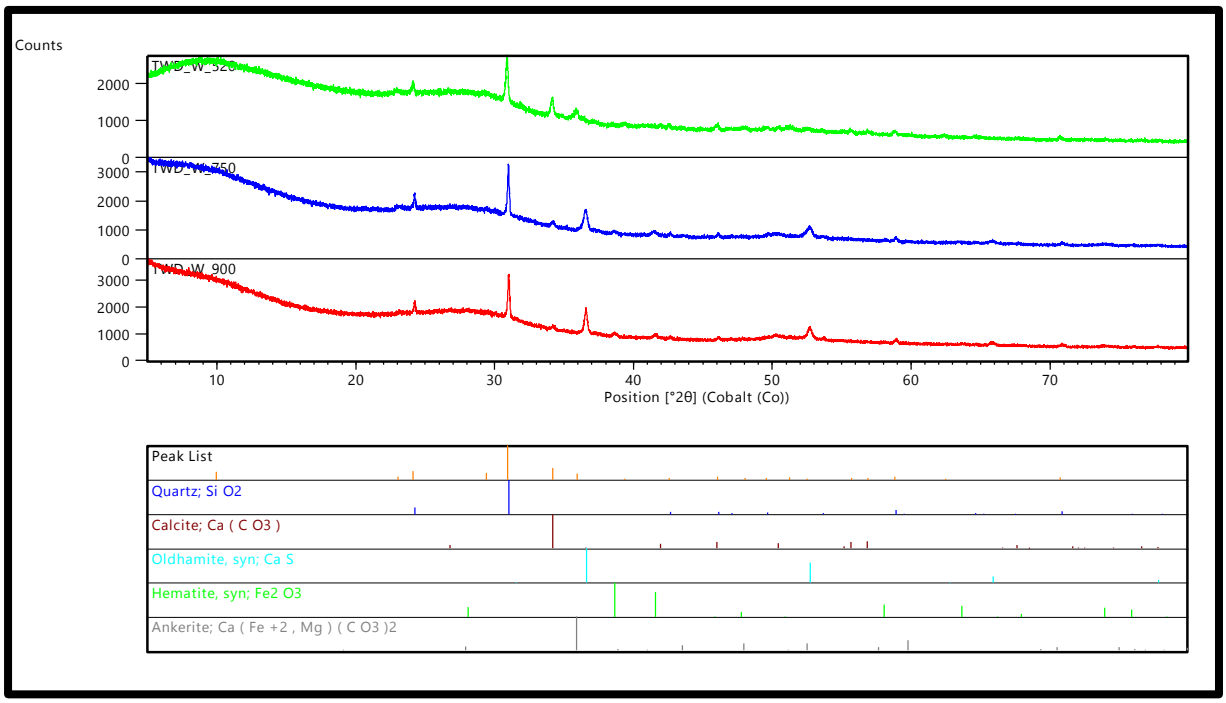

Figure C-7 TWD chars XRD spectra

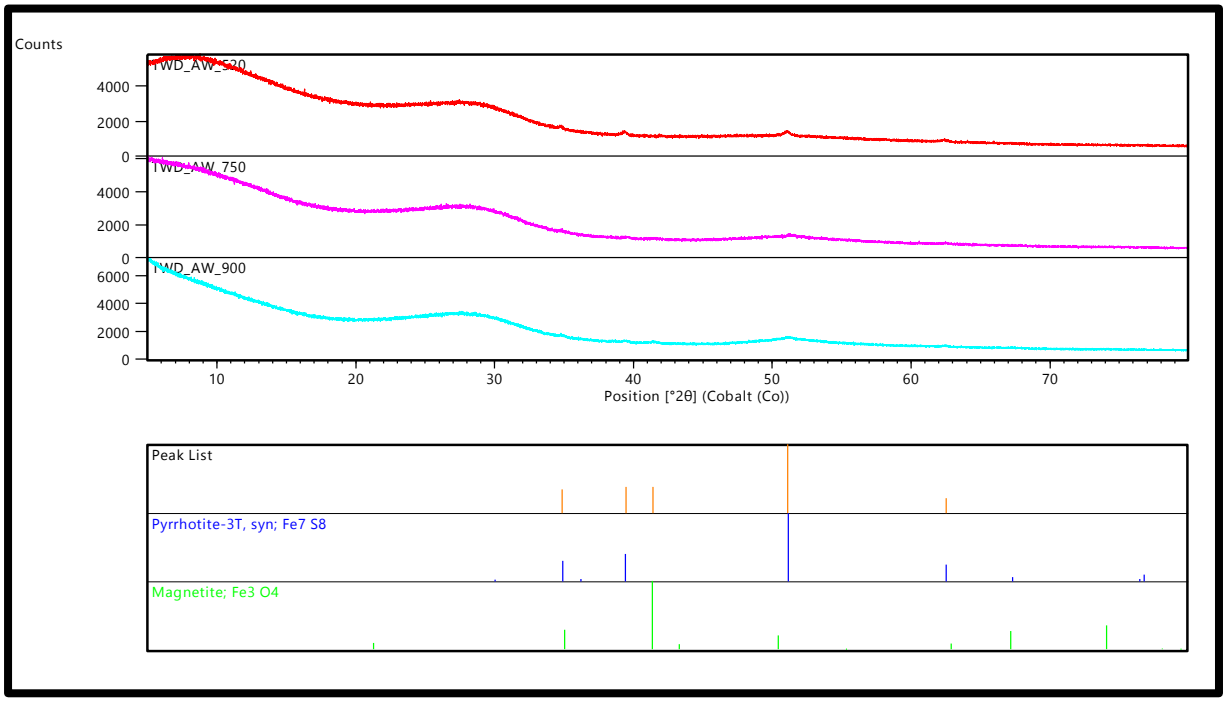

Figure C-8 AW TWD chars XRD spectra

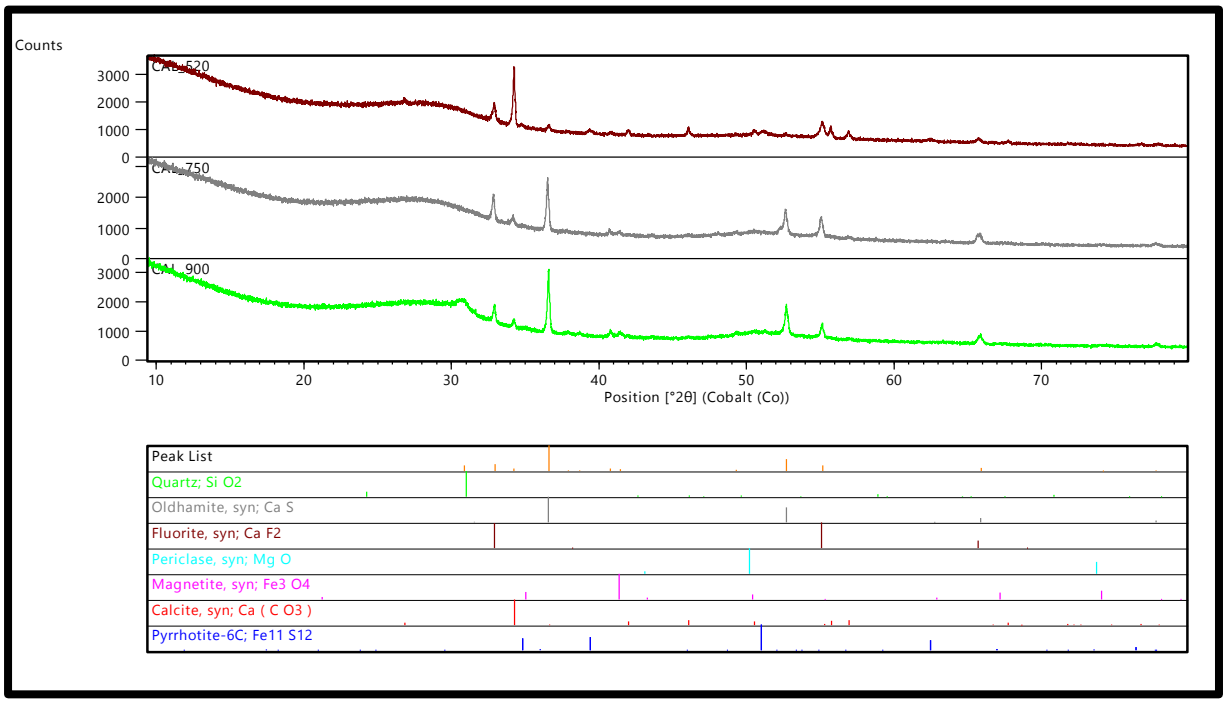

Figure C-9 AW Cal chars XRD spectra

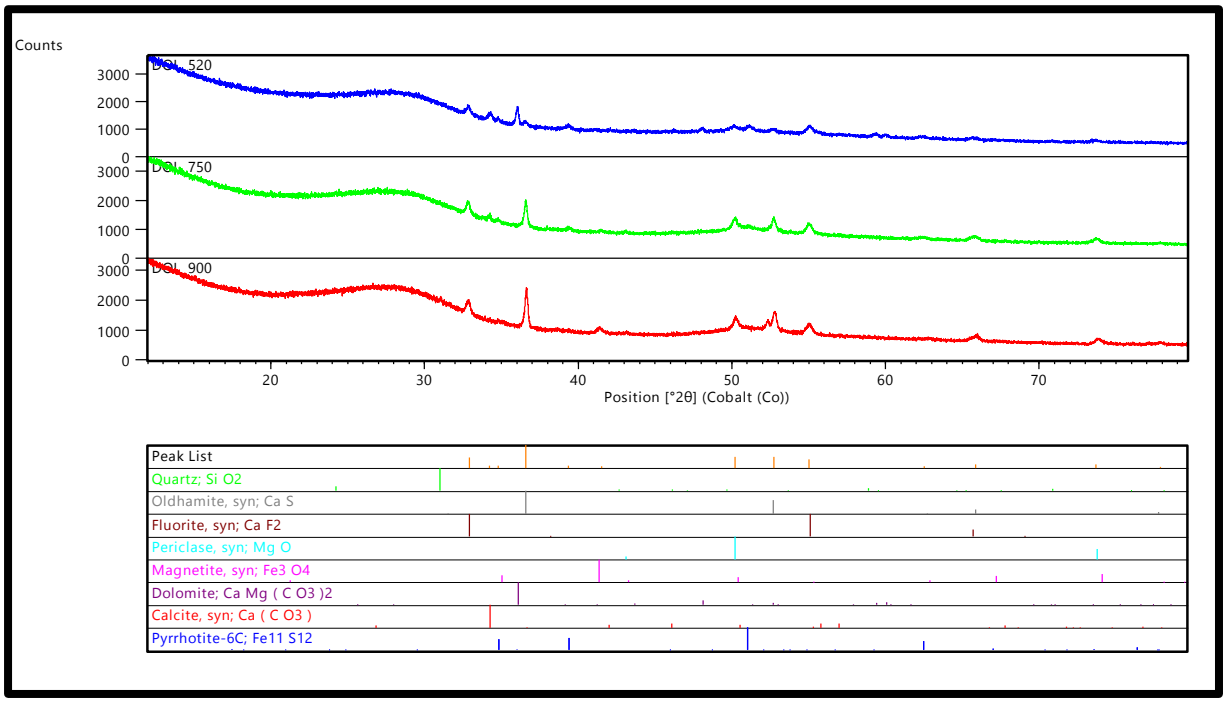

Figure C-10 AW Dol chars XRD spectra

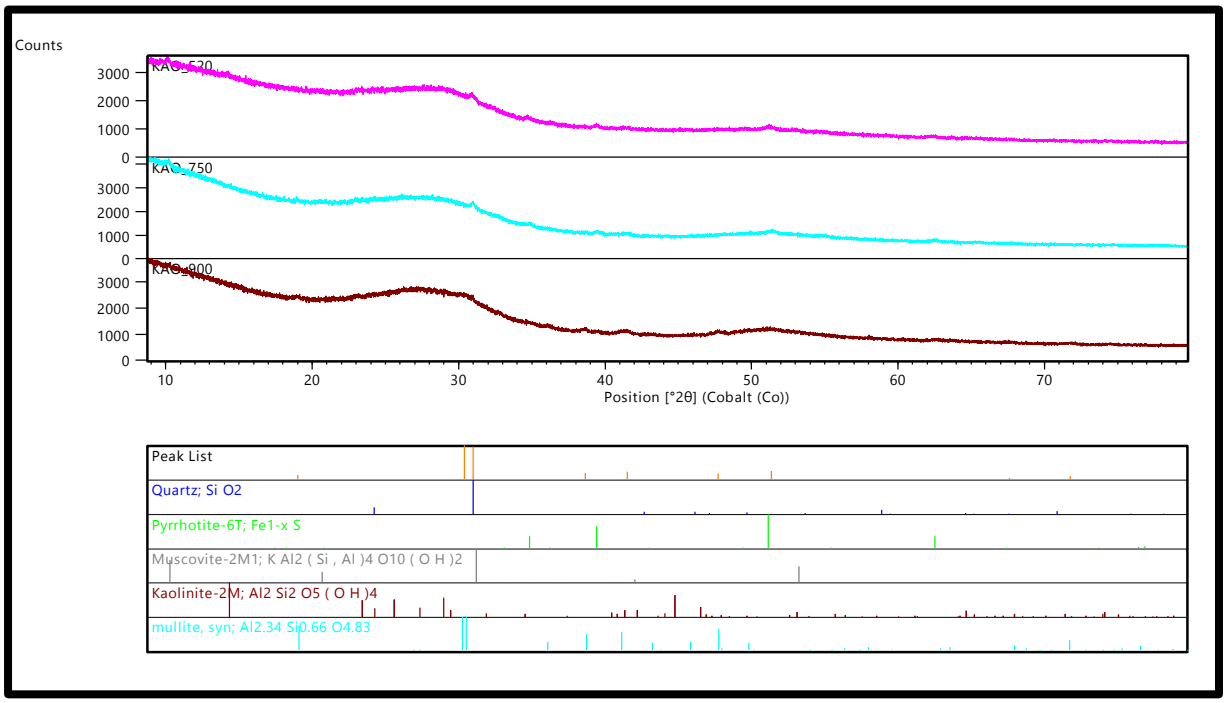

Figure C-11 AW Kao chars XRD spectra

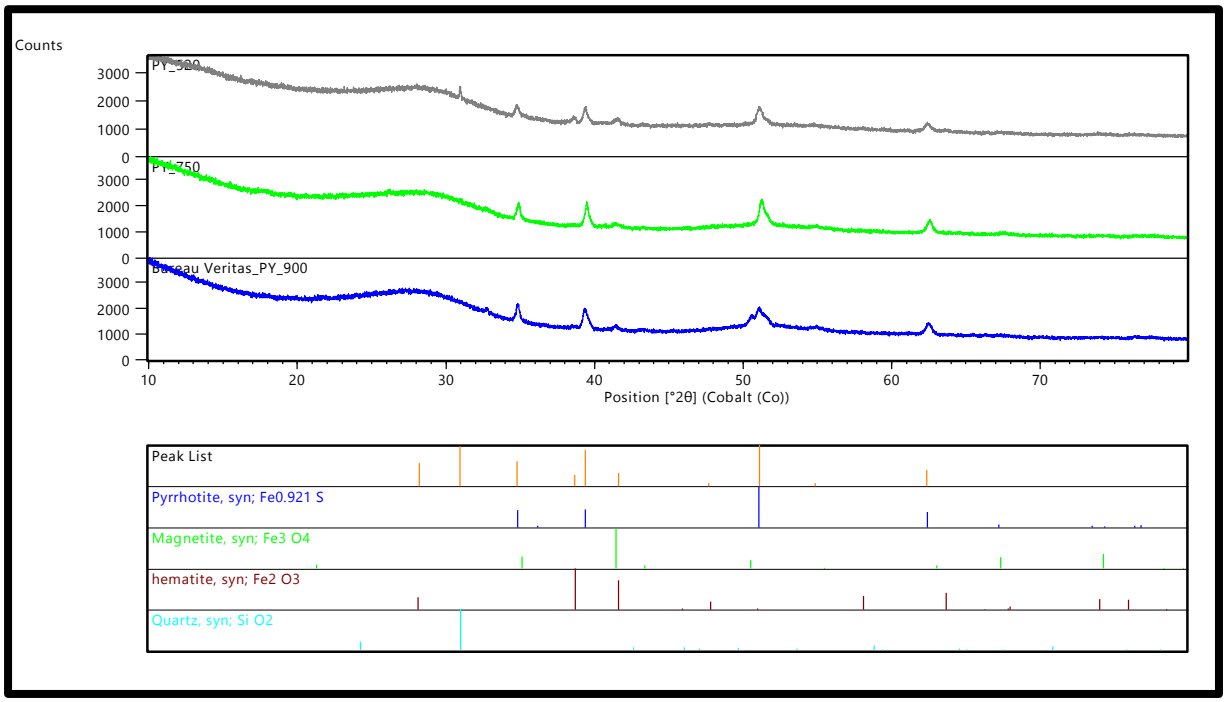

Figure C-12 AW Pyr chars XRD spectra

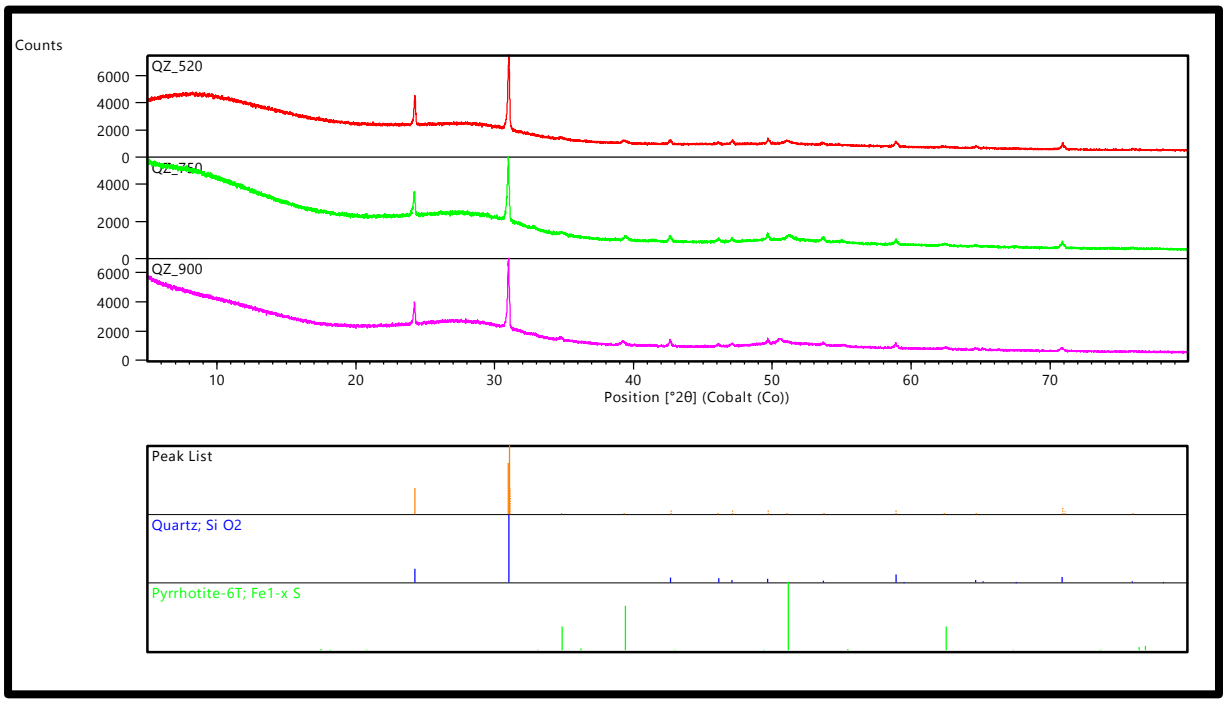

Figure C-13 AW Qz chars XRD spectra

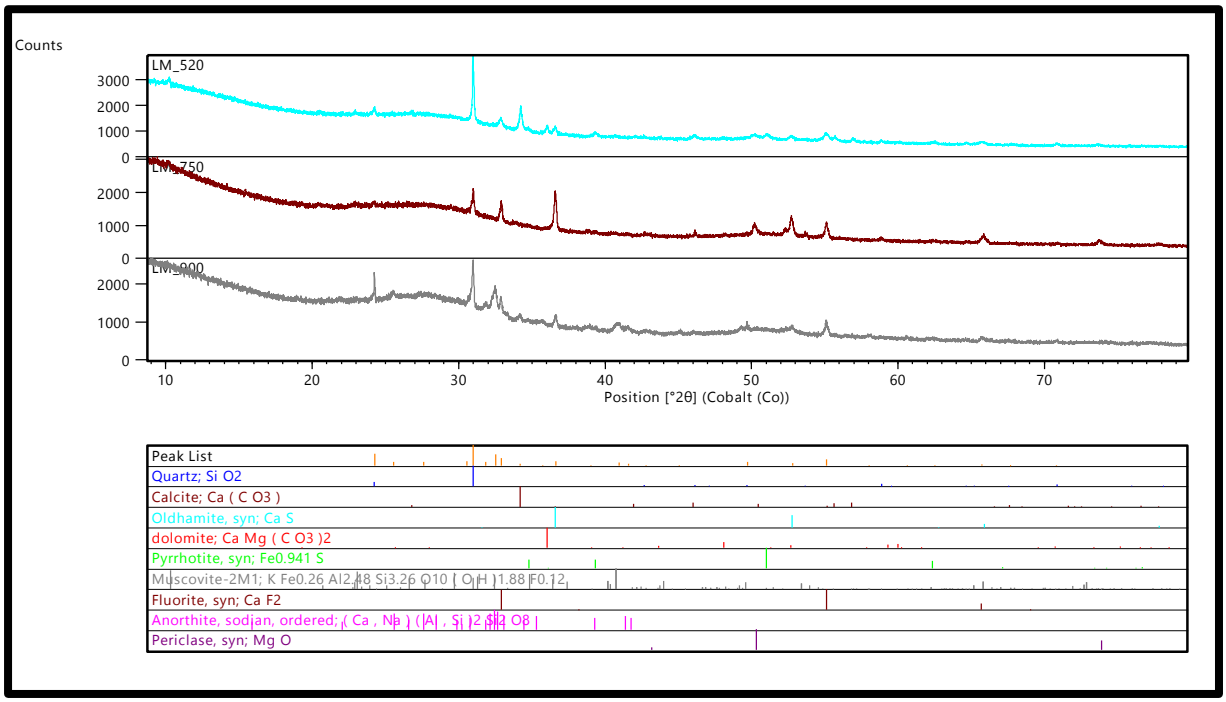

Figure C-14 LM chars XRD spectra

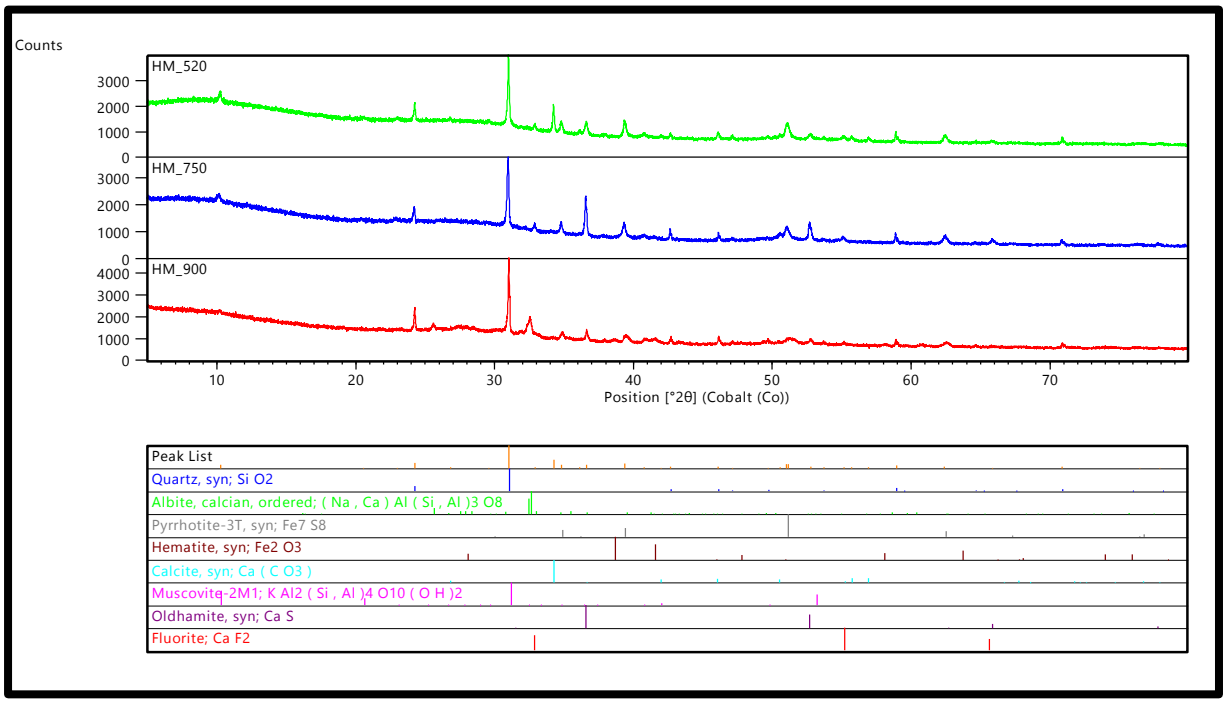

Figure C-15 HM chars XRD spectra

C-7 Qualifying experiments pyrolysis product yields

The as determined (Table C-14), mineral matter free basis (Table C-15) and dry, mineral matter free (Table C-16) pyrolysis products yield results for the qualifying experiments (Section 6.2.5) are reported.

Table C-14 Pyrolysis product yields for control experiments (as determined)

	TWD	TWD-Cal	TWD-Dol	TWD-Kao	TWD-Pyr	TWD-Qz
			wt%			
Water	6.9	7.3	7.5	7.0	7.0	6.7
Tar	7.3	6.2	6.5	7.8	7.0	7.2
Char	70.5	68.8	69.5	70.0	70.4	71.4
Gas	14.9	17.7	16.5	15.1	15.7	14.7
TOTAL	**100.0**	**100.0**	**100.0**	**100.0**	**100.0**	**100.0**

Table C-15 Pyrolysis product yields for control experiments (m.m.f.b.)

	TWD	TWD-Cal	TWD-Dol	TWD-Kao	TWD-Pyr	TWD-Qz
			wt%			
Water	8.9	9.2	8.6	8.6	8.3	8.6
Tar	7.1	7.4	9.0	7.9	8.2	8.4
Char	63.8	64.5	65.1	65.6	66.7	66.0
Gas	20.3	18.9	17.3	17.9	16.8	17.1
TOTAL	**100.0**	**100.0**	**100.0**	**100.0**	**100.0**	**100.0**

Table C-16 Pyrolysis product yields for control experiments (d.m.m.f.)

	TWD	TWD-Cal	TWD-Dol	TWD-Kao	TWD-Pyr	TWD-Qz
			wt%			
Tar	7.7	8.2	9.8	8.7	9.0	9.1
Char	70.0	71.0	71.3	71.7	72.7	72.2
Gas	22.2	20.8	18.9	19.6	18.3	18.7
TOTAL	**100.0**	**100.0**	**100.0**	**100.0**	**100.0**	**100.0**

C-8 FactSage evaluation of model coal-mineral mixtures

FactSage is a thermodynamic software package and it is mainly applied in the field of complex equilibrium and process simulation applications. The advantage provided by the software is that it can handle carbon reactions along with minerals, whilst the gas composition and atmosphere are varied (Van Dyk *et al.,* 2006). The software and the results produced by the use of this software will be evaluated in Chapter 6 of this study. For now, the results obtained for the various mineral mixtures and coal simulations will be evaluated as to motivate the manner in which the coal mineral mixtures were set up.

C-8.1 FactSage input data of coal-mineral mixtures

The input to the FactSage model that was used, was compiled using the results obtained from the coal characterisation. Three input data sets were evaluated:

I. Standard models. Input based on the proximate, ultimate and XRF ash analyses results, as done in previous studies in which FactSage was used for modelling of the heat treatment of coal (Hlatswayo, 2008; Van Dyk et al., 2008; Matjie et al., 2006; Van Dyk et al., 2006).
II. XRD models. Input based on the proximate, ultimate and mineral XRD analysis results.
III. QEMSCAN models. Input based on the proximate, ultimate and QEMSCAN analysis results.

The motivation for comparison of these three data sets resides in the fact that characterisation of the mineral phase by QEMSCAN gives the best overview of the mineral matter in its original form inside the coal matrix, whilst XRF ash analyses report all species as certain oxides. The author could also not find previous studies looking into these modelling methods. For Case I the minerals added for the mineral mixture were based on the XRD analyses results and on the QEMSCAN analyses results. These two methods of addition will be evaluated. The proximate, ultimate, XRF, XRD and QEMSCAN analyses results on the AW TWD coal was used as basis for the mineral mixture models. The amount of mineral matter to be added was determined by assuming a constant carbon value from the ultimate analysis results.

In Cases II and III all mineral phases were based on the composition as identified by XRD or QEMSCAN, without use of the XRF analysis results. The operating conditions for all three models were as follows: An inert atmosphere of N_2, starting at ambient temperature of 25°C and operating pressure as determined from the experimental setup of 0.88 bar. Table C-17 indicates the inputs used for the FactSage model. The amount of N_2 in the setup was calculated as outlined in Appendix B-1.

Table C–17 Input in FactSage of coal-mineral mixture models.

	Standard models			Models based on XRD		Models based on QEMSCAN	
	TWD	MM XRD	MM QEMSCAN	TWD	MM	TWD	MM
	mass of component (g)						
C	32.210	32.210	32.210	32.210	33.701	32.210	33.701
H	1.922	1.885	1.885	1.922	1.972	1.922	1.972
N	0.869	0.880	0.880	0.869	0.920	0.869	0.920
O	5.170	4.607	4.607	5.170	4.821	5.170	4.821
S	0.567	0.515	0.515	0.567	0.539	0.567	0.539
Moisture	2.099	0.964	0.964	2.099	1.008	2.099	1.008
Ash	7.162	0.836	0.836	7.162	7.162	7.162	7.162
Al2O3	1.806	0.125	0.125				
CaO	0.820	0.073	0.073				
Cr2O3	0.004	0.002	0.002				
Fe2O3	0.684	0.327	0.327				
K2O	0.046	0.004	0.004				
MgO	0.265	0.042	0.042				
MnO	0.008	0.000	0.000				
Na2O	0.046	0.010	0.010				
P2O5	0.105	0.002	0.002				
SiO2	2.564	0.043	0.043				
TiO2	0.124	0.048	0.048				
V2O5	0.005	0.002	0.002				
ZrO2	0.009	0.004	0.004				
Ba	0.041	0.021	0.021				
Sr	0.051	0.014	0.014				
SO3	0.584	0.120	0.120				
Calcite		0.592	1.096	0.305	0.448	0.600	0.672
Dolomite		1.182	2.381	1.219	1.194	1.297	1.454
Kaolinite		4.836	4.008	3.733	3.655	2.188	2.452
Pyrite		0.111	0.150	0.686	0.671	1.912	1.200
Quartz		1.382	0.617	1.067	1.044	0.380	0.407
Aragonite				0.152			
Apatite						0.212	0.004
Gibbsite						0.190	0.008
Siderite						0.061	0.000
Illite						0.208	0.001
Microcline						0.080	0.000
Rutile						0.033	0.007
TOTAL	**50.000**	**50.000**	**50.000**	**50.000**	**50.000**	**50.000**	**50.000**

C-8.2 FactSage – Results and Discussion of model coal-mineral mixtures

From Table C-18 and Figure C-16 it can be seen that the best correlations between gas composition of the TWD coal and the model mineral mixtures were obtained by addition according to the standard model setup as used by previous authors in FactSage, with mineral matter accounted for by use of the QEMSCAN results.

Table C–18 Cumulative mol % yield of CO, H_2, CH_4 and CO_2 gas species for different modelled cases

	Standard models			XRD Models		QEMSCAN Models	
	TWD	MM XRD	MM QS	TWD	MM	TWD	MM
Gas species	Cumulative mol %						
520°C							
CO	0.8	0.7	0.8	0.8	0.7	0.8	0.7
H_2	18.6	18.6	18.6	18.5	18.5	18.3	18.6
CH_4	71.1	72.2	71.1	70.5	73.0	70.5	72.8
CO_2	9.5	8.5	9.6	10.2	7.8	10.4	7.9
750°C							
CO	8.8	8.5	8.9	9.1	8.2	9.1	8.2
H_2	42.5	43.0	42.4	42.1	43.2	41.8	43.1
CH_4	40.5	41.2	40.5	40.1	41.7	40.2	41.7
CO_2	8.2	7.4	8.2	8.7	6.8	8.9	7.0
900°C							
CO	14.7	14.1	14.8	15.1	13.6	15.2	13.8
H_2	49.8	50.5	49.6	49.2	50.9	48.9	50.7
CH_4	29.5	30.0	29.4	29.2	30.4	29.3	30.4
CO_2	6.1	5.5	6.1	6.5	5.1	6.6	5.2

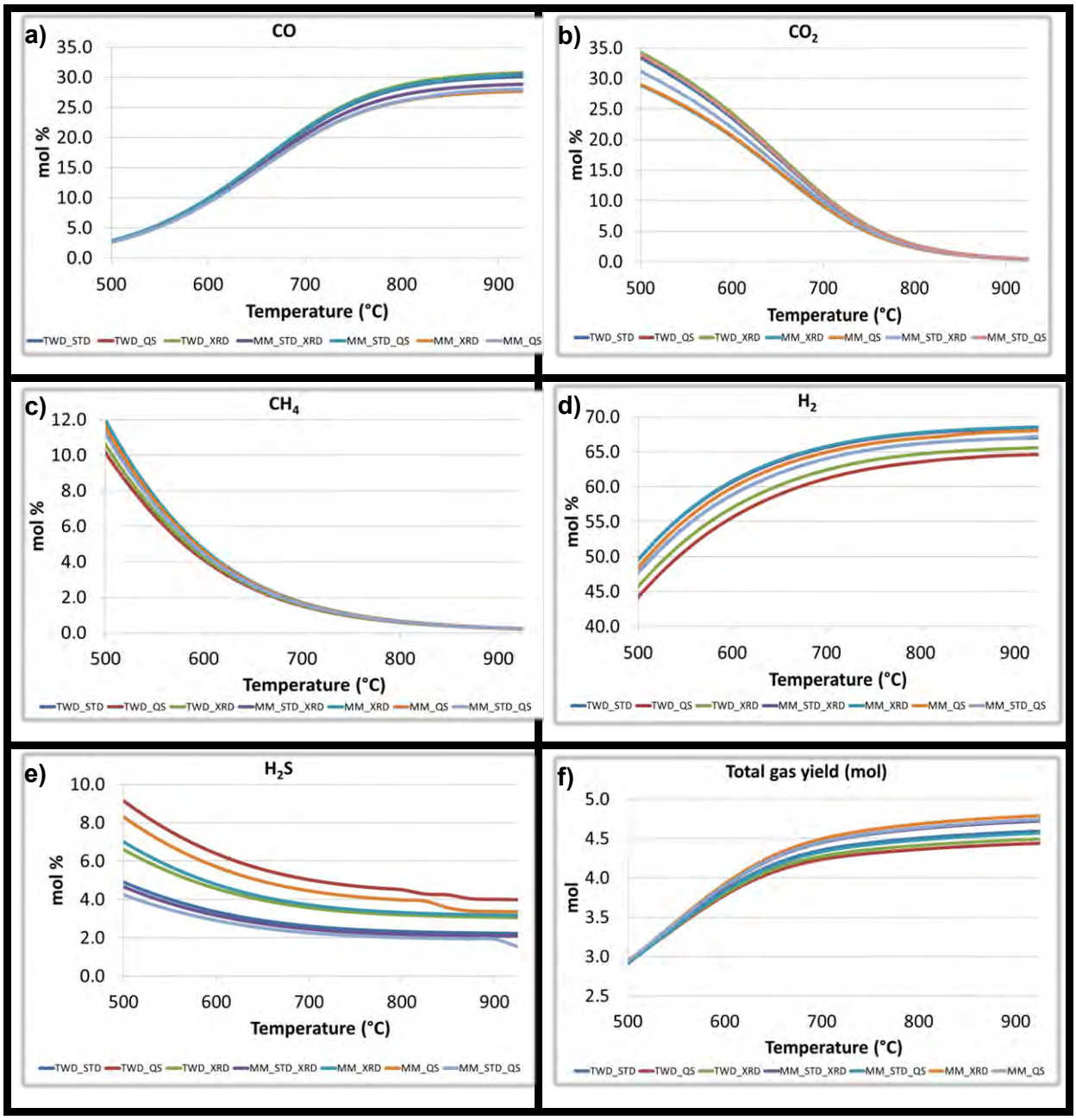

Figure C–18 Gas evolution profiles from FactSage data for different models a) CO, b) CO_2, c) CH_4, d) H_2, e) H_2S and f) Total gas yield for the different models.

C-9 Highveld ROM coal analyses (Govender, 2005).

Govender (2005) characterised a typical coal sample from the Highveld coal field before any washing (beneficiation) took place. This was used as basis for the make-up of a high ash percentage mineral mixture.

Table C-19 indicates the standards used for analyses of the coal sample as reported by Govender (2005).

Table C-19 Standards used in the analyses of Highveld ROM coal (Govender, 2005)

Analysis	Standard	Company
Proximate analysis	Moisture content (SABS 924); Ash content (ISO 1171); Volatile matter (ISO 562), Fixed carbon (by difference)	Coal and Mineral Technologies laboratory
Ultimate analysis	C,H,N (ASTM D5373); Total Sulphur (D4239)	Coal and Mineral Technologies laboratory
Ash composition	ASTM D3582	Coal and Mineral Technologies laboratory
XRD	Siemens D500 X-ray goniometer with Cu tube, variable slit and secondary graphite monochromator	Council for Geoscience laboratory
CCSEM		Van Alphen Consultancy

C-9.1 Chemical coal analyses

C-9.1.1 Proximate analyses results

Table C-20 indicates the proximate results as reported by Govender (2005).

Table C-20 Proximate analysis results (Govender, 2005)

	Highveld ROM				
	Unit	***A.D[a]***	***D.B.[b]***	***D.A.F.[c]***	***D.M.M.F.[d]***
Inherent moisture	wt%	3.0	0	0	0
Ash	wt%	25.5	14.9	0	0
Volatile matter (VM)	wt%	25.3	32.8	38.5	39.1
Fixed carbon (FC)*	wt%	46.2	52.3	61.5	60.9
TOTAL	wt%	**100**	**100**	**100**	**100**
Fuel ratio (FC/VM)		-	-	-	1.6

[a]A.D.= air dry; [b]D.B.= dry basis, [c]D.A.F. = dry, ash free basis, [d]D.M.M.F. = dry, mineral matter free basis

C-9.1.2 Ultimate analysis results

Table C-21 indicates the proximate results as reported by Govender (2005).

Table C-21 Ultimate analysis results (Govender, 2005)

	Unit	*D.A.F.*[b]
Total sulphur	wt%	1.9
Carbon	wt%	78.6
Hydrogen	wt%	4.4
Nitrogen	wt%	2.0
Oxygen (by difference)	wt%	13.1
TOTAL		**100**

[b]*D.A.F. = dry, ash free basis*

C-9.2 Mineralogical analyses results

Mineralogical analyses done by Govender (2005) include XRF ash analysis, Mineral XRD analysis and CCSEM analysis.

C-9.2.1 XRF Ash analysis

Table C-22 indicates the XRF ash analysis as reported by Govender (2005).

Table C-22 XRF Ash analysis results (Govender, 2005)

Ash species	wt% *(d.a.f.*)*
Al_2O_3	25.00
CaO	7.80
Fe_2O_3	5.90
K_2O	1.04
MgO	2.01
Na_2O	0.47
P_2O_5	0.80
SiO_2	50.1
TiO_2	1.29
SO_3	5.53
Total	**100.00**

** d.a.f. = dry, ash free basis*

C-9.2.2 Mineral XRD analysis

Table C-23 indicates the Mineral XRD analysis as reported by Govender (2005).

Table C-23 Mineral XRD results (Govender, 2005)

Mineral species	wt%
Quartz	19
Kaolinite	54
Calcite	3
Dolomite	8
Pyrite	6
Mica	8
TOTAL	**100**

C-9.2.3 CCSEM Mineral analysis

Table C-24 indicates the CCSEM mineral analysis as reported by Govender (2005).

Table C-24 CCSEM mineral analysis (Govender, 2005)

Mineral species	wt%
Sulphates/Gibbsite	0.1
Pyrite	5.1
Siderite	0.1
Calcite	3.4
Dolomite	1.9
Apatite	0.0
Kaolinite	12.7
Quartz	5.3
Illite/Muscovite	1.3
Microcline	0.33
Rutile	0.1
Other	0.3
TOTAL	**30.6**

C-10 Statistical models

The Q-Q plots for the derived are provided.

C-10.1 Gas yield

The Q-Q plot for the gas yield model is provided in Figure C-19

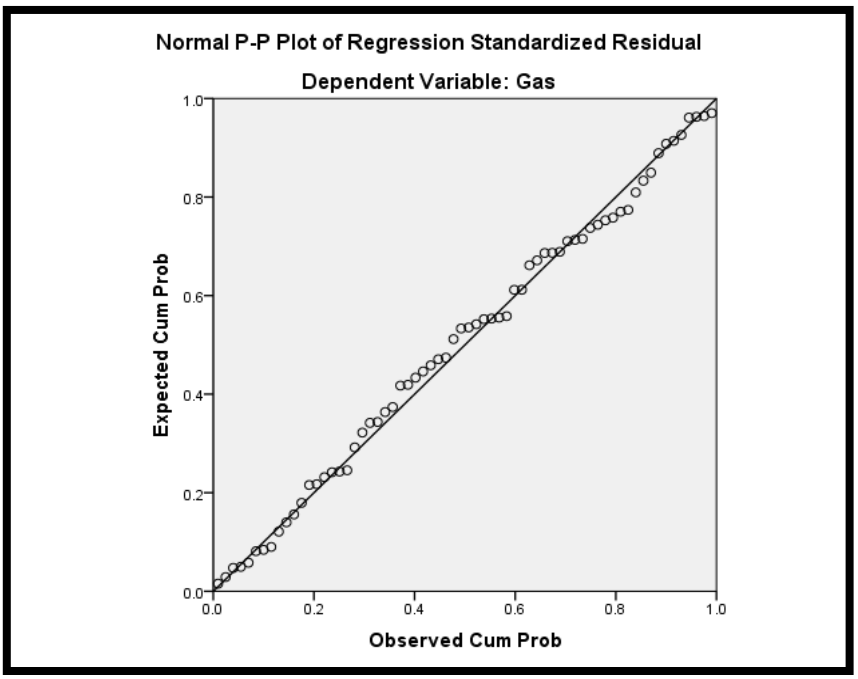

Figure C–19 Q-Q plot for Gas yield model.

C-10.2 Tar yield

The Q-Q plot for the tar yield model is provided in Figure C-20.

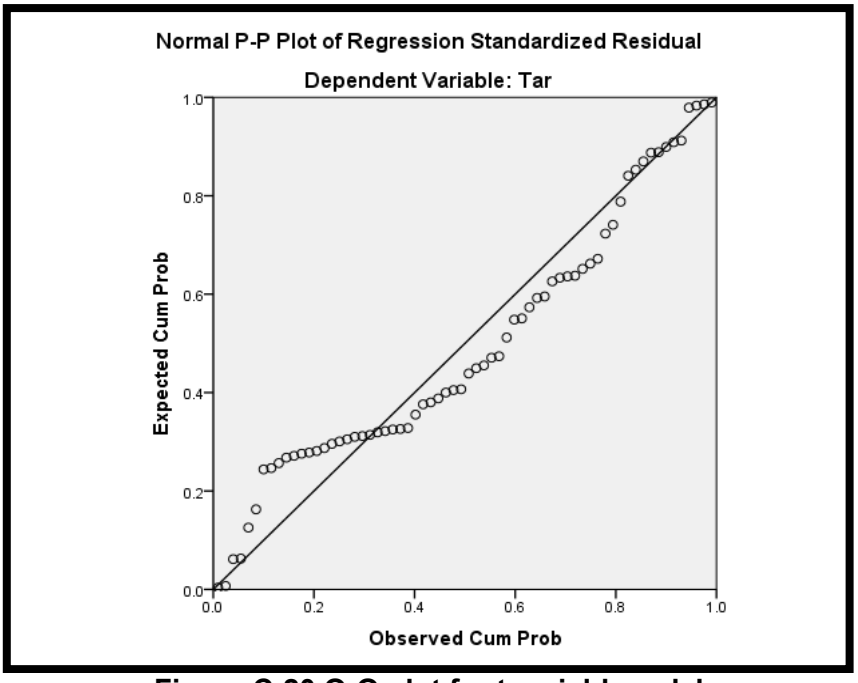

Figure C-20 Q-Q plot for tar yield model

C-10.3 Char yield

The Q-Q plot\ for the char yield model is provided in Figure C-21

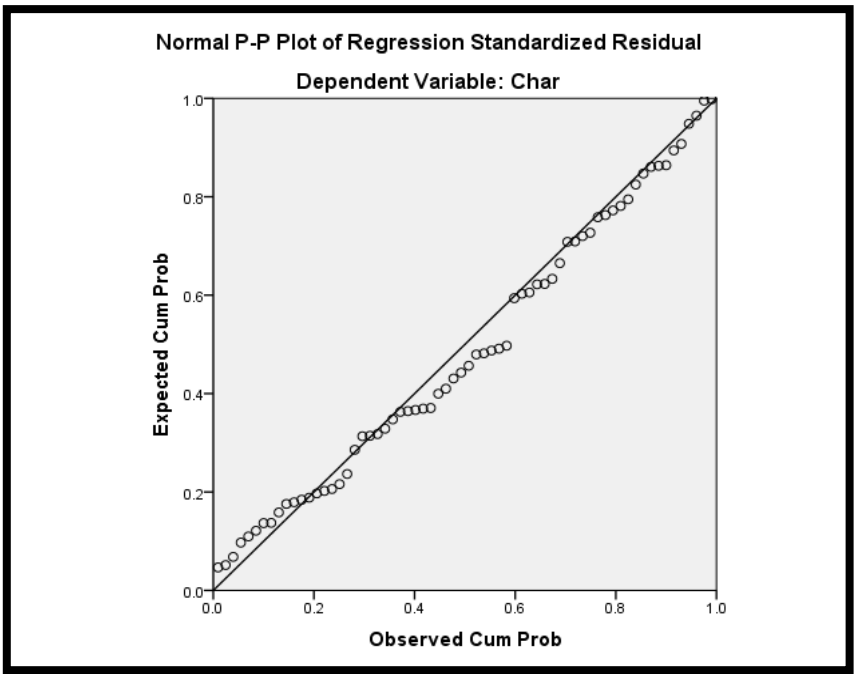

Figure C-21 Q-Q plot for char yield model

C-10.4 Gas composition

C-10.4.1. H_2 yield

The Q-Q plot for the H_2 yield model is Figure C-22

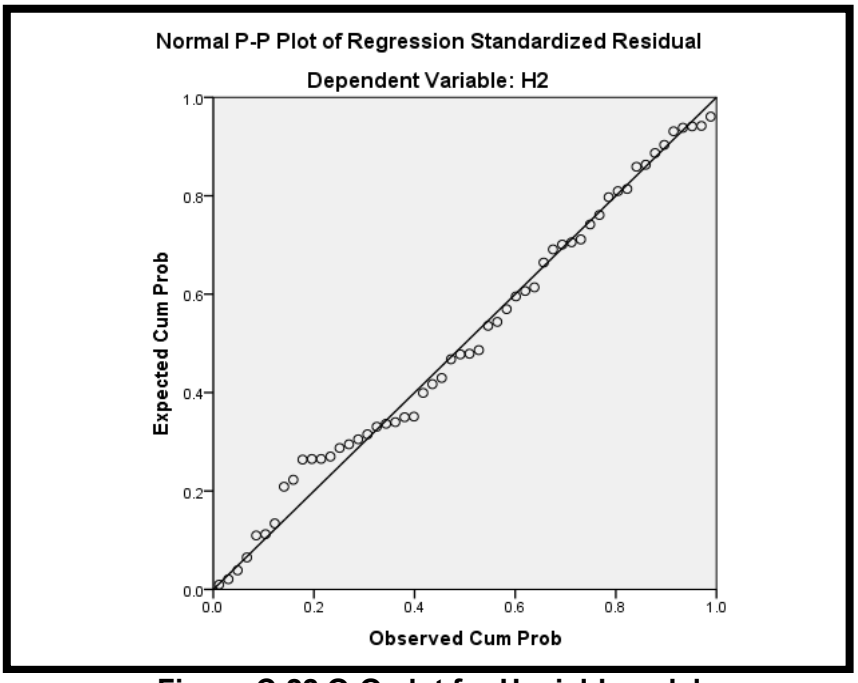

Figure C-22 Q-Q plot for H_2 yield model

C-10.4.2. CO yield

The Q-Q plot or the CO yield model is provided in Figure C-23.

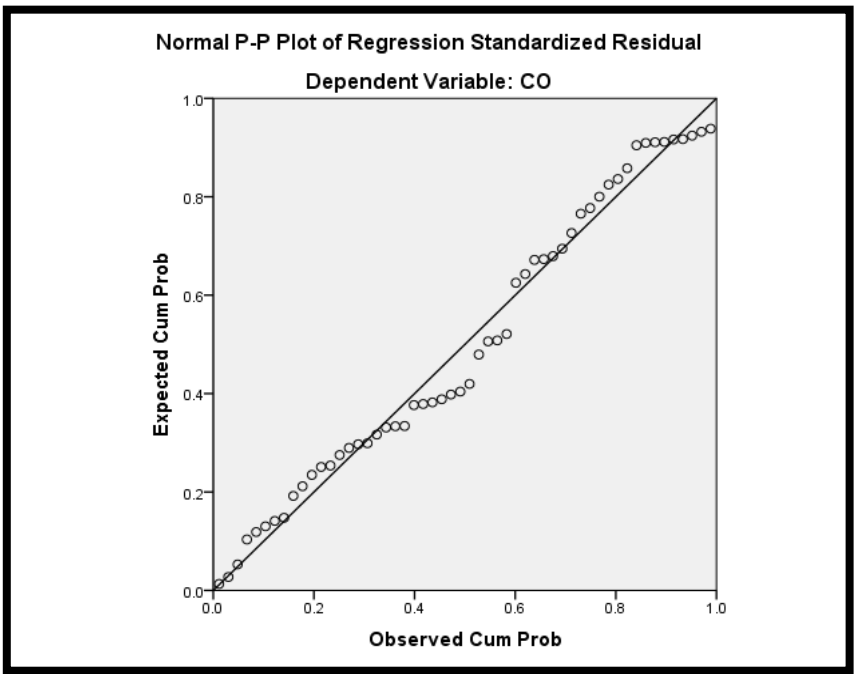

Figure C-23 Q-Q plot for CO yield model

C-10.4.3. CO_2 yield

The Q-Q plot for the CO_2 yield model is provided in Figure C-24.

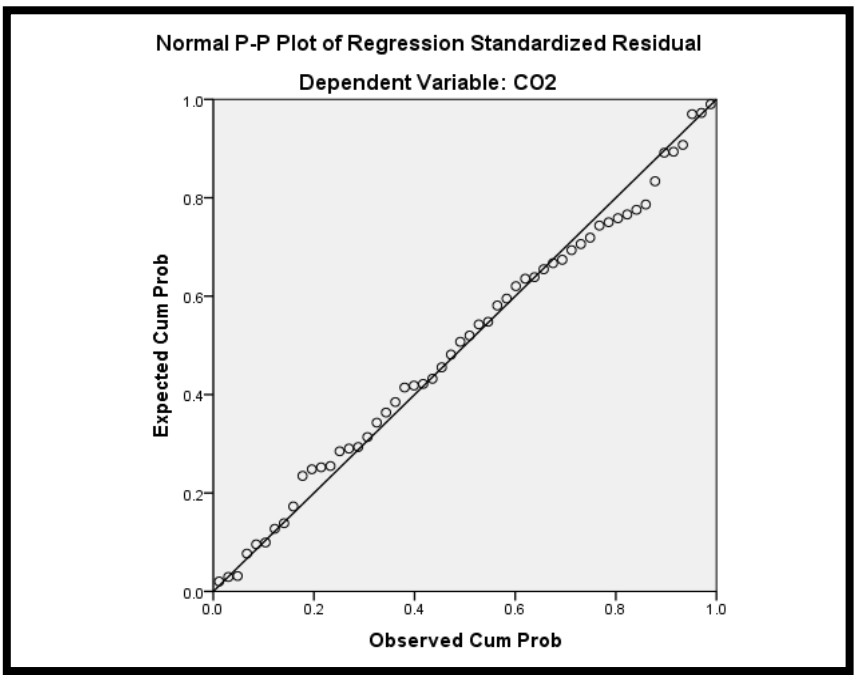

Figure C-24 Q-Q plot for CO_2 yield model

C-10.4.4. CH_4 yield

The Q-Q plot for the CH_4 yield model is provided in Figure C-25.

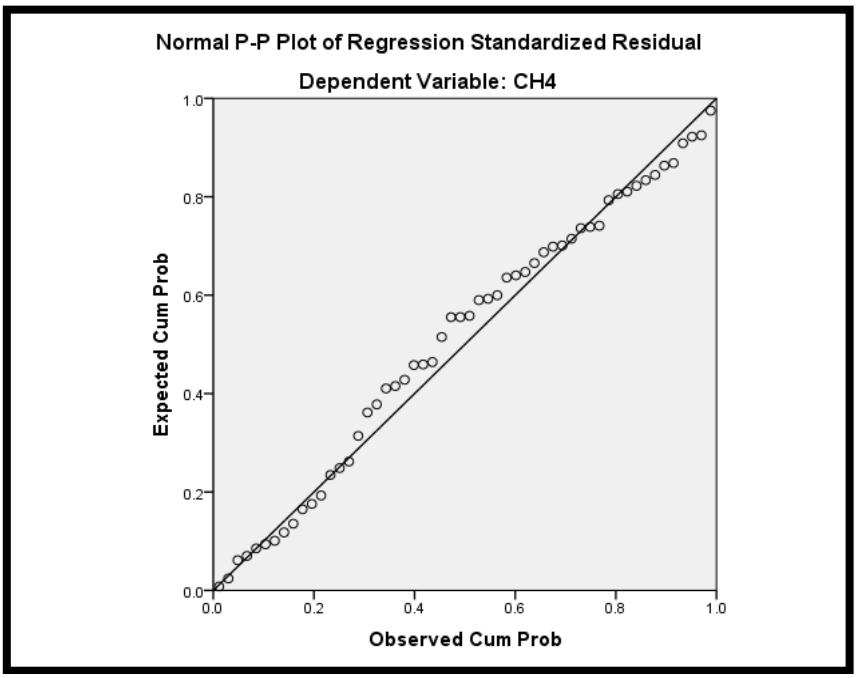

Figure C-25 Q-Q plot for the CH_4 yield model.

Appendix D: Publications